

https://dspace.org/

Design and synthesis of aldol addition catalytic peptides

Peme, Thabo

2021
https://hdl.handle.net/10539/32434

Downloaded from a DSpace repository. https://dspace.org/



UNIVERSITY OF THE
WITWATERSRAND,
JOHANNESBURG

DESIGN AND SYNTHESIS OF ALDOL ADDITION CATALYTIC PEPTIDES

Thabo Peme

Supervisor: Dr Maya Makatini

Co-supervisor: Prof Dean Brady

DECLARATION

I hereby confirm that the work presented in this report is my original work, and to the best of my knowledge, it has not been submitted previously or concurrently for any degree at any other institution. This entire work was conducted by me under the supervision of Dr Maya Makatini and Prof Dean Brady. It is submitted for examination for the degree of Doctor of Philosophy at the University of Witwatersrand



Thabo Peme

DEDICATION

*This PhD thesis is dedicated to my loving parents Maria and Lucas, and my siblings for their prayers, endless love, courage and support which always propel me move forward in life***.**

ACKNOWLEDGEMENTS

First and foremost, I would like to thank my Lord and saviour Jesus Christ, for granting me the strength, health, protection, ability, and wisdom to carry out this project. To you Lord belong all the glory, majesty, power and honour.

I would like to express my sincere gratitude to my supervisor Dr Maya Makatini, for giving me the opportunity to be her student and carry out this project. I'm grateful for your endless support, input, guidance and courage throughout this entire journey. Thank you for giving me the opportunity to express myself, to be confident and broaden my research skills. I will be forever thankful for this opportunity; God bless you mightily. A special appreciation to my co-supervisor Prof Dean Brady for all his input and support throughout this PhD. Thank you for all your efforts to make this work a success.

I am also thankful to Dr Wanyama Juma for his advices and willingness to help. You were always there to assist, even when it was not convenient. God bless you abundantly for your kindness.

I would like to say a big thank you to the Organic staff, Prof Charles de Koning, Prof Jo Michael, and Prof Moira Bode and Dr Amanda Rousseau, for their help and suggestions during organic group meetings and providing conducive research space.

I also would like to express my gratitude the mass spec team. Thapelo Mbhele, you such an amazing being! thank you for your patience and kind assistance in training me to be knowledgeable in LC-MS. Thank you to Eric Morifi and Refilwe Moepa for the continuous access to mass spec lab. A similar appreciation to the Dr Izak Kotźe and Dr Hendrik Henning for the support on the use of NMR instruments.

A special thanks to Prince Shumbula for his help in carrying out the AuNPs experiments and their analysis and Prof Moloto for the access to the lab facilities. A big thank you to Prof Sayed and Dr Ikechukwu for their assistance with Circular Dichroism experiments. I would like to thank Dr Vinu and Dr Robin for their help in analysis and interpretation of enzymes structures.

A special thanks to my colleagues; Pious Shuro, Khanani Machumela, Ntombi Ngqinayo, Lesotho Ntlamo, Refilwe Moepa, Sinazo Cobongela and Thapelo Mbhele for their inputs in group meetings and creating a friendly research environment

To my fellow organic mates both past and present: Dr Seanego, Dr Juma, Dr Kennedy, Dr Charles, Dr Memory, Mudzuli, Phathu, Dennis, Robin, Songz, Tebogo, Gciniwe, Amy, Xolani, Fatima, Kamo, Edward, Fatema, Adelaide, Mpumi, thank you for the wonderful times we shared in the lab.

I would like to thank the department of Chemistry support staff, glass blower; Mr Dzara, admin staff: Khwezi, Thuli, sis Getty, Amanda, and the chemical store guys; David and Elias.

A very special appreciation to my lovely parents Maria and Lucas for their endless support, courage and for raising me to be the man I am today. My siblings, Tlami, Dineo, Kefilwe, Phemelo and Thati, I thank God for your lives, I'm a proud brother. I'm also grateful to my Pastors in CE Braamfontein church; Pastor France and Albert, thank your sirs for nurturing my faith with the word of God.

To Wendy Machaba, I thank God for sending you my way. You have been so supportive in many ways since the day we met. When I started the write-up, my laptop broke and you eagerly offered your laptop which I used to compile this work. God bless you.

Lastly, I would like to express my special thanks to CSIR inter-bursary support for funding and the University of Witwatersrand for providing great research facilities to carrying out this project.

ABSTRACT

The aldol reaction is regarded as one of the most prominent carbon-carbon bond forming organic reactions. For many decades enzymes have gained considerable attention as useful catalysts for this reaction, due to their fascinating properties such as their high selectivity and mild reactions conditions. Although enzymes are efficient catalysts, they still suffer from limitations such as narrow substrate tolerance, pH specificity and high cost; there is therefore a need for catalysts that mimic enzyme activity but have fewer drawbacks. Synthetic peptides, because of their structural similarity to enzymes, synthetic accessibility and diverse molecular structures; have emerged as the ideal candidate to realize an enzyme-like catalyst. The design of a peptide catalyst possessing secondary structural units (such as the alpha-helix and beta turn) can produce a novel, enzyme-like organocatalyst. The structural units of the peptides in this study incorporates the beta turn and catalytic amino acids taken from the active site of the fructose-1,6-bisphosphate aldolase (FBPA) enzyme. The peptide sequence also consists of cysteine residues that can form strong interactions with the gold surface via the thiol groups. The immobilization of catalyst onto gold nanoparticle (AuNPs) has been proven to restrict conformational flexibility of catalysts thereby improving their catalytic activity and reusability. The overall aim of this study is to design and synthesize peptides catalysts based on the structure and activity of the FBPA enzyme.

Twelve mimetic peptides based on the catalytic active site of the FBPA enzyme [TP_Asp (**1**), TP_ADLys (**2**), TP_ADA (**3**), TP_AspC (**4**), TP_ADLysC (**5**), TP_ADAC (**6**), TP_Glu (**7**), TP_GDLys (**8**), TP_GDA (**9**), TP_GluC (**10**), TP_GDLysC (**11**) and TP_GDAC (**12**)] were designed and synthesized using the solid phase peptide synthesis strategy.

NMR (nuclear magnetic resonance spectroscopy) and CD (circular dichroism) were used to determine possible folding patterns and secondary structural features. Both experiments provided confirmation that the peptides are not linear but possesses secondary structural elements.

The screened selected peptides showed catalytic activity and the aldol products were obtained in low yields (up to 44%), excellent enantioselectivity (up to 94%) and moderate diastereoselectivity (65:35). The influence of water, substrate scope, catalyst loading and effect of solvents on the reactions were investigated. An increase in catalyst loading did not significantly improve the yields. The addition of water to the reaction medium to enhanced

both the yields and selectivities. Substituting the organic solvent with a 100 mM phosphate (pH=8.0) buffer afforded improved catalytic activity (38 % yield) and enantioselectivity (up to 80% ee) because of the structural conformation that the peptide adopts in the solution. Aromatic aldehydes bearing a halogen group were shown to be inappropriate substrates for the peptide aldol catalyzed reaction while nitro substituted aromatic aldehydes are acceptable substrates for the peptide-promoted aldol reaction

Different AuNPs particle sizes (16, 15 and 12 nm) were successfully conjugated to the peptide and characterized using surface plasmon resonance (SPR) and transmission electron microscopy (TEM). The AuNPs did not significantly improve the catalytic activity of the peptide. However, the use of peptide-capped AuNPs lead to a significant improvement of the enantioselectivity (up to 94%) and a moderate improvement of the diastereoselectivity of (62/48 anti/syn) for the reaction between *p*-nitrobenzaldehyde and cyclohexanone. This was attributed to the change in the peptide conformation caused by its interactions with the gold metal surface

In conclusion, the buffer solution and the conjugation of the peptide onto AuNPs induced peptide structural conformations with improved selectivity.

OUTLINE

Herein, the study is presented in four parts. The first part of this thesis provides a formal description of the design and synthesis of novel peptide catalysts for the asymmetric aldol reaction. Twelve mimetic peptides based on the catalytic active site of the FBPA enzyme [TP_Asp (**1**), TP_ADLys (**2**), TP_ADA (**3**), TP_AspC (**4**), TP_ADLysC (**5**), TP_ADAC (**6**), TP_Glu (**7**), TP_GDLys (**8**), TP_GDA (**9**), TP_GluC (**10**), TP_GDLysC (**11**) and TP_GDAC (**12**)] were designed and synthesized using the solid phase peptide synthesis strategy.

The second part involves the structural elucidation and characterization of the designed peptide analogues **1** and **2** using NMR (nuclear magnetic resonance) and CD (circular dichroism) to determine possible folding patterns and secondary structural features. The CD experiments indicated that the peptides exist as random coil structures that move towards the beta-sheet and alpha-helix conformations. The long/medium range NOEs (nuclear Overhauser effect) correlations in the NMR experiments revealed the existence of a bent conformation. Both the CD and NMR experiments provided a complementary confirmation that the peptides are not linear but possesses secondary structural elements.

The third part of this dissertation describes the preliminary test and application of the peptide catalysts for asymmetric aldol reactions. The selected peptides **1**, **2**, **3**, **4**, **7**, **8**, **9** and **11** screened showed catalytic activity towards the aldol reaction between cyclic, linear aldehydes and ketones. The influence of water, substrate scope, catalyst loading and effect of solvents on the reactions were investigated. The addition of water to the reaction medium enhanced both the yields and selectivities. The corresponding aldol products between acetone and aromatic aldehydes were obtained in low yields (up to 16%), excellent enantioselectivity (up to 93%) and an increase in catalyst loading did not significantly improve the yield. Aldol reactions between cyclohexanone and aromatic aldehydes in organic solvents exhibited poor catalytic activity (25% yield), enantioselectivity (up to 31% ee) and diastereoselectivity (64/36). Substituting the organic solvent with 100 mM phosphate (pH=8.0) afforded improved catalytic activity (38% yield), enantioselectivity (80% ee) because of the structural conformation that the peptide adopts in the solution. The aldol reaction between aromatic aldehydes bearing electron-withdrawing groups in ketone as a solvent afforded moderate yields (up to 42%), poor enantioselectivity (up to 20%) and moderate diastereoselectivity (up to 59/41; anti/syn). Hence, it can be concluded that the aromatic aldehydes bearing a halogen group are

inappropriate substrates for the peptide aldol catalyzed reaction while nitro substituted aromatic aldehydes are acceptable substrates for the peptide-promoted aldol reaction.

The fourth section involves the immobilization of peptide **2** onto gold nanoparticles (AuNPs) in order to improve the catalytic activity, stability and its reusability of peptide catalyst. AuNPs were successfully synthesized using the Turkevich method. Different particle sizes (16, 15 and 12 nm) in diameter were successfully conjugated to the peptide. The peptide conjugation to AuNPs was characterized using surface plasmon resonance (SPR) and transmission electron microscopy (TEM). The aldol reaction between *p*-nitrobenzaldehyde and cyclohexanone catalyzed by peptide-capped AuNPs indicated that AuNPs did not have much influence on the catalytic activity of the peptide. However, the use of peptide-capped AuNPs lead to a significant improvement on the enantioselectivity (up to 94%) and moderate diastereoselectivity of 62:38 (anti/syn) for the reaction between *p*-nitrobenzaldehyde and cyclohexanone. This was attributed to the change in conformation caused by the peptide interaction with the gold metal surface.

In conclusion novel aldol addition reaction peptides and AuNPs-peptide catalysts were successfully designed, synthesized and characterized. All the screened peptide exhibited moderate aldol reaction between *p*-nitrobenzaldehyde and cyclohexanone (Table 4-5), peptide-capped AuNPs afforded aldol products with improved enantioselectivity (up to 94%) and moderate diastereoselectivity (62:38). The use of a buffered solution proved to enhance the catalytic activity and selectivity of the peptide and that of the peptide-AuNPs catalyzed aldol reaction. The use of buffered solution induced the structural conformation of peptides and also improved the selectivity of peptide capped-AuNPs.

LIST OF TABLES

Table 2- 1: The peptide sequences with amino acid derived from the catalytic active site of the FBPA enzyme 44

Table 2- 2: Detailed summary of the cyclized peptide catalysts containing aspartic acid 54

Table 2- 3: Detailed summary of the cyclized peptide catalysts containing glutamic acid.....61

Table 3- 1: NMR chemical shifts (ppm) of identified spin assignment for TP_Asp using TOCSY spectrum.....79

Table 3- 2: NMR chemical shifts (ppm) of identified spin systems used for the initial assignment.....81

Table 3- 3: NMR chemical shifts (ppm) observed through NOEs intra-residue connectivity.82

Table 3- 4: NMR chemical shifts (ppm) of individual spin assignment for TP_Asp. 83

Table 3- 5: NMR chemical shifts (ppm) of identified spin assignment for TP_ADLys using TOCSY spectrum. 85

Table 3- 6: NMR chemical shifts (ppm) of individual spin assignment for TP_ADLys.....86

Table 4- 1: Peptide catalyzed aldol reactions between acetone and substituted aromatic aldehydes[a] 103

Table 4- 2: Aldol reaction between cyclohexanone and various aromatic aldehydes catalyzed by peptides[a] 105

Table 4- 3: Aldol reaction of cyclohexanone and *p*-nitrobenzaldehyde catalyzed by 4 mol% peptide catalysts in different solvents [a] 107

Table 4- 4: Aldol reaction between acetone and cyclohexanone using 8 mol% peptide catalyst[a] 110

Table 4- 5: Aldol reaction of cyclohexanone and *p*-nitrobenzaldehyde catalyzed by 8 mol% peptide catalyst in different solvents[a] 111

Table 4- 6: Recovery and reuse of catalyst TP_ADLys in aldol reaction[a] 113

Table 5- 1**:** The average size and standard deviation for produced nanoparticles.....132

Table 5- 2: Aldol reactions screening of *p*-nitrobenzaldehyde and cyclohexanone catalyzed by peptide-supported AuNPs[a] 134

Table 5- 3: Aldol reactions between *p*-nitrobenzaldehyde and cyclohexanone catalyzed by peptide-supported AuNPs[a] 136

Table 5- 4: Recovery and reuse of peptide capped AuNPs[a] 138

LIST OF SCHEMES

Scheme 1- 1: The direct catalytic asymmetric aldol reaction. 2

Scheme 1- 2: Types of beta turn motifs. 7

Scheme 1- 3: Mechanism of Type I Schiff base forming aldolase represented by the RAMA (Rabbit muscle aldolase**)** and the Type II zinc enolate mechanism represented by the fuculose-1-phosphate enzyme aldolase, bottom. P =OPO_3^{2-} 11

Scheme 1- 4: Mechanism of Fructose-1, 6-bisphosphate aldolase based on the structure of the DHAP Schiff-base intermediate. 14

Scheme 1- 5: Asymmetric aldol reaction reported by List *et al.* 16

Scheme 1- 6: The asymmetric cyanation of benzaldehyde to a cyanohydrine. 17

Scheme 1- 7: Peptide mediated kinetic resolution of functionalized racemic alcohols 18

Scheme 1- 8**:** Kofoed's peptide catalyzed enantioselective aldol reaction of *p*-nitrobenzaldehyde and acetone. 19

Scheme 1- 9: AuNPs-supported proline-catalyzed asymmetric aldol reactions. 23

Scheme 2- 1: Total synthesis of hydroxybrevicomins from aldol reaction catalyzed by an antibody 38C2. 38

Scheme 2- 2: A) Peptide dendrimer catalyzed aldol reaction, B) L2D1 Peptide dendrimer used. 39

Scheme 2- 3: Bayat's rational design of mimetic peptides based on the AKR active site. 40

Scheme 2- 4: General procedure for the SPPS peptide synthesis; where a=20% piperidine/DMF, b=DIPEA/HBTU/Fmoc-AA, and d=TFA/TIS/EDT/H_2O, X or Y=different amino acid side chain, R=amino acids. 46

Scheme 4- 1: Aldol reaction between cyclic and linear aldehyde and DHAP using RAMA. . 93

Scheme 4- 2: Aldol reactions catalyzed by RAMA using DHAP as a donor ketone: Reaction **1**, 1 mg RAMA, 20 % DMSO/TEA buffer (pH 7.0); Reaction 3-6, 3 mg (9.5×10-5 mol) RAMA, DHAP (0.05 mmol, 8.5 mg), TRIS-buffer pH 7.6, rt for 24-72 h. 95

Scheme 4- 3: Water as solvent in organocatalytic asymmetric aldol reactions, (A) Hayashi's proline catalyzed aldehyde–ketone aldol reaction in water, (B) Rahman's small proline-based dipeptide in aqueous medium. 97

Scheme 4- 4: Aldol test reactions for selected peptides, using (A) linear aldehydes and (B) aromatic aldehydes with acetone. 99

Scheme 4- 5: Aldol test reaction for selected peptides, using (A) linear aldehydes with cyclopentanone and (B) aromatic aldehydes cyclopentanone, (C) linear aldehydes with cyclohexanone, (D) aromatic aldehydes with cyclohexanone. 101

LIST OF FIGURES

Figure 1- 1: A crystal structure depicting hydrophobic groups packed inside (red), and hydrophilic hydroxyl groups outside the enzyme molecule. 4

Figure 1- 2: Ribbon diagram of the crystal structure of aldolase enzyme depicting the α-alpha helices (cerulean), β-sheets (purple), and active site residues bonded to the substrate (shown as spheres) [PDB code: 2ALD]....5

Figure 1- 3: An α-helix that is stabilized by internal hydrogen bonding. 6

Figure 1- 4: Free energy profile diagram for both enzyme-catalyzed and uncatalyzed reactions. The symbols; E represents the enzyme, S is the free substrate, S* the free transition state, ES represents the enzyme-substrate complex, ES* is the enzyme-transition state, EP is the enzyme-product complex and P the free product state 9

Figure 1- 5: The active sites residues of FBPA shown as stick form (on the right) 12

Figure 1- 6: 3D Structure depicting the FBPA active site residues interaction with the substrate molecule (2FBP) [some residues chains (side or main) are omitted for picture clarity] 13

Figure 1- 7: Modes of action of proline catalysis. 16

Figure 1- 8: Resin-supported peptide catalyst 19

Figure 1- 9: An N-terminal hydrogen bond replace with C-C bond obtained from a ring closing metathesis (RCM) reaction.....21

Figure 1- 10: β-hairpin with Asp-Gly β-turn promoter done by Ramírez-Alvarado *et al*. 21

Figure 1- 11: Peptide sequence of E3H15 conjugated to Gold nanoparticles.[111] 23

Figure 2- 1: Amino acids sequence of the *Drosophila melanogaster* FBPA enzyme obtained from the UniProt protein database. 41

Figure 2- 2: The amino acid residues of the FBPA active site 42

Figure 2- 3: Structural representation of TP_Asp peptide, showing a turn and catalytic motif site. 45

Figure 2- 4: Illustration of the difference between HATU and HBTU....47

Figure 2- 5: LC-MS spectrum for the fully synthesized crude TP_Asp 48

Figure 2- 6: Folded structure of TP_Asp using *d*e novo peptide structure prediction (RPBS Web Portal), depicting L-lysine side chain (yellow) pointing out. 49

Figure 2- 7: Common peptide secondary structure conformations....50

Figure 2- 8 : LC-MS spectrum for 1st purification of peak 1 for TP_ADA peptide 51

Figure 2- 9: Different ways of peptide cyclization. 52

Figure 2- 10: Amino acid sequence for peptide catalyst TP_Glu 55

Figure 2- 11: LC-MS spectrum for the 1st purification of TP_Glu peak 1 56
Figure 2- 12: LC-MS spectrum for TP_Glu peak 1 after 2nd purification 56
Figure 2- 13: Amino acid sequence for peptide catalyst TP_Glu, with D Lys highlighted in red 57
Figure 2- 14: LC-MS spectrum for TP_GDLys peak 2 after 1st purification 58
Figure 2- 15: LC-MS spectrum for TP_GDLys peak 2 after 2nd purification 59
Figure 2- 16: LC-MS spectrum for TP_GDA peak 3 after 2nd purification.....60
Figure 3- 1: Circular dichroism studies for TP_ADLys and TP_Asp peptides in 200 mM phosphate buffer solution (B) and percentage of peptide structure 73
Figure 3- 2: Circular dichroism spectra of TP_ADLys and TP_Asp peptides in water (W) and their secondary structure analysis 74
Figure 3- 3**:** 1D ^{1}H NMR spectra of TP_ADLys peptide effect of temperature variations 76
Figure 3- 4: Structural representation of TP_Asp. 77
Figure 3- 5: The partial ^{1}HN-Hα fingerprint region of 2D the TOCSY spectrum TP_Asp of the peptide, showing individual spin system patterns (full spectrum is provided in Appendix II, Figure S.3-6).....78
Figure 3- 6: TP_Asp peptide structure with arrows indicating long correlation using ROESY 84
Figure 4- 1: A series of selected peptides screened for aldol reaction catalytic activity. 98
Figure 4- 2: LC-MS chromatograph depicting the formation of A1 product in 3 hours. 99
Figure 4- 3: LC-MS chromatograph depicting the formation of A2 product in 30 minutes. 102
Figure 5- 1: Proposed structure of TP_ADLys peptide bounded to AuNP with its two cysteine residues. 125
Figure 5- 2: An image of a reaction mixture changing colour, due to the addition of the citrate solution, from (a) pale yellow to (b) pink/red. 127
Figure 5- 3**:** UV-vis absorption spectra showing LSPR band for citrate-capped AuNP (black line) and peptide-AuNPs (red line). 129
Figure 5- 4: TEM images for citrate-AuNPs and peptide-capped AuNPs (a) AuNP-20, (b) AuNP-20P, (c) AuNP-30, (d) AuNP-30P, (e) AuNP-50 and (f) AuNP-50P. 130
Figure 5- 5: Particle size distribution of citrate capped AuNPs and peptide-functionalised AuNPs obtained from TEM images. 131

LIST OF ABBREVIATIONS

δ	chemical shift
AAs	amino acids
Ala (A)	alanine
Aib	aminoisobutyric acid
Arg (R)	arginine
Asp (D)	aspartic acid
Au	gold
AuNPs	gold nanoparticles
Boc	Tert-Butyl-Oxycarbonyl
cat	catalyst
CD	circular dichroism
COSY	correlation spectroscopy
Cys (C)	cysteine
d	doublet
dd	doublet of doublets
DCM	dichloromethane
DHA	dihydroxyacetone
DHAP	dihydroxyacetone phosphate
DIPEA	N,N-diisopropylethylamine
DMF	N,N-dimethylformamide
DMSO	dimethyl sulfoxide
dr	diastereomeric ratio
EDT	1,2-Ethanedithiol
ee	enantiomeric excess
ESI	electrospray Ionisation
EtOAc	ethyl acetate
Et_2O	diethyl ether
FBPA	fructose-1,6-bisphosphate Aldolase
FBP	fructose-1,6-bisphosphate
Fmoc	9-Fluorenylmethoxycarbonyl
Glu (E)	glutamic acid
Gly (G)	glycine
HATU	1-[Bis(dimethylamino)methylene]-1H-1,2,3-triazolo[4,5-b]pyridinium 3-oxide hexaflourophosphate
HBTU	(2-(1H-benzotrial-1-yl-1,1,3,3-tetramethyluronium hexafluorophosphate
HMBC	heteronuclear multiple quantum coherence
HPLC	high performance liquid chromatography
HRMS	high resolution mass spectrometry
h	hour
HSQC	heteronuclear single quantum coherence

IPA	isopropyl alcohol
FT-IR	Fourier-transform infrared
LC-MS	liquid chromatography-mass spectrometry
LSPR	localised surface plasmon resonance
Lys (K)	lysine
J	coupling constant
m	multiplet
MBHA	rink Amide 4-methylbenzhydrylamine
MeCN	acetonitrile
MeOH	methanol
mg	milligram
mL	milliliter
min	minute
mM	millimolar
Mol	molar
MS	mass spectrometry
m/z	mass charge
NMP	N-methylpyrrolidone
NMR	nuclear magnetic resonance
NOE	nuclear Overhauser effect
NOESY	nuclear Overhauser effect spectroscopy
nm	nanometer
NPs	nanoparticles
PDB	Protein Data Bank
pep	peptide
s	singlet
SPPS	Solid phase peptide synthesis
Ser (S)	serine
t	triplet
TEA	triethylamine
TEM	transmission electron microscopy
TFA	trifluoroacetic acid
TLC	thin layer chromatography
TIS	Triisopropyl silane
TMS	Tetramethylsilane
TOCSY	total correlation spectroscopy
RAMA	rabbit muscle aldolase
R_f	retardation factor
r.t.	room temperature
ROESY	rotating frame Overhauser effect spectroscopy
TRIS	tris(hydroxymethyl)aminomethane
Tyr (Y)	tyrosine
q	quartet
μL	microliter

Table of Contents

DECLARATION II
DEDICATION III
ACKNOWLEDGEMENTS IV
ABSTRACT VI
OUTLINE VIII
LIST OF TABLES X
LIST OF SCHEMES XI
LIST OF FIGURES XII
LIST OF ABBREVIATIONS XIV
Chapter 1 1
Introduction 1
1.1 Background 1
1.2 Aldol reaction 2
1.3 Enzyme structures 4
1. 3.1. α-Helices 5
1.3.2 β-Turn structures, β-Sheets and β-hairpins 6
1.4 Enzyme catalysis 7
1.4.2 Transition state theory 8
1.5 Aldolases 10
1.5.1 Fructose-1, 6-bisphosphate aldolase enzyme 12
1.5.2 Mechanism of the Fructose-1, 6-bisphosphate aldolase 13
1.6 L-Proline as Type I micro Aldolase' 15
1.7 Peptides as organocatalysts 17
1.7.1 Peptides as catalyst for asymmetric aldol reactions 18
1.8 Design considerations and previous work 20
1.8.1 Stabilisation of Peptides using gold nanoparticles (AuNPs) 22
1.8.2 Design of cyclic and AuNPs supported catalytic peptides 24
1.9 Aims and Objectives of the project 24
1.10 References 25
Chapter 2 36
Design and synthesis of novel peptide-based catalysts 36

2.1 Introduction 36
2.2 Previous research on different enzyme mimic approaches 37
2.3 Enzyme mimics based on peptides with secondary structure 40
2.4 Peptide catalyst design 41
2.4.1 General considerations 41
2.4.2.1 Helical motif proposed structures (Helix design) 42
2.4.2.2 Turn motif proposed structures 43
2.4.2.3 D-Amino acids 43
2.5 Results and discussion 45
2.5.1 Synthesis of TP_Asp 45
2.5.1.1 Purification of TP_Asp 48
2.5.2 Synthesis of TP_ADLys 49
2.5.2.1 Purification of TP_ADLys 50
2.5.3 Synthesis of TP_ADA 50
2.5.3.1 Purification of TP_ADA 51
2.5.4 Importance of peptides cyclization 52
2.5.5 Cyclization of Aspartic containing peptides 53
2.5.5.1 Purification of cyclized Aspartic containing peptide catalyst 53
2.5.6 Synthesis of TP_Glu 54
2.5.6.1 Purification of TP_Glu 55
2.5.7 Synthesis of TP_GDLys 57
2.5.7.1 Purification of TP_GDLys 57
2.5.8 Synthesis and purification of TP_GDA 59
2.5.9 Cyclization and purification of Glutamic containing peptides 60
2.6 Peptides scale up 61
2.7 Concluding remarks 62
2. 8 References 63
Chapter 3 70
Structural Elucidation of peptides 70
3.1 Introduction 70
3.1.1 NMR Studies 70
3.1.2 Circular Dichroism studies 71
3.2. Results and discussion 72

3.2.1 Conformational studies of peptides using circular dichroism 72
3.2.2 Characterization of peptides by NMR 75
3.2.2.1 NMR temperature variations experiments 76
3.2.2.2 NMR structure elucidation of the TP_Asp peptide 77
3.2.2.3 Spin system assignment of amino acid residues for TP_Asp 78
3.2.2.4 Sequential spin specific assignment 80
3.2.2.5 Determination of the secondary structural elements of TP_Asp 83
3.2.2.6 NMR structure elucidation and spin systems assignment for TP_ADLys 84
3.2.2.7 Assessment of secondary structural elements for TP_ADLys 86
3.3 Concluding remarks 87
3.4 References 88
Chapter 4 92
Peptides as organocatalysts for direct aldol addition reactions 92
4.1 Introduction 92
4.2 Preliminary investigation of the Fructose-1,6-bisphosphate aldolase (FBPA) enzyme aldol reaction catalysis 93
4.3 Peptides screening and optimization of aldol reactions conditions 96
4.4 Results and discussions 98
4.4.1 Screening of selected peptides for aldol reaction catalytic activity 98
4.4.2 Concluding remarks 102
4.5 Optimization of Aldol reaction conditions 103
4.5.1 Scope of reaction and substrate 103
4.4.2 Effect of solvents 106
4.4.3 The Effect of catalyst concentration (catalyst loading) on the aldol reaction 110
4.4.5 Catalyst reusability studies 113
4. 5 Concluding remarks 114
4. 9 References 115
Chapter 5 124
Peptide-capped AuNPs as catalyst for direct aldol reaction 124
5.1 Introduction 124
5.2 Affinity of peptides towards gold nanoparticles (AuNPs) 125
5.3 Results and discussions 126
5.3.1 Synthesis and functionalization of AuNPs 126

5.3.2. Characterization and instrumentation 128
5.3.2.1 UV-vis spectrophotometry 128
5.3.2.2 Transmission electron microscopy 130
5.3.3 Peptide-capped AuNPs as asymmetric aldol reaction catalyst 133
5.3.3.1 Catalyst screening 133
5.3.3.2 Optimization of reactions conditions 135
5.3.3.3 Catalyst recyclability studies 137
5.4. Concluding remarks 138
5.5 References 140
Chapter 6 150
Conclusion and recommendations 150
Chapter 7 152
Experimental Procedures 152
7.1 Materials and methods 152
7.2. Instrumentation and general techniques 152
7.3 General procedure for the synthesis of peptides 154
7.3.1 General procedure for the automated and manual SPPS synthesis 154
7.3.2 General procedure for the determining loading capacity 155
7.3.3 General procedure for the synthesis of peptides 155
7.3.4 General procedure for cleaving peptides from the resin 156
7.3.5 Cyclisation of peptides 156
7.4 Typical procedures for Aldol reaction 156
7.4.1 Preliminary aldol reaction investigation using Fructose-1,6-bisphosphate aldolase (FBPA)-RAMA 156
7.4.2 General procedure for the aldol reaction preliminary test using acetone 156
7.4.3 General procedure for the aldol reaction preliminary test using cyclic ketone 157
7.4.4 Aldol reactions in acetone in the presence of water 157
7.5 Procedures for the aldol reactions between aromatic aldehydes and cyclohexanone 157
7.5.1 Aldol reaction between cyclohexanone and aromatic aldehydes (homogenous) 157
7.5.2 Aldol reaction between cyclohexanone and aromatic aldehydes (heterogenous) 158
7.5.3 General procedure for aldol reaction between cyclohexanone and aromatic aldehydes in organic solvent 158
7.6 General procedure for the synthesis of gold nanoparticle (AuNPs) 158

7.7 Typical procedure for the functionalization of TP_ADLys peptide to AuNPs.....159
7.8 General procedure for aldol reaction using peptide-capped AuNPs.....159
7.9.1 Catalyst recyclability for peptide catalyzed aldol reaction.....159
7.9.1 Catalyst recyclability for peptide-AuNPs catalyzed aldol reactions.....160
7.10 Characterization of Aldol Products.....160
7. 11 References.....163
APPENDICES.....164
Appendix I - Supplementary information for Chapter 2.....165
Appendix II- Supplementary information for Chapter 3.....192
Appendix III - Supplementary information for Chapter 4.....204

Chapter 1

Introduction

1.1 Background

The use of organic compounds as asymmetric catalysts compliments the traditional use of organometallic and biological approaches in asymmetric catalysis. Organocatalysis is regarded as the use of small, low-molecular weight organic compounds, predominately comprising of carbon, oxygen, hydrogen, sulphur, and phosphorus, to accelerate chemical reactions. It has recently gained a lot of attention in the synthesis of chiral molecules and has been designated the third general approach to the catalytic production of enantio-pure compounds.[1,2] In comparison to other commonly used catalytic methods in organic chemistry, organocatalysts have several advantages which include; non-toxicity to biological systems, they are readily available, are more stable and easier to synthesize.[1–3] Generally organocatalysts catalyze chemical reactions by the following mechanisms:

a) Activation of the reaction based on the nucleophilic/electrophilic properties of the catalyst, where the chiral catalyst is not consumed in the reaction process and no parallel regeneration is required,
b) Activation of the reaction by organic molecules, which form reactive intermediates, whereby the chiral catalyst is consumed and requires regeneration in a parallel catalytic cycle,
c) A phase transfer reaction, normally under this mechanism, the chiral catalyst forms a host-guest complex with the substrate and shuttles between the standard organic solvent and a second phase,
d) The fourth mechanism involves molecular-cavity-accelerated asymmetric transformations, where the catalyst selects between the competing substrates, depending on size and structure criteria. In most cases, the rate of acceleration of a given reaction is similar to the Lewis acid/base acid activation.[4,5]

The use of peptides as organocatalysts has attracted an interest recently due to various reasons, such as: 1. their building blocks have inherent chirality, functional diversity, and are easily

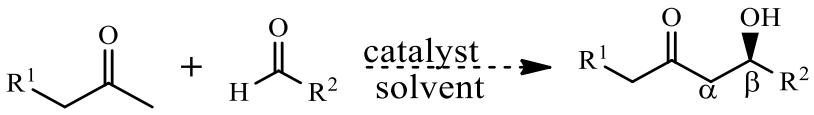
available; 2. they emulate action of natural enzymes; 3. they are very easy to synthesize via the solid phase approach; and lastly, they provide high stability.[2,6,7] When compared to enzymes, and organometallic catalyst, peptides tolerate a broader range of substrates and solvents, are also less-toxic and less-sensitive towards oxidation and moisture.[4,8–10] Although peptides are promising organocatalysts, they were limited by low yields until the recent work by Akagawa *et al*.[11,12] They reported a series of resin supported catalytic peptides which can efficiently catalyze various asymmetric reactions, yielding products with enantiomeric excess of up to 99%. Their successful design incorporates a β-turn and helical motif. The turn structure consists of five terminal residues and controls the enantioselectivity, while hydrophobic helical part enhances the reactions and stabilizes the whole peptide structure under aqueous conditions.

In this study we are particularly interested in designing and synthesizing aldol reaction peptide based organocatalysts with the following structural features:

- A turn motif to influence the conformation of the peptide and to enhance selectivity.
- A helical or catalytic motif to catalyze and improve the stereochemical control of the reaction.
- Gold nanoparticles to decrease conformational flexibility of the peptide and to also improve the catalytic efficiency and reusability of the peptide catalyst.

1.2 Aldol reaction

The aldol reaction is simply defined as the addition of an enolate donor to a carbonyl acceptor and it is one of the most important carbon-carbon bond forming organic reaction.[10,13,14] In this reaction a donor and an acceptor carbonyl component are coupled to generate one or two stereocenters resulting in a β-hydroxy-carbonyl (aldol) product (**Scheme 1-1**).



Scheme 1- 1: The direct catalytic asymmetric aldol reaction.[13]

One of the main goals in organic chemistry is to understand the reaction mechanism in order to design and discover new catalysts. However, some difficulties are often encountered because one must address intermediates that are structurally complex and of high energy.[15] Over the years, the aldol reaction has presented many challenges, such as the issues of chemo-, regio-, diastereo-, and enantioselectivity, which spurred the development of many stoichiometric

processes to address these problems.[13,16] This in turn led to the development of catalytic methods that avoid the production of stoichiometric by-products and provide an atom economical alternative for these important transformations.[17–19]

Generally, the control of stereochemistry is performed diastereomerically, either by using chiral aldehydes as starting material or stoichiometric chiral auxiliaries attached to the donor enolate.[20,21] In this approach, firstly, a chiral auxiliary is attached to the prochiral substrate through a covalent bond. This is then followed by performing a diastereoselective reaction before the auxiliary is cleaved to afford an enantioenriched product, together with the auxiliary which is recovered from the crude mixture. Controlling stereochemistry using chiral auxiliaries as substrates often present some limitations; and this includes utilizing one equivalent of the chiral auxiliary for chemical transformation which is very expensive and difficult to recover.[20,22] It also introduces additional steps to install and remove the chiral auxiliary.[23] Furthermore, these methods also include chiral Lewis acids and chiral Lewis bases, which requires the pre-activation of the donor to a more reactive species.[21,23] This has led chemists to look at the direct mechanism of the aldolase enzyme to enable them to design direct catalysts without limitations. To date, various catalysts for the aldol reactions have been reported, which includes enzymes, catalytic antibodies and organocatalysts. This study however intends to mimic the aldolase enzymes using catalytic peptides.

Enzymes have gained much recognition as useful catalysts in organic synthesis.[1] Their hydrophobic cavities are important in accelerating reactions through the capture of organic substrates as well as achieving highly stereoselective reactions.[24] Enzymes are usually highly chemo-, regio-, diastereo- and enantioselective. The use of enzymes has several advantages over chemical methods. Due to their selectivity, protecting group chemistry can be kept at minimum. Most enzymes operate best in mild conditions at room temperature in aqueous solution around pH 7, and because of this, their reactions are often compatible with each other. This makes it possible to combine enzymes in a one-pot and achieve a multistep reaction.[20,25] The application of enzymes in aqueous solution, plus the catalytic activity free of toxic heavy metals, and their biodegradability makes them an exceptional environmentally acceptable option, even though in certain instances the reaction is limited to a narrow range of substrates.[20,26]

The complex high-molecular structure of enzyme has an important role in the selective binding of the substrate by generating clefts or pockets wherein a molecule may only fit in a specific

orientation.[27] The enzymatic activity of enzymes is not only prompted by their topological structure. However, certain amino acids are arranged in space such that some functional groups remain in close proximity to act in a concerted manner to perform catalysis. In some cases the presence of cofactors such as metal ions, porphyrin, or flavin adenine dinucleotide, amongst others play a role in their structural and binding abilities.[20,27,28] These functional groups are spatially arranged within the inner secondary structural framework of polypeptides, such as the alpha helix (α) and beta (β) sheet (**Figure 1-1**).[11,26,29]

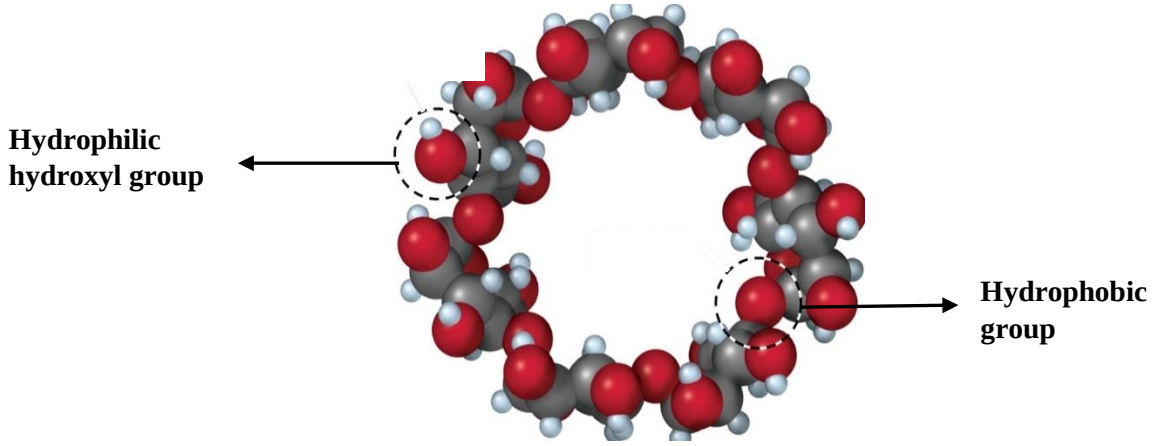


Figure 1- 1: A crystal structure depicting hydrophobic groups packed inside (red), and hydrophilic hydroxyl groups outside the enzyme molecule.[30]

Most enzyme structures are composed of about 60-500 amino acids residues in length, and normally a protein of this size has a vast number of potential primary sequences individually capable of specific folding patterns (thereby producing binding pockets and catalytically active sites).[28,31]

1.3 Enzyme structures

The catalytic function of enzymes is based on the complicated three-dimensional framework consisting of secondary structures such as the α-helix, β-sheet and turn moieties,[31,32] (**Figure 1-2**)

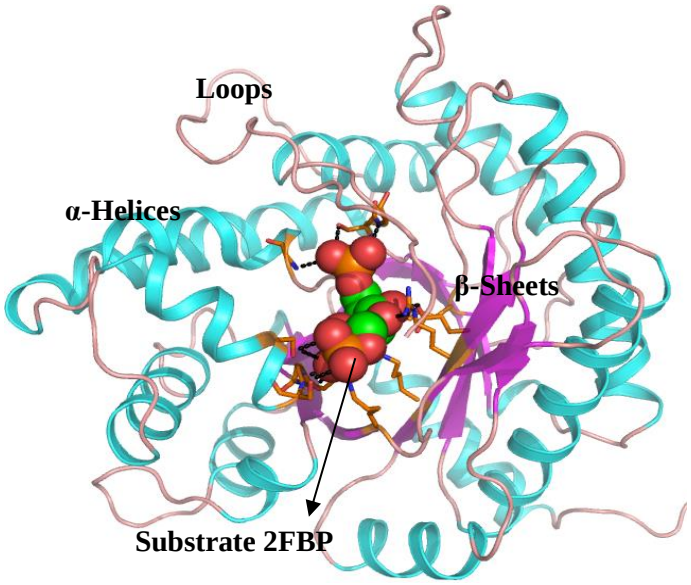


Figure 1- 2: Ribbon diagram of the crystal structure of aldolase enzyme depicting the α-alpha helices (cerulean), β-sheets (purple), and active site residues bonded to the substrate (shown as spheres) [PDB code: 2ALD]

1. 3.1. α-Helices

The α- helix is the most prevalent secondary protein structure. α-Helices, which are situated within the protein's surface,[33] play a vital role in the shape of sequence-selective recognition motifs for protein-protein and protein-nucleic acid interactions. More than 30% of the protein structure is helical in nature.[33–35] Helix lengths are normally short (consisting of about 8−20 residues) and they consist of 3-6 residues per turn.[33,34] The α- helical structure is characterized by the intramolecular hydrogen bond between the C=O bond of the *i*th residue and the N-H of the *i* + 4th amino acid residue of the peptide chain. Helices are considered to have 3 distinct faces because the side chain from certain residues overlaps every 3-4 residues as shown in (**Figure 1-3**). The α-helices bind along a specific face using residues in one of the following three motifs; *i*, *i* + 3, *i* + 4; *i*, *i* + 3, *i* + 7; or *i*, *i* + 4, *i* + 7.[33,34,36,37] Most of the side chains of amino acids in alpha-helices are situated in close proximity since they reside on the same face of the helix. The main role of the α-helix is thus, conformational hindrance of the side chains and steric hindrance.[33,38] The stabilization of the α-helix is achieved through non-covalent interactions such as ion pairs π-stacking or hydrophobic effects in proteins. Stabilization of peptide helices can also be accomplished by covalently tethering sides chains that are close together on the surface of the helix.[33,34,39,40] One can propose that the interest in the design and synthesis of the α-helical mimetic is motivated by; (i) having an understanding of the role

played by the α-helices in protein folding, (ii) the key role of the α-helices in mediating interactions in enzymes, protein-DNA and protein-RNA interactions.

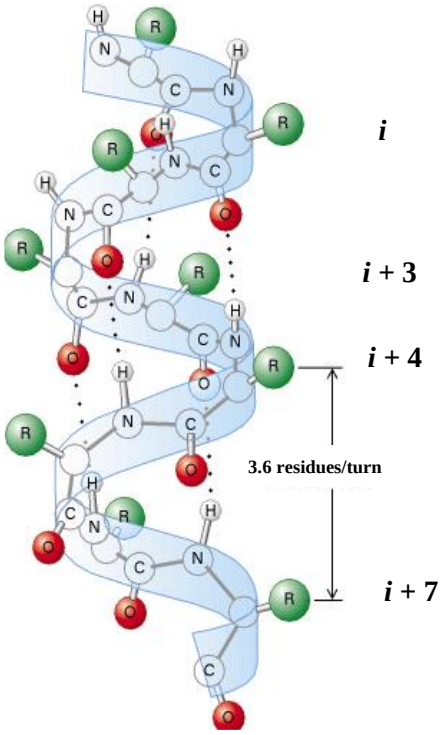


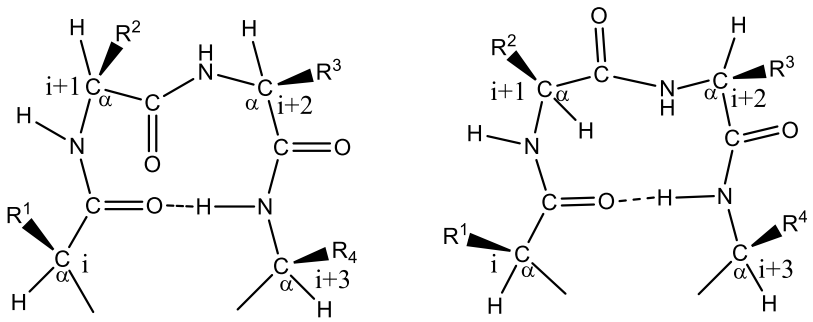
Figure 1- 3: An α-helix that is stabilized by internal hydrogen bonding.[40]

1.3.2 β-Turn structures, β-Sheets and β-hairpins

A turn is a structural motif or site where the peptide chain reverses its overall direction. Turn motifs in enzymes are responsible for determining the conformations and specificity of the active site and binding site. In most instances, they also play a role in protein folding and protein stability.[33,37,41] Classification of turns is based on the preferred φ, ψ angles of the backbone chain, the position of the stabilizing hydrogen bond and the length of the chain in which the turn occurs.[41,42] The β-sheets or β-hairpins are the common features in protein structures responsible for changing the polypeptide chain direction by nearly 180°.[33,37] They roughly account for 28% of the whole protein structure. Just like the α-helices, β-sheets are also responsible for protein conformational stability and protein-protein interactions, and are also important in secondary structural features which are essential for biological activities.[43,44] β-sheets are classified as either parallel, antiparallel or mixed. β-hairpins can be classified as a subset of β-sheets.[45]

As β-sheet motifs, β-hairpins are formed by antiparallel strands that are joined by a short connecting loop. The antiparallel β-strands in both β-hairpins and β-sheets are connected by

structures known as β-Turns. β-Turns constitute the most prevalent type of turns,[37,44,45] and they are formed by four consecutive amino acid residues arranged in such a way that the carbonyl oxygen atoms of the first residue (i) and the amide NH proton of the third residue (i+3) come closer in space.[37,41] There are two major classes of four-residues β-turn which are commonly observed, Type I and Type II. The variation of these classes is mostly on the orientation of the peptide bond between the *i* +1 and *i* + 2 residues (usually called corner residues), as shown in (**Scheme 1-2**), which are said to consequently affect the positions of their side chains.[37,46–48] β-turns play a role in stabilizing the sheet and the initiation of the formation of the β-hairpin or β-sheets.



Scheme 1- 2: Types of beta turn motifs.[48]

Furthermore, the secondary and tertiary 3-dimensional (3D) structures of enzymes are stabilized by noncovalent interactions such as hydrogen bonding, Van der Waals interactions, hydrophobic effects and steric interactions.[36] An understanding of the 3D folded structures presents an opportunity to design small molecules to mimic the recognition surface involved in selectivity and efficiency, and also perhaps help in our case to develop systems capable of catalyzing aldol reactions for a wide array of substrates.

1.4 Enzyme catalysis

The word ‘enzyme’ was first used by a German physiologist Wilhem Küne in 1878, to describe the ability of yeast to produce alcohol from sugars, and it is derived from the Greek words *en* (meaning ‘within’) and *zume* (meaning 'yeast’). It was in the late nineteenth century and early twentieth century that significant advances were achieved in extraction, characterization and commercialization and exploitation of most enzymes.[32,49] Enzymes are nature’s biomolecules developed many years ago to catalyze chemical reactions. Due to their ability to perform these reactions in an exceptional regio- and stereoselective manner (as discovered by Nobel prize

winner John Cornforth), most chemists have been inspired to explore their synthetic equivalence.[49–51]

The function of an enzyme is to bind and preorganize the active geometry, thus stabilizing the transition state electrostatically. Generally, it is known that the rate of acceleration of enzymes is mostly due to the transition-state stabilization. Inside the active site, the catalytic residues are accurately oriented in space so as to accommodate well-orchestrated, and very often highly stabilized, transition states.[29,52,53] Therefore, the active site preorganization provides a vital kinetic advantage, which itself is enforced and buttressed by the folded structure of protein. The exploration of the three-dimensional structures of enzymes provides detailed knowledge about the architecture of enzymes and their interaction with the reactants. However, it is not adequate to account for the enzymes abilities from static structures, therefore a better understanding of principles behind enzyme catalysis is necessary for designing novel enzyme-like mimics that can rival natural enzymes in terms of specificity and reaction rate accelerations. Within the context of this thesis, which involves the design and synthesis of artificial enzyme, it is therefore important to give a discussion on the principles behind enzyme catalysis.

1.4.2 Transition state theory

The mainstream of enzyme catalysis is mostly based on the transition state theory. The transition state theory originates mostly from Erying and Polany's work (1935),[54,55] and relates the relationship between enzyme-catalyzed chemical reactions kinetics to thermodynamics.[32,54,55] The enzyme's catalytic ability relies upon a decrease in energy difference between the ground state and transition state. The characteristic features of an enzyme-catalyzed reaction experimentally follow saturation or Michaelis-Menten kinetics, which involves a reaction pathway between an enzyme (E) and a substrate (S), which can be represented by the following equation (Equation 1).[32,52,56,57]

$$E + S \rightleftharpoons ES \rightleftharpoons ES^* \rightleftharpoons EP \rightleftharpoons E + P$$

Equation 1: Illustration of enzymatic reaction pathway

The first step in the mechanism involves the formation of an enzyme-substrate (ES) binary complex, which undergoes a series of chemical conversions to yield the active complex. The final stages include the conversion of substrate to the final product still bound to the enzyme (EP), which then is released to yield the product (P) and the now unbound enzyme.[52,56] The

functional groups of an enzyme that are involved in substrate binding and catalysis can be determined with the aid of site mutagenesis together with kinetic analysis. To gain a better understanding of the rate enhancement and specificity of enzymatic reactions, the structure of the reactive centres of these enzyme molecules, the active site, its relationship to the structures of the substrate molecules in their ground and transition states in forming the ES and ES* binary complexes, need to considered. This can be achieved by using the energy profile of the enzyme-catalyzed and uncatalyzed reaction of a substrate S, (**Figure 1-4**).[52,56,57]

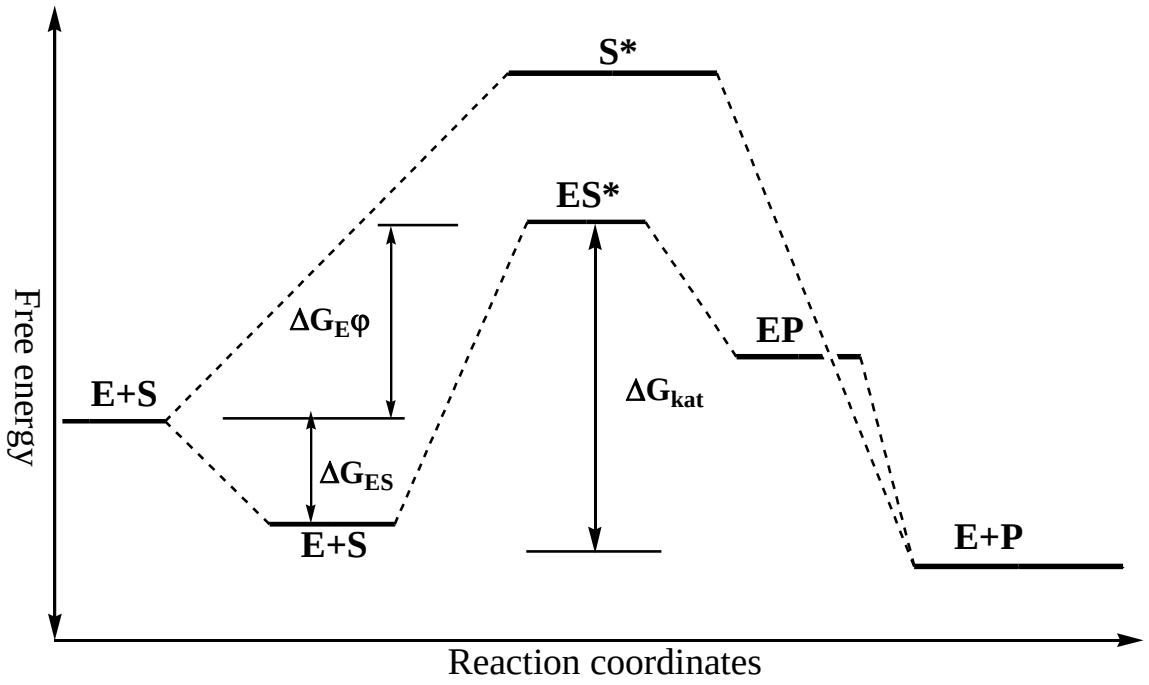


Figure 1- 4: Free energy profile diagram for both enzyme-catalyzed and uncatalyzed reactions. The symbols; E represents the enzyme, S is the free substrate, S* the free transition state, ES represents the enzyme-substrate complex, ES* is the enzyme-transition state, EP is the enzyme-product complex and P the free product state.[52]

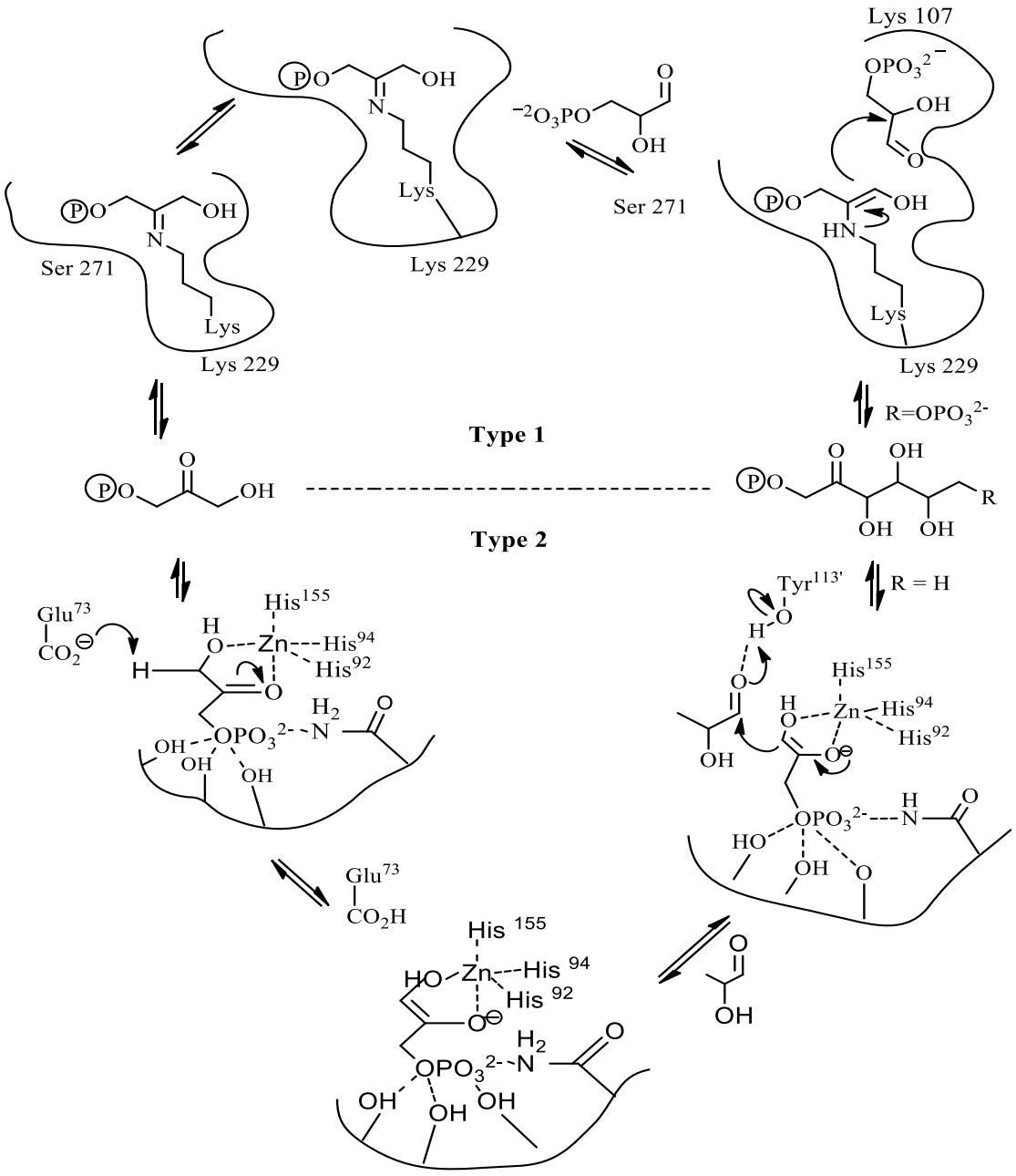
In the absence of an enzyme, the formation of a product from substrates occurs by overcoming a higher energy barrier which is needed to reach the transition state S*. However, in the presence of an enzyme the reaction proceeds through the formation of the ES complex and the binding energy associated with the ES complex formation can to some extent, be utilized to drive the transition state. When the binding has occurred, the molecular forces in the bound molecule simultaneously destabilizes the ground state configuration and this energetically favours the transition-state and the complex occurs at a lower energy (**Figure 1-4)** than the free S* state.[52,56]

The next stage in the reaction involves the formation of another intermediate state, the enzyme-product complex, EP, which comes before the final product (P) is released. It should be noted that the initial and final states have the same energy for both uncatalyzed and catalyzed reactions. Nevertheless, the overall activation energy barrier is significantly reduced in the enzyme-catalyzed case. ΔG_{kcat} is the amount of energy needed to reach the transition-state, whereas ΔG_{ES} is the net enefrgy gain associated with the enzyme-free substrate binding energy. The overall activation energy $\Delta G_{ES\varphi,}$ comprises of ΔG_{kcat} less the substrate binding energy $\Delta G_{ES.}$[52,56]

1.5 Aldolases

Aldolases are members of a specific class of enzymes called lyases (EC 4) that are present in all living organisms. There are over 30 aldolases which have been identified, and majority of these catalyze the reversible stereoselective addition of a ketone donor to an aldehyde acceptor. Two distinct classes of aldolases have been identified; the type I aldolases which are mostly found in animals and higher plants, and the type II aldolases which are found in bacteria and fungi. Type I aldolases follow the enamine mechanism, in which an enzyme lysine residue activates the donor by forming a Schiff base as an intermediate in the active site, which subsequently add regio-specifically to the acceptor.[20,25,49,58,59]

Type II aldolases catalyze the aldol reaction using the Zn^{2+} co-factor, which acts as a Lewis acid in the active site (**Scheme 1-3**). Since we want to create an enzyme mimic that does not require a metal cofactor, we utilized the Type I enamine-forming mechanism.



Scheme 1- 3: Mechanism of Type I Schiff base forming aldolase represented by the RAMA (Rabbit muscle **aldolase**) and the Type II zinc enolate mechanism represented by the fuculose-1-phosphate enzyme aldolase, bottom. Ⓟ =OPO_3^{2-}.[20]

The stereoselectivity in both types of aldolases is controlled by the enzyme and does not depend on the structure or stereochemistry of the substrate, making room for highly predictable products. Such exceptional features make the aldolase a useful tool in the synthesis of chiral compounds, such as carbohydrates, amino acids, and their analogues. Aldolases can be classified according to their donor and substrate specificity,[49,58] namely;

1. Pyruvate/2-oxobutyrate aldolases,
2. Dihydroxyacetone phosphate (DHAP) aldolases,
3. Dihydroxyacetone (DHA) aldolases,
4. Acetaldehyde aldolases,
5. Glycine/alanine aldolases

This study focuses on the DHAP aldolases, specifically Fructose-1,6-bisphophate aldolase

1.5.1 Fructose-1, 6-bisphosphate aldolase enzyme

Fructose-1, 6-bisphosphate aldolase (FBPA) is an enzyme of a glycolytic pathway that catalyzes the reversible reaction of fructose-1, 6-bisphosphate (FBP) and fructose-1-phosphate (FP) to dihydroxyacetone phosphate (DHAP) and either glyceraldehyde 3-phosphate (G3P) or glyceraldehyde.[53,60–65] Eukaryotic FBPA is a homotetramer with subunits that adopt the parallel $(\beta/\alpha)_8$-(TIM)-barrel folding.[62,64] The mechanism of FBPA follows the Type I and Type II mechanisms. There's a notable degree of similarity between the Type I human aldolase active site amino acids to that of both the rabbit and *Drosophila melanogaster*.[66] Among the Type I enzymes that are found in mammals there are three tissue-specific isozymes with the same molecular masses and catalytic mechanisms,[67–70] which are aldolase A (expressed in the muscle and red blood cell), aldolase B (expressed in the liver, kidney and small intestine), and aldolase C (expressed in the brain, smooth muscle, and neuronal tissue). All these isozymes have strictly conserved residues in the active site, comprising of Asp33, Arg42, Lys107, Lys146, Glu34, Glu187, Ser271 and Arg303, as well Lys229 which forms the Schiff-base intermediate (**Figure 1-5)** when bonded to the substrate fructose-1,6-bisphosphate (FBP).

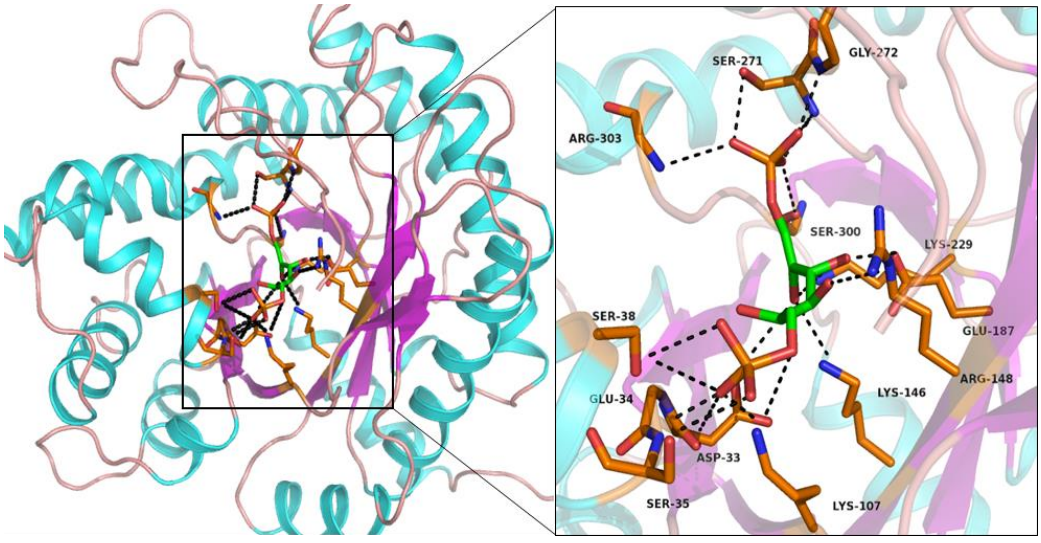


Figure 1- 5: The active sites residues of FBPA shown as stick form (on the right)

1.5.2 Mechanism of the Fructose-1, 6-bisphosphate aldolase

The catalytic function of the C-terminus, determines the orientation and flexibility of the substrate binding within the active site of this enzyme. The phosphate group of the substrate, interacts strongly with both the Schiff base Lys 229 and with Arg303, (**Figure 1-6**). The aldol cleavage in this enzyme proceeds through a number of distinct enzyme-substrate intermediates, including a carbinolamine, imine (Schiff base), and an enamine/carbanion.[60]

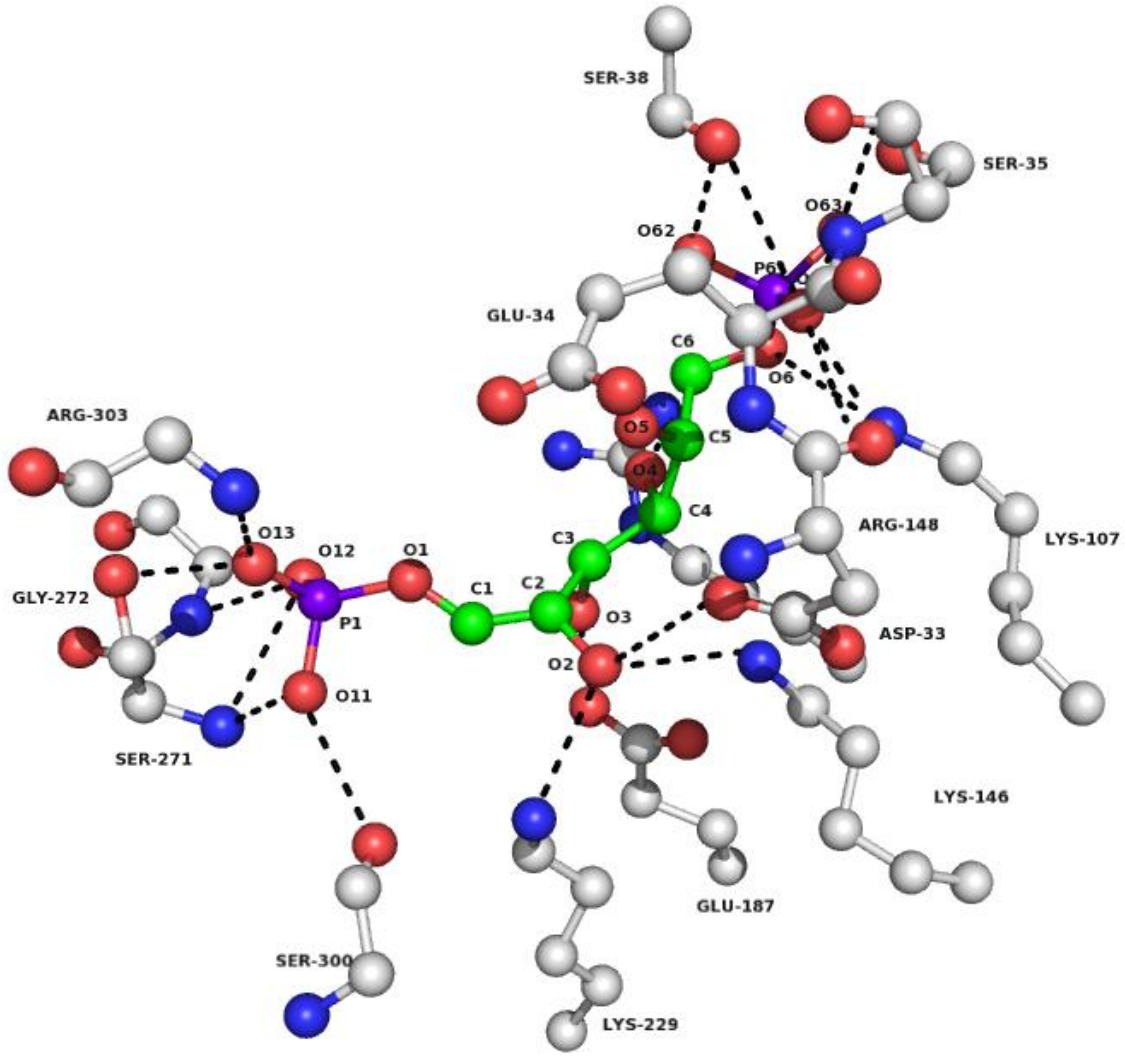
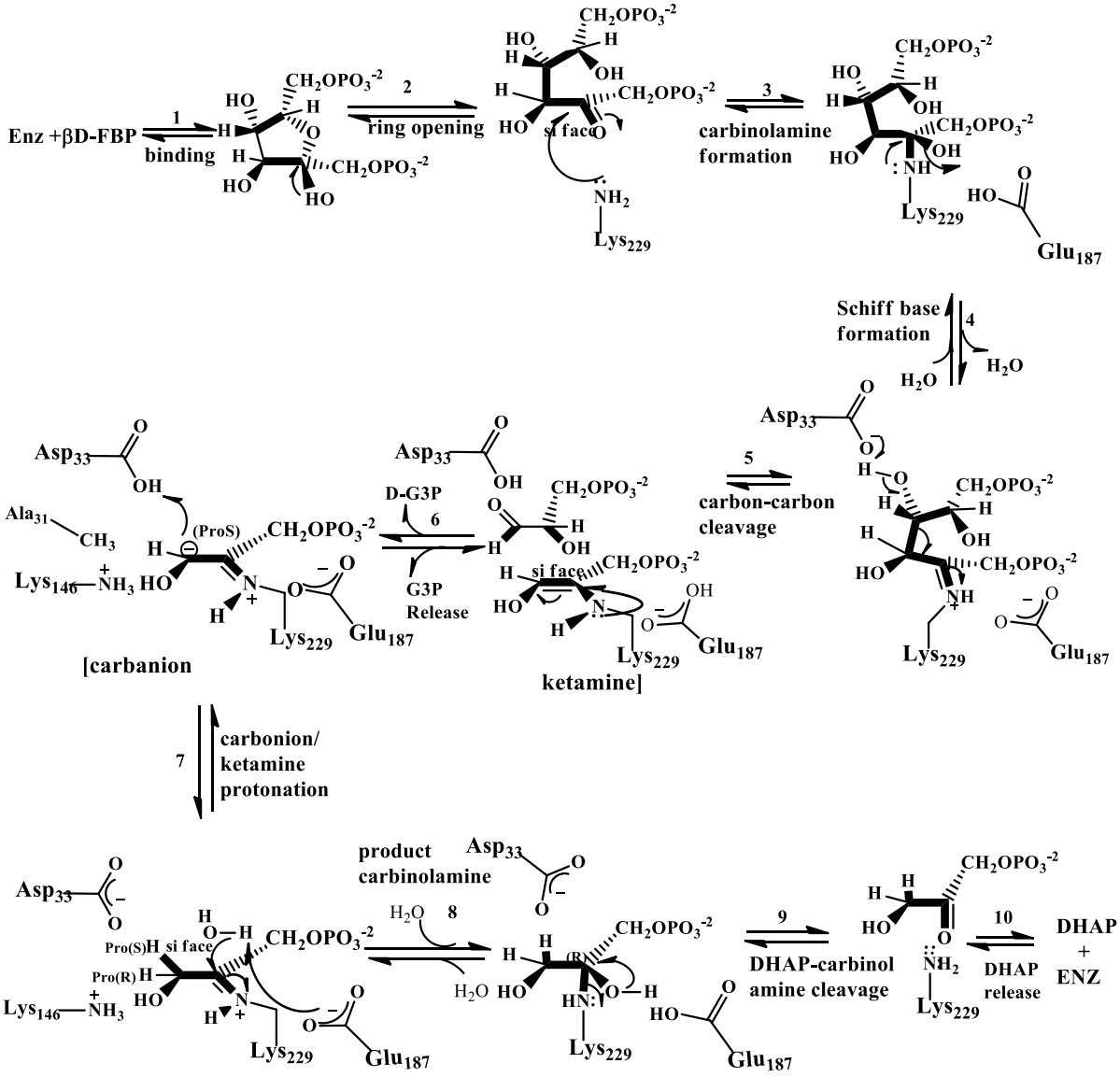


Figure 1- 6: 3D Structure depicting the FBPA active site residues interaction with the substrate molecule (2FBP) [some residues chains (side or main) are omitted for picture clarity]

The first step in this aldol cleavage reaction involves nucleophilic attack on the carbonyl carbon atom of an aldehyde or ketone substrate by a reactive lysine residue. The pK_a of lysine in aqueous solution is approximately 10.5, and at a physiological pH it is positively charged. Nonetheless, an uncharged lysine is observed at around a neutral pH. This suggests that the

pKa of the reactive lysine residue must be excited considerably in the active-site environment, so as to deprotonate it and make it more basic.[62] The Lys 229 residue attacks the carbonyl carbon of the substrate on the *si*-face by the ϵ-amino group, forming the carbinolamine followed by the dehydration to form Schiff base (imine), also shown in (**Scheme 1-4**).



Scheme 1- 4: Mechanism of Fructose-1, 6-bisphosphate aldolase based on the structure of the DHAP Schiff-base intermediate.[62]

The hydrolysis or reverse reaction for this imine is acid-catalyzed by Glu187, which is in close proximity to the hydroxyl group on the C2 sugar carbon. Glu187 also plays a role in orientating the lysine and stabilizing the charges during the formations of a Schiff base. Once the C2-hydroxyl is protonated, it will leave as water, or it can be deprotonated for a *re*-face attack of the imine in the reverse reaction.[60,62,64] The *si*-face of the imine is unavailable to solvent and

sterically hindered by enzymatic residues in the active site, leaving only the *re*-face exposed to solvent.

Lys146 interacts with substrates using the nitrogen of its main chain. Electron sink C2 makes a facile proton abstraction at C4-hydroxyl and Asp33 which is in close proximity to Lys146 acts as a base in the reaction. The interaction of lysine with the substrate involves the deprotonated form. The C3-C4 bond cleavage is followed by the release of the first product G3P and the carbanion/enamine is formed at the active site. Protonated Asp33 then donates a *si*-face proton to the resulting amine.[62] Arg-303 has been proposed to be involved in the binding of the cyclic form of the substrate and it is important to note that in a naturally occurring mutation that causes hereditary fructose intolerance, Arg-303 is substituted with Trp. Arg303 forms part of the phosphate-binding site of the enzyme, and is also associated with positioning the flexible C-terminus.[65] In the unbound structure, Arg303 forms a salt bridge with Glu34, and in the liganded structure it interacts with the C1-phosphate as shown in **Scheme 1-4**. Lys 107 forms part of the C6-phosphate binding, as it interacts with the O6 of the 6-phosphate molecule. The Ser35 and Ser38 side chain hydroxyl group interacts with the C6-phosphate residues. The C1-phosphate binding site involves protein backbone interactions (nitrogen atoms) of Ser271, Gly272 and Gly302 (not shown here for picture clarity) interacting with the nitrogen of Arg303.

1.6 L-Proline as Type I micro Aldolase'

For many years, a number of researchers have focused on proline-catalyzed aldol reactions which resemble the Type I aldolase mechanism.[10,71–75] The natural abundance of proline,[71,74,76] its confined phi angle that constrains the secondary structure; its ability to function as a bifunctional catalyst due to the carboxylic acid and amino group acting as a base and acid respectively; and finally the cyclic, pyrrolidine-based amino acid, has certainly made it the first choice for any enamine-catalyzed reaction including direct aldol reaction, (**Figure 1-7**).

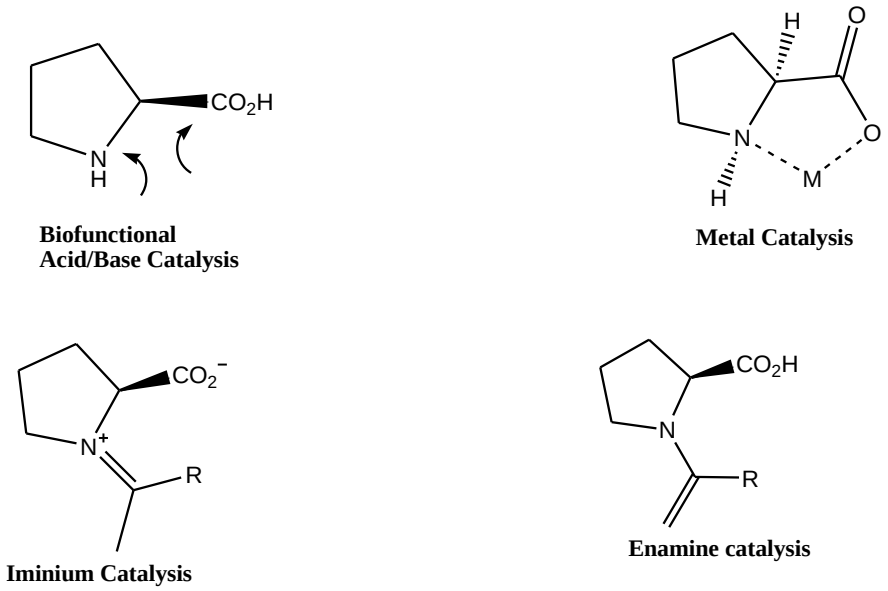
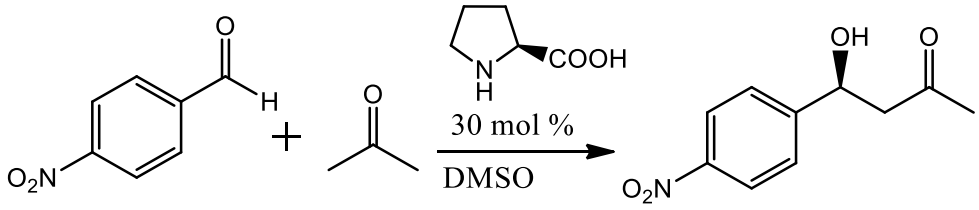


Figure 1- 7: Modes of action of proline catalysis.[77]

List *et al.*,[71] were the first group who reported that L-Proline can be applied as an effective catalyst for an intermolecular aldol reaction between acetone and aryl-, alkyl-substituted aldehyde acceptors in year 2000. They demonstrated that the upon addition of 30 mol % proline to *p*-nitrobenzaldehyde and acetone, the desired aldol products were achieved in 54–97% yield and enantioselectivities ranging from 60–90% ee (**Scheme 1-5**). From their studies they also discovered that DMSO was the most appropriate solvent in affording good yields and enantioselectivity.



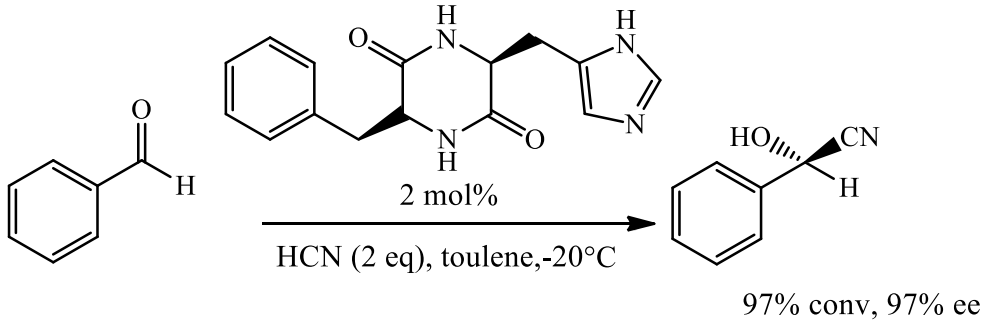
Scheme 1- 5: Asymmetric aldol reaction reported by List *et al.*[71]

Despite its applications in carrying out a wide array of asymmetric aldol reactions, there's still a lot of work to be done towards the development of other organocatalysts. Some limitations of proline based catalysis include, long reaction times, poor results with certain substrates and its low solubility in reactions.[13] This opens a door for the design and development of catalysts with increased lipophilicity that may lead to improved yields.

1.7 Peptides as organocatalysts

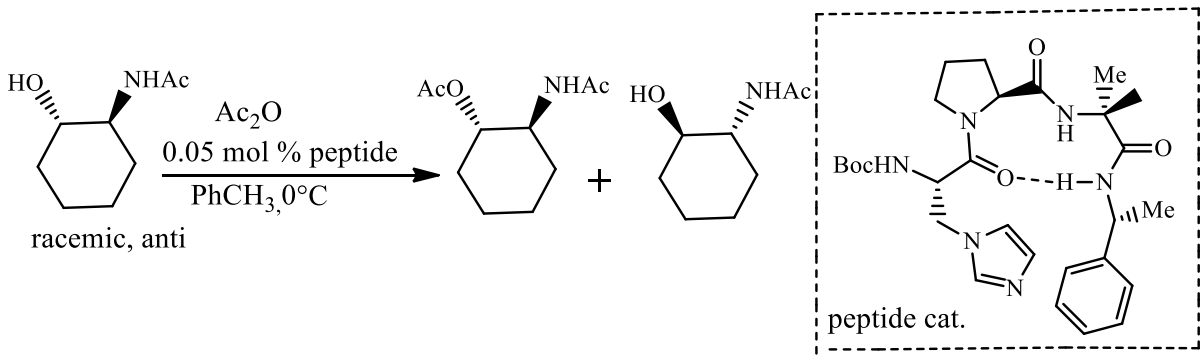
Amino acids, which are the building blocks of peptides, have provided several routes leading to attractive organic transformations in asymmetric catalysis, acting both as auxiliary scaffolds and catalysts. Peptides comprising of two to ten amino acids have emerged as simple yet exceptionally well-defined chiral catalyst for various enantioselective methods.[78–83]

Inoue and co-workers were the first group in early 1980s to report on peptides as organocatalysts. They demonstrated the catalytic use of the diketopiperazine cyclo (Phe-His) dipeptide in the cyanation of benzaldehyde (**Scheme 1-6**).[84] Only few reports followed after, and hence the application of peptides as asymmetric catalyst remained mostly dormant for almost two decades.



Scheme 1- 6: The asymmetric cyanation of benzaldehyde to a cyanohydrine.[84]

Miller and co-workers in 1998, reported on methylimidazole containing peptides for asymmetric kinetic resolution of functionalized racemic alcohols, which yielded excellent enantioselectivities (**Scheme 1-7**). Their work also gave important insight regarding the peptide-substrate complex which was of a great benefit to the context of biological catalysis.[85] Subsequently a lot of researchers have reported peptides as organocatalysts, and since this current project focuses on peptides as organic catalyst in asymmetric aldol reaction, a brief summary of selected reactions will be discussed.

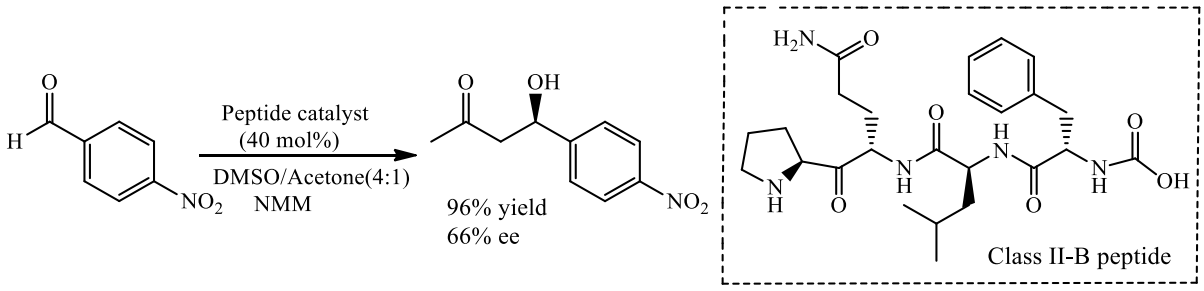


Scheme 1- 7: Peptide mediated kinetic resolution of functionalized racemic alcohols.[85]

1.7.1 Peptides as catalyst for asymmetric aldol reactions

The main advantage of using chemical peptides synthesis over recombinant protein synthesis, is the extended set of amino acids and other building blocks which can be incorporated, which include D-amino acids as well as a wide range of non-proteinogenic amino acids.[86] Small peptides, which are simplified enzymes, have gained a lot of application as catalyst in organocatalytic reactions. Short peptides which consist of 2-4 amino acid residues, as well as a secondary amine N-terminus, have effectively been applied as successful catalyst in asymmetric aldol reactions. Peptides offer many sites for structural and functional diversity that can be utilized to produce optimized catalysis. Due to their structural diversity which can be easily attained by changing sequences of amino acids and acid monomers, peptides have attracted attention as promising candidates for organocatalysis.[11,12,14,16,17,24,87] Compared to complete enzymes, peptides are more stable and are less substrate specific.

Resin supported peptides for asymmetric organocatalysis are typically short consisting of few residues.[86,88–91] Peptides with N-terminal ending propyl residue, having a secondary amino group can be utilized as cyclic amine catalysts to promote the enamine and imine –ion mechanisms.[92] Kofoed and co-workers were the first group to report on peptide-catalyzed asymmetric aldol reactions in 2003, wherein they demonstrated that the reaction between acetone and *p*-nitrobenzaldehyde progressed in the presence of a proline-based peptide and a mixture of acetone and DMSO, yielding moderate enantioselectivies and excellent yield. They further expanded their work; investigating various classes of peptides, specifically class IA and IB containing primary amines and class IIA and class IIB consisting secondary amines (**Scheme 1-8**). From this they postulated that class IIB peptides with N-terminal prolines as the secondary amine substituent, gave the best yield and enantioselectivity.[93]



Scheme 1- 8**:** Kofoed's peptide catalyzed enantioselective aldol reaction of *p*-nitrobenzaldehyde and acetone.[93]

Most of the work done on peptides as catalysts involve relatively simple peptides structures, usually consisting of few residues, only few studies have been done on well-designed peptide catalysts incorporating secondary structures such as α- helices for asymmetric organocatalytic reactions.[27] It is reported that a peptide having secondary structural motifs may yield better catalytic peptide performance.[92] Akagawa and their group,[11,24,87,94] developed a peptide catalyst with a free N-terminal, five amino acid residues, a turn motif, D-Pro-Aib, (Aib: 2-amino isobutyric acid) and a helical motif (**Figure 1-8**)

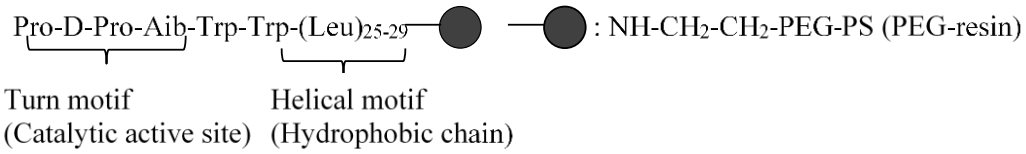


Figure 1- 8: Resin-supported peptide catalyst.[11]

From the developed peptide catalyst, they postulated that, in the peptide sequence, the beta turn motif and helical unit are required for promoting enhanced enantioselectivity. They also discussed how the presence of the helical part significantly improves the stereochemical control of the reaction when the moiety is at a distance from the terminal propyl group in the catalytic centre.[24] Since peptide structures and the substituents of the peptide side chains can be easily modified by altering amino acid monomers,[89] one can anticipate that the scope for exploring peptide catalyst can be extended to polypeptide sequences of many different enzyme molecules.

1.8 Design considerations and previous work

Designing a peptide catalyst by combining secondary structural motifs to form an appropriate reaction site can produce a novel, enzyme like organocatalyst with high catalytic abilities as reported by Akagawa and co-workers.[87] In this current study, we endeavour to design and synthesize FBPA enzyme peptides mimics that can catalyze the aldol addition reaction. However, arranging these peptide sequences into 3D structures can be energetically demanding, and the simple excision of short peptides from a parent protein may lead to loss of organized secondary structures.[36,95–97] This challenge has been previously addressed by other researchers by developing various strategies for nucleation and stabilization of short peptides sequences into helices, and these includes: helix capping,[38,98] non-natural amino acid,[39] side chain constraints,[99] and hydrogen bond surrogates (HBS).[95,96] The chemical and physical properties of short peptides are often hampered by the inability of most linear peptides to sustain an alpha helical conformation in solution due to weak hydrogen bonds.[39] Stabilisation of peptides in the helical structure not only reduces their heterogeneity,[87] but also substantially increases their resistance to proteolysis. The traditional strategy for stabilizing the α-helical conformation in peptides uses covalent bonds between the *i* and *i* + 4 or *i* and *i* + 7 residues. More emphasis has been on the incorporation of disulphide bonds bridges *via* oxidation of Cys residues and the formation of the amide bond between the side chain of Lys and Glu/Asp residues at selected positions.[39,95,99] Patgiri and co-workers,[95] reported short α helices stabilised by the hydrogen bond surrogate approach, which involves the introduction of an $i \rightarrow i + 4$ carbon-carbon bonds through a ring-closing metathesis (RCM) reaction, (**Figure 1-9**). They hypothesized that the metathesis-based methods afford a stable and irreversible bond in comparison to the hydrazone strategy and is applicable to a broader range of peptide sequence

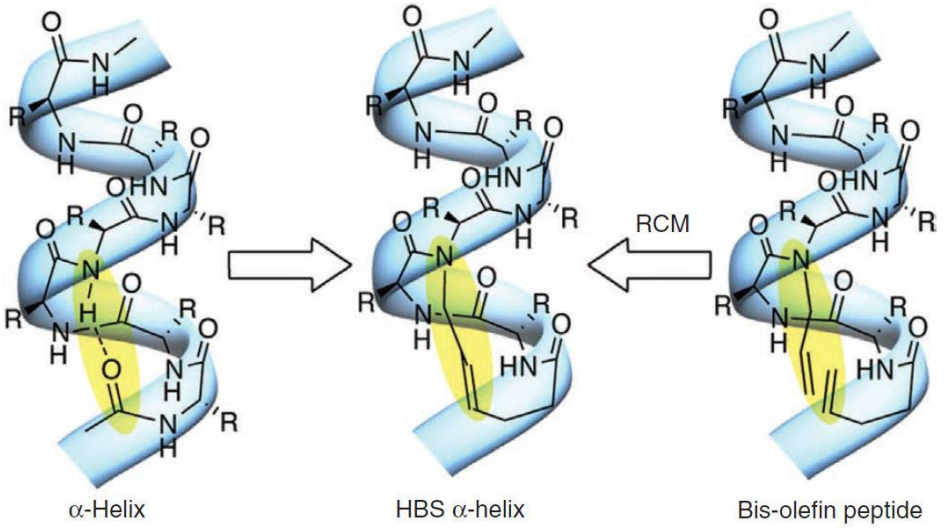


Figure 1- 9: An N-terminal hydrogen bond replace with C-C bond obtained from a ring closing metathesis (RCM) reaction.[95]

There are also several reports in stabilizing the turn structure of enzyme. One of the simple ways is to create a β-turn by incorporating non-bulky achiral amino acid such as glycine. Blanco's group[100] proposed that incorporating Aspartic acid and Glycine into the β-turn structure resulted in successful formation of β-hairpin in water. The β-hairpin and L-Asp-Gly dipeptide turn promoter are shown below in (**Figure 1-10**).

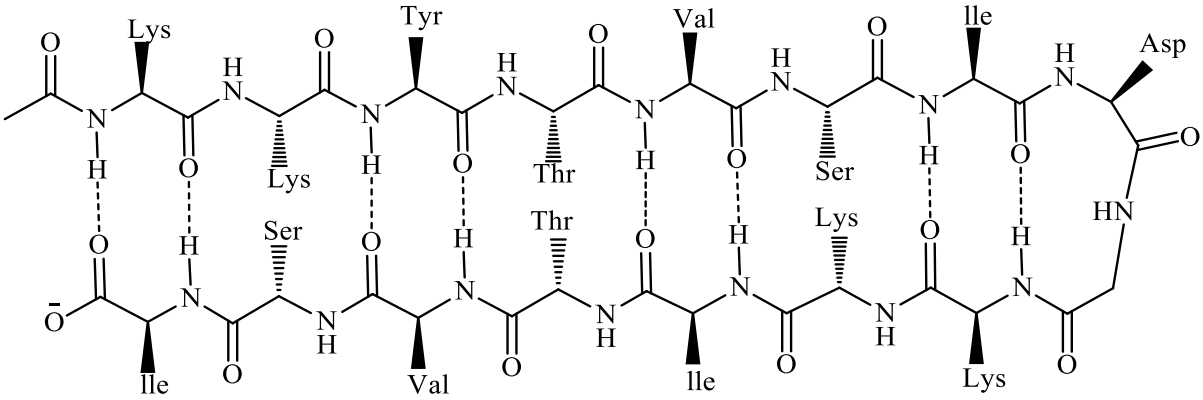


Figure 1- 10: β-hairpin with Asp-Gly β-turn promoter done by Ramírez-Alvarado *et al*. [100]

Other reports of different types of β-turn design, also include the replacement of an asparagine residue with D-proline[100] and the use of Aib (2-aminoisobutyric acid) combined with D-α-amino acids or achiral α-amino acid (as reported by Balaram and co-workers).[101] Although a lot has been achieved in the stabilization of peptides, the above methods are significant in pharmaceutical studies (i.e. drug delivery, drug development, stabilization again proteolysis);

and not much work has been done for stabilization of peptides as an organocatalysts. One way that enzymes are often stabilized is to immobilise them on solid substrates. One way that enzymes are often stabilized is to immobilize them on solid substrates. Among the powerful approaches utilized to create artificial enzyme, the application of gold nanoparticles (AuNPs) conjugated to a monolayer of thiols has proven to be a great tool.[102,103] This project involves the conjugation of peptides to gold nanoparticles.

1.8.1 Stabilisation of Peptides using gold nanoparticles (AuNPs)

Gold particles that are of nanometre scale (gold nanoparticles, AuNPs) have gained special attention for the application in various fields like biology, chemistry, engineering and medicine. They are therefore of a particular interest in this study due to their remarkable properties, such as biocompatibility and ease of surface functionalization. AuNPs also have an excellent ability to conjugate to organic compounds and bio-molecules, making them useful in biochemical sensing and bio-catalysis.[104–108] The conjugation of gold nanoparticles to peptides produces biocompatible and stable multifunctional systems.[104,109]

A peptide sequence with two cysteine thiolates at different positions or a thiolate and a guanidine group of Arg, has the ability to induce peptide-nanoparticle coupling. The coupling of peptides to gold nanoparticles has been shown to decrease conformational flexibility, and this difference in flexibility upon conjugation relies on the amino acids sequence of the peptide. AuNPs also possess the ability to control the conformational entropy of the peptide,[105] by introducing more constrains to the structure. It is worthy to note that the high density surrounding the nanoparticles has a tendency to generate micro-environments. The use of AuNPs has been shown to produce high catalytic efficiencies by several orders of magnitude greater than those of non-conjugated peptide variants, and to also generate new catalytic activities, where the monomeric peptide shows no catalytic activity.[110]

There are quite a few reports concerning the conjugation of AuNPs to peptide for application in asymmetric aldol reactions. Mikolajczak *et al*,[111] reported a peptide-nanoparticle conjugate whose activity was regulated by a conformational change in a self-assembled monolayer. From their work they demonstrated that the formed peptide monolayer at the gold nanoparticle surface increases the ester hydrolysis by an order of magnitude and triggers cooperative His-Glu interactions resulting in an increased catalytic efficiency (**Figure 1-11**).

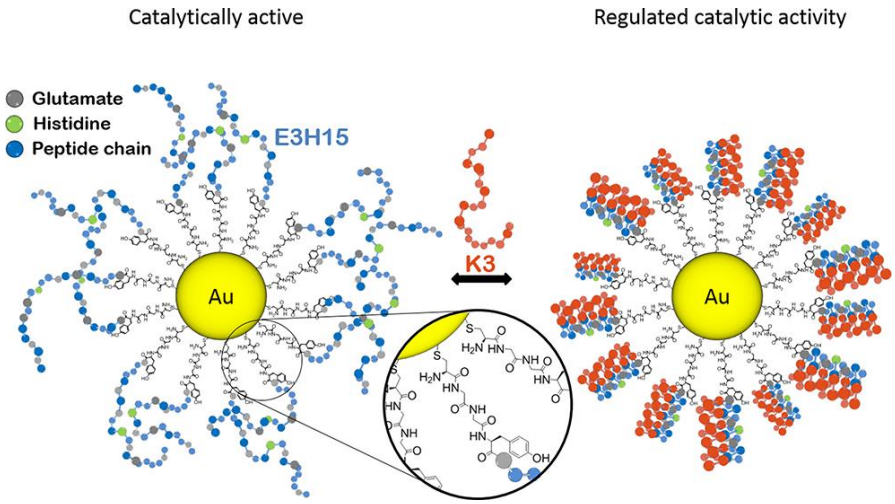
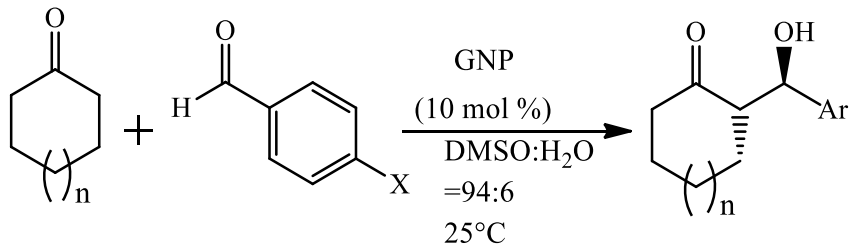


Figure 1- 11: Peptide sequence of E3H15 conjugated to Gold nanoparticles.[111]

Another inspiring work was demonstrated by Sóti and group,[112] where they reported on catalyst recycling efficiency of Proline-functionalized GNPs for asymmetric aldol reaction of benzaldehyde derivative and cyclic donors, resulting in high yield and enantioselectivities (**Scheme 1-9**).



Scheme 1- 9: AuNPs-supported proline-catalyzed asymmetric aldol reactions.[112]

Despite the exceptional improvements made by researchers thus far, organocatalysts still possess some limitations in industrial use due to their poor solubility in organic solvents. Polar solvents such as DMF, DMSO and NMP have been the solvents of choice for most work done, although they are considered problematic for large scale synthesis due to not being environmentally "green". Hence, there is still a need for soluble organocatalysts. This study focuses on the design of soluble peptide-based catalysts that mimic the Fructose-1,6-bisphophate aldolase.

1.8.2 Design of cyclic and AuNPs supported catalytic peptides

Our design of the aldolase synzymes which is explained in detail in Chapter 2, includes a β-turn motif consisting of amino acids (aa) extracted from the turn motif of the aldolase enzyme sequence (aa: 344-347), a helical portion mimicking both the helical motif amino acids and active site amino acids. This approach was motivated by the work done by Akagawa and co-workers (Section 1.7.1), who postulated that both the beta turn and helical units are necessary for the high enantioselectivity. The active site consists of proton donating and accepting amino acids (Arg, Lys, Asp and Glu). The selection of these amino acids was guided by the aldolase enamine mechanism pathway explained above in Section 1.5.2.

The linear peptide's conformational flexibility allows the peptide to assume random structures in aqueous solutions, instead of the desired α-helices and β-turn structures. To overcome this problem, cyclization was introduced by forming a disulphide bridge between the Cysteine thiolates. Cyclization can significantly reduce the peptide's degree of freedom thus producing a peptide with a better defined and more fixed shape. Cyclization of peptides using amide condensation (lactam or amide bond formation) and thiol oxidation of side chains, can also promote peptide stability.[37,113] To decrease conformation flexibility and improve catalytic efficiency in uncyclized peptides, the peptides were also conjugated to AuNPs.

1.9 Aims and Objectives of the project

The aim of this current study is to design and synthesize peptide based structural and activity mimics of the aldolase enzyme, namely Fructose-1, 6-bisphosphate aldolase (FBP aldolase) to catalyze aldol addition reactions. This leads to the following objectives.

- The design and synthesis of peptide sequences with aldol addition reaction catalytic properties
- The synthesis of stable cyclic peptides using the solid phase peptides synthesis strategy (SPPS)
- The synthesis of AuNPs and AuNPs-peptides conjugates
- Determination of 3D structures of the synthesized peptides using Nuclear magnetic resonance (NMR) spectroscopy and circular dichroism (CD)
- Synthesis and characterization of β-hydroxy-carbonyl (aldol) products from the aldol addition reactions catalyzed by synthesized peptides and AuNPs-peptide conjugates.
- Determination of optimal reaction conditions of peptide catalyzed aldol reactions

1.10 References

(1) Zou, W.; Ibrahem, I.; Dziedzic, P.; Sundén, H.; Córdova, A. Small Peptides as Modular Catalysts for the Direct Asymmetric Aldol Reaction: Ancient Peptides with Aldolase Enzyme Activity. *Chem. Commun.* **2005**, No. 39, 4946–4948. https://doi.org/10.1039/b509920j.

(2) Bayat, S.; Tejo, B. A.; Abdulmalek, E.; Salleh, A. B.; Normi, Y. M.; Abdul Rahman, M. B. Rational Design of Mimetic Peptides Based on Aldo-Ketoreductase Enzyme as Asymmetric Organocatalysts in Aldol Reactions. *RSC Adv.* **2014**, *4* (73), 38859–38868. https://doi.org/10.1039/c4ra04866k.

(3) Melchiorre, P.; Marigo, M.; Carlone, A.; Bartoli, G. Asymmetric Aminocatalysis - Gold Rush in Organic Chemistry. *Angew. Chemie - Int. Ed.* **2008**, *47* (33), 6138–6171. https://doi.org/10.1002/anie.200705523.

(4) Darko, P. I.; Moisan, L. Enantioselective Organocatalysis. *Angew. Chemie Int. Ed.* **2001**, *40* (20), 3726–3748. https://doi.org/10.1016/j.drudis.2006.11.004.

(5) Fu, G. C. Enantioselective Nucleophilic Catalysis with "Planar-Chiral" Heterocycles. *Acc. Chem. Res.* **2000**, *33* (6), 412–420. https://doi.org/10.1002/chin.200036271.

(6) Jarvo, E. R.; Miller, S. J. Amino Acids and Peptides as Asymmetric Organocatalysts. *Tetrahedron* **2002**, *58* (13), 2481–2495. https://doi.org/10.1016/S0040-4020(02)00122-9.

(7) Tsogoeva, S. Short Peptides and Peptide-Like Enzyme Mimics - Efficient Organic Catalysts in Asymmetric Synthesis. *Lett. Org. Chem.* **2005**, *2* (3), 208–213. https://doi.org/10.2174/1570178053765285.

(8) Berkessel, A.; Groger, H. *Asymmetric Organocatalysis- From Biomimetic Concepts to Applications in Asymmetric Synthesis*; John Wiley & Sons, 2005.

(9) Seayad, J.; List, B. Asymmetric Organocatalysis. *Org. Biomol. Chem.* **2005**, *3* (5), 719–729. https://doi.org/10.1007/978-3-642-19472-6_6.

(10) Gröger, H.; Wilken, J. The Application of l -Proline as an Enzyme Mimic and Further New Asymmetric Syntheses Using Small Organic Molecules as Chiral Catalysts. **2001**, *40* (3), 529–532.

(11) Akagawa, K.; Fujiwara, T.; Sakamoto, S.; Kudo, K. Efficient Asymmetric r -Oxyamination of Aldehydes by Resin-Supported Peptide Catalyst in Aqueous Media. *Org. Lett.* **2010**, *12* (4), 1804–1807.

(12) Akagawa, K.; Sugiyama, M.; Kudo, K. Asymmetric Michael Addition of Boronic Acids to a γ-Hydroxy- α,β-Unsaturated Aldehyde Catalyzed by Resin-Supported Peptide. *Org. Biomol. Chem.* **2012**, *10*, 4839–4843. https://doi.org/10.1039/c2ob25431j.

(13) Trost, B. M.; Brindle, C. S. The Direct Catalytic Asymmetric Aldol Reaction. *Chem. Soc. Rev.* **2010**, *39* (5), 1600–1632. https://doi.org/10.1039/b923537j.

(14) Córdova, A.; Zou, W.; Dziedzic, P.; Ibrahem, I.; Reyes, E.; Xu, Y. Direct Asymmetric Intermolecular Aldol Reactions Catalyzed by Amino Acids and Small Peptides. *Chem. -A-European J.* **2006**, *12* (20), 5383–5397. https://doi.org/10.1002/chem.200501639.

(15) Wagner, J.; Lerner, R. A.; Barbas, C. F. Efficient Aldolase Catalytic Antibodies That Use the Enamine Mechanism of Natural Enzymes. *Science (80-.).* **1995**, *270* (5243), 1797–1800. https://doi.org/10.1126/science.270.5243.1797.

(16) Trost, B. M.; Fleming, I. *Comprehensive Organic Synthesis*, 1st Editio.; Pergamon Press, 2007.

(17) Trost, B. M. Atom Economy-A Search for Synthetic Efficiency. *Science (80-.).* **1988**, *254* (5037), 1471–1477.

(18) Carreira, E. M.; Fettes, A.; MartI, C. Catalytic Enantioselective Aldol Addition Reactions. *Org. React.* **2004**, *67*, 1–216.

(19) Rainer Mahrwald. *Aldol Reactions*; Springer Heidelberg Dordrecht London New York, 2009.

(20) Machajewski, T. D.; Wong, C. The Catalytic Asymmetric Aldol Reaction. *Angew. Chemie - Int. Ed.* **2000**, *39*, 1352–1372.

(21) List, B. *Asymmetric Organocatalysis*; Meijere, Armin deJean-Marie Lehn, K. N. S. V. L., University, U. H., Eds.; Springer Heidelberg Dordrecht London New York, 2010.

(22) Davies, S. G.; Fletcher, A. M.; Thomson, J. E. Direct Asymmetric Syntheses of Chiral Aldehydes and Ketones via N-Acyl Chiral Auxiliary Derivatives Including Chiral Weinreb Amide Equivalents. *Chem. Commun.* **2013**, *49* (77), 8586–8598.

https://doi.org/10.1039/b000000x.

(23) Lerner, R. A.; Tramontano, A. Antibodies as Enzymes. *Trends Biochem. Sci.* **1987**, *12* (C), 427–430. https://doi.org/10.1016/0968-0004(87)90208-8.

(24) Akagawa, K.; Akabane, H.; Sakamoto, S.; Kudo, K. Organocatalytic Asymmetric Transfer Hydrogenation in Aqueous Media Using Resin-Supported Peptide Having a Polyleucine Tether. *Org. Lett.* **2008**, *10* (10), 2035–2037.

(25) Gijsen, H. J. M.; Qiao, L.; Fitz, W.; Wong, C. Recent Advances in the Chemoenzymatic Synthesis of Carbohydrates and Carbohydrate Mimetics. *Chem. Rev.* **1996**, *96* (1), 443–473.

(26) Garcia-Viloca, M.; Gao, J.; Karplus, M.; Truhlar, D. G. How Enzymes Work: Analysis by Modern Rate Theory and Computer Simulations. *Science (80-.).* **2004**, *303* (5655), 186–195. https://doi.org/10.1126/science.1088172.

(27) Davie, E. A. C.; Mennen, S. M.; Xu, Y.; Miller, S. J. Asymmetric Catalysis Mediated by Synthetic Peptides. *Chem. Rev.* **2007**, *107* (12), 5759–5812. https://doi.org/10.1021/cr068377w.

(28) Palmer, T. *Understanding Enzymes*, Third edti.; Ellis Horwood: New York London, 1991.

(29) Wong, C. .; Whitesides, G. . *Enzymes in Synthetic Organic Chemistry*; Pergamon Press, 1994; Vol. 12. https://doi.org/10.1055/s-1994-25719.

(30) Slonczewski, J. L.; Foster, J. W. *Microbiology : An Evolving Science*, Second Edi.; North & Company, Inc., 2011.

(31) Duncan, K. L.; Ulijn, R. V. Short Peptides in Minimalistic Biocatalyst Design. *Biocataysis* **2015**, *1* (1), 67–81. https://doi.org/10.1515/boca-2015-0005.

(32) Robinson, P. K. Enzymes : Principles and Biotechnological Applications. *Essay Biochem* **2015**, *59*, 1–41. https://doi.org/10.1042/BSE0590001.

(33) Keri, G.; Toth, I. *MOLECULAR PATHOMECHANISMS AND NEW TRENDS IN DRUG RESEARCH*, First edit.; Francis, T., Ed.; Taylor & Francis: London and New york, 2003.

(34) Garner, J.; Harding, M. M. Design and Synthesis of α-Helical Peptides and Mimetics. *Org. Biomol. Chem.* **2007**, *5* (22), 3577–3585. https://doi.org/10.1039/b710425a.

(35) Qian, H.; Schellman, J. A. Helix-Coil Theories: A Comparative Study. *J. Phys. Chem.* **1992**, *96* (10), 3987–3994.

(36) Henchey, L. K.; Jochim, A. L.; Arora, P. S. Contemporary Strategies for the Stabilization of Peptides in the a -Helical Conformation. *Curr. Opin. Chem. Biol.* **2008**, *12* (6), 22–26. https://doi.org/10.1016/j.cbpa.2008.08.019.

(37) Rizo, J. Constrained Peptides: Models of Bioactive Peptides and Protein Substructures. *Annu. Rev. Biochem.* **1992**, *61* (1), 387–418. https://doi.org/10.1146/annurev.biochem.61.1.387.

(38) Garner, J.; Harding, M. M. Design and Synthesis of a -Helical Peptides and Mimetics. *Org. Biomol. Chem.* **2007**, *5* (22), 3577–3585. https://doi.org/10.1039/b710425a.

(39) Lyu, P. C.; Sherman, J. C.; Chen, A.; Kallenbach, N. R. α-Helix Stabilization by Natural and Unnatural Amino Acids with Alkyl Side Chains. *Proc. Natl. Acad. Sci. U. S. A.* **1991**, *88* (12), 5317–5320. https://doi.org/10.1073/pnas.88.12.5317.

(40) Yin, H.; Lee, G.; Hamilton, A. D.; Mimetics, A. Alpha-Helix Mimetics in Drug Discovery. *Drug Discov. Res.* **2007**, 280–298.

(41) Wilmot, C. .; Thornton, J. M. β-Turns and Their Distortions: A Proposed New Nomenclature. *Protein Eng.* **1990**, *3* (6), 479–493.

(42) Miiller, G.; Gurrath, M.; Kurz, M.; Kessler, H. BVI Turns in Peptides and Proteins : A Model Peptide Mimicry. *PROTEINS Struct. Funct. Genet.* **1993**, *15* (3), 235–251.

(43) Sibanda, B. L.; Thornton, J. M. β-Hairpin Families in Globular Proteins. *Nature* **1985**, *316* (6024), 170–174.

(44) Schneider, J. P.; Kelly, J. W. Templates That Induce Alpha-Helical , Beta-Sheet , and Loop Conformations. *Chem. Rev.* **1995**, *95* (6), 2169–2187.

(45) Müller, G.; Gurrath, M.; Kurz, M.; Kessler, H. BVI Turns in Peptides and Proteins: A Model Peptide Mimicry. *Proteins Struct. Funct. Bioinforma.* **1993**, *15* (3), 235–251. https://doi.org/10.1002/prot.340150303.

(46) Hutchinson, E. G.; Thornton, J. M. A Revised Set of Potentials for ,& Turn Formation in Proteins. *Protein Eng.* **1994**, *3* (12), 2207–2216.

(47) Sibanda, B. L.; Blundell, T. L.; Thornton, J. M. Conformation of β-Hairpins in Protein

Structures A Systematic Classification with Applications to Modelling by Homology , Electron Density Fitting and Protein Engineering. *J. Mol. Biol.* **1989**, *206* (4), 759–777.

(48) Metrano, A. J.; Abascal, N. C.; Mercado, B. Q.; Paulson, E. K.; Hurtley, A. E.; Miller, S. J. Diversity of Secondary Structure in Catalytic Peptides with β - Turn- Biased Sequences. *J. Am. Chem. Soc.* **2017**, *139* (1), 492–516. https://doi.org/10.1021/jacs.6b11348.

(49) Drauz, K.; Gröger, H.; May, O. *Enzyme Catalysis in Organic Synthesis, Third Edition*, Third Edit.; Wiley-VCG Verlag & Co, 2012; Vol. 1. https://doi.org/10.1002/9783527639861.

(50) Reetz, M. T. Biocatalysis in Organic Chemistry and Biotechnology: Past, Present, and Future. *J. Am. Chem. Soc.* **2013**, *135* (34), 12480–12496. https://doi.org/10.1021/ja405051f.

(51) Benkovic, S. J.; Hammes-Schiffer, S. A Perspective on Enzyme Catalysis. *Science (80-.).* **2003**, *301* (5637), 1196–1202. https://doi.org/10.1126/science.1085515.

(52) Kirby, A. J. Enzyme Mechanisms, Models, and Mimics. *Angew. Chemie (International Ed. English)* **1996**, *35* (7), 706–724. https://doi.org/10.1002/anie.199607061.

(53) Smith, A. J. T.; Müller, R.; Toscano, M. D.; Kast, P.; Hellinga, H. W.; Hilvert, D.; Houk, K. N. Structural Reorganization and Preorganization in Enzyme Active Sites: Comparisons of Experimental and Theoretically Ideal Active Site Geometries in the Multistep Serine Esterase Reaction Cycle. *J. Am. Chem. Soc.* **2008**, *130* (46), 15361–15373. https://doi.org/10.1021/ja803213p.

(54) Eyring, H. The Activated Complex in Chemical Reactions. *J. Chem. Phys.* **1935**, *3* (2), 107–115. https://doi.org/10.1063/1.1749604.

(55) Evans, M. G.; Polanyi, M. Some Applications of the Transition State Method to the Calculation of Reaction Velocities, Especially in Solution. *Trans. Faraday Soc.* **1935**, *31*, 875–894. https://doi.org/10.1039/tf9353100875.

(56) Copeland, R. A. *Enzymes. A Practical Introduction to Structure, Mechanism, and Data Analysis, Second Ed.*, Second Edi.; WILEY-VCH, 2001; Vol. 291. https://doi.org/10.1006/abio.2001.5023.

(57) Ma, B.; Kumar, S.; Tsai, C. J.; Hu, Z.; Nussinov, R. Transition-State Ensemble in

Enzyme Catalysis: Possibility, Reality, or Necessity? *J. Theor. Biol.* **2000**, *203* (4), 383–397. https://doi.org/10.1006/jtbi.2000.1097.

(58) Horecker, B. L.; Tsolas, O.; Lai, C. Y. Aldolases. *Enzymes* **1972**, *7* (C), 213–258. https://doi.org/10.1016/S1874-6047(08)60450-3.

(59) Wong, C. Enzymatic Catalysts in Organic Synthesis. *Science (80-.).* **1989**, *244* (4909), 1145–1152.

(60) Dalby, A. R.; Tolan, D. R.; Littlechild, J. A. The Structure of Human Liver Fructose-1,6-Bisphosphate Aldolase. *Acta Crystallogr. Sect. D Biol. Crystallogr.* **2001**, *57* (11), 1526–1533. https://doi.org/10.1107/S0907444901012719.

(61) Gardberg, A.; Sankaran, B.; Davies, D.; Bhandari, J.; Staker, B.; Stewart, L. Structure of Fructose Bisphosphate Aldolase from Encephalitozoon Cuniculi. *Acta Crystallogr. Sect. F Struct. Biol. Cryst. Commun.* **2011**, *67* (9), 1055–1059. https://doi.org/10.1107/S1744309111021841.

(62) Choi, K. H.; Shi, J.; Hopkins, C. E.; Tolan, D. R.; Allen, K. N. Snapshots of Catalysis: The Structure of Fructose-1,6-(Bis)Phosphate Aldolase Covalently Bound to the Substrate Dihydroxyacetone Phosphate. *Biochemistry* **2001**, *40* (46), 13868–13875. https://doi.org/10.1021/bi0114877.

(63) Arakaki, T. L.; Pezza, J. A.; Cronin, M. A.; Hopkins, C. E.; Zimmer, D. B.; Tolan, D. R.; Allen, K. N. Structure of Human Brain Fructose 1,6-(Bis)Phosphate Aldolase: Linking Isozyme Structure with Function. *Protein Sci.* **2009**, *13* (12), 3077–3084. https://doi.org/10.1110/ps.04915904.

(64) Lorentzen, E.; Siebers, B.; Hensel, R.; Pohl, E. Mechanism of the Schiff Base Forming Fructose-1,6-Bisphosphate Aldolase: Structural Analysis of Reaction Intermediates. *Biochemistry* **2005**, *44* (11), 4222–4229. https://doi.org/10.1021/bi048192o.

(65) Dalby, A.; Dauter, Z.; Littlechild, J. A. Crystal Structure of Human Muscle Aldolase Complexed with Fructose 1 , 6-Bisphosphate : Mechanistic Implications. *Protein Sci.* **1999**, *8* (2), 291–297.

(66) Littlechild, J. A.; Watson, H. C. A Data-Based Reaction Mechanism for Type I Fructose Bisphosphate Aldolase. *Trends Biochem. Sci.* **1993**, *18* (2), 36–39. https://doi.org/10.1016/0968-0004(93)90048-R.

(67) Sygusch, J.; Beaudry, D.; Allaire, M. Molecular Architecture of Rabbit Skeletal Muscle Aldolase at 2.7 Å Resolution. *Proc. Natl. Acad. Sci.* **1987**, *84* (22), 7846–7850.

(68) Hester, G., Brenner-Holzach, O., Rossi, F.A., Struck-Donatz, M., Winterhalter, K.H., Smit, J.D.G. and Piontek, K. The Crystal Structure of Fructose-1, 6-Bisphosphate Aldolase FromDrosophila Melanogaster at 2.5 A˚ Resolution. *Front. Bioeng. Biotechnol. Lett.* **1991**, *292* (1–2), 237–242.

(69) Lorentzen, E.; Siebers, B.; Hensel, R.; Pohl, E. Mechanism of the Schiff Base Forming Fructose-1 , 6-Bisphosphate Aldolase : Structural Analysis of Reaction Intermediates. *Biochemistry* **2005**, *44* (11), 4222–4229.

(70) Sherawat, M.; Dean, R.; Allen, K. N. Structure of a Rabbit Muscle Fructose-1, 6-Bisphosphate Aldolase A Dimer Variant. *Acta Crystallogr. Sect. D Biol. Crystallogr.* **2008**, *64* (5), 543–550. https://doi.org/10.1107/S0907444908004976.

(71) List, B.; Lerner, R. A.; Iii, C. F. B.; Torrey, N.; Road, P.; Jolla, L.; December, R. V. Proline-Catalyzed Direct Asymmetric Aldol Reactions. *J. Am. Chem. Soc.* **2000**, *122* (10), 2395–2396.

(72) List, B.; Pojarliev, P.; Castello, C. Proline-Catalyzed Asymmetric Aldol Reactions between Ketones and α-Unsubstituted Aldehydes. *Org. Lett.* **2001**, *3* (4), 573–575. https://doi.org/10.1021/ol006976y.

(73) List, B. Enamine Catalysis Is a Powerful Strategy for the Catalytic Generation and Use of Carbanion Equivalents. *Acc. Chem. Res.* **2004**, *37* (8), 548–557. https://doi.org/10.1021/ar0300571.

(74) List, B.; Hoang, L.; Martin, H. J. New Mechanistic Studies on the Proline-Catalyzed Aldol Reaction. *Proc. Natl. Acad. Sci. U. S. A.* **2004**, *101* (16), 5839–5842. https://doi.org/10.1073/pnas.0307979101.

(75) Bahmanyar, S.; Houk, K. N. The Origin of Stereoselectivity in Proline-Catalyzed Intramolecular Aldol Reactions. *J. Am. Chem. Soc.* **2001**, *123* (51), 12911–12912. https://doi.org/10.1021/ja011714s.

(76) Alcaide, B.; Almendros, P. The Direct Catalytic Asymmetric Aldol Reaction. *European J. Org. Chem.* **2002**, *2002* (10), 1595–1601. https://doi.org/10.1002/1099-0690(200205)2002:10<1595::AID-EJOC1595>3.0.CO;2-M.

(77) Dalko, P. I.; Moisan, L. In the Golden Age of Organocatalysis. *Angew. Chemie - Int. Ed.* **2004**, *43* (39), 5138–5175. https://doi.org/10.1002/anie.200400650.

(78) Wiesner, M.; Revell, J. D.; Wennemers, H. Tripeptides as Efficient Asymmetric Catalysts for 1,4-Addition Reactions of Aldehydes to Nitroolefins–A Rational Approach. *Angew. Chemie* **2008**, *120* (10), 1897–1900. https://doi.org/10.1002/ange.200704972.

(79) Wennemers, H. Peptides as Asymmetric Catalysts for Aldol Reactions. *Chimia (Aarau).* **2007**, *61* (5), 276–278. https://doi.org/10.2533/chimia.2007.276.

(80) Tsogoeva, S. B.; Wei, S. (S)-Histidine-Based Dipeptides as Organic Catalysts for Direct Asymmetric Aldol Reactions. *Tetrahedron Asymmetry* **2005**, *16* (11), 1947–1951. https://doi.org/10.1016/j.tetasy.2005.04.027.

(81) Revell, J. D.; Wennemers, H. Functional Group Requirements within the Peptide H-Pro-Pro-Asp-NH2 as a Catalyst for Aldol Reactions. *Tetrahedron* **2007**, *63* (35), 8420–8424. https://doi.org/10.1016/j.tet.2007.06.010.

(82) Córdova, A.; Zou, W.; Dziedzic, P.; Ibrahem, I.; Reyes, E.; Xu, Y. Direct Asymmetric Intermolecular Aldol Reactions Catalyzed by Amino Acids and Small Peptides. *Chem. - A Eur. J.* **2006**, *12* (20), 5383–5397. https://doi.org/10.1002/chem.200501639.

(83) Tanaka, F.; Fuller, R.; Barbas, C. F. Development of Small Designer Aldolase Enzymes: Catalytic Activity, Folding, and Substrate Specificity. *Biochemistry* **2005**, *44* (20), 7583–7592. https://doi.org/10.1021/bi050216j.

(84) Oku, J.; Ito, N.; Inoue, S. Asymmetric Cyanohydrin Synthesis Catalyzed by Synthetic Dipeptides, 2. *Die Makromol. Chemie* **1982**, *183* (3), 579–586. https://doi.org/10.1002/macp.1982.021830307.

(85) Miller, S. J.; Copeland, G. T.; Papaioannou, N.; Horstmann, T. E.; Ruel, E. M. Kinetic Resolution of Alcohols Catalyzed by Tripeptides Containing the N-Alkylimidazole Substructure [6]. *J. Am. Chem. Soc.* **1998**, *120* (7), 1629–1630. https://doi.org/10.1021/ja973892k.

(86) Groß, A.; Hashimoto, C.; Sticht, H.; Eichler, J. Synthetic Peptides as Protein Mimics. *Front. Bioeng. Biotechnol.* **2016**, *3*, 211. https://doi.org/10.3389/fbioe.2015.00211.

(87) Akagawa, K.; Suzuki, R.; Kudo, K. Effect of the Helical Tether of a Resin-Supported

Peptide Catalyst for Friedel – Crafts-Type Alkylation in Water. *Adv. Synth. Catal.* **2012**, *354* (7), 1280–1286. https://doi.org/10.1002/adsc.201100950.

(88) Notz, W.; Tanaka, F.; Barbas, C. F. Enamine-Based Organocatalysis with Proline and Diamines: The Development of Direct Catalytic Asymmetric Aldol, Mannich, Michael, and Diels-Alder Reactions. *Acc. Chem. Res.* **2004**, *37* (8), 580–591. https://doi.org/10.1021/ar0300468.

(89) Wiesner, M.; Revell, J. D.; Tonazzi, S.; Wennemers, H. Peptide Catalyzed Asymmetric Conjugate Addition Reactions of Aldehydes to Nitroethylene - A Convenient Entry into Γ2-Amino Acids. *J. Am. Chem. Soc.* **2008**, *130* (17), 5610–5611. https://doi.org/10.1021/ja801027s.

(90) Seebach, D.; Beck, A. K.; Bierbaum, D. J. The World of β- And γ-Peptides Comprised of Homologated Proteinogenic Amino Acids and Other Components. *Chem. Biodivers.* **2004**, *1* (8), 1111–1239. https://doi.org/10.1002/cbdv.200490087.

(91) Seebach, D.; Matthews, J. L. β-Peptides: A Surprise at Every Turn. *Chem. Commun.* **1997**, *1* (21), 2015–2022. https://doi.org/10.1039/a704933a.

(92) Akagawa, K.; Suzuki, R.; Kudo, K. Development of a Peptide-Based Primary Aminocatalyst with a Helical Structure. *Asian J. Org. Chem.* **2014**, *3* (4), 514–522. https://doi.org/10.1002/ajoc.201400028.

(93) Kofoed, J.; Nielsen, J.; Reymond, J. L. Discovery of New Peptide-Based Catalysts for the Direct Asymmetric Aldol Reaction. *Bioorganic Med. Chem. Lett.* **2003**, *13* (15), 2445–2447. https://doi.org/10.1016/S0960-894X(03)00498-0.

(94) Akagawa, K.; Akabane, H.; Sakamoto, S.; Kudo, K. Asymmetric Transfer Hydrogenation in Aqueous Media Catalyzed by Resin-Supported Peptide Having a Polyleucine Tether. *Tetrahedron: Asymmetry* **2009**, *20* (4), 461–466. https://doi.org/10.1016/j.tetasy.2009.02.036.

(95) Patgiri, A.; Menzenski, M. Z.; Mahon, A. B.; Arora, P. S. Solid-Phase Synthesis of Short α-Helices Stabilized by the Hydrogen Bond Surrogate Approach Anupam. *Nat. Protoc.* **2015**, *5* (11), 1857–1865. https://doi.org/10.1038/nprot.2010.146.Solid-phase.

(96) Wang, D.; Liao, W.; Arora, P. S. Enhanced Metabolic Stability and Protein- Binding Properties of Artificial a Helices Derived from a Hydrogen-Bond Surrogate: Application

to Bcl-XL. *Angew. Chemie Int. Ed.* **2005**, *44* (40), 6525–6529. https://doi.org/10.1002/anie.200501603.

(97) Lifson, S.; Roig, A. On the Theory of Helix-Coil Transition in Polypeptides. *J. Chem. Phys.* **1961**, *34* (6), 1963–1974. https://doi.org/10.1063/1.1731802.

(98) Austin, R. E.; Maplestone, R. A.; Sefler, A. M.; Liu, K.; Hruzewicz, W. N.; Liu, C. W.; Cho, H. S.; Wemmer, D. E.; Bartlett, P. A. A Template for Stabilizatgion of a Peptide α-Helix: Synthesis and Evaluation of Conformational Effects by Circular Dichroism and NMR. *J. Am. Chem. Soc.* **1997**, *119* (28), 6461–6472. https://doi.org/10.1021/ja964231a.

(99) Phelan, J. C.; Skelton, N. J.; Braisted, A. C.; McDowell, R. S. A General Method for Constraining Short Peptides to an α-Helical Conformation. *J. Am. Chem. Soc.* **1997**, *119* (3), 455–460. https://doi.org/10.1021/ja9611654.

(100) Ramírez-Alvarado, M.; Blanco, F. J.; Serrano, L. De Novo Design and Structural Analysis of a Model β-Hairpin Peptide System. *Nat. Struct. Biol.* **1996**, *3* (7), 604–612. https://doi.org/10.1038/nsb0796-604.

(101) Aravinda, S.; Shamala, N.; Rajkishore, R.; Gopi, H. N.; Balaram, P. A Crystalline β-Hairpin Peptide Nucleated by a Type I′ Aib-D-Ala β-Turn: Evidence for Cross-Strand Aromatic Interactions. *Angew. Chemie - Int. Ed.* **2002**, *41* (20), 3863–3865. https://doi.org/10.1002/1521-3773(20021018)41:20<3863::AID-ANIE3863>3.0.CO;2-A.

(102) Mocanu, A.; Cernica, I.; Tomoaia, G.; Bobos, L. D.; Horovitz, O.; Tomoaia-Cotisel, M. Self-Assembly Characteristics of Gold Nanoparticles in the Presence of Cysteine. *Colloids Surfaces A Physicochem. Eng. Asp.* **2009**, *338* (1–3), 93–101. https://doi.org/10.1016/j.colsurfa.2008.12.041.

(103) Mikolajczak, D. J.; Koksch, B. Carbonic Anhydrase Mimics. *Catalysts* **2019**, *9* (11), 903.

(104) Porta, F.; Speranza, G.; Dal, V.; Francescato, P.; Scar, G. Gold Nanoparticles Capped by Peptides. *Mater. Sci. Eng. B* **2007**, *140* (3), 187–194. https://doi.org/10.1016/j.mseb.2007.03.019.

(105) Wu, R. H.; Nguyen, T. P.; Marquart, G. W.; Miesen, T. J.; Mau, T.; Mackiewicz, M. R.

A Facile Route to Tailoring Peptide-Stabilized Gold Nanoparticles Using Glutathione as a Synthon. *Molecules* **2014**, *19* (5), 6754–6775. https://doi.org/10.3390/molecules19056754.

(106) Ocampo-garcía, B. E.; Ramírez, F. D. M.; Ferro-flores, G.; León-rodríguez, L. M. De; Santos-cuevas, C. L.; Morales-avila, E.; Arteaga, C.; Murphy, D.; Pedraza-lópez, M.; Medina, L. A.; Camacho-lópez, M. A. Tc-Labelled Gold Nanoparticles Capped with HYNIC-Peptide / Mannose for Sentinel Lymph Node Detection. *Nucl. Med. Biol.* **2011**, *38* (14539), 1–11. https://doi.org/10.1016/j.nucmedbio.2010.07.007.

(107) Doyen, M.; Goole, J.; Bartik, K.; Bruylants, G. Amino Acid Induced Fractal Aggregation of Gold Nanoparticles : Why and How. *J. Colloid Interface Sci.* **2016**, *464*, 160–166. https://doi.org/10.1016/j.jcis.2015.11.017.

(108) Turkevich, J.; Stevenson, P. C.; Hillier, J. A Study of the Nucleation and Growth Processes in the Synthesis of Colloidal Gold. *Discuss. Faraday Soc.* **1951**, *11* (c), 55–75. https://doi.org/10.1039/DF9511100055.

(109) Lévy, R. Peptide-Capped Gold Nanoparticles: Towards Artificial Proteins. *ChemBioChem* **2006**, *7* (8), 1141–1145. https://doi.org/10.1002/cbic.200600129.

(110) Lee, K. H.; Marty Ytreberg, F. Effect of Gold Nanoparticle Conjugation on Peptide Dynamics and Structure. *Entropy* **2012**, *14* (4), 630–641. https://doi.org/10.3390/e14040630.

(111) Mikolajczak, D. J.; Heier, J. L.; Schade, B.; Koksch, B. Catalytic Activity of Peptide-Nanoparticle Conjugates Regulated by a Conformational Change. *Biomacromolecules* **2017**, *18* (11), 3557–3562. https://doi.org/10.1021/acs.biomac.7b00887.

(112) Sóti, P. L.; Yamashita, H.; Sato, K.; Narumi, T.; Toda, M.; Watanabe, N.; Marosi, G.; Mase, N. Synthesis of a Self-Assembling Gold Nanoparticle-Supported Organocatalyst for Enamine-Based Asymmetric Aldol Reactions. *Tetrahedron* **2016**, *72* (16), 1984–1990. https://doi.org/10.1016/j.tet.2016.02.065.

(113) Davies, J. S. The Cyclization of Peptides and Depsipeptides. *J. Pept. Sci.* **2003**, *9* (8), 471–501. https://doi.org/10.1002/psc.491.

Chapter 2

Design and synthesis of novel peptide-based catalysts

2.1 Introduction

Chemists and biochemists have long been fascinated by the exceptional correlation between the secondary structure of enzymes and how they function in living organisms, which is mainly due to the influence of the arrangement of amino acid sequences. Today, volumes of available information about chemical and biological data, information about sequences, catalytic residues, functions, structures, kinetics, binding affinity, metabolic pathways and bioinformatics detailing the evolution of enzymes is accessible through literature and databases. The databases that focus on enzymes or proteins in general, were developed from the information primarily found in literature (UniProt,[1] wwPDB,[2] IntEnz,[3] ExplorNZ,[4] pFam,[5] CSA,[6] BRENDA,[7] PLD,[8] KEGG,[9] BioPath,[10] Promise and MBD[11]). This has created the possibility of mimicking protein folding patterns or even the active site of an enzyme using a limited number of selected amino acids which are still able to form the desired structural conformation.

As already discussed, in the previous chapter, the catalytic function of enzymes is based on the tertiary structure of the polypeptide chain, which is made up of secondary motifs such as β-turns and α-helices. The combination of these structural frameworks provides the catalytic active site for an efficient and selective reaction. There is a lot of effort being devoted to the modification of enzyme activities in an attempt to meet the needs of organic chemical synthesis.[12] Generally approaches to enzyme mimics are divided into three categories namely;

1. The design approach, which incorporates the design of macromolecular receptors having the appropriate functionality of mimicking the binding and microenvironment of the active site,
2. The catalytic selection approach which uses combinatorial chemistry to generate a library of catalysts for screening and lastly the,

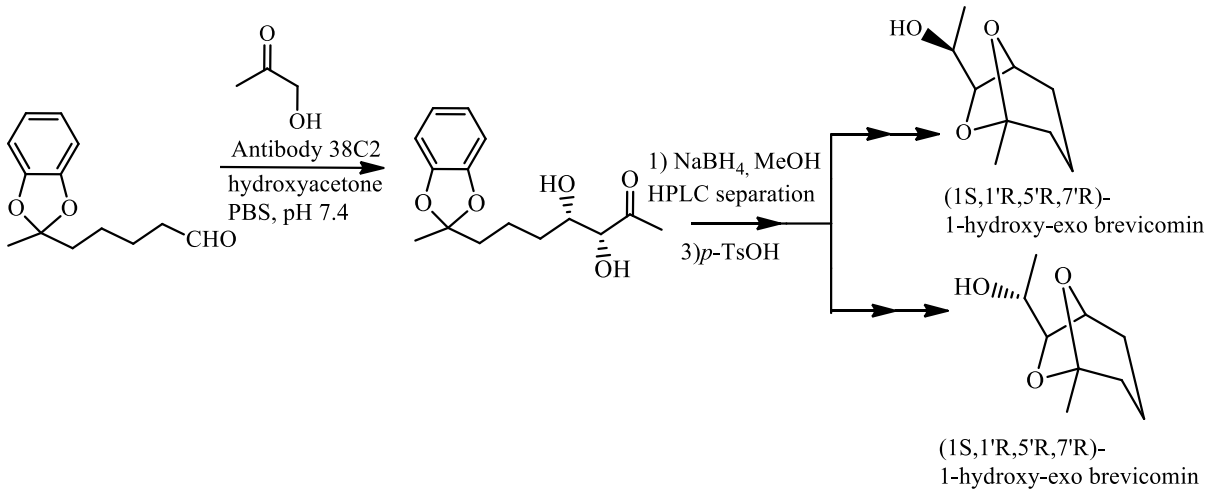
3. Transition state analogue selection approach, where a library of hosts is produced in the presence of a transition state analogue (TSA), and the best host that exhibits the highest binding affinity is then chosen from the library.[12,13]

Herein is a brief discussion of some previous work which was based on these approaches to create enzyme mimics, especially the application in asymmetric aldol reaction. In this study, the design approach is employed.

2.2 Previous research on different enzyme mimic approaches

Transitional state analogue approach; Most researchers have concentrated on this approach and synthesized molecules mimicking the enzyme transition states.[12] Catalytic antibodies, which are well known to catalyze reactions, are developed from the transition state analogues. Notably catalytic antibodies are renowned for catalyzing the asymmetric aldol reaction using the class I aldolase mechanism (Section 1.5.2). The mechanism uses the epsilon-amino group of Lys to form an enamine with the ketone substrate, subsequently reacting with the second substrate (aldehyde) to form a new carbon-carbon bond.

Lerner and group reported highly enantioselective polyclonal antibodies which were obtained from the hapten (a small molecule that binds to proteins and stimulates an immune response) binding site.[14] They proposed that these antibodies can catalyze the aldol reaction by forming Schiff bases with appropriate compounds that can undergo both the aldol and retro-aldol reactions similar to the enamine mechanism followed by the natural Class I aldolases. Furthermore, they reported a total synthesis of (1R, 1'R, 5'R, 7'R)- and (1S, 1'R, 5'R, 7'R)-1-hydroxy-exo-brevicomin with high enantioselectivity (**Scheme 2-1**) from aldol reaction catalyzed by the antibody 38C.

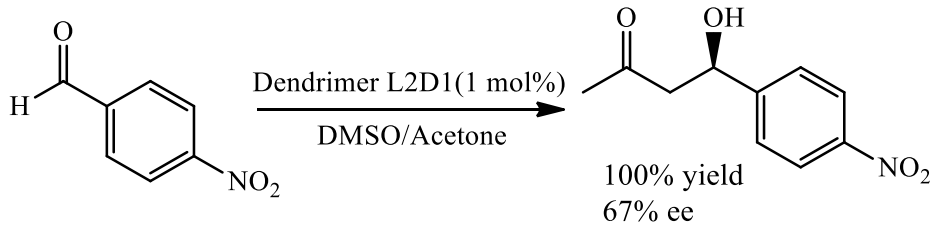


Scheme 2- 1: Total synthesis of hydroxybrevicomins from aldol reaction catalyzed by an antibody 38C2.[14]

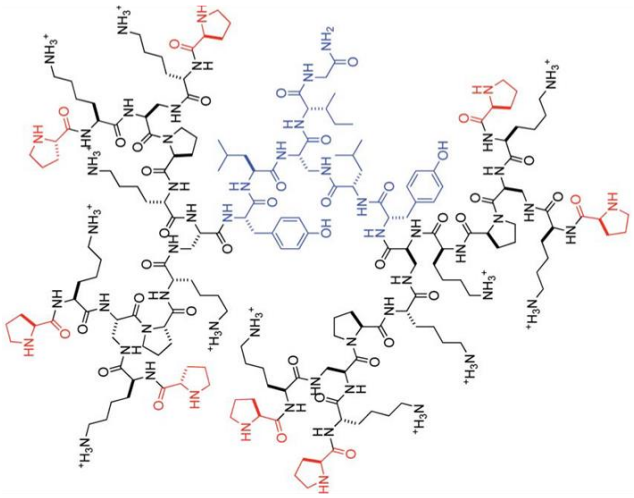
Even though antibodies have proved to be useful tool in modern synthetic chemistry, they are limited by the mode of preparation and use. The method of production requires the use of mice and highly specialized techniques. Other draw backs include the isolation which is often tedious, moreover they are also unstable at high temperature and lack chemical robustness which is a necessity in chemical reactions.[12]

The catalytic selection approach is the second approach that has been widely applied in enzyme mimics. It offers an opportunity for large numbers of various compounds to be synthesized within a short period of time. One of the strategies commonly applied in this approach, is combinatorial chemistry, which mimics natural evolution where a library of possible catalysts is generated and are directly screened for enzyme-like activity.[13] Kofoed and co-workers,[15] reported a peptide dendrimer-catalyzed aldol reaction, applying a dendrimer that was obtained using functional selection from a dendrimer combination libraries. Complete reaction conversion was reached in 3 hours with 1 mol % of catalyst and the obtained aldol products had an enantiomeric excess (%ee) of 67 % (**Scheme 2-2**).

A)



B)



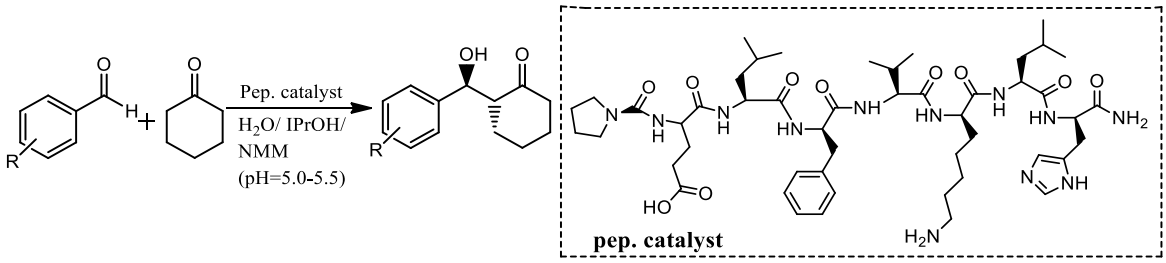
Scheme 2- 2: A) Peptide dendrimer catalyzed aldol reaction, B) **L2D1** Peptide dendrimer used.[15]

The directed evolution of enzymes has also been reported as a novel screening method for the catalytic selection approach. It uses screening methods to identify the mutations within the enzyme which are responsible for catalytic abilities. These mutants are then expressed in suitable host, and then screened for enantioselectivity in the reaction of interest using fascinating techniques such as infrared thermography.[12,16] There are other examples of work done using this technique in other organic reactions, such as the reduction of Baylis-Hillman adducts,[17] kinetic resolution of esters[18] and Diels-Alder cycloadditions between anthracene (diene) and maleimide (dienophile).[19] Even though there is no disputing the potential of directed evolution, dendrimers and combinatorial libraries strategies, these strategies can be extremely time-consuming.

The design approach has been utilized a lot in recent years. It focuses on the design of macromolecular receptors which have appropriately placed functional groups to mimic amino acids residues identified to be involved in enzyme catalyzed reactions.[12,16] The highlight of this approach has been on the design and synthesis utilizing functionalized cyclodextrins as an

aromatic acceptor, although recently cyclophanes also have shown some remarkable results.[13] Yuan and co-workers have developed a variety of mono- and unsymmetrical β-functional cyclodextrins and possible aldolase class I enzyme mimics.[20] They suggested that the designed catalyst can mimic the amino groups of class I aldolases with large reaction acceleration rate and substrate selectivity. However, the use of cyclodextrins has certain drawbacks, they are disadvantaged by their susceptibility to acid hydrolysis, while their rigidity puts a limit on the range of aromatic substrates that can be tolerated.

Rational design uses a priori knowledge of enzyme function, often combining structural information and a basic mechanistic picture of the chemical reaction being catalyzed. The goal normally, is to create new activity or vary the stereochemistry and regioselectivity of existing enzymes with the introduction of a fairly small number of mutations.[13] Bayat *et al.* reported the rational design of mimetic peptides based on the aldol-ketoreductase (AKR) enzyme as an asymmetric organocatalyst in aldol reaction (**Scheme 2-3**).[21] Their synthesized peptides proved to be excellent multifunctional organocatalysts with high yields of up to 97% and enantioselectivities of 98%.



Scheme 2- 3: Bayat's rational design of mimetic peptides based on the AKR active site.[21]

Even though some impressive results have been obtained using this strategy, the following limitation needs to be addressed; the approaches that involves laborious and time-consuming synthetic steps and in addition, a little defect in the design can sometimes led to the complete loss of activity.[12]

2.3 Enzyme mimics based on peptides with secondary structure

Peptide catalysts have a number of advantages over single amino acids because of their diverse structure, functionality and ability to preserve the characteristics of small molecule catalyst.[21–23] Peptides are a considerable alternative to the small, rigid organocatalysts and enzymes. Thus, designing peptide-based catalysts having secondary structural moieties can yield efficient selective organocatalysts.

2.4 Peptide catalyst design

2.4.1 General considerations

For the design of our novel peptide catalysts, we are interested in the amino acids (AAs) residues in the active site of the Fructose-1,6-bisphophate aldolase (FBPA) enzyme. We hypothesize that the incorporation of certain AAs from β-turns, and α-helices of the active site of the FBPA enzyme will yield a peptide with a secondary structure that can interact with most organic substrates in an aqueous media to yield aldol products.[24,25] We also postulate that the use of unnatural amino acid (D-amino acids) residues, would enhance the activity of the peptide catalyst. D-amino acids can alter the conformation of the peptide structure,[26,27] and this might result in a different or closer alignment of the peptide to the substrate.

2.4.2 Synthesis of catalytic peptides based on helical and β-turn structural resides

The AAs used in the design of the catalytic and turn motifs were adopted from the *D. melanogaster* aldolase enzyme structure obtained from the UniProt protein database (EC 4.1.3.12; Gene code: Ad1), **Figure 2-1**. Other sources of information about the catalytic and turn motif residues were accessed from the Protein Data bank (PDB).

```
        10         20         30         40         50
MTTYFNYPSK ELQDELREIA QKIVAPGKGI LAADESGPTM GKRLQDIGVE
        60         70         80         90        100
NTEDNRRAYR QLLFSTDPKL AENISGVILF HETLYQKADD GTPFAEILKK
       110        120        130        140        150
KGIILGIKVD KGVVPLFGSE DEVTTQGLDD LAARCAQYKK DGCDFAKWRC
       160        170        180        190        200
VLKIGKNTPS YQSILENANV LARYASICQS QRIVPIVEPE VLPDGDHDLD
       210        220        230        240        250
RAQKVTETVL AAVYKALSDH HVYLEGTLLK PNMVTAGQSA KKNTPEEIAL
       260        270        280        290        300
ATVQALRRTV PAAVTGVTFL SGGQSEEEAT VNLSAINNVP LIRPWALTFS
       310        320        330        340        350
YGRALQASVL RAWAGKKENI AAGQNELLKR AKANGDAAQG KYVAGSAGAG
       360
SGSLFVANHA Y
```

Figure 2- 1: Amino acids sequence of the *Drosophila melanogaster* FBPA enzyme obtained from the UniProt protein database.

2.4.2.1 Helical motif proposed structures (Helix design)

The designed sequences are based on the physical and chemical properties of catalytic amino acids. This refers to the different functional roles of amino acid residues which are involved in the catalytic activity of FBPA (**Figure 2-2**). These roles include stabilization, steric constraints, substrate activation, proton abstraction/donation, hydrogen, electron shuttling and covalent (nucleophilic/electrophilic) catalysis. It is noteworthy that most residues can perform more than one function, and the roles mentioned herein does not put any restriction on other roles.

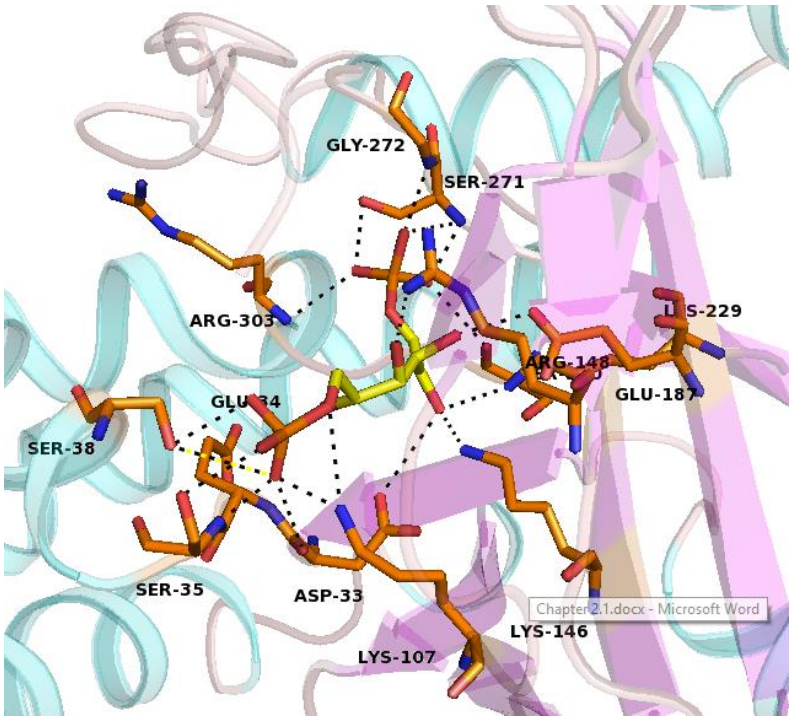


Figure 2- 2: The amino acid residues of the FBPA active site

- Arginine (Arg) was chosen due to its stabilizing effect, and as already emphasized in the previous chapter it is involved in the cyclic binding of the substrate and electrostatic stabilization. The side chain of arginine is known to engage in electrostatic interactions and hence has the ability to accurately position substrates for catalysis.[28–30]
- Cysteine (Cys) which undergoes oxidation forms disulphide bridges between two cysteines and hence provides stabilization.[29]
- Tyrosine (Tyr) which possesses a hydroxyl group (-OH) and an aromatic group is involved in proton shuttling and in the increase of electrostatic interactions that results in a stabilization effect.

- Aspartic acid (Asp) and Glutamic acid (Glu) were selected due to their carboxylic functional group on the side chains which are involved in acid/base roles i.e. proton donating/abstracting. An extra CH_2 linker inserted between the Cα and carboxylate group in Glu enable higher efficiency for acting as a base/catalyst than Asp, whilst Glu is more of an activator when compared to Asp.[31–35]
- Glycine (Gly) and Alanine (Ala) have hydrophobic (non-polar) side chains resulting in the hydrophobic interactions needed for an enzyme to perform the catalysis in their folded structure. Both Gly and Ala have an ability to form turns and thus stabilize helices. Ala also has a greater stabilizing affinity when compared to Gly because it can bury deeper into more non-polar regions upon folding, resulting in lower backbone entropy.[31,33]
- Serine (Ser) is chosen for its ability to stabilize enzyme structures

2.4.2.2 Turn motif proposed structures

In choosing the amino acid sequence of the turn motif, the same criteria explained above in Section 2.4.2.1 were utilized.

Amino acids 344-347 were selected for the turn motif

Turn
CRYKE**GSAG**KEYRC

- 344-347

2.4.2.3 D-Amino acids

D-Amino acids (D-AAs), are regarded as the "unnatural" enantiomers of amino acids since they are not utilized for the ribosomal protein synthesis.[27] It is well known that they are found as constituents of natural peptides and are naturally produced by microorganism, using non-ribosomal mechanisms of synthesis.[26] Due to their functional diversity and structural versatility, they have gained great use in the design of peptide and protein structures.[27,36] Furthermore, because of their conformational preference they are employed in peptide synthesis to restrict local conformations of peptide chains and to facilitate the formation of prime beta-turns. Studies have also shown that a peptide sequence consisting of L-and D-amino acids can be induced to form ambidextrous helical structures.[26,37,38] Peptides with catalytic motifs, β turns motifs and D-amino acids that were designed and synthesized in this study are outlined below in **Table 2-1**.

Table 2- 1: The peptide sequences with amino acid derived from the catalytic active site of the FBPA enzyme

Peptide	Sequence	Indications
TP_Asp	CRYK**D**GSAGK**D**YRC	Asp(D) with all L-AAs
TP_ADLys	CRY**K**DGSAG**K**DYRC	Asp(D) with L-AAs, but L-Lys is replaced with D-Lys
TP_ADA	**CRYKDGSAGKDYRC**	Asp (D), but L-AAs are replaced with D-AAs
TP_AspC	CRY**K**DGSAG**K**DYRC	Asp (D), but L-Lys is replaced with D-Lys, **cyclised**
TP_ADLysC	CRYKDGSAGKDYRC	Asp(D) with all L-AAs, **cyclised**
TP_ADAC	**CRYKDGSAGKDYRC**	Asp (D), replacing all L-AAs with D-AAs, **cyclised**
TP_Glu	CRYKEGSAGKEYRC	Using Glu (E) with L-AAs
TP_GDLys	CRYK**E**GSAGK**E**YRC	Using Glu but L-Lys is replaced with D-Lys
TP_GDA	**CRYKEGSAGKEYRC**	Using Glu, but L-AAs are replaced with D-AAs
TP_GluC	CRYKEGSAGKEYRC	Glu with L-AAs, **cyclised**
TP_GDLysC	CRY**K**EGSAG**K**EYRC	Glu, but L-Lys is replaced with D-Lys, **cyclised**
TP_GDAC	**CRYKEGSAGKEYRC**	Using Glu, all D-AAs, **cyclised**

D-AAs =represented by bold and blue colour

2.5 Results and discussion

2.5.1 Synthesis of TP_Asp

As discussed above, our goal was to design peptide catalysts with a turn motif and a catalytic site, as shown in (**Figure 2-3**).

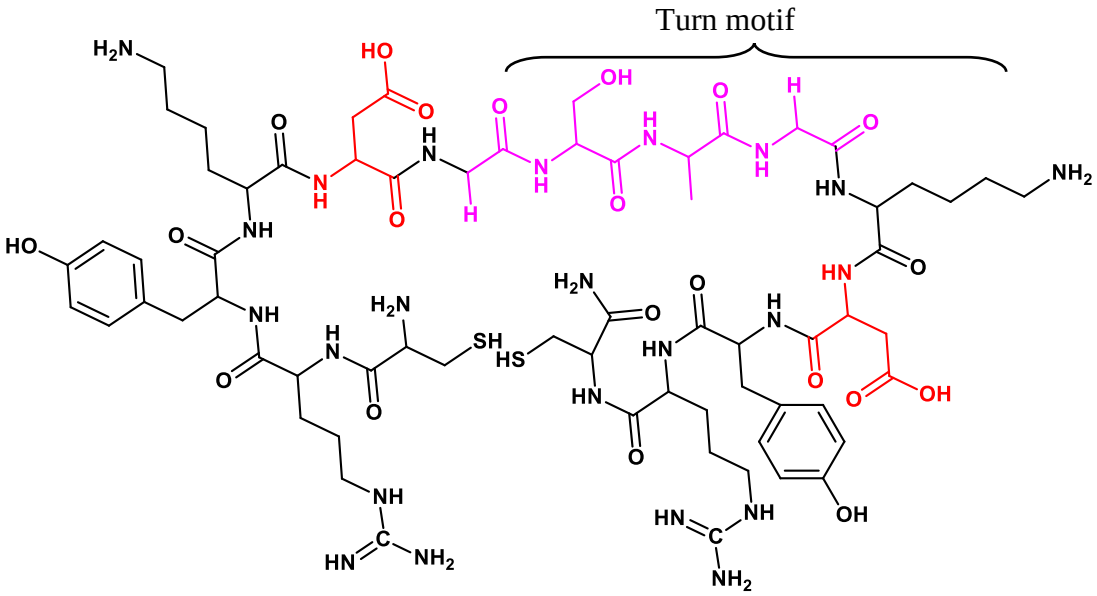
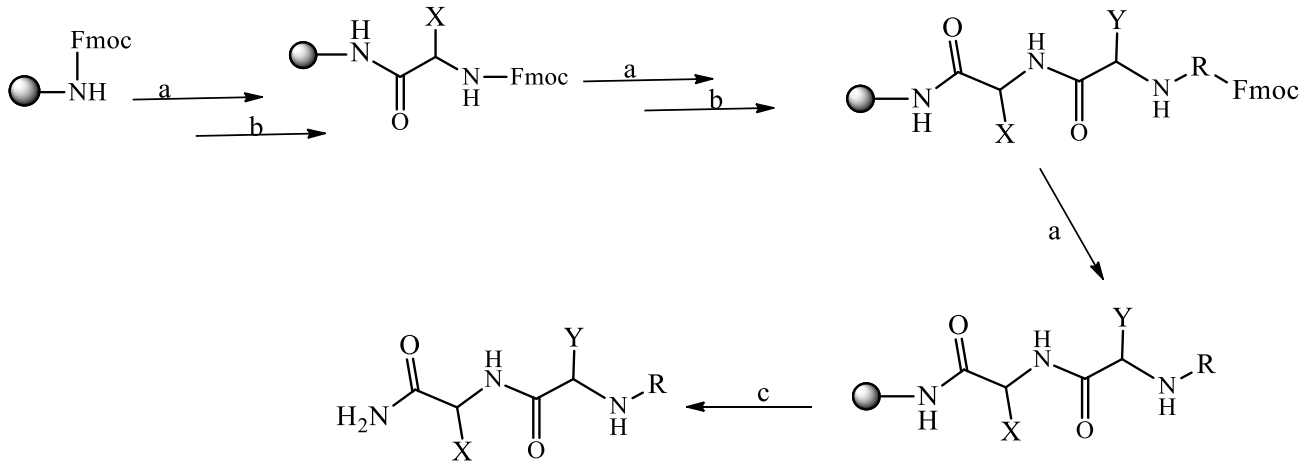


Figure 2- 3: Structural representation of TP_Asp peptide, showing a turn and catalytic motif site.

Peptides were synthesized manually and automatically using the Fmoc-(Fluorenylmethyloxycarbonyl) Solid-Phase Peptide Synthesis (SPPS) strategy (**Scheme 2-4**). The full synthetic procedures are outlined in Section 7.31.

The first attempt towards the synthesis of the (TP_Asp peptide) was carried out using a PS3 peptide synthesizer on a MBHA (4-methylbenzhydrylamine) rink amide resin (0.45 mmol/g, 1-0.6 g) in order to obtain an amide ending at the C-terminal. The first step involved the deprotection of Fmoc of the resin using a 20% piperidine/DMF solution to expose the free amino group. After the deprotection of the resin, the first amino acid cysteine (2.0 M) and coupling reagents (1.90 M HBTU (2-(1H-benzotrial-1-yl-1,1,3,3-tetramethyluronium hexafluorophosphate) and 1.0 M DIPEA (N, N Diisopropylethylamine) were added. The coupling times were varied between 20-30 minutes. The synthesis was left to run overnight.



Scheme 2- 4: General procedure for the SPPS peptide synthesis; where a=20% piperidine/DMF, b=DIPEA/HBTU/Fmoc-AA, and d=TFA/TIS/EDT/H_2O, X or Y=different amino acid side chain, R=amino acids.

The peptide was cleaved from the resin and analyzed using liquid chromatography-mass spectrometry (LC-MS), but the desired mass was not obtained. The coupling time was then increased to 40 minutes and the coupling was monitored sequentially using LC-MS, however at the 6th amino acid (Glycine), there was incomplete coupling. Glycine is a small flexible residue without a side chain therefore it could not have encountered steric hindrance. Difficulties are often encountered in peptide synthesis as the peptide chain grows, and they are often associated with aggregation, which can either be due to inter-or intra- molecular interactions or β-sheet secondary structure formation.[39,40] Hence, we attributed the incomplete coupling of glycine to the aggregation of the peptide.

Another attempt was made using a different coupling reagent HATU (1-[Bis(dimethylamino)methylene]-1H-1,2,3-triazolo[4,5-b]pyridinium 3-oxide hexafluorophosphate). HATU has been proven to reduce epimerization during coupling and it is also very efficient in coupling sterically hindered sequences. HATU and HBTU are both known to react with the carboxylic end of the AA to form active esters, which react with the amine of the resin bound peptide.[41,42] HATU (1.9 M) was utilized as a coupling reagent and the reactions were monitored by LC-MS. It was observed in this experiment that at the 9th amino acid (also Glycine), the coupling was inefficient as the mass of the 8th amino acid was observed. After the 9th AA, the coupling efficiency was infinitesimal up to the 11th AA (Lysine). It is reported that extreme steric hindrance leads to reduced accessibility and cause a reduction in reaction rates for both the coupling (acylation) and deprotection steps, thus the

observed decrease in coupling efficiency was attributed to the turn motif.[43–45] Consequently, the desired peptide products are frequently contaminated by deletion sequences.[46]

Another approach involved double coupling and an increase in coupling times to 40 minutes in order to obtain acceptable acylation yields. This was also monitored sequentially by LC-MS. It is presumed that HATU yields faster coupling rates because of the presence of a pyridine nitrogen atom in the cyclic ring, which lowers the energy of the tetrahedral transition state by hydrogen bonding to the attacking amine (**Figure 2-4**).[41,47] Despite these exceptional properties of HATU in peptides synthesis, it is expensive. One of the goals of this study was to create less expensive catalysts, hence the double coupling experiments were performed using HBTU due to its availability and affordability.

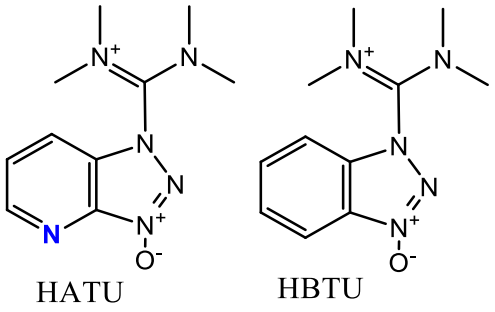


Figure 2- 4: Illustration of the difference between HATU and HBTU

Double coupling was carried out for all the amino acids in a peptide sequence for 45 minutes per coupling. However, whilst monitoring the reactions it was observed that the 6th and 9th AA were not completely coupled and were then triple coupled (**method 1**). Studies have shown that coupling glycine (a hydrophobic amino acid) into the peptide sequence as the peptide chain grows can be problematic, due to its small structural nature which induces agglomeration.[48,49] After numerous exertions to find a working approach for the synthesis, to improve the coupling efficiency and to obtain the complete synthesis of the peptide catalyst, the synthesis of the peptide was successful and was confirmed by LC-MS. The sample was dissolved in 60/40 (Water/acetonitrile, (H_2O/MeCN)) for analysis by LC-MS and the calculated mass for TP_Asp is 1620,70 g/mol whilst the half mass found was $[M+2H]^{2+}$ 810.8719 m/z at the retention time (t_R) of 7.63 min (**Figure 2-5**). A 20 minutes gradient elution method (5-50% MeCN) was utilized with the following solvent system: Solvent A: H_2O with 0.1% formic acid; solvent B: MeCN with 0.1% formic acid.

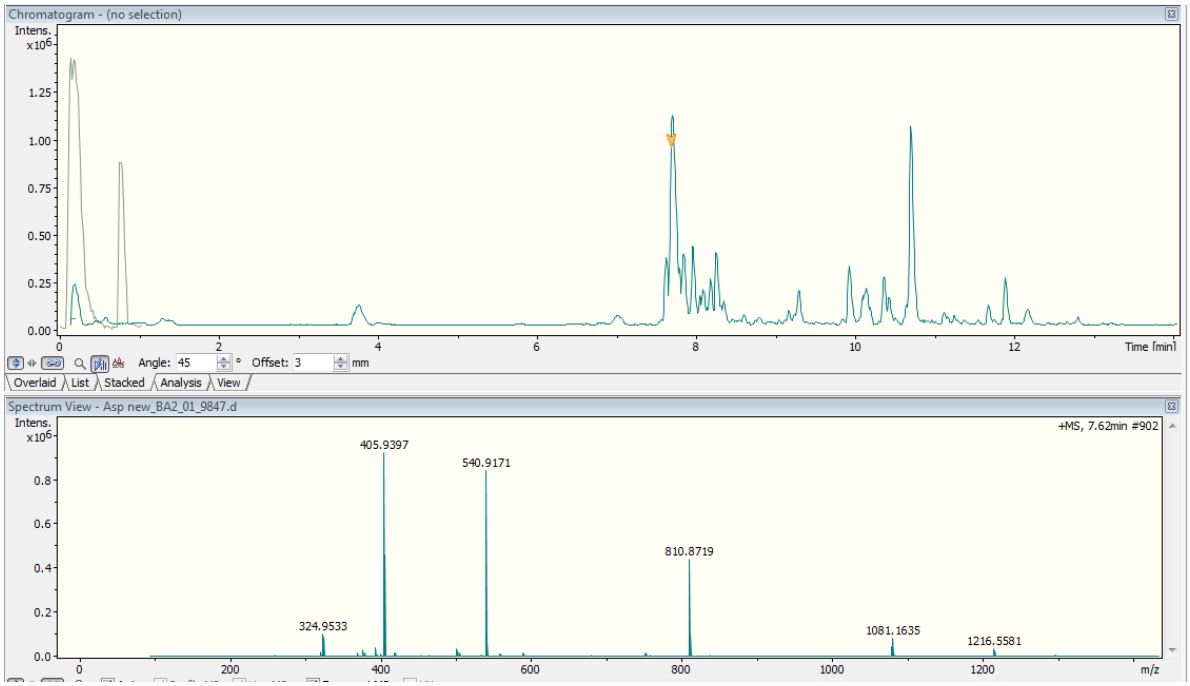


Figure 2- 5: LC-MS spectrum for the fully synthesized crude TP_Asp

2.5.1.1 Purification of TP_Asp

First attempt: A gradient elution method consisting of a buffered (0.1% formic acid), acetonitrile and buffered water was employed as the mobile phase in the purification of TP_Asp. After numerous runs with different elution gradient methods and flow rates, it was observed that 2-50% acetonitrile (**method 1-1**) in 15 minutes at a flow rate of 15 min/ml was the best method for the separation of the analyte. Due to the polar nature of the peptide, it was dissolved in less than 50% of acetonitrile in water.

Four of the fractions collected from the preparative-HPLC had the same masses with different retention times of 5.49, 6.58, 6.65 and 6.68 minutes respectively. Peptides are known to be very flexible and can exist as ensemble of conformations in solution, especially linear peptides. This is because of the formation of secondary structures that occur during the initial stages of protein folding.[50,51] We therefore postulate that the collected fractions with the analyte of interest are the result of peptide folding in solution. The average percentage yield of the 4 conformers was determined after drying the peptide using the rotary-evaporator, resulting in a mass of 293 mg and a yield of 55.7%.

2.5.2 Synthesis of TP_ADLys

In the synthesis TP_ADLys, the same synthetic approach as described above was followed except that the L-lysine residues in the 5th and 11th positions were replaced by D-Lysine (**method 2**). Lysine is one of the key AA in FBPA catalysis since it is responsible for the formation of the Schiff base through the enamine mechanism. D-amino acids are known to react faster than their L-counterparts by one tenth (1-5µmol) min/mg. Incorporating a D-AAs into a peptide chain also imposes local conformational restrictions.[50,51]

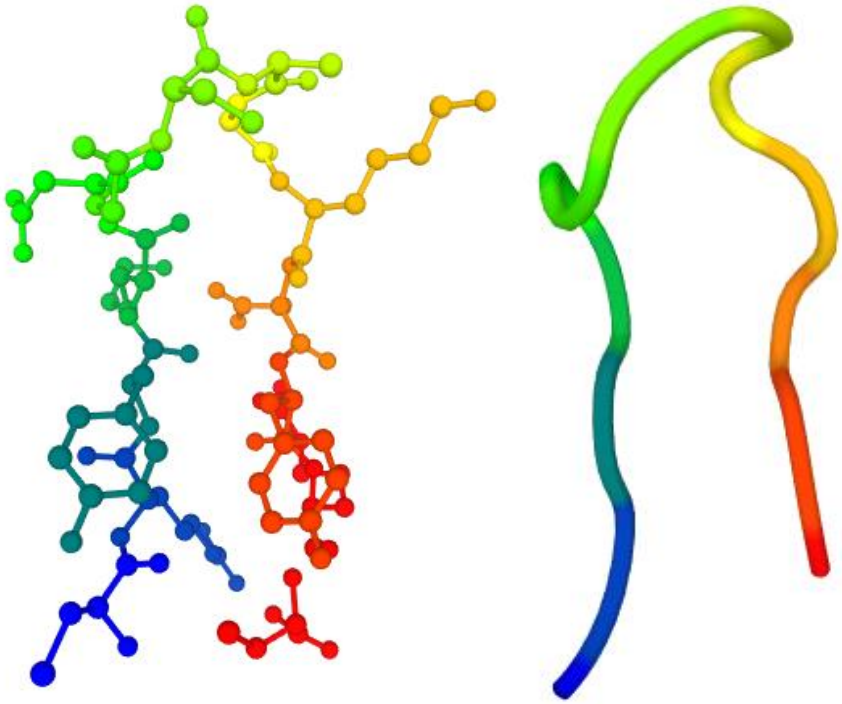


Figure 2- 6: Folded structure of TP_Asp using *d*e novo peptide structure prediction (RPBS Web Portal), depicting L-lysine side chain (yellow) pointing out.

D-Lys changes the orientation of the side chain so it can point inside the pocket of the catalyst. It can therefore efficiently hold and interact with the substrate more easily when compared to L-Lys which is pointing outward as shown in **Figure 2-6** above.

Furthermore, the other purpose of incorporating D-Lys was also to investigate whether it would have any effect on the enhancement of stereoselectivity. After the successful synthesis of TP_ADLys, the peptide was cleaved from the resin using a TFA cocktail (94% TFA, 2.5% EDT, 2.5%, H_2O, 1.0% TIS) followed by precipitation with cold diethyl ether. It was dissolved in 60/40 (water, acetonitrile) for analysis by LC-MS.

2.5.2.1 Purification of TP_ADLys

A slight modification of the method described in section 2.5.1.1 was made. We employed a gradient elution method consisting of water and acetonitrile, buffered with 0.1% formic acid as the mobile phase. Acetonitrile ratio was allowed to increase from 5% to 50% in 10 minutes and held constant at 50% for a further 20 minutes (**method 2-1)**. It was observed that there were 4 peaks with the same mass of interest, again suggesting the formation conformers.

After the successful purification of TP_ADLys, the four collected peaks were analyzed by LC-MS and they eluted at different retention times of 6.50, 6.62, 6.65 and 6.53 minutes respectively. The calculated or expected HRMS (ESI^+) *m/z* mass was 1620.71 $C_{66}H_{104}N_{22}O_{23}S_2$, and found the mass was 1620.7377 $[M+H]^+$. The average percentage purity of analyte peaks as determined using LC-MS was 89.25%. After purification, the solvents were removed using the rotary-evaporator resulting in the mass of 498 mg and a yield of 62.40%

2.5.3 Synthesis of TP_ADA

The peptide sequence is the same as that the peptides mentioned in Sections 2.6.1.1 and 2.6.2.1, except that all amino acids are D-amino acids (**method 3**). This peptide was designed to investigate the influence of D-amino acids on the structural conformation and catalysis. Due to their conformation preferences, they can be incorporated into peptide sequence to restrict the range of local conformations of the peptide thus nucleating folding and secondary structure formation (**Figure 2-7**).[26,52,53] It was initially hypothesized that an all D-amino acid peptide sequence will restrict or influence favourable conformations and perhaps improve catalytic efficiency.[26,52]

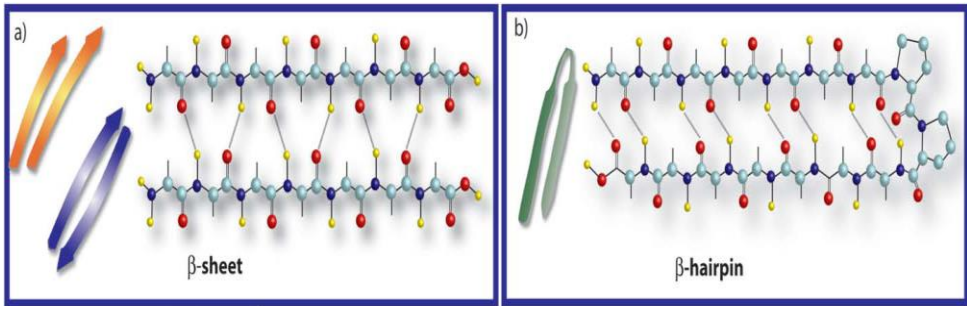


Figure 2- 7: Common peptide secondary structure conformations[54]

The peptide was synthesized automatically following the same strategy mentioned in Section 2.5.1, using double coupling for all AAs in the sequence while monitoring every coupling step using the LC-MS. The full peptide was cleaved off the resin and dissolved in MeCN/H_2O and analyzed using the LC-MS.

2.5.3.1 Purification of TP_ADA

In an attempt to purify TP_ADA, several modifications were introduced to the purification methods above. However, none yielded a good separation of the analyte as there were still some impurities co-eluting with the desired peptide when monitored by LC-MS. Even after the mobile phase system was varied, by replacing acetonitrile with methanol (MeOH) and also changing the prep-HPLC column, the purity was still low. The gradient elution method; 5-50% acetonitrile in 20 minutes at a flow rate of 15 min/ml (**method 3-1**) gave somewhat better separation, and was then applied for the purification. Four peaks with the same mass (conformers) were obtained, it was further observed that most of analyte peaks co-eluted with some impurities thereby compromising the percentage purity of the peptide, as shown in (**Figure 2-8**).

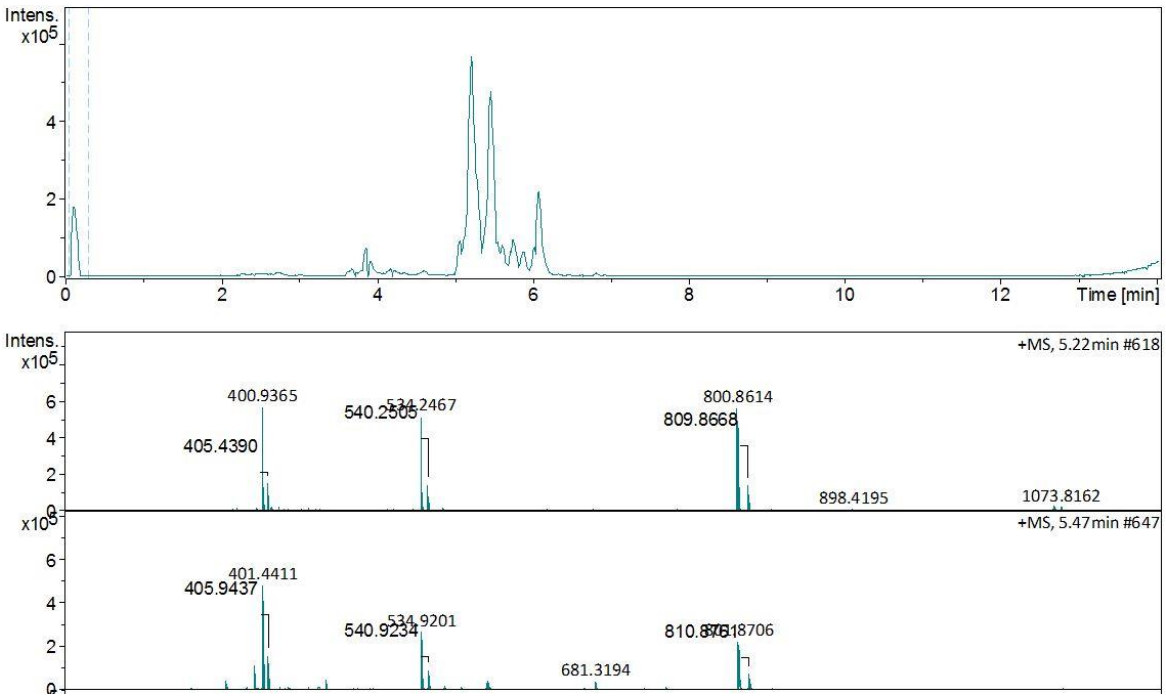


Figure 2- 8 : LC-MS spectrum for 1st purification of peak 1 for TP_ADA peptide

The challenges experienced during the purification were caused by the altered conformation of the peptide D-amino acid peptide.[52,55] Thus, the peptide was subjected to re-purification to eliminate impurities. The same prep-HPLC method (**method 3-1**) was applied for the second purification and 4 analyte peaks were collected again. Upon purification, the peptide was analyzed using LC-MS and individual peaks had retention times of 5.22, 5.21,5.23 and 7.5 minutes for peak 1, 2, 3 and 4 respectively, whilst the average percentage purity was calculated to be 56.3%. However, after the second purification the purity did not significantly improve but the yield decreased. Due to low yields, we did not attempt the 3rd purification. The peptide was lyophilized following the removal of organic solvents using a rotary evaporator, resulting in a mass of 69.7 mg and a yield of 9.2%

2.5.4 Importance of peptides cyclization

The structural stability of an artificial enzyme plays an essential role in determining the catalytic efficiency of artificial enzyme. It is reported that poor conformational stability of peptides may result in poor cooperativity between catalytic centers and substrates.[56] Cyclization is normally applied in order to synthesize more rigid peptide structures, with enhanced conformational stability. Peptide cyclization provides stability by decreasing the entropy and facilitating a favourable local interaction. Peptides can be cyclized in four different ways, depending on the functional group: head-to-tail (C-terminus to N-terminus), head-to-side chain, side chain-to tail, or side chain-to side chain (**Figure 2-9**).[57–61]

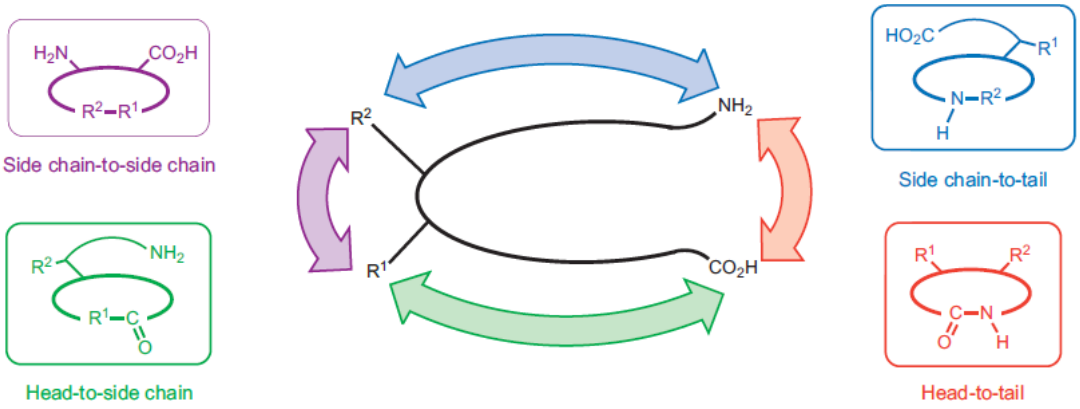


Figure 2- 9: Different ways of peptide cyclization.[59]

There are several cyclization techniques which can be employed to stabilize peptides, namely:[59] *amide condensation* (amide bond formation or lactam bond); *on resin cyclization*; *thiol oxidation* (disulfide bridges) and *solution phase cyclization*. In this study, cyclization through *thiol oxidation* or disulfide bridges will be utilized because the other above-mentioned techniques involve numerous steps, that are time consuming and therefore costly. A disulfide bridge is formed between two thiol groups (SH) from the side chain of cysteine or cysteine analogues.

2.5.5 Cyclization of Aspartic containing peptides

The synthesis of peptides; TP_AspC, TP_ADLysC and TP_ADAC was performed using the same synthetic approach adopted above in **methods 1** to **3** respectively. Upon successful synthesis of the peptides, as confirmed by LC-MS, the resin bound peptides were cyclized using iodine for 3 hours. It was observed that the cyclization was not efficient as there were still some fragments of the uncyclized peptide. After several attempts, it was observed that increasing the cyclization time and reducing the iodine concentration improved cyclization efficiency of the peptide.

2.5.5.1 Purification of cyclized Aspartic containing peptide catalyst

Upon successful cyclization of the peptides, they were cleaved from the resin and dissolved in 60/40 (H_2O/MeCN) and injected onto a C-18 prep-HPLC column for separation. The separation method was modified since the cyclic nature of the peptides altered their interaction with the mobile phase causing a change in the elution time and separation when compared to the linear peptides. The purification of the cyclized peptide was performed using a gradient elution adopted in **method 1-1**. The peptides co-eluted with some impurities, thus a second purification was done eluting with 3-50% MeCN in 15 minutes at a flow rate of 15 min/ml (**method 4-1**). The mass spectra of the collected analyte peaks showed the presence of insignificant impurities, although peptides yields were lower after the second purification. A summary of the spectral data of all the TP_Asp cyclized peptides after successful purification are tabulated in **Table 2-2** below.

The cyclization did not reduce the number of isolated conformations and this could possibly mean that the conformations are formed during the synthesis and not in solution after the cleavage.

Table 2- 2: Detailed summary of the cyclized peptide catalysts containing aspartic acid

Cyclized peptides	Sequence	Calculated Mass	Half mass found $[M+2H]^{2+}$	R_t/min	Av. yield/ %
TP_AspC	CRYKDGASGKDYRC	$C_{66}H_{102}N_{22}O_{23}S_2$ 1618.70	810. 8829	P1=5.22 P2=7.79 P3=7.66 P4=7.80	10.1
TP_ADLysC	CRYKDGASGKDYRC	$C_{66}H_{102}N_{22}O_{23}S_2$ 1618.70	809. 8806	P1=5.25 P2=5.42 P3=5.28 P4=6.69	16.8
TP_ADAC	CRYKDGASGKDYRC	$C_{66}H_{102}N_{22}O_{23}S_2$ 1618.70	809.9170	P1=5.38 P2=7.79 P3=7.66 P4=7.80	6.5

P=Peak

2.5.6 Synthesis of TP_Glu

The aim behind the design of TP_Glu was to investigate the nucleophilic effect of glutamic acid on the catalysis (**Figure 2-10**). Both glutamic and aspartic acid have similar properties (hydrophilic character), except that glutamic acid has a higher molecular weight due to an extra methylene (-CH_2) on its side chain group.[62,63] Studies have shown that even though Glu and Asp perform nucleophilic functions, glutamic acid is more likely to act as a general base/acid than aspartic acid.[62] We therefore envisaged that utilizing the better activating glutamic acid would facilitate an efficient proton abstraction compared to aspartic acid.

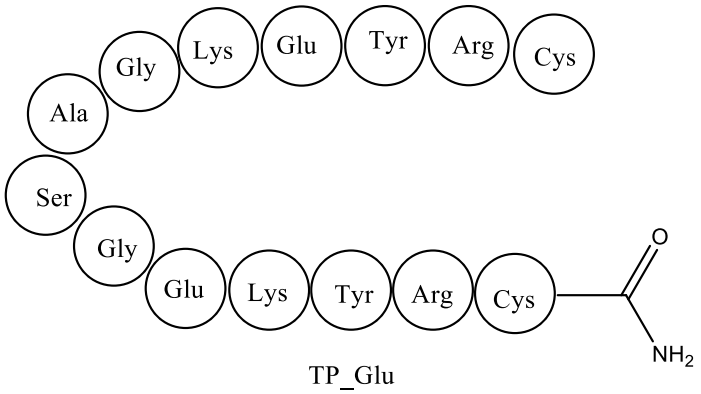


Figure 2- 10: Amino acid sequence for peptide catalyst TP_Glu

TP_Glu peptide was first synthesized using the method outlined in Section 2.5.1. However, whilst monitoring the reaction by LC-MS, it was observed that the 10th amino acid did not completely couple even after it was double coupled. This was attributed to the bulkiness of the glutamic acid side chain protecting group which can cause steric hindrance. Glutamic acid was then coupled for the 3rd time (triple coupling) (**method 4**), before the rest of the amino acid residues were added. The completion of the synthesis was confirmed by LC-MS and the peptide was dissolved in 60/40 (H_2O/MeCN).

2.5.6.1 Purification of TP_Glu

Modifications were made to **method 1-1** and **method 2-2**; and a gradient elution method utilizing 3-60% acetonitrile (**method 5-1**) in 20 minutes at a flow rate of 15 min/ml was selected for the separation of the analyte. Similar to what was observed with TP_Asp, 4 conformers were collected. The analyte peaks were characterized by LC-MS and the peptide co-eluted with impurities, (**Figure 2-11**).

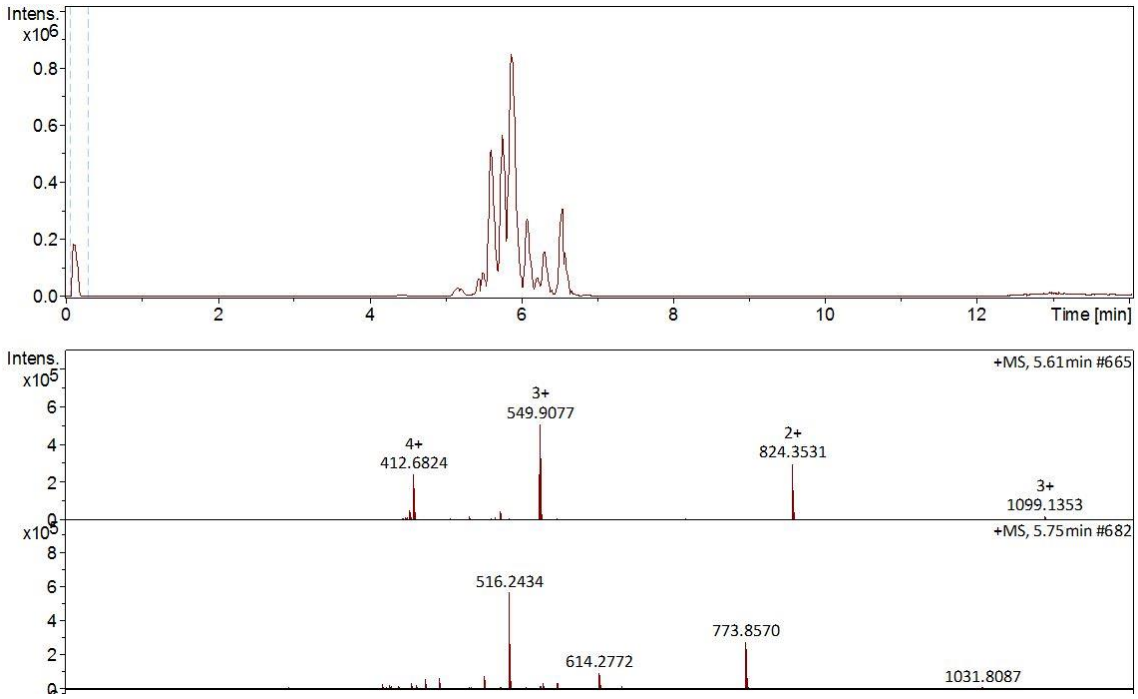


Figure 2- 11: LC-MS spectrum for the 1st purification of TP_Glu peak 1

The collected analyte peaks were combined and re-purified using **method 5-1** and an improvement in the purity was observed (**Figure 2−12**), although there was a decrease in yield. The overall purity was 70.0% while the purity calculated for individual peaks was 87.3, 74.5, 69.2 and 63.4% for peak 1, 2, 3 and 4 respectively. The calculated mass for TP_Glu $C_{68}H_{108}N_{22}O_{23}S_2$ was 1646.74 Daltons and the half mass found was $[M+2H]^{2+}$ 824.2697. The solvents were removed using a rotary evaporator and the peptide (198.4 mg) was resuspended in cold diethyl ether, resulting in a final percentage yield of 32.4%. The retention times of analyzed peaks were within the range of 7-8 minutes, (**Figure 2-12**).

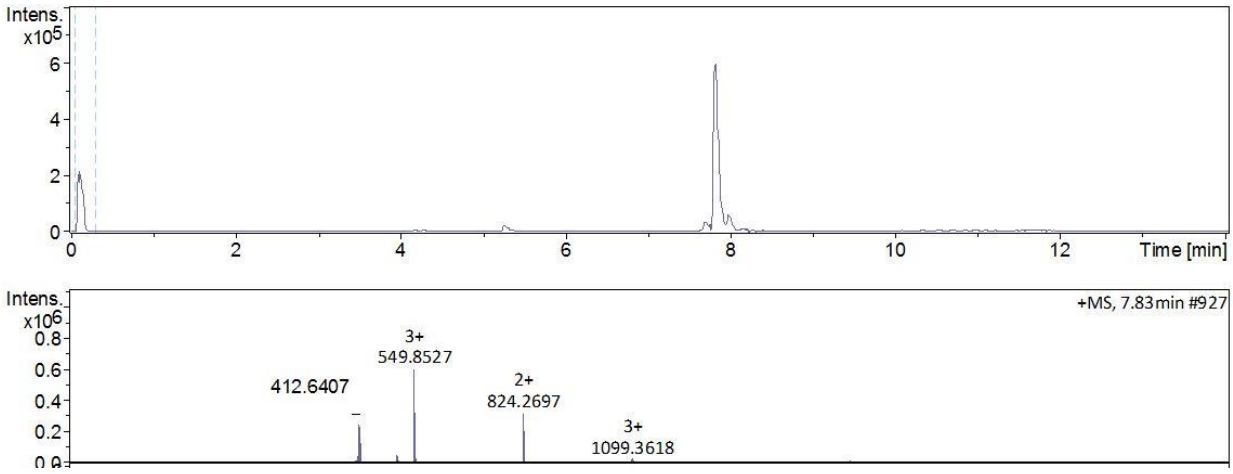


Figure 2- 12: LC-MS spectrum for TP_Glu peak 1 after 2nd purification

2.5.7 Synthesis of TP_GDLys

In the design of TP_GDLys, the same amino acid sequence used in the synthesis of TP_Glu was employed except that L-lysine in the 4th and 10th positions were replaced with D-lysine (**Figure 2-13**). The motivation for the incorporation of D-lysine follows the similar reasoning outlined in Section 2.5.2; hence we therefore envisaged that incorporating D-lysine onto the sequence, will have an enhancement effect on the catalytic efficiency. The full peptide mass was confirmed by LC-MS following peptide cleavage from resin the using the method described in Section 7.3.4

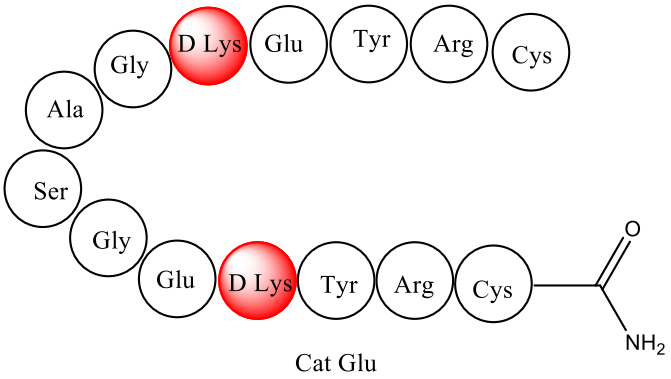


Figure 2- 13: Amino acid sequence for peptide catalyst TP_Glu, with D Lys highlighted in red

2.5.7.1 Purification of TP_GDLys

The purification of TP_GDLys was performed by prep-HPLC following the separation method discussed in Section 2.5.6.1. The solvents were removed after purification using the rotary-evaporator resulting in a mass of 151.3 mg and yield of 25.0%. Upon completion of the first purification, it was noticed that there were quite a few impurities which co-eluted with the analyte of interest, (**Figure 2-14**), hence further purification was required.

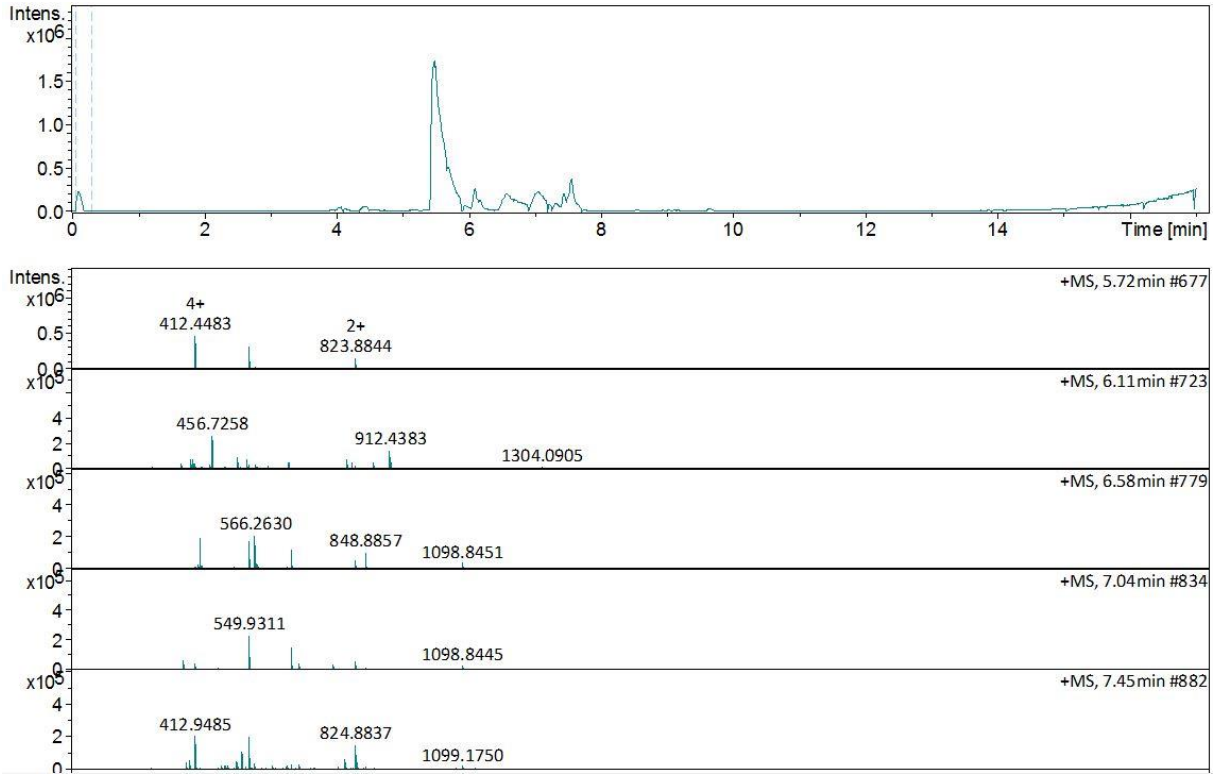


Figure 2- 14: LC-MS spectrum for TP_GDLys peak 2 after 1st purification

The second purification was performed employing **method 4-1** and, upon completion of purification, the solvent was dried off and analyte peaks analyzed by LC-MS as shown in (**Figure 2-15**). The average percentage purity of all collected peaks was found to be 84.83%, while the percentage purity calculated for the individual peaks was 76.8, 86.6, 89.6 and 86. 2% for 1, 2, 3 and 4 respectively. The calculated molecular mass for TP_GDLys $C_{68}H_{108}N_{22}O_{23}S_2$ was 1646.74 Daltons and the half mass found $[M+2H]^{2+}$ was 824.1098. The final percentage yield was 32.4%, which was obtained after the peptide (198.4 mg) was resuspended in cold diethyl ether.

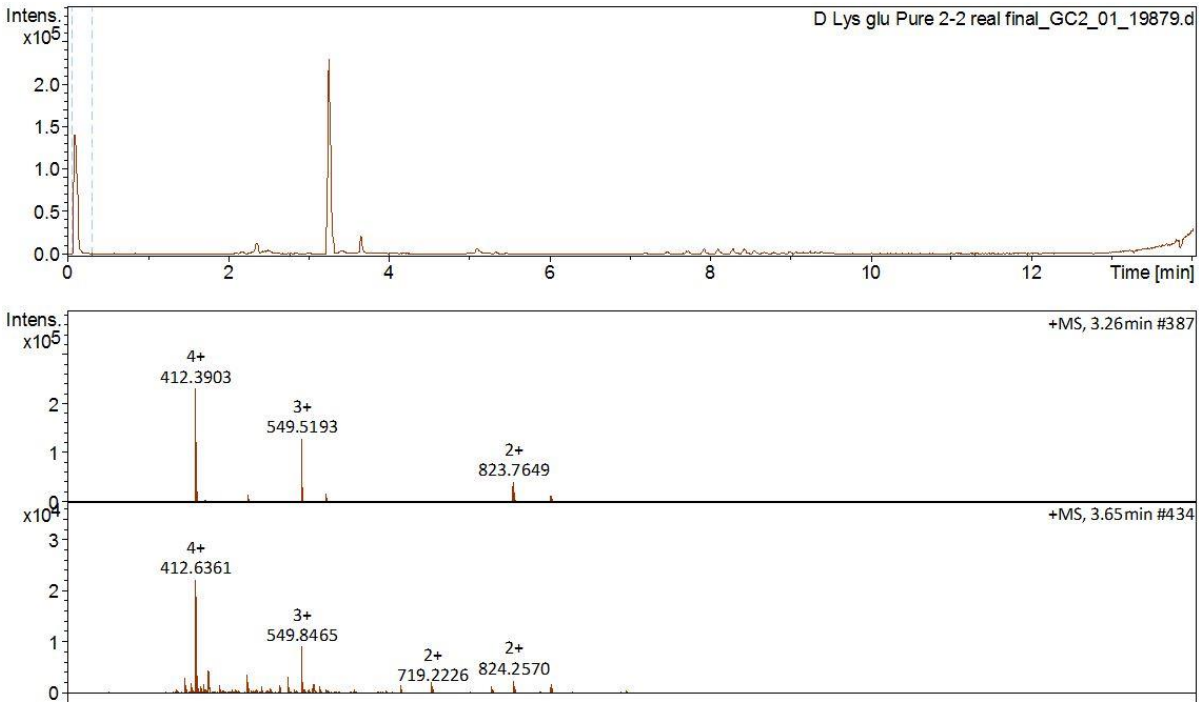


Figure 2- 15: LC-MS spectrum for TP_GDLys peak 2 after 2nd purification

2.5.8 Synthesis and purification of TP_GDA

This peptide was designed using the same amino acid sequence outlined in Section 2.5.6 but with all D-amino acids. The purpose of this design was to investigate the roles of D-amino acids in the enhancement of catalytic efficiency. A similar synthetic strategy (**method 3**) was adopted for the synthesis of the peptide, and upon completion the peptide was cleaved from the resin and purified using the prep-HPLC employing **method 4-1**. The purification was performed twice, and the calculated molecular mass was $C_{68}H_{108}N_{22}O_{23}S_2$ 1648.74 m/z, whilst the half mass found was $[M+2H]^{2+}$ 824.7649 m/z. The overall purity was determined by LC-MS and found to be 69.8%. The retention times of analyzed peaks were within the range 7-8 minutes (**Figure 2-16**).

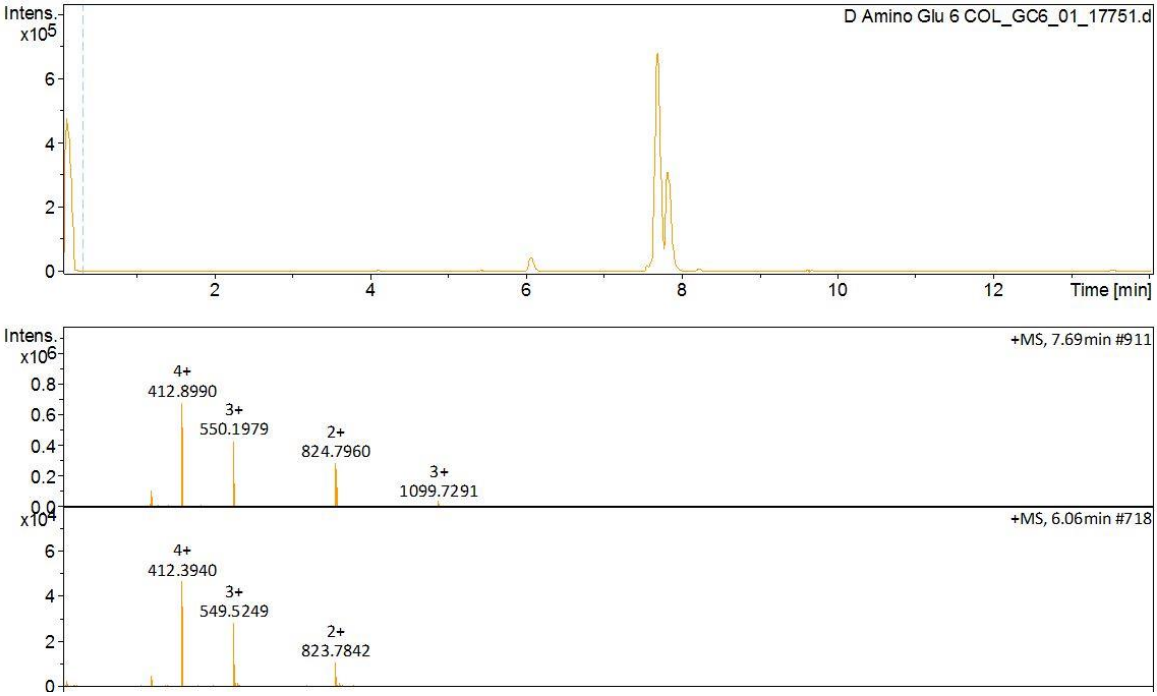


Figure 2- 16: LC-MS spectrum for TP_GDA peak 3 after 2nd purification

2.5.9 Cyclization and purification of Glutamic containing peptides

During the SPPS synthesis of linear peptides, the cysteine thiol groups are protected by groups which can be orthogonally cleaved prior to cyclization. These protecting groups such as Trt (S-triphenylmethyl) and Acm (S-Acetamidomethyl) can easily be removed with molecular iodine.

For the cyclization of TP_ Glu, TP_GDLys and TP_GDA, the peptides were first synthesized on the Rink (MBHA) following the synthetic strategy outlined in Section 2.5.7. The resin bond peptides were cyclized using the iodine cyclization method explained in detail in Section 7.3.5. Some difficulties were encountered due incomplete cyclization as confirmed by LC-MS. This could be attributed to a high degree of secondary structural conformations, causing different folding patterns within the peptide. Previous studies have demonstrated that difficulties are often encountered in cyclizing peptide rich in Arg(s) and Lys(s), due to steric hindrance and bulkiness of these molecules.[56] **Table 2-2**, details the summarized LC-MS data of the cyclized peptides.

Table 2- 3: Detailed summary of the cyclized peptide catalysts containing glutamic acid

Cyclised peptide	Sequence	Calculated Molecular Mass	Half mass found $[M+2H]^{2+}$	R_t/min	Av. Yield %
TP_GluC	CRYKEGASGKEYRC	$C_{68}H_{106}N_{22}O_{23}S_2$ 1646.7300	823.8775	P1=5.42 P2=5.58 P3=5.55 P4=5.61	7.2
TP_GDLysC	CRYKEGASGKEYRC	$C_{68}H_{106}N_{22}O_{23}S_2$ 1646.7300	823.8789	P1=4.62 P2=4.64 P3=4.72 P4=4.76	10.2
TP_GDAC	CRYKEGASGKEYRC	$C_{68}H_{106}N_{22}O_{23}S_2$ 1646.7300	824.7964	P1=5.29 P2 =5.42 P3=5.53 P4=5.72	5.7

P=peak

2.6 Peptides scale up

In an attempt to improve the synthesis and to ensure complete aminoacylations and increased yield of the peptide catalyst, the peptides were synthesized manually. Peptide synthesis using an automated peptide synthesizer has certain advantages such as continuous coupling without stopping, and it also allows for multiple and parallel syntheses. Nonetheless, the synthesis of peptides using an automatic synthesizer has certain disadvantages. These include; mechanical errors which are often associated with skipping amino acids and stopping synthesis in the middle of a reaction, inability to fully dissolve all the reagents (AAs, coupling reagents) and insufficient dispensing of the reaction mixture to the reaction vessel resulting in low coupling efficiency thus compromising the yield of the peptide. The challenges mentioned were encountered during the synthesis of the peptides using the automatic peptide synthesizer, and therefore peptides were further synthesized manually.

2.7 Concluding remarks

In summary we were able to successfully design a suitable synthetic route for the synthesis of peptide catalysts using both automatic and manual SPPS strategy. The peptides synthesized comprised of both the natural and unnatural AAs. Some of the linear peptide chains were also cyclized to restrict the freedom of rotation. Peptide sequences with unnatural amino acids (D-amino acids) and the cyclized peptides were difficult to synthesize and purify due to the secondary structure formation and were obtained in low yields. Peptide folding during chain elongation also created a peptide structure that sterically hinders the coupling of the incoming amino acid.

The formation of conformational isomers was confirmed by LC-MS 4 as peaks having the same molecular weight were obtained during purification. All the peptides synthesized in sufficient yields were screened for aldol reaction catalytic activity. Further studies such as; the catalytic activity, selectivity and structural analysis studies, were done with peptides with good yields (TP_Asp and TP_ADLys). The next two chapters (Chapter 3 and 4) will focus on these peptides.

2. 8 References

(1) Apweiler, R. The Universal Protein Resource (UniProt). *Nucleic Acids Res.* **2008**, *36* (SUPPL. 1), 190–195. https://doi.org/10.1093/nar/gkm895.

(2) Berman, H.; Henrick, K.; Nakamura, H. Announcing the Worldwide Protein Data Bank. *Nat. Struct. Biol.* **2003**, *10* (12), 980. https://doi.org/10.1038/nsb1203-980.

(3) Fleischman, A.; Darsow, M.; Degtyarenko, K.; Fleischmann, W.; Boyce, S.; Axelsen, K. B.; Bairoch, A.; Schomburg, D.; F.Tipton, K.; Apweiler, R. IntEnz, the Integrated Relational Enzyme Database. *Nucleic Acids Res.* **2004**, *32* (90001), 434D – 437. https://doi.org/10.1093/nar/gkh119.

(4) McDonald, A. G.; Boyce, S.; Moss, G. P.; Dixon, H. B. F.; Tipton, K. F. ExplorEnz: A MySQL Database of the IUBMB Enzyme Nomenclature. *BMC Biochem.* **2007**, *8* (4), 1–7. https://doi.org/10.1186/1471-2091-8-14.

(5) Bateman, A. The Pfam Protein Families Database. *Nucleic Acids Res.* **2002**, *30* (1), 276–280. https://doi.org/10.1093/nar/30.1.276.

(6) Porter, C. T.; Bartlett, G. J.; Thornton, J. M. The Catalytic Site Atlas: A Resource of Catalytic Sites and Residues Identified in Enzymes Using Structural Data. *Nucleic Acids Res.* **2004**, *32* (90001), 129D – 133. https://doi.org/10.1093/nar/gkh028.

(7) I. Schomburg; C. Antje; C. Ebeling; Gremse, M.; Heldt, C.; D.Schomburg. BRENDA, the Enzyme Database: Updates and Major New Developments. *Nucleic Acids Res.* **2004**, *32* (90001), 431D – 433. https://doi.org/10.1093/nar/gkh081.

(8) Puvanendrampillai, D.; Mitchell, J. B. O. L/D Protein Ligand Database (PLD): Additional Understanding of the Nature and Specificity of Protein-Ligand Complexes. *Bioinformatics* **2003**, *19* (14), 1856–1857. https://doi.org/10.1093/bioinformatics/btg243.

(9) Kanehisa, M. From Genomics to Chemical Genomics: New Developments in KEGG. *Nucleic Acids Res.* **2006**, *34* (90001), D354–D357. https://doi.org/10.1093/nar/gkj102.

(10) Reitz, M.; Sacher, O.; Tarkhov, A.; Trümbach, D.; Gasteiger, J. Enabling the Exploration of Biochemical Pathways. *Org. Biomol. Chem.* **2004**, *2* (22), 3226–3237. https://doi.org/10.1039/b410949j.

(11) Degtyarenko, K. N.; North, A. C. T.; Findlay, J. B. C. PROMISE: A Database of Bioinorganic Motifs. *Nucleic Acids Res.* **1999**, *27* (1), 233–236. https://doi.org/10.1093/nar/27.1.233.

(12) Motherwell, W. B.; Bingham, M. J.; Six, Y. Recent Progress in the Design and Synthesis of Artificial Enzymes. *Tetrahedron* **2001**, *57* (22), 4663–4686. https://doi.org/10.1016/S0040-4020(01)00288-5.

(13) Maeda, Y.; Makhlynets, O. V; Matsui, H.; Korendovych, I. V. Design of Catalytic Peptides and Proteins Through Rational and Combinatorial Approaches. *Annu. Rev. Biomed. Eng.* **2016**, *18*, 311–328. https://doi.org/10.1146/annurev-bioeng-111215-024421.

(14) List, B.; Shabat, D.; Iii, C. F. B.; Lerner, R. A. Enantioselective Total Synthesis of Some Brevicomins Using Aldolase Antibody 38C2. *Chem. Eur. J.* **1998**, *4* (5), 881–885.

(15) Kofoed, J.; Darbre, T.; Reymond, J. L. Artificial Aldolases from Peptide Dendrimer Combinatorial Libraries. *Org. Biomol. Chem.* **2006**, *4* (17), 3268–3281. https://doi.org/10.1039/b607342e.

(16) Bolt, A. Directed Evolution of Aldolases for Exploitation in Synthetic Organic Chemistry. **2008**, *474*, 318–330. https://doi.org/10.1016/j.abb.2008.01.005.

(17) Walton, A. Z.; Conerly, W. C.; Pompeu, Y.; Sullivan, B.; Stewart, J. D. Biocatalytic Reductions of Baylis À Hillman Adducts. *Acs Catal.* **2011**, *1* (9), 989–993.

(18) Reetz, M. T. Directed Evolution of Selective Enzymes and Hybrid Catalysts. *Tetrahedron* **2002**, *58* (32), 6595–6602.

(19) Griffiths, A. D.; Agresti, J. J.; Kelly, B. T.; Ja, A. Selection of Ribozymes That Catalyse Multiple-Turnover Diels – Alder Cycloadditions by Using in Vitro Compartmentalization. *Proc. Natl. Acad. Sci.* **2005**, *102* (45), 8–13.

(20) Yuan, D. Q.; Dong, S. D.; Breslow, R. Cyclodextrin-Based Class I Aldolase Enzyme Mimics to Catalyze Crossed Aldol Condensations. *Tetrahedron Lett.* **1998**, *39* (42), 7673–7676. https://doi.org/10.1016/S0040-4039(98)01717-1.

(21) Bayat, S.; Tejo, B. A.; Abdulmalek, E.; Salleh, A. B.; Normi, Y. M.; Abdul Rahman, M. B. Rational Design of Mimetic Peptides Based on Aldo-Ketoreductase Enzyme as Asymmetric Organocatalysts in Aldol Reactions. *RSC Adv.* **2014**, *4* (73), 38859–38868.

https://doi.org/10.1039/c4ra04866k.

(22) Akagawa, K.; Kudo, K. Development of Selective Peptide Catalysts with Secondary Structural Frameworks. *Acc. Chem. Res.* **2017**, *50* (10), 2429–2439. https://doi.org/10.1021/acs.accounts.7b00211.

(23) Wennemers, H. Asymmetric Catalysis with Peptides. *Chem. Commun.* **2011**, *47* (44), 12036–12041. https://doi.org/10.1039/c1cc15237h.

(24) Akagawa, K.; Kudo, K. Development of Selective Peptide Catalysts with Secondary Structural Frameworks. *Acc. Chem. Res.* **2017**, *50* (10), 2429–2439. https://doi.org/10.1021/acs.accounts.7b00211.

(25) Metrano, A. J.; Abascal, N. C.; Mercado, B. Q.; Paulson, E. K.; Hurtley, A. E.; Miller, S. J. Diversity of Secondary Structure in Catalytic Peptides with β - Turn- Biased Sequences. *J. Am. Chem. Soc.* **2017**, *139* (1), 492–516. https://doi.org/10.1021/jacs.6b11348.

(26) Mahalakshmi, R.; Balaram, P. The Use of D-Amino Acids in Peptide Design. In *D-Amino Acids: A New Frontier in Amino Acid and Protein Research− Practical Methods and Protocols*; 2006 Nova Science Publishers, Inc, 2007; pp 415–430.

(27) Pollegioni, L.; S. Servi. *Unnatural Amino Acids: Methods and Protocol*; Human Press :New York, NY, USA, 2013.

(28) Sygusch, J.; Beaudry, D.; Allaire, M. Molecular Architecture of Rabbit Skeletal Muscle Aldolase at 2.7-A Resolution. *Proc. Natl. Acad. Sci. U. S. A.* **1987**, *84* (22), 7846–7850. https://doi.org/10.1073/pnas.84.22.7846.

(29) Maurady, A.; Zdanov, A.; De Moissac, D.; Beaudry, D.; Sygusch, J. A Conserved Glutamate Residue Exhibits Multifunctional Catalytic Roles in D-Fructose-1,6-Bisphosphate Aldolases. *J. Biol. Chem.* **2002**, *277* (11), 9474–9483. https://doi.org/10.1074/jbc.M107600200.

(30) Tittmann, K. Sweet Siblings with Different Faces: The Mechanisms of FBP and F6P Aldolase, Transaldolase, Transketolase and Phosphoketolase Revisited in Light of Recent Structural Data. *Bioorg. Chem.* **2014**, *57*, 263–280. https://doi.org/10.1016/j.bioorg.2014.09.001.

(31) Holliday, G. L.; Mitchell, J. B. O.; Thornton, J. M. Understanding the Functional Roles

of Amino Acid Residues in Enzyme Catalysis. *J. Mol. Biol.* **2009**, *390* (3), 560–577. https://doi.org/10.1016/j.jmb.2009.05.015.

(32) Gijsen, H. J. M.; Qiao, L.; Fitz, W.; Wong, C. Recent Advances in the Chemoenzymatic Synthesis of Carbohydrates and Carbohydrate Mimetics. *Chem. Rev.* **1996**, *96* (1), 443–473.

(33) Harris, T. K.; Turner, G. J. Structural Basis of Perturbed PKa Values of Catalytic Groups in Enzyme Active Sites. *IUBMB Life* **2002**, *53* (2), 85–98. https://doi.org/10.1080/10399710290038972.

(34) Garner, J.; Harding, M. M. Design and Synthesis of α-Helical Peptides and Mimetics. *Org. Biomol. Chem.* **2007**, *5* (22), 3577–3585. https://doi.org/10.1039/b710425a.

(35) Bartlett, G. J.; Porter, C. T.; Borkakoti, N.; Thornton, J. M. Analysis of Catalytic Residues in Enzyme Active Sites. *J. Mol. Biol.* **2002**, *324* (1), 105–121. https://doi.org/10.1016/S0022-2836(02)01036-7.

(36) Pollegioni, L.; Rosini, E.; Molla, G. Advances in Enzymatic Synthesis of D-Amino Acids. *Int. J. Mol. Sci.* **2020**, *21* (9). https://doi.org/10.3390/ijms21093206.

(37) Melchionna, M.; E. Styan, K.; Marchesan, S. The Unexpected Advantages of Using D-Amino Acids for Peptide Self- Assembly into Nanostructured Hydrogels for Medicine. *Curr. Top. Med. Chem.* **2016**, *16* (18), 2009–2018. https://doi.org/10.2174/1568026616999160212120302.

(38) Beck-Sickinger, A. G.; Gaida, W.; Schnorrenderg, G.; Lang, R.; Jung, G. Neuropeptide Y: Identification of the Binding Site. *Int. J. Pept. Protein Res.* **1990**, *36* (6), 522–530. https://doi.org/10.1111/j.1399-3011.1990.tb00991.x.

(39) Tickler, A. K.; Wade, J. D. Overview of Solid Phase Synthesis of "Difficult Peptide" Sequences. *Curr. Protoc. Protein Sci.* **2007**, *50* (1), 18.8.1-18.8.6. https://doi.org/10.1002/0471140864.ps1808s50.

(40) Bacsa, B.; Horváti, K.; Bõsze, S.; Andreae, F.; Kappe, C. O. Solid-Phase Synthesis of Difficult Peptide Sequences at Elevated Temperatures: A Critical Comparison of Microwave and Conventional Heating Technologies. *J. Org. Chem.* **2008**, *73* (19), 7532–7542. https://doi.org/10.1021/jo8013897.

(41) Valeur, E.; Bradley, M. Amide Bond Formation : Beyond the Myth of Coupling

Reagents. *Chem. Soc. Rev.* **2009**, *38* (2), 606–631. https://doi.org/10.1039/b701677h.

(42) Albericio, F.; Bofill, J. M.; El-Faham, A.; Kates, S. A. Use of Onium Salt-Based Coupling Reagents in Peptide Synthesis. *J. Org. Chem.* **1998**, *63* (26), 9678–9683. https://doi.org/10.1021/jo980807y.

(43) Chakraborty, P.; Zuckermann, R. N.; Foundry, T. M.; Berkeley, L. Coarse-Grained, Foldable, Physical Model of the Polypeptide Chain. *Proc. Indian Acad. Sci. Chem. Sci.* **110AD**, *2013* (33), 10–15. https://doi.org/10.1073/pnas.1305741110/-/DCSupplemental.www.pnas.org/cgi/doi/10.1073/pnas.1305741110.

(44) Marcelino, A.M.C. and Gierasch, L. . Roles of β-Turns in Protein Folding: From Peptide Models to Protein Engineering. *Biopolym. Orig. Res. Biomol.* **2012**, *89* (5), 308–391. https://doi.org/10.1002/bip.20960.Roles.

(45) Hou, W.; Liu, X. Z. C. Progress in Chemical Synthesis of Peptides and Proteins. *Trans. Tianjin Univ.* **2017**, *23* (5), 401–419. https://doi.org/10.1007/s12209-017-0068-8.

(46) Kolesanova, E. F.; Sanzhakov, M. A.; Kharybin, O. N. Development of the Schedule for Multiple Parallel "Difficult" Peptide Synthesis on Pins. *Int. J. Pept.* **2013**, *2013*. https://doi.org/10.1155/2013/197317.

(47) Montalbetti, C. A. G. N.; Falque, V. Amide Bond Formation and Peptide Coupling. *Tetrahedron* **2005**, *61* (46), 10827–10852. https://doi.org/10.1016/j.tet.2005.08.031.

(48) Ludwick, A. G.; Jelinski, L. W.; Dumais, J. J.; Live, D.; Kintanar, A. Association of Peptide Chains during Merrifield Solid-Phase Peptide Synthesis. A Deuterium NMR Study. *J. Am. Chem. Soc.* **1986**, *108* (21), 6493–6496. https://doi.org/10.1021/ja00281a007.

(49) Masuda, K.; Ooyama, H.; Shikano, K.; Kondo, K.; Furumitsu, M.; Iwakoshi-Ukena, E.; Ukena, K. Microwave-Assisted Solid-Phase Peptide Synthesis of Neurosecretory Protein GL Composed of 80 Amino Acid Residues. *J. Pept. Sci.* **2015**, *21* (6), 454–460. https://doi.org/10.1002/psc.2756.

(50) Yan, Y.; Zhang, D.; Huang, S. Y. Efficient Conformational Ensemble Generation of Protein-Bound Peptides. *J. Cheminform.* **2017**, *9* (1), 1–13. https://doi.org/10.1186/s13321-017-0246-7.

(51) Dyson, H. J.; Wright, P. E. Peptide Conformation and Protein Folding. *Curr. Opin.*

Struct. Biol. **1993**, *3* (1), 60–65. https://doi.org/10.1016/0959-440X(93)90203-W.

(52) Yu, Y.; Hu, C.; Xia, L.; Wang, J. Artificial Metalloenzyme Design with Unnatural Amino Acids and Non-Native Cofactors. *ACS Catal.* **2018**, *8* (3), 1851–1863. https://doi.org/10.1021/acscatal.7b03754.

(53) Wong, C. H.; Wang, K. T. New Developments in Enzymatic Peptide Synthesis. *Experientia* **1991**, *47* (11–12), 1123–1129. https://doi.org/10.1007/BF01918376.

(54) Dasgupta, A.; Mondal, J. H.; Das, D. Peptide Hydrogels. *RSC Adv.* **2013**, *3* (24), 9117–9149. https://doi.org/10.1039/c3ra40234g.

(55) Aravinda, S.; Shamala, N.; Roy, R. S.; Balaram, P. Non-Protein Amino Acids in Peptide Design. *Proc. Indian Acad. Sci. Chem. Sci.* **2003**, *115* (5-6 SPEC. ISS.), 373–400. https://doi.org/10.1007/bf02708230.

(56) Wong, Y. M.; Masunaga, H.; Chuah, J. A.; Sudesh, K.; Numata, K. Enzyme-Mimic Peptide Assembly to Achieve Amidolytic Activity. *Biomacromolecules* **2016**, *17* (10), 3375–3385. https://doi.org/10.1021/acs.biomac.6b01169.

(57) Atassi, M. Z.; Manshouri, T. Design of Peptide Enzymes (Pepzymes): Surface-Simulation Synthetic Peptides That Mimic the Chymotrypsin and Trypsin Active Sites Exhibit the Activity and Specificity of the Respective Enzyme. *Proc. Natl. Acad. Sci. U. S. A.* **1993**, *90* (17), 8282–8286. https://doi.org/10.1073/pnas.90.17.8282.

(58) Zheng, L.; Marcozzi, A.; Gerasimov, J. Y.; Herrmann, A. Conformationally Constrained Cyclic Peptides: Powerful Scaffolds for Asymmetric Catalysis. *Angew. Chemie - Int. Ed.* **2014**, *53* (29), 7599–7603. https://doi.org/10.1002/anie.201403829.

(59) White, C. J.; Yudin, A. K. Contemporary Strategies for Peptide Macrocyclization. *Nat. Chem.* **2011**, *3* (7), 509–524. https://doi.org/10.1038/nchem.1062.

(60) Wang, X. Y.; Wang, Q.; Huang, X. Y.; Wang, T.; Yu, X. Q. Synthesis of Small Cyclic Peptides Containing the Disulfide Bond. *Arkivoc* **2006**, *2006* (11), 148–154. https://doi.org/10.3998/ark.5550190.0007.b14.

(61) Hill, T. A.; Shepherd, N. E.; Diness, F.; Fairlie, D. P. Constraining Cyclic Peptides to Mimic Protein Structure Motifs. *Angew. Chemie - Int. Ed.* **2014**, *53* (48), 13020–13041. https://doi.org/10.1002/anie.201401058.

(62) Lee, D. Y.; Kim, K. A.; Yu, Y. G.; Kim, K. S. Substitution of Aspartic Acid with Glutamic Acid Increases the Unfolding Transition Temperature of a Protein. *Biochem. Biophys. Res. Commun.* **2004**, *320* (3), 900–906. https://doi.org/10.1016/j.bbrc.2004.06.031.

(63) Bayat, S.; Tejo, B. A.; Salleh, A. B.; Abdulmalek, E.; Normi, Y. M.; Abdul Rahman, M. B. Asymmetric Michael Reaction Catalyzed by Mimicked Peptides. *Catal. Letters* **2014**, *144* (2), 222–228. https://doi.org/10.1007/s10562-013-1156-6.

Chapter 3

Structural Elucidation of peptides

3.1 Introduction

The development of an organocatalyst requires an understanding of the 3-dimensional structure and mechanism of the catalyst. The three-dimensional structure of peptides is usually characterized using several experimental techniques such nuclear magnetic resolution (NMR), X-ray crystallography, Fourier transform infrared (FT-IR) spectroscopy and circular dichroism (CD). Even though techniques like X-ray crystallography provide absolute elucidation of peptides and proteins, they can be laborious. This is because they require high-quality single crystals for analysis, which are not easy to attain for peptides.[1] In addition, x-ray studies usually do not address the issue of conformational flexibility and dynamic inter-conversion of peptide and protein structures.[2]

In this section we describe, the structural analysis of the peptides using NMR and circular Dichroism (CD) in order to determine the conformations of the synthesized peptides. As already mentioned in Chapter 2, TP_Asp and TP_ADLys will be selected for the structural elucidation in this chapter.

3.1.1 NMR Studies

The peptide secondary structure is stabilized by inter- and intra-molecular hydrogen bonds which lead to structural motifs such as, α-helices, β-sheets and β-turns.[2] Solution NMR spectroscopy of peptides has been proven to be a powerful tool in providing information regarding a peptide's structural conformation. The amide proton signal region is essential for the understanding of the peptide organization.[3,4] Due to the large number of hydrogen atoms in peptides, one dimensional ^{1}H NMR is mutually crowded with overlapping lines. Therefore, two dimensional (2D) and three-dimensional (3D) NMR experiments are used.[5] With the use of chemical shifts alone, one can provide a generalised 3D structural picture of the peptide. The conformation studies of peptide NMR depends mostly on the nuclear Overhauser effects (NOE) and coupling constant.[3,5] The NOE experiments show cross peaks interactions involved by measuring interproton interaction within a distance of 5 Å or less, whereas coupling

constants provides information about torsion angles.[4,5] NOE is expressed by a relationship between $\omega\tau_c$, where ω is the spectrometer frequency and τ_c is rotational correlation time of the molecule. When the molecular weight of the molecule increases; the rotational correlation (τ_c) also increases and this further result in a decrease in NOE enhancement. This is generally a concern for peptide molecules with a molecular mass around 1000 to 1200 Da which falls within the region $\omega\tau_c \approx 1.2$. There is little or no NOE enhancement around that region, and ROESY(rotational-frame Overhauser effect spectroscopy) is often used to overcome this challenge.[5–8] Correlation spectroscopy (COSY) and total correlation spectroscopy (TOCSY) are also important NMR experiments. Their mechanism involves scalar couplings whose magnitudes depend on the number of the intervening protons (generally 3 or smaller) in the dihedral angle about the central bond.[5,9,10]

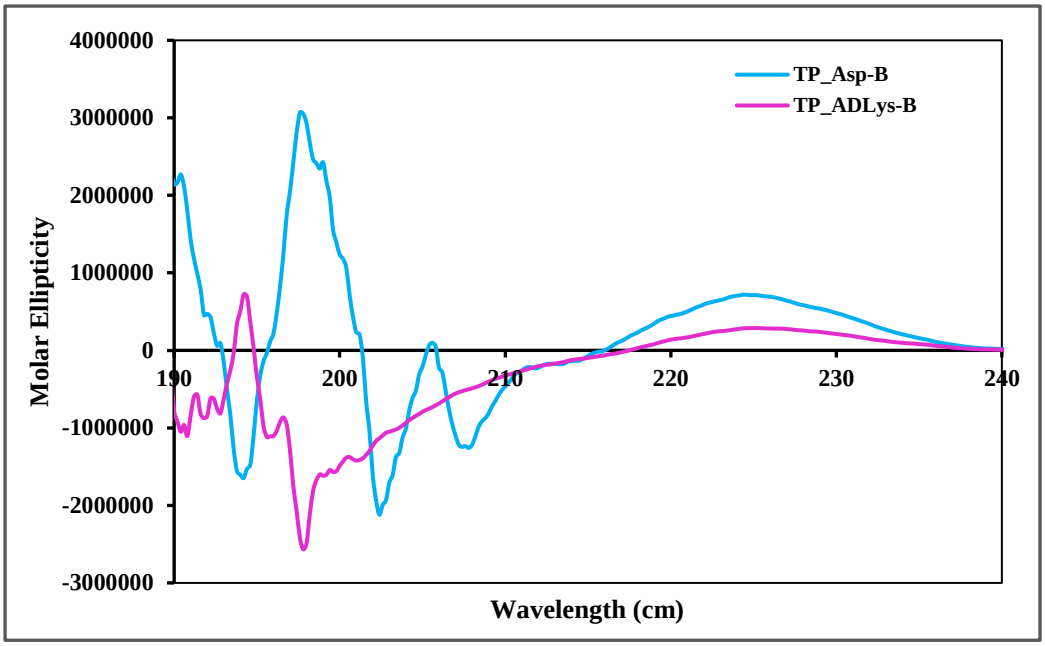
3.1.2 Circular Dichroism studies

Circular dichroism (CD) is another important technique used to determine the conformation of peptides in solution. CD spectroscopy is normally employed in the analysis of optically active chiral molecules and is based on the excitation of electronic transmissions of proteins, nucleic acids and peptides chiral groups. In this technique, a sample is irradiated with circularly polarized light and the difference in absorbance of the right- and left-handed circularly polarized components is measured.[11–13] The difference in secondary structural components of peptides and proteins, such as; the alpha helix, beta sheets, and beta turn are analyzed in the far band UV region of 260-190 nm. Around this band, CD measures the ellipticity of peptide with polarized light.[11,14,15] Optically active compounds, chiral entities and amide bonds in a polypeptide backbone, absorb at different extents depending on the two dihedral angles ϕ and ψ.[11,16] The amides of the polypeptide backbone have different absorptions depending on the hydrogen bonding or non-hydrogen bonded state of the amides.[17] CD experiments are generally performed in solution of high dilution of approximately (<1 mM) to avoid peptide aggregation.

3.2. Results and discussion

3.2.1 Conformational studies of peptides using circular dichroism

The method used for CD experiments is explained in detail in section 7.2 The CD results for both TP_Asp and TP_ADLys peptides in buffered solution are represented in **Figure 3-1** below. The pH and the net charge of the peptide affect the electrostatic interactions and therefore influence the degree of ionization and function of the peptide.[18,19] Furthermore, buffered solutions are normally employed because they are known to have a strong influence on the peptide stability and structure.[18–22] Water was also chosen as a solvent because the peptide is assumed to adopt an extended conformation due to extensive solvation.[23,24] On this basis, the CD experiments were performed in both a 200 mM phosphate buffer and water in order to compare the difference in structural conformation of the peptides. It is reported in literature that a peptide β-sheet structure, usually shows a minimum absorption around 215 nm and a relatively strong maximum absorption at 195 nm. α-Helical structures exhibit two pronounced minima bands at 208 and 222 nm and a maximum at 198 nm, whereas the random coil has a minimum at 198 and a small positive band at 217 nm.[13,25] As seen in the **Figure 3-1** below, the CD spectrum for **TP_ADLys** shows an absorption minima around 202 and 194 nm, and a maximum band at 198 nm, which suggest random coil that deviates to a β-sheet conformation.



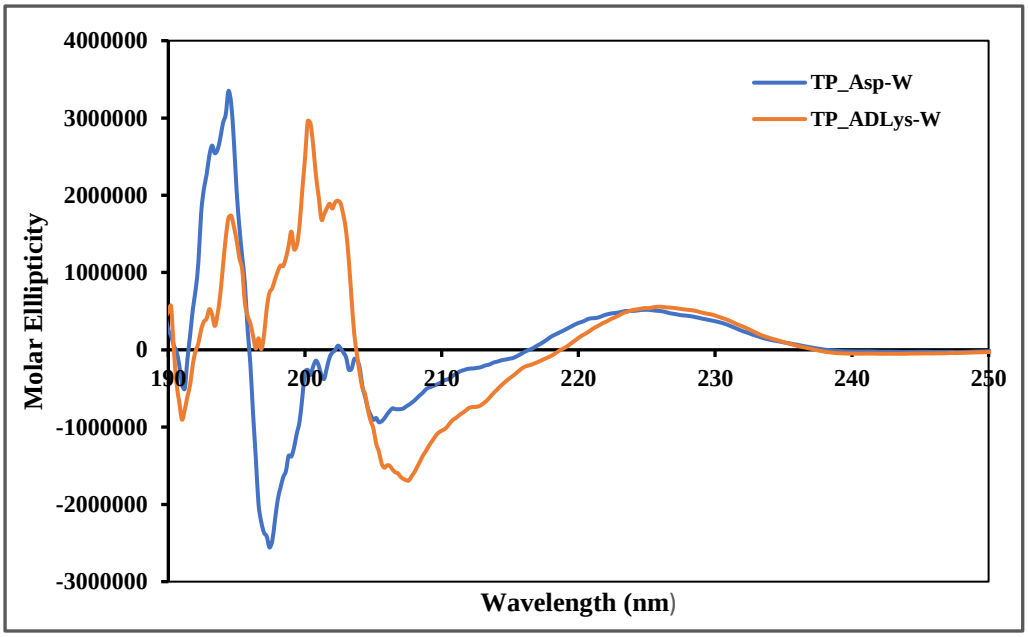
Secondary structure	TP_ADLys-B (%)	TP_Asp-B (%)
Helix	7.7	23.3
Beta	36.2	8.9
Turn	12.4	12.4
Random	41.7	39.4

Figure 3- 1: Circular dichroism studies for **TP_ADLys** and **TP_Asp** peptides in 200 mM phosphate buffer solution (**B**) and percentage of peptide structure

The CD data was further analyzed using the online program to estimate peptide secondary structure formation, available at http://perry.freeshell.org/raussens.html. The results revealed that the most dominant percentage of the peptide structure for **TP_ADLys** was 41.7% random, followed by 36.1 % beta sheet conformation and 12.7 and 7.7% turn and helix conformation respectively. Random coil formation corresponds to π-π* and n-π transitions bands and is referred to as the lack of ordered secondary structure.[15,26]

A similar trend was observed for the **TP_Asp** spectrum, which resembles a random coil with the negative absorption maxima at 198 nm. In addition, the secondary structure estimate shows that the highest percentages of the structure were 39.4% random, 23.9% helix and with almost equal amount of turn and beta structures.

The CD experiments were repeated in unbuffered water to investigate the difference in structural conformation of the peptides (**Figure 3-2)**.



Secondary structure	TP_ADLys-W (%)	TP_Asp-W (%)
Helix	25.1	63.32
Beta	14.6	12.09
Turn	12.5	8.71
Random	37.8	15.88

Figure 3- 2: Circular dichroism spectra of **TP_ADLys** and **TP_Asp** peptides in water (**W**) and their secondary structure analysis

The obtained results in water for **TP_ADLys**, depict a random coil structures going to a helix conformation. Furthermore, the obtained data exhibits relatively strong absorption maxima around 194 and 204 nm suggesting β-sheets and α-helix conformation respectively with a minimum peak at 208 nm. The CD spectroscopy results for **TP_Asp** in water display a minimum absorption with two negative peaks around 204 and 197 nm, which is a characteristic of an α-helix structure. Analysis indicates that the majority of the structural elements were α-helix (63.32%), with nearly equal percentages of random (15.88%) and beta structures (12.09%).

Solvation of the peptide backbone is proposed to be an important factor in determining the thermodynamic helical propensities and the thermodynamic stability of the solvent-chain contact.[27] Reported modelling and computation studies have demonstrated that CD experiments of polypeptide in that water allow favourable folding conditions that enable interior chain interactions thus maximizing chain packing.[23,24,27,28] Furthermore, it is also

suggested that helices are preferred in water, since hydrogen bonding promotes favourable chain-solvent interactions.[24,28] Notably, when the CD measurements are performed in water α-helical structures seem to dominate for both **TP_Asp** and **TP_ADLys** peptides. These results further demonstrate that the ability of the peptides to assume secondary structure with mixtures of conformations is influenced by the solvent. From this study, it can be concluded that the CD measurements reveals that TP_Asp possesses an alpha-helix conformation followed by random coil; whereas with TP_ADLys, adopts a beta sheet that deviates to a random coil pattern. This is an indication that indeed replacing l-lysine with unnatural d-lysine, altered the peptide conformation.

As already shown earlier in Chapter 2, during purification the peptides were isolated as conformational isomers. The obtained CD results prove the existence of possible different conformations of the TP_Asp and TP_ADLys peptides in solution.

3.2.2 Characterization of peptides by NMR

To determine the optimal conditions for the NMR experiments for better resolution and dispersion of peaks; the experiments were recorded at different temperatures and mixing times for TOCSY, NOESY and ROESY. The detailed conditions used for the aforementioned experiments are specified in Section 7.1. The varied mixing times recorded for the NOESY were 150, 200 and 250 ms; and 100, 150, 200, 250 and 300 ms for the ROESY experiments. The mixing time duration usually determines the visibility and spectral quality. At short mixing times, the magnetisation and spin diffusion have less time to travel down the side. This result in more intense α-protons peaks than the β-protons along the amide shift, which will further be more pronounced than the γ-proton. Longer mixing time are thus necessary in order to be able to obtain a better dispersion of protons at high shifts such as δ and γ protons. Furthermore it is reported that peak areas increase with increase in mixing time.[7,29,30]

There was poor or no dispersion of chemical shifts in the NOESY spectrum in both varied conditions (temperature and mixing time). Both peptides studied have a molecular mass of 1600 g/mol, which falls in the region $\omega\tau_c \approx 1.2$. As indicated in Section 3.1.1, there is little or no NOE enhancement for molecules around this region. Consequently, NOESY experiments were not successful. The NOE assignments will therefore be based on the ROESY spectra recorded with 200 ms at 300K.

3.2.2.1 NMR temperature variations experiments

The amide protons are known to readily exchange with the deuterium of the solvent to form intermolecular hydrogen bonds with solvent molecules. In such instances the energy of the hydrogen bond involved is low; and therefore, small thermal energy provided through sample heating is sufficient enough to the break them. On the hand, the intramolecular hydrogen bonds formed by shielded protons are relatively higher and thus higher temperature is required to break them.[8,31–33] This is the principle behind temperature variance in NMR studies. The amide protons involved in an intermolecular bonding of the shielded has a temperature coefficient value of (<3 ppb/K), whereas intramolecular hydrogen bond has a value of >5 ppb/K. Temperature variations experiments in NMR usually provide insight into the phenomena of underlying chemical shifts dispersion. Moreover, variations in temperature influence the resolution of peaks that are considerably overlapping, that is, they may provide better resolution upon variance; and may also facilitate the conformation equilibrium of peptides which relies on the energy involved.[8,31]

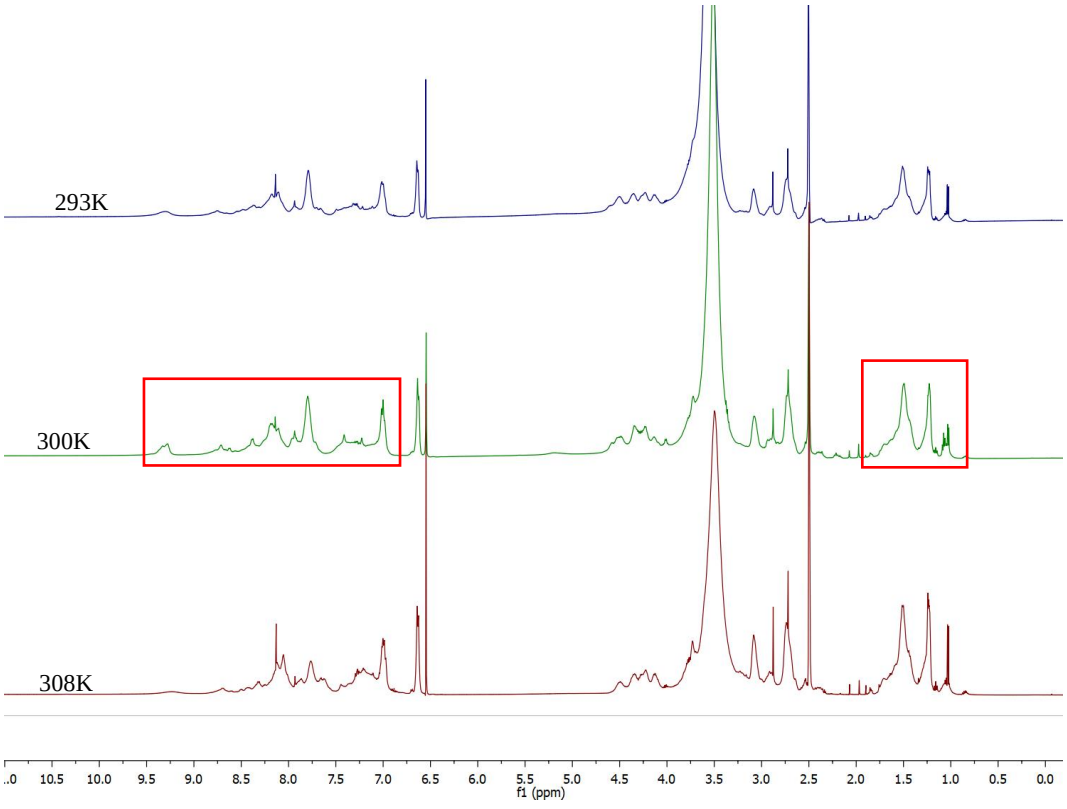


Figure 3- 3**:** 1D ^{1}H NMR spectra of TP_ADLys peptide effect of temperature variations

To investigate the influence of temperature variations on the spectral quality (line width) and cross peaks resolution; the experiments were performed at 293K to 308K **(Figure 3-3)**. The

broadening of the resonance peaks at low temperature (293K) could not be effectively induced as some peaks were not observed or properly resolved around the amide region. This is indicative of the exchange between the two species, forming intermolecular hydrogen bonds with the solvent. The amide protons became more pronounce as the temperature was increased to 300K. The temperature could not be further adjusted beyond 308K, since the spectral dispersion of peaks become less pronounced beyond this temperature, especially for the TOCSY and ROESY spectrum (spectra shown in **Appendix II**, **Figure S.3-20 and S.3-22**). It is reported that at higher temperature there may be disruption in structure or loss of secondary structure of peptides due thermal instability of 3D structure. In addition, when the experiments were performed at 308K, there was poor resolution of aliphatic protons as shown in figure. This study indicates the magnetic environment changes with variation in temperatures, thus influencing the spectral dispersion. At 300K, the structure of many multiplets in the spectrum appear to be relatively resolved and was thus this temperature was chosen for all the analysis of peptide structures in this study.

3.2.2.2 NMR structure elucidation of the TP_Asp peptide

As already stated in Chapter 2, both peptides (TP_Asp and TP_ADLys) consist of 14 amino acids, except that L-lysine was replaced with D-lysine in peptide TP_ADLys. The TP_Asp peptide (using a three-letter code) follows the sequence; Cys-Arg-Tyr- Lys-Asp-Gly-Ser-Ala-Gly-Lys-Asp-Tyr-Arg-Cys; and **Figure 3-4** below depicts the structure.

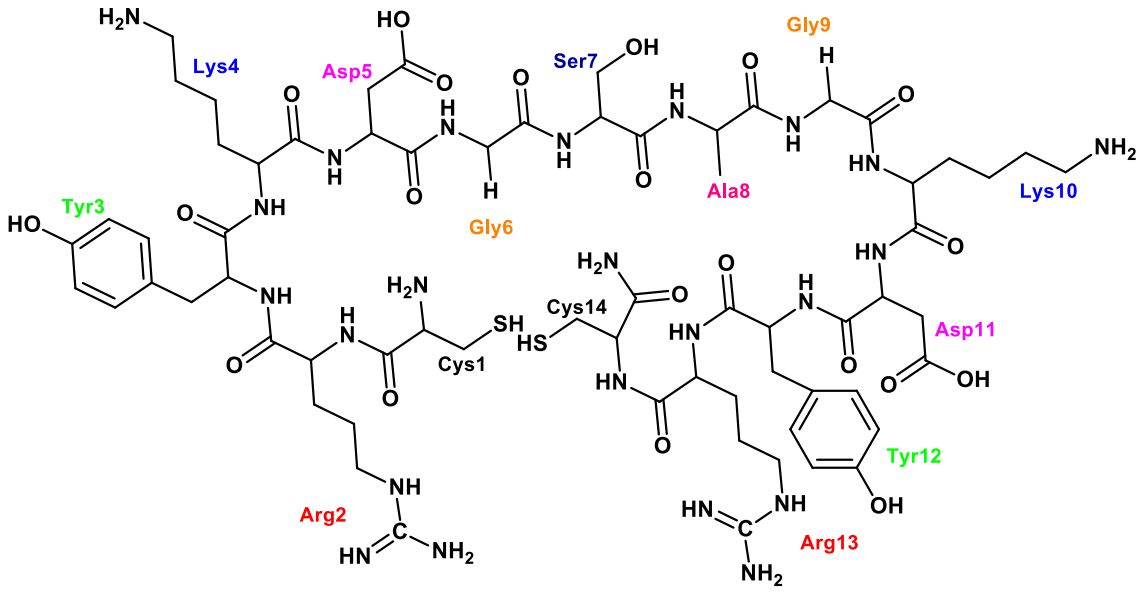


Figure 3- 4: Structural representation of TP_Asp.

3.2.2.3 Spin system assignment of amino acid residues for TP_Asp

The individual spin systems were assigned based on the COSY and TOCSY spectra. This technique was developed by Wüthrich *et al.*[4] and relies on the differences in the amino acid side chains (fingerprint region) that results in different spectra patterns. Each specific residue possesses a unique pattern connecting an amide to its backbone C^{α} proton and the remaining sidechain protons. Identification of each side chains spin system helps in identifying the specific amino acid residue present.[34,35] The TOCSY spectrum of TP_Asp showing the fingerprint region of amide protons-f2 (7.5-8.67 ppm) and alpha-aliphatic region-f1 (1.0-4.60 ppm) is shown in **Figure 3-5**..

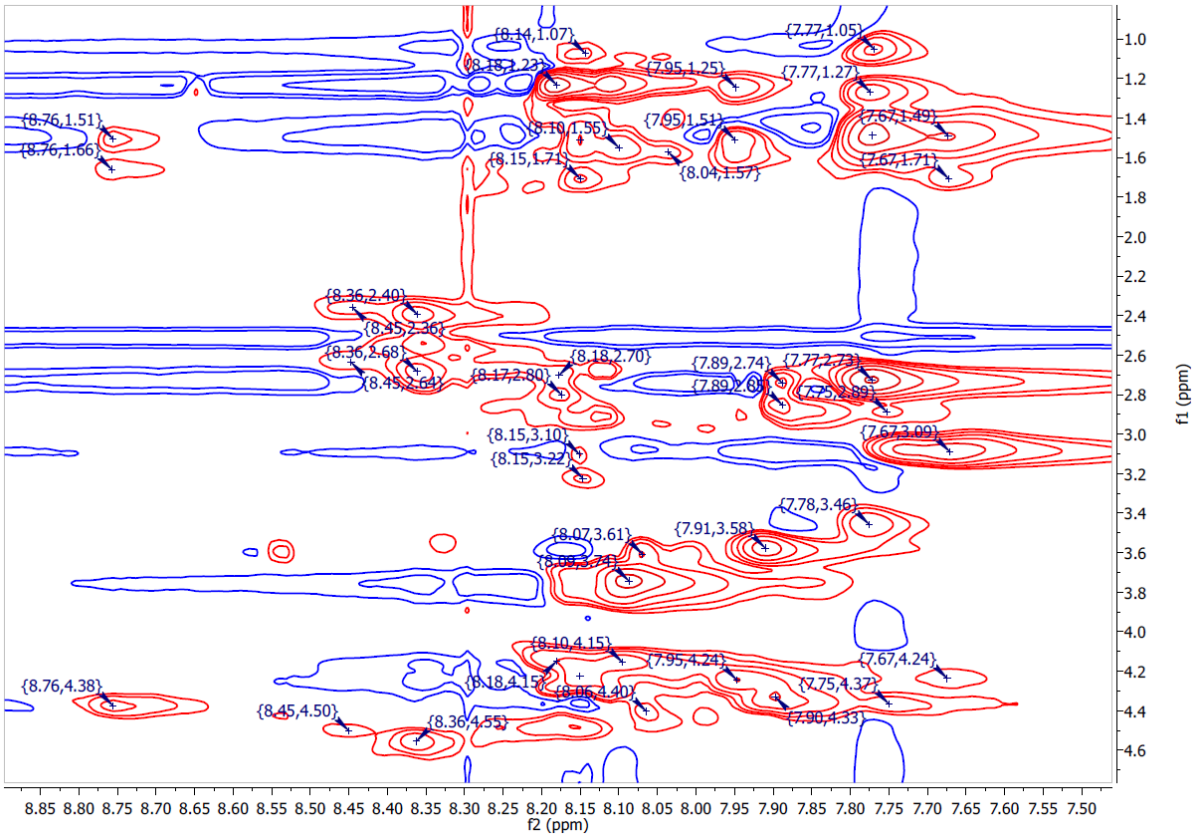


Figure 3- 5: The partial ^{1}HN-Hα fingerprint region of 2D the TOCSY spectrum TP_Asp of the peptide, showing individual spin system patterns (full spectrum is provided in **Appendix II, Figure S.3-6**)

The long spin system residues such as Arg and Lys; which consists of γ and δ protons in their side chains, were unambiguously identified from TOCSY spectra. Moreover, Gly residues, which have only two α-protons whose chemical shift appears around 3.5-4 ppm, were also not difficult to identify. In contrast, residues corresponding to an AMX spin system (for examples

Tyr, Cys, Asp, Ser) were quite difficult to assign using either COSY or TOCSY spectra. This is due to the fact that the backbone of these amino acid residues contains one α-protons and two β-protons with similar spin patterns.

Furthermore, some residues could be not unambiguously located on the TOCSY spectrum due to severe overlaps and some missing cross peaks in the fingerprint region. This can be attributed to low intensity due to the small NH-αCH coupling constant or large line width.[2] It is suggested in literature that overlapping components in the TOCSY spectrum may result in cancellation of some cross peak intensities.[2,8] Excessive overlaps of most cross peaks were also caused by the repeating residues in the peptide sequence and this also limited the assignment of most spin systems from the COSY spectrum. Consequently, since TOCSY is more sensitive than the COSY and offers a better resolution,[2] it was chosen for the spin system analysis. **Table 3-1** gives a summary of all identified chemical shifts for the amino acid residues. On the basis of the difficulties mentioned above it was not possible to fully complete the exact assignment of some individual AMX spin systems using the TOCSY spectrum. Therefore, the fingerprint backbone region of the ROESY spectrum was used to identify neighbouring amino acids. The 2D ^{1}H-^{13}C HSQC (Heteronuclear single quantum coherence) spectrum (aliphatic region) was also used to assign Cα of the corresponding spin systems.

Table 3- 1: NMR chemical shifts (ppm) of identified spin assignment for TP_Asp using TOCSY spectrum

Residue	**H-NH**	**^{1}Hα**	**Cα**	**^{1}Hβ**	**^{1}Hγ**	**^{1}Hδ**	**^{1}Hε**
1	8.75	4.38	55.04	1.51, 1.66			
2	8.45	4.5	52.12	2.64, 2.36	8.45		
3	8.36	4.55	49.95	2.69, 2.39			
4	8.18	4.48	52.31	2.80, 2.70	1.23		
5	8.15	4.22	52.84	3.23, 3.10	1.71	1.52	1.07
6	8.10	4.15	52.89	1.51			
7	8.08	3.74	42.4				
8	8.07	4.4	55.02	3.61			
9	7.91	3.58	62.16				
10	7.95	4.24	52.88	1.51, 1.25			
11	7.89	4.33	55.07	2.85, 2.74			
12	7.77	4.37	53.01	3.46, 2.73	1.49	1.27	1.05
13	7.75	4.37	55.03	2.88			
14	7.68	4.24	45.72	3.08	1.71		

3.2.2.4 Sequential spin specific assignment

The NMR sequential walk technique used to assign peptide residues is normally performed using a NOESY/ROESY spectrum, since each residue will have a unique pattern showing a connection of its amide proton to its backbone C^{α} proton and its side chain protons.[8,30] To complete the sequential residue assignment, the "sequential walk" in the ^{1}HN(i)-^{1}Hα fingerprint backbone region of the 2D ^{1}H ROESY spectrum was performed to confirm the primary structure of the peptides. However, due to some difficulties already mentioned above such as severe overlaps and missing peaks, this technique could not be successfully utilized to perform a complete sequential spin assignment of the peptide. A 2D ^{1}H ROESY NMR spectrum for TP_Asp peptide showing the amide backbone of the fingerprint region, is attached in **Appendix II, Figure S.3-16**. The next strategy was to utilise the NOEs (nuclear Overhauser effect) of the observed neighbouring amino acid residues, (for example; $^{1}H_{i}^{N}$-$^{1}H^{N}_{i+1}$ and $^{1}H_{i}^{\alpha}$ - $^{1}H^{N}_{i+1}$) in the ^{1}H-ROESY spectrum.

As already discussed in Section 3.2.2.3, amino acids with long side chains such as Lys and Arg could be unambiguously identified from TOCSY spectrum on the basis of their spin systems having γ and δ protons. However, at this point their exact positions in the peptide chain were not assigned; but were only identified and used as a starting reference point for sequential analysis. Similar basis was used for the identification of the two Gly residues. A preview of the identified spin systems used for the initial assignments are shown in **Table 3-2**.

Table 3- 2: NMR chemical shifts (ppm) of identified spin systems used for the initial assignment.

Residue	H-NH	^{1}Hα	Cα	^{1}Hβ	^{1}Hγ	^{1}Hδ	^{1}Hε	Known res
1								
2/13	8.18	4.48	52.31	2.80, 2.70	1.23			Arg
3								
4/	8.15	4.22	52.84	3.23, 3.10	1.71	1.52	1.07	Lys
5								
6/9	7.91	3.58	62.16					Gly
7								
8								
9/6	8.08	3.74	42.4					Gly
10/4	7.77	4.37	53.01	3.46, 2.73	1.49	1.27	1.05	Lys
11								
12								
13/2	7.68	4.24	45.72	3.08	1.71			Arg
14								

The assigment procedure was further continued using neighbouring NOEs connecivities in the ROESY spectrum. As a starting point; the NH resonance at 7.91 ppm was assumed to represent Gly6. A ROESY correlation between the peak 7.91 ppm and the alpha proton 4.33 ppm suggest a dαN(i,i+1) connectivity between these crosspeaks and the alpha proton was attributed to the aspartic acid (Asp) residue located at position 5, which is in close proximity to the Gly amide proton. On that basis, another sequential connectivity between 7. 89 (Asp5-HN) resonance peak and 4.55 ppm (7.89;4.55) was also observed, and 4.55 ppm was assgined to the alpha proton of tyrosine (Tyr3), a dαN(i,i+2) relationship. Identification of Arg2 was based on the sequential connectivity, dαN(i,i+1), between 8.36 ppm (Tyr3-HN) and 4.24 ppm, which is the alpha proton of Arg with the HN resonance peak at 7.68 ppm. A correlation, dαβ(i,i+1), between Arg2 (Hβ-3.08) and 7.75 ppm was observed in the ROESY spectrum and the resonance, 7.75 ppm was therefore assigned as the amide proton of Cys1. Asp11 was assigned using a correlation between (Asp11HN-7.95; Gly9Hα-3.74) cross-peaks, a dαN(i,i-2) connectivity. The resonance at 3.74 ppm, is identified to belong to one of the Gly amino acids, Gly9, since Gly6 has already been assigned. Another sequential correlation between the NH resonance of Lys (HN-7.77) with 4.55 ppm, (7.77; 4.50 ppm), dαN(i,i+2) was observed and the alpha proton

4.50 ppm was assigned to Tyr12. The summary of the identified sequential correlation observed are shown below in **Table 3-3**.

Table 3- 3: NMR chemical shifts (ppm) observed through NOEs intra-residue connectivity.

Residue	**H-NH**	**^{1}Hα**	**Cα**	**^{1}Hβ**	**^{1}Hγ**	**^{1}Hδ**	**^{1}Hε**	**ROESY**	**Assigned**
1	7.75	4.37	55.03	2.88				(3.08;7.75)	Cys1
2	7.68	4.24	45.72	3.08	1.71				Arg2
3	8.36	4.55	49.95	2.69, 2.39				(8.36;4.25)	Tyr3
4	8.15	4.22	52.84	3.23, 3.10	1.71	1.52	1.07		
5	7.89	4.33	55.07	2.85, 2.74				(7.89;4.55)	Asp5
6	7.91	3.58	62.16					(7.93;4.33)	Gly6
7									
8									
9	8.08	3.74	42.4						
10	7.77	4.37	53.01	3.46, 2.73	1.49	1.27	1.05		
11	7.95	4.24	52.88	1.51, 1.25				(7.95;3.74)	Asp11
12	8.45	4.5	52.12	2.64, 2.36				(7.77;4.50)	Tyr12
13	8.18	4.48	52.31	2.80, 2.70	1.23				
14									

As previously mentioned in Section 2.6.1.1, the residues Gly, Ala and Ser, forms part of the turn motif in our peptide. The unique backbone of the alanine spin pattern can be identified unambiguously from the TOCSY spectrum, since it has one shielded β-proton. And in addition, since there is only one alanine residue in the peptide sequence, this would mean it occupies position 7 with an alpha proton of 4.15 ppm. Identification of serine residue is also based on the fact that it has a distinct spin pattern from other AMX spin systems, with two deshielded β-protons resonance. The remaining amino acid with an alpha proton at 4.38 ppm was assigned based on its correlation with amide proton of Arg, Arg13-HN; (8.18; 4.38), a dαN(i,i+1) correlation. This was attributed to the alpha proton of Cys14 (4.38 ppm). The complete sequential assignment of the amino residues is summarized in **Table 3-4**.

Table 3- 4: NMR chemical shifts (ppm) of individual spin assignment for TP_Asp.

Residue	H-NH	^{1}Hα	Cα	^{1}Hβ	^{1}Hγ	^{1}Hδ	^{1}Hε	ROESY
Cys1	7.75	4.36	55.03	2.88				(3.08;7.75)
Arg2	7.68	4.24	45.72	3.08	1.71			
Tyr3	8.36	4.55	49.95	2.69, 2.39				(8.36;4.25)
Lys4	8.15	4.22	52.84	3.23, 3.10	1.71	1.52	1.07	
Asp5	7.89	4.33	55.07	2.85, 2.74				(7.89;4.55)
Gly6	7.91	3.58	62.16					(7.93;4.33)
Ser7	8.07	4.4	55.02	3.61				
Ala8	8.1	4.15	52.89	1.51				
Gly9	8.08	3.74	42.4					
Lys10	7.77	4.37	53.01	3.46, 2.73	1.49	1.27	1.05	
Asp11	7.95	4.24	52.88	1.51, 1.25				(7.95;3.74)
Tyr12	8.45	4.5	52.12	2.64, 2.36				(7.77;4.50)
Arg13	8.18	4.48	52.31	2.80, 2.70	1.23			(8.18; 4.38)
Cys14	8.75	4.38	55.04	1.51, 1.66				

3.2.2.5 Determination of the secondary structural elements of TP_Asp

The secondary structure or backbone interactions that stabilize the peptide, can be characterized by the presence of long-range Hα-Hα or NH-Hα interactions.[8,36] Of particular interest, a long-range correlation NOEs between the amide proton of Ala8, Ala8(HN-8.10 ppm) and Arg13(Hβ-1.23). This observation suggests that the structure is not linear but adopt a certain conformation. It is worthy to mention, however, that due difficulties mentioned above, such as severe overlaps and missing cross-peaks, as well as finding virtually identical chemical shifts on the ROESY spectrum, this suggested structural conformation is not a conclusive structural elucidation. For example, the Hα-shift values of Arg2(Hα-4.24) and Asp11(Hα-4.24) or Lys4(Hα-4.22) are quite close, and differentiating a correlation between these spins systems can thus be difficult. **Figure 3-6** below represents the possible long-range correlation observed.

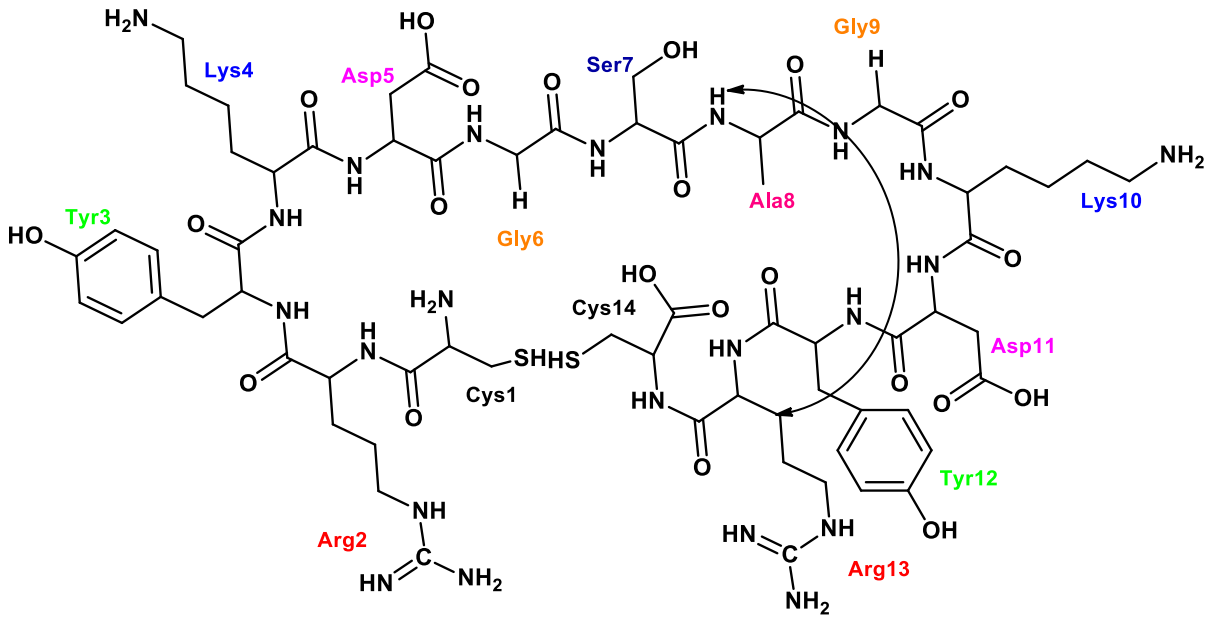


Figure 3- 6: TP_Asp peptide structure with arrows indicating long correlation using ROESY

3.2.2.6 NMR structure elucidation and spin systems assignment for TP_ADLys

The structural elucidation for TP_ADLys was performed using the same approach mentioned in Sections 3.2.2.3 and 3.2.2.4 and the corresponding supporting documents are available in **Appendix II**. The summary of identified chemical shifts of the amino acid residues from the amide fingerprint backbone region obtained using a 2D ^{1}H TOCSY spectrum are shown in **Table 3-5**. The 2D ^{1}H-^{13}C HSQC spectrum was also used to assign the Cα of the individual spin systems. After the identification of the spin systems, the sequence specific resonance assignment was carried using intra-residual couplings.

Table 3- 5: NMR chemical shifts (ppm) of identified spin assignment for TP_ADLys using TOCSY spectrum.

Residue	**H-NH**	**^{1}Hα**	**Cα**	**^{1}Hβ**	**^{1}Hγ**	**^{1}Hδ**	**^{1}Hε**
1	8.75	4.37	52.84	1.69, 1.52			
2	8.18	4.48	52.85	2.8	1.23		
3	8.45	4.5	49.87	2.63, 2.36			
4	7.78	4.36	43.84	3.52, 2.73	1.5	1.27	1.06
5	7.91	4.33	53.02	2.83, 2.89			
6	7.92	3.58	64.63				
7	8.06	4.59	49.87	3.61			
8	8.10	4.15	52.83	1.56			
9	8.09	3.74	48.58				
10	8.15	4.23	52.86	3.11,3.23	1.72	1.53	1.06
11	7.94	4.24	45.63	1.51, 1.24			
12	8.37	4.55	49.67	2.69, 2.40			
13	7.69	4.24	48.94	3.08	1.71	1.5	
14	7.75	4.36	55.08	2.89			

Following the same approach as above, the sequential assignment was initiated by first identifying spin systems with distinct and recognizable side chains (such as Arg, Lys, Gly). Since there are only two glycine residues in the peptide sequence; the next step was to assume that the spin system with amide protons of resonance 7.91 ppm is glycine. The observed dNα(i,i+1) connectivity, between 7.91 and 4.33 ppm (7.91, 4.34), was then attributed to the NH Gly6 and Hα-Asp 5 correlation and the resonance at 4.33 ppm was assigned to the alpha proton of Asp5. With the aid of a ^{1}H ROESY spectrum, the corresponding sequential residues were identified and the observed correlations are presented in **Table 3-6.**

Table 3- 6: NMR chemical shifts (ppm) of individual spin assignment for TP_ADLys

Residue	H-NH	^{1}Hα	Cα	^{1}Hβ	^{1}Hγ	^{1}Hδ	^{1}Hε	ROESY
Cys1	7.75	4.36	55.08	2.89				
Argr2	7.69	4.24	48.94	3.08	1.71	1.5		(3.08;7.75)
Tyr3	8.37	4.55	49.67	2.69, 2.40				(8.37;4.24)
Lys4	8.15	4.23	52.86	3.11,3.23	1.72	1.53	1.06	
Asp5	7.91	4.33	53.02	2.83, 2.89				(7.91;4.55)
Gly6	7.92	3.58	64.63					(7.92;4,33)
Ser7	8.06	4.41	49.87	3.61				
Ala8	8.1	4.15	52.83	1.56				
Gly9	8.09	3.74	48.58					
Lys10	7.77	4.36	43.84	3.52, 2.73	1.5	1.27	1.06	(7.77;4.50)
Asp11	7.94	4.24	45.63	1.51, 1.24				(7.94;3.74)
Tyr12	8.45	4.5	49.87	2.63, 2.36				
Arg13	8.18	4.48	52.85	2.8	1.23			(8.18: 4.37)
Cys14	8.75	4.37	52.84.02	1.69, 1.52				

3.2.2.7 Assessment of secondary structural elements for TP_ADLys

Using ROESY ^{1}H NMR spectra, the NOEs interaction observed was between Ala8(HN-8.10) to Asp11(Hβ-1.24), which suggest that the peptide is not linear (**Figure 3-7**).

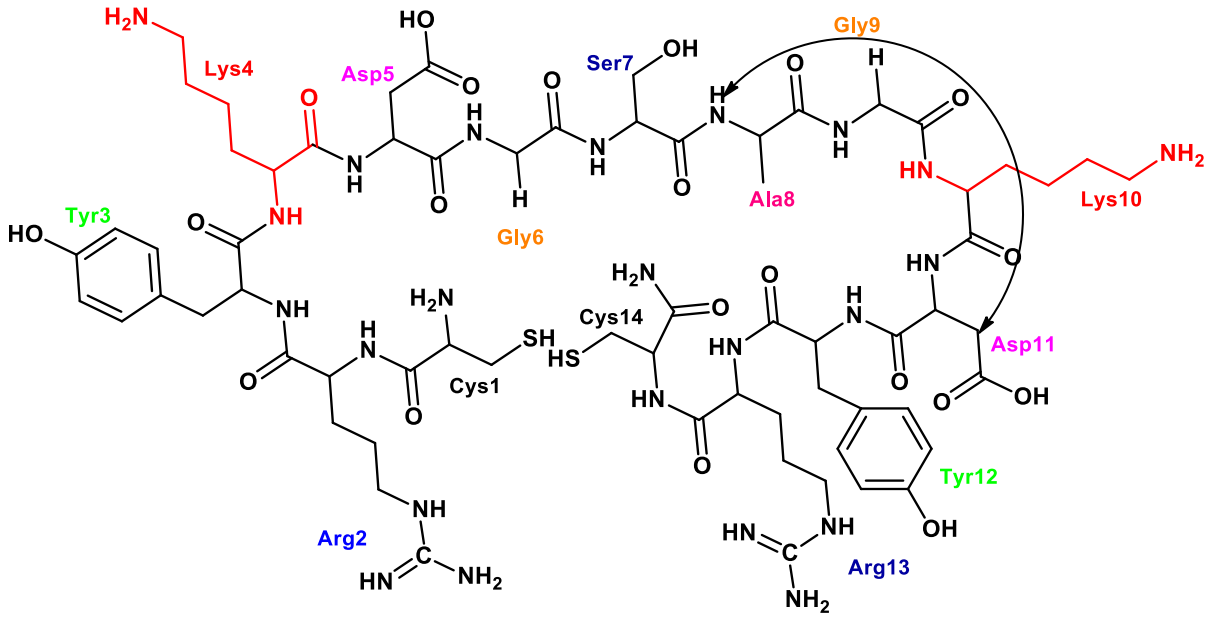


Figure 3-7:TP_ADLys peptide structure with arrows indicating long correlations using ROESY NOEs (black lines)

For both peptides, not many long-range NH-Hα and Hα-Hα NOEs correlations were observed. Furthermore, the intensities of the long/medium range NOEs correlations were lower than those of the sequential cross peaks. Although it is difficult to provide a conclusion structure conformation of the peptides, one can propose that the structure is not linear from one distinct medium NOEs range correlation observed.

3.3 Concluding remarks

CD experiments suggest that the peptides predominately form a helix-structure with a random coil conformation when measurements were performed in water or a buffered aqueous solution. The 2D ^{1}H NMR (ROESY and TOCSY) experiments proved to be important complementary tools in the elucidation of the secondary peptide structures. The observed of long/medium-range ROESY correlations together with the CD results provide summative confirmation that indeed the peptides are not linear but adopted a random-helical conformation for TP_Asp, and random-beta sheets conformation for TP_ADLys peptide.

Despite varying experimental conditions for NMR studies, satisfactory spectra were still not obtained to help provide conclusive structural conformation. Future NMR experiments will therefore be conducted using an advanced NMR instruments with well-shielded, high field magnets such as 600 or 700 MHz.

3.4 References

(1) Surewicz, W. K.; Mantsch, H. H.; Chapman, D. Determination of Protein Secondary Structure by Fourier Transform Infrared Spectroscopy: A Critical Assessment. *Biochemistry* **1993**, *32* (2), 389–394. https://doi.org/10.1021/bi00053a001.

(2) Gomathi, L.; Subramanian, S. Elucidation of Secondary Structures of Peptides Using High Resolution NMR. *Current Science*. 1996, pp 553–567.

(3) Cavanagh, J.; Fairbrother, W.; A. G. Palmer, I.; Range, M.; Skelton, N. J. *Protein NMR Spectroscopy Principle and Practice*, Second Edi.; Elsevier Academic Press, 2007.

(4) Wuthrich, K. Protein Structure Determination in Solution by NMR Spectroscopy. *J. Biol. Chem.* **1990**, *265* (36), 22059–22062. https://doi.org/10.1142/9789812795830_0001.

(5) Thiele, C. M.; Petzold, K.; Schleucher, J. EASY ROESY: Reliable Cross-Peak Integration in Adiabatic Symmetrized ROESY. *Chem. - A Eur. J.* **2009**, *15* (3), 585–588. https://doi.org/10.1002/chem.200802027.

(6) Nuclear, T.; Medical, H. Structure Determination of a Tetrasaccharide: Transient Nuclear Overhauser Effects in the Rotating Frame. *J. Am. Chem. Soc.* **1984**, *106* (3), 811–813.

(7) Hwang, T.L. and Shaka, A. . Cross Relaxation without TOCSY: Transverse Rotating-Frame Overhauser Effect Spectroscopy. *J. Am. Chem. Soc.* **1992**, *114* (8), 3157–3159.

(8) Raghothama, S. REVIEWS NMR of Peptides. *J. Indian Inst. Sci.* **2010**, *90* (1), 90.

(9) Thomas, W. A. NMR and Conformations of Amino Acids, Peptides and Proteins. **1970**, 1–41.

(10) Guthrie, D. J. 1H Nuclear Magnetic Resonance (NMR) in the Elucidation of Peptide Structure. *Methods Mol. Biol.* **1997**, *73*, 163–184. https://doi.org/10.1385/0-89603-399-6:163.

(11) Kelly, S.; Price, N. The Use of Circular Dichroism in the Investigation of Protein Structure and Function. *Curr. Protein Pept. Sci.* **2005**, *1* (4), 349–384. https://doi.org/10.2174/1389203003381315.

(12) Greenfield, N.; Fasman, G. D. Computed Circular Dichroism Spectra for the Evaluation of Protein Conformation. *Biochemistry* **1969**, *8* (10), 4108–4116. https://doi.org/10.1021/bi00838a031.

(13) Johnson, W. C. Protein Secondary Structure and Circular Dichroism: A Practical Guide. *Proteins Struct. Funct. Bioinforma.* **1990**, *7* (3), 205–214. https://doi.org/10.1002/prot.340070302.

(14) Greenfield, N. J. Methods to Estimate the Conformation of Proteins and Polypeptides from Circular Dichroism Data. *Anal. Biochem.* **1996**, *10* (235), 1–10.

(15) Creighton, T. E. *Proteins : Structures and Molecular Properties*, 2nd Editio.; W.H. Freeman, New York, 1993.

(16) Micsonai, A.; Wien, F.; Kernya, L.; Lee, Y. H.; Goto, Y.; Réfrégiers, M.; Kardos, J. Accurate Secondary Structure Prediction and Fold Recognition for Circular Dichroism Spectroscopy. *Proc. Natl. Acad. Sci. U. S. A.* **2015**, *112* (24), E3095–E3103. https://doi.org/10.1073/pnas.1500851112.

(17) Greenfield, N. J. Using Circular Dichroism Spectra to Estimate Protein Secondary Structure. *Nat. Protoc.* **2007**, *1* (6), 2876–2890. https://doi.org/10.1038/nprot.2006.202.

(18) Zapadka, K. L.; Becher, F. J.; Gomes dos Santos, A. L.; Jackson, S. E. Factors Affecting the Physical Stability (Aggregation) of Peptide Therapeutics. *Interface Focus* **2017**, *7* (6). https://doi.org/10.1098/rsfs.2017.0030.

(19) Zbacnik, T. J.; Holcomb, R. E.; Katayama, D. S.; Murphy, B. M.; Payne, R. W.; Coccaro, R. C.; Evans, G. J.; Matsuura, J. E.; Henry, C. S.; Manning, M. C. Role of Buffers in Protein Formulations. *J. Pharm. Sci.* **2017**, *106* (3), 713–733. https://doi.org/10.1016/j.xphs.2016.11.014.

(20) Kopec, J.; Schneider, G. Comparison of Fluorescence and Light Scattering Based Methods to Assess Formation and Stability of Protein-Protein Complexes. *J. Struct. Biol.* **2011**, *175* (2), 216–223. https://doi.org/10.1016/j.jsb.2011.04.006.

(21) Tyler-Cross, R.; Schirch, V. Effects of Amino Acid Sequence, Buffers, and Ionic Strength on the Rate and Mechanism of Deamidation of Asparagine Residues in Small Peptides. *J. Biol. Chem.* **1991**, *266* (33), 22549–22556.

(22) Kheddo, P.; Tracka, M.; Armer, J.; Dearman, R. J.; Uddin, S.; Van Der Walle, C. F.; Golovanov, A. P. The Effect of Arginine Glutamate on the Stability of Monoclonal Antibodies in Solution. *Int. J. Pharm.* **2014**, *473* (1–2), 126–133. https://doi.org/10.1016/j.ijpharm.2014.06.053.

(23) Pappu, R. V; Rose, G. D. A Simple Model for Polyproline II Structure in Unfolded States of Alanine-Based Peptides. *Protein Eng.* **2002**, *11*, 2437–2455. https://doi.org/10.1110/ps.0217402.Folding.

(24) Avbelj, F.; Baldwin, R. L. Role of Backbone Solvation and Electrostatics in Generating Preferred Peptide Backbone Conformations : Distributions of Phi. *Proc. Natl. Acad. Sci. U. S. A.* **2003**, *100* (10), 5742–5747.

(25) Tilstra, L.; Mattice, W. . *The β Sheet ⇌ Coil Transition of Polypeptides, as Determined by Circular Dichroism. In: Fasman G.D. (Eds) Circular Dichroism and the Conformational Analysis of Biomolecules*, eds.; Springer, Boston, MA, 1996. https://doi.org/https://doi.org/10.1007/978-1-4757-2508-7_8.

(26) Fuchs, P. F. J.; Bonvin, A. M. J. J.; Bochicchio, B.; Pepe, A.; Alix, A. J. P.; Tamburro, A. M. Kinetics and Thermodynamics of Type VIII β-Turn Formation: A CD, NMR, and Microsecond Explicit Molecular Dynamics Study of the GDNP Tetrapeptide. *Biophys. J.* **2006**, *90* (8), 2745–2759. https://doi.org/10.1529/biophysj.105.074401.

(27) Avbelj, F.; Baldwin, R. L. Role of Backbone Solvation in Determining Thermodynamic β Propensities of the Amino Acids. *Proc. Natl. Acad. Sci. U. S. A.* **2002**, *99* (3), 1309–1313.

(28) Avbelj, F.; Luo, P.; Baldwin, R. L. Energetics of the Interaction between Water and the Helical Peptide Group and Its Role in Determining Helix Propensities. *Proc. Natl. Acad. Sci. U. S. A.* **2000**, *97* (20), 10786–10791.

(29) James, T. L. Relaxation Matrix Analysis of 2D NMR Data. *Prog. Nucl. Magn. Reson. Spectrosc.* **1990**, *22* (1), 83–100.

(30) Jones, C.; Mulloy, B.; Thomas, A. H.; Williamson, M. P. Peptide Structure Determination by NMR. In *Spectroscopic Methods and Analyses*; 2003; pp 69–86. https://doi.org/10.1385/0-89603-215-9:69.

(31) Trainor, K.; Palumbo, J. A.; Mackenzie, D. W. S.; Meiering, E. M. Temperature Dependence of NMR Chemical Shifts : Tracking and Statistical Analysis. *Protein Sci.* **2020**, *29* (1), 306–314. https://doi.org/10.1002/pro.3785.

(32) Andersen, N. H.; Neidigh, J. W.; Harris, S. M.; Lee, G. M.; Liu, Z.; Tong, H. Extracting Information from the Temperature Gradients of Polypeptide NH Chemical Shifts. 1. The Importance of Conformational Averaging. *J. Am. Chem. Soc.* **1997**, *119* (36), 8547–8561.

https://doi.org/10.1021/ja963250h.

(33) Tinoco, L. W.; Fraga, J. L.; Anobom, C. D.; Zolessi, F. R.; Obal, G.; Toledo, A.; Pritsch, O.; Arruti, C. Structural Characterization of a Neuroblast-Speci Fi c Phosphorylated Region of MARCKS. *Biochim. Biophys. Acta (BBA)-Proteins Proteomics* **2020**, *1844* (4), 837–849. https://doi.org/10.1016/j.bbapap.2014.02.016.

(34) Wilson, D.; Daly, N. L. Nuclear Magnetic Resonance Seq (NMRseq): A New Approach to Peptide Sequence Tags. *Toxins (Basel).* **2018**, *10* (11), 437. https://doi.org/10.3390/toxins10110437.

(35) Bodenhausen, G.; Wiithrich, K. Improved Spectral Resolution in COSY 1H NMR Spectra of Proteins via Double Quantum Filtering. *Biochem. Biophys. Res. Commun.* **1983**, *117* (2), 479–485. https://doi.org/10.1016/0006-291x(83)91225-1.

(36) Skelton, N. J.; Garcia, K. C.; Goeddel, D. V.; Quan, C.; Burnier, J. P. Determination of the Solution Structure of the Peptide Hormone Guanylin: Observation of a Novel Form of Topological Stereoisomerism. *Biochemistry* **1994**, *33* (46), 13581–13592. https://doi.org/10.1021/bi00250a010.

Chapter 4

Peptides as organocatalysts for direct aldol addition reactions

4.1 Introduction

Chemistry plays a huge role in improving the quality of life by providing various products, however this has resulted in the depletion of non-renewable resources and pollution, hence the introduction of green and sustainable chemistry.[1] The development of catalytic routes leading to the synthesis of complex organic molecules, led by both industrial and academic discoveries of efficient selective catalysts for a wide range of liquid- and multi-phase organic transformations, has in past years grown tremendously.[2,3] Most of these developments, often coincide with efforts made by pharmaceutical and chemical industries, who have been in pursuit of rationalizing the cost of manufacturing and waste disposal in an increasing ecologically aware and economically competitive market. The area of organocatalysis, which also has witnessed an immense growth over the years, has received great attention because of its green chemistry advantages such as its high efficiency, economic feasibility and ecological sustainability and its analogy to eon-perfected enzyme catalysis.[4–7]

Due to the rise in demand for optically pure compounds, a lot of work has been done to improve and develop efficient stereoselective methodologies. For many years, transition-metal complexes and enzymes have been known to be the only two main classes for proficient asymmetric catalysis.[8] It was only a few years ago that a change in this perception occurred as chemists realized that simple organic molecules could be considered as highly effective and remarkably enantioselecitve catalysts for various important chemical transformations.[9]

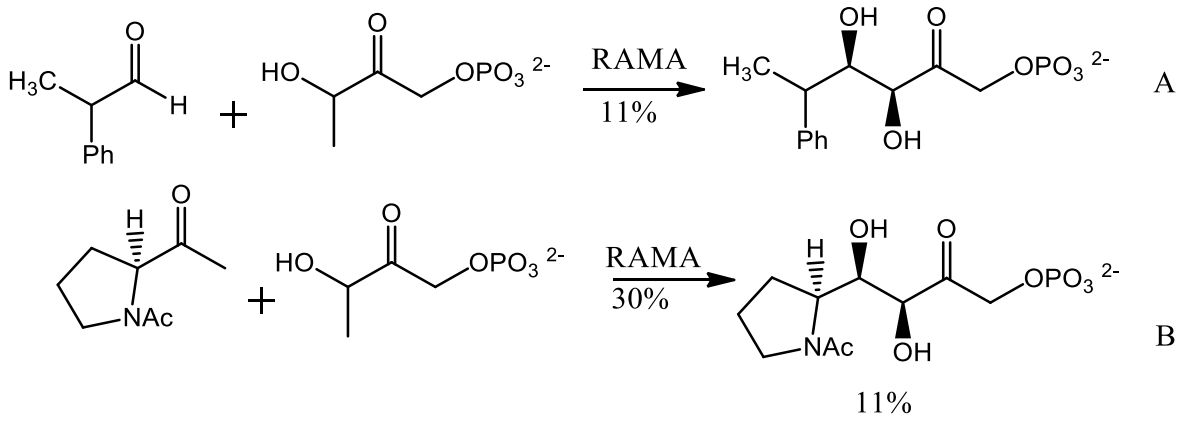
The primary aim of this project is to catalyze carbon-carbon forming reactions utilizing peptides as organocatalysts, and we are specifically interested in the aldol reaction, since it is considered to be one of the most versatile and widely used reactions for the construction of carbon-carbon bonds in organic synthesis.[4–7,10–12] There has been a huge progress in the development of enantioselective and efficient catalysts for this reaction, as discussed in Chapter 1.

In this chapter the following is described: (a) Screening of TP_Asp and TP_ADLys peptides for aldol addition reaction catalytic, (b) Catalysis in aqueous media and some common organic solvents

4.2 Preliminary investigation of the Fructose-1,6-bisphosphate aldolase (FBPA) enzyme aldol reaction catalysis

In this section we explore the use of the fructose-1,6-bisphosphate enzyme from Rabbit Muscle Aldolase (RAMA), EC 4.1.2.13, in an aldol reaction. As discussed earlier in Chapter 1, the fructose-1,6-bisphosphate aldolase enzyme catalyzes the reversible cleavage of fructose to glyceraldehyde and dihydroxyacetone phosphate (DHAP). There are a number of reports that cover the class I aldolase from rabbit skeletal muscle, especially the mechanism and the application in organic synthesis.[13–16] RAMA is known to accept a broad spectrum of aldehydes as electrophilic acceptor substrates for the aldol reaction but only accepts DHAP or its close analogues as a donor substrate for the nucleophilic component.[13,14,17–19] RAMA was chosen for this study because is it commercially available, selective and the mostly studied aldolase enzyme.

There are few available reports on the application of RAMA as a catalyst in organic synthesis. One such report is by Whitesides and co-workers,[19] who reported on D-fructose-1,6-bisphosphate aldolase as a useful catalyst for the stereoselective aldol reaction between DHAP and various aldehydes. They demonstrated from their work that cyclic aldehydes yielded low aldol products when compared to linear aldehydes which produced high yields with a low catalyst loading (**Scheme 4-1**).



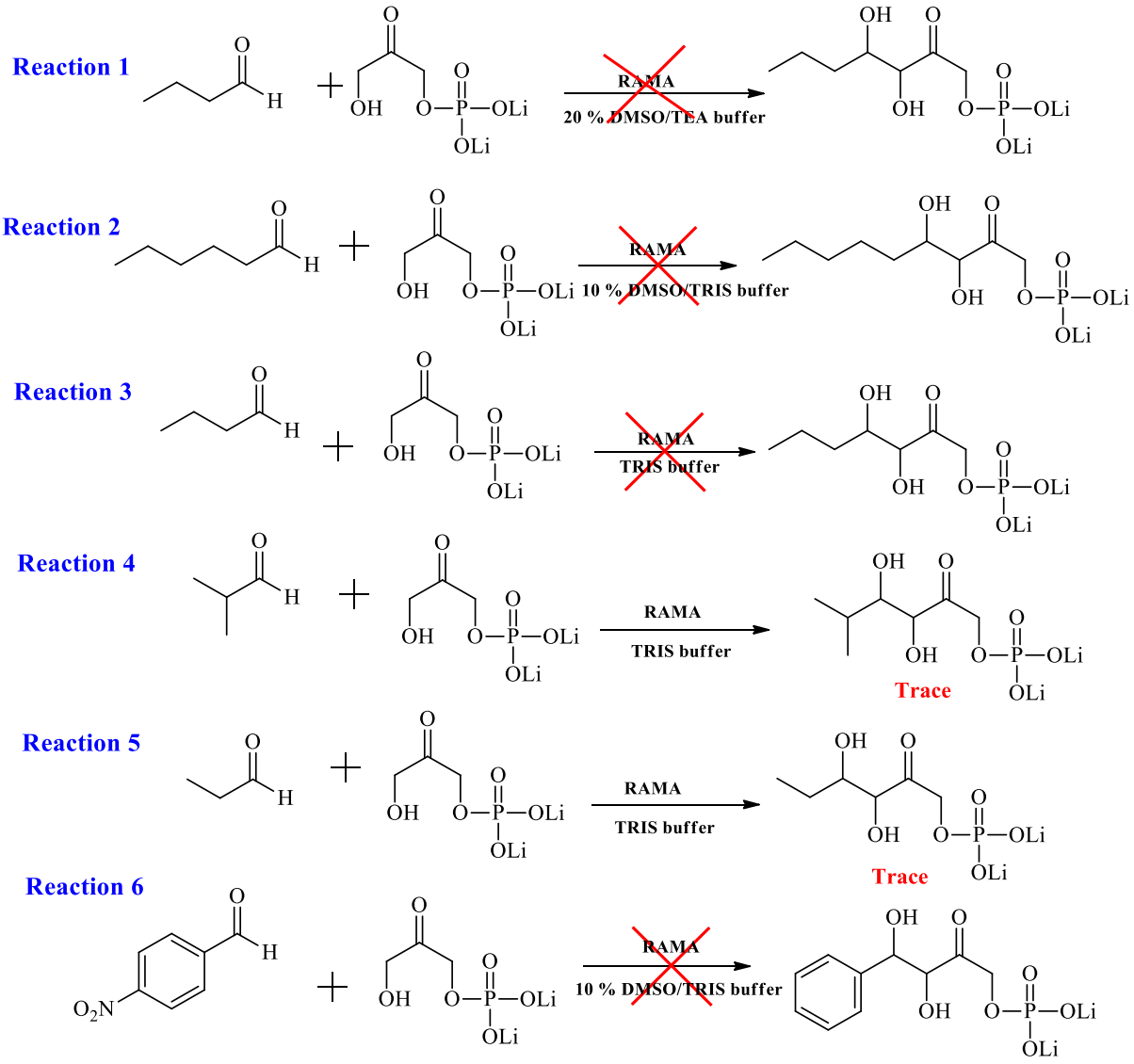
Scheme 4- 1: Aldol reaction between cyclic and linear aldehyde and DHAP using RAMA.[19]

The following observations were made regarding acceptable reactions conditions and substrate tolerance; i) The substituted aldehydes with leaving groups at the β -position to the carbonyl are appropriate substrates, ii) Aliphatic aldehydes are acceptable substrates but steric hindrance next to the aldehyde may reduce reactivity and finally, iii) Simple aldehydes, for example, isobutyraldehyde, are reported to be either poor or unreactive, whereas aldehydes with unsaturation in conjugation with the carbonyl group are not tolerated.[13,20,21] Even though DHAP is commercially available it is expensive, therefore efficient and reliable reaction conditions method are required in undertaking such reactions.

In the first attempt, we utilized DHAP, butyraldehyde as a donor substrate, a 20% DMSO/triethylamine (TEA) buffer, 1mg (4.5×10^{-5} mol%) of RAMA and the reaction was left to stir for over 48 hours (**Scheme 4-2**, reaction 1) while it was consistently monitored by TLC. A trace amount of the expected product was observed after 48 hours. This may be attributed to the small amount (4.5×10^{-5} mol%) of catalyst (RAMA) used.

A literature review of the successful applications of RAMA in aldol reactions revealed that RAMA tolerates 10-20% of DMSO (v: v) especially when used with the TEA buffer which can also assist its activity. In addition, 20% ethanol was also reported as one of the favourable solvents.[13] The reaction medium for this enzyme reaction is very important because of the sensitivity of DHAP to pH, temperature and chemical instability. A large deviation from the optimal pH could results in epimerization and breakdown of DHAP.[14,17,18]

Further attempts to improve the reaction conditions for the aldol reaction using RAMA were made by varying substrates (acceptor aldehydes) and co-solvents, (**Scheme 4-2**, Reactions 3–6). Linear aldehydes were chosen based on the discussion above that they are favoured over cyclic or aromatic aldehydes and their reactions are easily reproducible and they are friendly to use. Tris-buffer was chosen instead of TEA buffer because it was reported in literature,[20,21] to be an acceptable reaction medium for the aldolase enzyme. DMSO was added to reactions 2 and 6 to assists with solubility of the aforementioned aldehydes.



Scheme 4- 2: Aldol reactions catalyzed by RAMA using DHAP as a donor ketone: **Reaction 1**, 1 mg RAMA, 20 % DMSO/TEA buffer (pH 7.0); **Reaction 3-6**, 3 mg (9.5×10-5 mol) RAMA, DHAP (0.05 mmol, 8.5 mg), TRIS-buffer pH 7.6, rt for 24-72 h.

The reactions performed in the TRIS buffer (reactions, 4 and 5) using short chain linear aldehydes yielded trace amounts of product. Studies have shown that the effectiveness of DHAP decreases over time in the reaction further hindering the reaction rate.[14] Aromatic aldehydes substituted with electron withdrawing groups were previously reported to be the most reactive substrates, however they were inactive in this study. Moreover, linear aldehydes with long chain (reaction 2) proved also to be inappropriate substrates for this reaction. It was observed that changing the solvent or buffer did not have any major influence in facilitating a speedy conversion of the aldehyde. The effectiveness of DHAP is proposed to have decreased over time in enzymatic reaction thus impeding the overall aldol reactions due to its instability

and thus impeding the overall reaction yield.[14] Therefore the observed reactions outcomes (**Scheme 4-2)** could be caused by low concentrations of DHAP used and its instability.

Most of the reported work in literature for the DHAP dependent aldolases enzymes have focused on the synthesis of carbohydrates,[19,22–27] and there are not many studies on its application in aldol reactions. This limited the comparison of the results obtained in this work with those in literature, to provide more plausible rationale of the outcomes. Due to the fact that both the enzyme and DHAP substrate are expensive, the reactions could not be further optimized.

The challenges experienced with this reaction include some of the limiting factors experienced with most enzymes such as they are expensive; they function at a specific pH, and they are also substrate specific. Hence, there is a need to design catalytic peptide mimics that can be utilized in organic reactions, that are not necessarily pH depended or substrate specific. The catalytic activity of the synthesized peptides will be investigated in aldol reactions in the next section.

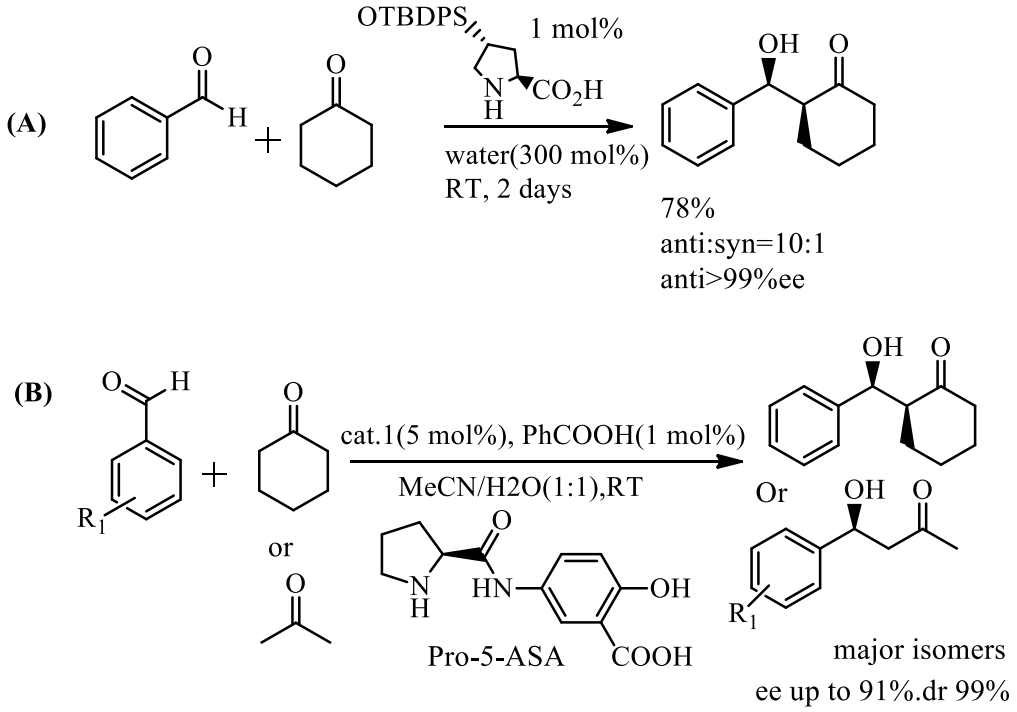
4.3 Peptides screening and optimization of aldol reactions conditions

The choice of solvent or solvent mixture, plays a crucial role in the optimization of reaction conditions, as it has a strong impact on the yields and enantioselectivities. Reaction conditions play a vital role in influencing the reaction kinetics and the evolution of the transition state. For example, previously reported computational and experimental studies have shown that double hydrogen-bond interactions with the carbonyl oxygen increase the rate of activation of the electrophile activation and the rigidity of the transition state rather than a single hydrogen-bond.[28–33] Moreover such interactions have the ability to cause an increase in strength and directionality, enhance enantioselectivity and in addition contribute to the effectiveness of the catalyst. In non-aqueous solvents organocatalysts use specific hydrogen bonding, charge-charge and dipole-charge interactions to align the catalyst to the substrate. However in water, organocatalysts utilizes hydrophobic interactions because the high dielectric constant of water screens the charge-to-charge interaction and water molecules compete for hydrogen bonding.[32,34–36] Water molecules are also thought to bring the organic reagents close to each other, leading to hydrophobic hydration.[34,35]

The development of environmentally friendly organic reactions is an important aspect in synthetic chemistry. The use of water ‘as solvent’ or co-solvent in chemical reactions has attracted a lot of attention due to its potential and advantages such as safety, low cost,

availability, efficiency, reactivity when compared to common organic solvents, and lastly its impact on the environment that avoids issues of pollution which are inherent with common organic solvents.[5,7,33,37,38] However it is worth noting that the use of excess amount of water in reactions often results in low yield and poor selectivity, while a small addition of water can accelerate the reaction and improves selectivity.[5,7,10,38–43]

The use of water in aldol reactions is also propose to alters the catalyst activity by interrupting ionic interactions and hydrogen bonds which influences stabilization of transition state of the reaction. Most of the work reported involving the use of water 'as a solvent or in excess as co-solvent with other organic solvents in organocatalyst has focused mostly on proline or substituted proline,[18,19,22,23] and short peptides (di-or tri-peptides)[5,10,40,46] (**Scheme 4-3**) and polypeptides catalysts.[47] In this current study we anticipate that the designed peptides can be employed in different organic solvents in a presence of small amount of water due to their solubility. The peptides completely dissolve in 60% water/40% acetonitrile, therefore, the effect of water (addition) on the reaction medium and its influence on the catalyst will be investigated.



Scheme 4- 3: Water as solvent in organocatalytic asymmetric aldol reactions, (A) Hayashi's proline catalyzed aldehyde–ketone aldol reaction in water,[23] (B) Rahman's small proline-based dipeptide in aqueous medium.[5]

4.4 Results and discussions

4.4.1 Screening of selected peptides for aldol reaction catalytic activity

The synthesized peptide catalysts described in Chapter 2, were tested for aldol reaction catalytic activity. As already mentioned in Chapter 2 some peptides were obtained in low yields and hence they could not be evaluated for catalytic activity. The list of peptides that were tested are shown in (**Figure 4-1**). A table detailing all the amino acid sequences and the variations of the peptides listed has already been provided in Section 2.4.2.2, **Table 2-1**.

In our first screening reaction, linear aldehydes were chosen for their simple structures that dissolve in water; and in addition; they were also selected based on the discussion provided Section 2. 9, regarding the acceptable reaction conditions and substrate tolerance of FBPA enzymes. Acetone was selected as a solvent since short peptides may perform significantly better in the aldol reaction medium when acetone (ketone) is used as co-solvent, as reported by Tang *et al*,[41] and Wennemers *et al*.[48] Furthermore, the solvents system (reaction medium) was selected based on the possibility of recovering the catalyst at the end of the reaction. Hence the first reaction utilized acetone as the solvent of choice, with linear aliphatic aldehydes as the reactant.

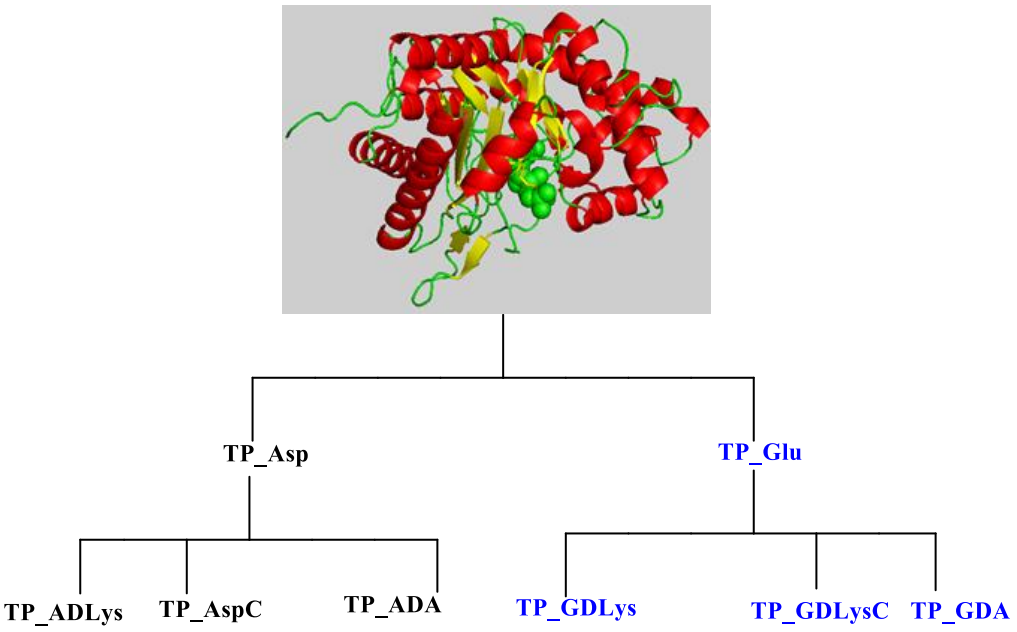
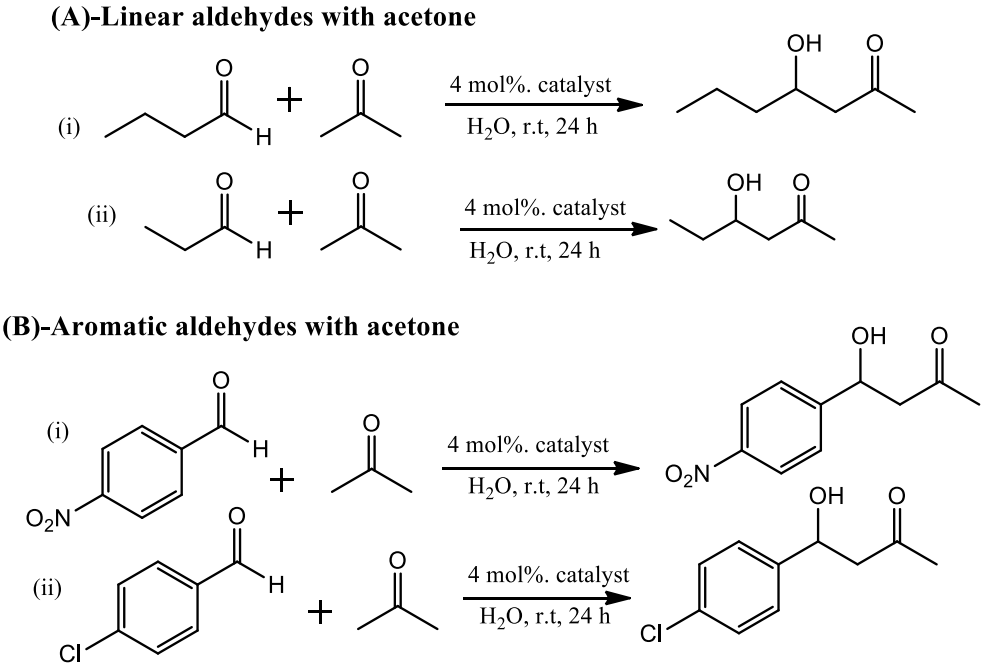


Figure 4- 1: A series of selected peptides screened for aldol reaction catalytic activity.

The test reactions were performed using 3 equivalences of acetone in water and 4 mol% of peptides (**Scheme 4-4**), and in addition we had some control experiments, where the same reactions conditions were used but without the peptide.



Scheme 4- 4: Aldol test reactions for selected peptides, using (A) linear aldehydes and (B) aromatic aldehydes with acetone.

The reaction's progress was monitored by LC-MS, in intervals of 30 min, 3 h, 7 h and 24 h. It was observed that aliphatic aldehydes were poor substrates as the formation of the product only occurred after 7 hours, whereas with aromatic aldehydes the product had already formed within the first 3 hours (**Figure 4-2**).

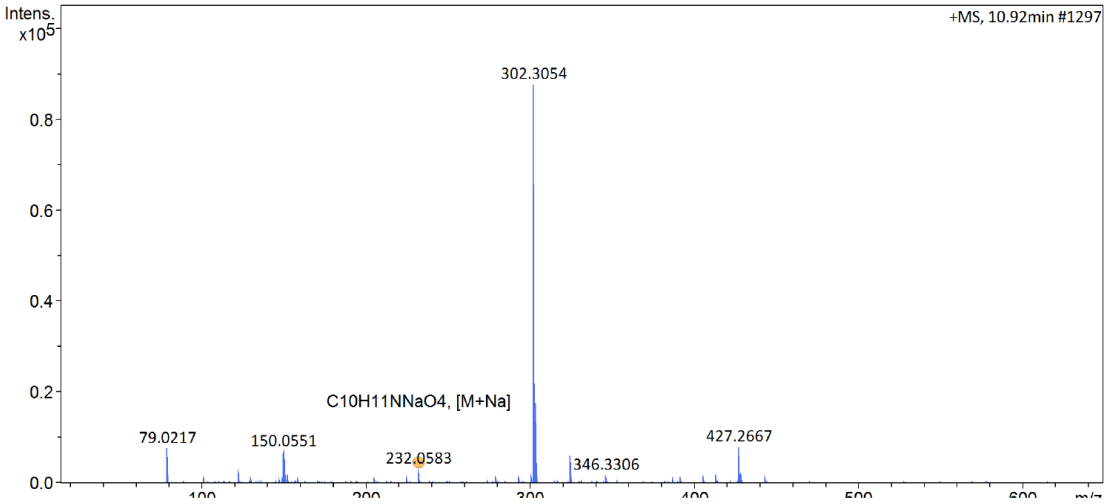


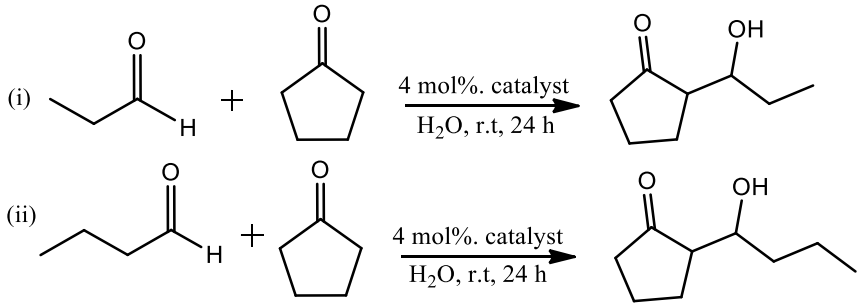
Figure 4- 2: LC-MS chromatograph depicting the formation of **A1** product in 3 hours.

It was astonishing to note that aromatic aldehydes reacted faster than aliphatic aldehydes as this was a different behaviour compared to the natural FBPA enzyme, which favourably accepts aliphatic aldehydes as substrates over aromatics. The aliphatic substrates were also not completely consumed when compared to the aromatics where most of the aldehyde was converted to the product.

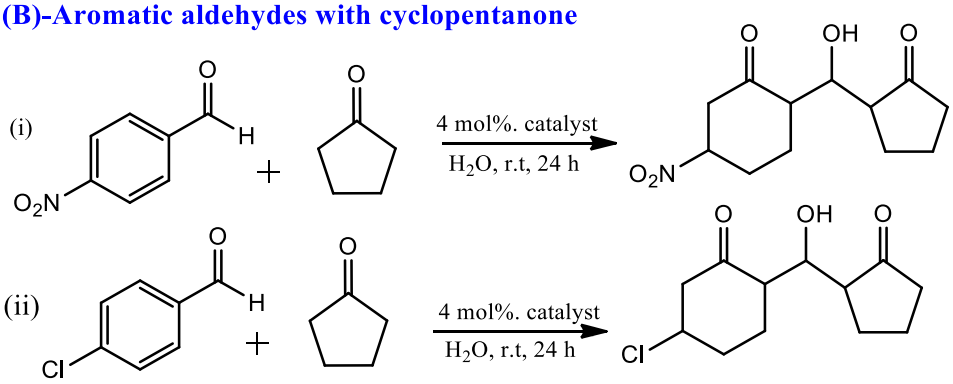
The *para*-nitro-substituted aldehyde showed better conversion when compared to *para*-chloro-substituted aldehydes. There was no formation of product in the control experiments within 24 hours, thus confirming the catalytic activity of the peptides. It is worth mentioning that the peptide reactions did not go to completion in 24 hours, but however 24 hours was just chosen as the end for the initial screening. TLC was also used to monitor the qualitative and semi-qualitative formation of the product.

In the next stage of aldol screening, the activity of cyclic ketones with both aliphatic and aromatic aldehydes **Scheme 4-5** below, was investigated. The control experiments were also conducted, where the reactions were performed in the absence of the peptide. The reactions (both the control experiments and peptide reactions) were also monitored in time intervals of 30 minutes, 3, 7 and 24 hours respectively while stirring in the orbital shaker. The formation of the product was only observed after 7 hours for the aliphatic aldehydes. We propose that this catalytic system may not be compatible with linear aliphatic aldehydes as they showed slower reactivity with both cyclopentanone and cyclohexanone. The obtained results were also in agreement with what is reported in literature.[49] There was also no remarkable differences between the two aliphatic aldehydes (propanal and butyraldehyde). This outcome could also suggest that the reaction conditions needed to be modified by increasing both the reaction time and the amount of catalyst to improve the reactivity.

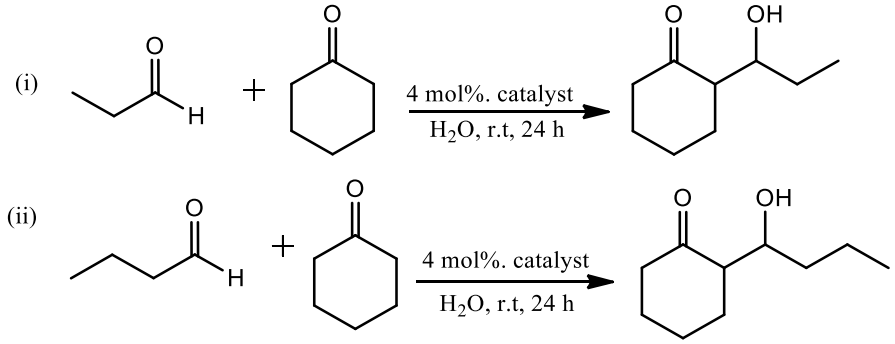
(A)-Linear aldehydes with cyclopentanone



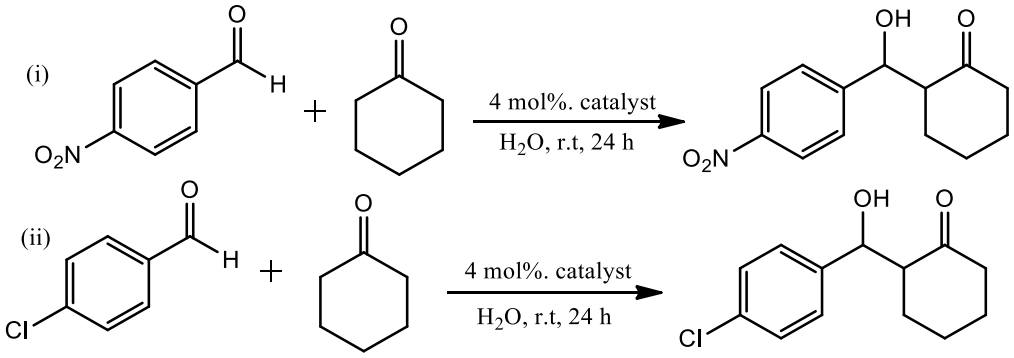
(B)-Aromatic aldehydes with cyclopentanone



(C)-Linear aldehydes with cyclohexanone



(D)-Aromatic aldehydes with cyclohexanone



Scheme 4- 5: Aldol test reaction for selected peptides, using (A) linear aldehydes with cyclopentanone and (B) aromatic aldehydes cyclopentanone, (C) linear aldehydes with cyclohexanone, (D) aromatic aldehydes with cyclohexanone.

Aromatic aldehydes have been widely used in many reports,[10] pertaining to aldol reactions, especially those containing electron withdrawing groups.[4,39,50–52] An electron withdrawing substituent on aromatic aldehydes accelerates the rate of formation of the enamine intermediate unlike electron donating groups or unsubstituted aromatic aldehydes.[41,51,52] They showed moderate results with cyclopentanone and cyclohexanone and rapid formation of products within the first 30 minutes for the reaction between the aromatic aldehyde and cyclic ketone, **Figure 4-3**.

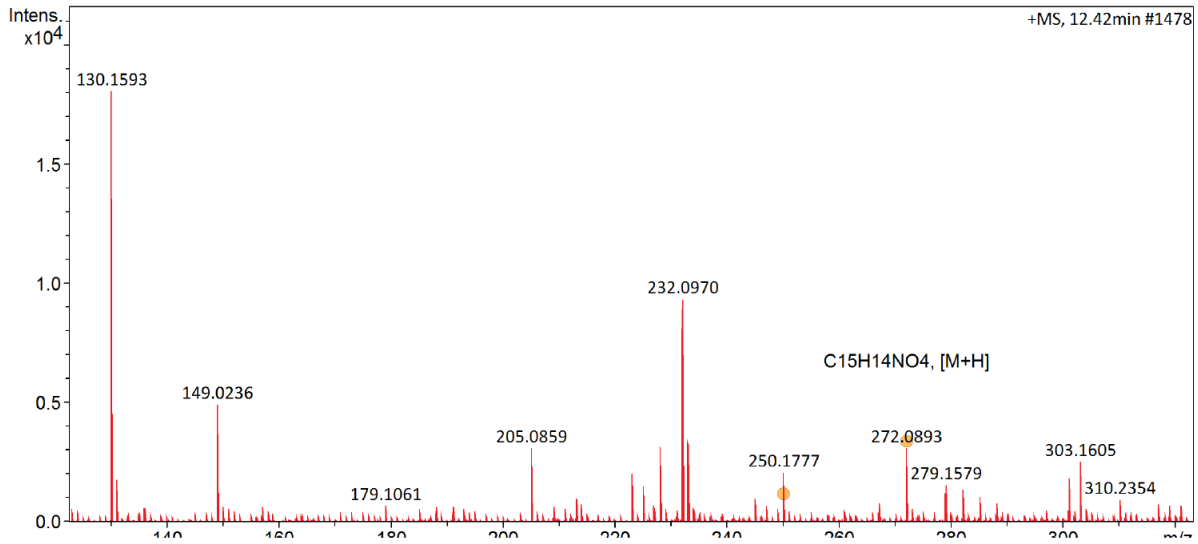


Figure 4- 3: LC-MS chromatograph depicting the formation of **A2** product in 30 minutes.

Cyclopentanone and cyclohexanone are known as good acceptable donors for the aldol reaction[41,45,53] and, cyclohexanone is used in benchmark reactions for the development of new catalysts in most asymmetric aldol reactions. There was no outstanding difference between the two reactions in Scheme 4-3 **(B)** and **(D)**, although some reports,[54] suggest that cyclohexanone gives better activity than cyclopentanone. It is noteworthy to point out that in all the control experiments, there was no formation of aldol product within 24 hours.

4.4.2 Concluding remarks

All selected peptides were successfully screened for aldol reaction catalytic activity and interestingly, they all showed positive results. The aldol reaction between aliphatic aldehyde and acyclic ketone proceeded at a slower rate, while that of aromatic aldehydes and acetone proceeded at a moderate rate. This observation suggests that aliphatic aldehydes were poor or unfavourable substrates and therefore needed longer reaction time and more catalyst. The peptide catalysts are more active towards both cyclic aldehyde and ketones. The effect of water

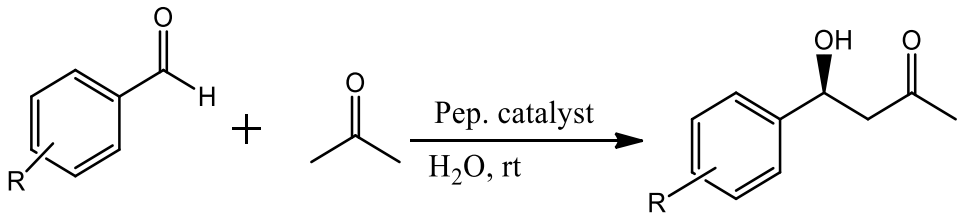
on the yields and enantioselectivity at this point cannot be determined since the product was not isolated and will be discussed in the next section.

4.5 Optimization of Aldol reaction conditions

4.5.1 Scope of reaction and substrate

Based on the results obtained from the above, the catalytic activity was further explored by varying the reaction conditions for reaction between acetone and *p*-nitrobenzaldehyde **Table 4-1** (Entries 1-9).

Table 4- 1: Peptide catalyzed aldol reactions between acetone and substituted aromatic aldehydes[a]



Entry	Catalyst	R	Solvent	Time (h)	Yield (%)[b]	ee (%)[c]
1	TP_Asp	4-NO_2	Acetone/H_2O	48	16	70
2		2-NO_2	Acetone/H_2O	48	13	12
3	TP_ADLys	4-NO_2	Acetone/H_2O	48	15	82
4		2-NO_2	Acetone/H_2O	48	10	7
5		4-Cl_4	Acetone/H_2O	48	14	85
6[d]	TP_Asp	4-NO_2	DMSO/H_2O	72	Trace	-
7[d]		2-NO_2	DMSO/H_2O	72	Trace	-
8[d]	TP_ADLys	4-NO_2	DMSO/H_2O	72	Trace	-
9[d]		2-NO_2	DMSO/H_2O	72	Trace	-

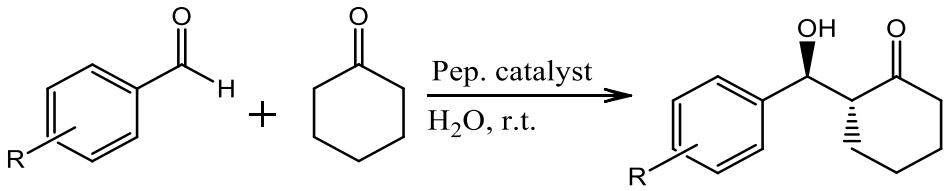
[a] The reaction was performed using aldehyde (0.25 mmol), pep.catalyst (4 mol %), dissolved in 0.75 mL of 3:1 acetone/water (molar ratio 30:42; acetone/water), at r.t. for 48 h. [b] Isolated yield. [c] ee values determined by chiral-phase HPLC analysis. [d] reaction was performed using acetone (0.628 mmol, 50 µL), 0.75 mL DMSO/H2O (0.5173 mL DMSO, 0.237 mL water).

From the obtained results it can be seen that when acetone/water was used the conversions were quite low (entries 1-5), despite increasing the reaction time to 48 hours. This outcome demonstrates the negative effect of water which might be in competition with the donor acetone in hydrogen bonding. Despite low yields when reactions were performed in acetone and *p*-nitrobenzaldehyde, good selectivity with the ee of 70 and 81% (entries 1 and 3) were obtained. Similar results were reported in literature.[39,52] The aldol reactions proceeded slowly with low yields and good ee's when performed in acetone (up to 20% yield and 65% ee was obtained by Córdova *et al*).[39]

Poor enantioselectivities (up 12%) were observed when *o*-nitrobenzaldehyde was used (entries 2, 4), however there was a significant improvement in ee of up 85%, when *p*-chlorobenzaldehyde was utilized (entry 5). In another attempt to improve the reaction conditions while using the same catalyst, acetone/water was replaced with DMSO/H_2O. Unfortunately, only traces of the product were detected on the TLC (entries 6-7) and increasing the reaction time did not improve the yield. Although DMSO is commonly used for most of the studies reported on aldol reactions,[42,43,53,55] some studies have shown that acyclic ketones may be poor substrates in DMSO.[55,56] At this moment the reaction mechanism is unclear and therefore the transition state is not fully understood for a plausible hypothesis to be suggested.

In the preliminary investigation (Section 4.4.1) it was observed that aldol reactions with acetone proceeded at a slower rate when compared to cyclic ketones. Thus the reaction with cyclic ketones were optimized. Cyclic ketones generally have low solubility in water, and therefore their reactions are normally performed in a biphasic water/ketone system or heterogenous mixtures comprising a water emulsion or a suspension.[45,56–58] The experimental results in **Table 4-2** below, indicate that a large volume of water (entries 1-3), is not favourable for the reaction, as the mixture becomes immiscible and this results in the increase in the reaction time and decrease in the overall catalytic activity of the peptides.[58]

Table 4- 2: Aldol reaction between cyclohexanone and various aromatic aldehydes catalyzed by peptides[a]



Entry	Catalyst	R	Time (h)	Yield (%)[b]	ee (%)[c]	dr (anti:syn)[d]
1[e]	TP_ADLys	4-NO_4	48	NR	-	-
2[e]		2-NO_2	48	NR	-	-
3[e]		4-Cl	48	NR	-	-
4	TP_Asp	4-NO_2	48	17	7	43:57
5		2-NO_2	48	11	9	47:53
6		4-Cl	48	Trace	-	-
7		4-Br	48	Trace	-	-
8		4-H	48	Trace	-	-
9	TP_ADLys	4-NO_2	48	15	5	49:51
10		2-NO_2	48	13	14	22:78
11		4-Cl	48	Trace	-	-
12		4-Br	48	Trace	-	-
13		4-H	48	Trace	-	-

[a]The reaction was performed using aldehyde (0.157 mmol), pep. catalyst (4 mol%), 0.45 mL of solvent, ketone/water 20:1 (v/v) for 48 h at r.t. [b] Isolated yield. [c] ee values determined by chiral-phase HPLC analysis.[d] Determined by ^{1}H NMR analysis of the crude product. [e] the reaction was performed in ketone/water 10:1 (v/v).

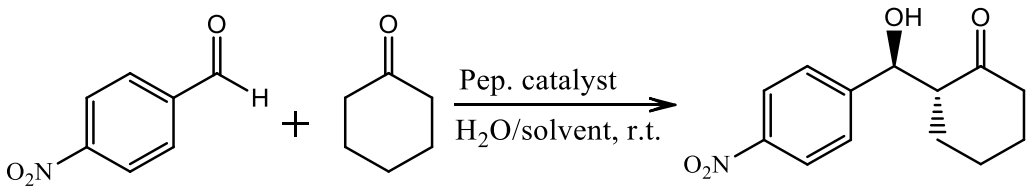
Another attempt was made with reduced amount of water and a positive outcome resulted from this modification (entries 4 and 5). The beneficial influence of reducing water, allows the dissolution of cyclohexanone consequently creating monophasic system and a homogenous aldol reaction.[45,58] In addition, this also proved that the partition coefficient has somewhat has an influence in establishing the optimal reaction conditions. Even though this attempt gave considerably better results, the products were obtained in low yields with poor selectivities for both aldehydes. Cheng and Luo did similar work whereby the ketone was used in excess as co-solvent and obtained low selectivities. They further revealed that an acid additive is needed to attain good stereoselectivity.[49] However this hypothesis was not examined in this study, but

can be considered for future studies. Furthermore, it was also observed that aromatic aldehydes bearing a halogen group (entries 6-7 and 11-12) required longer reaction time or more catalyst loading as only trace amounts of the product were observed for both peptides. Similar results were also obtained in literature,[7,56] where the halogenated aldehydes yielded no reaction or required longer reaction time. Between the two nitrobenzaldehydes (*para*-nitrobenzaldehyde and *ortho*-nitrobenzaldehyde), there was an insignificant difference in their yields, but it can be seen that *p*-nitrobenzaldehyde is slightly higher than *o*-nitrobenzaldehyde. This suggests that due to steric hindrance, the nitro- group which is located at the ortho position might be unfavourable for the nucleophilic attack.[59] There was also no significant difference between catalytic activity of the two peptides catalyst, due to the fact the yields or selectivity are within the same range.

4.4.2 Effect of solvents

The effect of various organic solvents was examined with *p*-nitrobenzaldehyde and cyclohexanone as substrates. It can be seen from the results, that polar aprotic solvents such as chloroform ($CHCl_3$) and acetonitrile (MeCN) were not suitable for the peptide catalyzed aldol reactions (**Table 4-3**, entries 1, 2,10 and 11) as no reaction occurred even after 96 hours.

Table 4- 3: Aldol reaction of cyclohexanone and *p*-nitrobenzaldehyde catalyzed by 4 mol% peptide catalysts in different solvents [a]



Entry	Catalyst	Solvent	Time (h)	Yield (%) [b]	ee (%) [c]	dr (anti:syn) [d]
1	TP_ADLys	MeCN/H_2O	96	NR	-	-
2		$CHCl_3$/H_2O	96	NR	-	-
3		IPA/H_2O	72	<10	-	-
4		DMSO	72	12	5	48:52
5		DMF	96	NR	-	
6		DMSO/H_2O	72	16	14	57:43
7		DMF/H_2O	96	<9[e]	-	-
8		H_2O/DMSO	72	<8[e]	-	-
9		Brine	72	13	39	31:69
10	TP_Asp	MeCN/H_2O	96	NR	-	-
11		$CHCl_3$/H_2O	96	NR	-	-
12		IPA/H_2O	72	<9[e]	-	-
13		DMSO	72	11	8	45:55
14		DMF	96	NR	-	
15		DMSO/H_2O	72	13	20	63:37
16		DMF/H_2O	96	Trace	-	-
17		H_2O/DMSO	72	<7[e]	-	-
18		Brine	72	14	12	37:63

[a] The reaction was performed using *p*-nitrobenzaldehyde (0.157 mmol, 24 mg), cyclohexanone (0.628 mmol, 70 µL), pep .catalyst (4 mol%) and dissolved in 0.75 mL (0.5173 mL solvent and 0.237 mL water) at r.t [b] Isolated yield. [c] ee values determined by chiral-phase HPLC analysis. [d] Determined by ^{1}H NMR analysis of the crude product [e] Estimated by TLC.

Some enzyme catalysts are sensitive towards several organic solvents, in such a way that they are more unstable in polar water miscible-solvents than in water-immiscible solvents.[60,61] For entries 1, 2, 10 , and 11 the outcome is attributed to low solubility of the peptide in $CHCl_3$, causing a decrease in the reaction rate, whereas with acetonitrile the decrease could be caused by weak hydrogen bonds that it forms with both the peptide and substrate. The reaction in polar wet protic solvent, particularly isopropanol (IPA), proceeded at a slow rate as only trace amounts of the product was observed after several days (entries 3 and 12). This outcome may

suggest longer reaction times are required for the formation of the product. The aforementioned solvents were selected in this study because they are readily available in the lab and they have been reported in literature[4,52] to yield aldol products with high yields and good selectivity. Although high-boiling organic solvents such as DMSO and DMF are commonly used in aldol reactions studies they are often considered problematic for large-scale synthesis due to inconvenient work-up, solvent removal and recovery steps.[51] The influence of these solvents on a small-scale reaction synthesis were then investigated.

As shown in **Table 4-3**, (entries 5 and 14) when plain DMF was used there was no reaction even after 96 hours, however when a small amount of water was added (entries 7 and 16) a trace amount of the product was observed. When plain DMSO was used (entries 4 and 13), only a small amount of product was isolated. This presumably due to high viscosity of DMSO or even DMF, it might hinder free efficient interaction between the peptide and substrates. Although the use of DMSO in proline-catalyzed reactions often yields better results,[59,62,63] other reports suggest no reaction or longer reaction time when anhydrous DMSO is applied.[56] Other authors also reported on the aldol reaction between *p*-nitrobenzaldehyde and cyclohexanone performed in anhydrous/wet DMSO and obtained good yields and high selectivities (up to >80% yields and ee).[7,39,47,59] Such findings would imply the mode of activity of our peptide in this system is quite different. Moreover, it can be noted that some promising results were observed when DMSO/H_2O was used (entries 6 and 15) with the yields of 16 and 15%. It was also intriguing to observe a considerable improvement in the ee, to 14 and 20% respectively and moderate diastereoselectivities. These observations also illustrated that the addition of water to peptide promoted aldol reaction has some effect on influencing both the yields and stereoselectivities. The presence of small amount of water is proposed to influence the hydrogen bonding, which then alters the reaction mechanism and stereochemistry.[39,64] Certain enzyme catalysts are reported to be less reactive in anhydrous solvents than in water due to constrained conformational stability.[60] For this reason, water is essential in binding to the surface of the enzyme, to exhibit both conformational flexibility and enzymatic activity. It is also believed that water affects the hydrogen bonding of the acidic moiety and the backbone of the peptide transition state, which facilitate highly ordered transition states in aqueous conditions.[42,60] Therefore, we postulate that the role of water in this reaction medium, is of significant importance in influencing the reaction rate, and therefore improving the hydrogen bonding for the stabilization of the transition state and ground state of the substrate.

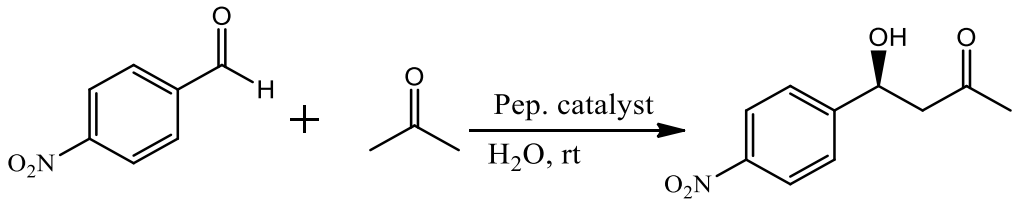
The reactions were then carried out using higher equivalence of water in DMSO (entries 8 and 17). The reaction still proceeded slowly, causing a decrease in both the reaction rate and yields, as only trace amounts of the product was obtained. Brine is often applied as an alternative to milliQ water when investigating the aqueous environment for reaction optimizations, and to also explore tolerance of catalyst towards the complex aqueous environment. It is reported that brine influences the reaction to proceed faster than in concentrated organic phase due to salting-out-effect.[65–67] Gryko and co-workers also demonstrated that the use of NaCl can accelerate the organocatalyzed aldol reaction in water by accelerating the aggregation of the organic material in concentrated hydrophobic pockets.[68] In an attempt to examine these hypotheses, the reactions were performed in brine solution (entries 9 and 18). It was observed that a brine solution is able to facilitate the aldol reaction, as yields of 13 and 14% were observed after 72 hours as well as an improvement in both ee% and diastereoselectivity (when employing TP_ADLys peptide, entry 9).

In summary, it was proven that the selected peptide catalysts are able to catalyze aldol reactions in some of the commonly used organic solvents and ketones. Both ketones (acetone and cyclohexanone) seem to be the most favourable medium for faster reactions than other organic solvents. The direct aldol reaction between acetone and *p*-nitrobenzaldehyde yielded no results in organic solvents. In addition, reactions performed in acetone have longer reaction times with good enantioselectivies. Halogenated aromatic aldehydes and unsubstituted benzaldehyde could not be successfully employed as substrates when reacted with cyclohexanone as they afforded long reaction times with only traces of the product observed. Moreover, these studies demonstrated that the reactions of aromatic aldehydes bearing electron-withdrawing substituent were acceptable as they afforded improved yields with moderate selectivities. Polar aprotic solvents (DMF and MeCN) were inappropriate medium for aldol reactions between cyclohexanone and substituted aromatic aldehydes. The addition of water to the reaction medium using either ketone or organic solvents proved to have little effect on the yields and selectivities. In the next set of experiments for further optimization of reaction to improve the yields, focus was given to the reactions with satisfactory results in Table **4-4**. The catalyst loading was increased to 8 mol%, while keeping the solvent mixture and reaction conditions the same.

4.4.3 The Effect of catalyst concentration (catalyst loading) on the aldol reaction

The first reaction between *p*-nitrobenzaldehyde and acetone was performed with an 8 mol% peptide catalyst (**Table 4-4**, entries 1 and 2). As mentioned earlier a reaction between by acetone and *p*-nitrobenzaldehyde forms aldol adducts with high enantioselectivities but the reaction times are long while the yields are low. Having establish acetone as the best solvent medium for this reaction, we then investigated the influence of catalyst loading so as to improve the results in **Table 4-1**. Unfortunately, increasing the catalyst did not improve the yields, even after the reaction was left stirring for over 48 hours.

Table 4- 4: Aldol reaction between acetone and cyclohexanone using 8 mol% peptide catalyst[a]



Entry	Catalyst	Solvent	Time (h)	Yield (%)[b]	ee (%)[c]
1	TP_ADLys	acetone	48	15	93
2	TP_Asp	acetone	48	13	91

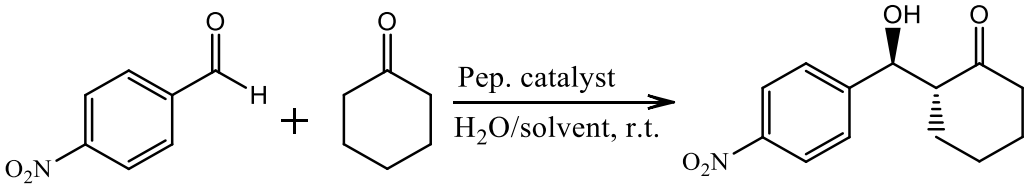
[a] The reaction was performed using *p*-nitrobenzaldehyde (0.157 mmol, 24 mg) and pep. catalyst (8 mol %) and dissolved in 0.75 mL of 3:1 acetone/water (molar ratio 30:42; acetone/ water), and the reaction mixture was stirred for 24 hrs at r.t. [b] Isolated yield. [c] ee values determined by chiral-phase HPLC analysis.

The reaction yielded products with good enantioselectivities (up to 93%) but there was no improvements on the reaction times. As mentioned in Section 4.5.1, there is a lot of similar results reported in literature where acetone is used in excess or as solvent, and the reaction affords low yields with good or excellent enationatioselectives.[39,56,69–74] Despite much work done on this reaction, there is not much explanation or emphasis provided for this observation, even when large catalyst loading of up to 30 mol% was used; there was still longer reaction times with low yields.

Subsequently, in another attempt to improve the results in **Table 4-2** and **4-3**, we then optimized the reaction conditions to investigate the influence of catalyst concentration on the aldol reaction between *p*-nitrobenzaldehyde and cyclohexanone. The reactions were carried out

in a few selected solvents which afforded better results in **Table 4-3** and the results are summarized in **Table 4-5**.

Table 4- 5: Aldol reaction of cyclohexanone and *p*-nitrobenzaldehyde catalyzed by 8 mol% peptide catalyst in different solvents[a]



Entry	Catalyst	Solvent	Time (h)	Yield (%)[b]	ee (%)[c]	dr(anti:syn)[d]
1[e]	TP_Asp	Ketone	48	42	20	38:62
2		DMSO	72	21	8	54:44
3		DMSO/H_2O	72	25	16	65:35
4		Brine	72	24	37	43:57
5[e]	TP_ADLys	Ketone	48	40	6	59:41
6		DMSO	72	20	6	58:42
7		DMSO/H_2O	72	27	31	64:36
8		Brine	72	23	65	64:36
9[f]		Buffer	72	38	80	57:43
10	Plain (buffer)	Buffer	120	Trace	-	-

[a] The reaction was performed using *p*-nitrobenzaldehyde (0.157 mmol, 24 mg), cyclohexanone (0.628 mmol, 70 µL), pep. catalyst (8 mol%), and dissolved in 0.75 mL (0.5173 mL solvent and 0.237 mL water) at r.t. [b] Isolated yield. [c] ee values were determined by chiral-phase HPLC analysis.[d] Determined by ^{1}H NMR analysis of the crude product. [e] The reaction was performed in ketone(cyclohexanone)/water 20:1 (v/v). [f] The reaction was performed in phosphate buffer (pH 8.0)

Compared to the results obtained with 4 mol%; some noticeable increase in the yields was observed when cyclohexanone with small amount of water was used (entries 1 and 5), yields of 40 and 42% for both peptide catalyst in 48 hours were obtained. The reactions further afforded much improved enantioselectivity and diastereoselectivity for the TP_Asp catalyst, whereas with TP_ADLys an ee of 6% was obtained with moderate diastereoselectivity. There were some notable results in entries 2, 6, when plain DMSO was used, although the reaction still proceeded slowly it gave moderate yields. In addition, when small amount of water was added to DMSO (entries 3 and 7), there was a significant improvement of the yields (up to 31% ee) and diastereoselectivity (65:45). A further increase in the yields was observed when the

reaction was performed in a brine solution (entries 4 and 8), with quite reasonable ee (up to 65%) and dr (64:36) values were obtained.

The effect of the pH was also investigated. At neutral pH both peptides (TP_Asp and TP_ADLys) have a charge of 2.9 and the calculated isoelectric point ($pI_{calculated}$) which is the pH where the net charge of the peptide is zero found to be 9.6 when determined using a peptide calculator.[†]

It is also understood that most enzymatic catalytic reactions are dependent upon the pH of the reaction medium to function efficiently and for obtaining optimal enantioselectivity.[75–77] Based on this, we then attempted the aldol reaction in buffered aqueous media, using 100mM phosphate buffer at pH of 8.0. Although the buffering capacity of the phosphate buffer is reported to be maximal near 7 and low around 9,[78] some reasonable results were observed, a 38% conversion, a stereoselectivity (ee) of 80% and a diastereoselectivity of 57:43. High stereoselectivity has been previously reported for biocatalysts facilitating asymmetric aldol reactions in buffer solutions (pH=4.0-8.0).[77] A pH of 8 was selected because studies have shown that for the best results the pH must be kept above the peptide's pI for better stability. In this study the use of a buffer solutions beyond a pH of 9 is restricted because the aldol reaction may become base-catalyzed around this pH.[79,80] Thus a pH of 8 was selected as a compromise

In order to ascertain the influence of the buffer, a reaction with the buffer in the absence of the peptide (entry 10) was conducted and it only showed trace amount of the product after 120 hours. Thus the activity observed (entry 9) could be attributed to the structural conformation assumed by the peptide in the buffer. According to the results obtained in Chapter 3 the peptide assumed a random coil structure in a buffered solution and this may result in an efficient interaction with the substrate and selectivity. Lower pHs were not investigated because the lysine residue will be protonated and less nucleophilic. The low yield and longer reaction time observed for entry 9 can be accounted for by poor dissolution of the substrates, since the reaction was only carried out in an aqueous buffer.

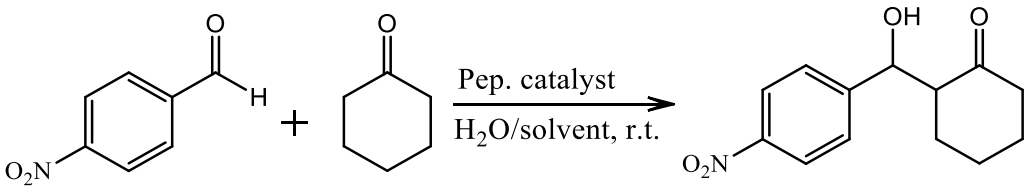
In summary, these findings prove that catalyst loading plays a vital role in influencing the aldol reaction yields and selectivities. Thus, the concentration of 8 mol% of the peptide will be chosen as the optimum for further investigation.

[†] PepCalc.com - Peptide property calculator

4.4.5 Catalyst reusability studies

The catalyst was easily recovered at the end of each reaction, through precipitation by adding diethyl ether (Et_2O) to the combined water layers. The catalyst recovery studies were performed for the TP_ADLys peptide selected aldol reactions. The summary of the results, using *p*-nitrobenzaldehyde and cyclohexanone as substrates are summarized in **Table 4-6**. The reactions were similar to the ones reported in **Table 4-5** (entries 1-5 and 9).

Table 4- 6: Recovery and reuse of catalyst TP_ADLys in aldol reaction[a]



Entry	Catalyst	Solvent	Time (h)	Yield (%)[b]	ee (%)[c]	dr (anti:syn)[d]
1	TP_DLys	DMSO	72	Trace	-	-
2		DMSO/H_2O	72	Trace	-	-
3		Brine	72	Trace	-	-
4[e]		Ketone	72	Trace	-	-
5[f]		Buffer	72	13	81	61:39

[a] The reaction was performed using *p*-nitrobenzaldehyde (0.157 mmol, 24 mg), cyclohexanone (0.628 mmol, 70 µL), and dissolved in 0.75 mL (0.5173 mL DMSO and 0.237 mL water) at r.t .[b] Isolated yield. [c] ee values determined by chiral-phase HPLC analysis.[d] Determined by 1H NMR analysis of the crude product [e] The reaction was performed in ketone/water 20:1 (v/v).[f] The reaction was performed in phosphate buffer(pH 8.0)

The results indicate that the reusability of catalyst was unsatisfactory in DMSO, brine or ketone, as only a trace amount of the product was observed after 72 hours (entries 1-2 and 3-4). This suggests the peptide cannot be efficiently reused as there is loss of catalytic activity. However, when the reaction was performed in a buffered solution, promising results were observed as yield of 13% was obtained (entry 5), and as already mentioned above, the buffer at this pH might have an effect in influencing the favourable structural conformation. Despite a longer reaction time and low yield when compared to the 38% that was obtained from the first use (**Table 4-5**, entry 9), the reaction was still achieved in high selectivities of 81% ee and dr of 81:19. There was trace amount of the product for the control experiment (entry 6) performed in a buffered solution in the absence of the peptide.

4. 5 Concluding remarks

Peptides that mimic the fructose-1,6-phosphate aldolase can catalyze the direct aldol reaction and afford moderate yields and selectivity. Aldol reactions between acetone and aromatic aldehydes afforded low yields of the product (up to 16%), excellent enantioselectivity (up 93%) and an increase in the catalyst loading did not significantly improve the yield. Aldol reactions between cyclohexanone and aromatic aldehydes in organic solvents exhibited poor catalytic activity (25% yield), enantioselectivity (up to 31% ee) and diastereoselectivity (64/36). The reaction between aromatic aldehydes bearing electron-withdrawing groups in ketone as a solvent afforded moderate yields (up to 42%), poor enantioselectivity (up to 20%) and moderate diastereoselectivity (up to 59/41).

Hence, it can be concluded that aromatic aldehydes bearing a halogen group are inappropriate substrates for the peptide aldol catalyzed reaction while nitro substituted aromatic aldehydes are acceptable substrates for the peptide-promoted aldol reaction.

The results clearly indicate that the solvent medium has an influence on the catalytic activity. The addition of small amount of water accelerated the reaction rate which improved the yields, thus suggesting that the water is compatible with the peptide catalysts. This also shows the influence of water on the reaction it stabilizes the transition state through the formation of hydrogen bonds with the catalyst. The aldol reaction promoted by brine solution, proved that the salting out effect can accelerate the reaction rate and improve the yield, enantioselectivity and diastereoselectivity. The 100 mM phosphate buffer (pH of 8.0) solution yielded products with good enantioselectivity and this was attributed to the structural conformation that the peptide adopts in the solution.

There are strategies as discussed in Section 1.8.1 that can improve catalytic activity and enhance the conformation entropy of short and polypeptides. Hence, in an effort to further improve on the yields, the peptides were immobilized on gold nanoparticles and the results are reported in the next chapter.

4. 9 References

(1) Bhandari, M.; Raj, S. Practical Approach to Green Chemistry. *Int. J. Pharm. Pharm. Sci.* **2017**, *9* (4).

(2) Blackmond, D. G.; Armstrong, A.; Coombe, V.; Wells, A. Water in Organocatalytic Processes : Debunking the Myths. *Angew. Chemie - Int. Ed.* **2007**, *46*, 3798–3800. https://doi.org/10.1002/anie.200604952.

(3) Wieczorek, R.; Adamala, K.; Gasperi, T.; Polticelli, F.; Stano, P. Small and Random Peptides: An Unexplored Reservoir of Potentially Functional Primitive Organocatalysts. the Case of Seryl-Histidine. *Life* **2017**, *7* (2), 1–24. https://doi.org/10.3390/life7020019.

(4) Yi, Y.; Zhi, G.; Yanhong, H. E. Biocatalytic Direct Asymmetric Aldol Reaction Using Proteinase from Aspergillus Melleus. *Sci. China Chem.* **2013**, *56* (7), 939–944. https://doi.org/10.1007/s11426-013-4874-0.

(5) Bayat, S.; Bakar, A.; Emilia, S.; Malek, A.; Yousefi, S. Design of a Simple Organocatalysts for Asymmetric Direct Aldol Reactions in Aqueous Medium. *Catal. Letters* **2015**, *145* (9), 1750–1755. https://doi.org/10.1007/s10562-015-1583-7.

(6) Bayat, S.; Abd, E.; Yahaya, N. M.; Bakar, A.; Ario, B.; Basyaruddin, M.; Rahman, A. Asymmetric Aldol Reactions Catalyzed by the Promiscuous Aldo – Ketoreductase Enzyme. *Tetrahedron Lett.* **2014**, *55*, 6303–6306. https://doi.org/10.1016/j.tetlet.2014.09.012.

(7) Jiang, Z.; Yang, H.; Han, X.; Luo, J.; Wong, M. W.; Lu, Y. Direct Asymmetric Aldol Reactions between Aldehydes and Ketones Catalyzed by L-Tryptophan in the Presence of Water. *Org. Biomol. Chem.* **2010**, *8* (6), 1368–1377. https://doi.org/10.1039/b921460g.

(8) Ramo, D. J.; Yus, M. In the Arena of Enantioselective Synthesis , Titanium Complexes Wear the Laurel Wreath. *Chem. Rev.* **2006**, *106* (6), 2126–2208.

(9) Dalko, P. I.; Moisan, L. In the Golden Age of Organocatalysis. *Angew. Chemie - Int. Ed.* **2004**, *43* (39), 5138–5175. https://doi.org/10.1002/anie.200400650.

(10) Lei, M.; Shi, L.; Li, G.; Chen, S.; Fang, W.; Ge, Z.; Li, R. Dipeptide-Catalyzed Direct Asymmetric Aldol Reactions in the Presence of Water. *Tetrahedron* **2007**, *63*, 7892–

7898. https://doi.org/10.1016/j.tet.2007.05.077.

(11) Li, L.; Xu, L.; Ju, Y.; Lai, G. Asymmetric Direct Aldol Reactions Catalyzed by a Simple Chiral Primary Diamine – Br⊘nsted Acid Catalyst in / on Water. *Synth. Commun.* **2009**, *7911* (39), 764–774. https://doi.org/10.1080/00397910802431131.

(12) Zou, W.; Ibrahem, I.; Dziedzic, P.; Sundén, H.; Córdova, A. Small Peptides as Modular Catalysts for the Direct Asymmetric Aldol Reaction: Ancient Peptides with Aldolase Enzyme Activity. *Chem. Commun.* **2005**, No. 39, 4946. https://doi.org/10.1039/b509920j.

(13) Bednarski, M. D.; Simon, E. S.; Bischofberger, N.; Fessner, W. D.; Kim, M. J.; Lees, W.; Saito, T.; Waldmann, H.; Whitesides, G. M. Rabbit Muscle Aldolase as a Catalyst in Organic Synthesis. *J. Am. Chem. Soc.* **1989**, *111* (2), 627–635. https://doi.org/10.1021/ja00184a034.

(14) Iturrate, L.; í a-Junceda, E. . Dihydroxyacetone Phosphate - Dependent Aldolases in the Core of Multi - Step Processes. In *Multi-Step Enzyme Catalysis: Biotransformations and Chemoenzymatic Synthesis*; 2008; pp 61–81.

(15) Wong, C. -H; Halcomb, R. L.; Ichikawa, Y.; Kajimoto, T. Enzymes in Organic Synthesis: Application to the Problems of Carbohydrate Recognition (Part 1). *Angew. Chemie Int. Ed. English* **1995**, *34* (5), 412–432. https://doi.org/10.1002/anie.199505211.

(16) Brockamp, H. P.; Kula, M. R. Staphylococcus Carnosus Aldolase as Catalyst for Enzymatic Aldol Reactions. *Tetrahedron Lett.* **1990**, *31* (49), 7123–7126. https://doi.org/10.1016/S0040-4039(00)97257-5.

(17) Dean, S. M.; Greenberg, W. A.; Wong, C. H. Recent Advances in Aldolase-Catalyzed Asymmetric Synthesis. *Adv. Synth. Catal.* **2007**, *349* (8–9), 1308–1320. https://doi.org/10.1002/adsc.200700115.

(18) Charmantray, F.; El Blidi, L.; Gefflaut, T.; Hecquet, L.; Bolte, J.; Lemaire, M. Improved Straightforward Chemical Synthesis of Dihydroxyacetone Phosphate through Enzymatic Desymmetrization of 2,2-Dimethoxypropane-1,3-Diol. *J. Org. Chem.* **2004**, *69* (26), 9310–9312.

(19) Wong, C. H.; Whitesides, G. M. Synthesis of Sugars by Aldolase-Catalyzed Condensation Reactions. *J. Org. Chem.* **1983**, *48* (19), 3199–3205.

https://doi.org/10.1021/jo00167a012.

(20) Schoevaart, R.; Van Rantwijk, F.; Sheldon, R. A. Class I Fructose-1,6-Bisphosphate Aldolases as Catalysts for Asymmetric Aldol Reactions. *Tetrahedron Asymmetry* **1999**, *10* (4), 705–711. https://doi.org/10.1016/S0957-4166(99)00044-0.

(21) Schoevaart, R.; Rantwijk, F. Van; Sheldon, R. A. Stereochemistry of Nonnatural Aldol Reactions Catalyzed by DHAP Aldolases. *Biotechnol. Bioeng.* **2000**, *70* (3), 349–352.

(22) Fessner, W. -D; Sinerius, G.; Schneider, A.; Dreyer, M.; Schulz, G. E.; Badia, J.; Aguilar, J. Diastereoselective Enzymatic Aldol Additions: L-Rhamnulose and L-Fuculose 1-Phosphate Aldolases from E. Coli. *Angew. Chemie Int. Ed. English* **1991**, *30* (5), 555–558. https://doi.org/10.1002/anie.199105551.

(23) Wong, C. -H; Halcomb, R. L.; Ichikawa, Y.; Kajimoto, T. Enzymes in Organic Synthesis: Application to the Problems of Carbohydrate Recognition (Part 2). *Angew. Chemie Int. Ed. English* **1995**, *34* (5), 521–546. https://doi.org/10.1002/anie.199505211.

(24) Lees, W. J.; Whitesides, G. M. Diastereoselectivity (Enantioselectivity) of Aldol Condensations Catalyzed by Rabbit Muscle Aldolase at C-2 of RCHOHCHO If R Has an Appropriately Placed Negatively Charged Group. *J. Org. Chem.* **1993**, *58* (7), 1887–1894. https://doi.org/10.1021/jo00059a047.

(25) Liu, K. K. C.; Kajimoto, T.; Chen, L.; Zhong, Z.; Ichikawa, Y.; Wong, C. H. Use of Dihydroxyacetone Phosphate Dependent Aldolases in the Synthesis of Deoxyazasugars. *J. Org. Chem.* **1991**, *56* (22), 6280–6289. https://doi.org/10.1021/jo00022a013.

(26) Peters, J.; Brockamp, H. P.; Minuth, T.; Grothus, M.; Steigel, A.; Kula, M. R.; Elling, L. Combined Chemoenzymatic Synthesis of 20-6-Deoxy-α-L-Sorbofuranosyl-D-Glucose. *Tetrahedron: Asymmetry* **1993**, *4* (6), 1173–1182. https://doi.org/10.1016/S0957-4166(00)80226-8.

(27) Durrwachter, J. R.; Drueckhammer, D. G.; Nozaki, K.; Sweers, H. M.; Wong, C. H. Enzymatic Aldol Condensation/Isomerization as a Route to Unusual Sugar Derivatives. *J. Am. Chem. Soc.* **1986**, *108* (24), 7812–7818. https://doi.org/10.1021/ja00284a053.

(28) Wang, S.; Meng, X.; Zhou, H.; Liu, Y.; Secundo, F.; Liu, Y. Enzyme Stability and Activity in Non-Aqueous Reaction Systems : A Mini Review. *Catalysts* **2016**, *6* (32), 1–16. https://doi.org/10.3390/catal6020032.

(29) Nagy, P. I. Competing Intramolecular vs . Intermolecular Hydrogen Bonds in Solution. *Int. J. Mol. Sci.* **2014**, *15* (1), 19562–19633. https://doi.org/10.3390/ijms151119562.

(30) Knowles, R. R.; Jacobsen, E. N. Attractive Noncovalent Interactions in Asymmetric Catalysis: Links between Enzymes and Small Molecule Catalysts. *Proc. Natl. Acad. Sci. U. S. A.* **2010**, *107* (48), 20678–20685. https://doi.org/10.1073/pnas.1006402107.

(31) Taylor, M. S.; Jacobsen, E. N. Reaction Mechanisms Asymmetric Catalysis by Chiral Hydrogen-Bond Donors Angewandte. *Angew. Chemie - Int. Ed.* **2006**, *45*, 1520–1543. https://doi.org/10.1002/anie.200503132.

(32) Zhao.Q, Lam.Y, Kheirabadi. M, Xu. C, Houk. K.N, S. C. . Hydrophobic Substituent Effects on Proline Catalysis of Aldol Reactions in Water. *J. Org. Chem.* **2013**, *77* (10), 4784–4792. https://doi.org/10.1021/jo300569c.Hydrophobic.

(33) Yorulmaz, T.; Aydogan, F.; Yolacan, C. New and Effective Proline-Based Catalysts for Asymmetric Aldol Reaction in Water. *Synth. Commun.* **2017**, *47* (1), 78–85. https://doi.org/10.1080/00397911.2016.1252988.

(34) Gruttadauria, M.; Giacalone, F.; Noto, R. Water in Stereoselective Organocatalytic Reactions. *Adv. Synth. Catal.* **2009**, *351* (1–2), 33–57. https://doi.org/10.1002/adsc.200800731.

(35) Lindström, U. M. Stereoselective Organic Reactions in Water. *Chem. Rev.* **2002**, *102* (8), 2751–2772. https://doi.org/10.1021/cr010122p.

(36) Raj, M.; Singh, V. K. Organocatalytic Reactions in Water. *Chem. Commun.* **2009**, No. 44, 6687–6703. https://doi.org/10.1039/b910861k.

(37) Mase, N.; Nakai, Y.; Ohara, N.; Yoda, H.; Takabe, K.; Tanaka, F.; Barbas, C. F. Organocatalytic Direct Asymmetric Aldol Reactions in Water. *J. Am. Chem. Soc.* **2006**, *128* (3), 734–735. https://doi.org/10.1021/ja0573312.

(38) Hayashi, Y. In Water or in the Presence of Water? *Angew. Chemie - Int. Ed.* **2006**, *45*, 8103–8104. https://doi.org/10.1002/anie.200603378.

(39) Córdova, A.; Zou, W.; Dziedzic, P.; Ibrahem, I.; Reyes, E. Direct Asymmetric Intermolecular Aldol Reactions Catalyzed by Amino Acids and Small Peptides. *Chem. Eur. J.* **2006**, *12* (20), 5383–5397. https://doi.org/10.1002/chem.200501639.

(40) Bayat, S.; Tejo, B. A.; Salleh, A. B. U. B.; Abdmalek, E.; Normi, Y. M.; Basyaruddin, M.; Rahman, A. Various Polar Tripeptides as Asymmetric Organocatalyst in Direct Aldol Reactions in Aqueous Media. *Chirality* **2013**, *25* (11), 726–734. https://doi.org/10.1002/chir.

(41) Tang, Z.; Yang, Z.; Chen, X.; Cun, L.; Mi, A.; Jiang, Y.; Gong, L. A Highly Efficient Organocatalyst for Direct Aldol Reactions of Ketones with Aldedydes. *J. Am. Chem. Soc.* **2005**, *127* (25), 9285–9289.

(42) Córdova, A.; Zou, W.; Dziedzic, P.; Ibrahem, I.; Reyes, E.; Xu, Y. Direct Asymmetric Intermolecular Aldol Reactions Catalyzed by Amino Acids and Small Peptides. *Chem. - A Eur. J.* **2006**, *12* (20), 5383–5397. https://doi.org/10.1002/chem.200501639.

(43) Jiang, Z.; Liang, Z.; Wu, X.; Lu, Y. Asymmetric Aldol Reactions Catalyzed by Tryptophan in Water. *Chem. Commun.* **2006**, No. 26, 2801–2803. https://doi.org/10.1039/b606154k.

(44) Armando, C.; Notz, W.; Iii, C. F. B. Direct Organocatalytic Aldol Reactions in Buffered Aqueous Media . Direct Organocatalytic Aldol Reactions in Buffered Aqueous Media †. *Chem. Commun.* **2002**, *24*, 3024–3025. https://doi.org/10.1039/B207664K.

(45) Yujiro Hayashi, Tatsunobu Sumiya, Junichi Takahashi, Hiroaki Gotoh, Tatsuya Urushima, and M. S. Highly Diastereo- and Enantioselective Direct Aldol Reactions in Water. *Angew. Chemie - Int. Ed.* **2006**, *45* (6), 958–961. https://doi.org/10.1002/anie.200502488.

(46) Aratake, S.; Itoh, T.; Okano, T.; Usui, T.; Shoji, M.; Hayashi, Y. Small Organic Molecule in Enantioselective , Direct Aldol Reaction ‘“ in Water .”’ *Chem. Commun.* **2007**, *24*, 2524–2526. https://doi.org/10.1039/b702559a.

(47) Bayat, S.; Tejo, B. A.; Abdulmalek, E.; Salleh, A. B.; Normi, Y. M.; Abdul Rahman, M. B. Rational Design of Mimetic Peptides Based on Aldo-Ketoreductase Enzyme as Asymmetric Organocatalysts in Aldol Reactions. *RSC Adv.* **2014**, *4* (73), 38859–38868. https://doi.org/10.1039/c4ra04866k.

(48) Krattiger, P.; Kovasy, R.; Revell, J. D.; Ivan, S.; Wennemers, H. Increased Structural Complexity Leads to Higher Activity : Peptides as Efficient and Versatile Catalysts for Asymmetric Aldol Reactions. *Org. Lett.* **2005**, *7* (6), 1101–1103.

(49) Luo, S.; Xu, H.; Li, J.; Zhang, L.; Cheng, J. A Simple Primary-Tertiary Diamine-Brønsted Acid Catalyst for Asymmetric Direct Aldol Reactions of Linear Aliphatic Ketones. *J. Am. Chem. Soc.* **2007**, *129* (11), 3074–3075.

(50) Hayashi, Y.; Aratake, S.; Itoh, T.; Okano, T.; Sumiya, T.; Shoji, M. Dry and Wet Prolines for Asymmetric Organic Solvent-Free Aldehyde-Aldehyde and Aldehyde-Ketone Aldol Reactions. *Chem. Commun.* **2007**, No. 9, 957–959. https://doi.org/10.1039/b613262f.

(51) Bayat, S.; Tejo, B. A.; Abdulmalek, E.; Salleh, B.; Normi, Y. M.; Basyaruddin, M.; Rahman, A. Rational Design of Mimetic Peptides Based on Aldo- Ketoreductase Enzyme as Asymmetric Organocatalysts in Aldol Reactions. *RSC Adv.* **2014**, *4* (73), 38859–38868. https://doi.org/10.1039/C4RA04866K.

(52) Zhang, G.; Chen, Y.; Li, H.; Guan, Z.; He, Y. Earthworms as a Biocatalyst : In Asymmetric Aldol Reactions. *SLAS Discov. Adv. Life Sci. R&D* **2017**, *22* (9), 1162–1167. https://doi.org/10.1177/2472555217724437.

(53) Sakthivel, K.; Notz, W.; Bui, T.; Iii, C. F. B.; Scripps, T.; Torrey, N.; Road, P.; Jolla, L. Amino Acid Catalyzed Direct Asymmetric Aldol Reactions : A Bioorganic Approach to Catalytic Asymmetric Carbon - Carbon Bond-Forming Reactions. *J. Am. Chem. Soc.* **2001**, *123* (22), 5260–5267.

(54) Trost, B. M.; Brindle, C. S. The Direct Catalytic Asymmetric Aldol Reaction. *Chem. Soc. Rev.* **2010**, *39* (5), 1600–1632. https://doi.org/10.1039/b923537j.

(55) Wu, X.; Jiang, Z.; Shen, H. M.; Lu, Y. Highly Efficient Threonine-Derived Organocatalysts for Direct Asymmetrie Aldol Reactions in Water. *Adv. Synth. Catal.* **2007**, *349* (6), 812–816. https://doi.org/10.1002/adsc.200600564.

(56) D'Elia, V.; Zwicknagl, H.; Reiser, O. Short α/β-Peptides as Catalysts for Intra- and Intermolecular Aldol Reactions. *J. Org. Chem.* **2008**, *73* (8), 3262–3265. https://doi.org/10.1021/jo800168h.

(57) Mase, N.; Nakai, Y.; Ohara, N.; Yoda, H.; Takabe, K.; Tanaka, F.; Iii, C. F. B. Organocatalytic Direct Asymmetric Aldol Reactions in Water. *J. Am. Chem. Soc.* **2006**, *128* (3), 734–735.

(58) Lin, J. H.; Zhang, C. P.; Xiao, J. C. Enantioselective Aldol Reaction of Cyclic Ketones

with Aryl Aldehydes Catalyzed by a Cyclohexanediamine Derived Salt in the Presence of Water. *Green Chem.* **2009**, *11* (11), 1750–1753. https://doi.org/10.1039/b916583e.

(59) Pihko, P. M.; Laurikainen, K. M.; Usano, A.; Nyberg, A. I.; Kaavi, J. A. Effect of Additives on the Proline-Catalyzed Ketone-Aldehyde Aldol Reactions. *Tetrahedron* **2006**, *62* (2–3), 317–328. https://doi.org/10.1016/j.tet.2005.09.070.

(60) Kumar, A.; Dhar, K.; Kanwar, S. S.; Arora, P. K. Lipase Catalysis in Organic Solvents: Advantages and Applications. *Biol. Proced. Online* **2016**, *18* (1), 1–11. https://doi.org/10.1186/s12575-016-0033-2.

(61) Klibanov, A. M. Asymmetric Transformations Catalyzed by Enzymes in Organic Solvents. *Acc. Chem. Res.* **1990**, *23* (4), 114–120. https://doi.org/10.1021/ar00172a004.

(62) Nyberg, A. I.; Usano, A.; Pihko, P. M. Proline-Catalyzed Ketone-Aldehyde Aldol Reactions Are Accelerated by Water. *Synlett* **2004**, No. 11, 1891–1896. https://doi.org/10.1055/s-2004-831296.

(63) Llanes, P.; Sayalero, S.; Rodríguez-Escrich, C.; Pericàs, M. A. Asymmetric Cross- and Self-Aldol Reactions of Aldehydes in Water with a Polystyrene-Supported Triazolylproline Organocatalyst. *Green Chem.* **2016**, *18* (12), 3507–3512. https://doi.org/10.1039/c6gc00792a.

(64) Huang, J.; Zhang, X.; Armstrong, D. W. Highly Efficient Asymmetric Direct Stoichiometric Aldol Reactions on/in Water. *Angew. Chemie - Int. Ed.* **2007**, *46* (47), 9073–9077. https://doi.org/10.1002/anie.200703606.

(65) Huang, W.; Tian, H.; Xu, H. L -Valine Dipeptide Organocatalysts with Two Amide Units for the Direct Asymmetric Aldol Reaction in Brine. *Catal. Letters* **2011**, *141* (6), 872–876. https://doi.org/10.1007/s10562-011-0589-z.

(66) Tian, H.; Gao, J.; Xu, H.; Zheng, L.; Huang, W.; Liu, Q.; Zhang, S. Proline-Based Dipeptides as Efficient Organocatalysts for Asymmetric Aldol Reactions in Brine. *Tetrahedron: Asymmetry* **2011**, *22* (10), 1074–1080. https://doi.org/10.1016/j.tetasy.2011.06.017.

(67) Delaney, J. P.; Henderson, L. C. Investigating Ionic Effects Applied to Water Based Organocatalysed Aldol Reactions. *Int. J. Mol. Sci.* **2011**, *12* (12), 9083–9094. https://doi.org/10.3390/ijms12129083.

(68) Gryko, D.; Saletra, W. J. Organocatalytic Asymmetric Aldol Reaction in the Presence of Water. *Org. Biomol. Chem.* **2007**, *5* (13), 2148–2153. https://doi.org/10.1039/b703254d.

(69) Machajewski, T. D.; Wong, C.-H. The Catalytic Asymmetric Aldol Reaction. *Angew. Chemie Int. Ed.* **2000**, *39* (8), 1352–1375. https://doi.org/10.1039/b923537j.

(70) Berkessel, A.; Koch, B.; Lex, J. Proline-Derived N-Sulfonylcarboxamides: Readily Available, Highly Enantioselective and Versatile Catalysts for Direct Aldol Reactions. *Adv. Synth. Catal.* **2004**, *346* (9–10), 1141–1146. https://doi.org/10.1002/adsc.200404126.

(71) Zhao, J.; Chen, A.; Liu, Q. Enantioselective Direct Aldol Reactions Catalyzed by Cinchonine-Derived Prolinamides. *Chinese J. Chem.* **2009**, *27* (5), 930–936. https://doi.org/10.1002/cjoc.200990158.

(72) Luo, Z. Bin; Dai, L. X. Novel Small Organic Molecules for a Highly Enantioselective Direct Aldol Reaction. *Chemtracts* **2003**, *16* (14), 843–847. https://doi.org/10.1002/chin.200423282.

(73) Nakadai, M.; Saito, S.; Yamamoto, H. Diversity-Based Strategy for Discovery of Environmentally Benign Organocatalyst: Diamine-Protonic Acid Catalysts for Asymmetric Direct Aldol Reaction. *Tetrahedron* **2002**, *58* (41), 8167–8177. https://doi.org/10.1016/S0040-4020(02)00965-1.

(74) Tang, Z.; Yang, Z. H.; Chen, X. H.; Cun, L. F.; Mi, A. Q.; Jiang, Y. Z.; Gong, L. Z. A Highly Efficient Organocatalyst for Direct Aldol Reactions of Ketones with Aldedydes. *J. Am. Chem. Soc.* **2005**, *127* (25), 9285–9289. https://doi.org/10.1021/ja0510156.

(75) Xie, Z. B.; Wang, N.; Jiang, G. F.; Yu, X. Q. Biocatalytic Asymmetric Aldol Reaction in Buffer Solution. *Tetrahedron Lett.* **2013**, *54* (8), 945–948. https://doi.org/10.1016/j.tetlet.2012.12.022.

(76) Birolli, W. G.; Fonseca, L. P.; Porto, A. L. M. Aldol Reactions by Lipase From Rhizopus Niveus, an Example of Unspecific Protein Catalysis. *Catal. Letters* **2017**, *147* (8), 1977–1987. https://doi.org/10.1007/s10562-017-2121-6.

(77) Dziedzic, P.; Zou, W.; Háfren, J.; Córdova, A. The Small Peptide-Catalyzed Direct Asymmetric Aldol Reaction in Water. *Org. Biomol. Chem.* **2006**, *4* (1), 38–40.

https://doi.org/10.1039/b515880j.

(78) Zbacnik, T. J.; Holcomb, R. E.; Katayama, D. S.; Murphy, B. M.; Payne, R. W.; Coccaro, R. C.; Evans, G. J.; Matsuura, J. E.; Henry, C. S.; Manning, M. C. Role of Buffers in Protein Formulations. *J. Pharm. Sci.* **2017**, *106* (3), 713–733. https://doi.org/10.1016/j.xphs.2016.11.014.

(79) Tyler-Cross, R.; Schirch, V. Effects of Amino Acid Sequence, Buffers, and Ionic Strength on the Rate and Mechanism of Deamidation of Asparagine Residues in Small Peptides. *J. Biol. Chem.* **1991**, *266* (33), 22549–22556. https://doi.org/10.1016/S0021-9258(18)54607-X.

(80) Bayat, S.; Abd Malek, E.; Yahaya, N. M.; Salleh, A. B.; Tejo, B. A.; Abdul Rahman, M. B. Asymmetric Aldol Reactions Catalyzed by the Promiscuous Aldo-Ketoreductase Enzyme. *Tetrahedron Lett.* **2014**, *55* (46), 6303–6306. https://doi.org/10.1016/j.tetlet.2014.09.012.

Chapter 5

Peptide-capped AuNPs as catalyst for direct aldol reaction

5.1 Introduction

Nanoparticles (NPs) have gained a lot of attention in recent years, with wide applications in sensing, drug discovery, novel therapy, catalysis and in control of protein structure and activity.[1–4] The term nanoparticles refers to a particle of any material having dimensions of 100 nm or less, and properties that can distinguish it from the bulk material based on the size and surface effects.[1,3,5] In this study we are interested in gold nanoparticles (AuNPs) because of their size-and shape-depended properties and also they are easy to synthesize and modify. In addition, AuNPs can be simply functionalised using biomolecules possessing amines or thiols and phosphine moieties.[2,3,6]

As mentioned in Chapter 4, a high organocatalyst loading of up to 30 mol % is required for most of the asymmetric reactions in organic synthesis and this often presents challenges such as; purification of products and difficulties in separation of catalyst recovery from the reaction mixture.[7] Hence there is a need to recycle and re-use catalysts to ensure cost and environment friendly catalytic processes. The immobilization of catalysts onto solid-carriers have shown some impressive results.[8–10]

AuNPs conjugates with a monolayer of cysteine-containing peptides are known to have excellent molecular recognition and catalysis properties.[11,12] Peptides functionalized onto the surface of the gold nanoparticle have also been shown to form new functional nanoparticle with enzyme-like structure and properties.[13,14]

Designed peptides which are smaller and more robust than natural proteins make it simpler to facilitate convenient site-specific incorporation of functional groups for further modification and direct immobilization. In order to effectively employ NPs for biocatalysis, it is vital to have an understanding of the interactions of the amino acids with NPs. The conjugation of polypeptides to NPs has the ability to influence both the function and the structure, and this effect depends on the sequence of the peptide.[15] The coupling of peptides to AuNPs could also lead to more compact or extended structures depending of the amino acids sequence of the

peptide.[15–17] Furthermore, common properties influencing the adsorption behaviour of peptides includes, their size, net charge, stability of folded domain; and conformation.[18,15]

5.2 Affinity of peptides towards gold nanoparticles (AuNPs)

The key factors to consider in the immobilization of peptides onto gold nanoparticles are a compatible environment or surface for conjugation and an understand of the interaction between peptide and NPs. Amino acids are regarded as suitable agents for conjugation to gold nanoparticles. This is as a result of the presence of different functional group such as, -NH_2, -SH that have strong affinity for the gold surface.[19–21] Some of these amino acids are known to interact with the gold surface specifically through their side chains. They are also thought to attach to the surface of neighbouring AuNPs through hydrogen bonding leading to the aggregation of linear structures.[19,20] Cysteine is mostly likely to bind to the AuNPs through its thiol (–SH) group (**Figure 5-1**), and this bond is formed by the ligand exchange reaction between cysteine and citrate capped gold nanoparticles.[21,22]

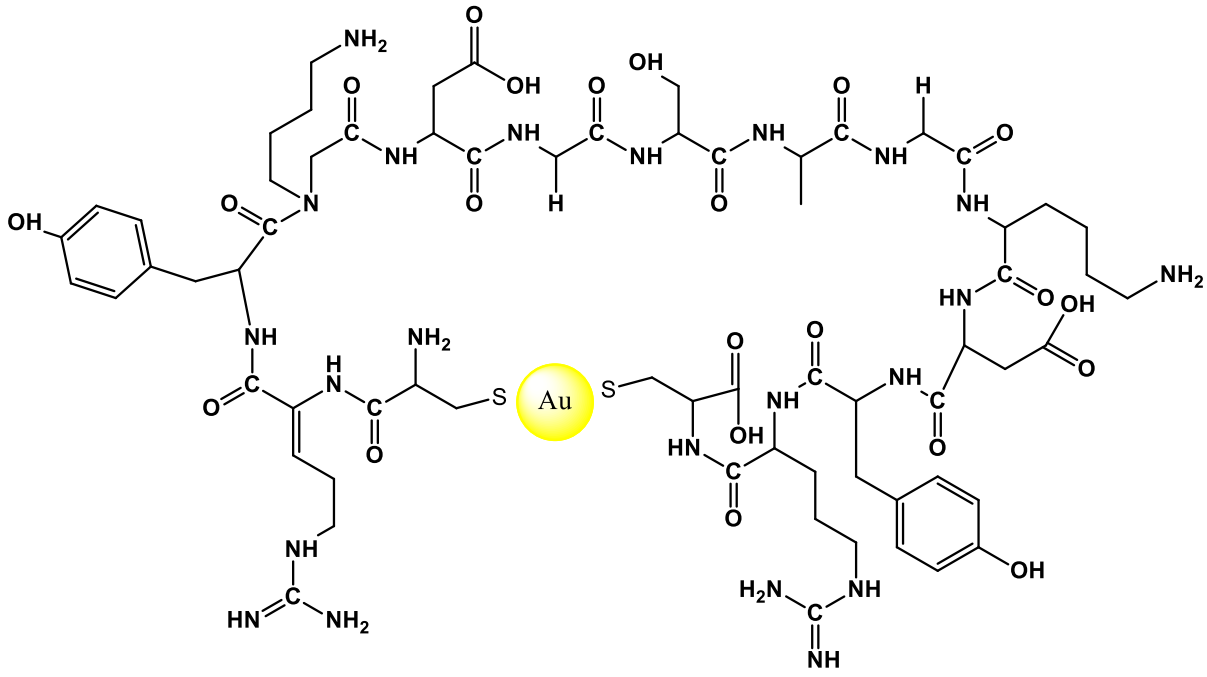


Figure 5- 1: Proposed structure of TP_ADLys peptide bounded to AuNP with its two cysteine residues.

The surface atoms of gold nanoparticles are known to be electrophilic, and therefore have a strong affinity for nucleophiles such as sulfur.[23] The cysteine sulphurs have a high affinity towards gold nanoparticles and its assembly effect can be attributed to the zwitterion type electrostatic interaction between the charged amine and acid group of cysteine molecule.[21] The

designed peptide sequence in this study takes into account such special features, with cysteine residues at the end of each) terminus, [C(-COOH) and N(-NH_2)] of the peptides. The studied peptide sequence possesses amino acids with hydrophobic side chains, [Alanine (A) and glycine (G)]; which are known to also promote self-assembly and stability of peptide in water.[24] These hydrophobic interactions together with hydrogen bonding of the amides backbone, are thought to provide efficient packing of the molecules on the NPs surface. In addition, such high molecule density on the NPs reduces molecules mobility thus promoting stability.[24,25]

To date, most of the work reported in literature involves immobilization of enzymes onto gold nanostructures in an attempt to improve enzymatic activity, stability and to change substrate specificity[26–29] or create enzyme mimics.[13,14,30] Studies involving conjugation of peptides to AuNPs have been focused on the detection of heavy metals,[31,32] and on biomedical applications for drug delivery and cellular uptake.[1,33–35] However, little has been reported on peptide-AuNPs regarding organic synthetic reactions,[36,37] and not much research has been conducted on peptide-capped AuNPs as for aldol reactions.[38]

In this chapter, we investigate the synthesis of gold nanoparticles conjugated to a catalytic cysteine-containing polypeptide (TP_ADLys). The catalytic activity and stability of the peptide-capped AuNPs will also be investigated on asymmetric aldol reaction. We envisage that the peptide-capped AuNPs, will produce a defined conformational peptide structure to improve catalytic efficiency, catalyst recovery and reduce the need for high catalyst loading.

5.3 Results and discussions

5.3.1 Synthesis and functionalization of AuNPs

Gold nanoparticles are generally synthesized by the reduction of hydrogen tetrachlorocuprate ($HAuCl_4$), using a reducing agent such as trisodium citrate or $NaBH_4$.[16,39,40] In this study citrate was chosen for the preparation of AuNPs. The reduction of gold chloride (III) using citrate has few advantages such as: the citrate can be readily replaced allowing easy functionalization of the particle and also the biomolecules (include peptides or proteins containing thiols amine and phosphine moieties) can be used for functionalization since the synthesis is performed in an aqueous medium.[41–43] In addition, citrate stabilized NPs are well-suited for application involving biomolecules since they are easily dispersed in water.[44–46] The gold nanoparticles were synthesized by addition of various ratios of citrate solution to aqueous solution of

$HAuCl_4$, as described in detail in Section 7.2. Different volumes of citrate solution were added to obtain different sizes of AuNPs and to also investigate the efficiency of the reductant which mostly depends on its concentration.[47] The reduction of gold salt (Au^{3+}) to Au^0 was verified by the appearance of colour change from pale yellow to pink/red (**Figure 5-2**), thus indicating the activation of nucleation and growth. The colour changes during the reaction, are related to the reaction kinetics of AuNPs synthesis.[48,49]

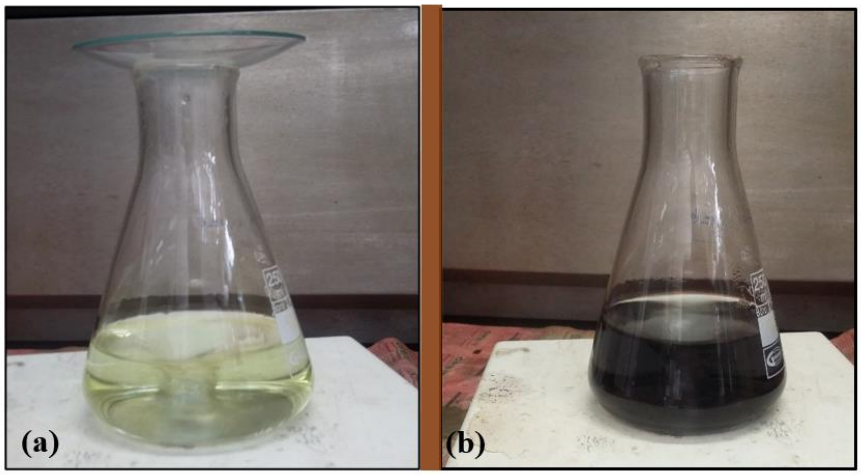


Figure 5- 2: An image of a reaction mixture changing colour, due to the addition of the citrate solution, from (a) pale yellow to (b) pink/red.

The poor interaction between the surface Au metal and the terminal carboxylic group of citrate molecule, permits easy postsynthetic treatment and further functionalization by binding to biomolecules (e.g. peptides).[50] Hence, after successful synthesis and characterization of AuNPs, they were immobilized on the uncyclized polypeptide (TP_DLys) having two free thiol groups on both ends. The functionalization was performed by varying both the volume of gold solutions and peptide concentrations, and this was confirmed by colour change from pink/red to pale pink solution.

5.3.2. Characterization and instrumentation

5.3.2.1 UV-vis spectrophotometry

Once the stable NPs were generated, they were investigated using various techniques. Initially, the optical properties of both the gold colloidal solutions and peptide-conjugated gold were monitored using UV-vis spectrophotometry. The electronic property of AuNPs, localized surface plasmon resonance (LSPR) confers a convenient preliminary indicator for surface functionalisation.[23] The LSPR observed wavelength (λ_{LSPR}) mostly depends upon the shape, size and distance between the adjacent nanoparticle and it is also affected by the changes in the dielectric environment.[51] For every run, the spectra background was corrected using milli-Q water since both samples were prepared in the same solvent system, so that the observed absorbance arises only from Au^{3+} nanoparticle and the Au^{3+}/peptide complex. The UV-vis absorption spectra of AuNPs and peptide-conjugated AuNPs are presented in **Figure 5-3**. The concentration of the peptide used for UV-vis and TEM analysis was 1.5 mol%. The absorption profile obtained for citrate capped-AuNPs reveal a damped localized LSPR band peaking around 518, 520 and 523 nm for AuNP-20, AuNP-30 and AuNP-50 respectively, thus confirming the formation of quasi-spherical AuNPs. [†] This is due to the effect of collective oscillations of conducting electrons when interacting with the electromagnetic radiation.[52] Furthermore, the magnitude of the shift differs with both the refractive index of the adsorbed layer and its thickness.[53,54] The gradual increase in shift of the AuNPs as the citrate volume increased, further demonstrated the dependence of LSPR on the size of the nanoparticle. Literature reports that a higher citrate ratio affords nanoparticles with smaller particles size.[55]

[†] AuNP-20→Denotes labelling for AuNPs using 20, 30 or 50ml citrate; AuNP-20P denotes labelling for peptide coupled to AuNPs using 20 ml citrate volume.

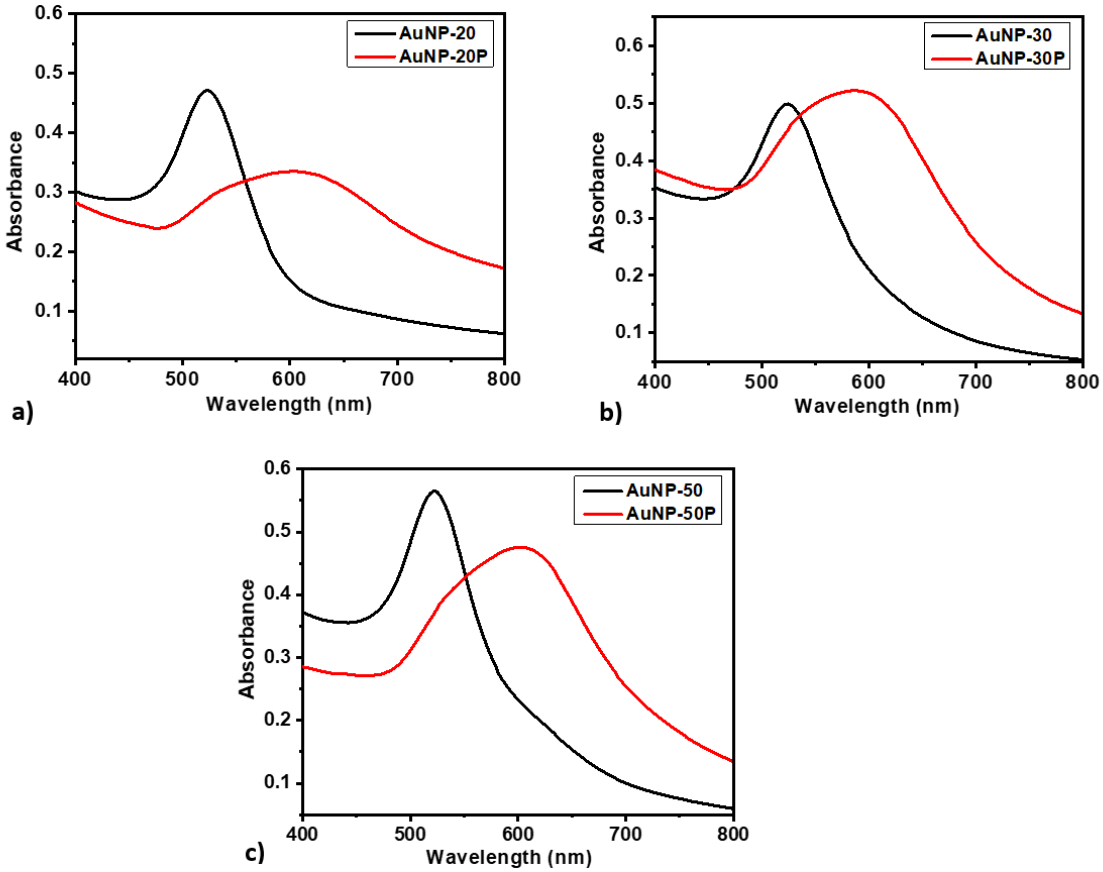


Figure 5- 3**:** UV-vis absorption spectra showing LSPR band for citrate-capped AuNP (black line) and peptide-AuNPs (red line).

When particles were capped with peptides, a broader absorbance shoulder is seen with a strong plasmon band at 605, 600, 595 nm for AuNP-20P, AuNP-30P and AuNP-50P respectively. The large LSPR shift observed suggests a strong interparticle interaction, confirming the conjugation of peptide to AuNPs. Additionally, this shift is due to the change in refractive index in the vicinity of the particle surface during the immobilization of the peptide.[56] The broader surface plasmon also indicates the change in dielectric constant which is attributed to the agglomeration of the nanoparticles. A change in dielectric environment close to the particles surface is thought to cause changes in the resonance conditions, which consequently gives rise to a shift both in the intensity and LSPR peak. Agglomeration is often caused by the intermolecular forces between the nanoparticles and peptide. These results further suggest the formation of more anisotropic nanoparticles due to broader size distribution.[56,57]

5.3.2.2 Transmission electron microscopy

TEM imaging and analysis is a technique used to determine the nanoparticle size formation and morphology such as changes in shape and diameter. **Figure 5-4** shows the TEM images of citrate capped-AuNPs and peptide functionalized AuNPs. The images of the citrate capped-NPs shown in **Figure 5-4 (a)-(c)** reveal roughly quasi-spherical particles in shape with a fairly narrow size distribution. Furthermore, the results also indicate that the particles are polycrystalline in nature. It can be observed that upon functionalization of the peptide, the particles are fairly dispersed because of the ionic nature of the peptide surface, causing a slight electrostatic repulson of the individual particles (**Figure 5-4 (d)-(f)**).

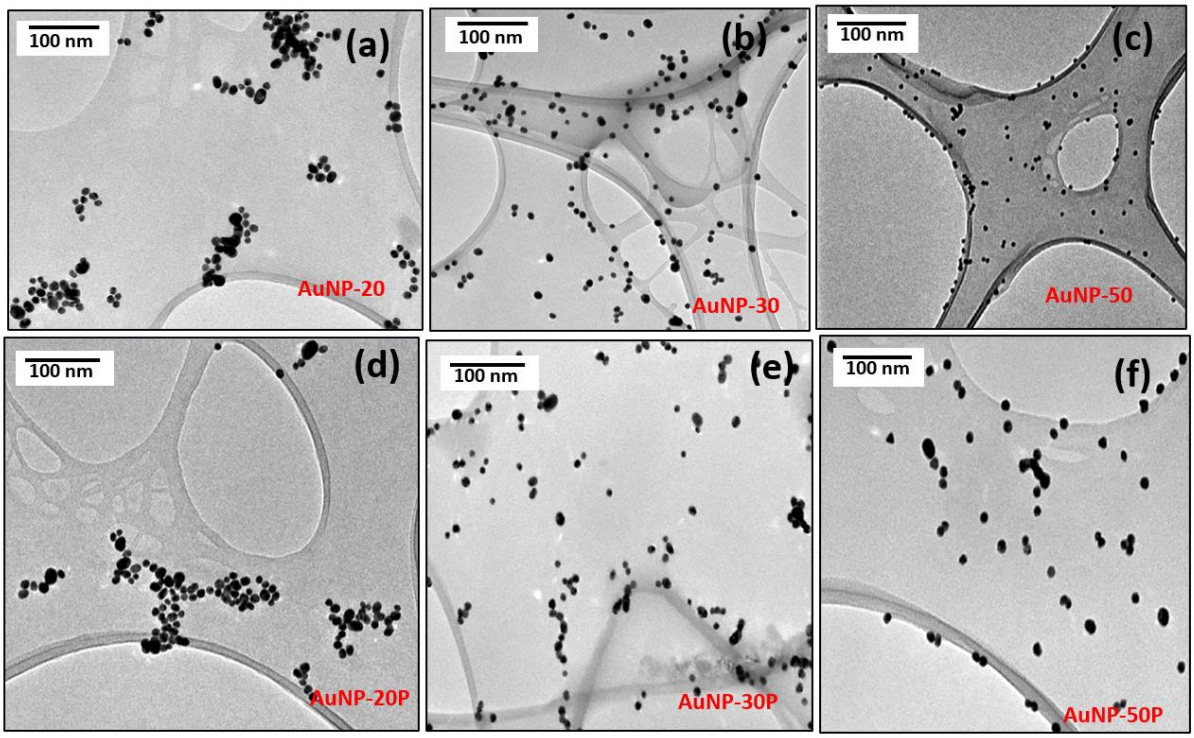


Figure 5- 4: TEM images for citrate-AuNPs and peptide-capped AuNPs (a) AuNP-20, (b) AuNP-20P, (c) AuNP-30, (d) AuNP-30P, (e) AuNP-50 and (f) AuNP-50P.

Figure 5-5 below depicts, the particle size distribution histograms of the citrate-AuNPs **(a)-(c)** and peptide functionalized AuNPs **(d)-(f),** used to measure the average diameter.

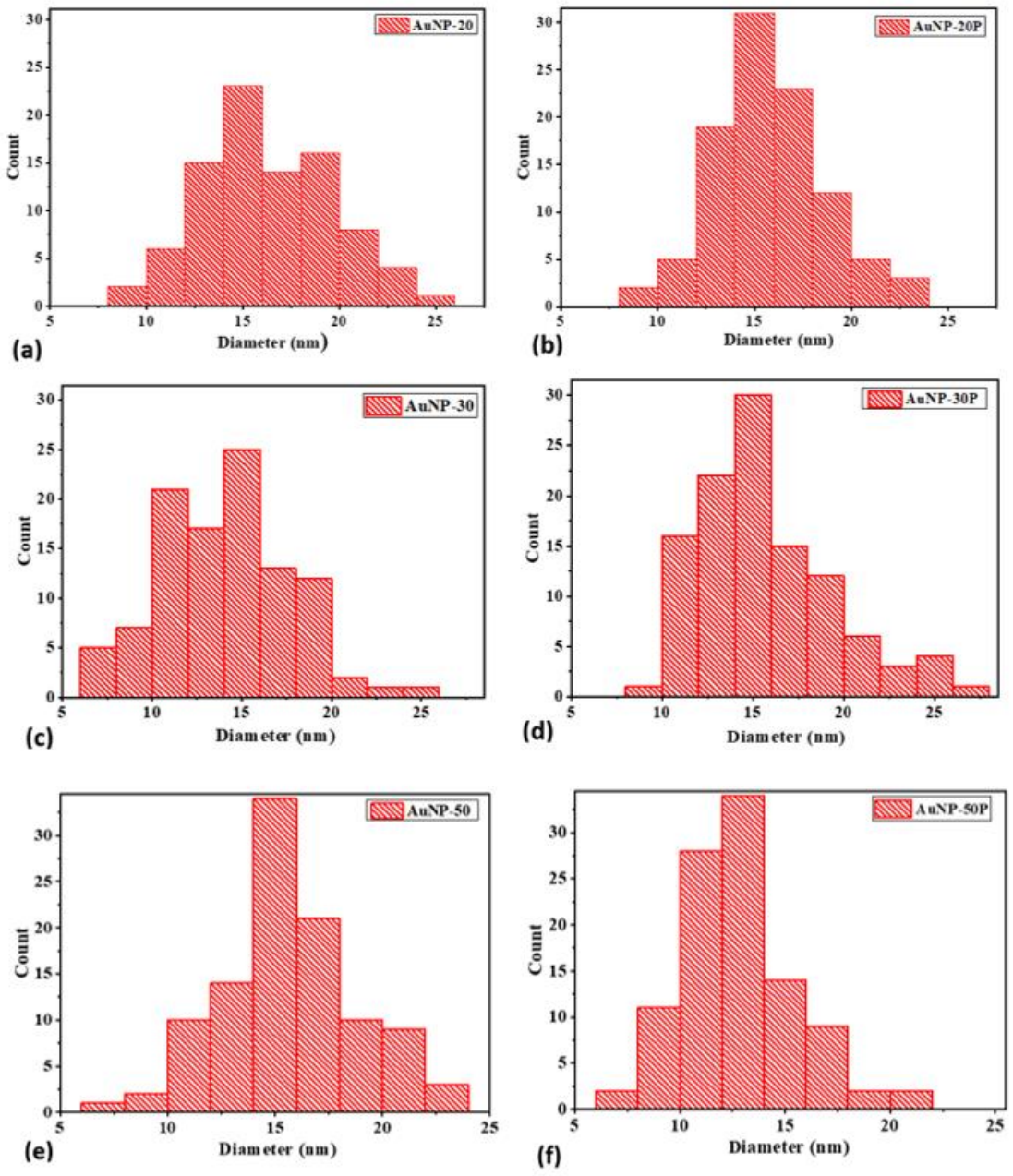


Figure 5- 5: Particle size distribution of citrate capped AuNPs and peptide-functionalised AuNPs obtained from TEM images.

The particle size distribution was obtained by measuring the average of at least 100 nanoparticles per image, using Image J software. Histograms provide a visual representation of the average size of the particles and how they differ. The summary of average particle size and diameter are given in **Table 5-1** below. The nanomaterials produced using 0.04 M of 20-, 30- and 50-mL of citrate has an average diameter (± one standard deviation) of 16±2.8, 16±4.74

and 13.5±2.9 nm, respectively. A relationship between the surface to volume ratio can be seen, as there is infinitesimal decrease in the average size as the citrate ratio increases. This effect can be attributed to a slight agglomeration of nanoparticles (**Figure 5-3**) prior to functionalization which can results in slow substitution reaction of the citrate.[58] One of the contributing factors leading to aggregation is high surface area to volume ratio which leads to thermodynamically unstable small Au clusters, as reported in literature.[49,59] Moreover, other studies postulate that aggregation is due to van der Waals forces and the tendency of Au(III) complexes to attract metallic Au surfaces.[39,60,61]

It is reported that large-surface to volume ratio of small-sized AuNPs facilitates the basis for the high adsorption capacity for peptides.[6] There was an interesting change in trend on the average particle size upon the conjugation of peptide, **Table 5-1)**, as it can be seen that there was a decrease in average diameter from 13.5±3.15–11.9±2.47. The observed results were consistent with what is reported in previous studies. This observation suggests that the binding affinity plays a vital role in governing the interactions between peptide and growing particles. The mechanism can also be explained in terms of the effect called "bridging flocculation, and this describes the binding of a peptide molecule to more than one particle at a time.[62] The chelate formed between the sulfhydryl group of the cysteine residue of the peptide and $Au3^{+}$ can also restrict growth of AuNPs by prohibit further nucleation of the free remaining gold ions.[47,63,64]

Table 5- 1**:** The average size and standard deviation for produced nanoparticles

Sample Name	Average diameter (nm)
AuNP-20ml	16±3
AuNP-Pp-20ml	15.8±2.8
AuNP-30ml	16±4.75
AuNP-Pp-30ml	15±3.75
AuNP-50ml	13.5±3.15
AuNP-Pp-50ml	11.9±2.1

5.3.3 Peptide-capped AuNPs as asymmetric aldol reaction catalyst

5.3.3.1 Catalyst screening

In this section, the catalytic activity of the previously synthesized Peptide capped-AuNPs is investigated. The advantages of using water as solvent has been mentioned before in Section 4.2.

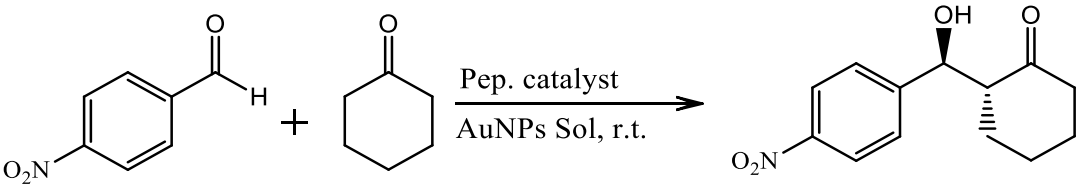
Literature reports that factors such as pH solution, ionic strength and composition of buffers can influence the interaction between peptides molecules and gold nanoparticles leading to irreversible aggregation when subject to centrifugation. This occurrence is explained in terms of the net charge and isoelectric point of the peptide.[42,62,65–68] Studies have also shown that when the pH of the solution is kept below the isoelectric point (pI) of the peptide it will induce the irreversible particle aggregation but, when the solution pH is kept above its pI, it will enable controlled particle stability.[62,65,67] As discussed, in Section 4.4.3, at neutral pH the peptide has net charge of 2.9 and calculated isoelectric point of 9.6. The use of buffer solutions beyond a pH of 9 is restricted because as indicated in Chapter 4 the aldol reaction may become base-catalyzed around this pH. Thus a pH of 8 was selected.

The peptide was immobilized to AuNPs in deionized water and aldol reactions were performed using the same aqueous solution in which the peptide capped-AuNPs were suspended in. The advantages of water-based strategies for the synthesis of AuNPs include; the possibility of immobilizing AuNPs in a variety of biomolecules (proteins, peptide, Abs(antibodies), etc.). In contrast, albeit in organic based synthetic methods NPs can be produced with better size control with quality nano-crystals but the functionalization of NPs to biomolecules is not possible in this medium. This is attributed to poor stability and dispersion of nanoparticles in this medium.[69–72] In addition, synthesis of AuNPs in this medium is often followed by stabilization with phosphine ligands,[73,74] organoamines[75,76] and alkanethiols,[77,78] which might hamper the application in this study since peptides will be used as conjugates. Thus, the synthesis of peptide-supported AuNPs in this study was conducted in aqueous solutions. The centrifuged solution of AuNPs was divided into 3 aliquots of 10 mL. Each aliquot was further divided into fractions of 1.5, 1.0 and 0.5 mL and added to different peptide concentration of 1.5, 2.8, 4.0 and 6 mol% and stirred for 3 hours at room temperature to allow the complete exchange of citrate with thiols on the particle surface. The ruby-red colour changed to a pale red colour and

the excess non-immobilized peptide was decanted with supernatant after centrifugation at 1500 rpm for 15 min.

The activity of the functionalized peptide-AuNPs was investigated using the benchmark reaction between *p*-nitrobenzaldehyde and cyclohexanone and the results are summarized in **Table 5-2**.

Table 5- 2: Aldol reactions screening of *p*-nitrobenzaldehyde and cyclohexanone catalyzed by peptide-supported AuNPs[a]



Entry	Citrate vol. (ml)	Vol of AuNPs (mL)	Pep.catalyst (mol%)	Time (h)	Yield (%)	ee (%)
1		1.5	1.5	96	NR	–
2	10	1.0	2.8	96	NR	–
3		0.5	4.0	96	NR	–
4		1.5	1.5	96	NR	–
5	20	1.0	2.8	96	NR	–
6		0.5	4.0	96	NR	–
7		1.5	1.5	96	NR	–
8	30	1.0	2.8	96	Trace	–
9		0.5	4.0	96	Trace	–
10		1.5	1.5	96	Trace	–
11	50	1.0	2.8	96	Trace	–
12		0.5	4.0	96	Trace	–

The reaction was performed using *p*-nitrobenzaldehyde (0.157 mmol, 24 mg), cyclohexanone (0.628 mmol, 70 µL), dissolved in 1.5 mL, 1.0 mL and 0.5 ml of AuNPs solution

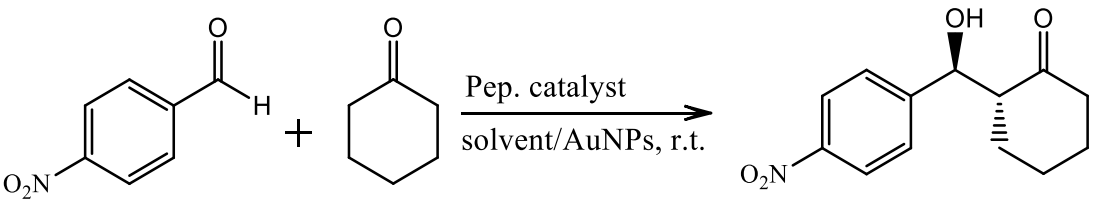
Repeated centrifugation of the mixture allowed for the removal of excess non-immobilized peptide. The catalytic activities were initially investigated with AuNP-20, AuNP-30, AuNP-50 mL and different peptide concentration. Regrettably, due to aggregation of AuNP-peptide conjugates at this concentration as seen in **Figure 5-3d**, no product was observed after 96 hours, when using 10- and 20-ml citrate-gold ratio (entries 1-6).

Subsequently, when reactions were performed in 30-and 50-ml citrate-gold ratio, trace amount of the product was observed (entries 8 to 12). Since an increase in citrate-gold ratio results in small nanoparticles size that interacts with the peptide to form conjugates (Figure 5-3f) that evenly disperse and can efficiently interact with the substrates. Due to poor solubility of the substrates which was assumed to contribute to the unfavourable results, further optimization of the reaction conditions will be discussed next. Different solvent media were used and the peptide concentration was increased.

5.3.3.2 Optimization of reactions conditions

The use of a ketone (cyclohexanone) as a solvent has been shown to promote aldol reactions more efficiently than organic solvents in this study and elsewhere (this has been discussed in detail in Section 4.4.2, **Table 4-2** and **4-5**). Importantly, DMSO as solvent has also been shown to be an effective solvent in the catalytic aldol reaction as already discussed (see Section 4.4.2, **Table 4-3** and **4-5**). Thus, for a better comparison of the results between unsupported and supported peptide catalyst, the aldol reaction between *p*-nitrobenzaldehyde and cyclohexanone were carried out in DMSO and cyclohexanone as solvents. The results obtained are summarized below in **Table 5-3**.

Table 5- 3: Aldol reactions between *p*-nitrobenzaldehyde and cyclohexanone catalyzed by peptide-supported AuNPs[a]



Entry	Citrate vol. (ml)	Solvent	Peptide.cat (mol%)	Time (h)	Yield (%)[b]	ee (%)[c]	dr (anti:syn)[d]
1	30	Ketone[a]	4	96	Trace	–	–
2			6	96	Trace	–	–
3	50		4	96	Trace	–	–
4			6	96	15	26	26:74
5	30	DMSO[e]	4	96	Trace	–	–
6			6	96	16	51	62:38
7	50		4	96	15	48	46:54
8			6	96	17	20	44:56
9	20	Buffer[f]	6	72	21	72	57:43
10	30		6	72	39	94	59:41
11	50		6	72	44	78	56:44

[a]The reaction was performed using *p*-nitrobenzaldehyde (0.157 mmol, 24 mg), 0.5 mL of cyclohexanone/AuNPs solution. [b] Isolated yield. [c] ee values determined by chiral-phase HPLC analysis.[d] Determined by 1 H NMR analysis of the crude product. [e] the reaction was performed using ketone (cyclohexanone) (0.628 mmol, 70 µL) in 1 mL DMSO, [f] reactions were performed using buffer solution in AuNPs solution (1:1) at r.t.

When the reactions were performed in a cyclohexanone/AuNPs system, only a trace amount of the product was observed, **Table 5-3**, entries 1 and 2. This outcome could be attributed to the low solubility of cyclohexanone in aqueous AuNPs solution, creating a biphasic system thus compromising the catalytic efficiency. Although poor yields were obtained when the reactions were performed with AuNP-Pp-50ml (entry 4) in cyclohexanone, the effect of AuNPs size on the selectivity of the reaction is notable. In the absence of a supported catalyst (**Table 4-2** entry 5), lower ee of less than 7% were obtained whereas with the peptide-AuNPs the enantioselectivity has improved and the ee of up to 26% were obtained. Moreover, there was an improvement in yields when wet DMSO was used, Entries 6, 7 and 8. These findings further

demonstrate that increasing the peptide concentration and modifying the solvent system can lead to an improvement in catalytic efficiency, albeit longer reaction time.

The biocatalytic performance for the AuNPs-peptide catalyzed aldol reactions was further evaluated in a buffered solution (entries 9-11). There was a significant improvement of both the yields (up to 42), enantioselectivity and moderate improvement of the diastereoselectivity (59:41) for the aldol reactions in buffered solutions. The influence of the solution is known to influence the controlled stability of the AuNPs and particles.[15,65,69,79,80] Furthermore, in Chapter 3 it was demonstrated that the peptide adopts a different conformation in a buffer solution and therefore the improvement in selectivity was attributed to the slight conformational change of the peptide resulting in proficient interaction of the substrate or stabilization of the reaction intermediates.[27,28,81]Studies have also shown that the gold to thiol bond (Au-S) changes from coordinate to a covalent bond in alkaline pH.[23,82]

In general, aldol reaction catalyzed by peptide-capped AuNPs produced aldol products with enhanced enantioselectivity and diastereoselectivity compared to the unsupported peptide catalysts in Chapter 4. These results were inconsistent with what is reported in literature by Sóti *et al.*,[38] where unsupported proline catalyst yielded high selectivity compared to the proline-supported AuNPs. Although there was an improvement in selectivity of the aldol product, it was unfortunate that the conjugation of peptide to AuNPs did not significantly improve the catalytic activity of the peptide even after an increase in the catalyst loading. Literature reports that, the polypeptide with a defined confirmation may lose structure as a consequence of its interaction with the metal surface.[15]

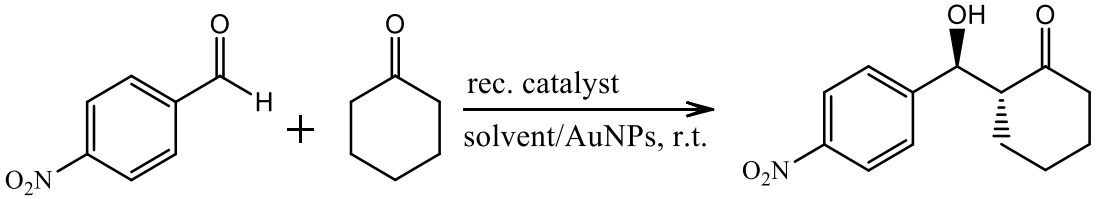
The synthesized peptides exist in approximately four conformations as reported in chapter 2 and it is possible that the conjugation of the peptide caused a change in structure of the more active conformation. The newly formed conjugated conformation has a more defined shape which results in better selectivity. Multiple interactions formed between the peptide and the interface, are thought to have a significant influence on the conformation of the peptide backbone.[15,83]

5.3.3.3 Catalyst recyclability studies

In order to investigate the reusability of the peptide-capped AuNPs, Et_2O and C_2H_5OH were added to the filtered aqueous layers obtained after extracting the crude product. The mixture was further centrifuged smoothly at 500 rpm once for 10 min and the AuNPs were recovered

after decantation. **Table 5-4** gives a summary of the results obtained from the recovered catalyst. These results suggest that AuNPs were not effective in facilitating the recovery of the catalyst as there was still mass loss; about 4-5 mg was recovered from 11.5 and 16.4 mg of the peptide initially used. Studies have shown that the decrease or loss of activity when recycling AuNPs supported catalyst be attributed to the irreversible aggregation of the nanoparticles during to extraction step.[7,27]

Table 5- 4: Recovery and reuse of peptide capped AuNPs[a]



Entry	Citrate conc.(ml)	Solvent	Time (h)	Yield (%)	ee (%)	dr (%)
1	50	Ketone	96	traces	-	-
2	30	DMSO	96	traces	-	-
3	50	DMSO	96	traces	-	-
4		DMSO	96	traces	-	-

[a]The reaction was performed using *p*-nitrobenzaldehyde (0.157 mmol, 24 mg), 0.5 mL of cyclohexanone/AuNPs solution. [b] The reaction was performed using cyclohexanone (0.628 mmol, 70 µL) in 0.75 mL DMSO/AuNPs solution at r.t.

5.4. Concluding remarks

In summary, the synthesis, characterization and catalytic activity of peptide-capped AuNPs was demonstrated. The nanomaterials were generated using a simple reduction approach while varying the gold-citrate ratio. It was observed that the nanoparticles were quasi-spherical in nature with a relatively narrow size distribution. Small size nanoparticles of approximately 12 nm (50 mL citrate), could serve as promising candidates for efficient peptide-conjugation. In comparison to the unsupported peptide catalyzed aldol reaction between *p*-nitrobenzaldehyde and cyclohexanone (Table 4-5), peptide-capped AuNPs afforded aldol products with improved enantioselectivity (up to 51%) and moderate diastereoselectivity (62:38). The use of buffered solution proved to enhance both the catalytic activity and selectivity of the peptide-AuNPs catalyzed aldol reaction. This was explained in terms of the slight change in conformation of the peptide-AuNPs resulting in efficient interaction with the substrates. When reactions were performed in cyclohexanone and DMSO as solvent there was no improvement of both the

catalytic activity and reusability of the catalyst. This outcome was attributed to the random coil structure of the peptide which could have caused weak interactions with gold surface

As previously mentioned, a lot of reported work on aldol reaction catalyzed AuNPs supported-catalysts have been mostly on proline and this therefore limited the amount of comparable available data to provide plausible mechanisms. Due to time constraints and challenges mentioned on the reproducibility of the peptide catalyst, no further modifications on the peptide-capped AuNPs and the aldol reactions conditions could be performed.

5.5 References

(1) Surujpaul, P. P.; Gutiérrez-wing, C.; Ocampo-garcía, B.; Ramírez, F. D. M.; Murphy, C. A. De. Gold Nanoparticles Conjugated to [Tyr 3] Octreotide Peptide. *Biophys. Chem.* **2008**, *138* (3), 83–90. https://doi.org/10.1016/j.bpc.2008.09.005.

(2) Ocampo-garcía, B. E.; Ramírez, F. D. M.; Ferro-flores, G.; León-rodríguez, L. M. De; Santos-cuevas, C. L.; Morales-avila, E.; Arteaga, C.; Murphy, D.; Pedraza-lópez, M.; Medina, L. A.; Camacho-lópez, M. A. Tc-Labelled Gold Nanoparticles Capped with HYNIC-Peptide / Mannose for Sentinel Lymph Node Detection. *Nucl. Med. Biol.* **2011**, *38* (14539), 1–11. https://doi.org/10.1016/j.nucmedbio.2010.07.007.

(3) Lee, K. H.; Marty Ytreberg, F. Effect of Gold Nanoparticle Conjugation on Peptide Dynamics and Structure. *Entropy* **2012**, *14* (4), 630–641. https://doi.org/10.3390/e14040630.

(4) Porta, F.; Speranza, G.; Dal, V.; Francescato, P.; Scar, G. Gold Nanoparticles Capped by Peptides. *Mater. Sci. Eng. B* **2007**, *140* (3), 187–194. https://doi.org/10.1016/j.mseb.2007.03.019.

(5) Stratakis, M.; Garcia, H. Catalysis by Supported Gold Nanoparticles: Beyond Aerobic Oxidative Processes. *Chem. Rev.* **2012**, *112* (8), 4469–4506. https://doi.org/10.1021/cr3000785.

(6) Liu, S.; Lämmerhofer, M. Functionalized Gold Nanoparticles for Sample Preparation: A Review. *Electrophoresis* **2019**, *40* (18–19), 2438–2461. https://doi.org/10.1002/elps.201900111.

(7) Khiar.N; Navas.R; Elhalem.E; Valdivia.V; Fernández.I. Proline-Coated Gold Nanoparticles as a Highly Efficient Nanocatalyst for the Enantioselective Direct Aldol Reaction in Water. *RSC Adv.* **2013**, *3* (12), 3861–3864. https://doi.org/10.1039/c3ra22955f.

(8) Gruttadauria, M.; Giacalone, F.; Noto, R. Supported Proline and Proline-Derivatives as Recyclable Organocatalysts. *Chem. Soc. Rev.* **2008**, *37* (8), 1666–1688. https://doi.org/10.1039/b800704g.

(9) Wang, B. G.; Ma, B. C.; Wang, Q.; Wang, W. Superparamagnetic Nanoparticle-Supported (S)-Diphenyl- Prolinol Trimethylsilyl Ether as a Recyclable Catalyst for

Asymmetric Michael Addition in Water. *Adv. Synth. Catal.* **2010**, *352* (17), 2923–2928. https://doi.org/10.1002/adsc.201000508.

(10) Haraguchi, N.; Kiyono, H.; Takemura, Y.; Itsuno, S. Design of Main-Chain Polymers of Chiral Imidazolidinone for Asymmetric Organocatalysis Application. *Chem. Commun.* **2012**, *48* (33), 4011–4013. https://doi.org/10.1039/c2cc18115k.

(11) Tauran, Y.; Brioude, A.; Coleman, A. W.; Rhimi, M.; Kim, B. Molecular Recognition by Gold, Silver and Copper Nanoparticles. *World J. Biol. Chem.* **2013**, *4* (3), 35. https://doi.org/10.4331/wjbc.v4.i3.35.

(12) Lévy, R. Peptide-Capped Gold Nanoparticles: Towards Artificial Proteins. *ChemBioChem* **2006**, *7* (8), 1141–1145. https://doi.org/10.1002/cbic.200600129.

(13) Pengo, P.; Baltzer, L.; Pasquato, L.; Scrimin, P. Substrate Modulation of the Activity of an Artificial Nanoesterase Made of Peptide-Functionalized Gold Nanoparticles. *Angew. Chemie* **2007**, *119* (3), 404–408. https://doi.org/10.1002/ange.200602581.

(14) Mikolajczak, D. J.; Koksch, B. Peptide-Gold Nanoparticle Conjugates as Artificial Carbonic Anhydrase Mimics. *Catalysts* **2019**, *9* (11), 903.

(15) Aili, D. and Stevens, M. M. Bioresponsive Peptide–Inorganic Hybrid Nanomaterials. *Chem. Soc. Rev.* **2010**, *39* (9), 3358–3370. https://doi.org/10.1039/b919449p.

(16) Lee, K. H.; Ytreberg, F. M. Effect of Gold Nanoparticle Conjugation on Peptide Dynamics and Structure. *Entropy* **2012**, *14* (4), 630–641. https://doi.org/10.3390/e14040630.

(17) Tang, Z.; Palafox-hernandez, J. P.; Law, W.; Hughes, Z. E.; Swihart, M. T.; Prasad, P. N.; Knecht, M. R.; Walsh, T. R. Biomolecular Recognition Principles for Bionanocombinatorics : An Integrated Approach To Elucidate Enthalpic and Entropic Factors. *ACS Nano* **2013**, *7* (11), 9632–9646. https://doi.org/10.1021/nn404427y.

(18) Nakanishi, K.; Sakiyama, T.; Imamura, K. On the Adsorption of Proteins on Solid Surfaces, a Common but Very Complicated Phenomenon. *J. Biosci. Bioeng.* **2001**, *91* (3), 233–244. https://doi.org/10.1016/S1389-1723(01)80127-4.

(19) Mandal, S.; Phadtare, S.; Sastry, M. Interfacing Biology with Nanoparticles. *Curr. Appl. Phys.* **2005**, *5* (2), 118–127. https://doi.org/10.1016/j.cap.2004.06.006.

(20) Zhang, J.; Chi, Q.; Nielsen, J. U.; Friis, E. P.; Andersen, J. E. T.; Ulstrup, J. Two-Dimensional Cysteine and Cystine Cluster Networks on Au(111) Disclosed by Voltammetry and in Situ Scanning Tunneling Microscopy. *Langmuir* **2000**, *16* (18), 7229–7237. https://doi.org/10.1021/la000246h.

(21) Mocanu, A.; Cernica, I.; Tomoaia, G.; Bobos, L. D.; Horovitz, O.; Tomoaia-Cotisel, M. Self-Assembly Characteristics of Gold Nanoparticles in the Presence of Cysteine. *Colloids Surfaces A Physicochem. Eng. Asp.* **2009**, *338* (1–3), 93–101. https://doi.org/10.1016/j.colsurfa.2008.12.041.

(22) Chai, F.; Wang, C.; Wang, T.; Ma, Z. L-Cysteine Functionalized Gold Nanoparticles for the Colorimetric Detection of Hg^{2+} Induced by Ultraviolet Light. *Nanotechnology* **2010**, *21* (2). https://doi.org/10.1088/0957-4484/21/2/025501.

(23) Natarajan, P.; Sukthankar, P.; Changstrom, J.; Holland, C. S.; Barry, S.; Hunter, W. B.; Sorensen, C. M.; Tomich, J. M. Synthesis and Characterization of Multifunctional Branched Amphiphilic Peptide Bilayer Conjugated Gold Nanoparticles. *ACS Omega* **2018**, *3* (9), 11071–11083. https://doi.org/10.1021/acsomega.8b01633.

(24) Lévy, R.; Thanh, N. T. K.; Christopher Doty, R.; Hussain, I.; Nichols, R. J.; Schiffrin, D. J.; Brust, M.; Fernig, D. G. Rational and Combinatorial Design of Peptide Capping Ligands for Gold Nanoparticles. *J. Am. Chem. Soc.* **2004**, *126* (32), 10076–10084. https://doi.org/10.1021/ja0487269.

(25) Pale-Grosdemange, C.; Simon, E. S.; Prime, K. L.; Whitesides, G. M. Formation of Self-Assembled Monolayers by Chemisorption of Derivatives of Oligo(Ethylene Glycol) of Structure $HS(CH_2)11(OCH_2CH_2)MOH$ on Gold. *J. Am. Chem. Soc.* **1991**, *113* (1), 12–20. https://doi.org/10.1021/ja00001a002.

(26) Wang, Q.; Yang, Z.; Gao, Y.; Ge, W.; Wang, L.; Xu, B. Enzymatic Hydrogelation to Immobilize an Enzyme for High Activity and Stability. *Soft Matter* **2008**, *4* (3), 550–553. https://doi.org/10.1039/b715439a.

(27) Ardao, I.; Comenge, J.; Benaiges, M. D.; Álvaro, G.; Puntes, V. F. Rational Nanoconjugation Improves Biocatalytic Performance of Enzymes: Aldol Addition Catalyzed by Immobilized Rhamnulose-1-Phosphate Aldolase. *Langmuir* **2012**, *28* (15), 6461–6467. https://doi.org/10.1021/la3003993.

(28) Wu, C. S.; Wu, C. T.; Yang, Y. S.; Ko, F. H. An Enzymatic Kinetics Investigation into the Significantly Enhanced Activity of Functionalized Gold Nanoparticles. *Chem. Commun.* **2008**, 42, 5327–5329. https://doi.org/10.1039/b810889g.

(29) Brennan, J. L.; Hatzakis, N. S.; Tshikhudo, T. R.; Dirvianskyte, N.; Razumas, V.; Patkar, S.; Vind, J.; Svendsen, A.; Nolte, R. J. M.; Rowan, A. E.; Brust, M. Bionanoconjugation via Click Chemistry: The Creation of Functional Hybrids of Lipases and Gold Nanoparticles. *Bioconjug. Chem.* **2006**, *17* (6), 1373–1375. https://doi.org/10.1021/bc0601018.

(30) Pengo, P.; Polizzi, S.; Pasquato, L.; Scrimin, P. Carboxylate - Imidazole Cooperativity in Dipeptide-Functionalized Gold Nanoparticles with Esterase-like Activity. *J. Am. Chem. Soc.* **2005**, *127* (6), 1616–1617.

(31) Slocik, J. M.; Zabinski, J. S.; Phillips, D. M.; Naik, R. R. Colorimetric Response of Peptide-Functionalized Gold Nanoparticles to Metal Ions. *Small* **2008**, *4* (5), 548–551. https://doi.org/10.1002/smll.200700920.

(32) Storhoff, J. J.; Elghanian, R.; Mucic, R. C.; Mirkin, C. A.; Letsinger, R. L. One-Pot Colorimetric Differentiation of Polynucleotides with Single Base Imperfections Using Gold Nanoparticle Probes. *J. Am. Chem. Soc.* **1998**, *120* (9), 1959–1964. https://doi.org/10.1021/ja972332i.

(33) Shukla, R.; Hill, E.; Shi, X.; Kim, J.; Muniz, M. C.; Baker, J. R. Tumor Microvasculature Targeting with Dendrimer-Entrapped Gold Nanoparticles. *Soft Matter* **2008**, *4* (11), 2160–2163. https://doi.org/10.1039/b810885d.

(34) Sun, L.; Liu, D.; Wang, Z. Functional Gold Nanoparticle - Peptide Complexes as Cell-Targeting Agents. *Langmuir* **2008**, *24* (18), 10293–10297. https://doi.org/10.1021/la8015063.

(35) Khamehchian, S.; Nikkhah, M.; Madani, R.; Hosseinkhani, S. Enhanced and Selective Permeability of Gold Nanoparticles Functionalized with Cell Penetrating Peptide Derived from Maurocalcine Animal Toxin. *J. Biomed. Mater. Res. Part A* **2016**, *104* (11), 2693–2700.

(36) Mikolajczak, D. J.; Heier, J. L.; Schade, B.; Koksch, B. Catalytic Activity of Peptide-Nanoparticle Conjugates Regulated by a Conformational Change. *Biomacromolecules*

2017, *18* (11), 3557–3562. https://doi.org/10.1021/acs.biomac.7b00887.

(37) Pengo, P.; Baltzer, L.; Pasquato, L.; Scrimin, P. Substrate Modulation of the Activity of an Artificial Nanoesterase. *Angew. Chemie* **2007**, *119* (3), 400–404. https://doi.org/10.1002/anie.200602581.

(38) Sóti, P. L.; Yamashita, H.; Sato, K.; Narumi, T.; Toda, M.; Watanabe, N.; Marosi, G.; Mase, N. Synthesis of a Self-Assembling Gold Nanoparticle-Supported Organocatalyst for Enamine-Based Asymmetric Aldol Reactions. *Tetrahedron* **2016**, *72* (16), 1984–1990. https://doi.org/10.1016/j.tet.2016.02.065.

(39) Turkevich, J.; Stevenson, P. C.; Hillier, J. A Study of the Nucleation and Growth Processes in the Synthesis of Colloidal Gold. *Discuss. Faraday Soc.* **1951**, *11* (c), 55–75. https://doi.org/10.1039/DF9511100055.

(40) Wu, R. H.; Nguyen, T. P.; Marquart, G. W.; Miesen, T. J.; Mau, T.; Mackiewicz, M. R. A Facile Route to Tailoring Peptide-Stabilized Gold Nanoparticles Using Glutathione as a Synthon. *Molecules* **2014**, *19* (5), 6754–6775. https://doi.org/10.3390/molecules19056754.

(41) Natarajan, P.; Sukthankar, P.; Changstrom, J.; Holland, C. S.; Barry, S.; Hunter, W. B.; Sorensen, C. M.; Tomich, J. M. Synthesis and Characterization of Multifunctional Branched Amphiphilic Peptide Bilayer Conjugated Gold Nanoparticles. *ACS Omega* **2018**, *3* (9), 11071–11083. https://doi.org/10.1021/acsomega.8b01633.

(42) Dahl, J. A.; Maddux, B. L. S.; Hutchison, J. E.; Dahl, J. A.; Maddux, B. L. S.; Hutchison, J. E. Toward Greener Nanosynthesis. *Chem. Rev.* **2007**, *107* (6), 2228–2269. https://doi.org/10.1021/cr050943k.

(43) Zarabi, M. F.; Arshadi, N.; Farhangi, A.; Akbarzadeh, A. Preparation and Characterization of Gold Nanoparticles with Amino Acids, Examination of Their Stability. *Indian J. Clin. Biochem.* **2014**, *29* (3), 306–314. https://doi.org/10.1007/s12291-013-0358-4.

(44) Verma, A.; Srivastava, S.; Rotello, V. M. Modulation of the Interparticle Spacing and Optical Behavior of Nanoparticle Ensembles Using a Single Protein Spacer. *Chem. Mater.* **2005**, *17* (25), 6317–6322. https://doi.org/10.1021/cm051483e.

(45) Chah, S.; Hammond, M. R.; Zare, R. N. Gold Nanoparticles as a Colorimetric Sensor

for Protein Conformational Changes. *Chem. Biol.* **2005**, *12* (3), 323–328. https://doi.org/10.1016/j.chembiol.2005.01.013.

(46) Page Faulk, W.; Malcolm Taylor, G. Communication to the Editors. An Immunocolloid Method for the Electron Microscope. *Immunochemistry* **1971**, *8* (11), 1081–1083. https://doi.org/10.1016/0019-2791(71)90496-4.

(47) Jia, Y.; Yan, X.; Guo, X.; Zhou, G.; Liu, P.; Li, Z. One Step Preparation of Peptide-Coated Gold Nanoparticles with Tunable Size. *Materials (Basel).* **2019**, *12* (13), 1–12. https://doi.org/10.3390/ma12132107.

(48) Grzelczak, M.; Pérez-Juste, J.; Mulvaney, P.; Liz-Marzán, L. M. Shape Control in Gold Nanoparticle Synthesis. *Chem. Soc. Rev.* **2008**, *37* (9), 1783–1791. https://doi.org/10.1039/b711490g.

(49) Tran, M.; DePenning, R.; Turner, M.; Padalkar, S. Effect of Citrate Ratio and Temperature on Gold Nanoparticle Size and Morphology. *Mater. Res. Express* **2016**, *3* (10), 1–10. https://doi.org/10.1088/2053-1591/3/10/105027.

(50) Piella, J.; Bastús, N. G.; Puntes, V. Size-Controlled Synthesis of Sub-10-Nanometer Citrate-Stabilized Gold Nanoparticles and Related Optical Properties. *Chem. Mater.* **2016**, *28* (4), 1066–1075. https://doi.org/10.1021/acs.chemmater.5b04406.

(51) Cottancin, E.; Celep, G.; Lermé, J.; Pellarin, M.; Huntzinger, J. R.; Vialle, J. L.; Broyer, M. Optical Properties of Noble Metal Clusters as a Function of the Size: Comparison between Experiments and a Semi-Quantal Theory. *Theor. Chem. Acc.* **2006**, *116* (4–5), 514–523. https://doi.org/10.1007/s00214-006-0089-1.

(52) Castro-Longoria, E.; Vilchis-Nestor, A. R.; Avalos-Borja, M. Biosynthesis of Silver, Gold and Bimetallic Nanoparticles Using the Filamentous Fungus Neurospora Crassa. *Colloids Surfaces B Biointerfaces* **2011**, *83* (1), 42–48. https://doi.org/10.1016/j.colsurfb.2010.10.035.

(53) Martinsson, E.; Sepulveda, B.; Chen, P.; Elfwing, A.; Liedberg, B.; Aili, D. Optimizing the Refractive Index Sensitivity of Plasmonically Coupled Gold Nanoparticles. *Plasmonics* **2014**, *9* (4), 773–780. https://doi.org/10.1007/s11468-013-9659-y.

(54) Chen, C. F.; Tzeng, S. Der; Chen, H. Y.; Lin, K. J.; Gwo, S. Tunable Plasmonic Response from Alkanethiolate-Stabilized Gold Nanoparticle Superlattices: Evidence of

near-Field Coupling. *J. Am. Chem. Soc.* **2008**, *130* (3), 824–826. https://doi.org/10.1021/ja0773610.

(55) Zong, J.; Cobb, S. L.; Cameron, N. R. Peptide-Functionalized Gold Nanoparticles: Versatile Biomaterials for Diagnostic and Therapeutic Applications. *Biomater. Sci.* **2017**, *5* (5), 872–886. https://doi.org/10.1039/c7bm00006e.

(56) Aili, D.; Enander, K.; Rydberg, J.; Nesterenko, I.; Björefors, F.; Baltzer, L.; Liedberg, B. Folding Induced Assembly of Polypeptide Decorated Gold Nanoparticles. *J. Am. Chem. Soc. Am. Chem. Soc.* **2008**, *130* (17), 5780–5788.

(57) Su, K.; Wei, Q.; Zhang, X. Interparticle Coupling Effects on Plasmon Resonances of Nanogold Particles. *Nano Lett.* **20033**, No. 8, 1087–1090.

(58) Mlambo, M.; Harris, R.A.; Mashazi, P.; Sabela, M., Kanchi, S.; Madikizela, L.M.; Shumbula, P.N.; Moloto, N.; Hlatshwayo, T.T. and Mdluli, P. . Computational and Experimental Evaluation of Selective Substitution of Thiolated Coumarin Derivatives on Gold Nanoparticles: Surface Enhancing Raman Scattering and Electrochemical Studies. *Appl. Surf. Sci.* **2017**, *396*, 695–704. https://doi.org/10.1016/j.apsusc.2016.11.011.

(59) Chow, M. K.; Zukoski, C. F. Gold Sol Formation Mechanisms: Role of Colloidal Stability. *Journal of Colloid And Interface Science*. 1994, pp 97–109. https://doi.org/10.1006/jcis.1994.1210.

(60) Wang, S.; Qian, K.; Bi, X.; Huang, W. Influence of Speciation of Aqueous HAuCl4 on the Synthesis, Structure, and Property of Au Colloids. *J. Phys. Chem. C* **2009**, *113* (16), 6505–6510. https://doi.org/10.1021/jp811296m.

(61) Ji, X.; Song, X.; Li, J.; Bai, Y.; Yang, W.; Peng, X. Size Control of Gold Nanocrystals in Citrate Reduction: The Third Role of Citrate. *J. Am. Chem. Soc.* **2007**, *129* (45), 13939–13948. https://doi.org/10.1021/ja074447k.

(62) Tullman, J. A.; Finney, W. F.; Lin, Y. J.; Bishnoi, S. W. Tunable Assembly of Peptide-Coated Gold Nanoparticles. *Plasmonics* **2007**, *2* (3), 119–127. https://doi.org/10.1007/s11468-007-9033-z.

(63) Celentano, M.; Jakhmola, A.; Profeta, M.; Battista, E.; Guarnieri, D.; Gentile, F.; Netti, P. A.; Vecchione, R. Diffusion Limited Green Synthesis of Ultra-Small Gold

Nanoparticles at Room Temperature. *Colloids Surfaces A Physicochem. Eng. Asp.* **2018**, *558* (July), 548–557. https://doi.org/10.1016/j.colsurfa.2018.09.030.

(64) Kamble, G. S.; Kolekar, S. S.; Han, S. H.; Anuse, M. A. Synergistic Liquid-Liquid Extractive Spectrophotometric Determination of Gold(III) Using 1-(2′,4′-Dinitro Aminophenyl)-4,4,6-Trimethyl-1,4-Dihydropyrimidine-2-Thiol. *Talanta* **2010**, *81* (3), 1088–1095. https://doi.org/10.1016/j.talanta.2010.02.002.

(65) Aili, D.; Enander, K.; Rydberg, J.; Lundström, I.; Baltzer, L.; Liedberg, B. Aggregation-Induced Folding of a de Novo Designed Polypeptide Immobilized on Gold Nanoparticles. *J. Am. Chem. Soc.* **2006**, *128* (7), 2194–2195. https://doi.org/10.1021/ja057056j.

(66) Moore, T. L.; Rodriguez-Lorenzo, L.; Hirsch, V.; Balog, S.; Urban, D.; Jud, C.; Rothen-Rutishauser, B.; Lattuada, M.; Petri-Fink, A. Nanoparticle Colloidal Stability in Cell Culture Media and Impact on Cellular Interactions. *Chem. Soc. Rev.* **2015**, *44* (17), 6287–6305. https://doi.org/10.1039/c4cs00487f.

(67) Fang, B.; Nakagawa, K. Effect of PH, Ionic Strength, and Freezing Treatment on a Colloidal Suspension of Egg White Aggregates. *Food Struct.* **2021**, *27* (April 2020), 100181. https://doi.org/10.1016/j.foostr.2021.100181.

(68) Barreto, Â.; Luis, L. G.; Girão, A. V.; Trindade, T.; Soares, A. M. V. M.; Oliveira, M. Behavior of Colloidal Gold Nanoparticles in Different Ionic Strength Media. *J. Nanoparticle Res.* **2015**, *17* (12), 1–13. https://doi.org/10.1007/s11051-015-3302-0.

(69) Amina, S. J.; Guo, B. A Review on the Synthesis and Functionalization of Gold Nanoparticles as a Drug Delivery Vehicle. *Int. J. Nanomedicine* **2020**, *15*, 9823–9857.

(70) Herizchi, R.; Abbasi, E.; Milani, M.; Akbarzadeh, A.; Herizchi, R.; Abbasi, E.; Milani, M.; Akbarzadeh, A. Current Methods for Synthesis of Gold Nanoparticles Current Methods for Synthesis of Gold Nanoparticles. *Artif. cells, nanomedicine, Biotechnol.* **2016**, *44* (2), 596–602. https://doi.org/10.3109/21691401.2014.971807.

(71) Mahato, K.; Nagpal, S.; Ayesha, M.; Ananya, S.; Pawan, S.; Maurya, K. Gold Nanoparticle Surface Engineering Strategies and Their Applications in Biomedicine and Diagnostics. *3 Biotech* **2019**, *9* (2), 1–19. https://doi.org/10.1007/s13205-019-1577-z.

(72) Egorova, E. A.; van Rijt, M. M.; Sommerdijk, N.; Gooris, G. S.; Bouwstra, J. A.; Boyle,

A. L.; Kros, A. One Peptide for Them All : Gold Nanoparticles. *ACS Nano* **2020**, *14* (5), 5874–5886. https://doi.org/10.1021/acsnano.0c01021.

(73) Petroski, J.; Chou, M. H.; Creutz, C. Rapid Phosphine Exchange on 1,5-Nm Gold Nanoparticles. *Inorg. Chem.* **2004**, *43* (5), 1597–1599. https://doi.org/10.1021/ic035304b.

(74) Weare, W. W.; Reed, S. M.; Warner, M. G.; Hutchison, J. E. Improved Synthesis of Small (d CORE ≈ 1 . 5 Nm). *J. Am. Chem. Soc.* **2000**, *122* (51), 12890–12891.

(75) Hiramatsu, H.; Osterloh, F. E. Communications A Simple Large-Scale Synthesis of Nearly with Exchangeable Surfactants. *Chem. Mater.* **2004**, *16* (13), 2509–2511.

(76) Manea, F.; Bindoli, C.; Polizzi, S.; Lay, L.; Scrimin, P. Expeditious Synthesis of Water-Soluble, Monolayer-Protected Gold Nanoparticles of Controlled Size and Monolayer Composition. *Langmuir* **2008**, *24* (8), 4120–4124. https://doi.org/10.1021/la703558y.

(77) Brust, M.; Bethell, D.; Schiffrin, D.; Whyman, R. Synthesis of Thiol-Derivatized Gold Nanoparticles in a 2-Phase Liquid- Liquid System Synthesis of Thiol-Derivatised Gold Nanoparticles in a Two-Phase Liquid-Liquid System. *J. Am. Chem. Soc.* **1994**, *7*, 801–802. https://doi.org/10.1039/c39940000801.

(78) Ingram, R. S.; Hostetler, M. J.; Murray, R. W. Poly-Hetero-ω-Functionalized Alkanethiolate-Stabilized Gold Cluster Compounds. *J. Am. Chem. Soc.* **1997**, *119* (39), 9175–9178. https://doi.org/10.1021/ja971734n.

(79) Ahmed, S. R.; Oh, S.; Baba, R.; Zhou, H.; Hwang, S.; Lee, J.; Park, E. Y. Synthesis of Gold Nanoparticles with Buffer-Dependent Variations of Size and Morphology in Biological Buffers. *Nanoscale Res. Lett.* **2016**, *11* (1), 1–11. https://doi.org/10.1186/s11671-016-1290-3.

(80) Busch, R. T.; Karim, F.; Weis, J.; Sun, Y.; Zhao, C.; Vasquez, E. S. Optimization and Structural Stability of Gold Nanoparticle-Antibody Bioconjugates. *ACS Omega* **2019**, *4* (12), 15269–15279. https://doi.org/10.1021/acsomega.9b02276.

(81) Eck, D.; Helm, C. A.; Wagner, N. J.; Vaynberg, K. A. Plasmon Resonance Measurements of the Adsorption and Adsorption Kinetics of a Biopolymer onto Gold Nanocolloids. *Langmuir* **2001**, *17* (4), 957–960. https://doi.org/10.1021/la001142+.

(82) Xue, Y.; Li, X.; Li, H.; Zhang, W. Quantifying Thiol-Gold Interactions towards the

Efficient Strength Control. *Nat. Commun.* **2014**, *5*, *1-9*. https://doi.org/10.1038/ncomms5348.

(83) Lundqvist, M.; Nygren, P.; Jonsson, B. H.; Broo, K. Induction of Structure and Function in a Designed Peptide upon Adsorption on a Silica Nanoparticle. *Angew. Chemie Int. Ed.* **2006**, *45* (48), 8169–8173. https://doi.org/10.1002/anie.200600965.

Chapter 6

Conclusion and recommendations

The main aim of this study was to design and synthesize aldol reaction catalyzing peptides based on the sequence, structural conformation and activity of the Fructose-1,6-bisphosphate aldolase enzyme.

Novel catalyst peptides were successfully designed, synthesized, and characterized. The synthesis of peptide catalysts consisting of all D-AAs presented some challenges during synthesis, cyclization and purification, thus they were obtained in low yields. This was attributed to the possible folding of the growing peptide chains, thus compromising the coupling efficiency. Therefore, for future studies it is recommended that computational studies and full NMR elucidation of the peptide in this study be obtained to determine the 3D conformation and structure activity relationship before the design of new peptides and synthetic routes. Once the 3D conformation is known, the regions with high folding can be synthesized as separate short peptides to avoid deletion sequences.

With the aid of NMR and CD the possible conformations and secondary structural features of TP_Asp and TP_ADLys were successfully elucidated. The folding patterns of TP_Asp and TP_ADLys were influenced by the solvent used as revealed by CD experiments. CD studies further demonstrated that TP_ADLys and TP_Asp peptides exist as random coils that deviate to beta-sheet and α-helical conformations in solution, respectively. Long- medium- range NOEs were used to determine structural conformations. Currently the information that was obtained for the HMBC and HSQC spectra from a 500 MHz instrument provided limited complementary information for secondary structural elucidation. For future NMR studies, an advanced NMR instrument such as 600 or 700 MHz should be used to acquire good quality 2D spectra to provide a conclusive secondary structure of peptides. Molecular dynamics (MD) simulation protocol should also be incorporated to obtain a complementary information regarding the folding of the peptides.

The catalytic peptides were tested for asymmetric aldol reaction catalytic activity and they showed activity towards a selected range of substrates including aliphatic and aromatic ketone/aldehydes. Reaction between acetone and aromatic aldehydes afforded aldol products

with low yields and good enantioselectivities (85-93%). Aldol products between aromatic aldehydes with cyclohexanone were obtained with low yields and selectivities. Selected organic solvents were found to be acceptable, offering aldol products with low yields, poor enantioselectivities and moderate diastereoselectivities. The addition of water proved to significantly improve the reaction rate and selectivities, and it was further demonstrated that the buffered solution achieved aldol products with very high ee and moderate diastereoselectivity. It is also worth highlighting that there was no significant difference observed in the catalytic activity between the aspartic acid containing peptide (TP_Asp) and glutamic acid containing peptide (TP_ADLys).

The synthesis, immobilization and catalytic performance of peptide capped AuNPs with a range of sizes (16, 15 and 12 nm in diameter) obtained by varying citrate ratio was demonstrated. AuNPs with quasi-spherical shape and narrow size distribution as suggested by TEM were obtained. Aldol reaction between *p*-nitrobenzaldehyde and cyclohexanone catalyzed by peptide-capped AuNPs was evaluated. Conjugating the catalyst onto peptide AuNPs did not enhance activity and reusability. However, a significant improvement in the selectivity was observed. These findings were associated with the change in peptide structure caused by the interaction of the peptide with AuNPs.

Smaller particles were observed to yield better results therefore a new approach utilizing stronger reducing agents such $NaBH_4$ that can produce monodisperse particles with smaller particle size should be investigated. Protocols which use stabilizing molecules in the synthesis of peptide-support AuNPs such as the Brust-Schiffrin (BS) synthesis should also be considered.

We have demonstrated the application of novel peptides in the catalysis of the commonly used benchmark aldol reaction between acetone and *p*-nitrobenzaldehyde with low yields but good enantioselectivities. The synthesized peptide had lower activity and selectivity when compared to the previously reported proline-based catalysts, but our findings provide information on the structural/conformational design and properties of the peptide catalysts. This information will be used in the design of peptidomimetic catalysts with an activated lysine.

Future work should involve computational studies to determine a plausible mechanism, structure of the transition state and the most active structural conformation of the peptide catalysts. This will assist in the optimization of the reaction conditions for future reactions.

Chapter 7

Experimental Procedures

7.1 Materials and methods

All solvents and reagents were obtained from commercial sources. Reagent used in the peptide synthesis such as diisopropylethylamine (DIPEA), piperidine, triisopropylsilane (TIS), formic acid, trifluoroacetic acid (TFA), 1,2-ethanedithiol (EDT) were purchased from Sigma-Aldrich South Africa, while Fmoc protected amino acids, (2-(1H-benzotriazol-1-yl-1,1,3,3-tetramethyluronium hexafluorophosphate (HBTU), 1-[Bis(dimethylamino)methylene]-1H-1,2,3-triazolo[4,5-b]pyridinium 3-oxide hexafluorophosphate (HBTU), Rink amide MBHA were purchased from DLD scientific. Organic solvents such as dimethyl formamide (DMF), methanol, acetonitrile, hexane, dimethyl sulfoxide and diethyl ether were supplied by Radchem and Pyramid Scientific. Solvents for column chromatography (ethyl acetate and hexanes) were purchased from Protea Chemicals (South Africa) and distilled before use to remove non-volatile components.

7.2. Instrumentation and general techniques

Peptide synthesis: peptides were synthesized on an automated Protein Technologies, Inc PS-3TM peptide synthesizer.

Purification of the peptides was achieved *via* an Agilent 1260 Infinity semi-preparative HPLC system with a UV/VIS detector and an automated fraction collector on a Kinetix® 5 μm B-C18, 100 Å (250 ×230 nm) column. A two-buffer system was employed; Buffer A consisted of 0.1% formic acid in H_2O and buffer B consisted of 0.1% formic acid in CH_3CN. A flow rate of 20 ml/min or 15 ml/min and UV wavelengths of 215 and 254 nm were utilized.

Analytical LC-MS analysis was carried out on an Ultra High Performance Liquid Chromatography (Thermo Scientific Ultimate 3000, RS diode array detectors)-High Resolution Mass Spectrometer (Bruker Compact quadruple time of-flight) coupled to Diode Array (215 and 254 nm). A two-buffer system was employed with a flow rate of 0.3 ml/min on a C18 column (5 μm, 100 Å, 4.60 mm × 150 mm). The buffer system utilized formic acid as

the ion-pairing agent, solvents-A (water with 0.1% formic acid) and solvent-B (acetonitrile with 0.1% formic acid acid).

Analytical thin layer chromatography (TLC) plates (0.2 mm silica gel 60 with fluorescent indicator UV_{254}) were obtained from Sigma-Aldrich. Aldol reactions were monitored using TLC and further visualization was done by staining with potassium permanganate ($KMnO_4$) solution followed by heating. The compounds were purified using column chromatography on normal silica gel (particle size 0.063-0.200 mm) and flash silica gel (particle size 0.040-0.063) purchased from Merck. Ethyl acetate and hexane were used as eluting solvents. Solvent ratios are reported as (30/70; volume by volume)

The enantiomeric excess (ee), was determined by chiral high performance liquid chromatography (HPLC) analysis on a Dionex HPLC Ultimate 3000 instrument (CHROMELEON version 6.80 software); coupled to a pump and photodiode array detector. A Lux 5μ cellulose-2 column was used for the analysis with hexane and isopropyl alcohol (IPA) as the mobile phase. Detailed solvent ratios are outlined in the experimental section below.

^{1}H-NMR spectra were recorded on a Bruker Avance 300 MHz, Bruker Avance 400 MHz and on Bruker III 500 MHz spectrometer. The chemical shifts (δ) values are reported in parts per million (ppm) relative to deuterated chloroform ($CDCl_3$, 7.26 ppm) and dimethyl sulfoxide (DMSO-$_{d6}$, 2.49 ppm) and referenced against the internal standard, tetramethylsilane (TMS, 0.00 ppm). The spectra were analyzed as first order and the values of the coupling constant (J) are reported as Hertz (Hz). Multiplicity of signals are expressed as: s=singlet, br s=broad singlet, d=doublet, dd=double doublet, t=triplet, q=quartet, m=multiplet.

^{13}C-NMR spectra were recorded on Bruker Avance 300 MHz, Bruker Avance 400 MHz and on Bruker III 500 MHz spectrometer. The chemical shifts values are reported in (ppm) relative to deuterated chloroform ($CDCl_3$, 77.2 ppm), (DMSO-$_{d6}$, 39.52 ppm) and TMS as an internal standard.

2D NMR spectra which include COSY, ^{13}C-HSQC, TOCSY, NOESY and ROESY experiments, were recorded at 293, 300, and 308 K on a 500 MHz NMR Bruker III 500 MHz spectrometer. All 2D spectra were recorded at the phase sensitive mode using time proportional phase increment (TPPI). The residual water peak of DMSO-d6 was suppressed by a presaturation pulse of 2 s duration. The first NOESY experiments were recorded with mixing time of 150, 200 and 250 ms; ROESY spectrum were recorded with mixing times of 100, 150,

200, 250 and 300 ms; while TOCSY was recorded with mixing times of 48, 64, 70, 80 and 100 ms; each increment was the sum of 32 scans with a relaxation delay of 2.0 s; 2048 data point were collected per experiment.

CD spectra were recorded on a JASCO J-18 spectropolarimeter between the range of 190 to 250 nm in the specified solvents (water and phosphate buffer), with 10 scans at 20°C. The quartz cuvette used had a pathlength of 0.2 cm with a resolution of 0,2 mm, a bandwidth of 1.0 nm and a sensitivity of 10-20 mdeg. The peptides (0, 00061 mol L^{-1}) were prepared in water and a 20mM phosphate buffer (pH 8). The value of absorption was measured as molar ellipticity per residue deg.cm^2. $dmol^{-1}$). The signals obtained were converted to mean residue ellipticity, [θ] using the equation below:

$$[\theta] = \frac{(MRW \times \theta)}{10 \times d \times c} \text{ deg.cm}^2\text{.dmol}^{-1}$$

where MWR is the mean residue weight, θ the observed ellipticity in degrees, c is peptide concentration in g/ml and d is the pathlength in cm.[1]

Transmission electron microscopy (TEM) analysis was done using FEI Tecnai-12 microscopy at an electron acceleration voltage of 200 KV and beam size of 10-100 nm. Sample analysis was carried out by placing a drop of the gold colloidal on carbon-coated copper TEM grids. The sample was transferred on the grid and allowed to dry in air for few minutes before analysis.

UV-vis was used to monitor optical properties of gold colloidal solution. The analysis was conducted using a Varian Cary Eclipse (Cary 50) UV-vis spectrophotometer; with a Quartz cuvette of 1cm optical length.

7.3 General procedure for the synthesis of peptides

7.3.1 General procedure for the automated and manual SPPS synthesis

Swelling, activation and coupling of the first amino acid

The Fmoc-rink amide resin, 600 mg, (0, 160 mmol/g) was swelled in DMF (10.0 mL) for 20 minutes in a 70 mL glass reaction vessel with fritted filters. The DMF was removed by suction and a 20% piperidine solution in DMF (5 mL) was added and mixed by bubbling for 5 minutes with inert nitrogen gas (N_2). The piperidine solution was then filtered out and the resin was washed with DMF (5×5 mL) for 30 sec second per each wash.

The first amino acid cysteine (1.20 mmol, 0.2 M), and coupling reagent HBTU (1.14 mmol, 0.19 M) were dissolved in a solution of 1.0 M DIPEA in DMF (6 mL) and added into the reaction vessel. An additional 6 mL of DMF was also added. The reaction mixture was allowed to react for 45 minutes while a gentle flow of N_2 was bubbled into the reaction. For double coupling, the resin was washed with (3×5 mL) DMF, and the coupling was repeated using the same mixture for 60 minutes. The resin was then washed with (3×5 mL) DMF, and (2×5mL) DCM. The resin was then dried by suction for 30 minutes. This was followed by the determination of resin loading capacity and the procedure is described below.[2]

The loading capacity was performed in order to calculate the exact moles of the amino acid attached to the resin.

7.3.2 General procedure for the determining loading capacity

Duplicates of the dried resin beads (5-10 mg) were weighed into two 2 mL plastic Eppendorf tubes. A solution of 20% piperidine in DMF (1.0 mL) was added to each Eppendorf tube and left to shake for 20 minutes at 90 rpm on the orbital shaker. The samples were then centrifuged for 2 minutes and 100 μL of the supernatant was transferred into a plastic centrifuge tube containing 10 mL of DMF. From this solution 1 mL was then transferred into a cuvette. The samples contained in a cuvette were checked for absorbance at a wavelength of 301 nm on a UV/Vis spectrometer three times (reading were obtained in a triplicates). DMF was ran as a blank to zero the background. The Loading Capacity was calculated using the following equation below.[3]

$$Loading\ capacity = \left(\frac{mmol}{g}\right) of\ resin = \left(\frac{101\ \times Absorbace}{7.8\ \times w}\right)$$

Where; A= Average absorbance and W=mg of resin.

7.3.3 General procedure for the synthesis of peptides

After the first coupling, the resin-bound amino acid was then treated with 2×5 mL 20 % piperidine in DMF for 10 minutes to remove the Fmoc protecting group from cysteine. The resin was washed with DMF (5×5 mL) before the second amino acid was coupled. A solution containing 6 mL of 1.0 M DIPEA, (1.14 mmol, 0.19 M) HBTU, and (1.02 mmol, 0.2 M) arginine was added to the resin. The reaction mixture was mixed gently by bubbling nitrogen

gas for 45 minutes. The remaining amino acids in the sequence were also coupled using the same procedure until the full peptide was synthesized.

7.3.4 General procedure for cleaving peptides from the resin

The resin bound peptide was washed with (3 ×5 mL) DMF and then (3×5 mL) DCM and dried by suction. A cleavage cocktail (10 mL) containing 94% TFA: 2.5%EDT:2.5%H_2O:1%TIS was then reacted with the resin bound peptide for 3 hrs. The cleavage solution was filtered off, and the resin was washed with 5 mL of TFA and the filtrated was divided into portions in and poured into 50 ml centrifuged tubes. Cold diethyl ether was added to the filtered solution upon which a white precipitate of the crude peptide was formed. The two samples were centrifuged at 5000 rpm for 10 minutes. The step was repeated 3 times with cold diethyl ether. The obtained white precipitate was then dissolved in 10 mL (60/40; H_2O/MeCN) for further analysis and purification.

7.3.5 Cyclisation of peptides

The cyclization of the peptide was performed when the peptide was still attached to the resin. Iodine (10 equivalence, moles determined using the resin loading capacity), was dissolved in DMF/H_2O (4:1) solution (10 mL). The resin bound peptide was transferred into the solution and left to react for 4 hours. Upon completion, the resin was washed with (3×10 mL) DMF, (2×10 mL) 2 % ascorbic acid/DMF, (3×10mL) DMF and (3×10 mL) DCM.

7.4 Typical procedures for Aldol reaction

7.4.1 Preliminary aldol reaction investigation using Fructose-1,6-bisphosphate aldolase (FBPA)-RAMA

To a 2mL Eppendorf vial containing a solution of a 0.2M triethanolamine (TEA) 1mL buffer (pH 7.0), DMSO (0.4 mL) and DHAP (8.5 mg, 0.05 mmol), the RAMA enzyme (4.5×10^{-5} and 9.5×10^{-5} mol%) was added and stirred for 20 minutes in an orbital shaker. The corresponding acceptor aldehyde (0.2 mmol) was then added and the resulting mixture was left to react for 48 hours at room temperature. The reaction progress was monitored using TLC.

7.4.2 General procedure for the aldol reaction preliminary test using acetone

To a solution of 0.75 mL (acetone/water,3:1) in a 2 mL Eppendorf tube, a catalyst (4 mol%) was added and the reaction was stirred for 15 min. An aldehyde (0.25 mmol, 38mg) was then

added and the reaction was stirred for 24 hours at room temperature. The reaction was monitored using TLC and LC-MS at of 30 minutes, 3, 7 and 24 hours. To monitor the reaction progress using LC-MS, 30μL of the reaction mixture was added into a 2 mL HPLC vial containing 1.5 mL of acetonitrile and analyzed.

7.4.3 General procedure for the aldol reaction preliminary test using cyclic ketone

In a 2 mL Eppendorf tube containing a ketone (0.45 mL), 4 mol % of the catalyst was added, followed by 40μL of water and the reaction was stirred for 15 minutes. This was followed by the addition of the acceptor aldehyde (0.25 mmol, 38mg) and the reaction mixture was left to stir for 24 hours at room temperature. The reaction was monitored by LC-MS; 30μL of the reaction mixture was added into a 2 mL HPLC vial containing 1.5 mL acetonitrile and analyzed

7.4.4 Aldol reactions in acetone in the presence of water

A peptide catalyst (0.0064 mmol, 4 mol%) was added to a vial containing 0.75 mL of 3:1 acetone/water and the mixture was stirred for 15 min. An acceptor aldehyde (0.157 mmol, 24 mg) was then added and the resulting reaction mixture was stirred vigorously at room temperature for 24-72 hours. The reaction was stopped upon completion as indicated by TLC and acetone was evaporated under reduced pressure. The crude product was extracted using (3 ×10 mL) ethyl acetate (EtOAc) and 2 mL water. The combined organic phases were dried over Na_2SO_4, and concentrated under reduced pressure. The crude product was then purified by flash silica gel column chromatography using ethyl acetate/hexane (1:3). The pure product was then subjected to chiral-phase HPLC analysis to determine the ee.

7.5 Procedures for the aldol reactions between aromatic aldehydes and cyclohexanone

7.5.1 Aldol reaction between cyclohexanone and aromatic aldehydes (homogenous)

A peptide catalyst (0.0064 mmol, 4 mol%) was added to the ketone (0.45 mL) in water (40μL) and stirred for 15 minutes. An acceptor aldehyde was then added and the resulting reaction mixture was left to stir for 24-72 hours at room temperature. The reaction was stopped upon completion as indicated by TLC. The reaction was quenched by extraction with (3×10 mL) EtOAc and brine solution (2 mL). The combined organic extract was washed with brine and dried with Na_2SO_4, filtered and concentrated *in vacuo*. Diastereomeric ratio of the crude product was determined by ^{1}H NMR analysis. The crude aldol product was purified by flash

silica-gel column chromatography using EtOAc/Hexane (1:3) and the desired aldol product was subjected to chiral-phase HPLC analysis to determine the ee.

7.5.2 Aldol reaction between cyclohexanone and aromatic aldehydes (heterogenous)

A peptide catalyst (0.0064 mmol, 4 mol%) was added to a solution of a ketone (0.450 mL) and 60 μL of water and stirred for 15 minutes. An acceptor aldehyde (0.157 mmol, 24 mg) was then added to reaction mixture which was stirred for 24-72 hours. The reaction was monitored by TLC and the reaction was quenched by extraction with (3×10 mL) EtOAc and (1×2 mL) brine solution. The combined organic layers were dried with Na_2SO_4, filtered and concentrated *in vacuo*. The crude product was purified by flash chromatography on silica gel using EtOAc: hexane (1:3).

7.5.3 General procedure for aldol reaction between cyclohexanone and aromatic aldehydes in organic solvent

A peptide catalyst (0.0064 mmol, 4 mol%) was added to a vial containing a 0.75 mL solvent mixture (0.5173 mL solvent and 0.237 mL water) and cyclohexanone (0.628 mmol, 70 μL) and the mixture was stirred for 15 minutes. An acceptor aldehyde (0.157 mmol, 24 mg) was then added to the reaction mixture which was stirred for 24 -72 hours. The reaction progress was monitored by TLC and was extracted with EtOAc (3×10 mL) and brine solution (1×2.0 mL). The combined organic layers were dried over Na_2SO_4 and concentrated in vacuo. Diastereomeric ratio of the crude product was determined by ^{1}H NMR analysis. The crude product was purified by flash chromatography on silica-gel with hexane/ethyl acetate (3:1). The pure products were then analyzed by the chiral HPLC and the ee values were determined.

7.6 General procedure for the synthesis of gold nanoparticle (AuNPs)

The synthesis of citrate capped AuNPs was conducted according to the procedures developed by Turkevich *et al*.[4] All glassware used were thoroughly cleaned with aqua regia(HCl/HNO_3) and rinsed with Millipore-Q water before use. An aqueous solution of tetrachloroauric acid ($HAuCl_4$) (1 mM, 250mL) was heated at 100 °C with vigorous mechanical stirring for 20 minutes. Once the solution started boiling an aqueous solution of trisodium citrate dihydrate (0.04 M, 10 mL) was then added dropwise while the reaction was stirred vigorously. The solution was allowed to boil for an additional 10 minutes to ensure complete reduction of $HAuCl_4$. A colour change from colourless to deep ruby-red indicating the formation of AuNPs was observed. The solution was gradually cooled down at room temperature for 3 hours.

To obtain different sizes of AuNPs various volumes of 10, 20, 30 and 50 mL aqueous tri-sodium citrate were added to the mixture. After cooling, the colloidal solutions of AuNPs were washed with water by centrifuging at 1500 rpm for 15 minutes using an Universal 320R centrifuge in order eliminate excess unreacted ions and the starting material in the supernatant. The concentrated dispersed AuNPs particles at the bottom of the centrifuge tube free of excess salts were diluted back to the original concentration with Millipore-Q water. The AuNPs solutions were transferred into glass vials wrapped with aluminium foil to avoid interactions with light which may cause in aggregation of the particles. The vials were stored in the fridge and could be used for over 6 months without aggregation.

7.7 Typical procedure for the functionalization of TP_ADLys peptide to AuNPs

The centrifuged solution of AuNPs was divided into 3 aliquots of 10 mL. This was further divided into fractions of 1.5 1.0 and 0.5 mL and were added to different peptide concentrations of (1.5, 2.8, 4 and 6 mol%) and stirred for 3 hours at room temperature to allow the complete exchange of citrate with thiols on the particle surface. The ruby-red colour changed to a pale red colour and excess non-immobilized peptide was removed by centrifugation at 1500 rpm for 15 min in a Universal 320R centrifuge.

7.8 General procedure for aldol reaction using peptide-capped AuNPs

The corresponding ketone (0.628 mmol, 70 μL) was added to a 2mL Eppendorf vial containing 1 mL of the DMSO/AuNP-pep solution (0.5:0.5 mL, v: v) and the mixture was stirred for 15 minutes. This was followed by the addition of the acceptor aldehyde (0.157 mmol, 24 mg) and the resulting mixture was stirred for 24-72 hours. Conversion of the product was monitored by TLC, upon which the reaction mixture was extracted with (3×5 mL) EtOAc and the combine organic phases were dried over Na_2SO_4 and concentrated *in vacuo*. Diastereomeric ratio of the crude product was determined by ^{1}H NMR analysis. The crude aldol product was purified using flash silica-gel column chromatography and EtOAc/Hexane (1:3) and the desired aldol product was subjected to chiral-phase HPLC analysis to determine the ee

7.9.1 Catalyst recyclability for peptide catalyzed aldol reaction

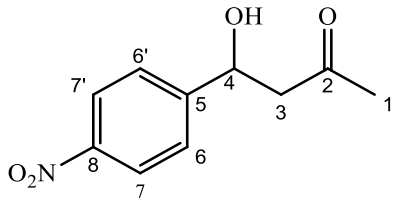
The filtered aqueous layers obtained after extraction of the crude product, were combined and washed with Et_2O (3 mL) and C_2H_5O (4 mL). The peptide was catalyst obtained was after drying and decantation of the resuspended mixture. The recycled peptide was added to a vial containing a 0.75 mL solvent mixture (0.5173 mL solvent and 0.237 mL water) and

cyclohexanone (0.628 mmol, 70 μL) and the mixture was stirred for 15 minutes. An acceptor aldehyde (0.157 mmol, 24 mg) was then added to the reaction mixture which was stirred for 24 -72 hours. The reaction progress was monitored by TLC.

7.9.1 Catalyst recyclability for peptide-AuNPs catalyzed aldol reactions

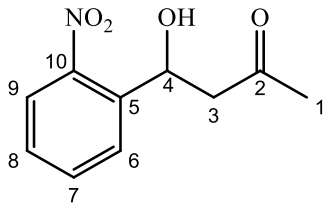
The filtered aqueous layers obtained after extraction of the crude product, were combined and washed with Et_2O (3 mL) and C_2H_5O (4 mL). The mixture was centrifuged at 500 rpm for 10 min and resuspended at 0°C. After decantation, the supported catalyst was dried and used in the next cycle. The recovered catalyst was added to the corresponding ketone (0.628 mmol, 70 μL) and 0.5 mL of DMSO in a 2 mL Eppendorf vial and the mixture was stirred for 15 minutes. This was followed by the addition of the acceptor aldehyde (0.157 mmol, 24 mg) and the resulting mixture was stirred for 24-96 hours.

7.10 Characterization of Aldol Products



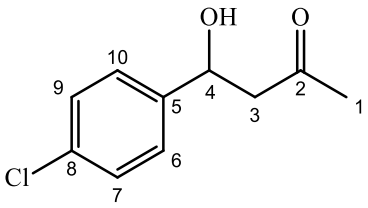
4-Hydroxy-4-(4'-nitrophenyl)-butan-2-one (TP_A1N4ACE)

Yellow solid: R_f = 0.27 (30% ethyl acetate/hexane). IR (V_{max}/cm^{-1}): 3459 (O-H), 3118 (=C-H), 3068 (C-H), 1574 (C=C), 1706(C=O), 1323(C-O). ^{1}H NMR (500 MHz, $CDCl_3$) δ: 8.22 (d, 2H, H-7& H-7'), 7.54 (d, 2H, H-6 and H-6'), 5.30 – 5.21 (m, 1H, H-4), 3.55 (brs, *J* = 3.3 Hz, 1H, OH), 2.87 – 2.77 (m, 2H, H-3), 2.23 (s, 3H, H-1).^{13}C NMR (126 MHz, $CDCl_3$) δ: 208.44(C-2), 126.45(C-6), 126.34(C-6'), 123.80(C-7) , 123.72(C-7') , 68.62(C-4) , 50.83(C-3) , 30.77(C-1).HRMS (ESI) *m/z*: Calculated for $C_{10}H_{11}NO_4$:209.068, found: 232.0910$[M+23]^+$



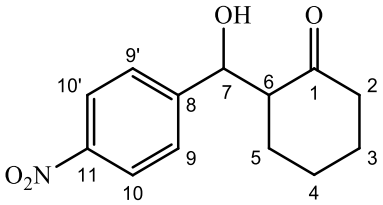
4-Hydroxy-4-(2'-nitrophenyl)-butan-2-one (TP_A2N2ACE)

colourless solid: R_f = 0.32 (30% ethyl acetate/hexane). IR (V_{max}/cm^{-1}): 3461 (O-H), 3068(=C-H), 2922 (C-H), 1609 (C=O), 1518 (C=C), 1333(C-O). ^{1}H NMR (500 MHz, CDCl3) δ 8.04 – 7.80 (m, 2H, H-9 and H-8), 7.77 – 7.58 (m, 1H, H-6), 7.50 – 7.38 (m, 1H, H-7), 5.68 (dd, 1H, H-4), 3.79 (brs, 1H, OH), 3.11 (d, 1H, H-3), 2.74 (dd, *J* = 17.8, 9.4 Hz, 1H, H-3), 2.24 (s, 2H H-1).^{13}C NMR (126 MHz, $CDCl_3$) δ: 208.76 (C-2), 147.12(C-10), 138.47(C-5), 133.82(C-7), 128.28(C-6), 128.19(C-9), 124.43(C-8), 65.60(C-4), 51.12(C-3), 30.43(C-1). HRMS (ESI) *m/z*: Calculated for $C_{10}H_{11}NO_4$:209.07, found: 232.0583 $[M+23]^+$



4-Hydroxy-4-(4'-chloropheny)-butan-2-one (TP_A3ClACE)

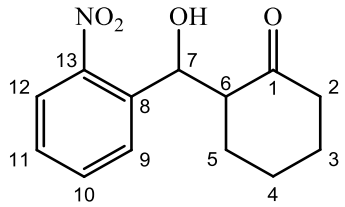
Colourless oil: R_f = 0.28 (30% ethyl acetate/hexane). IR (V_{max}/cm^{-1}): 3421 (O-H), 3117(=C-H), 2967 (C-H), 1701 (C=O), 1519 (C=C), 1315(C-O). ^{1}H NMR (500 MHz, $CDCl_3$) δ: 7.33 – 7.26 (m, 4H, Ar-H), 5.12 (d, *J* = 9.0, 3.4 Hz, 1H, H-4), 3.47 (brs, 1H, OH), 2.89 – 2.72 (m, 2H, H-3), 2.19 (s, 3H, H-1). ^{13}C NMR (126 MHz,) δ: 208.86, 141.25, 133.30, 128.65, 127.03, 69.16, 51.82, 30.76. HRMS (ESI) *m/z*: Calculated for $C_{10}H_{11}ClO_4$:198.0488, found: 221.0334 $[M+23]^+$



2-(Hydroxy(4-nitrophenyl)methyl)cyclohexanone (TP_A4N4CY)

Yellowish solid: R_f = 0.26 (30% ethyl acetate/hexane). IR (V_{max}/cm^{-1}): 3426(O-H), 3077(=C-H), 2949 (C-H), 1698 (C=O), 1524 (C=C), 1024(C-O). ^{1}H NMR (500 MHz, $CDCl_3$) δ: 8.21 (d, *J* = 8.9, 2.3 Hz, 2H,H-10 and H-10'), 7.50 (d, *J* = 7.5 Hz, 2H, H-9 and H-9'), 4.90 (d, *J* = 8.3, 3.0 Hz, 1H, H-7), 4.07 (brs, 1H, OH), 2.63 – 2.55 (m, 1H, H-6), 2.54 – 2.45 (m, 1H, H-2a), 2.41 – 2.31 (m, 1H, H-2b), 2.16 – 2.08 (m, 1H-H-3a), 1.72 – 1.64 (m, 1H-H-3b), 1.63 – 1.48 (m, 4H, H-4 and H-3). ^{13}C NMR (126 MHz, $CDCl_3$) δ: 214.73 (C-1), 147.96 (C-11), 127.87 (C-8), 126.59 (C-9 and C-9'), 123.52 (C-10 and C-10'), 74.05 (C-7), 70.14 (C-6),

57.20 (C-2), 42.69 (C-5), 30.77 (, 27.64 , 24.75 HRMS (ESI) *m/z*: Calculated for $C_{13}H_{15}NO_4$:249.1001, found 272.0890 $[M+23]^+$.



2-Hydroxy(2-nitrophenyl)methyl)cyclohexanone (**TP_A5N2CY**)

Yellow oil: R_f = 0.29 (30% ethyl acetate/hexane). IR (V_{max}/cm^{-1}): 3454(O-H), 2922 (=C-H), 2853 (C-H), 1693 (C=O), 1512 (C=C), 1199(C-O).^{1}H NMR (500 MHz, $CDCl_3$) δ: 7.94 – 7.72 (m, 2H), 7.64 (t, *J* = 7.7 Hz, 1H), 7.43 (t, *J* = 7.8 Hz, 1H), 5.45 (d, *J* = 7.0 Hz, 1H), 4.07 (d, *J* = 37.1 Hz, 0H), 2.82 – 2.68 (m, 1H), 2.51 – 2.28 (m, 2H), 1.92 – 1.52 (m, 5H), 1.26 (d, 2H). ^{13}C NMR (126 MHz, $CDCl_3$) δ 214.96 (C-1), 148.73 (C-13), 136.63 (C-8), 133.07 (C-10), 129.00 (C-9), 128.40 (C-12), 124.10 (C-11), 69.81 (C-7), 57.31 (C-6), 42.85 (C-2), 31.14 (C-5), 27.77 (C-3), 25.00 (C-4). Calculated for $C_{13}H_{15}NO_4$:249.1001, found 272.0890 $[M+23]^+$.

7. 11 References

(1) Kelly, S. M.; Jess, T. J.; Price, N. C. How to Study Proteins by Circular Dichroism. *Biochim. Biophys. Acta (BBA)-Proteins Proteomics* **2005**, *1751* (2), 119–139. https://doi.org/10.1016/j.bbapap.2005.06.005.

(2) Jensen, K.J., Shelton, P.T. and Pedersen, S. . (Ed). *Springer Protocols. Methods in Molecular Biology 1047: Peptide Synthesis and Applications*, Second Edi.; New York: Humana Press., 2013.

(3) Howl, J. (Ed). *METHODS IN MOLECULAR BIOLOGY:Peptide Synthesis and Applications*; Springer Science & Business Media., 2005; Vol. 298.

(4) Turkevich, J.; Stevenson, P. C.; Hillier, J. A Study of the Nucleation and Growth Processes in the Synthesis of Colloidal Gold. *Discuss. Faraday Soc.* **1951**, *11* (c), 55–75. https://doi.org/10.1039/DF9511100055.

APPENDICES

Appendix I - Supplementary information for Chapter 2

Appendix II - Supplementary information for Chapter 3

Appendix III - Supplementary information for Chapter 4

Appendix I - Supplementary information for Chapter 2

LC-MS spectra for selected compounds

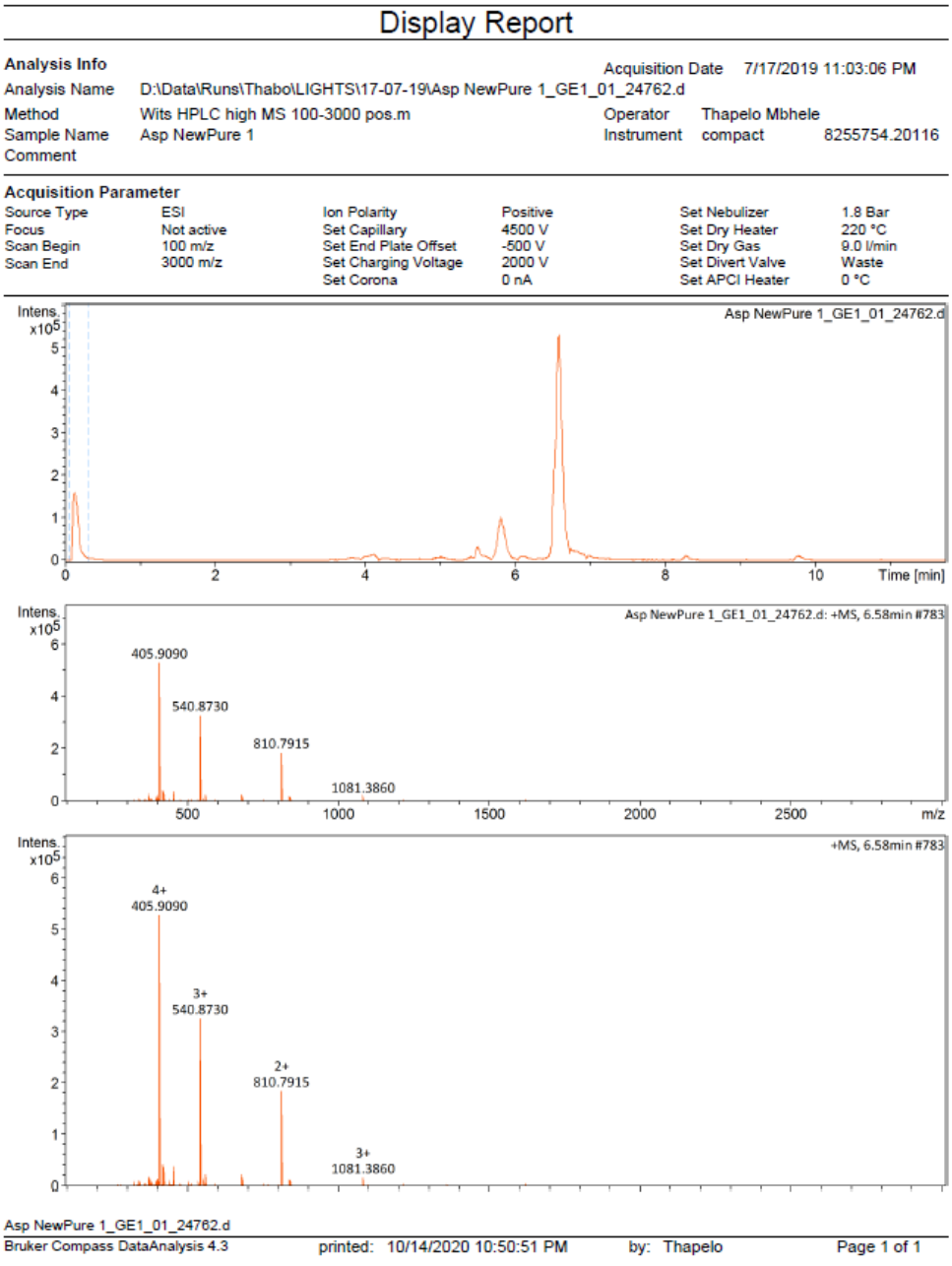


Figure S.2-1: LC-MS spectrum of TP_Asp conformation 1 (peak 1)

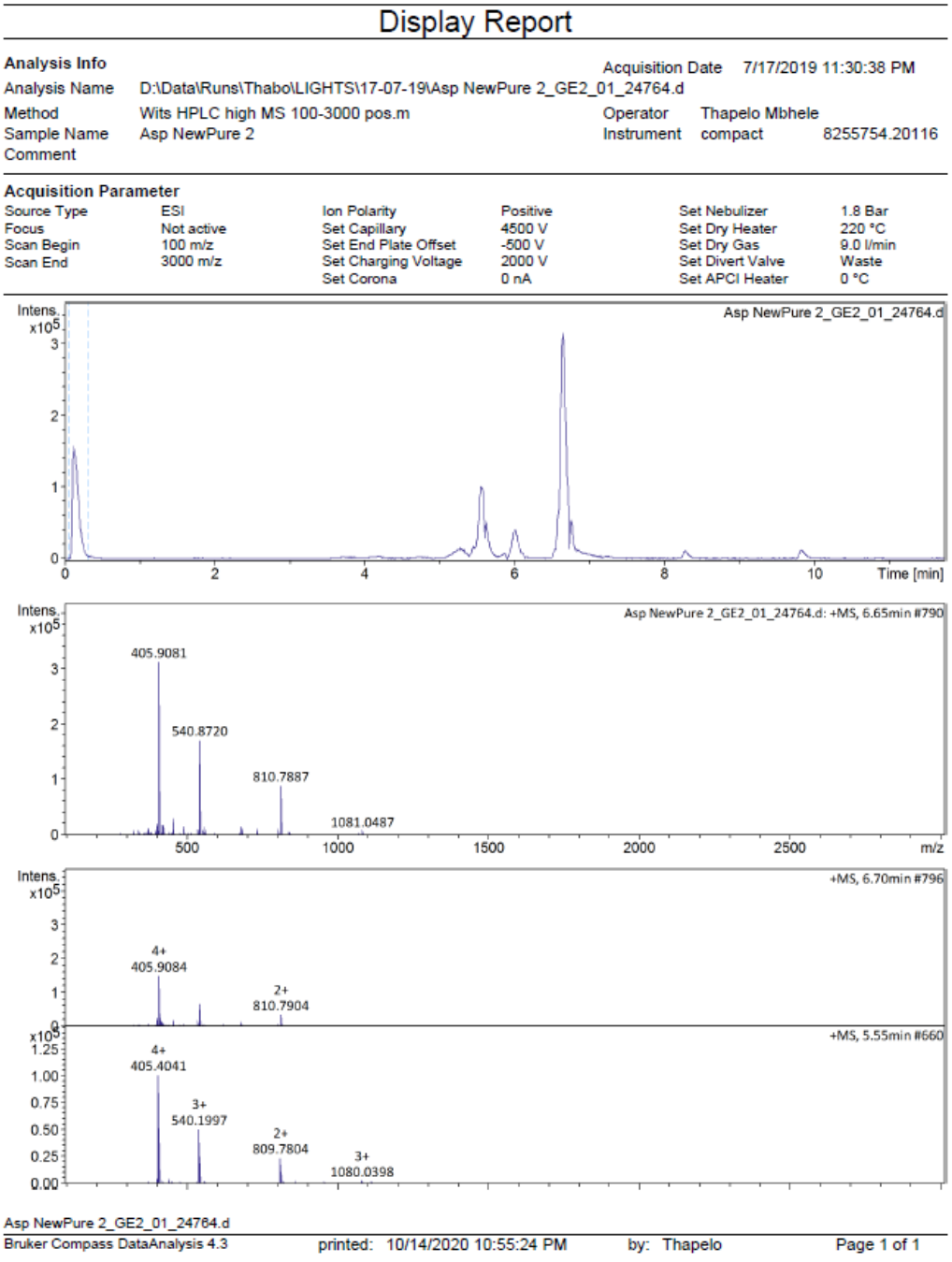


Figure S.2-2: LC-MS spectrum of TP_Asp conformation 2 (peak 2)

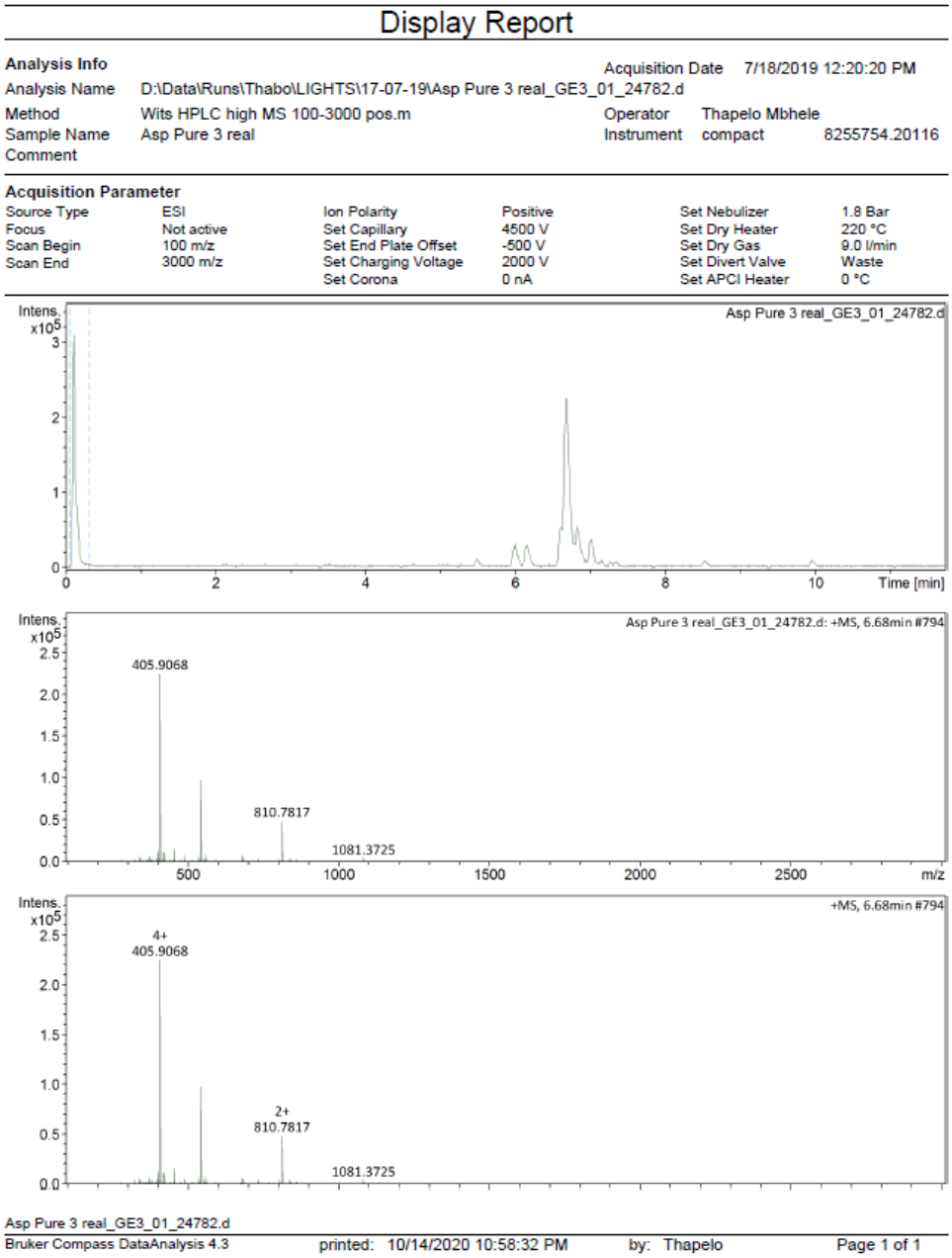


Figure S.2-3: LC-MS spectrum of TP_Asp conformation 3 (peak 3)

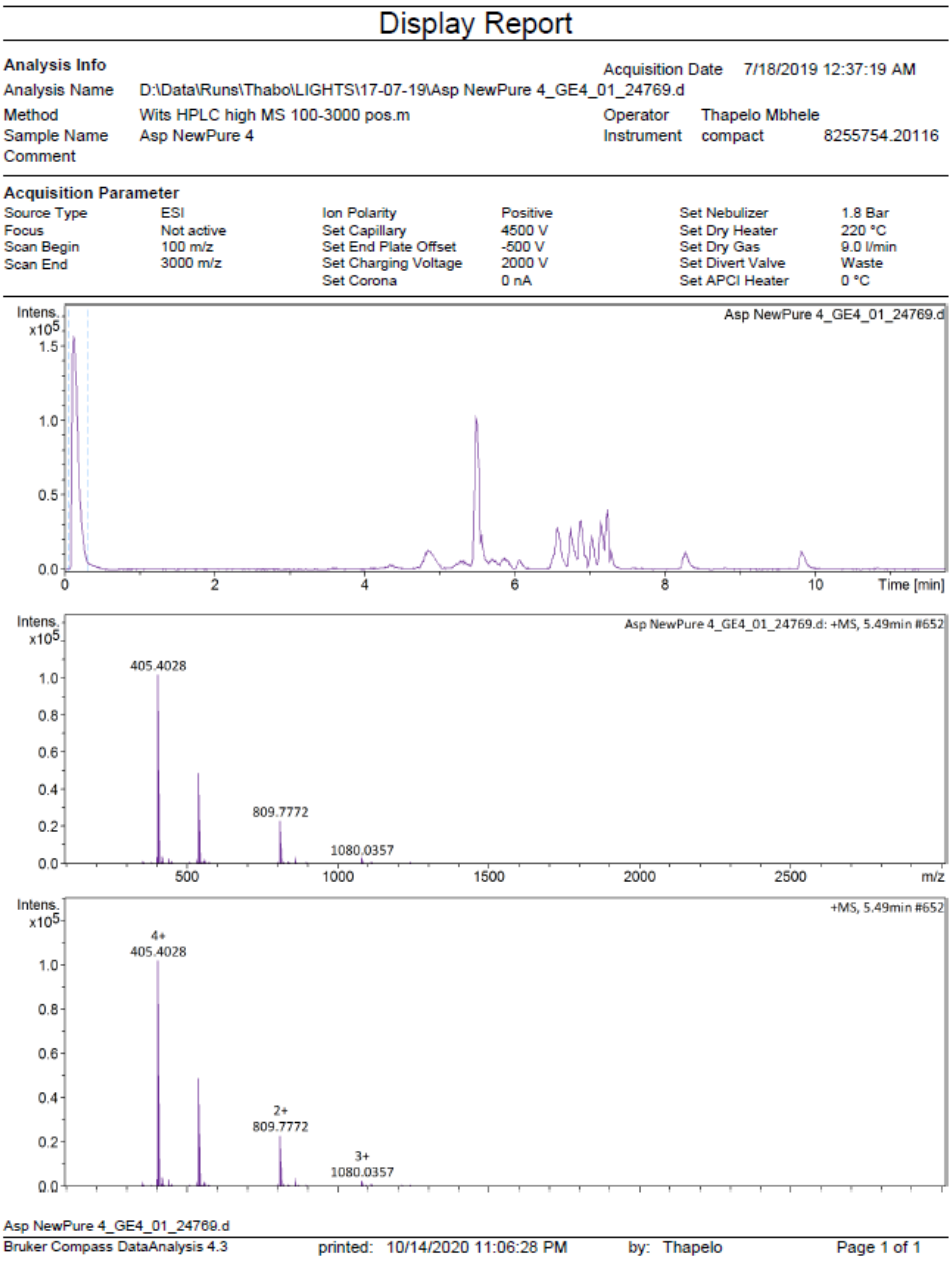


Figure S.2-4: LC-MS spectrum of TP_Asp conformation 4 (peak 4)

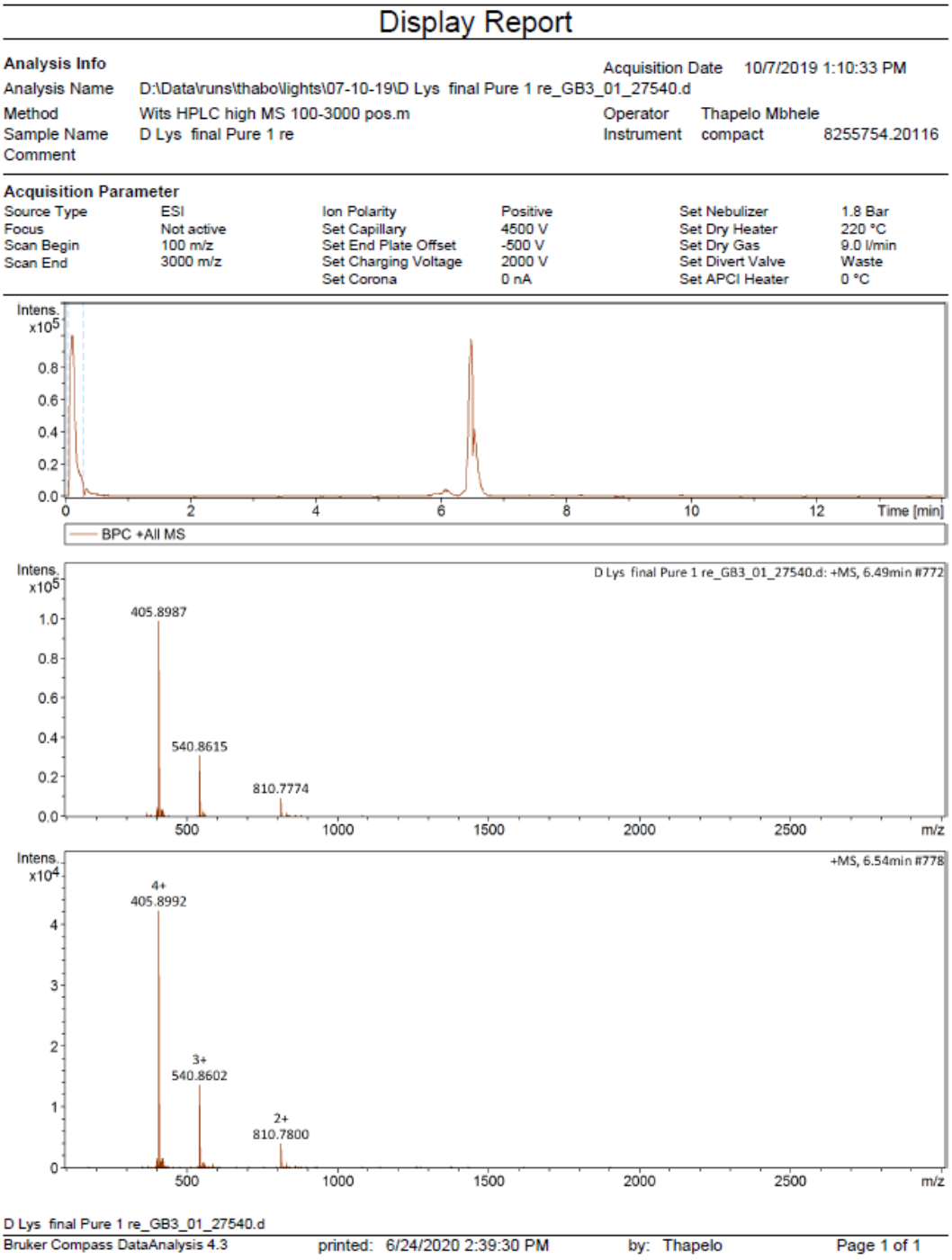


Figure S.2-5: LC-MS spectrum of TP_ADLys conformation 1 (peak 1)

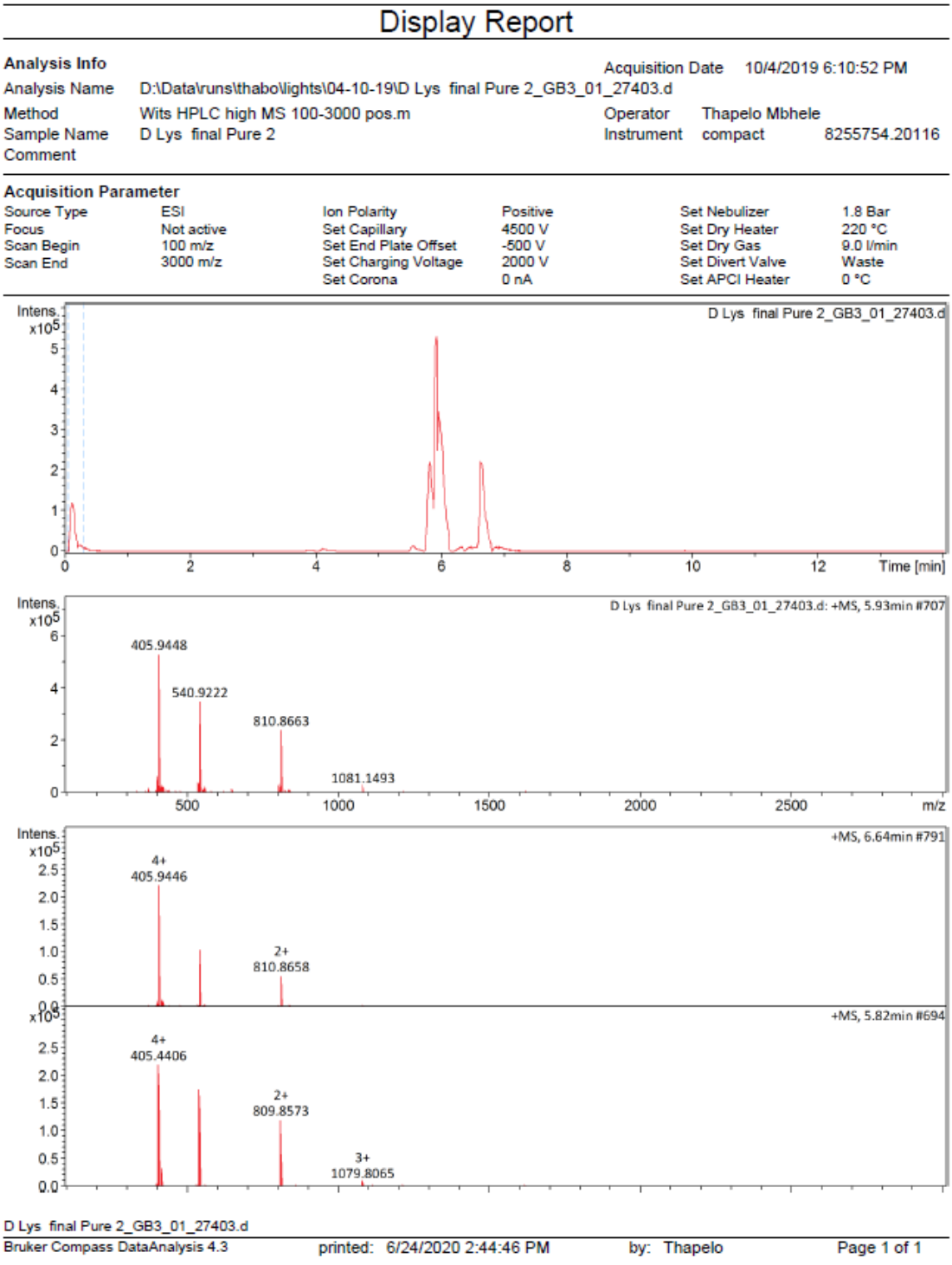


Figure S.2-6: LC-MS spectrum of TP_ADLys conformation 2 (peak 2)

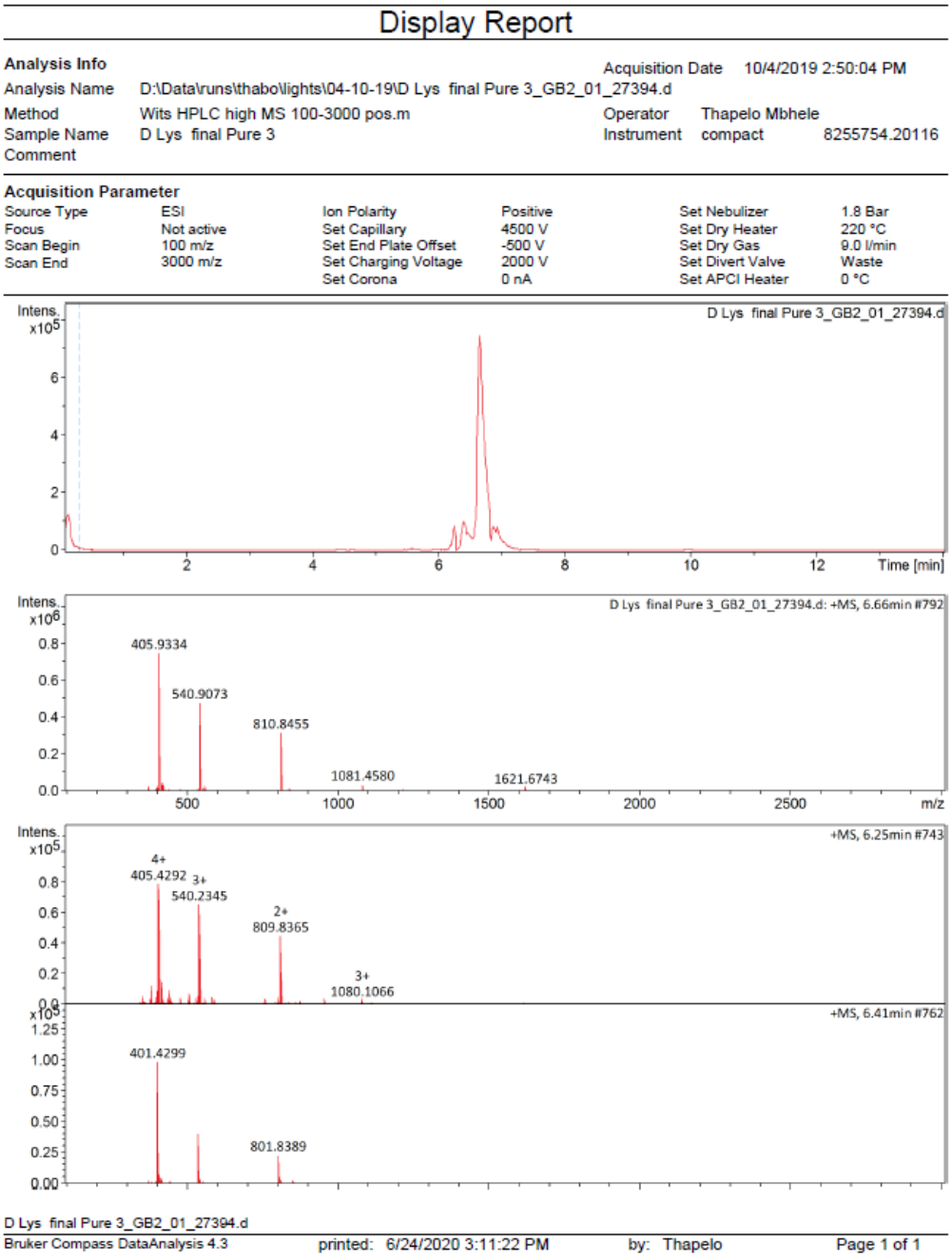


Figure S.2-7: LC-MS spectrum of TP_ADLys conformation 3 (peak 3)

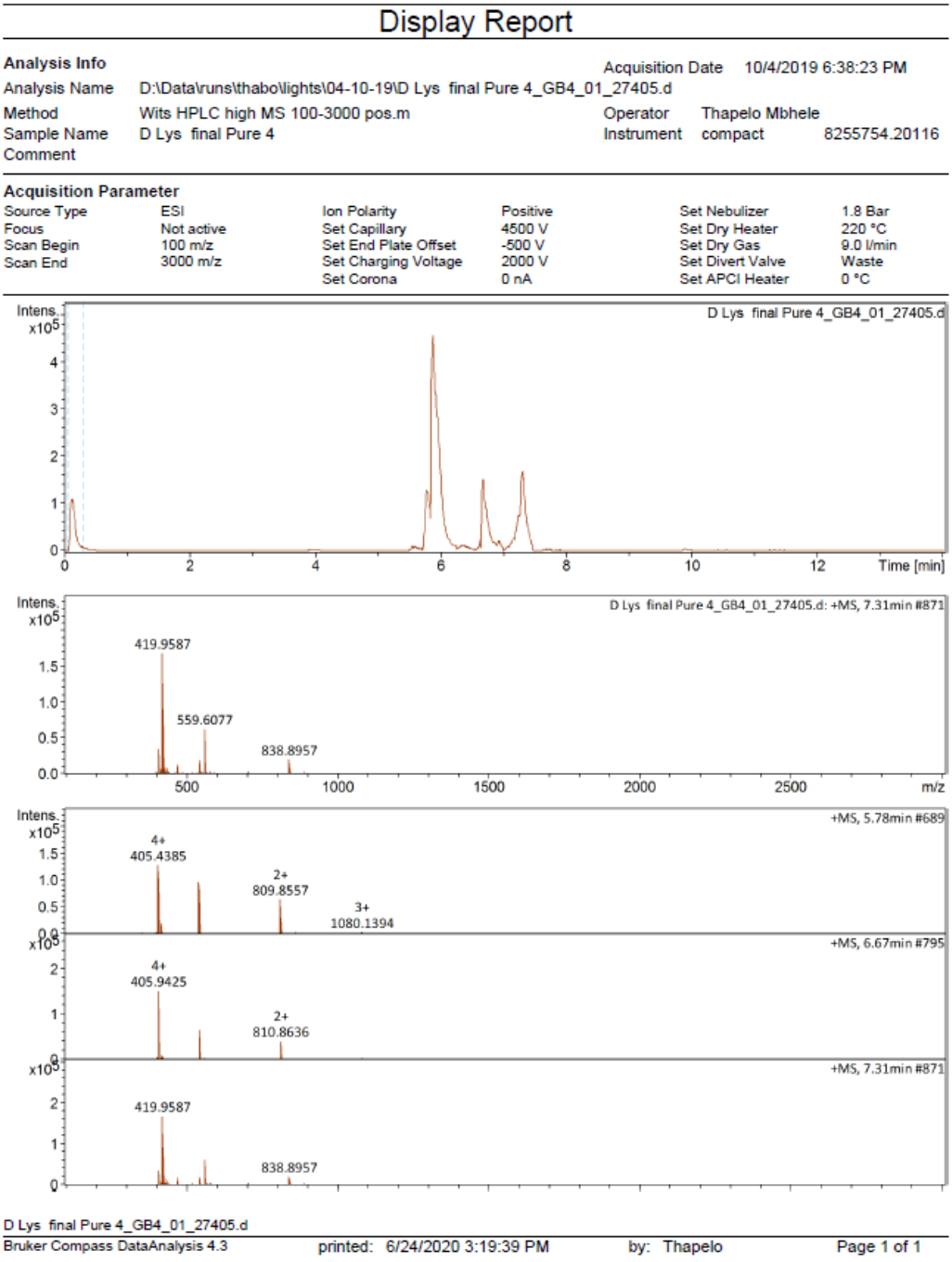


Figure S.2-8: LC-MS spectrum of TP_ADLys conformation 3 (peak 3)

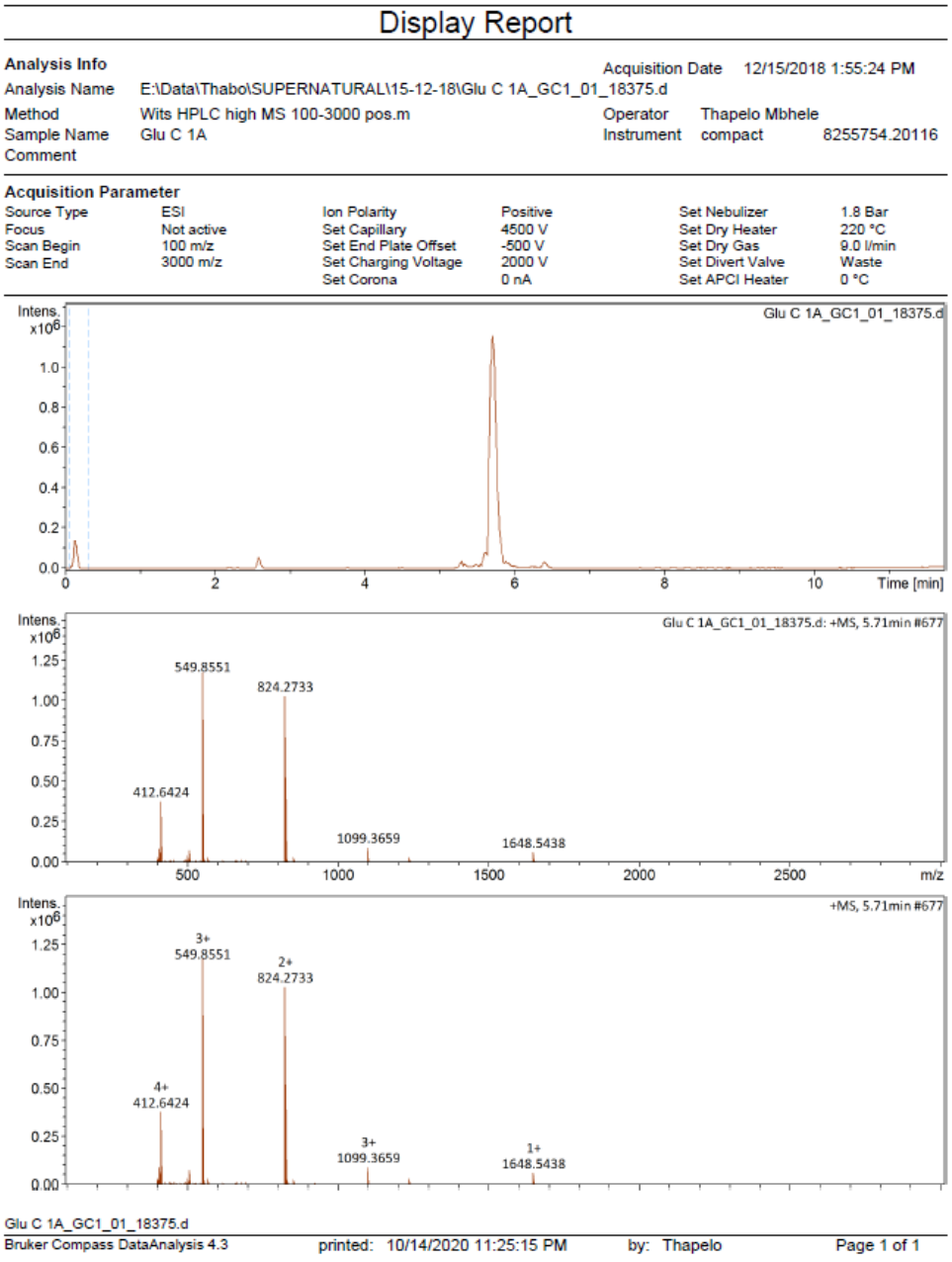


Figure S.2-9: LC-MS spectrum of TP_Glu conformation 1 (peak 1)

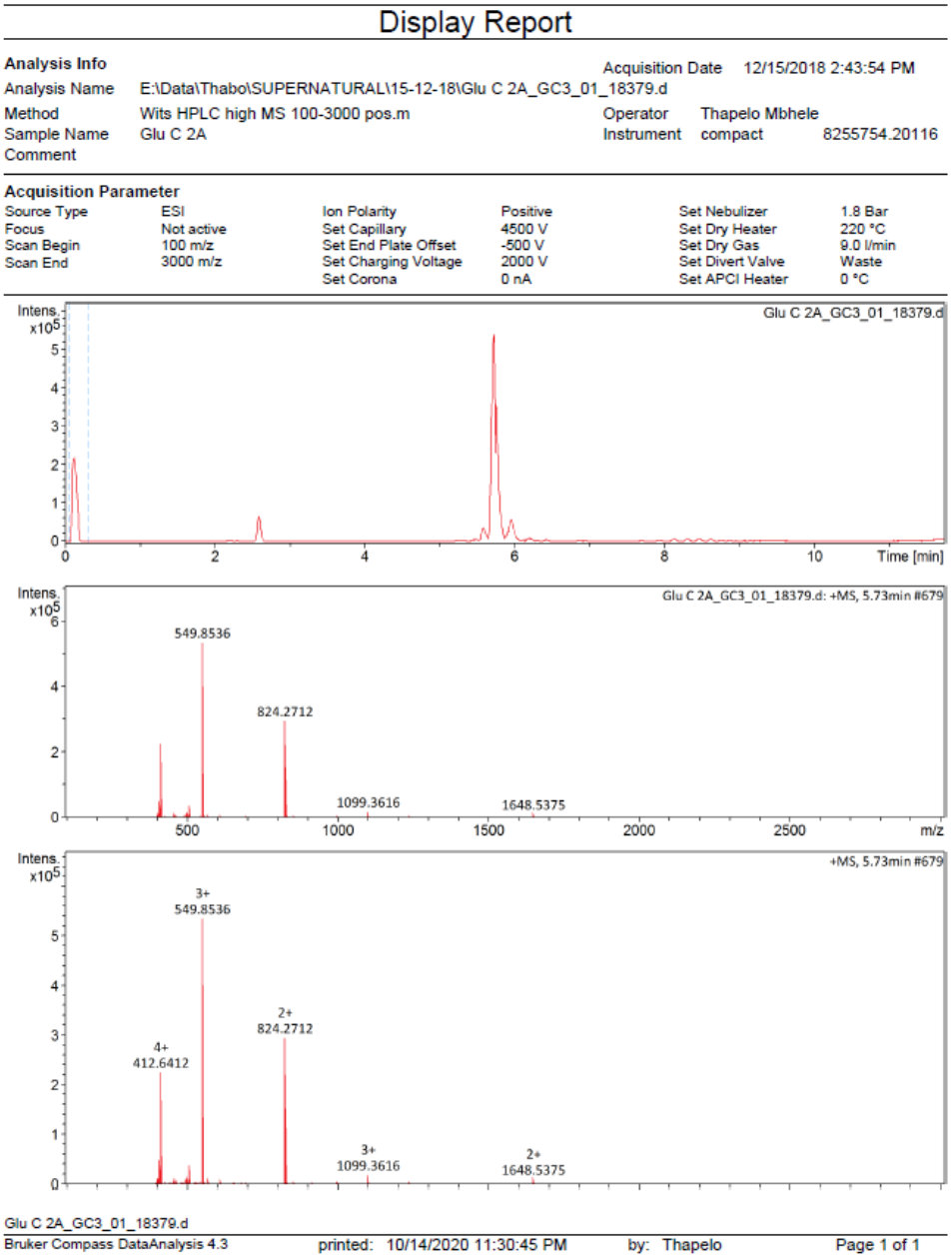


Figure S.2-10: LC-MS spectrum of TP_Glu conformation 2 (peak 2)

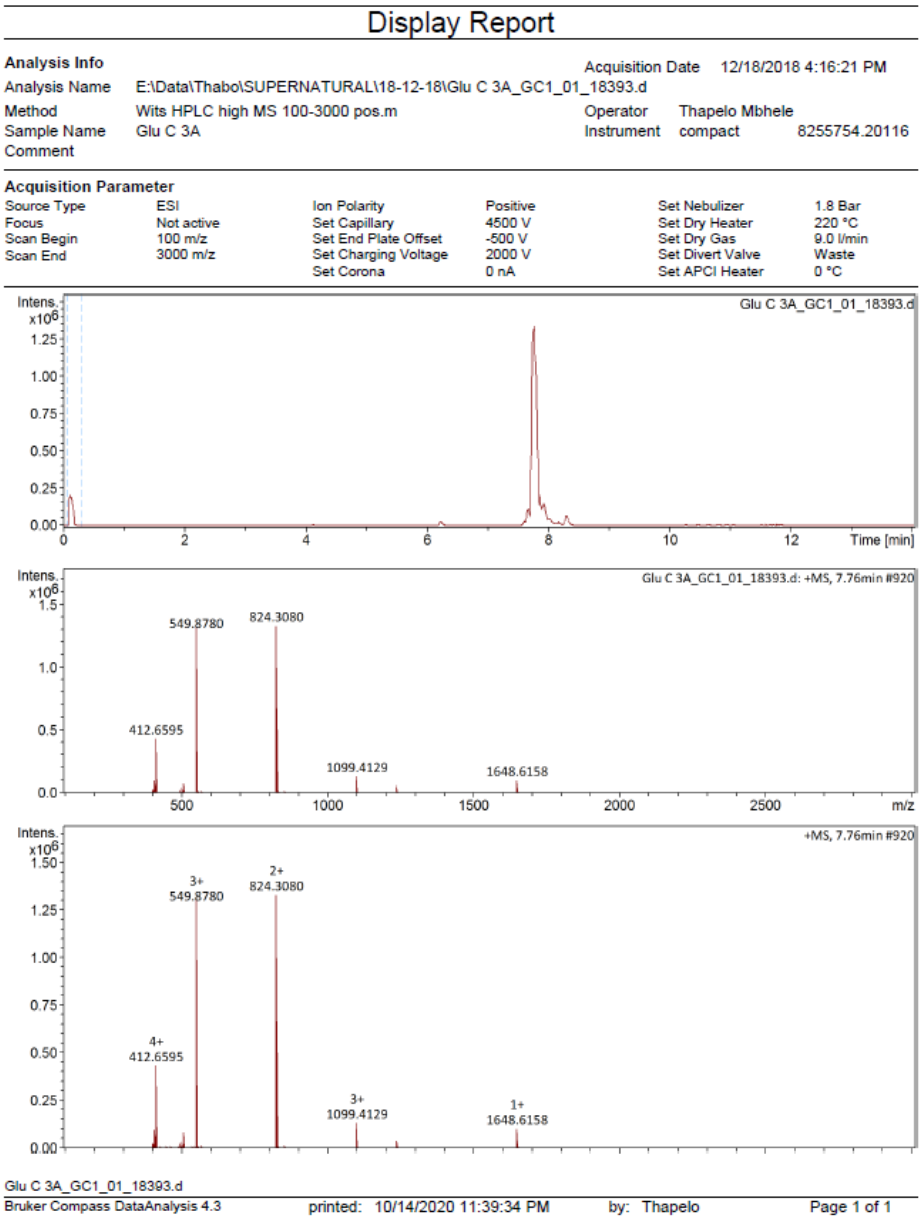


Figure S.2-11: LC-MS spectrum of TP_Glu conformation 3 (peak 3)

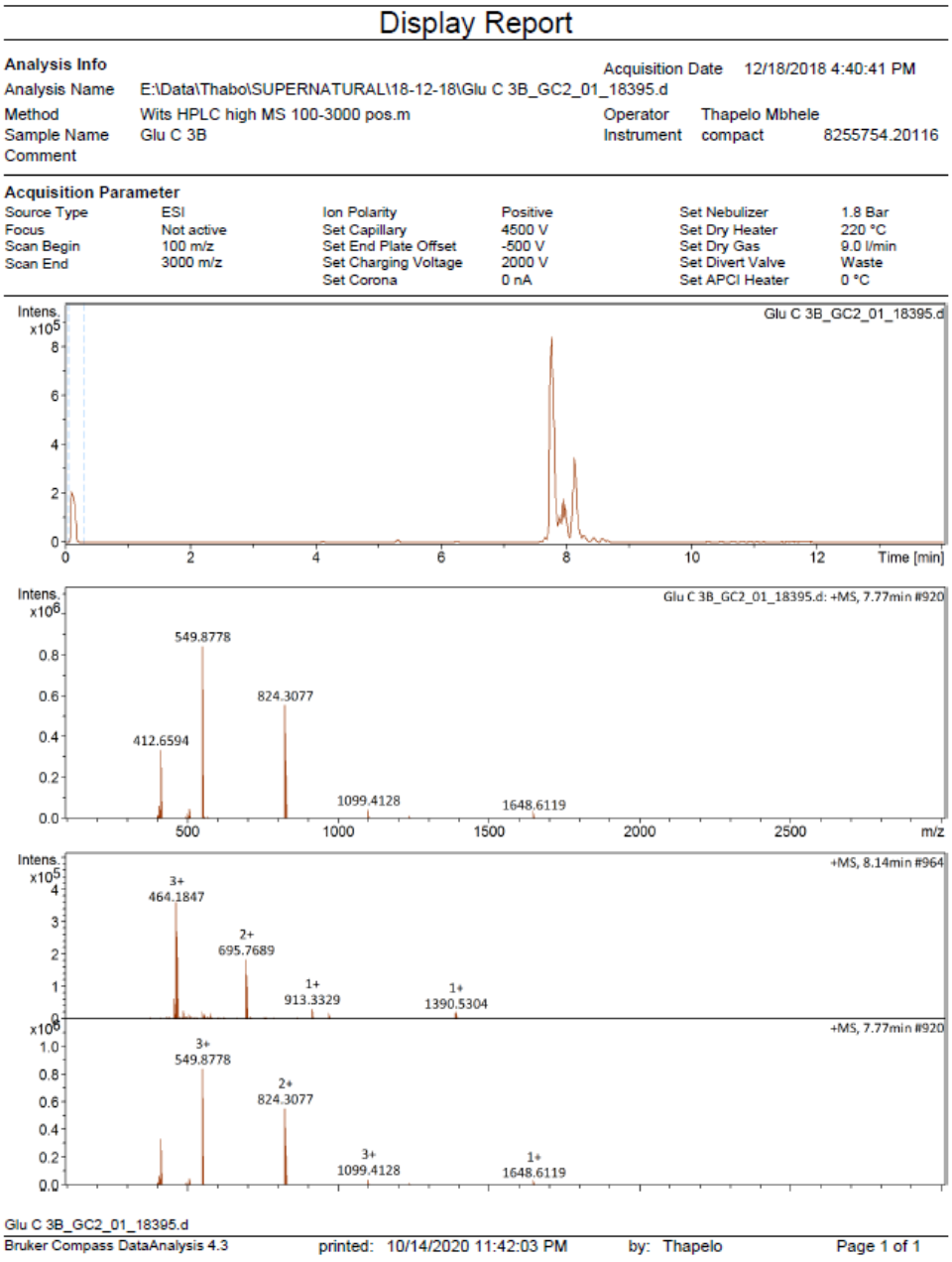


Figure S.2-12: LC-MS spectrum of TP_Glu conformation 4 (peak 4)

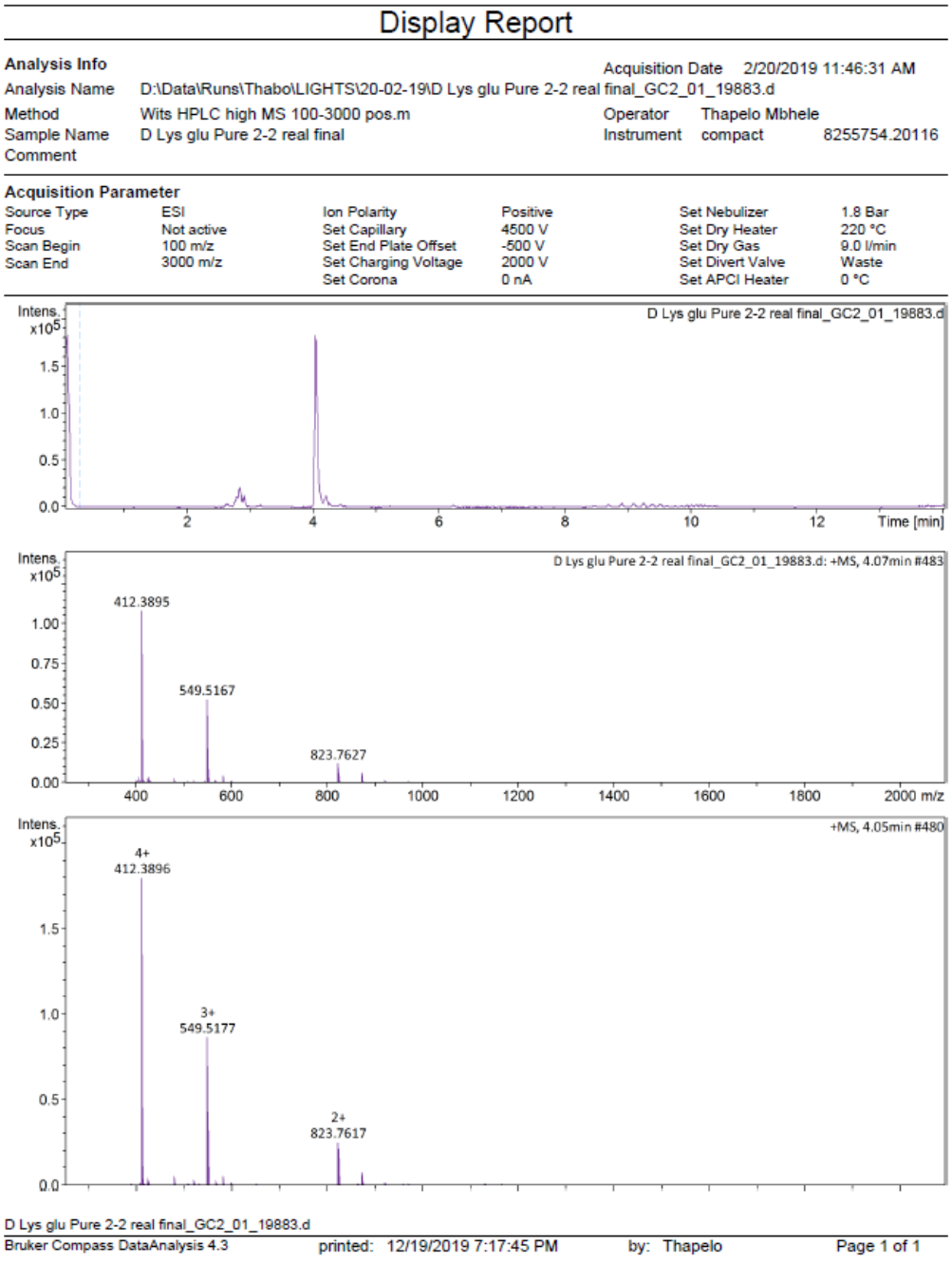


Figure S.2-13: LC-MS spectrum of TP_GDLys conformation 1 (peak 1)

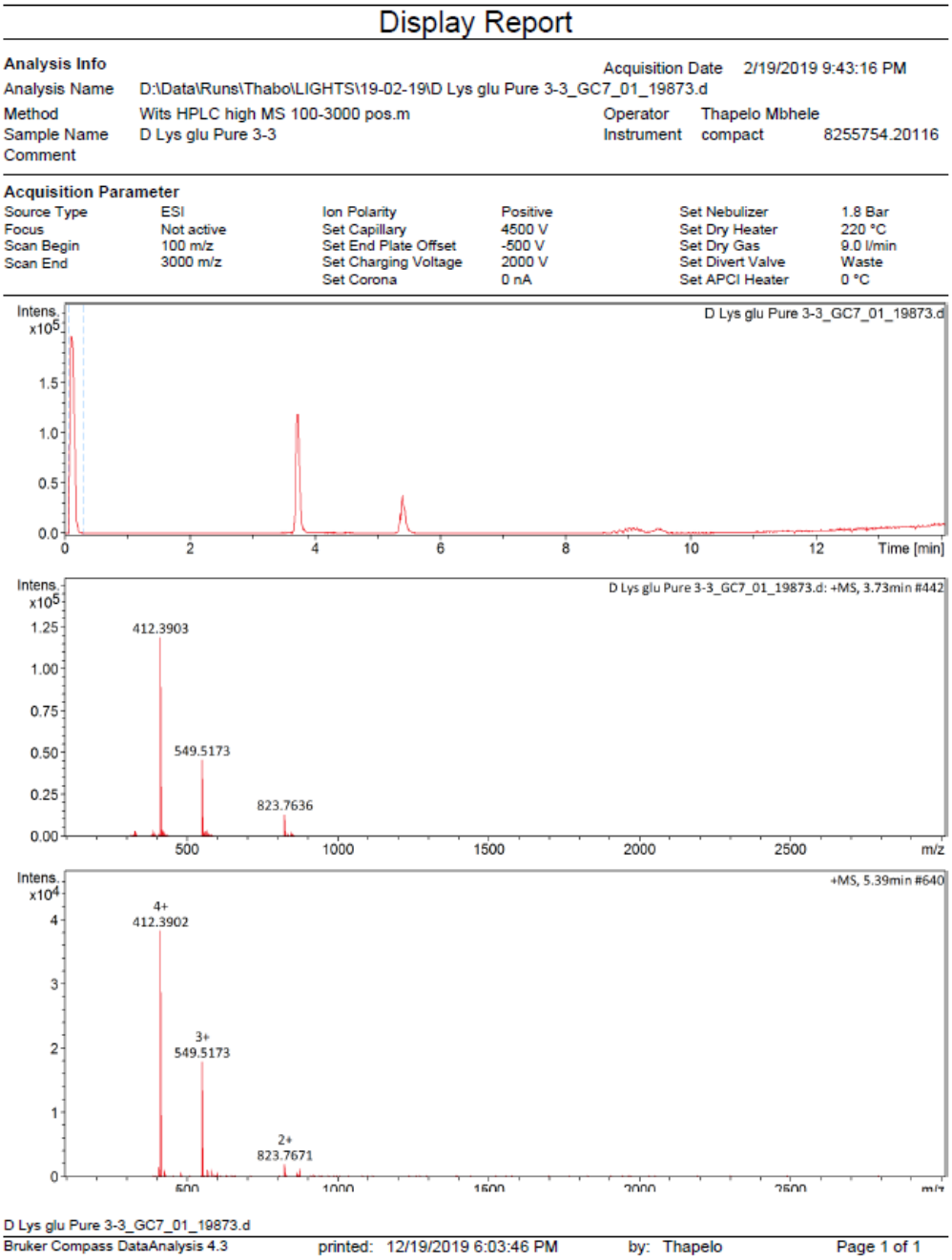


Figure S.2-14: LC-MS spectrum of TP_GDLys conformation 2 (peak 2)

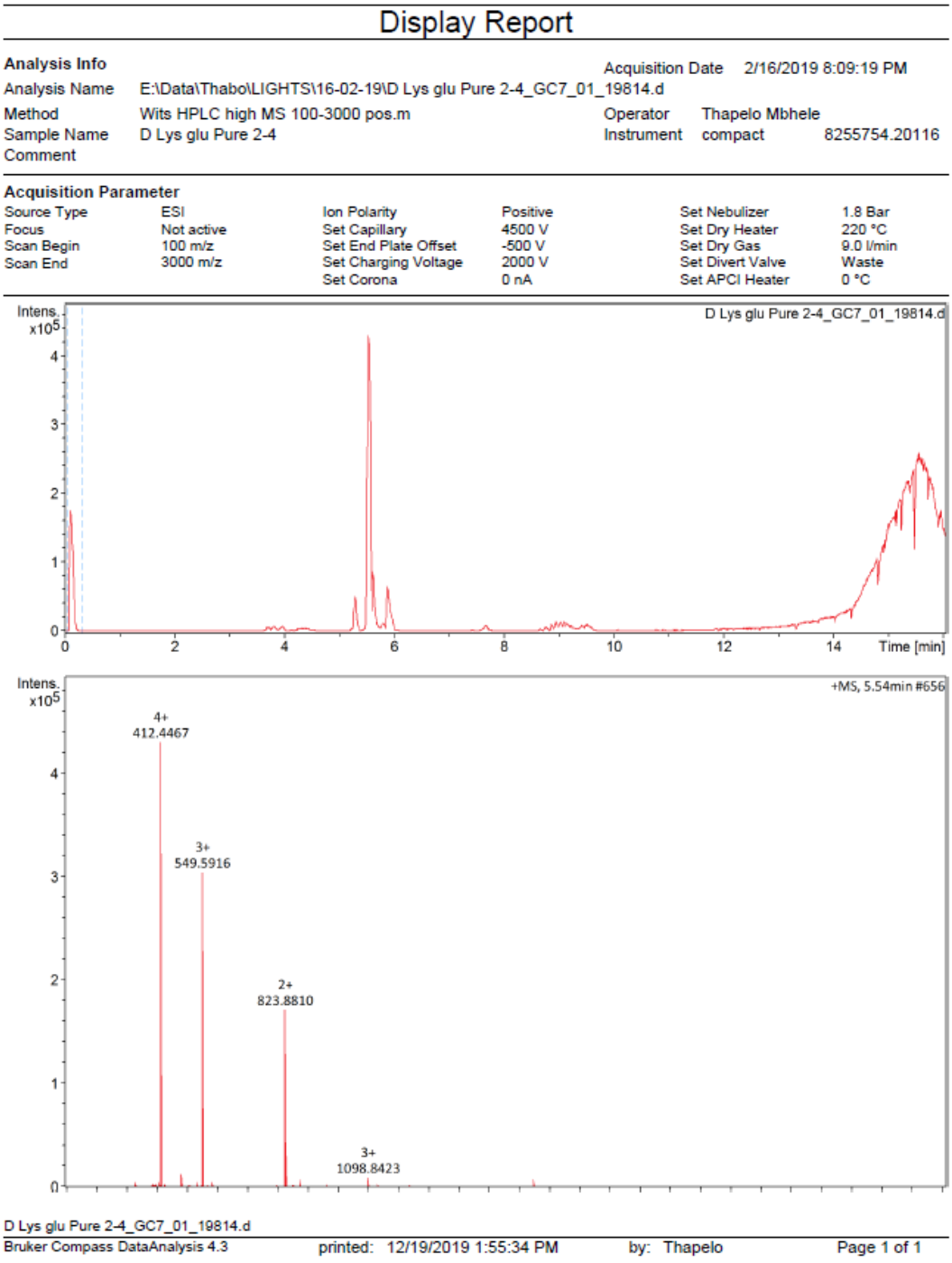


Figure S.2-15: LC-MS spectrum of TP_GDLys conformation 3 (peak 3)

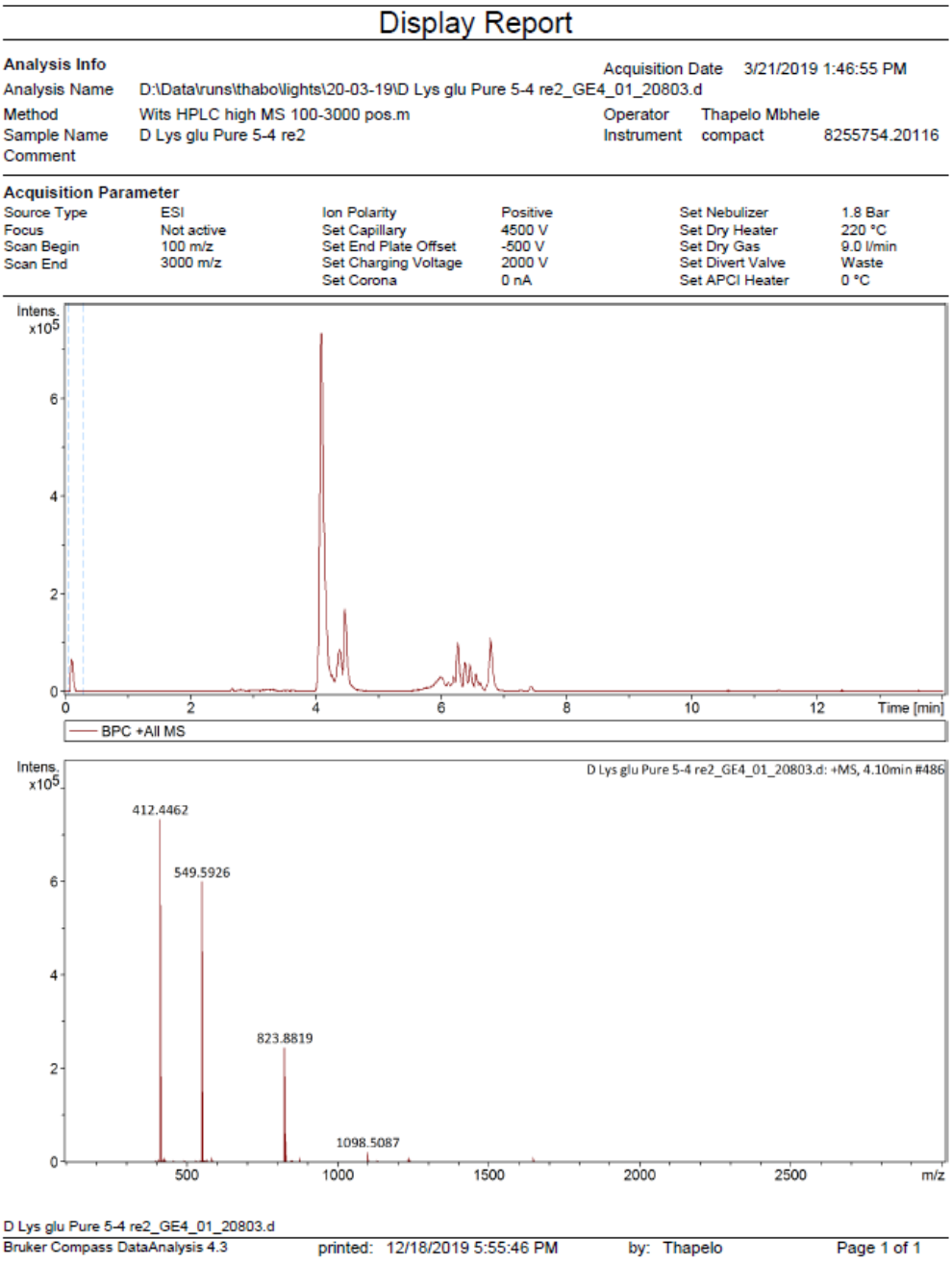


Figure S.2-16: LC-MS spectrum of TP_GDLys conformation 4 (peak 4)

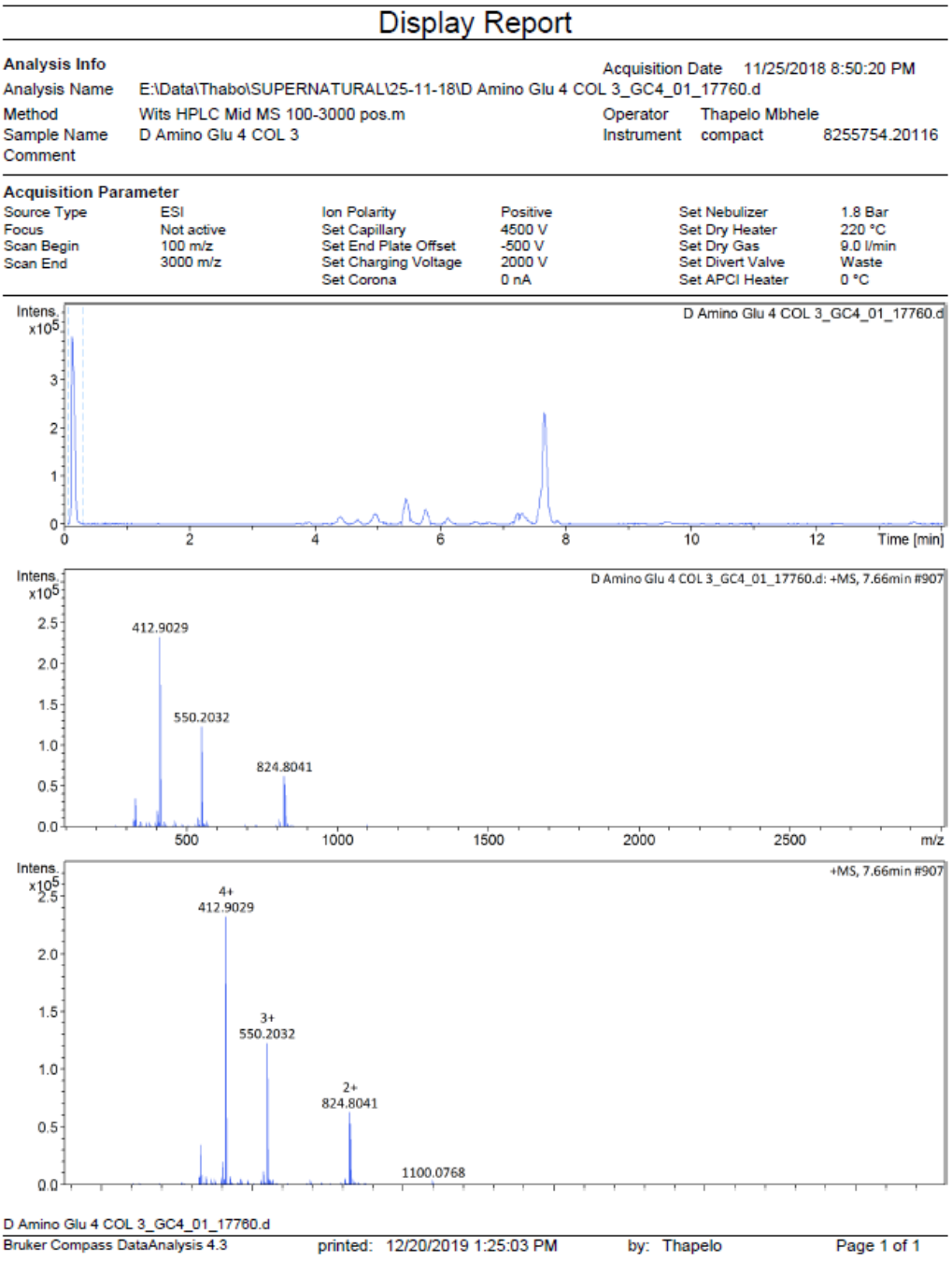


Figure S.2-17: LC-MS spectrum of TP_GDA conformation 1 (peak 1)

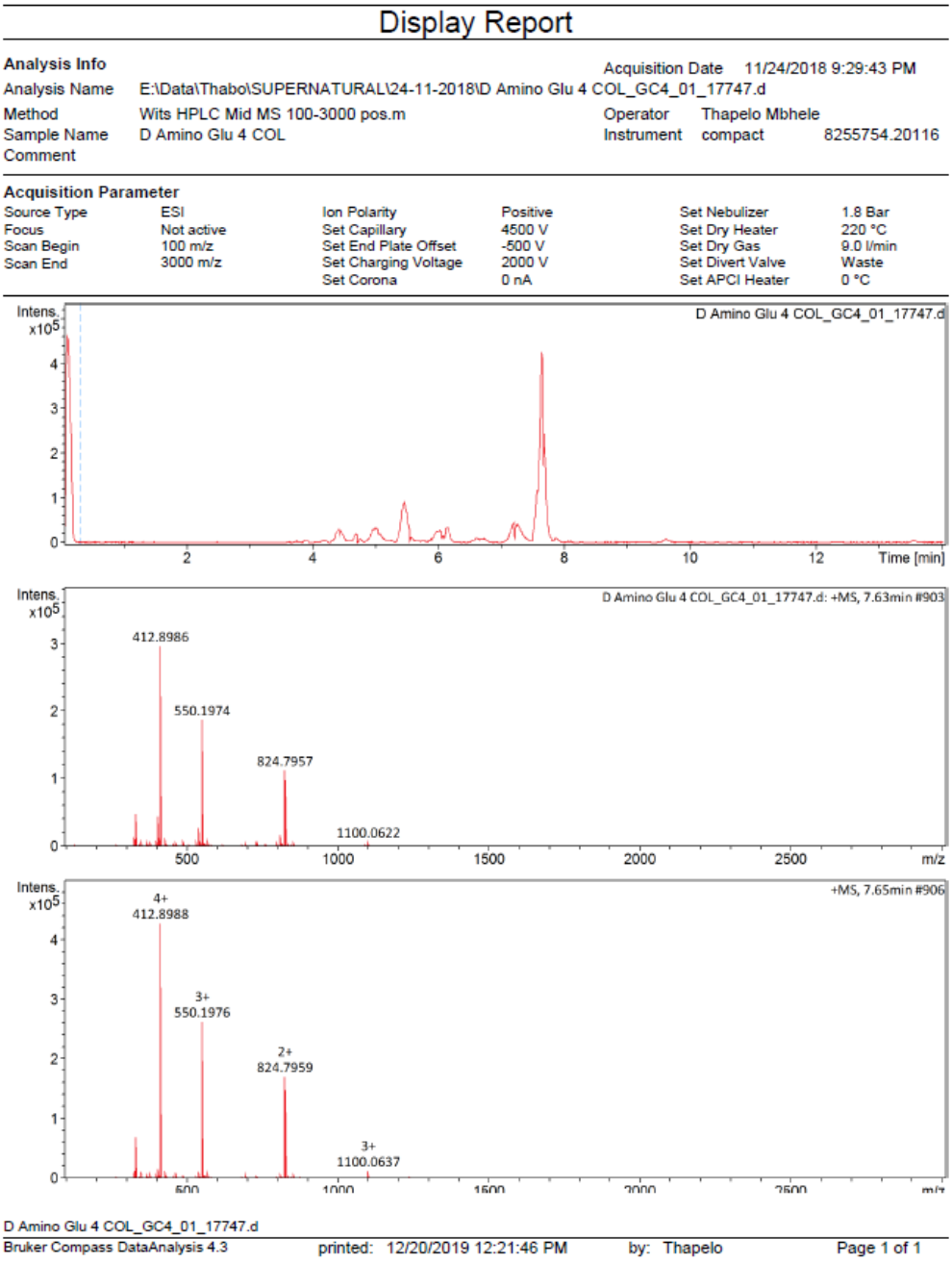


Figure S.2-18: LC-MS spectrum of TP_GDA conformation 2 (peak 2)

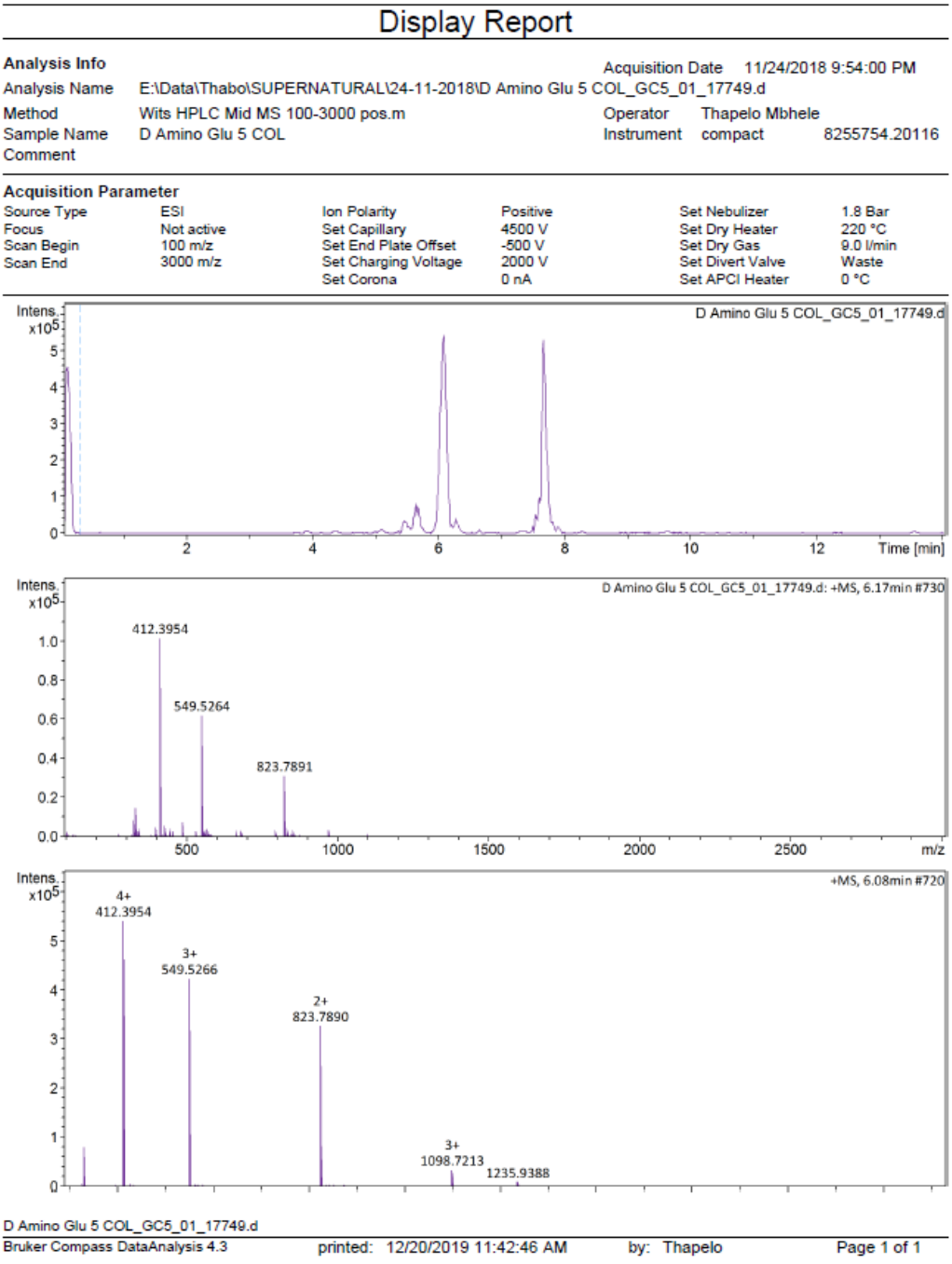


Figure S.2-19: LC-MS spectrum of TP_GDA conformation 3 (peak 3)

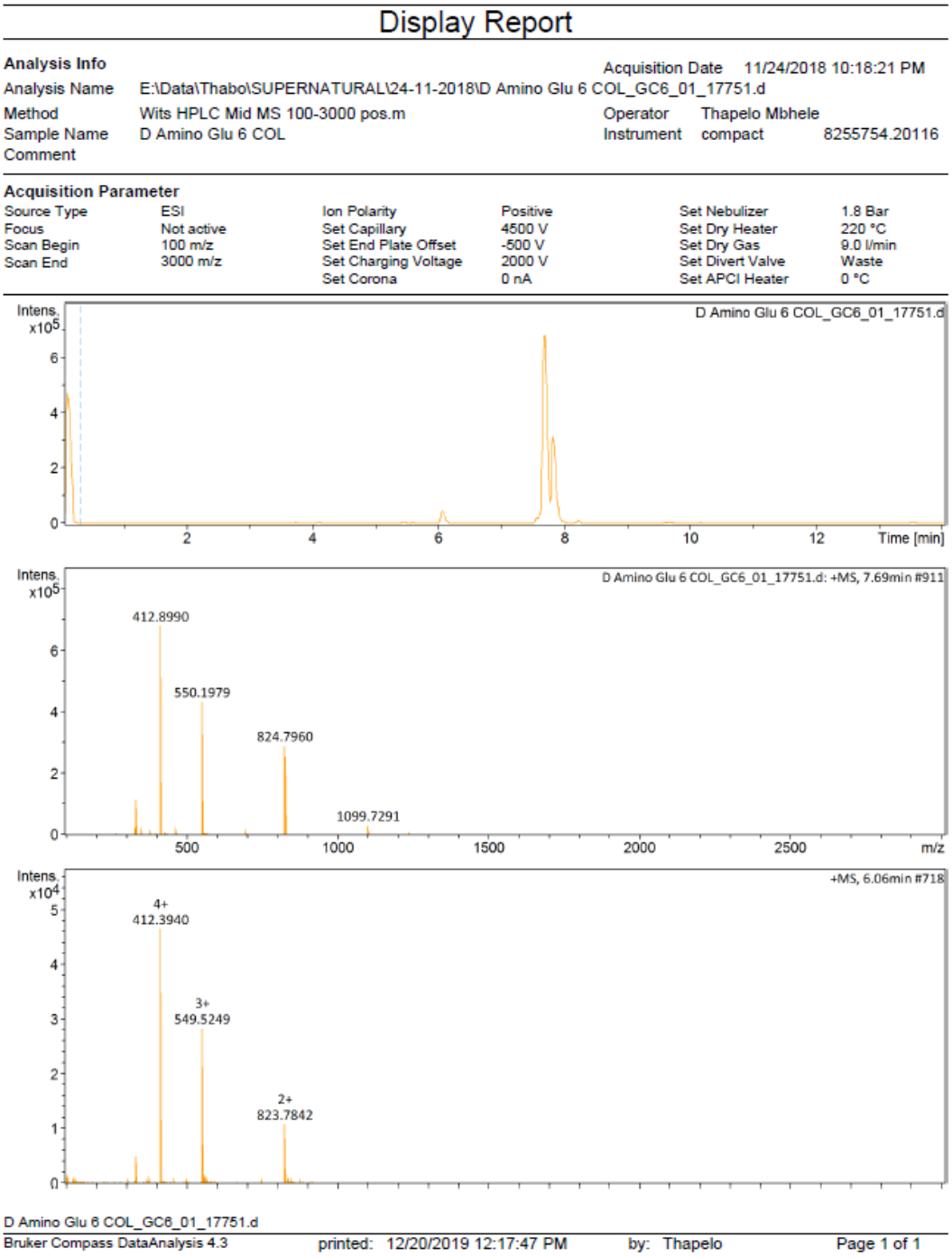


Figure S.2-20: LC-MS spectrum of TP_GDA conformation 4 (peak 4)

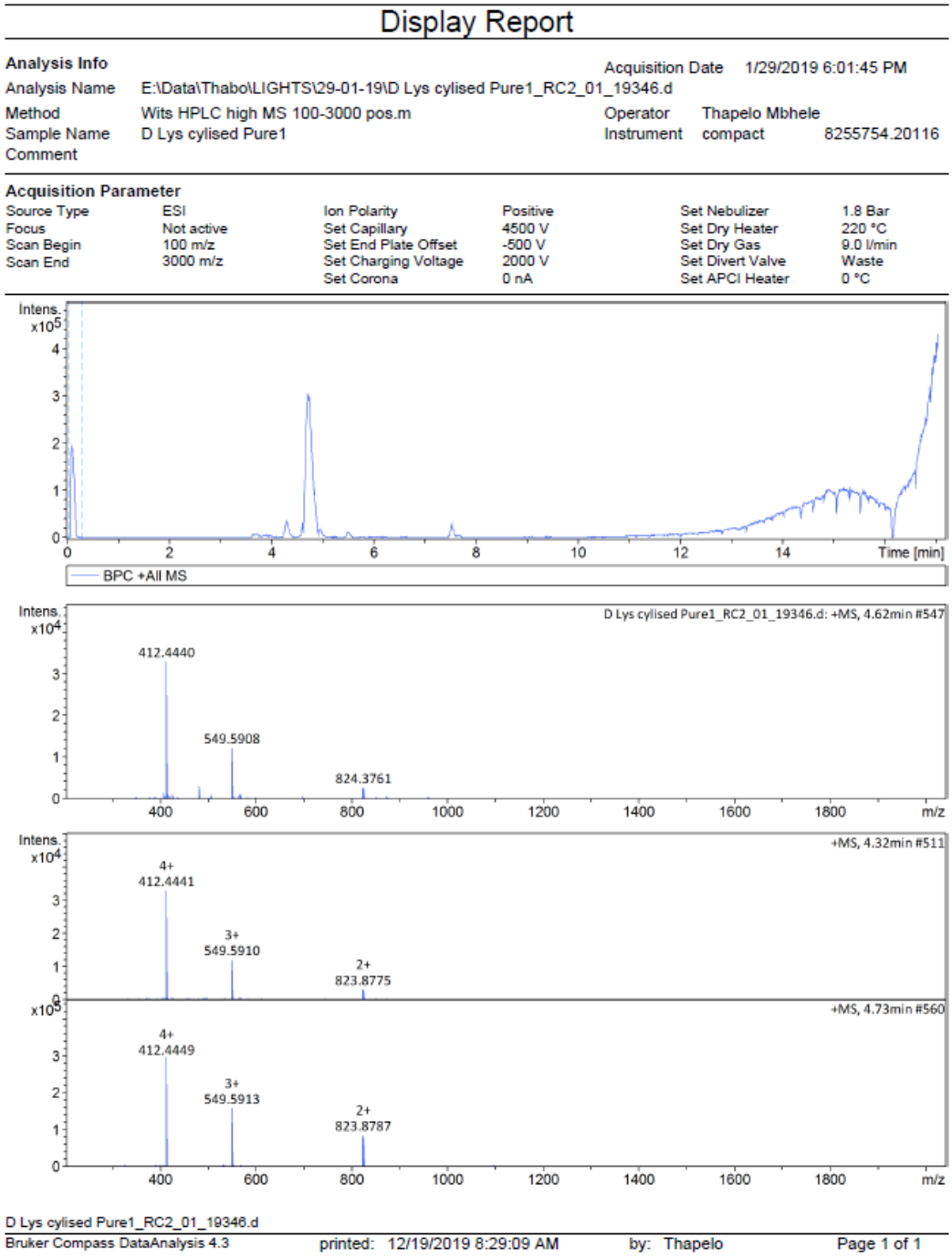


Figure S.21: LC-MS spectrum of TP_GLysC conformation 1 (peak 1)

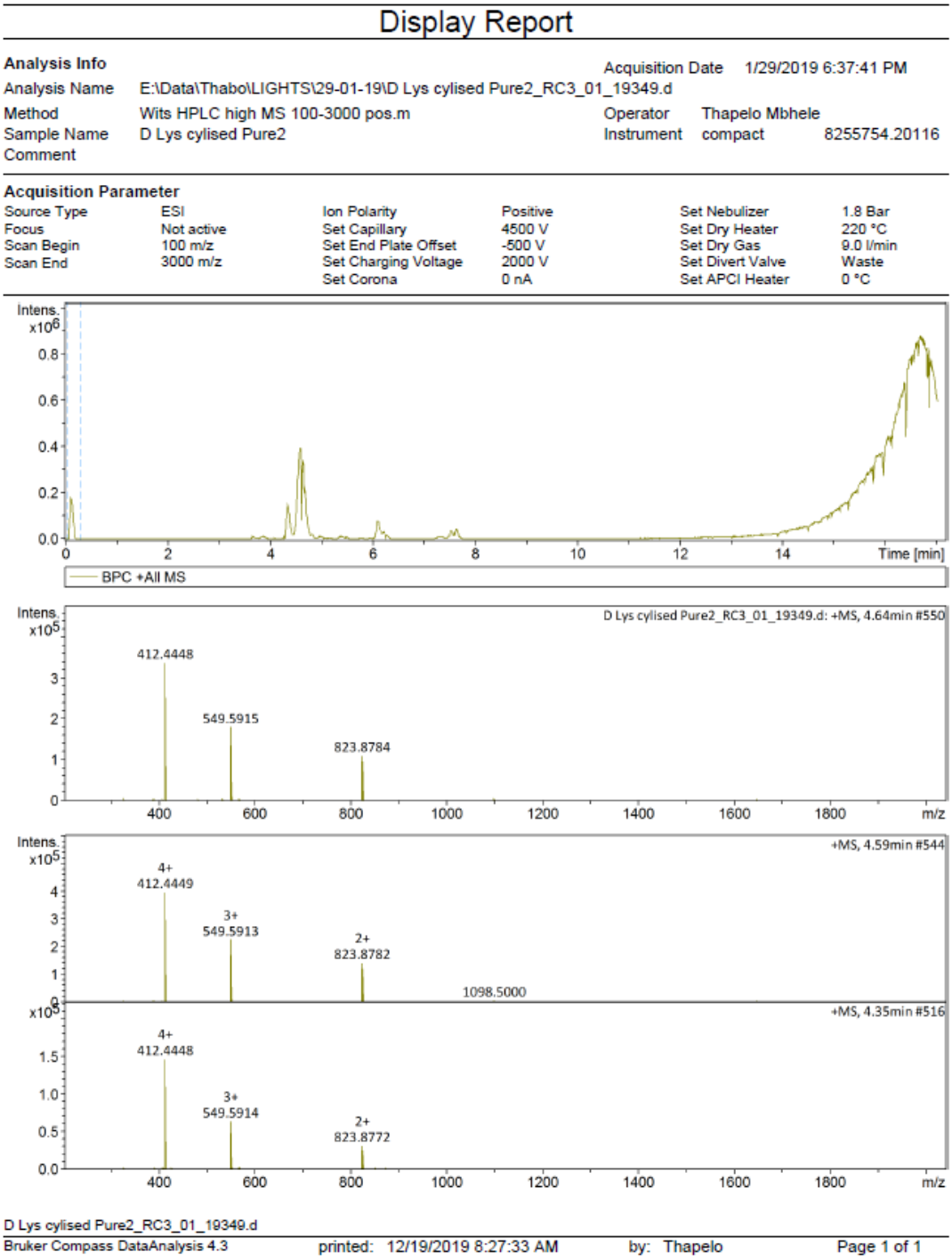


Figure S.2-22: LC-MS spectrum of TP_GLysC conformation 2 (peak 2)

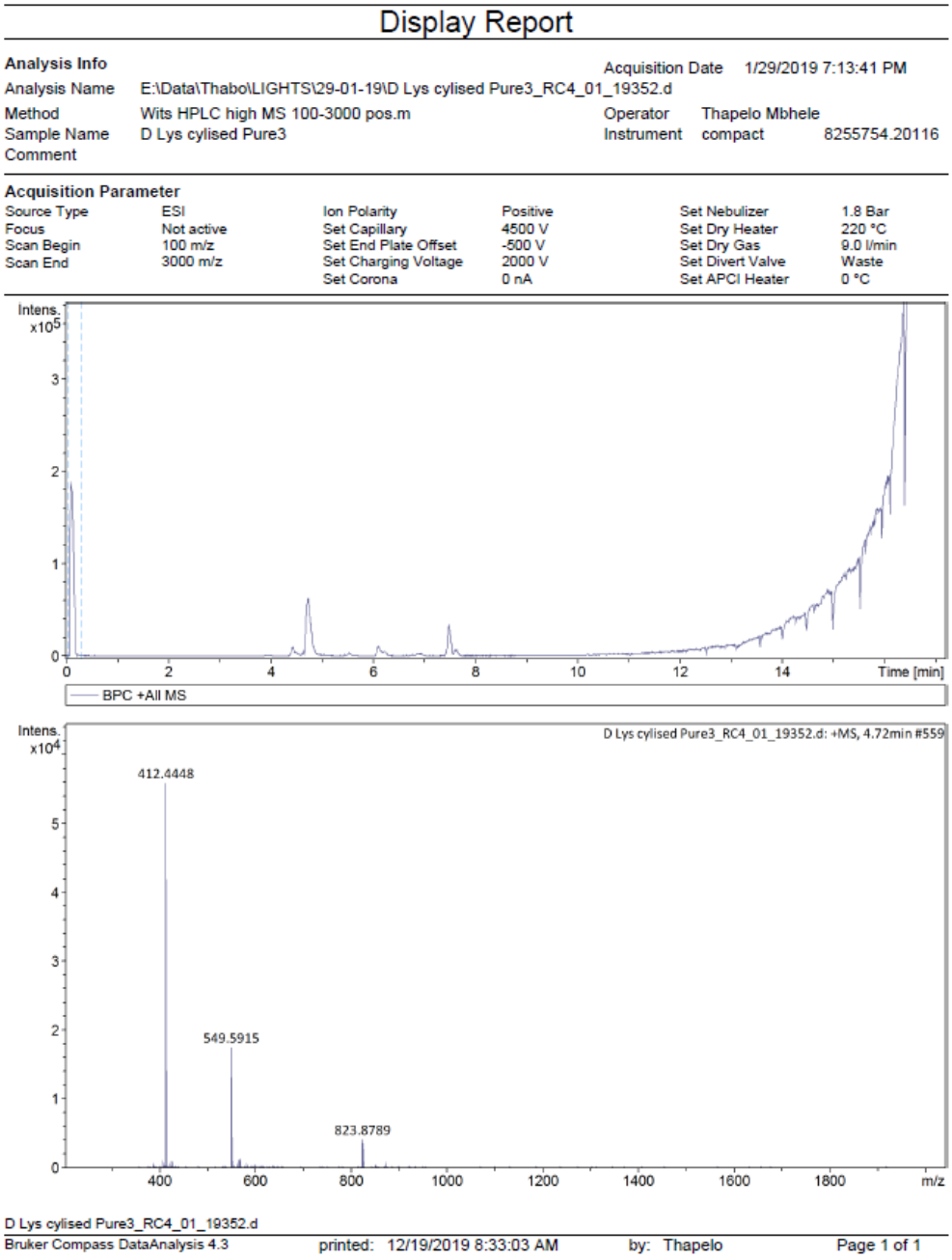


Figure S.2-23: LC-MS spectrum of TP_GLysC conformation 3 (peak 3)

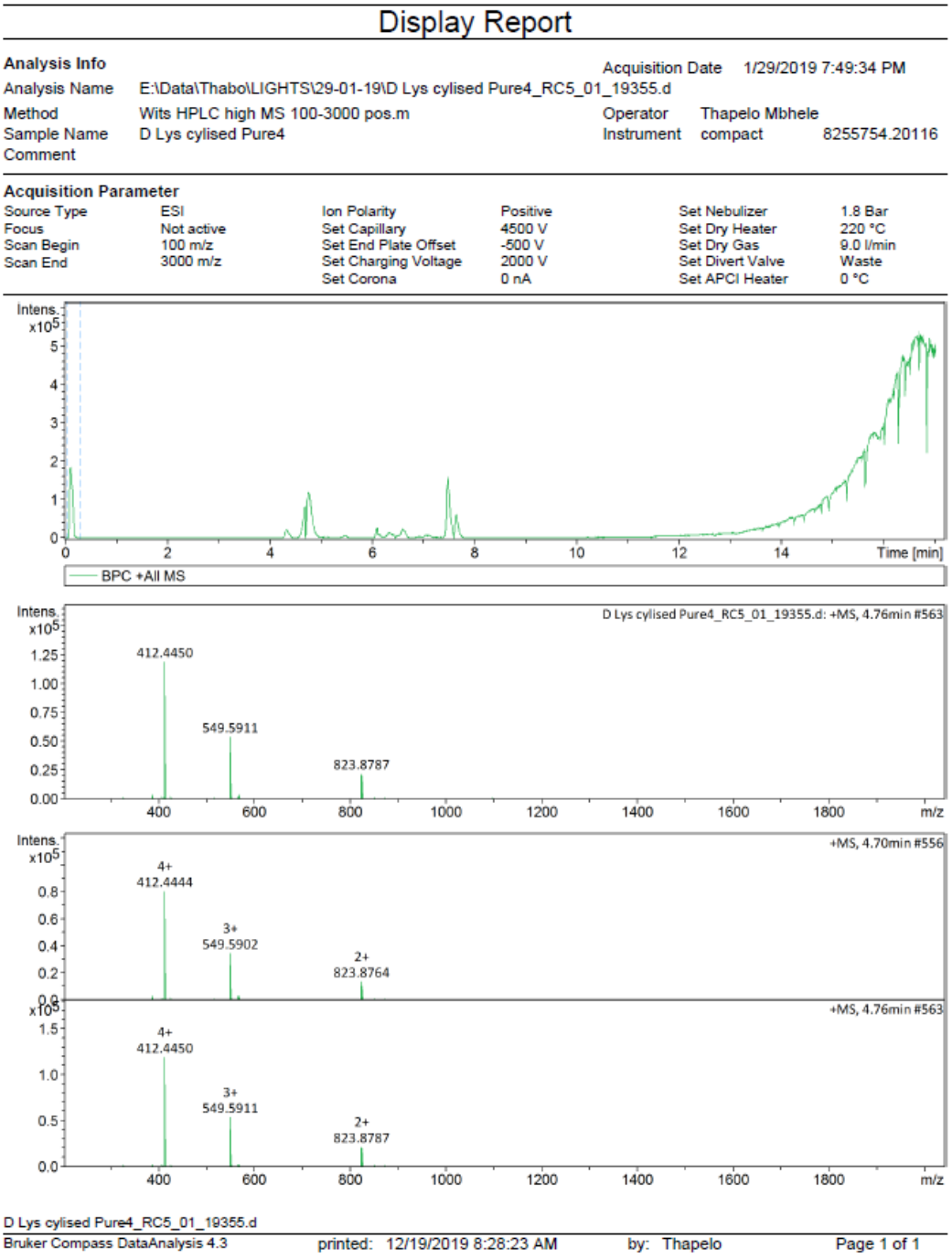


Figure S.2-25: LC-MS spectrum of TP_GLysC conformation 4 (peak 4)

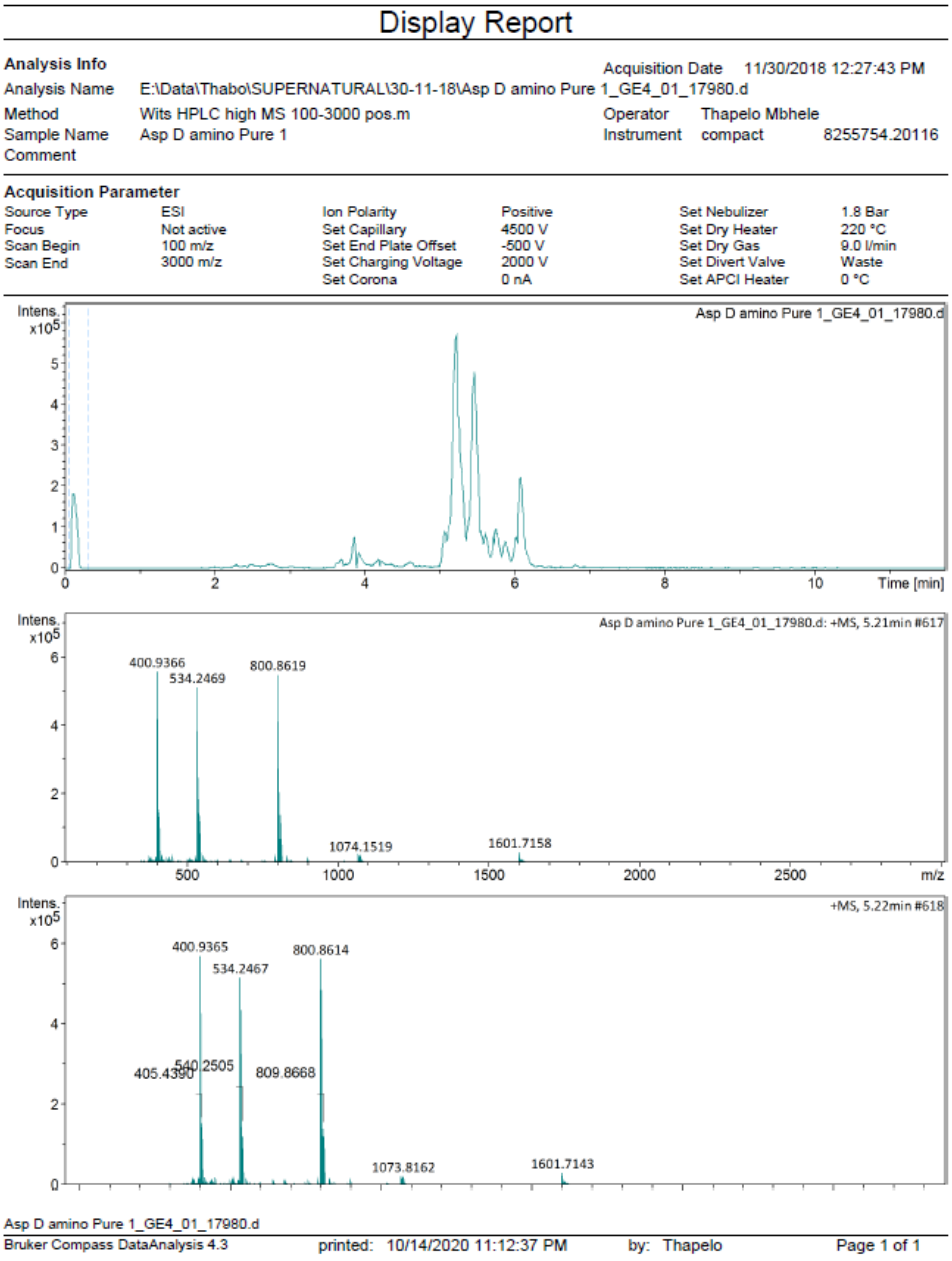


Figure S.2-26: LC-MS spectrum of TP_ADA conformation 1 (peak 1)

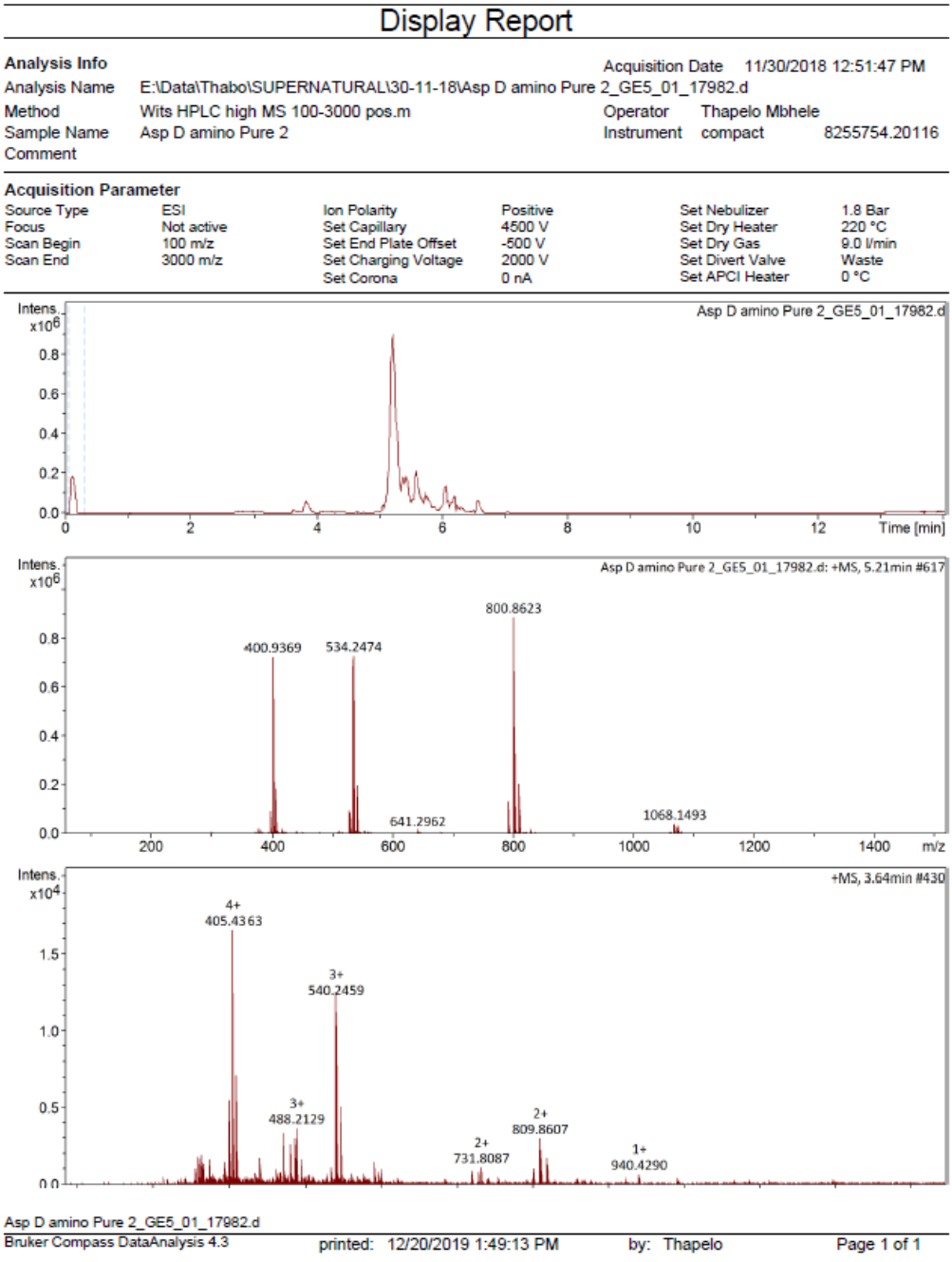


Figure S.2-27: LC-MS spectrum of TP_ADA conformation 2 (peak 2)

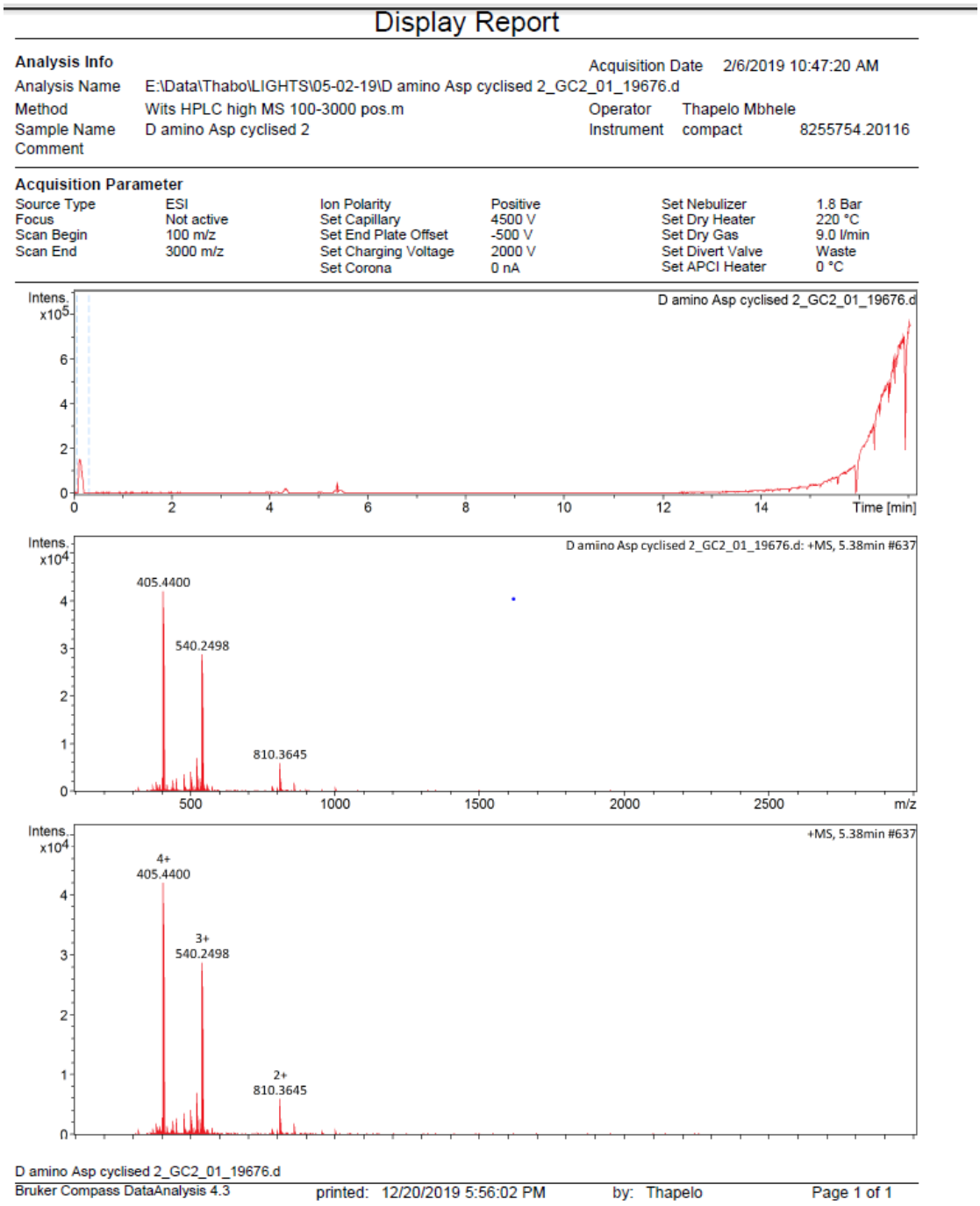


Figure S.2-28: LC-MS spectrum of TP_ADAC conformation 2 (peak 2)

Appendix II- Supplementary information for Chapter 3

NMR spectra for peptide structures

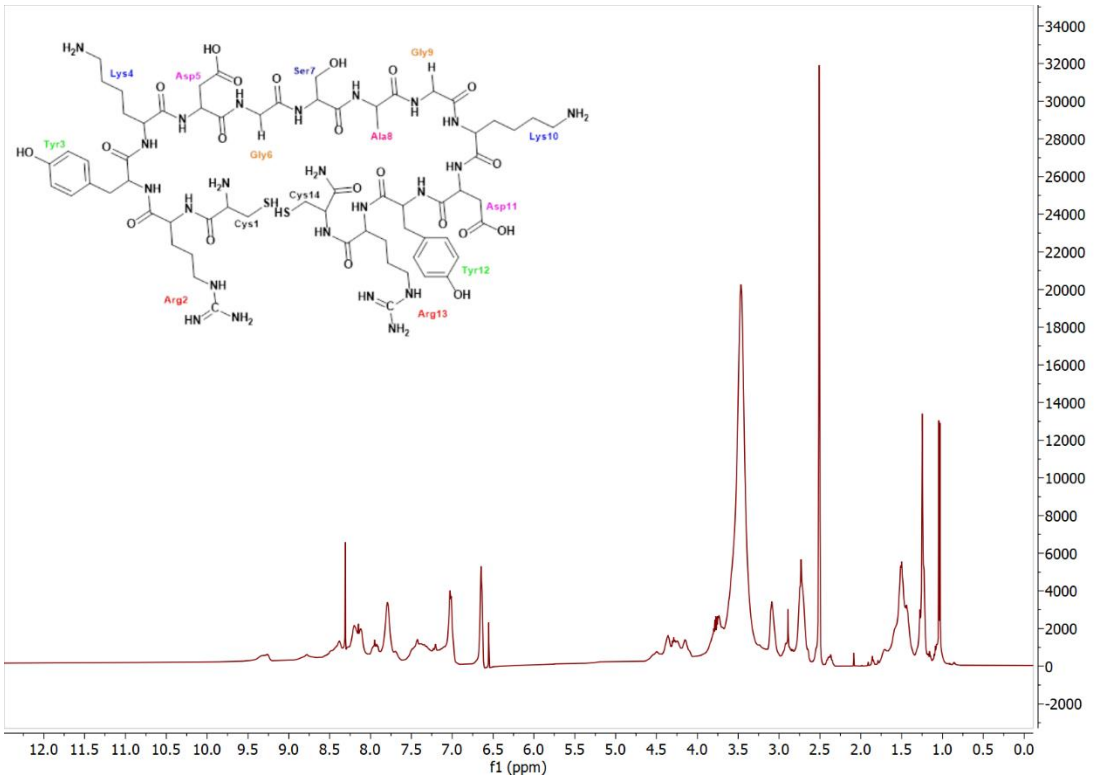


Figure S.3-1: ^{1}H NMR spectrum of TP_Asp peptide

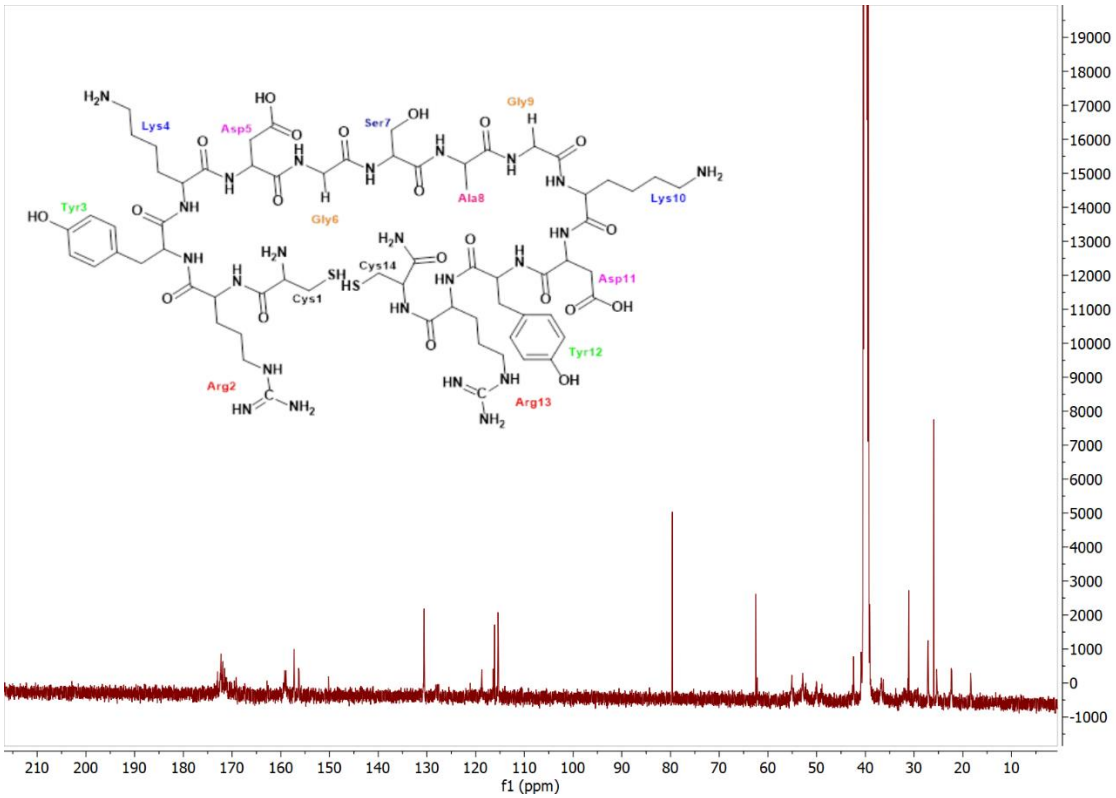


Figure S.3-2: ^{13}C NMR spectrum of TP_Asp peptide

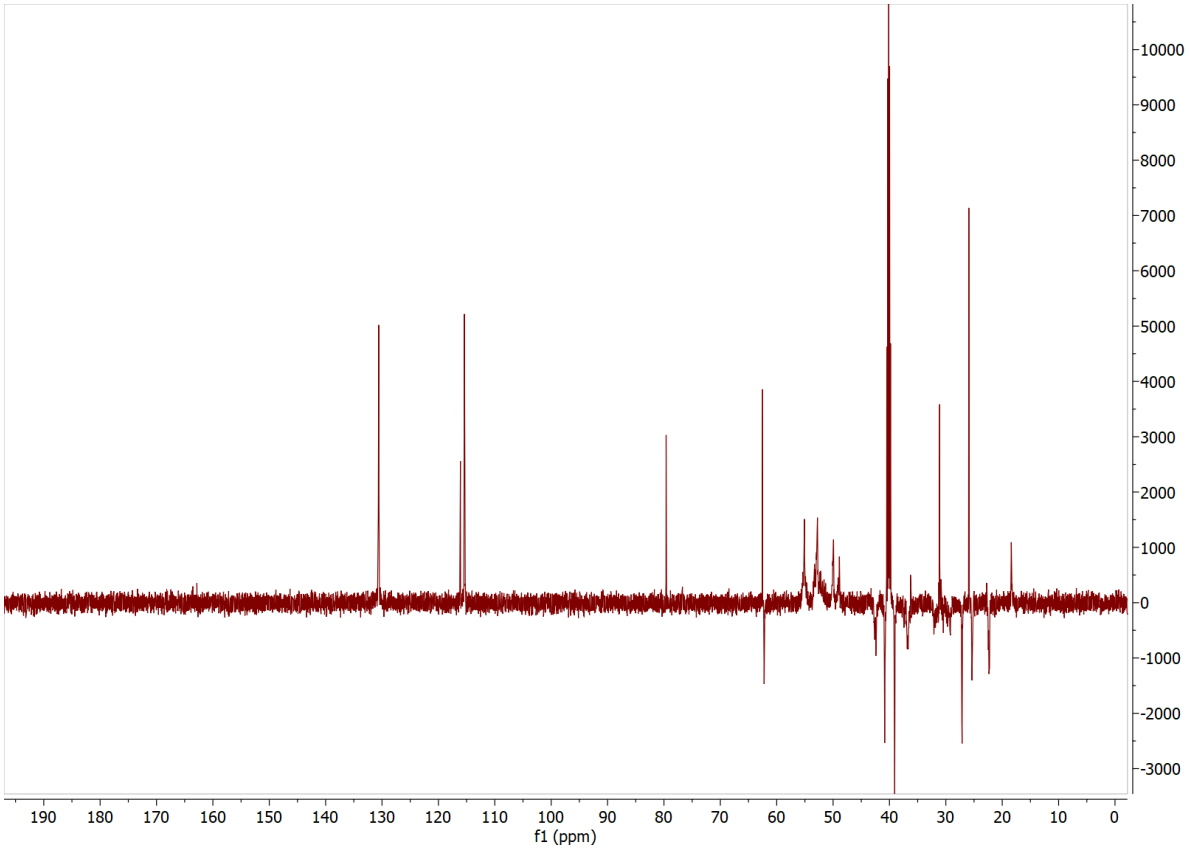


Figure S.3-3: DEPT 135 NMR spectrum of TP_Asp peptide

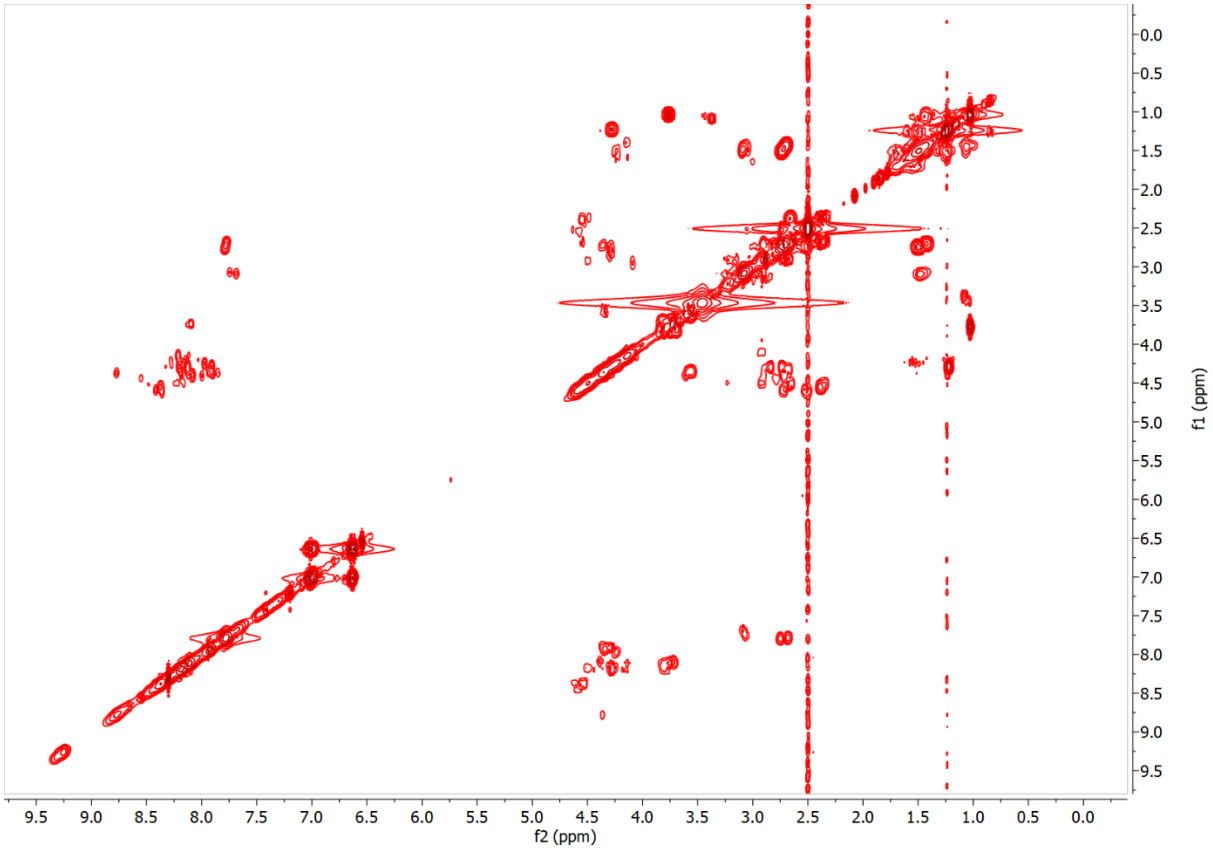


Figure S.3-4: 2D ^{1}H COSY NMR spectrum of TP_Asp peptide

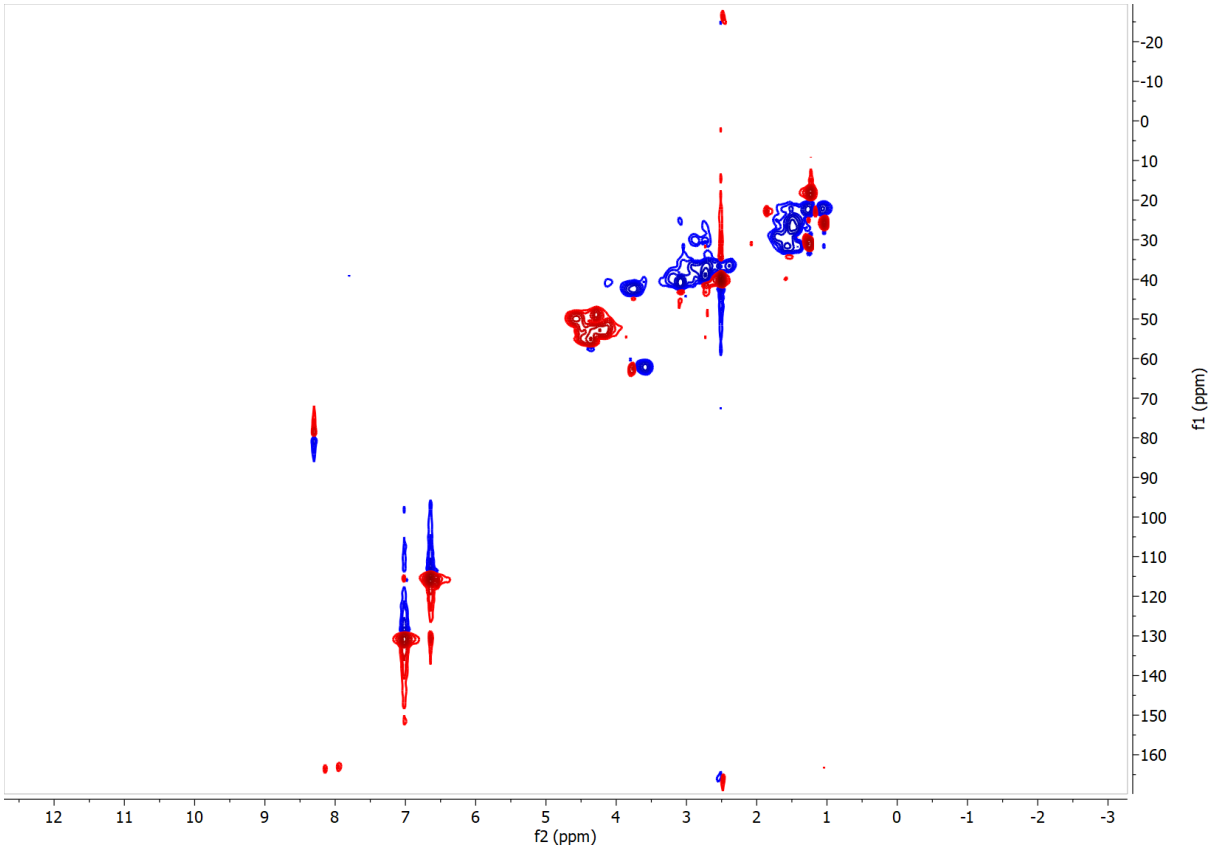


Figure S.3-5: HSQC NMR spectrum of TP_Asp peptide

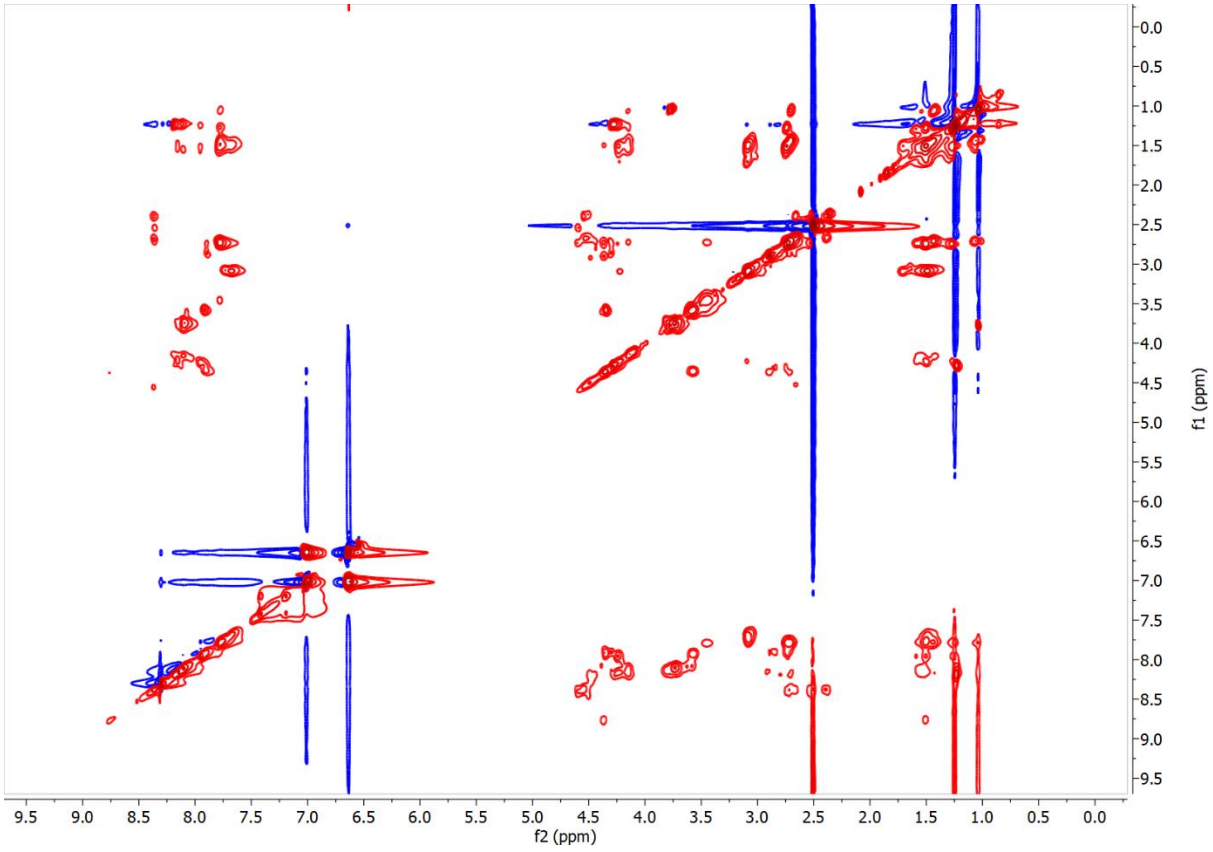


Figure S.3-6: 2D ^{1}H TOCSY NMR spectrum of TP_Asp peptide

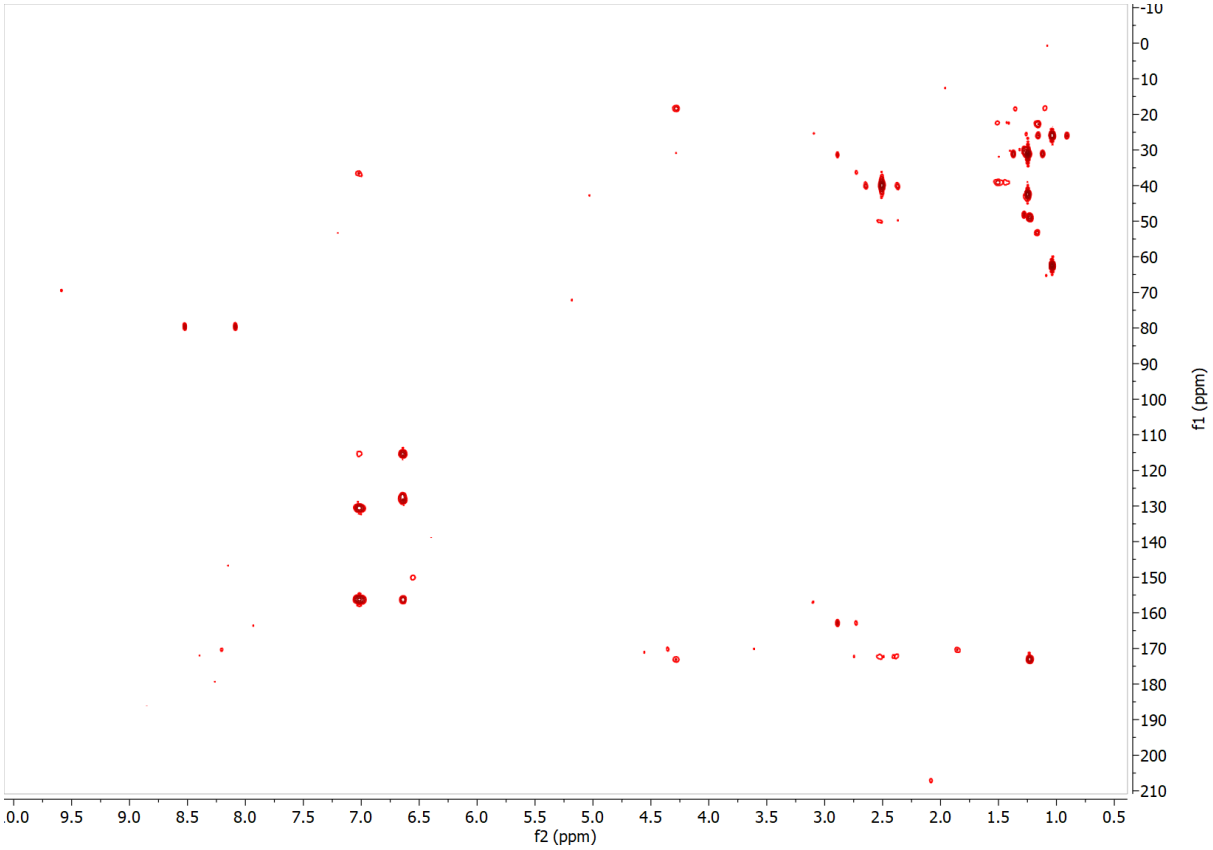


Figure S.3-7: HMBC NMR spectrum of TP_Asp peptide

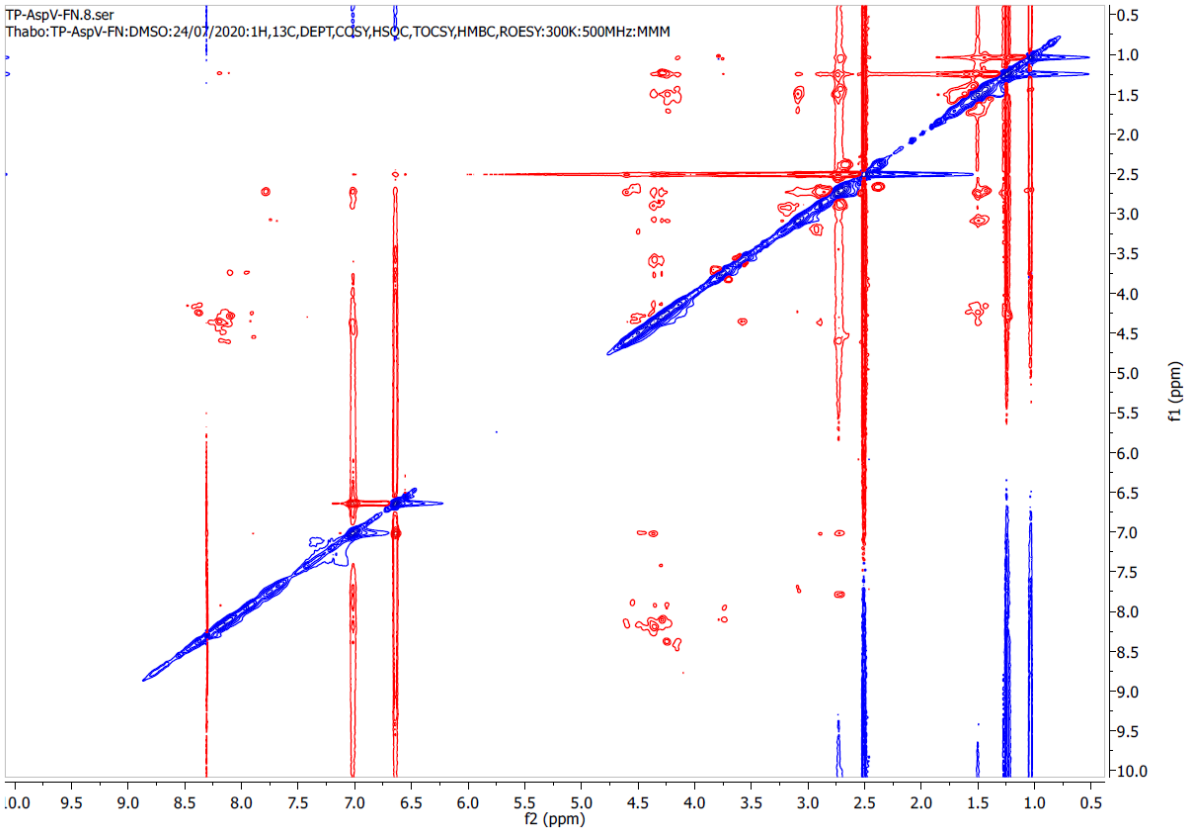


Figure S.3-8: 2D ^{1}H ROESY NMR spectrum of TP_Asp peptide

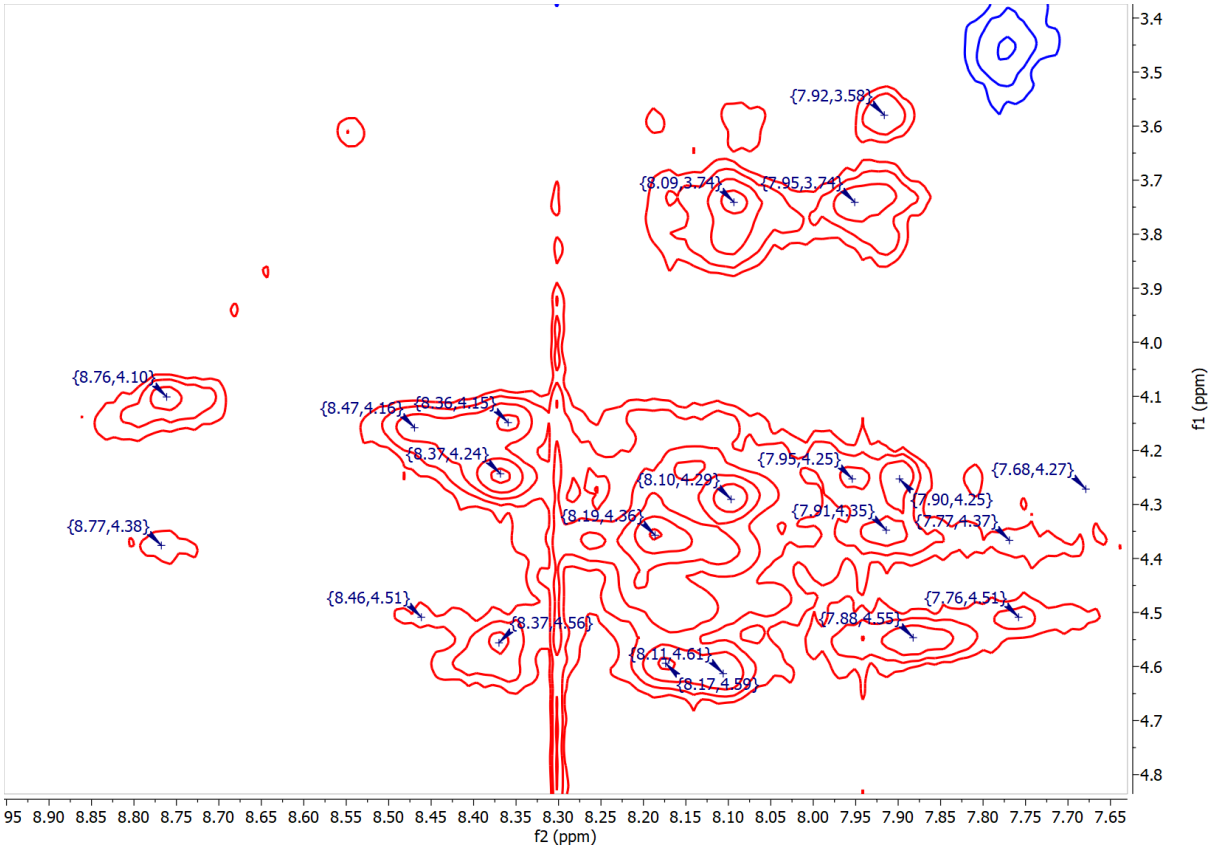


Figure S.3-9: 2D ^{1}H ROESY NMR spectrum of TP_ADLys peptide, ^{1}HN region

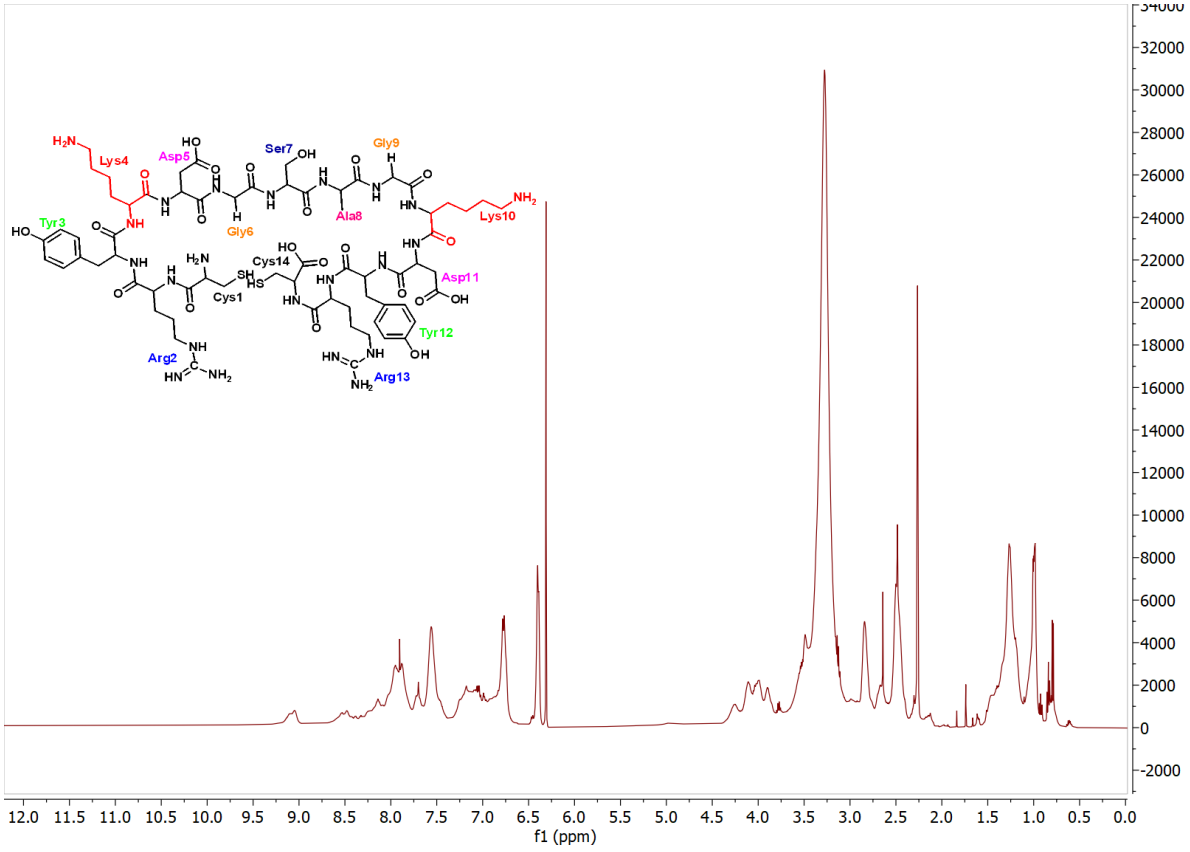


Figure S.3-10: ^{1}H NMR spectrum of TP_ADLys peptide

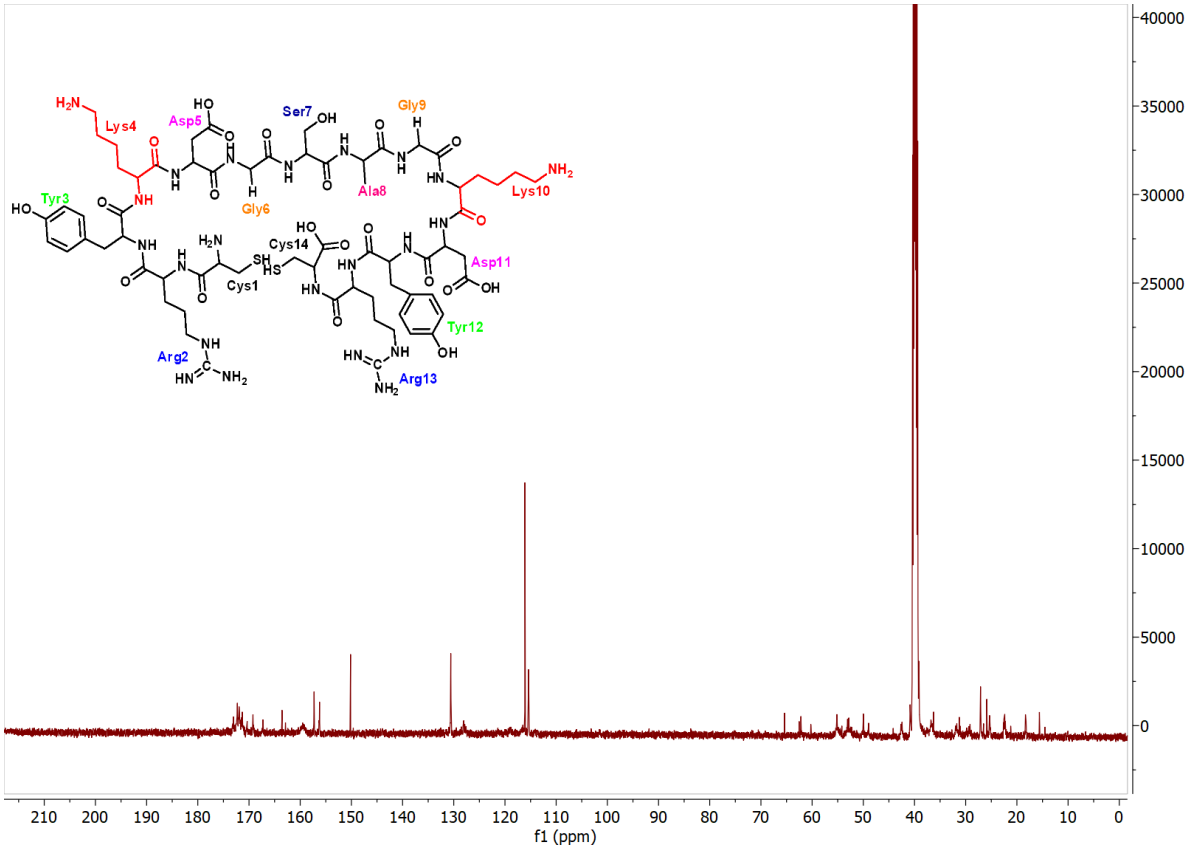


Figure S.3-11: ^{13}C NMR spectrum of TP_ADLys peptide

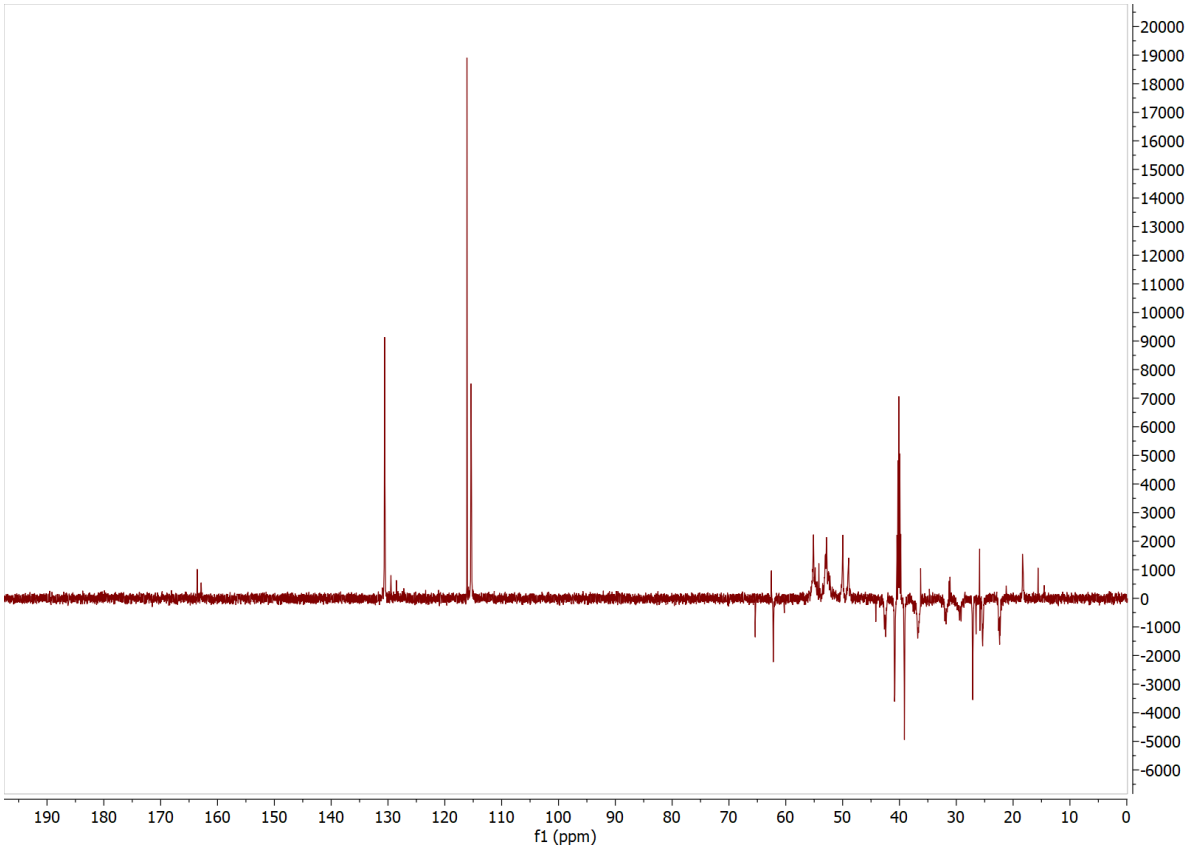


Figure S.3-12: DEPT 135 NMR spectrum of TP_ADLys peptide

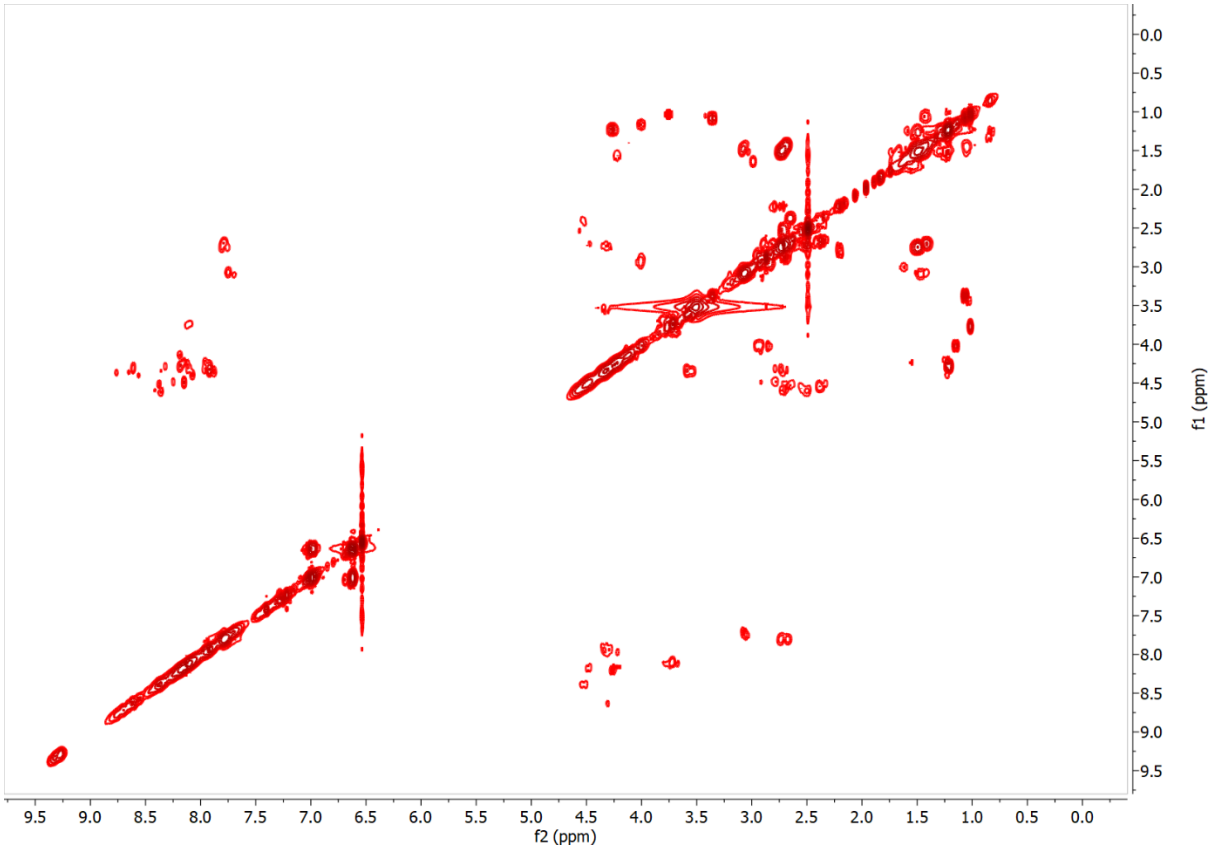


Figure S.3-13: 2D ^{1}H COSY NMR spectrum of TP_ADLys peptide

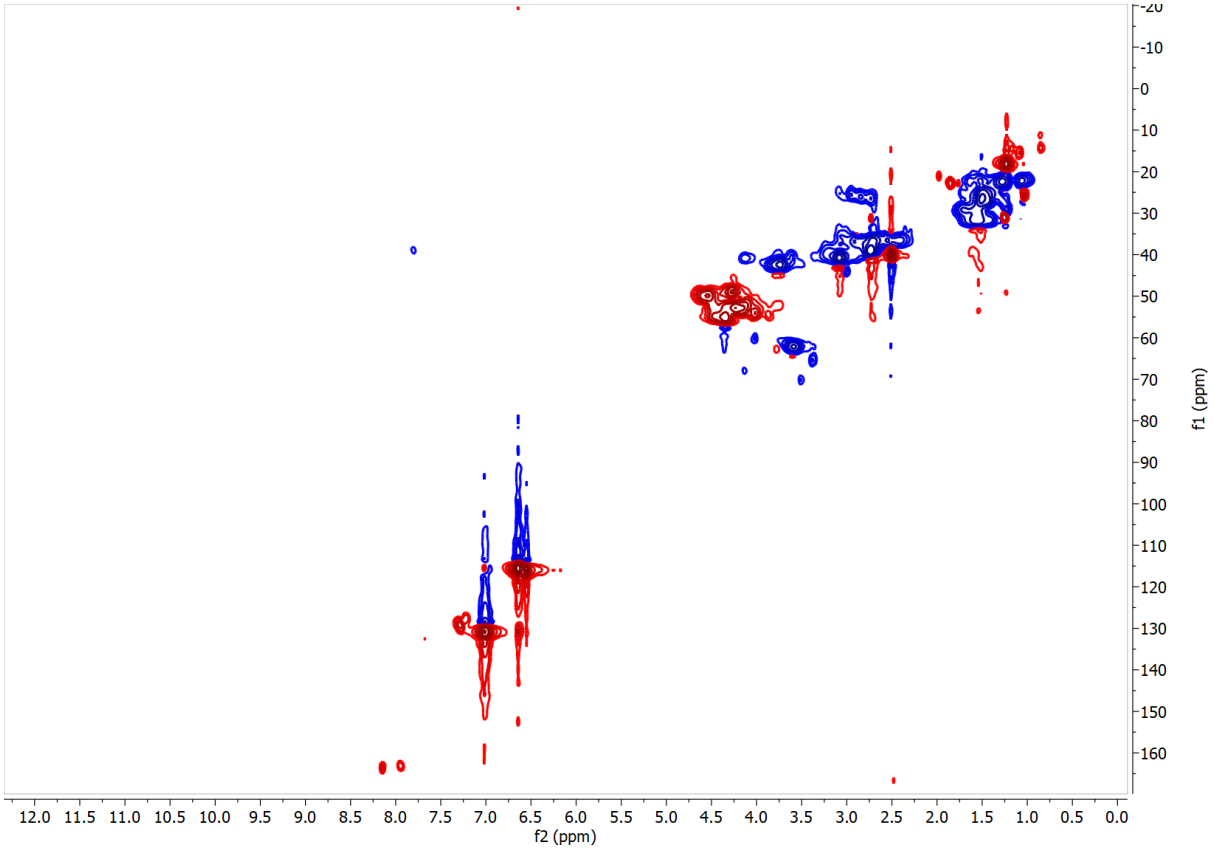


Figure S.3-14: HSQC NMR spectrum of TP_ADLys peptide

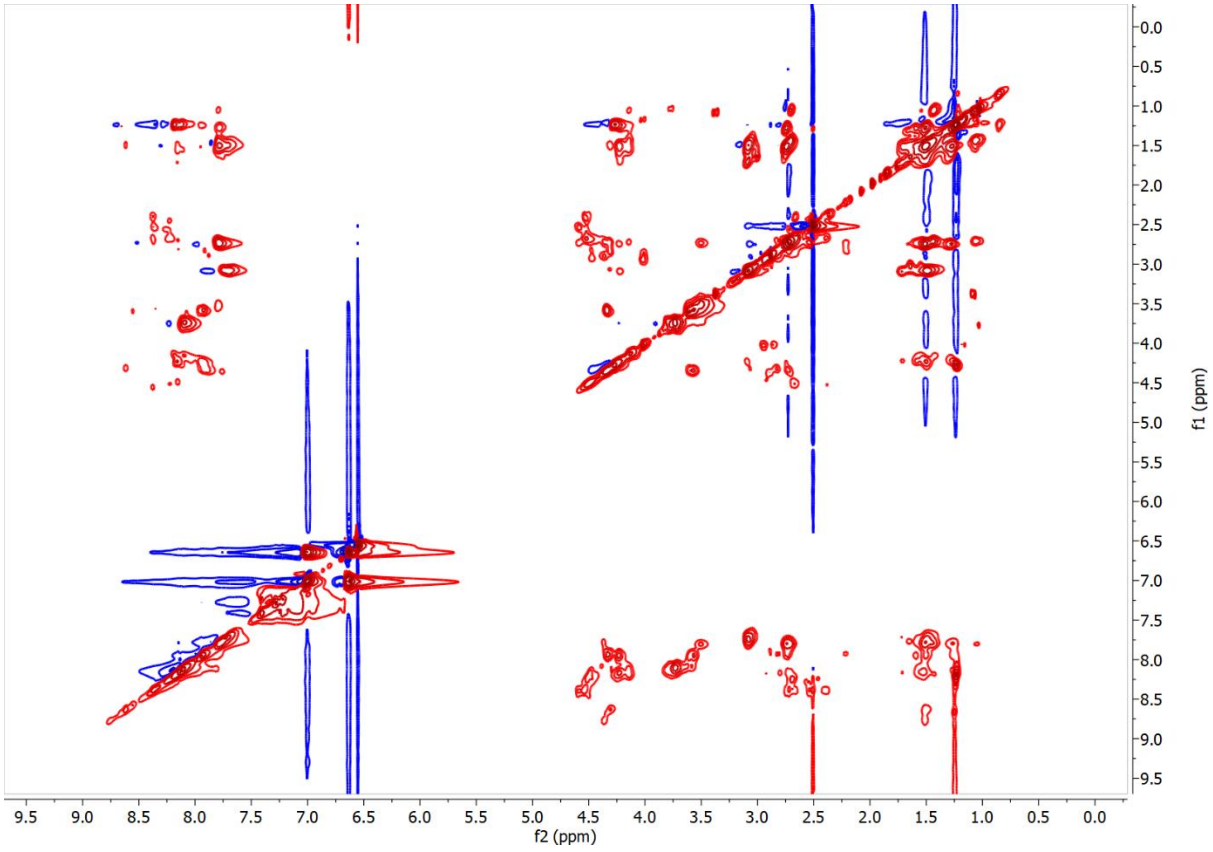


Figure S.3-15: 2D ^{1}H TOCSY spectrum of TP_ADLys peptide

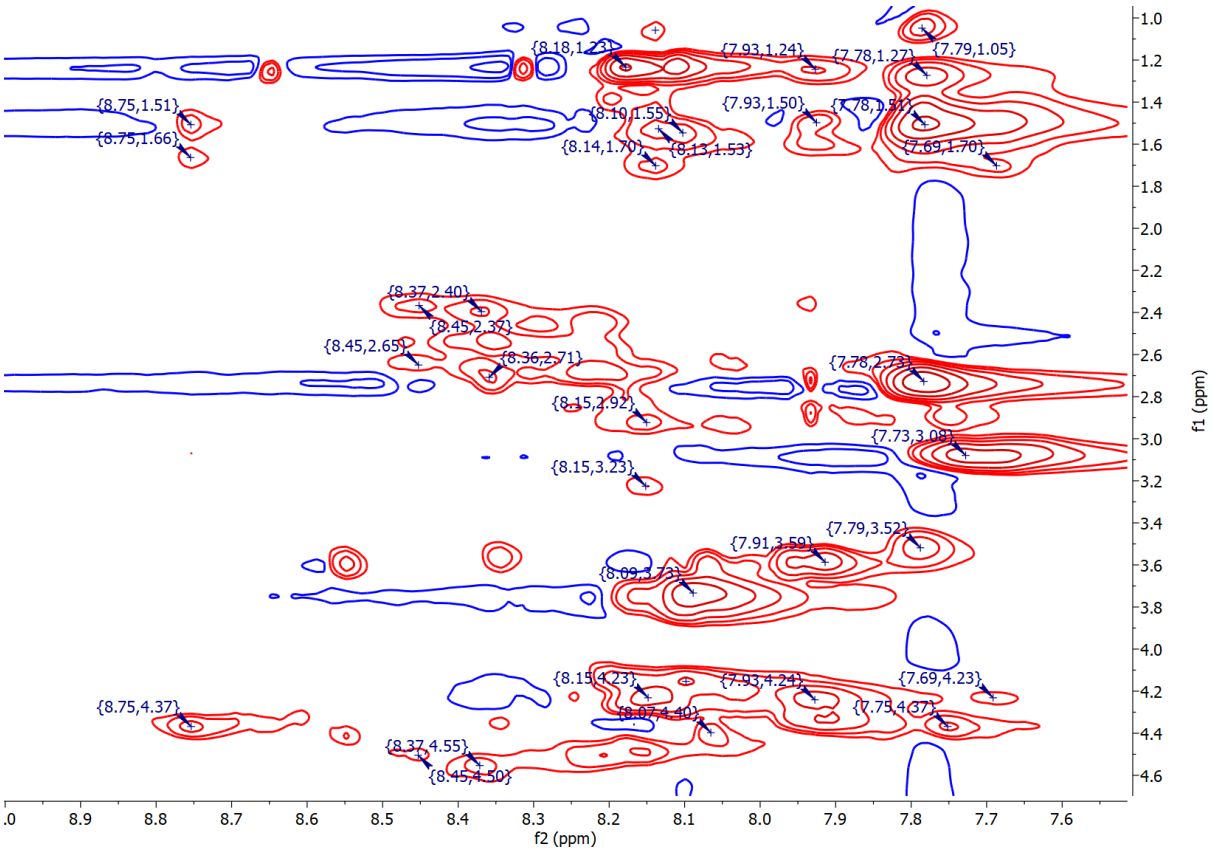


Figure S.3-16: 2D ^{1}H TOCSY spectrum of TP_ADLys peptide, ^{1}HN fingerprint region

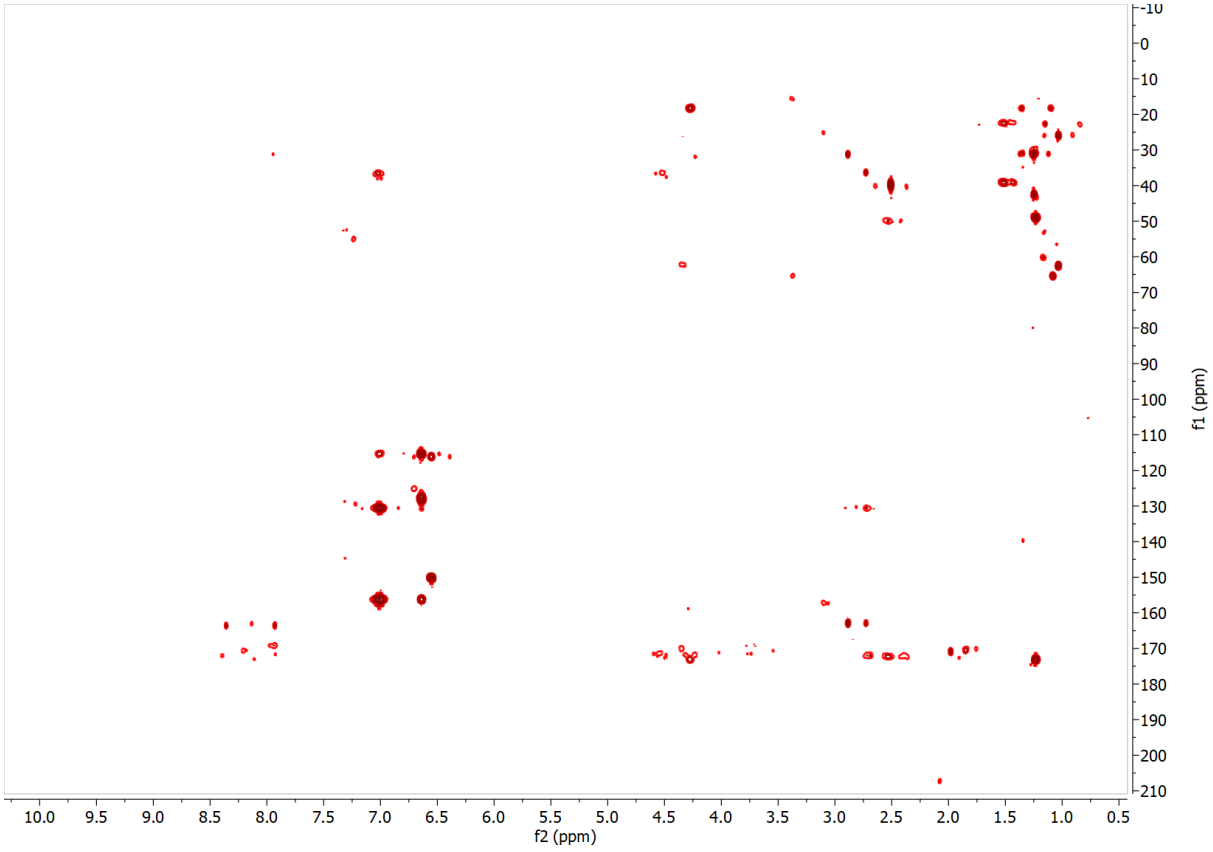


Figure S.3-17: HMBC NMR spectrum of TP_ADLys peptide

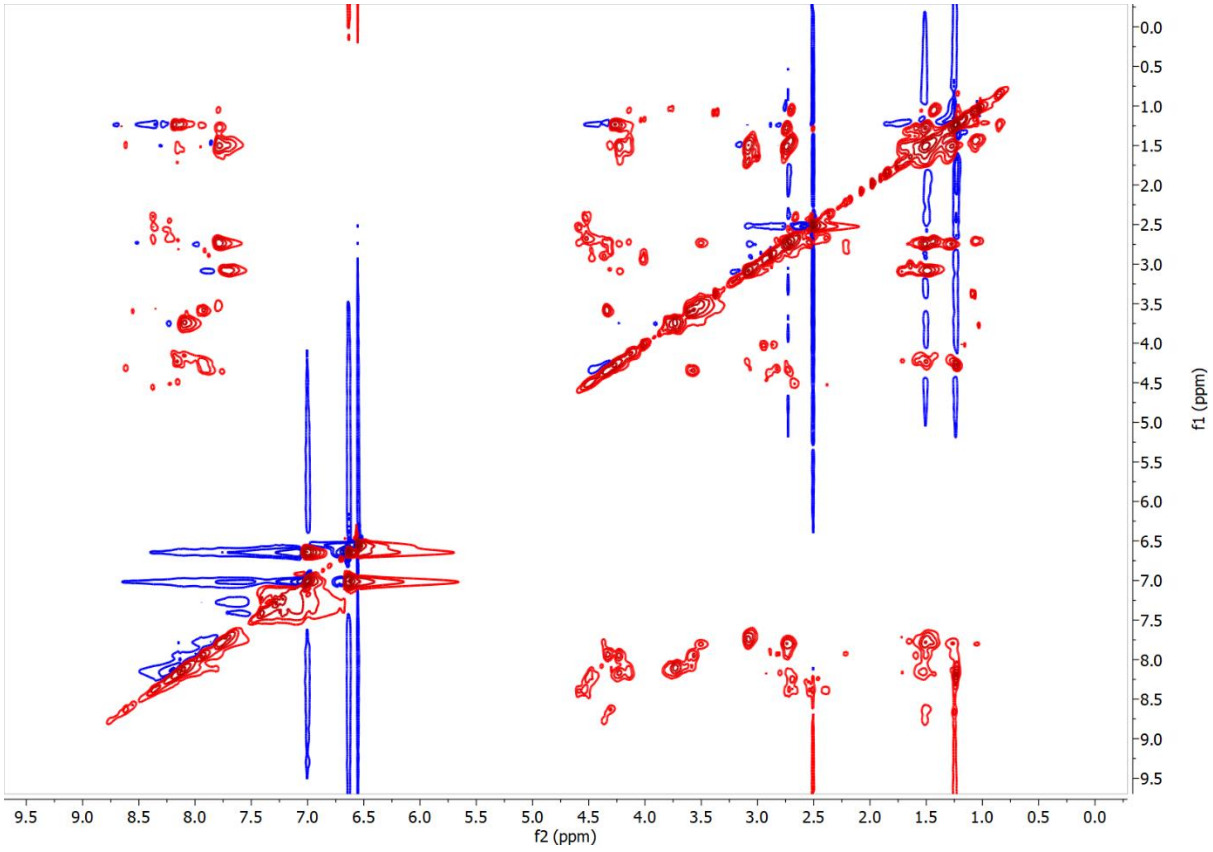


Figure S.3-18: 2D ^{1}H ROESY NMR spectrum of TP_ADLys peptide

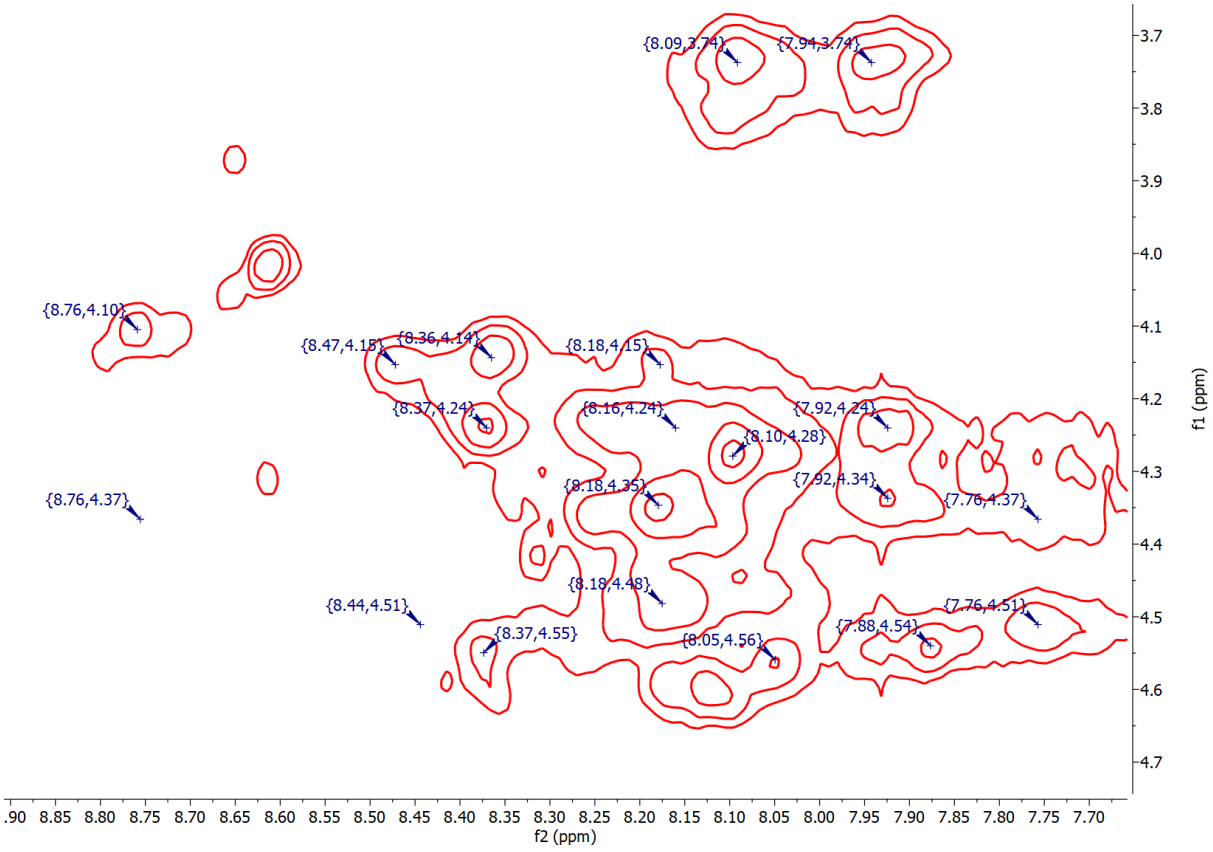


Figure S.3-19: 2D ^{1}H ROESY NMR spectrum of TP_ADLys peptide, ^{1}HN region

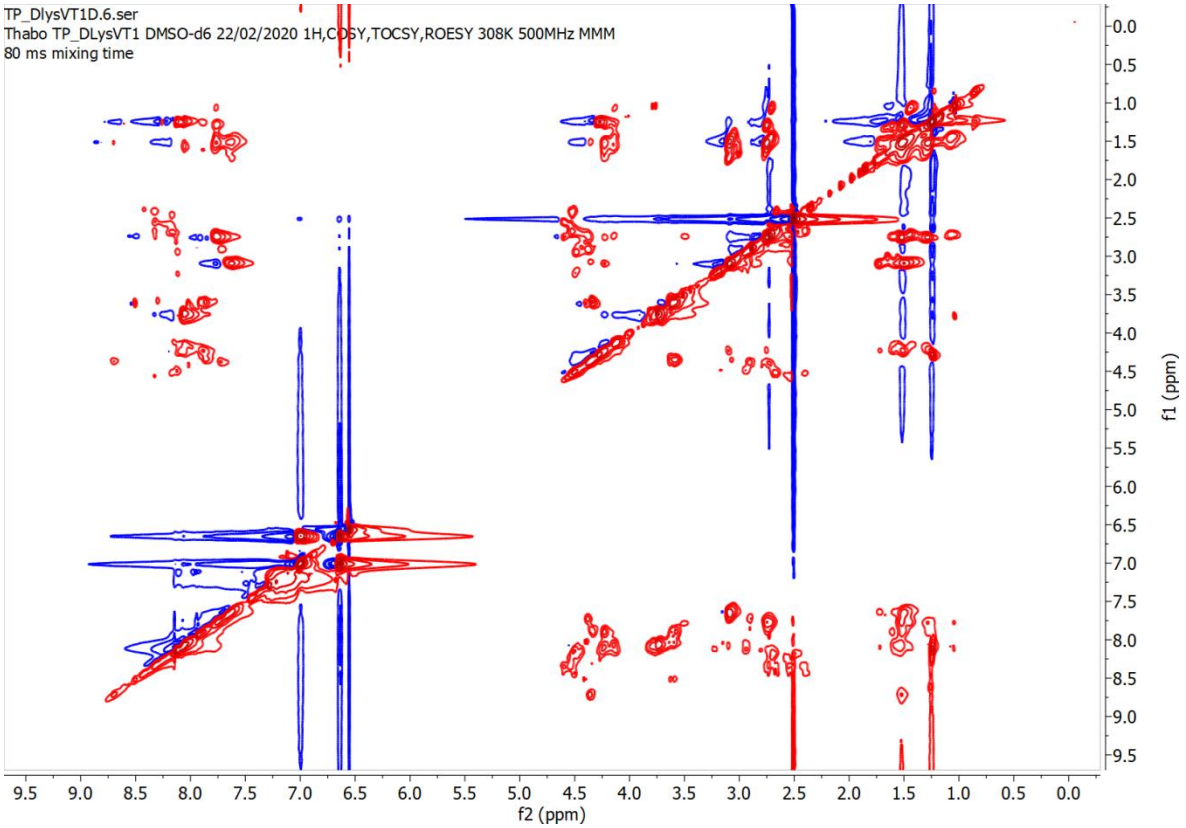


Figure S.3-20: 2D ^{1}H TOCSY spectrum of TP_ADLys peptide at **308K**

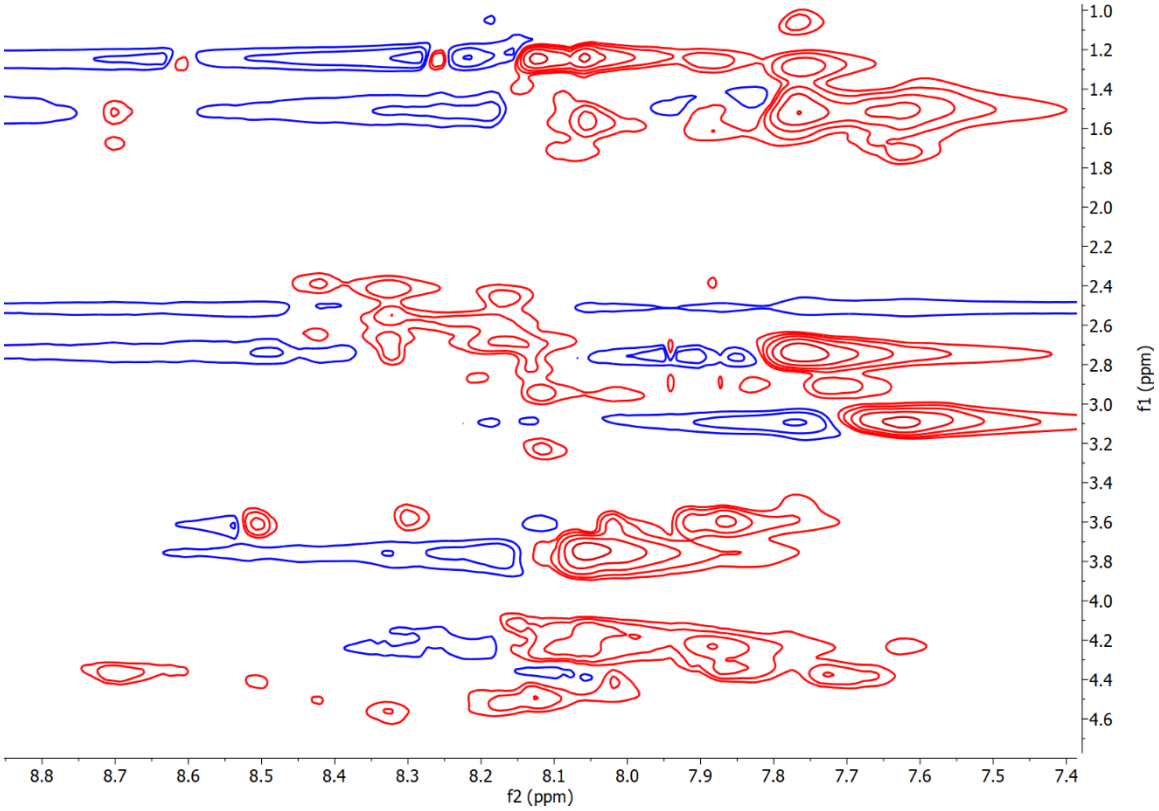


Figure S.3-21: 2D ^{1}H TOCSY spectrum of TP_ADLys peptide, ^{1}HN fingerprint region at 308K

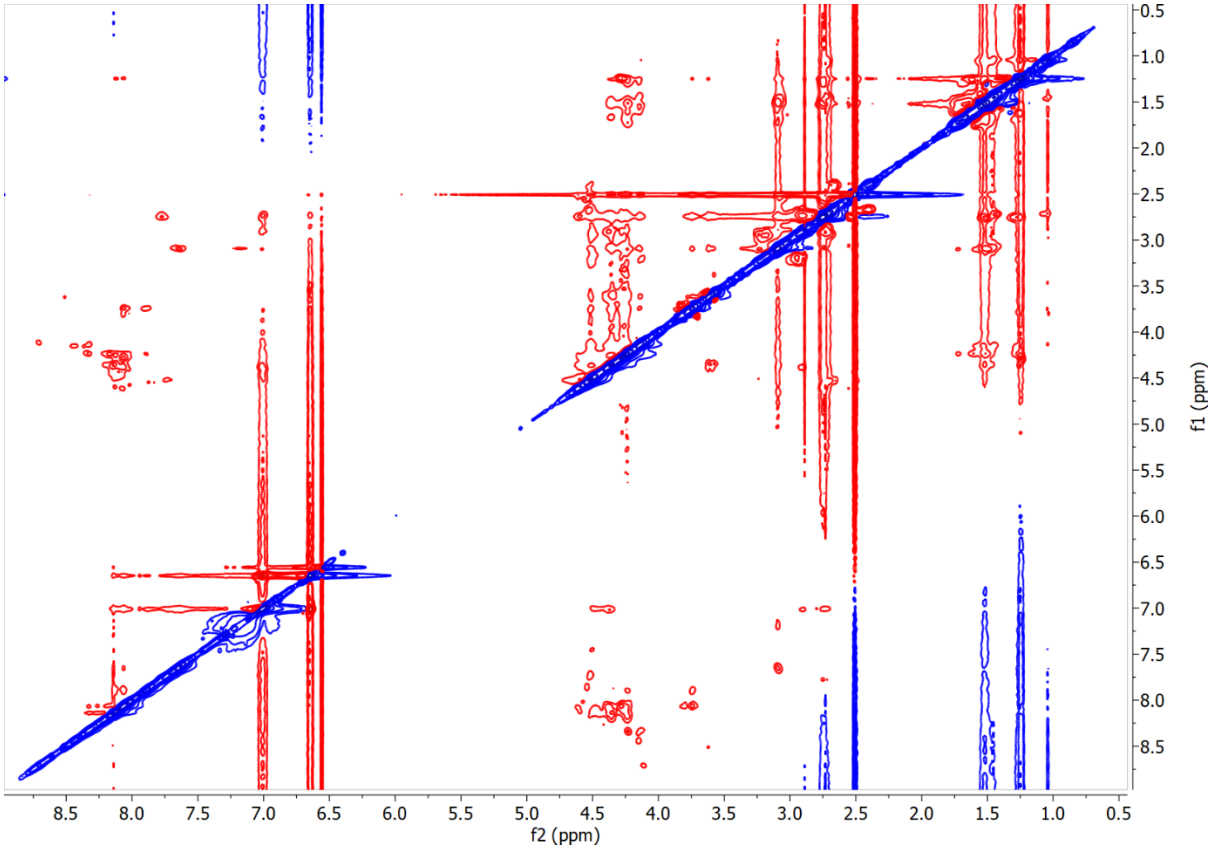


Figure-S.3-22: 2D ^{1}H ROESY spectrum of TP_ADLys peptide at **308K**

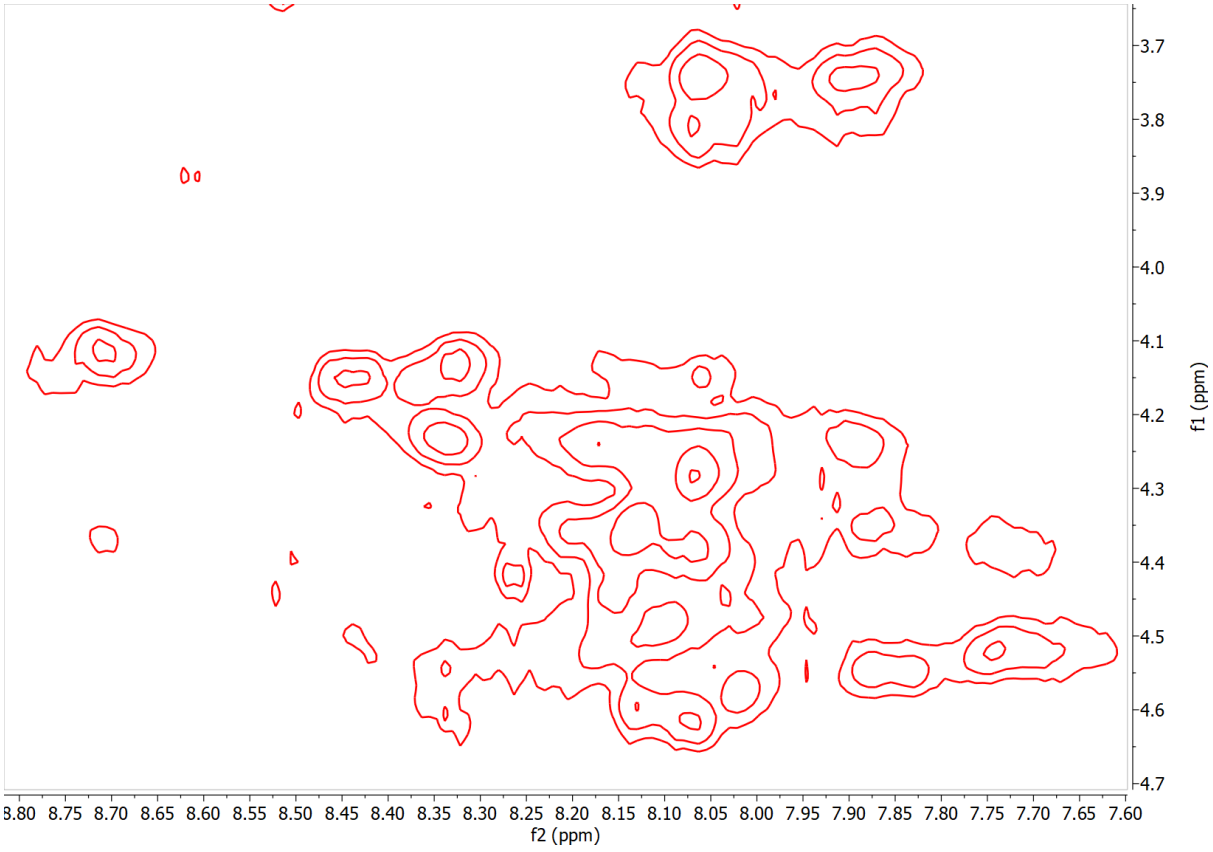


Figure S.3-23: 2D ^{1}H ROESY spectrum of TP_ADLys peptide, ^{1}HN fingerprint region at **308K.**

Appendix III - Supplementary information for Chapter 4

Selected NMR spectra for aldol products

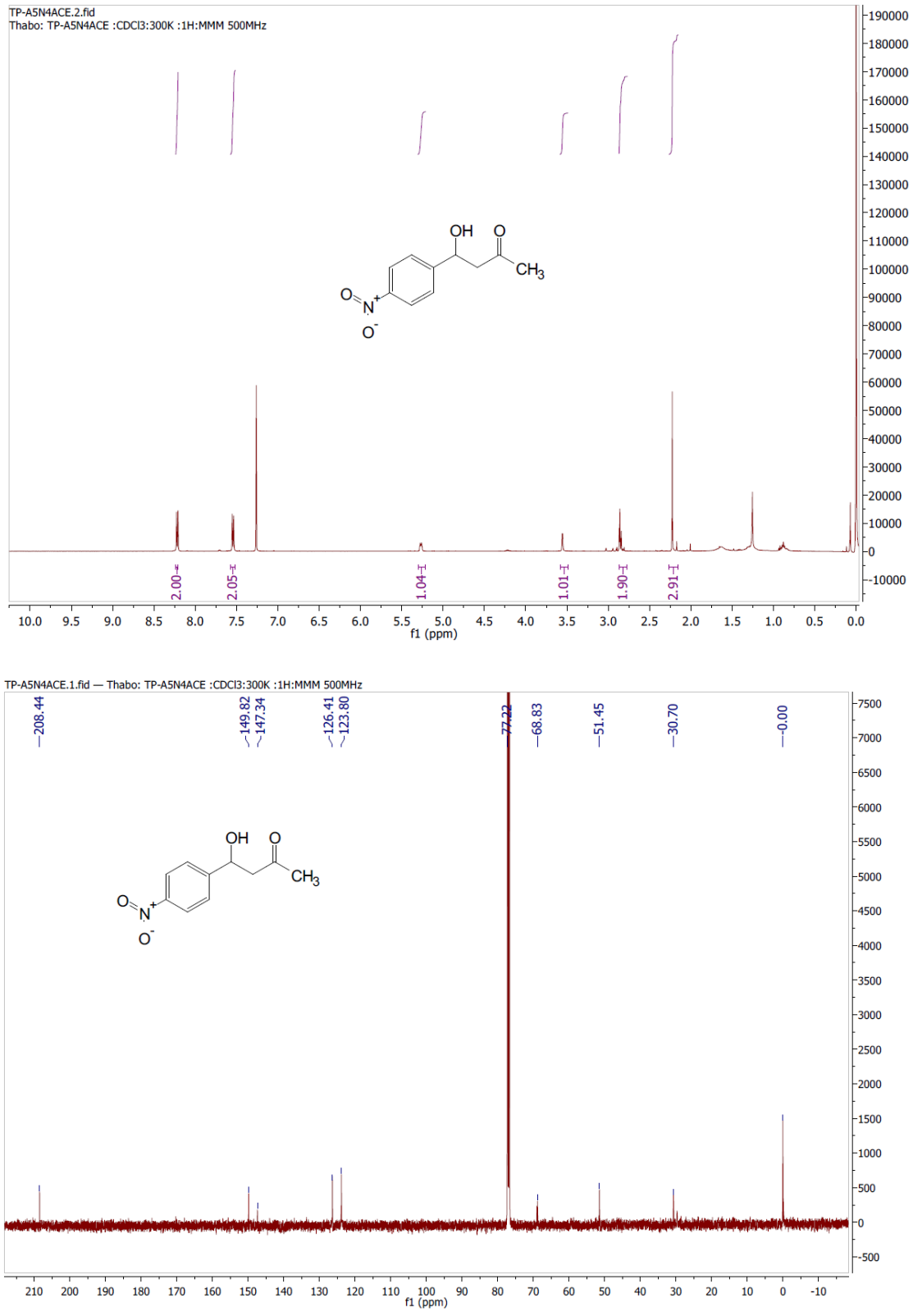


Figure S.4-1: ^{1}H and ^{13}C NMR spectra of the aldol product **TP_A1N4ACE**

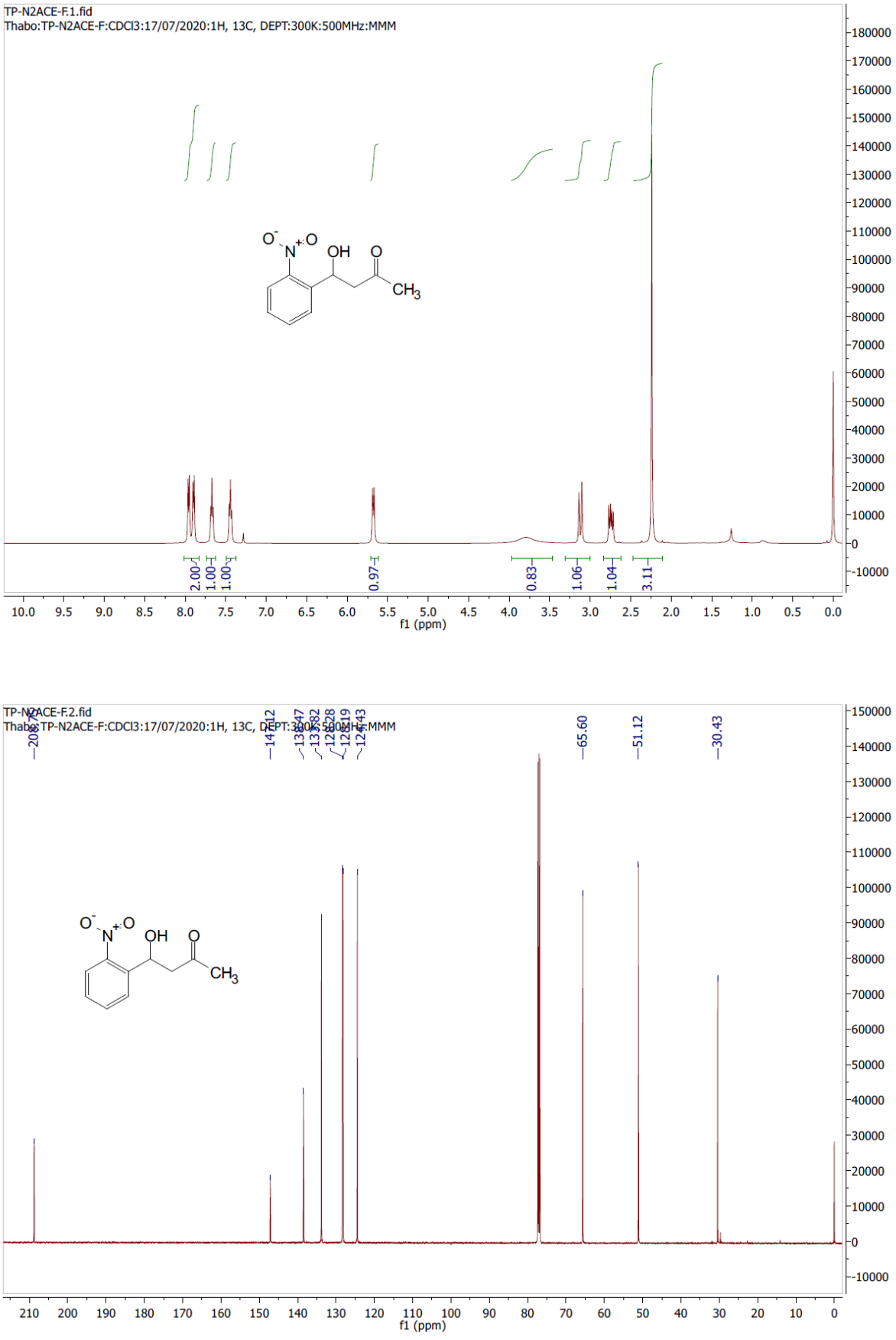


Figure S.4-2: ^{1}H and ^{13}C NMR spectra of the aldol product **TP_A2N2ACE**

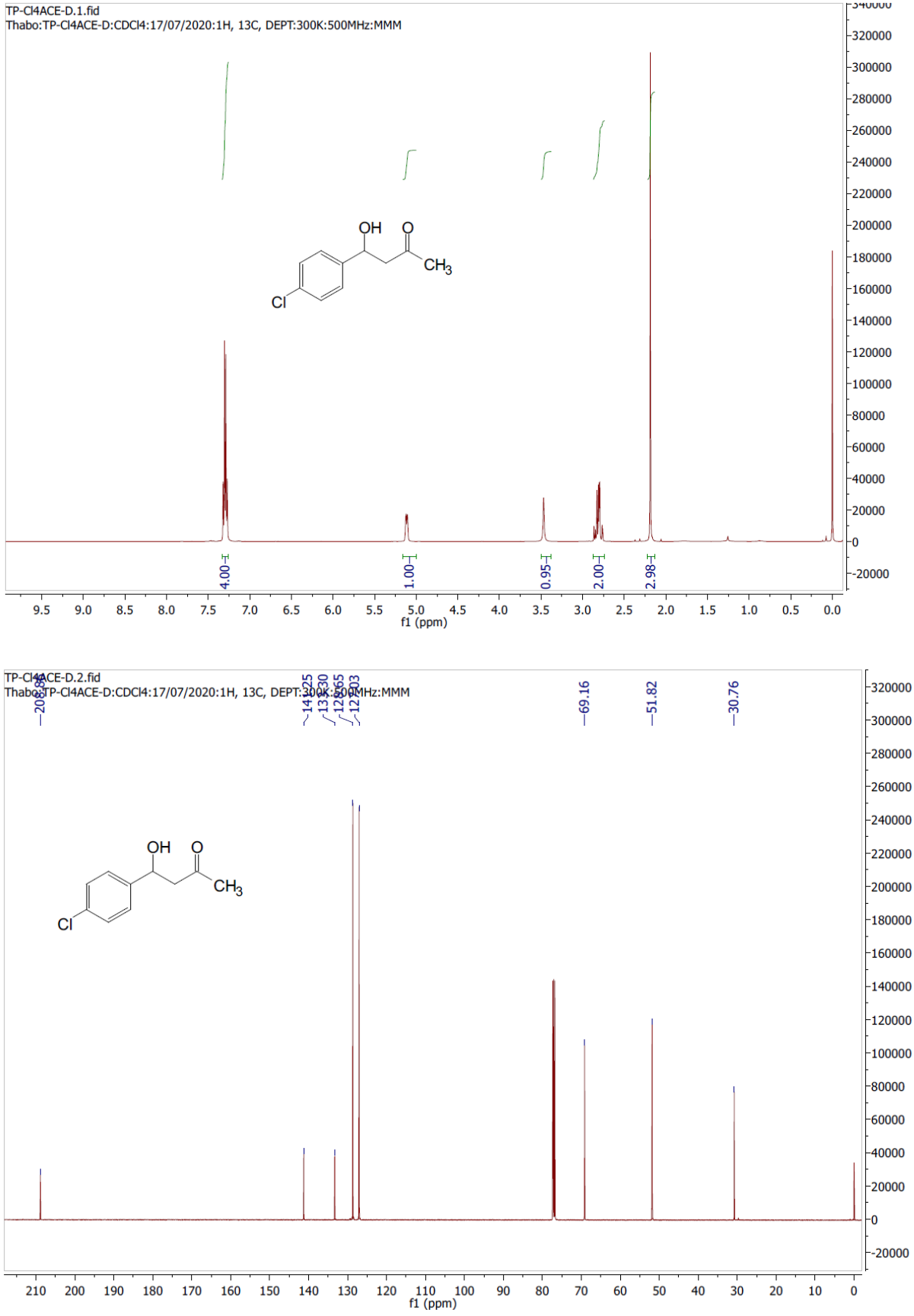


Figure S.4-3: ^{1}H and ^{13}C NMR spectra of the aldol product **TP_A3Cl4ACE**

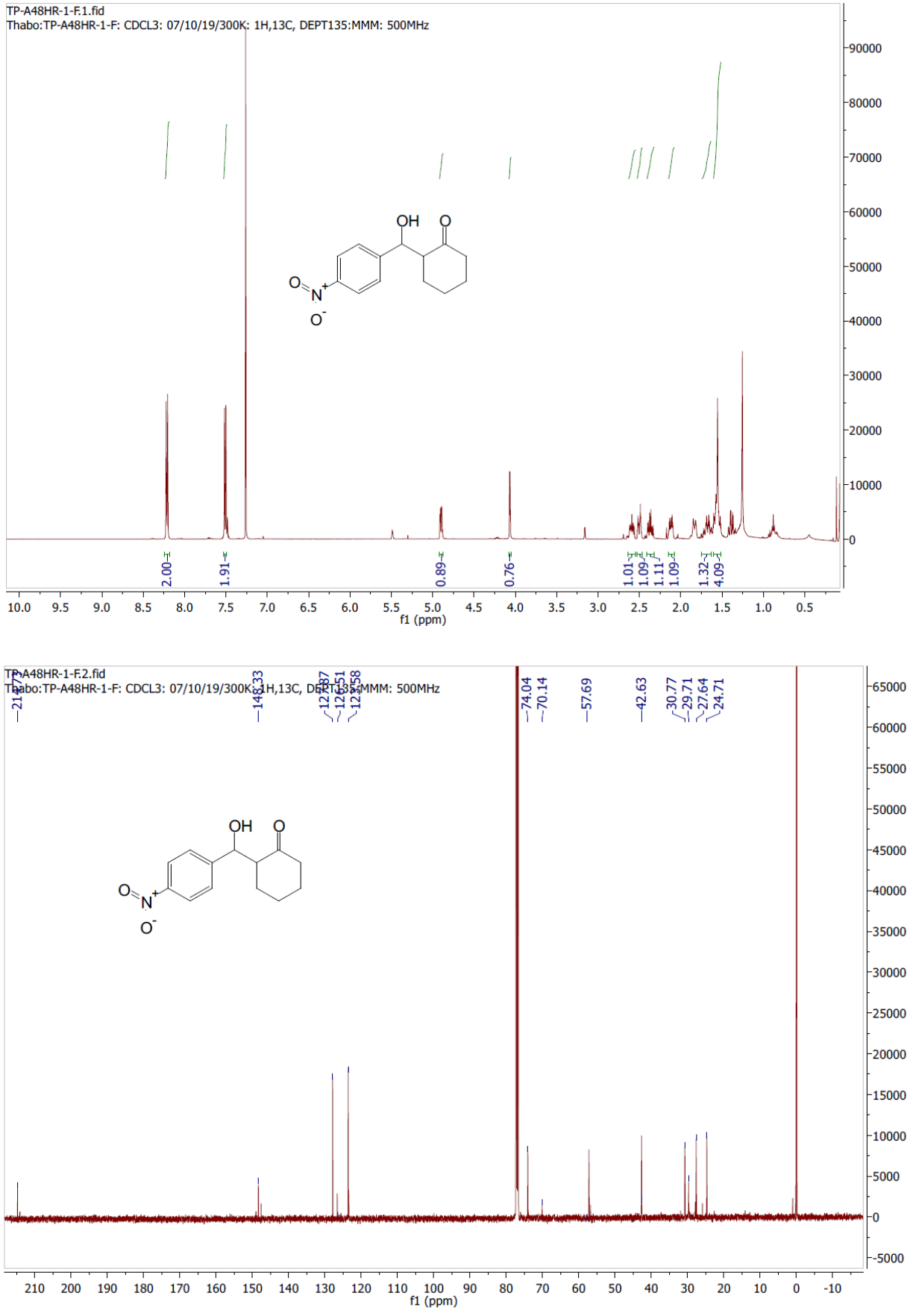
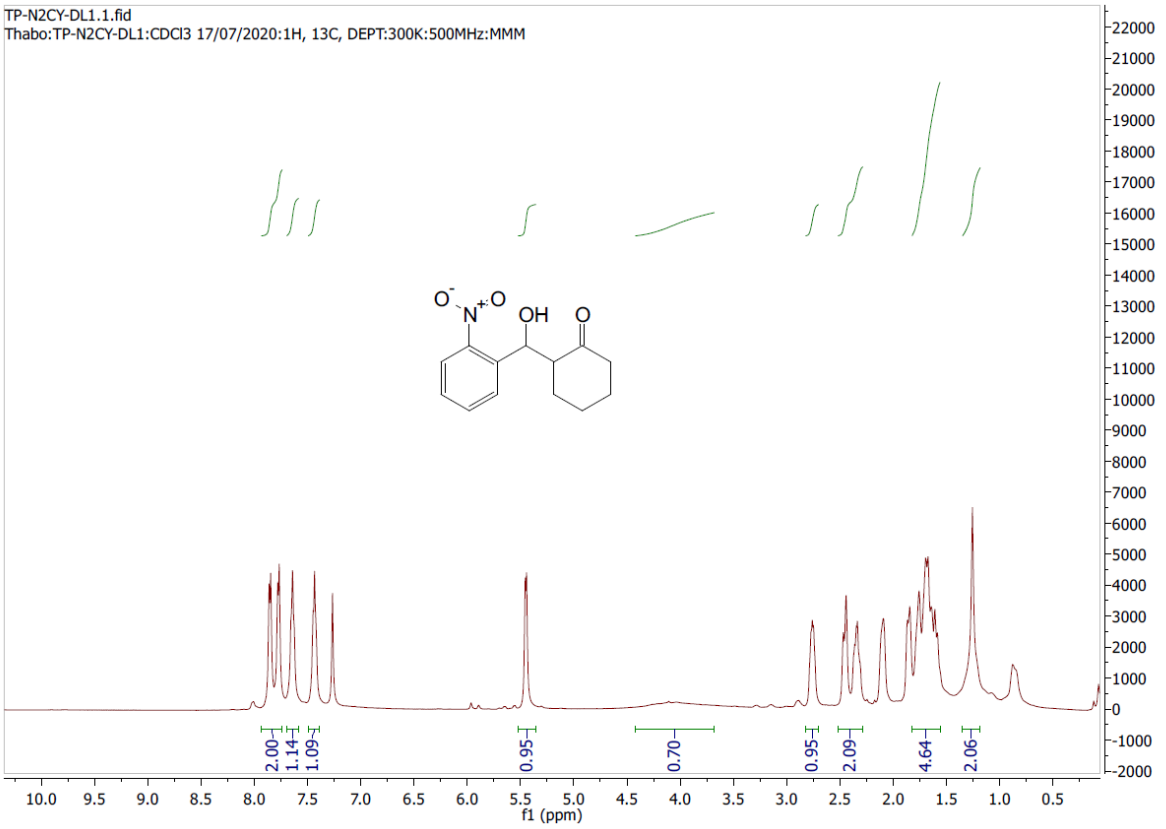


Figure S.4-4: ^{1}H and ^{13}C NMR spectra of the aldol product **TP_A4N4CY**



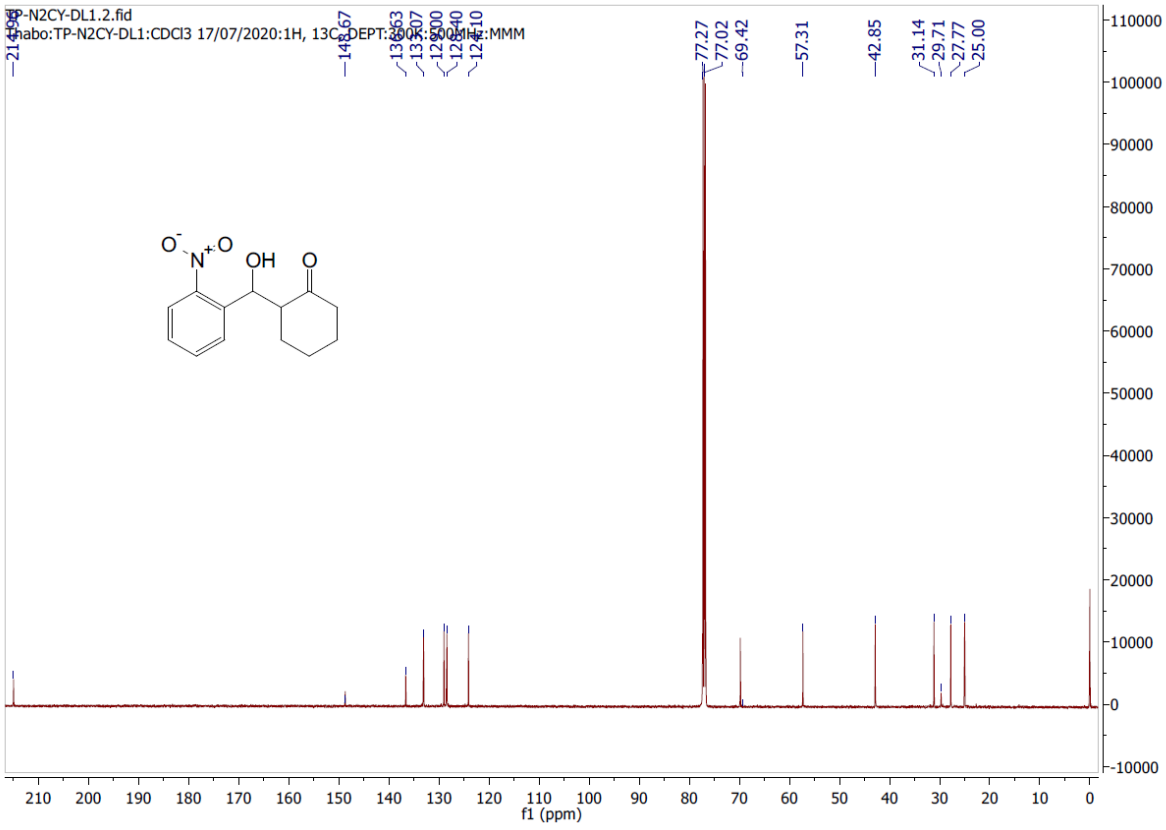
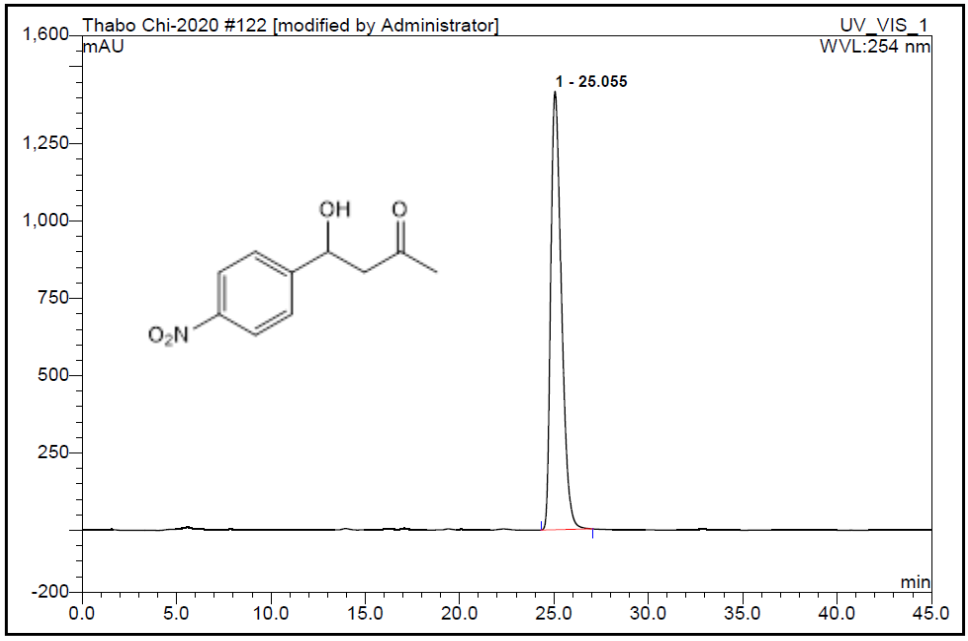


Figure S.4-5: ^{1}H and ^{13}C NMR spectra of the aldol product **TP_A5N2CY**

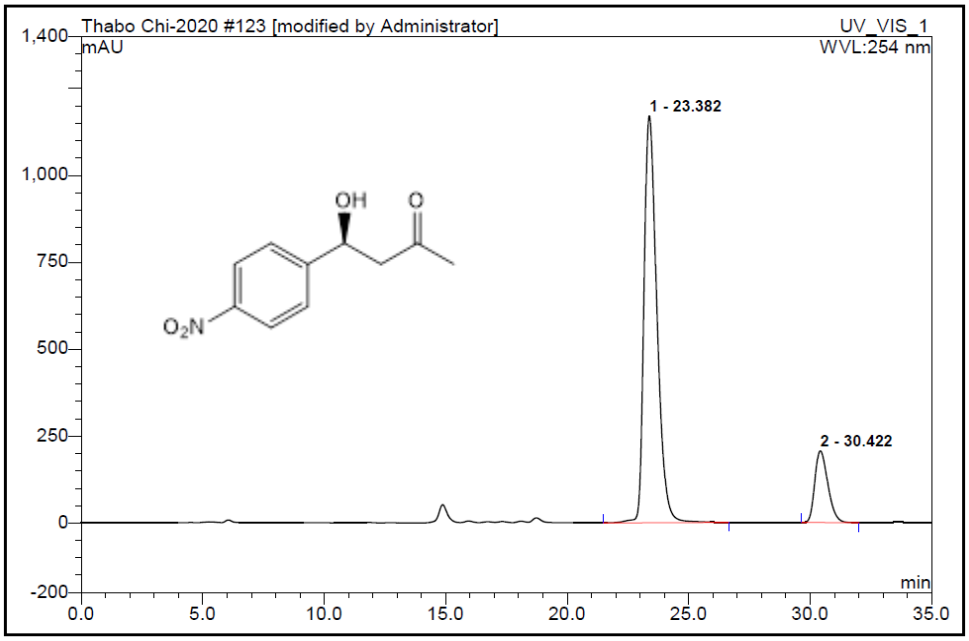
Selected chiral HPLC chromatograms for aldol products

Using Acetone as a solvent and substrate **(Table 4-1)**



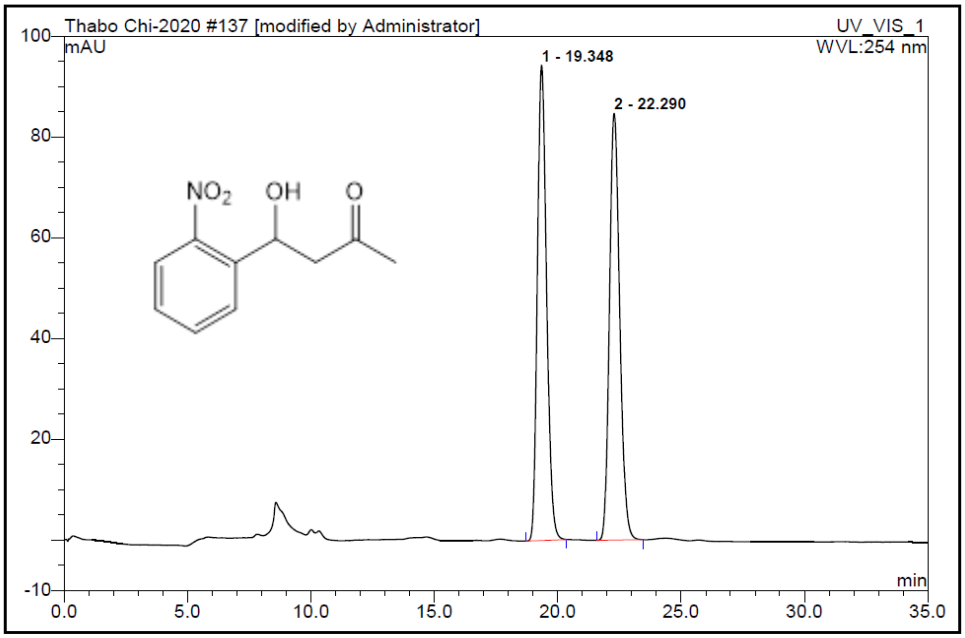
No.	Ret.Time min	Peak Name	Height mAU	Area mAU*min	Rel.Area %	Amount	Type
1	25.06	n.a.	1417.902	931.038	100.00	n.a.	BMB*
Total:			1417.902	931.038	100.00	0.000	

Figure S.4-S: Chiral HPLC chromatogram of **TP_A1N4ACE** –**standard**



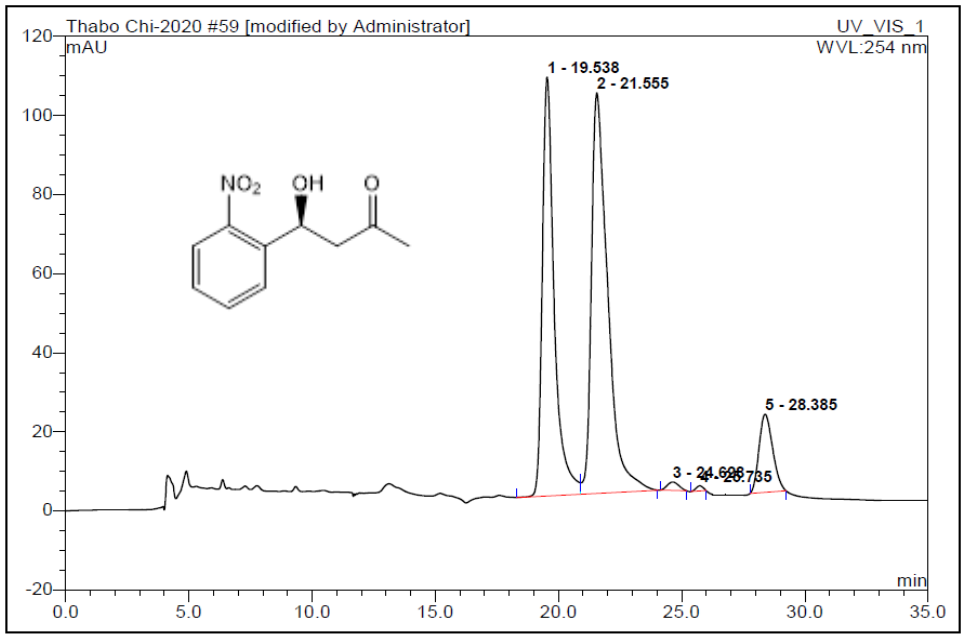
No.	Ret.Time min	Peak Name	Height mAU	Area mAU*min	Rel.Area %	Amount	Type
1	23.38	n.a.	1170.390	720.822	84.85	n.a.	BMB*
2	30.42	n.a.	206.183	128.699	15.15	n.a.	BMB
Total:			1376.573	849.521	100.00	0.000	

Figure S.4-6: Chiral HPLC chromatogram of **TP_A1.1N4ACE** (entry1)



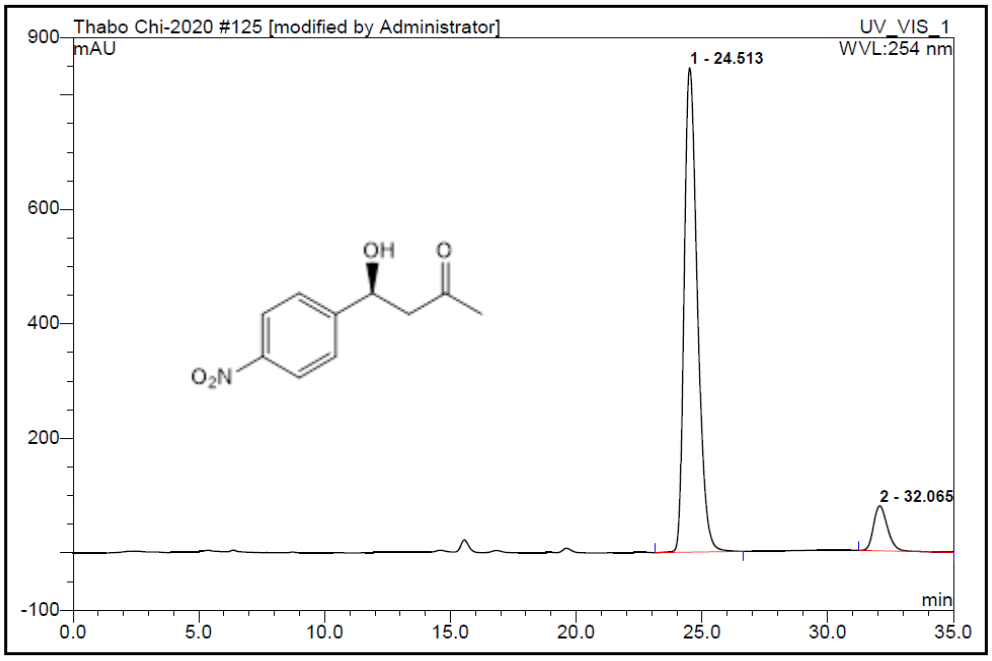
No.	Ret.Time min	Peak Name	Height mAU	Area mAU*min	Rel.Area %	Amount	Type
1	19.35	n.a.	94.329	40.831	49.99	n.a.	BMB*
2	22.29	n.a.	84.722	40.849	50.01	n.a.	BMB*
Total:			179.051	81.680	100.00	0.000	

Figure S.4-S2: Chiral HPLC chromatogram of **racemate TP_A2N2ACE-S2**



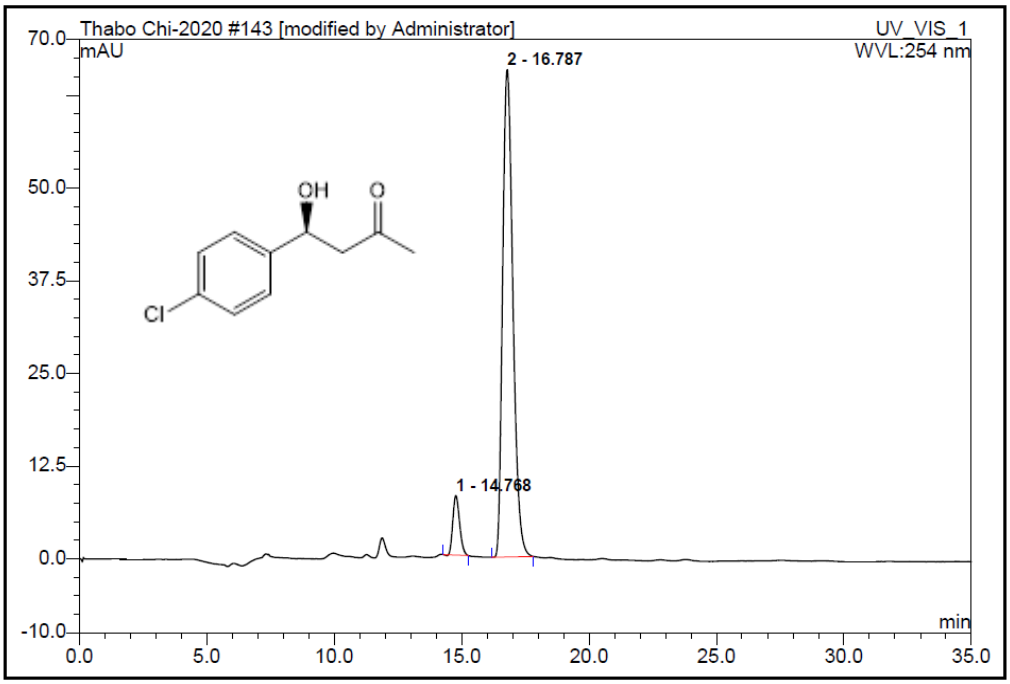
No.	Ret.Time min	Peak Name	Height mAU	Area mAU*min	Rel.Area %	Amount	Type
1	19.54	n.a.	105.908	59.370	39.25	n.a.	BM *
2	21.56	n.a.	101.309	77.648	51.34	n.a.	MB*
3	24.63	n.a.	2.125	1.156	0.76	n.a.	BMB*
4	25.74	n.a.	1.280	0.417	0.28	n.a.	BMB*
5	28.39	n.a.	19.739	12.653	8.37	n.a.	BMB*
Total:			230.360	151.244	100.00	0.000	

Figure S.4-7: Chiral HPLC chromatogram of **TP_A2.1N2ACE** (entry 2)



No.	Ret.Time min	Peak Name	Height mAU	Area mAU*min	Rel.Area %	Amount	Type
1	24.51	n.a.	846.014	515.043	91.14	n.a.	BMB*
2	32.07	n.a.	78.442	50.053	8.86	n.a.	BMB*
Total:			924.456	565.095	100.00	0.000	

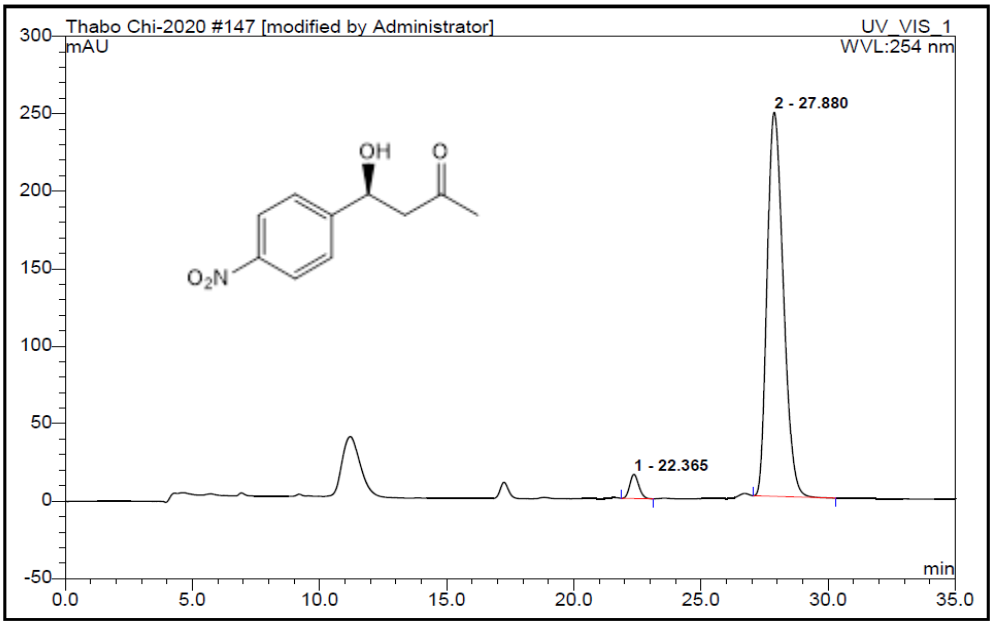
Figure S.4-8: Chiral HPLC chromatogram of **TP_A1.2N4ACE** (entry 4)



No.	Ret.Time min	Peak Name	Height mAU	Area mAU*min	Rel.Area %	Amount	Type
1	14.77	n.a.	8.036	2.462	7.43	n.a.	BMB*
2	16.79	n.a.	65.744	30.679	92.57	n.a.	BMB*
Total:			73.780	33.142	100.00	0.000	

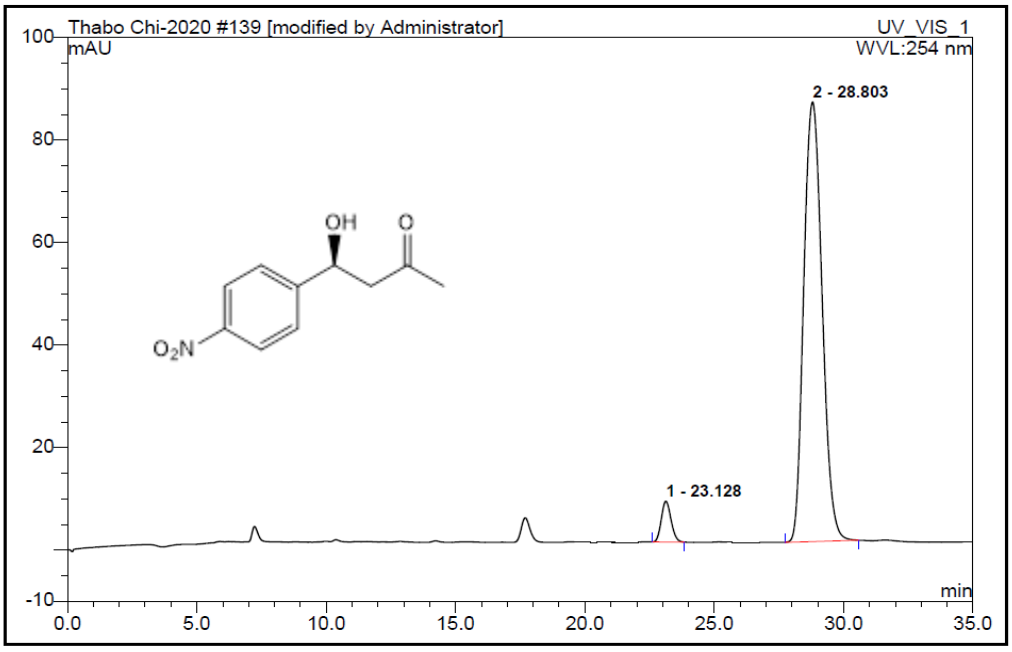
Figure S.4-9: Chiral HPLC chromatogram of **TP_A3Cl4ACE** (entry 5)

Using 8 mol% for reaction between Acetone and *p*-nitrobenzaldehyde **(Table 4-4)**



No.	Ret.Time min	Peak Name	Height mAU	Area mAU*min	Rel.Area %	Amount	Type
1	22.37	n.a.	15.513	6.386	3.37	n.a.	BMB*
2	27.88	n.a.	247.796	182.974	96.63	n.a.	BMB*
Total:			263.309	189.360	100.00	0.000	

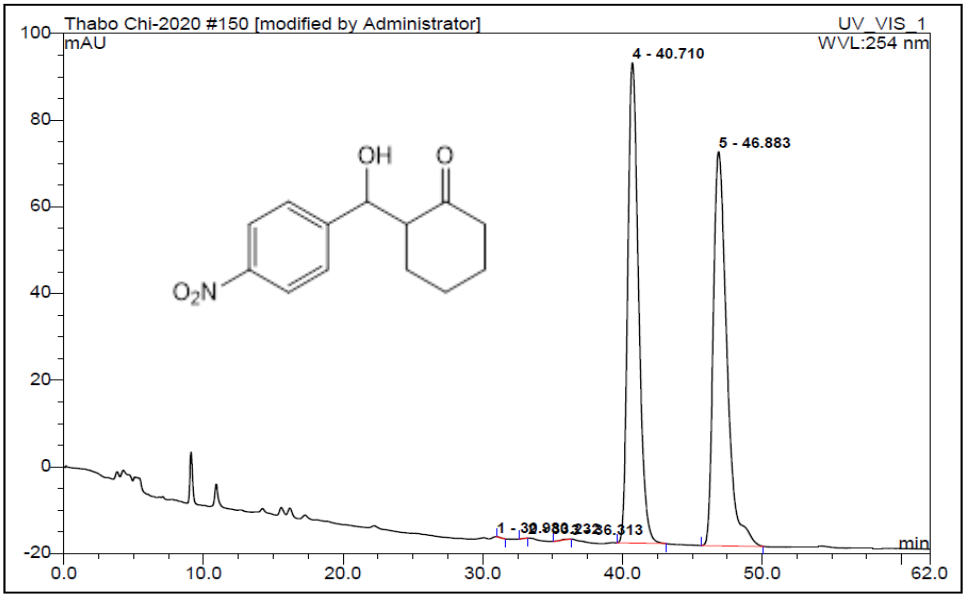
Figure S.4-10: Chiral HPLC chromatogram of **TP_A1.3N4ACE** (entry 1)



No.	Ret.Time min	Peak Name	Height mAU	Area mAU*min	Rel.Area %	Amount	Type
1	23.13	n.a.	7.962	3.480	4.71	n.a.	BMB*
2	28.80	n.a.	85.803	70.346	95.29	n.a.	BMB*
Total:			93.765	73.825	100.00	0.000	

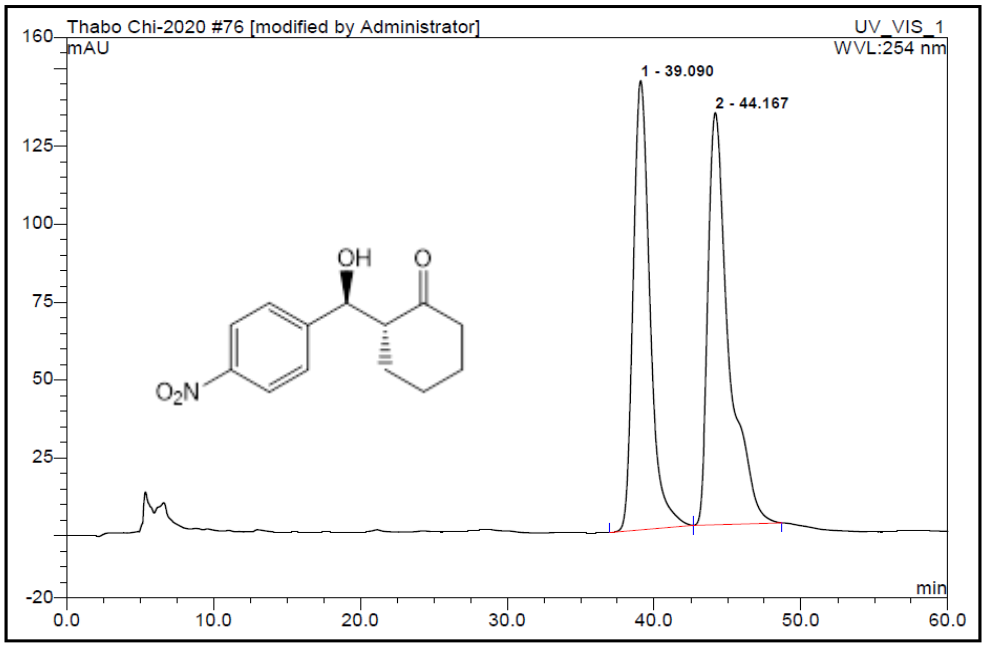
Figure S.4-11: Chiral HPLC chromatogram of **TP-A1.4N4ACE** (entry 2)

Effect of substrate: Reaction between cyclohexanone and aromatic aldehydes **(Table 4-2)**



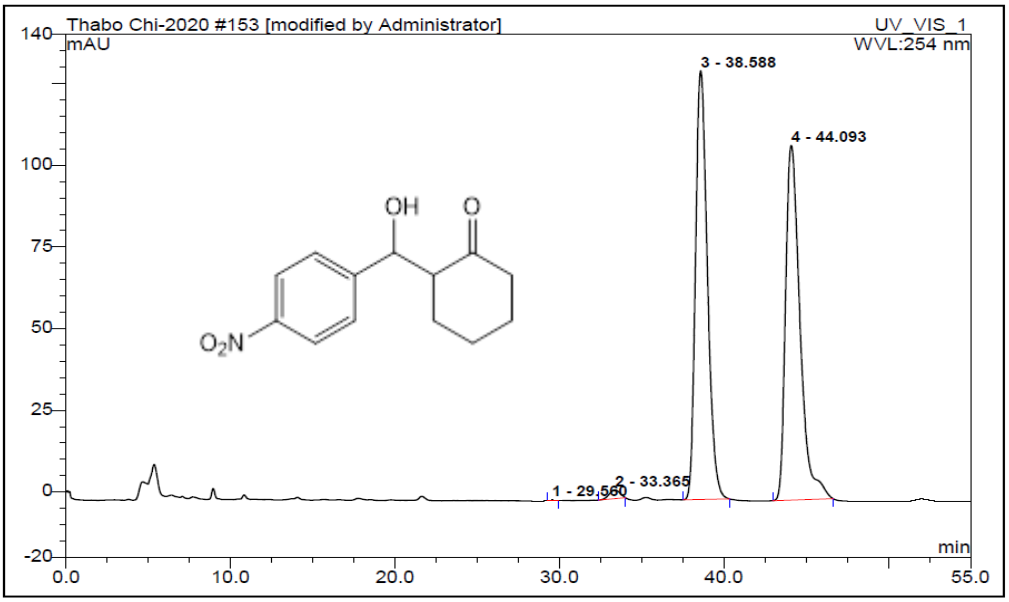
No.	Ret.Time min	Peak Name	Height mAU	Area mAU*min	Rel.Area %	Amount	Type
1	30.98	n.a.	0.011	0.002	0.00	n.a.	BMB*
2	33.23	n.a.	0.010	0.011	0.01	n.a.	BMB*
3	36.31	n.a.	0.008	0.046	0.02	n.a.	BMB*
4	40.71	n.a.	110.867	99.050	49.14	n.a.	BMB*
5	46.88	n.a.	90.970	102.454	50.83	n.a.	BMB
Total:			201.866	201.564	100.00	0.000	

Figure S.4-R: Chiral HPLC chromatogram of **racemate TP_A4N4CY-R1**



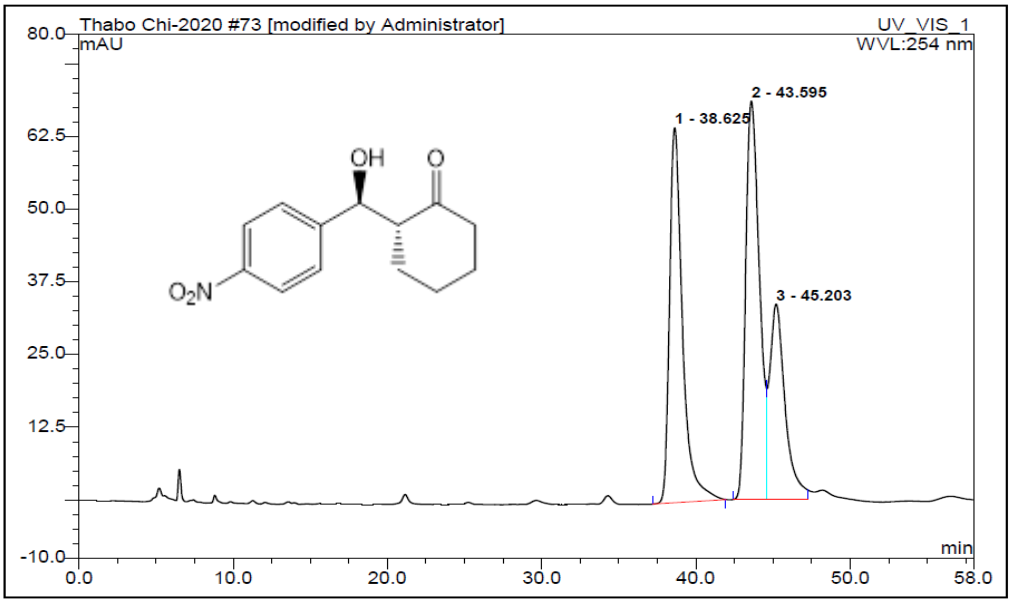
No.	Ret.Time min	Peak Name	Height mAU	Area mAU*min	Rel.Area %	Amount	Type
1	39.09	n.a.	144.164	191.099	46.64	n.a.	BMB*
2	44.17	n.a.	132.215	218.650	53.36	n.a.	BMB*
Total:			276.380	409.750	100.00	0.000	

Figure S.4-12: Chiral HPLC chromatogram of **TP_A4.1N4CY** (entry 4)



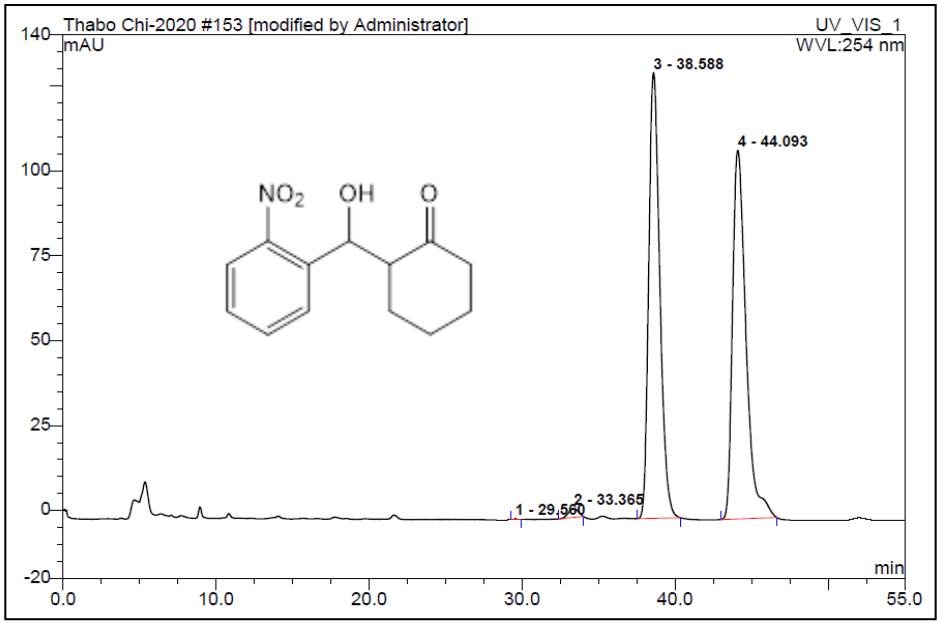
No.	Ret.Time min	Peak Name	Height mAU	Area mAU*min	Rel.Area %	Amount	Type
1	29.56	n.a.	0.181	0.069	0.03	n.a.	BMB*
2	33.37	n.a.	2.682	1.999	0.90	n.a.	BMB*
3	38.59	n.a.	131.271	109.853	49.38	n.a.	BMB*
4	44.09	n.a.	108.542	110.528	49.69	n.a.	BMB*
Total:			242.676	222.450	100.00	0.000	

Figure S.4-R: Chiral HPLC chromatogram of **racemate TP_A4N4CY-R4**



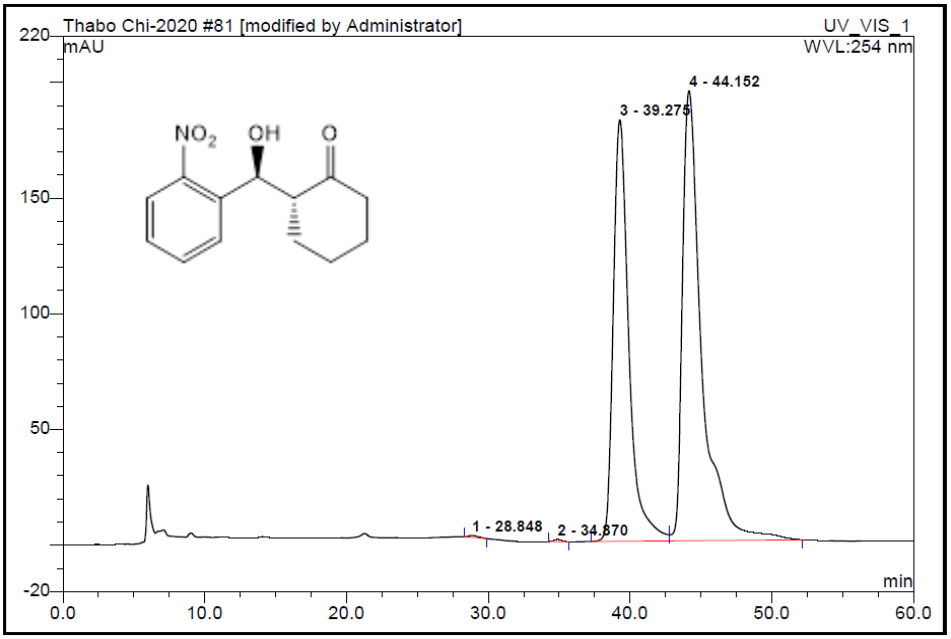
No.	Ret.Time min	Peak Name	Height mAU	Area mAU*min	Rel.Area %	Amount	Type
1	38.63	n.a.	64.448	62.770	36.38	n.a.	BMB*
2	43.60	n.a.	68.545	70.791	41.03	n.a.	BM *
3	45.20	n.a.	33.626	38.975	22.59	n.a.	M *
Total:			166.619	172.535	100.00	0.000	

Figure S.4-13: Chiral HPLC chromatogram of **TP_A4.2N4CY** (entry 9)



No.	Ret.Time min	Peak Name	Height mAU	Area mAU*min	Rel.Area %	Amount	Type
1	29.56	n.a.	0.181	0.069	0.03	n.a.	BMB*
2	33.37	n.a.	2.682	1.999	0.90	n.a.	BMB*
3	38.59	n.a.	131.271	109.853	49.38	n.a.	BMB*
4	44.09	n.a.	108.542	110.528	49.69	n.a.	BMB*
Total:			242.676	222.450	100.00	0.000	

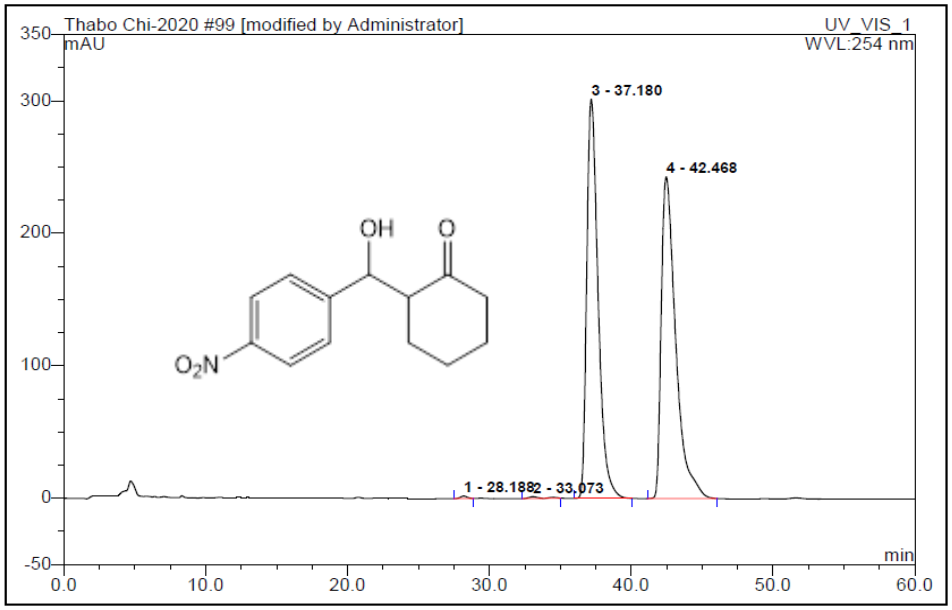
Figure S.4-R: Chiral HPLC chromatogram of **racemate TP_A5N2CY-RA5**



No.	Ret.Time min	Peak Name	Height mAU	Area mAU*min	Rel.Area %	Amount	Type
1	28.85	n.a.	0.923	0.717	0.13	n.a.	BMB
2	34.87	n.a.	0.962	0.630	0.12	n.a.	BMB*
3	39.28	n.a.	182.083	232.316	43.02	n.a.	BM *
4	44.15	n.a.	194.427	306.341	56.73	n.a.	MB*
Total:			378.395	540.004	100.00	0.000	

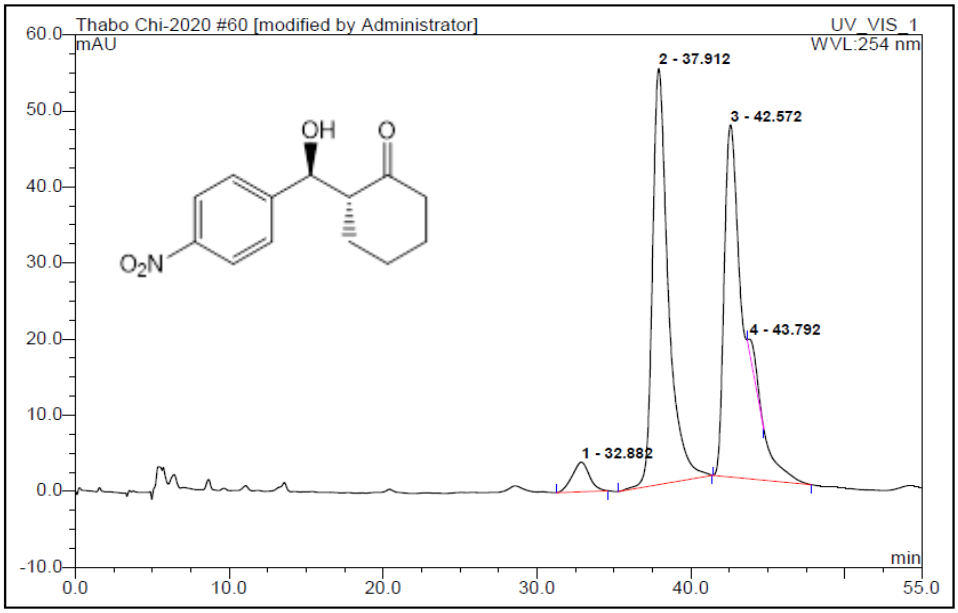
Figure S.4-14: Chiral HPLC chromatogram of **TP_A5.1N2CY** (entry 10)

Effect of solvents -Reaction between cyclohexanone and *p*-nitrobenzaldehyde (**Table 4-3)**



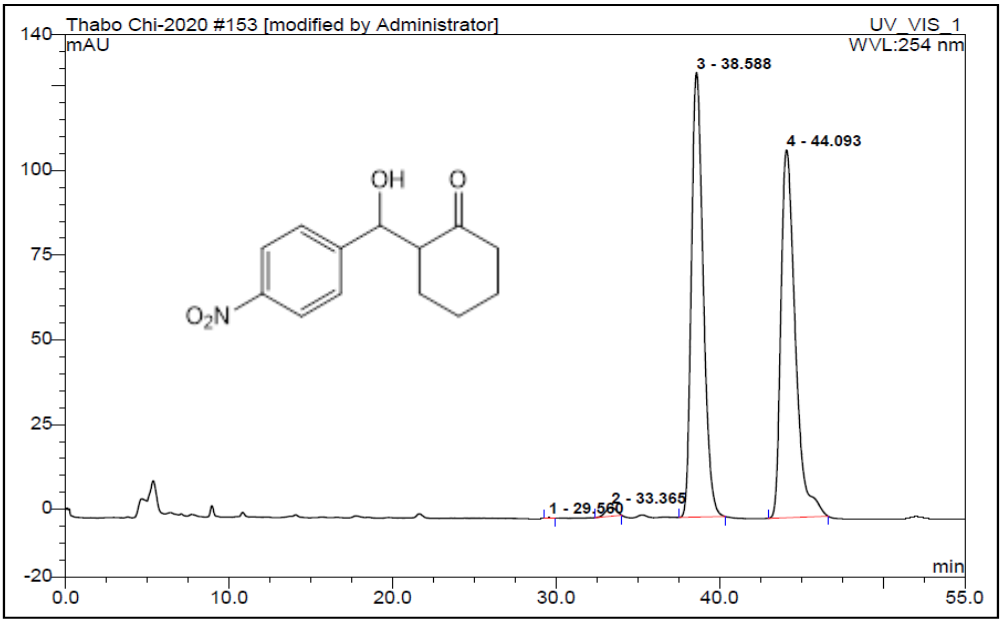
No.	Ret.Time min	Peak Name	Height mAU	Area mAU*min	Rel.Area %	Amount	Type
1	28.19	n.a.	1.891	1.030	0.18	n.a.	BMB*
2	33.07	n.a.	1.428	1.464	0.26	n.a.	BMB*
3	37.18	n.a.	301.322	280.012	49.20	n.a.	BMB*
4	42.47	n.a.	242.824	286.638	50.36	n.a.	BMB*
Total:			547.464	569.144	100.00	0.000	

Figure S.4-R: Chiral HPLC chromatogram of **racemate TP_A4N4CY-R5**



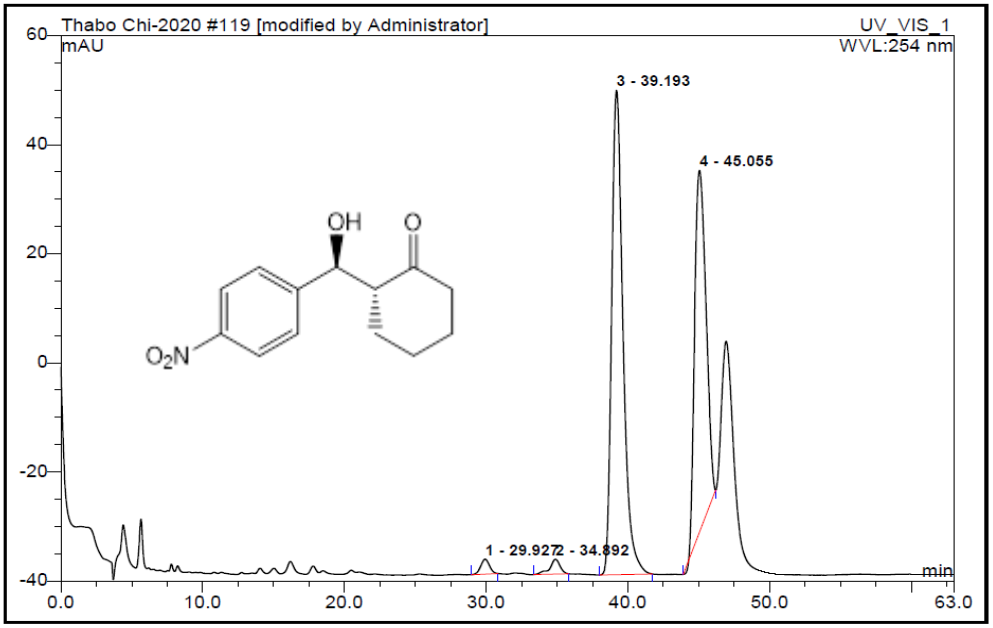
No.	Ret.Time min	Peak Name	Height mAU	Area mAU*min	Rel.Area %	Amount	Type
1	32.88	n.a.	3.885	5.043	3.48	n.a.	BMB*
2	37.91	n.a.	54.689	65.290	45.11	n.a.	BMB*
3	42.57	n.a.	46.283	72.571	50.14	n.a.	BMB*
4	43.79	n.a.	1.556	1.823	1.26	n.a.	Rd
Total:			106.413	144.727	100.00	0.000	

Figure S.4-15: Chiral HPLC chromatogram of **TP_A4.3N4CY** (entry 4)



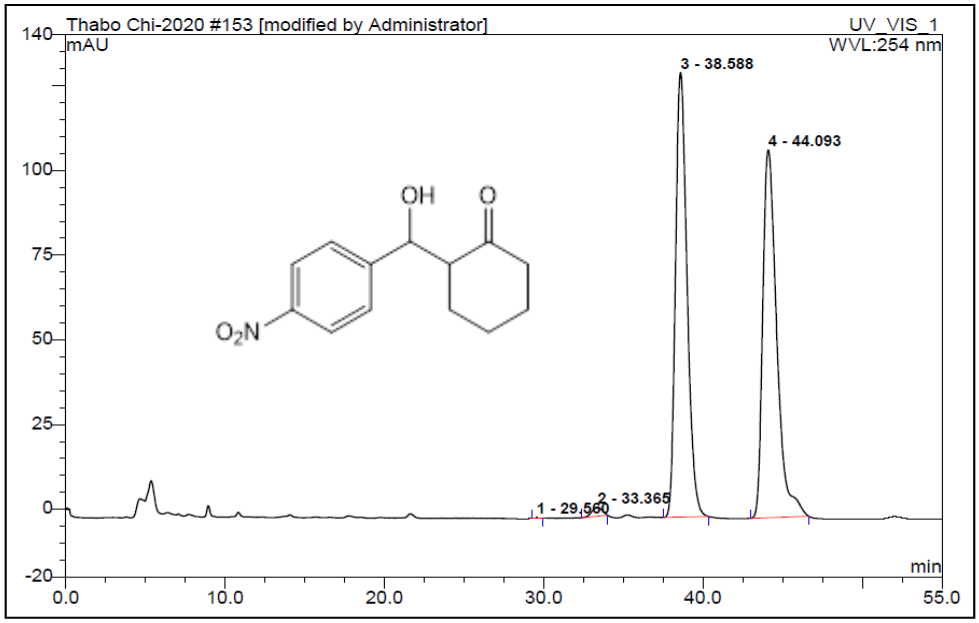
No.	Ret.Time min	Peak Name	Height mAU	Area mAU*min	Rel.Area %	Amount	Type
1	29.56	n.a.	0.181	0.069	0.03	n.a.	BMB*
2	33.37	n.a.	2.682	1.999	0.90	n.a.	BMB*
3	38.59	n.a.	131.271	109.853	49.38	n.a.	BMB*
4	44.09	n.a.	108.542	110.528	49.69	n.a.	BMB*
Total:			242.676	222.450	100.00	0.000	

Figure S.4-R: Chiral HPLC chromatogram of **racemate TP_A4N4CY-R6**



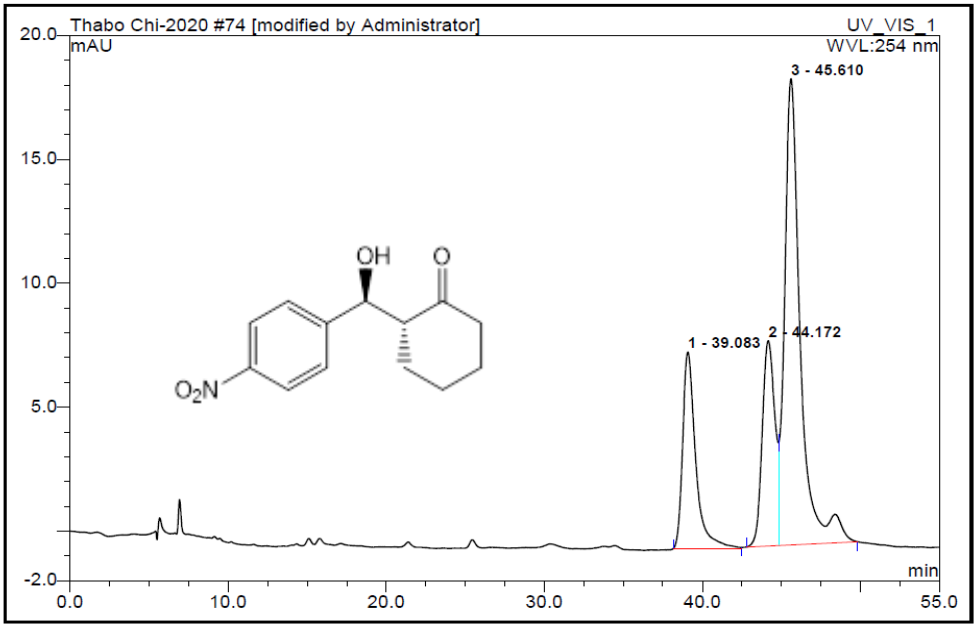
No.	Ret.Time min	Peak Name	Height mAU	Area mAU*min	Rel.Area %	Amount	Type
1	29.93	n.a.	2.726	1.960	1.32	n.a.	BMB*
2	34.89	n.a.	2.718	2.275	1.54	n.a.	BMB*
3	39.19	n.a.	88.765	82.427	55.70	n.a.	BMB*
4	45.06	n.a.	66.283	61.318	41.44	n.a.	BMB*
Total:			160.492	147.979	100.00	0.000	

Figure S.4-16: Chiral HPLC chromatogram of **TP_A4.4N4CY** (entry 6)



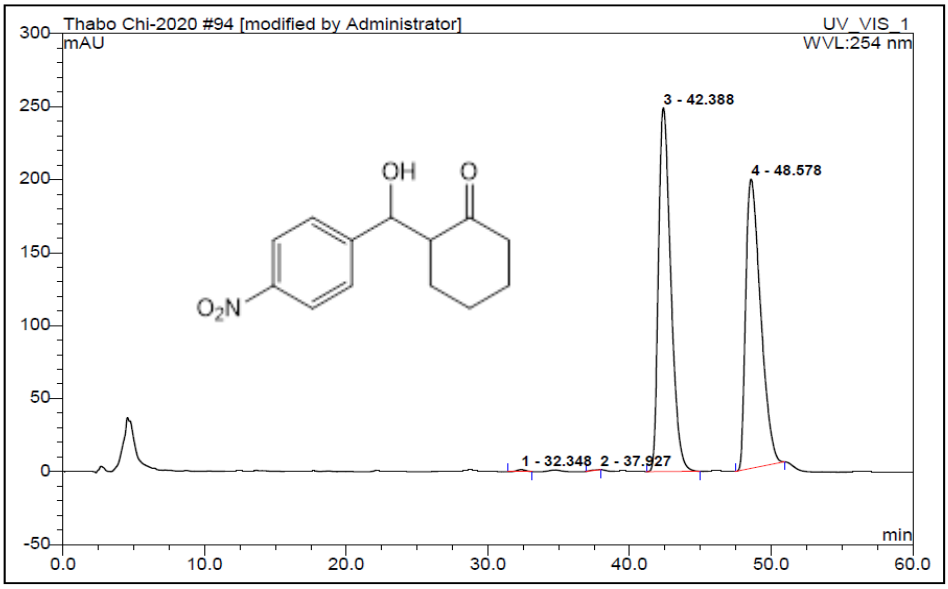
No.	Ret.Time min	Peak Name	Height mAU	Area mAU*min	Rel.Area %	Amount	Type
1	29.56	n.a.	0.181	0.069	0.03	n.a.	BMB*
2	33.37	n.a.	2.682	1.999	0.90	n.a.	BMB*
3	38.59	n.a.	131.271	109.853	49.38	n.a.	BMB*
4	44.09	n.a.	108.542	110.528	49.69	n.a.	BMB*
Total:			242.676	222.450	100.00	0.000	

Figure S.4-R: Chiral HPLC chromatogram of **racemate TP_A4N4CY-R7**



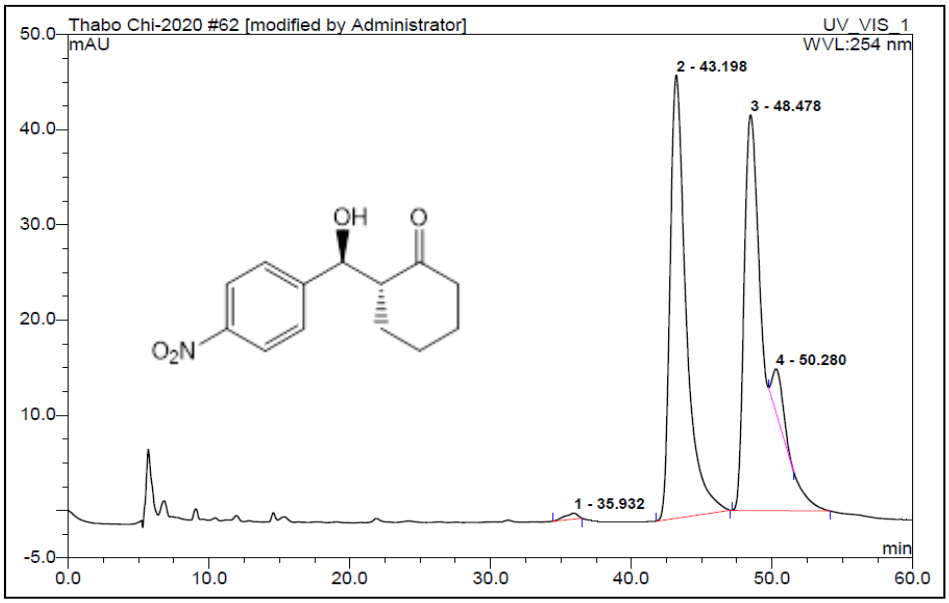
No.	Ret.Time min	Peak Name	Height mAU	Area mAU*min	Rel.Area %	Amount	Type
1	39.08	n.a.	7.925	7.582	20.41	n.a.	BM *
2	44.17	n.a.	8.280	7.602	20.46	n.a.	BM *
3	45.61	n.a.	18.812	21.974	59.14	n.a.	MB*
Total:			35.017	37.158	100.00	0.000	

Figure S.4-17: Chiral HPLC chromatogram of **TP_A4.5N4CY** (entry 9)



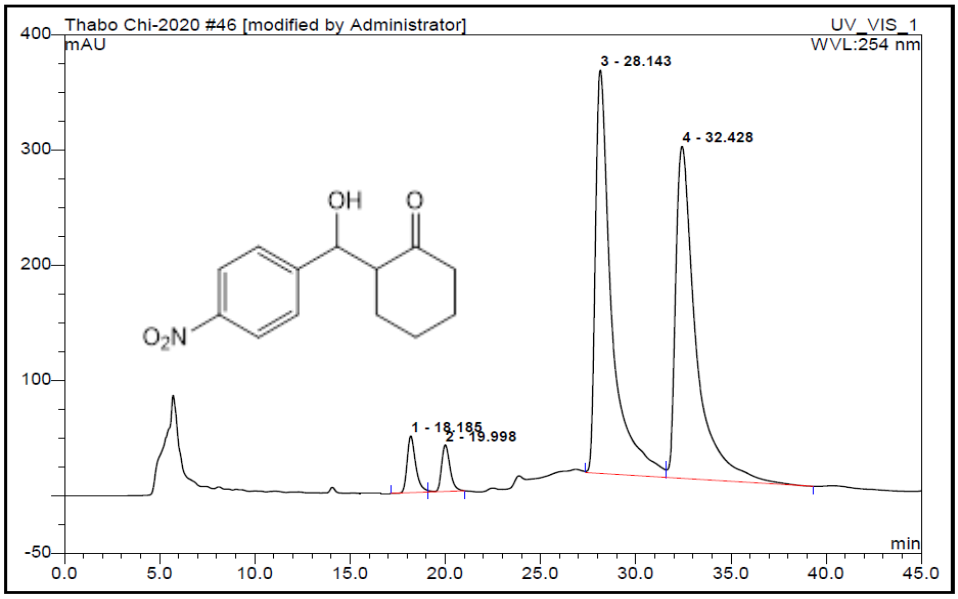
No.	Ret.Time min	Peak Name	Height mAU	Area mAU*min	Rel.Area %	Amount	Type
1	32.35	n.a.	1.387	0.998	0.20	n.a.	BMB*
2	37.93	n.a.	0.032	0.182	0.04	n.a.	BMB*
3	42.39	n.a.	249.159	251.603	50.91	n.a.	BMB*
4	48.58	n.a.	198.169	241.383	48.85	n.a.	BMB*
Total:			448.746	494.165	100.00	0.000	

Figure S.4-R: Chiral HPLC chromatogram of **racemate TP_A4N4CY-R8**



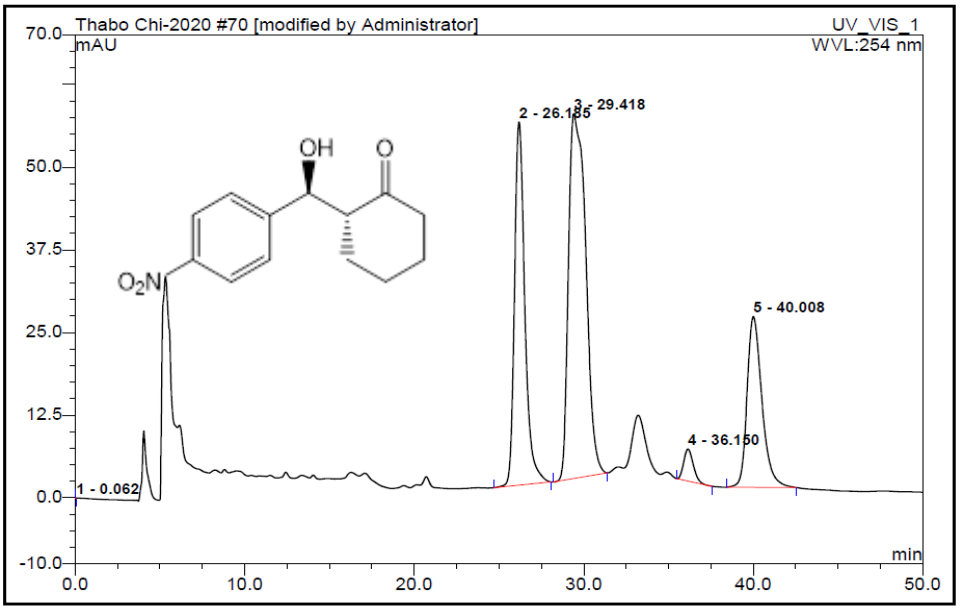
No.	Ret.Time min	Peak Name	Height mAU	Area mAU*min	Rel.Area %	Amount	Type
1	35.93	n.a.	0.625	0.676	0.48	n.a.	BMB*
2	43.20	n.a.	46.566	61.847	44.33	n.a.	BMB*
3	48.48	n.a.	41.579	72.831	52.20	n.a.	BMB*
4	50.28	n.a.	4.533	4.162	2.98	n.a.	Rd
Total:			93.304	139.516	100.00	0.000	

Figure S.4-18: Chiral HPLC chromatogram of **TP_A4.6N4CY** (entry 13)



No.	Ret.Time min	Peak Name	Height mAU	Area mAU*min	Rel.Area %	Amount	Type
1	18.19	n.a.	49.255	25.866	3.44	n.a.	BM *
2	20.00	n.a.	40.366	20.758	2.76	n.a.	MB*
3	28.14	n.a.	350.081	350.136	46.53	n.a.	M *
4	32.43	n.a.	288.095	355.814	47.28	n.a.	MB*
Total:			727.798	752.574	100.00	0.000	

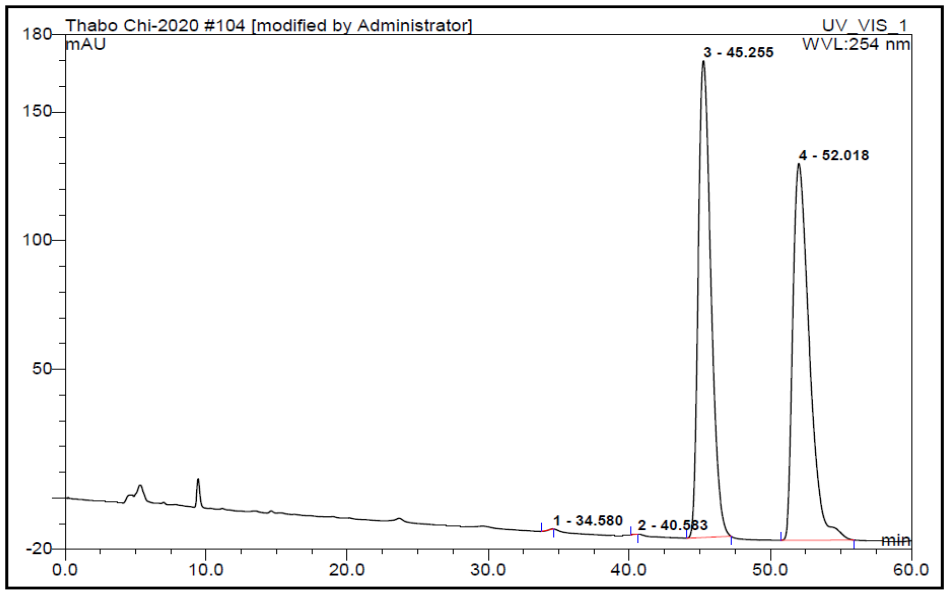
Figure S.4-R: Chiral HPLC chromatogram of **racemate TP_A4N4CY-R10**



No.	Ret.Time min	Peak Name	Height mAU	Area mAU*min	Rel.Area %	Amount	Type
1	0.06	n.a.	0.005	0.000	0.00	n.a.	BMB
2	26.19	n.a.	54.929	38.662	29.15	n.a.	BMB*
3	29.42	n.a.	55.175	64.604	48.70	n.a.	BMB*
4	36.15	n.a.	4.826	3.142	2.37	n.a.	BMB*
5	40.01	n.a.	25.817	26.244	19.78	n.a.	BMB*
Total:			140.752	132.652	100.00	0.000	

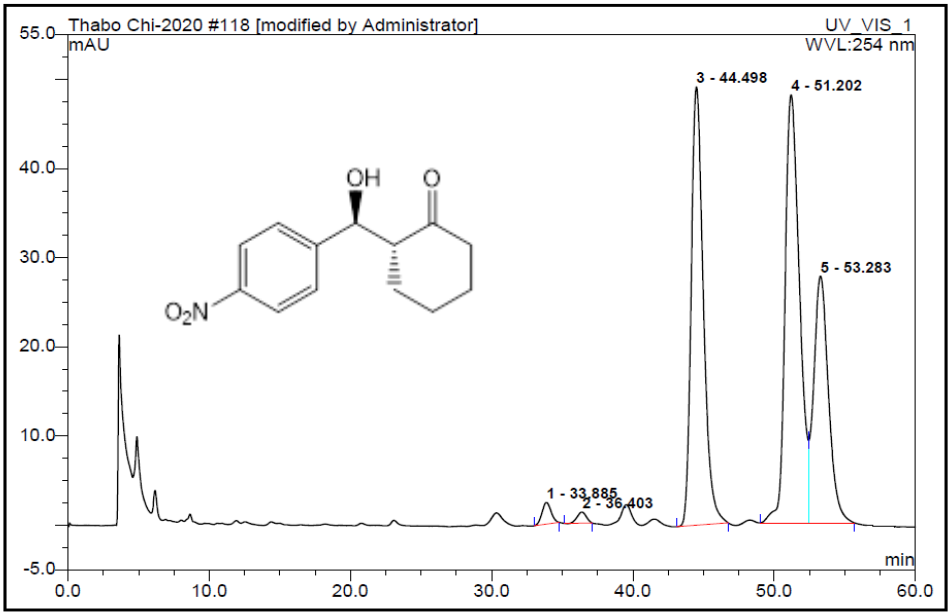
Figure S.4-19: Chiral HPLC chromatogram of **TP_A4.7N4CY** (entry 15)

Aldo products **using 8 mol%** between cyclohexanone and *p*-nitrobenzaldehyde **(Table 4-5)**



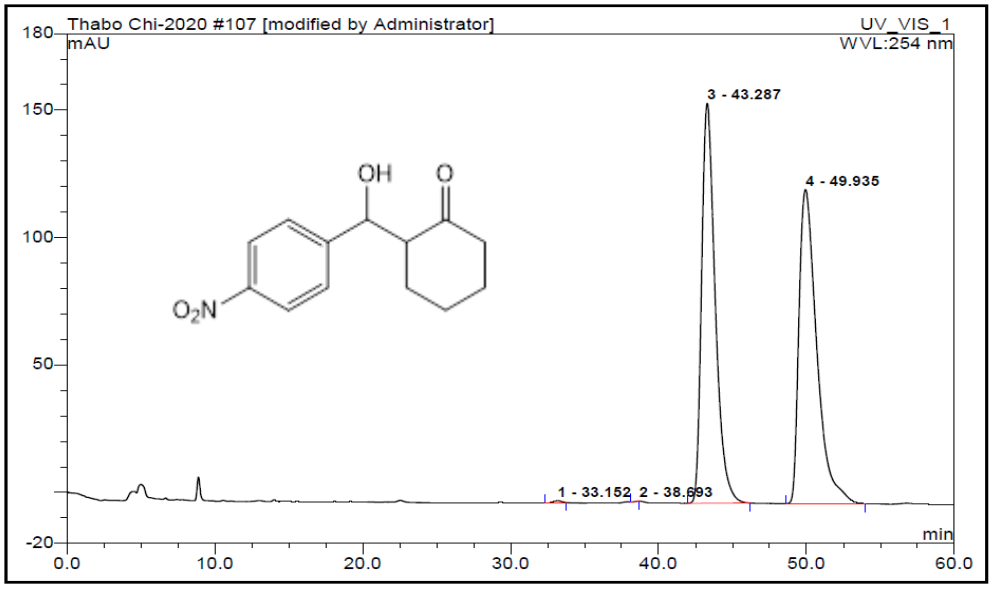
No.	Ret.Time min	Peak Name	Height mAU	Area mAU*min	Rel.Area %	Amount	Type
1	34.58	n.a.	0.066	0.017	0.00	n.a.	BMB*
2	40.58	n.a.	0.008	0.001	0.00	n.a.	BMB*
3	45.26	n.a.	185.230	193.103	49.21	n.a.	BMB*
4	52.02	n.a.	146.419	199.321	50.79	n.a.	BMB*
Total:			331.723	392.442	100.00	0.000	

Figure S.4-R: Chiral HPLC chromatogram of **racemate TP_A4N4CY-R13**



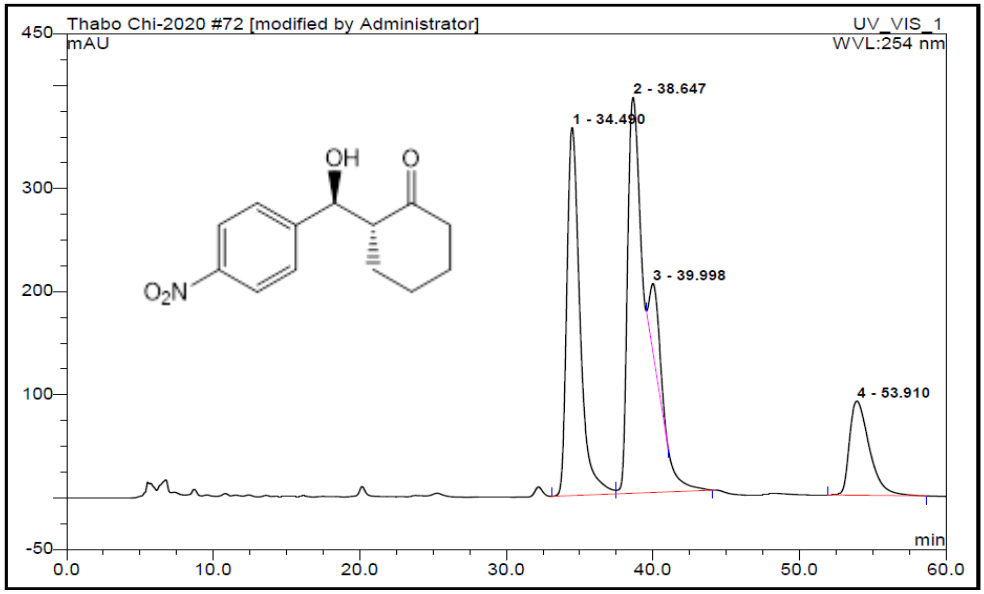
No.	Ret.Time min	Peak Name	Height mAU	Area mAU*min	Rel.Area %	Amount	Type
1	33.89	n.a.	2.422	1.802	1.26	n.a.	BMB*
2	36.40	n.a.	1.243	0.933	0.65	n.a.	BMB*
3	44.50	n.a.	49.146	49.059	34.41	n.a.	BMB*
4	51.20	n.a.	47.979	56.946	39.94	n.a.	BM
5	53.28	n.a.	27.664	33.849	23.74	n.a.	MB*
Total:			128.454	142.589	100.00	0.000	

Figure S.4-20: Chiral HPLC chromatogram of **TP_A4.10N4CY** (entry 5)



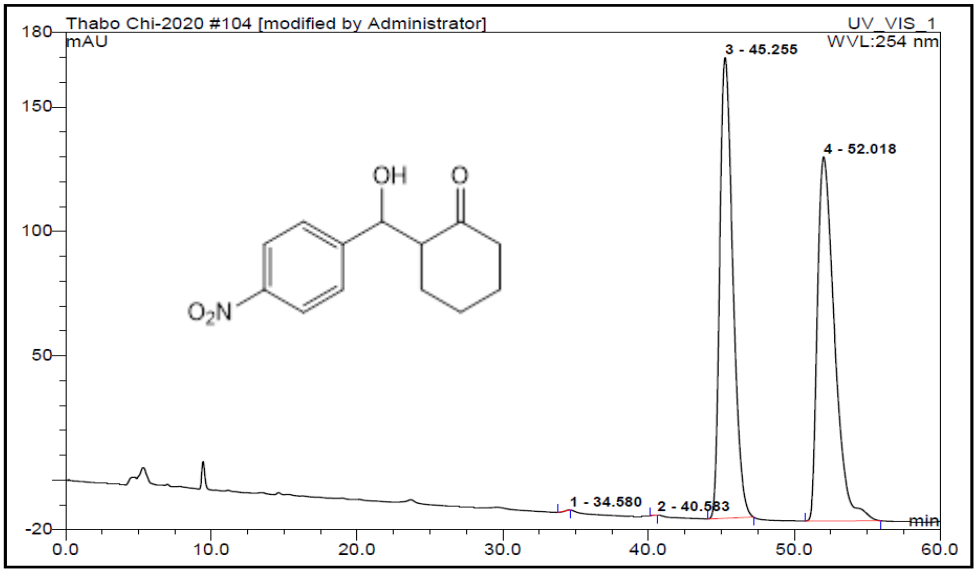
No.	Ret.Time min	Peak Name	Height mAU	Area mAU*min	Rel.Area %	Amount	Type
1	33.15	n.a.	0.855	0.598	0.18	n.a.	BM *
2	38.69	n.a.	0.010	0.003	0.00	n.a.	BMB*
3	43.29	n.a.	156.876	167.356	49.27	n.a.	BMB*
4	49.94	n.a.	123.206	171.693	50.55	n.a.	BMB
Total:			280.947	339.650	100.00	0.000	

Figure S.4-R: Chiral HPLC chromatogram of **racemate TP_A4N4CY-R12**



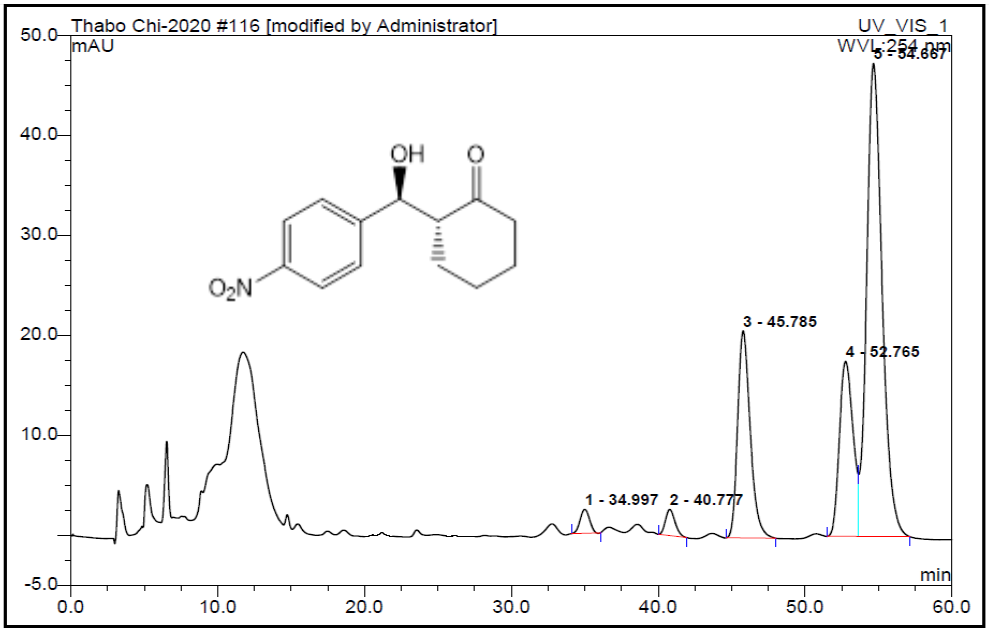
No.	Ret.Time min	Peak Name	Height mAU	Area mAU*min	Rel.Area %	Amount	Type
1	34.49	n.a.	356.697	372.865	31.78	n.a.	BM *
2	38.65	n.a.	383.506	603.075	51.40	n.a.	MB*
3	40.00	n.a.	66.234	53.515	4.56	n.a.	Rd
4	53.91	n.a.	91.311	143.847	12.26	n.a.	BMB*
Total:			897.748	1173.302	100.00	0.000	

Figure S.4-21: Chiral HPLC chromatogram of **TP_A4.9N4CY** (entry 1)



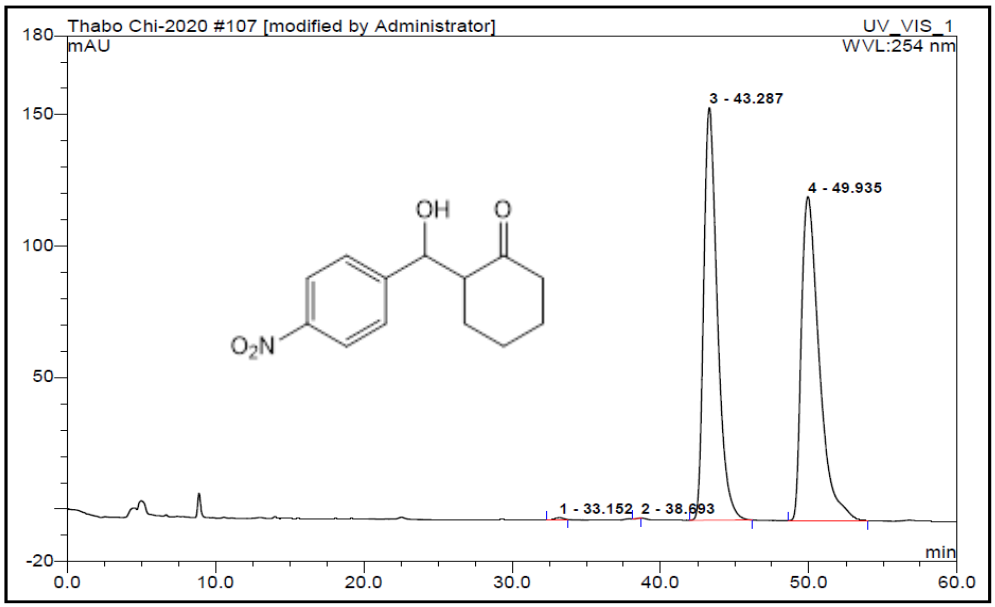
No.	Ret.Time min	Peak Name	Height mAU	Area mAU*min	Rel.Area %	Amount	Type
1	34.58	n.a.	0.066	0.017	0.00	n.a.	BMB*
2	40.58	n.a.	0.008	0.001	0.00	n.a.	BMB*
3	45.26	n.a.	185.230	193.103	49.21	n.a.	BMB*
4	52.02	n.a.	146.419	199.321	50.79	n.a.	BMB*
Total:			331.723	392.442	100.00	0.000	

Figure S.4-R: Chiral HPLC chromatogram of **racemate TP_A4N4CY-R15**



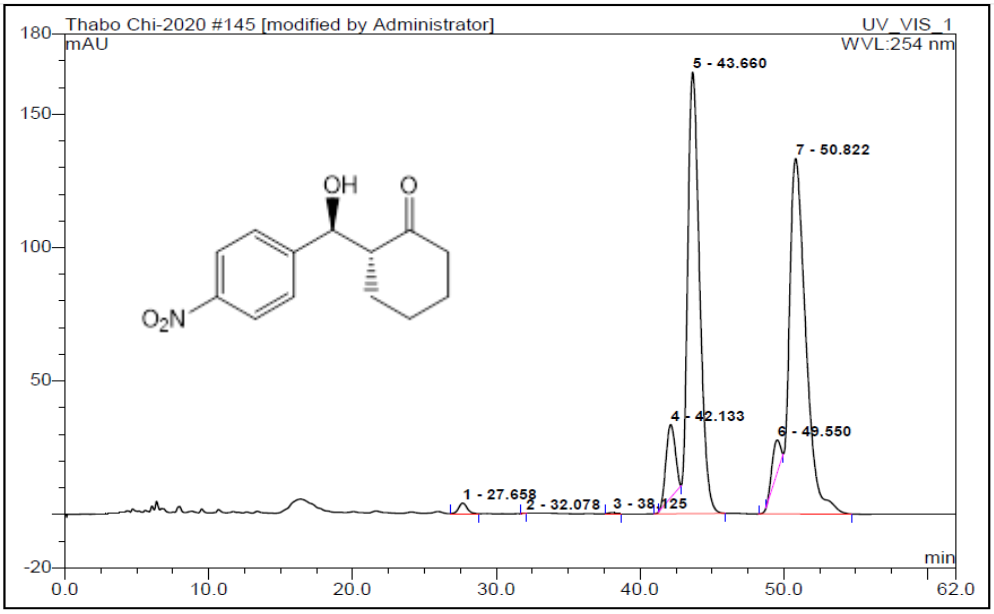
No.	Ret.Time min	Peak Name	Height mAU	Area mAU*min	Rel.Area %	Amount	Type
1	35.00	n.a.	2.391	1.759	1.73	n.a.	BMB*
2	40.78	n.a.	2.615	1.975	1.95	n.a.	BMB*
3	45.79	n.a.	20.731	20.635	20.34	n.a.	BMB*
4	52.77	n.a.	17.529	19.034	18.77	n.a.	BM *
5	54.67	n.a.	47.354	58.025	57.21	n.a.	MB*
Total:			90.620	101.428	100.00	0.000	

Figure S.4-22: Chiral HPLC chromatogram of **TP_A4.13N4CY** (entry 4)



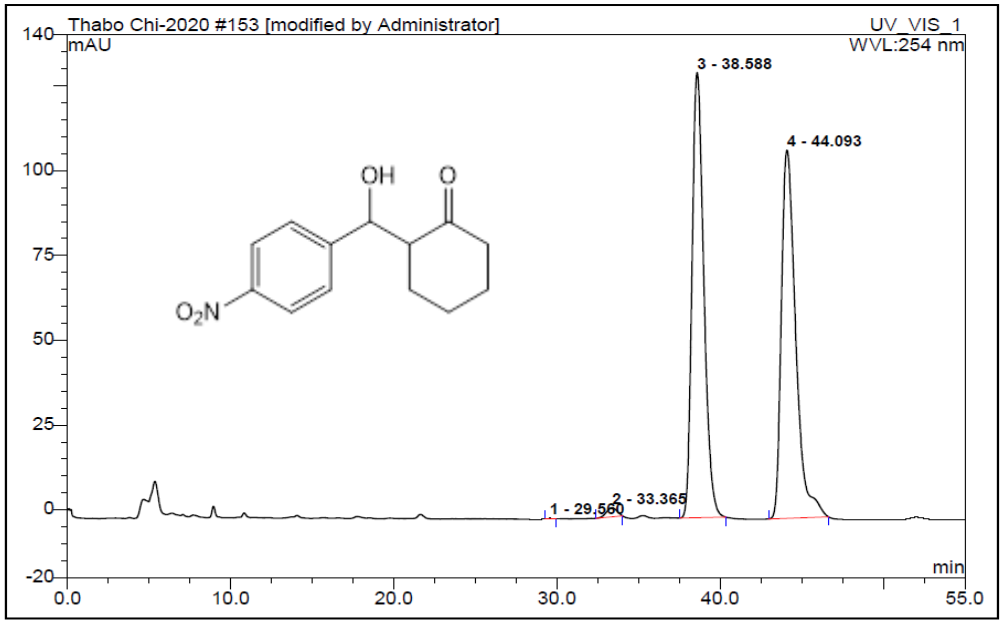
No.	Ret.Time min	Peak Name	Height mAU	Area mAU*min	Rel.Area %	Amount	Type
1	33.15	n.a.	0.855	0.598	0.18	n.a.	BM *
2	38.69	n.a.	0.010	0.003	0.00	n.a.	BMB*
3	43.29	n.a.	156.876	167.356	49.27	n.a.	BMB*
4	49.94	n.a.	123.206	171.693	50.55	n.a.	BMB
Total:			280.947	339.650	100.00	0.000	

Figure S.4-R: Chiral HPLC chromatogram of **racemate TP_A4N4CY-R14**



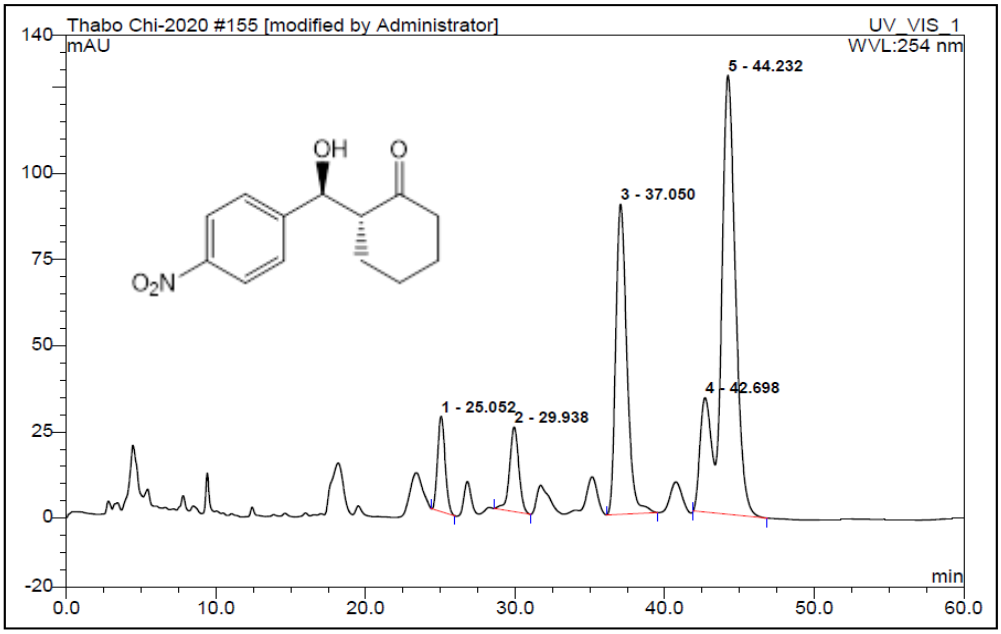
No.	Ret.Time min	Peak Name	Height mAU	Area mAU*min	Rel.Area %	Amount	Type
1	27.66	n.a.	3.954	2.686	0.69	n.a.	BMB*
2	32.08	n.a.	0.008	0.003	0.00	n.a.	BMB*
3	38.13	n.a.	0.484	0.284	0.07	n.a.	BMB*
4	42.13	n.a.	27.400	20.285	5.18	n.a.	Ru
5	43.66	n.a.	165.417	168.513	43.02	n.a.	BMB*
6	49.55	n.a.	12.085	8.313	2.12	n.a.	Ru
7	50.82	n.a.	133.210	191.609	48.92	n.a.	BMB*
Total:			342.558	391.692	100.00	0.000	

Figure S.4-23: Chiral HPLC chromatogram of **TP_A4.14N4CY** (entry 6)



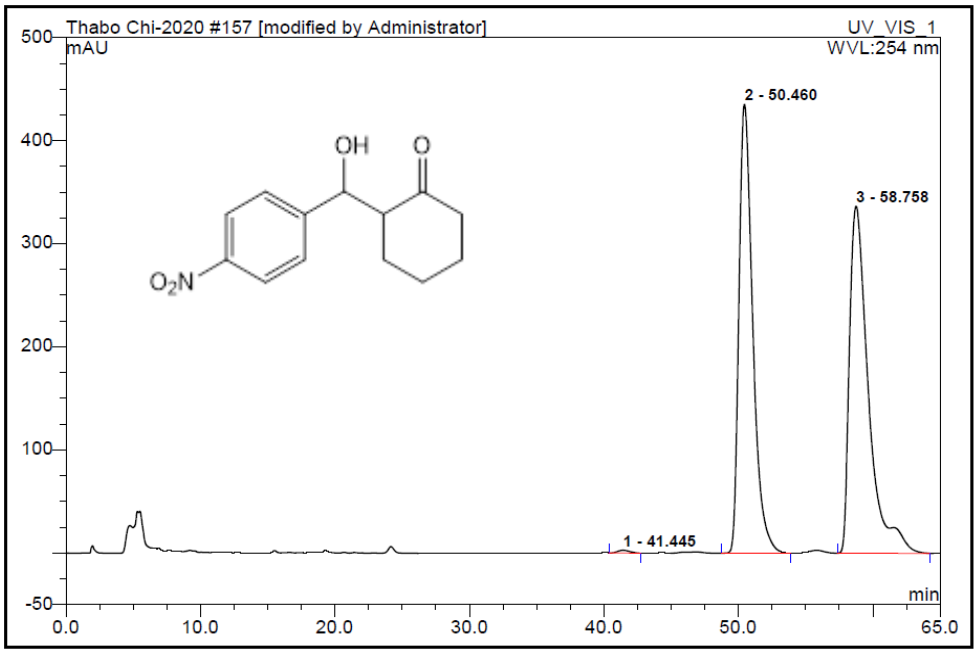
No.	Ret.Time min	Peak Name	Height mAU	Area mAU*min	Rel.Area %	Amount	Type
1	29.56	n.a.	0.181	0.069	0.03	n.a.	BMB*
2	33.37	n.a.	2.682	1.999	0.90	n.a.	BMB*
3	38.59	n.a.	131.271	109.853	49.38	n.a.	BMB*
4	44.09	n.a.	108.542	110.528	49.69	n.a.	BMB*
Total:			242.676	222.450	100.00	0.000	

Figure S.4-R: Chiral HPLC chromatogram of **racemate TP_A4N4CY-15**



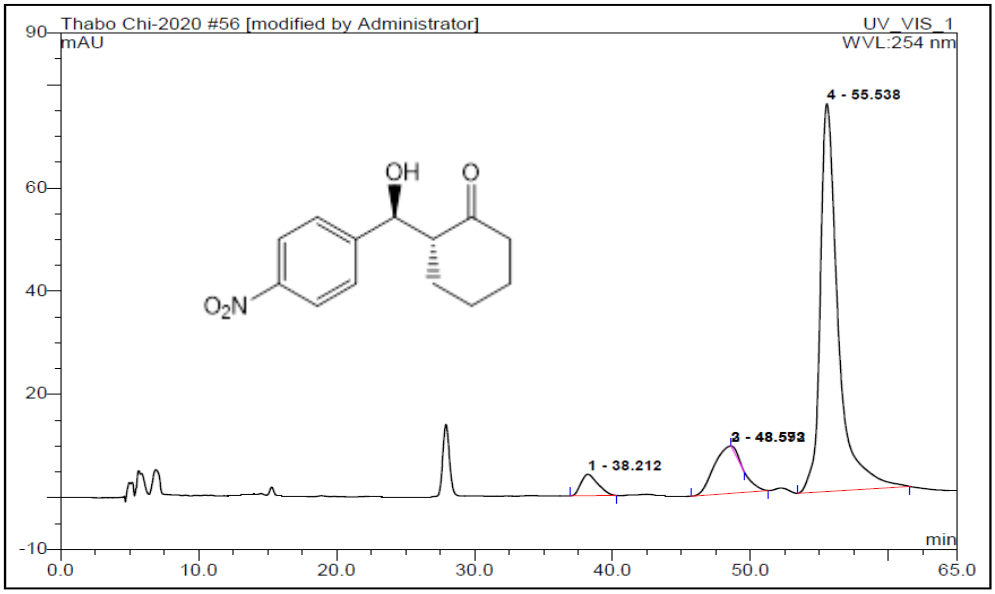
No.	Ret.Time min	Peak Name	Height mAU	Area mAU*min	Rel.Area %	Amount	Type
1	25.05	n.a.	27.625	16.077	5.92	n.a.	BMB*
2	29.94	n.a.	24.568	17.622	6.48	n.a.	BMB*
3	37.05	n.a.	89.999	77.484	28.51	n.a.	BMB*
4	42.70	n.a.	33.210	0.000	0.00	n.a.	BMb*
5	44.23	n.a.	127.454	160.564	59.09	n.a.	bMB*
Total:			302.857	271.747	100.00	0.000	

Figure S.4-24: Chiral HPLC chromatogram of **TP_A4.15N4CY** (entry 7)



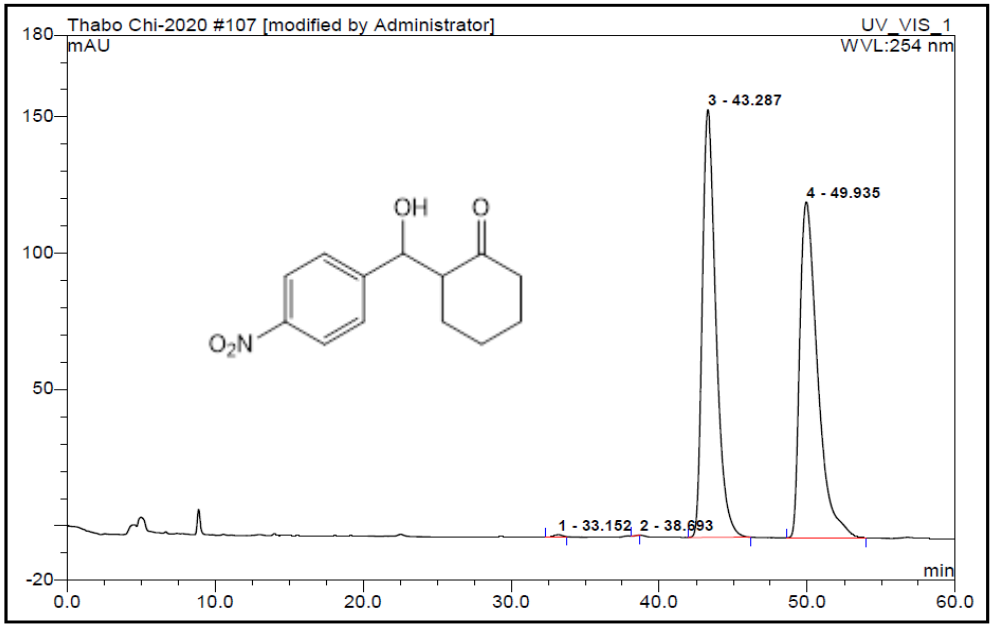
No.	Ret.Time min	Peak Name	Height mAU	Area mAU*min	Rel.Area %	Amount	Type
1	41.45	n.a.	2.604	2.643	0.25	n.a.	BMB*
2	50.46	n.a.	435.305	517.082	48.38	n.a.	BMB
3	58.76	n.a.	336.497	549.047	51.37	n.a.	BMB*
Total:			774.406	1068.772	100.00	0.000	

Figure S.4-R: Chiral HPLC chromatogram of **racemate TP_A4N4CY-R16**



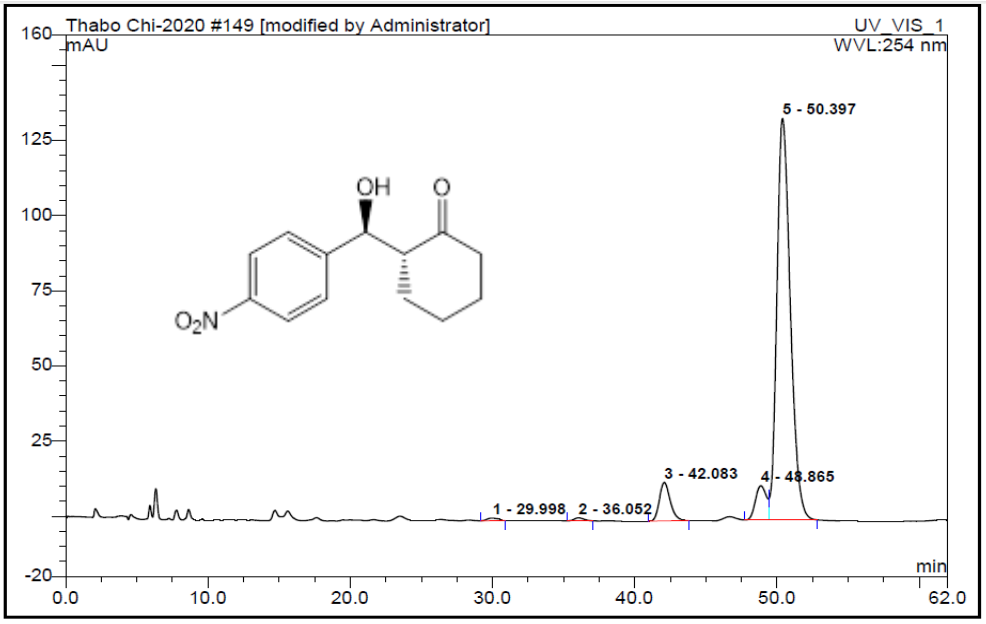
No.	Ret.Time min	Peak Name	Height mAU	Area mAU*min	Rel.Area %	Amount	Type
1	38.21	n.a.	4.138	5.849	4.16	n.a.	BMB*
2	48.57	n.a.	9.164	21.210	15.08	n.a.	BMB*
3	48.59	n.a.	0.036	0.496	0.35	n.a.	Rd
4	55.54	n.a.	75.124	113.102	80.41	n.a.	MB*
Total:			88.461	140.657	100.00	0.000	

Figure S.4-25: Chiral HPLC chromatogram of **TP_A4.16N4CY** (entry 8)



No.	Ret.Time min	Peak Name	Height mAU	Area mAU*min	Rel.Area %	Amount	Type
1	33.15	n.a.	0.855	0.598	0.18	n.a.	BM *
2	38.69	n.a.	0.010	0.003	0.00	n.a.	BMB*
3	43.29	n.a.	156.876	167.356	49.27	n.a.	BMB*
4	49.94	n.a.	123.206	171.693	50.55	n.a.	BMB
Total:			280.947	339.650	100.00	0.000	

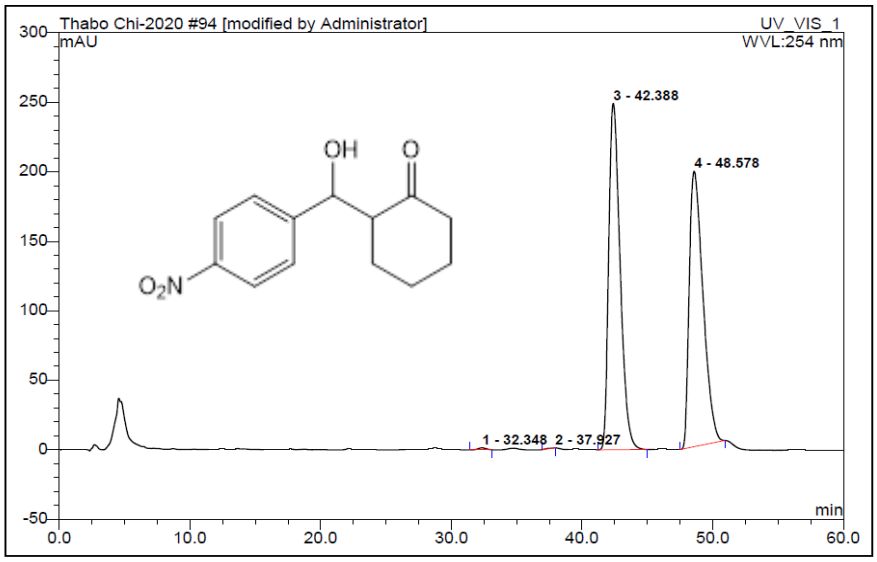
Figure S.4-R: Chiral HPLC chromatogram of **racemate TP_A4N4CY-R17**



No.	Ret.Time min	Peak Name	Height mAU	Area mAU*min	Rel.Area %	Amount	Type
1	30.00	n.a.	0.908	0.784	0.46	n.a.	BMB*
2	36.05	n.a.	1.048	0.807	0.48	n.a.	BMB*
3	42.08	n.a.	12.788	11.323	6.68	n.a.	BMB*
4	48.87	n.a.	11.390	9.960	5.87	n.a.	BM *
5	50.40	n.a.	133.447	146.715	86.51	n.a.	MB*
Total:			159.581	169.589	100.00	0.000	

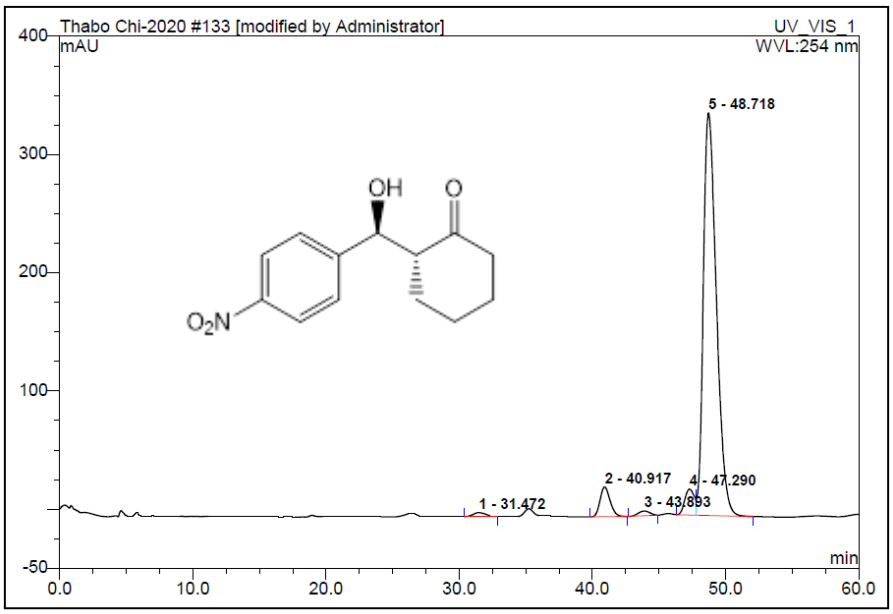
Figure S.4-26: Chiral HPLC chromatogram of **TP_A4.17N4CY** (entry 9)

Catalyst Recycling: Reaction between cyclohexanone and *p*-nitrobenzaldehyde (**Table 4-6**)



No.	Ret.Time min	Peak Name	Height mAU	Area mAU*min	Rel.Area %	Amount	Type
1	32.35	n.a.	1.387	0.998	0.20	n.a.	BMB*
2	37.93	n.a.	0.032	0.182	0.04	n.a.	BMB*
3	42.39	n.a.	249.159	251.603	50.91	n.a.	BMB*
4	48.58	n.a.	198.169	241.383	48.85	n.a.	BMB*
Total:			448.746	494.165	100.00	0.000	

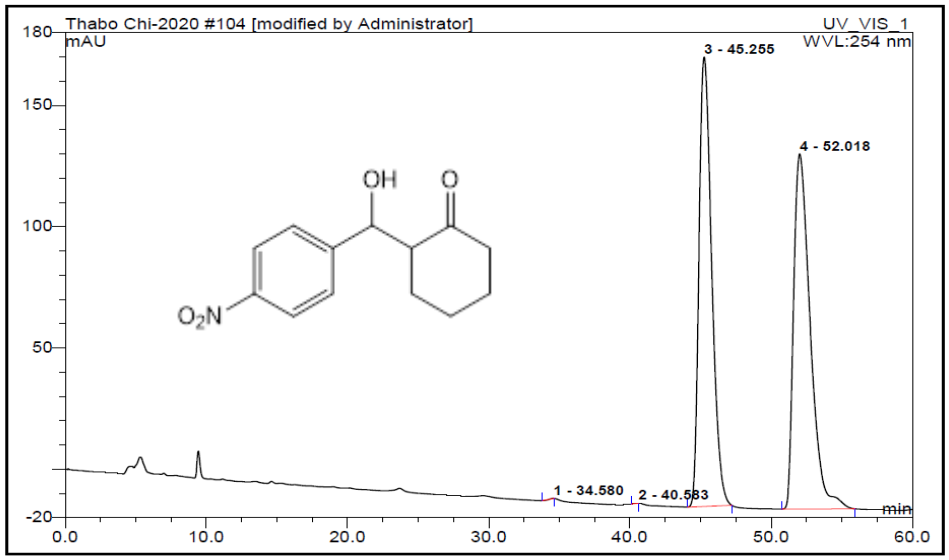
Figure S.4-R: Chiral HPLC chromatogram of **racemate TP_A4N4CY-R18**



No.	Ret.Time min	Peak Name	Height mAU	Area mAU*min	Rel.Area %	Amount	Type
1	31.47	n.a.	3.412	3.731	0.86	n.a.	BMB*
2	40.92	n.a.	25.122	21.977	5.07	n.a.	BMB*
3	43.89	n.a.	3.977	3.971	0.92	n.a.	BMB*
4	47.29	n.a.	21.839	17.770	4.10	n.a.	BM *
5	48.72	n.a.	340.588	386.386	89.06	n.a.	MB*
Total:			394.937	433.835	100.00	0.000	

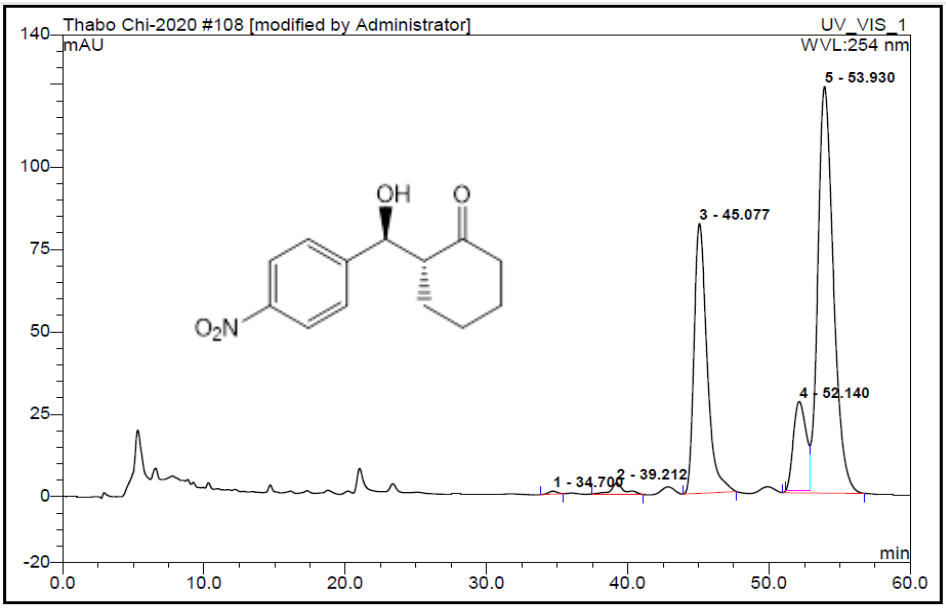
Figure S.4-27: Chira**l** HPLC chromatogram of **TP_A4.18N4CY** (entry 5)

Chiral chromatograms for aldol products obtained by **Peptide-AuNPs (Table 5-3)**



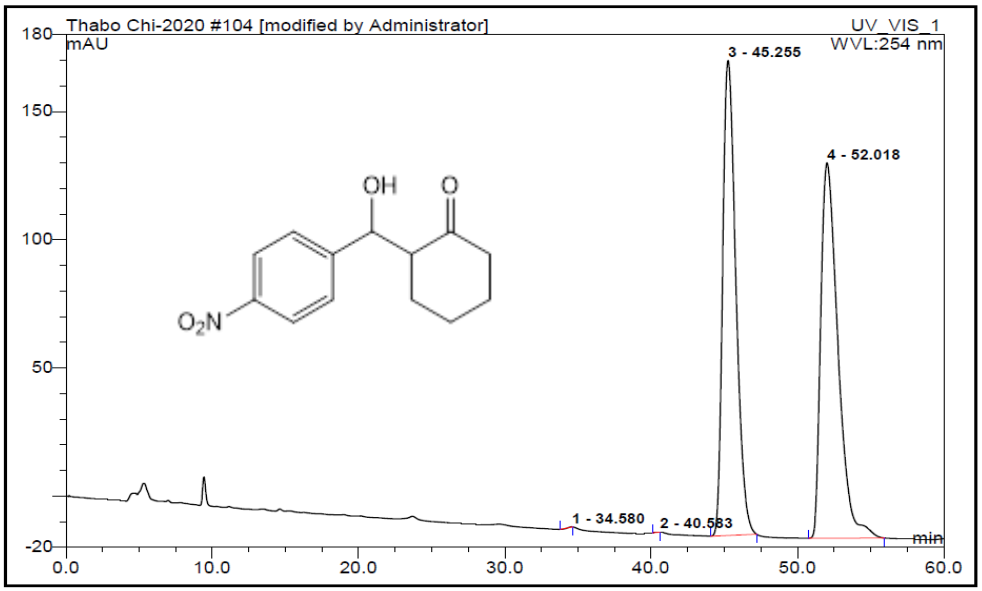
No.	Ret.Time min	Peak Name	Height mAU	Area mAU*min	Rel.Area %	Amount	Type
1	34.58	n.a.	0.066	0.017	0.00	n.a.	BMB*
2	40.58	n.a.	0.008	0.001	0.00	n.a.	BMB*
3	45.26	n.a.	185.230	193.103	49.21	n.a.	BMB*
4	52.02	n.a.	146.419	199.321	50.79	n.a.	BMB*
Total:			331.723	392.442	100.00	0.000	

Figure S.4-R: Chiral HPLC chromatogram of **racemate TP_A4N4CY-R19**



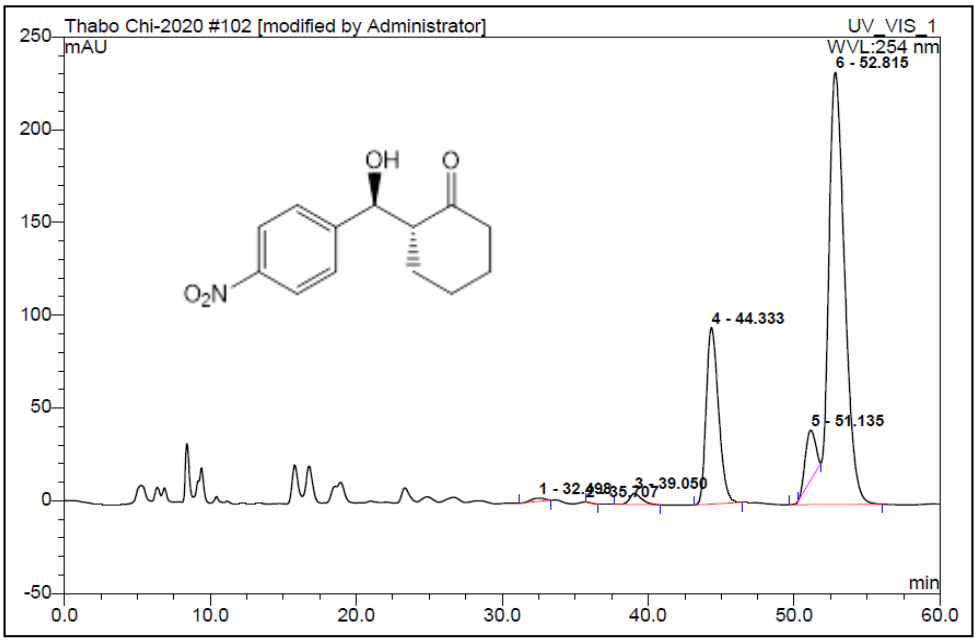
No.	Ret.Time min	Peak Name	Height mAU	Area mAU*min	Rel.Area %	Amount	Type
1	34.70	n.a.	0.901	0.655	0.23	n.a.	BMB*
2	39.21	n.a.	3.332	3.340	1.20	n.a.	BM *
3	45.08	n.a.	81.827	87.279	31.28	n.a.	BMB*
4	52.14	n.a.	26.870	27.948	10.02	n.a.	Ru*
5	53.93	n.a.	123.245	159.804	57.27	n.a.	BMB*
Total:			236.176	279.025	100.00	0.000	

Figure S.4-28: Chiral HPLC chromatogram of **TP_A4.19N4CY** (entry 4)



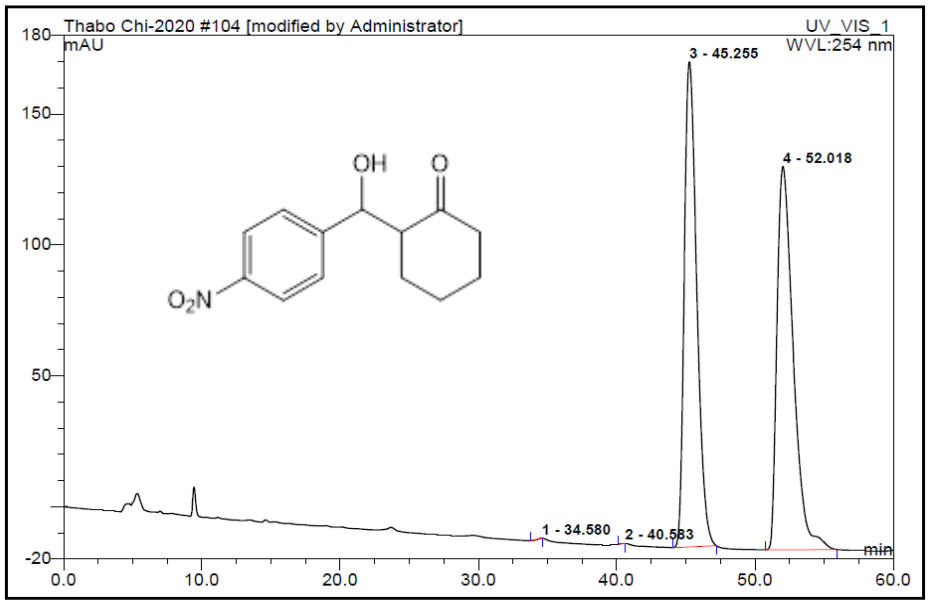
No.	Ret.Time min	Peak Name	Height mAU	Area mAU*min	Rel.Area %	Amount	Type
1	34.58	n.a.	0.066	0.017	0.00	n.a.	BMB*
2	40.58	n.a.	0.008	0.001	0.00	n.a.	BMB*
3	45.26	n.a.	185.230	193.103	49.21	n.a.	BMB*
4	52.02	n.a.	146.419	199.321	50.79	n.a.	BMB*
Total:			331.723	392.442	100.00	0.000	

Figure S.4-R: Chiral HPLC chromatogram of **racemate TP_A4N4CY-R20**



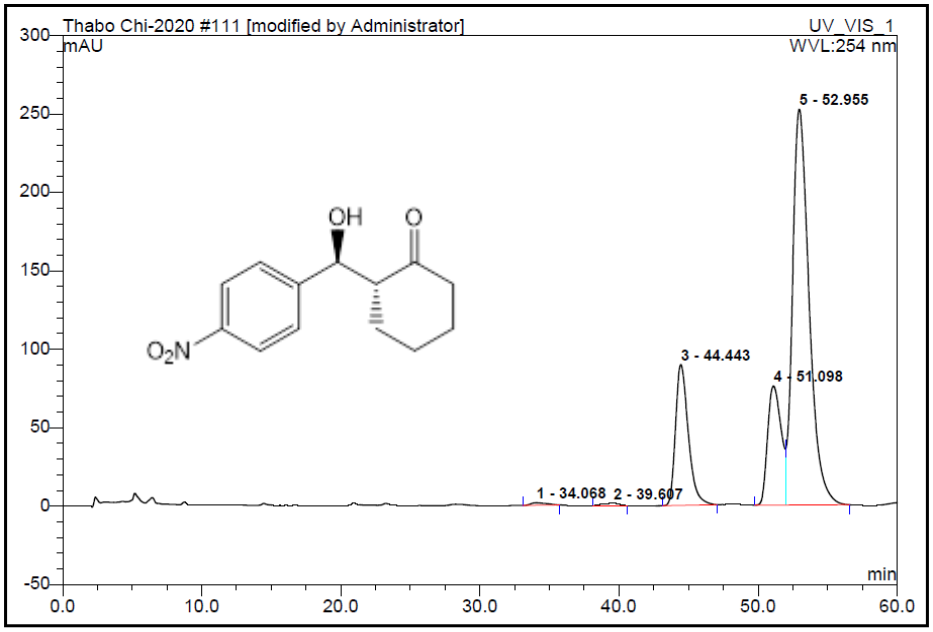
No.	Ret.Time min	Peak Name	Height mAU	Area mAU*min	Rel.Area %	Amount	Type
1	32.50	n.a.	1.778	1.933	0.44	n.a.	BMB*
2	35.71	n.a.	0.008	0.045	0.01	n.a.	BMB*
3	39.05	n.a.	6.032	5.823	1.34	n.a.	BMB
4	44.33	n.a.	95.063	93.130	21.41	n.a.	BMB*
5	51.14	n.a.	26.761	21.448	4.93	n.a.	Ru
6	52.82	n.a.	232.944	312.643	71.87	n.a.	BMB*
Total:			362.587	435.023	100.00	0.000	

Figure S.4-29: Chiral HPLC chromatogram of **TP_A4.20N4CY** (entry 6)



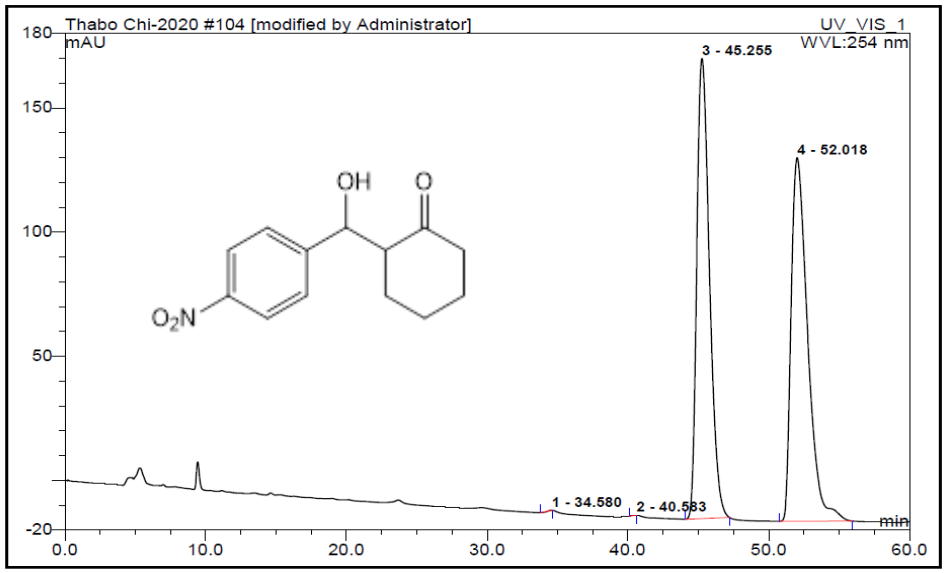
No.	Ret.Time min	Peak Name	Height mAU	Area mAU*min	Rel.Area %	Amount	Type
1	34.58	n.a.	0.066	0.017	0.00	n.a.	BMB*
2	40.58	n.a.	0.008	0.001	0.00	n.a.	BMB*
3	45.26	n.a.	185.230	193.103	49.21	n.a.	BMB*
4	52.02	n.a.	146.419	199.321	50.79	n.a.	BMB*
Total:			331.723	392.442	100.00	0.000	

Figure S.4-R: Chiral HPLC chromatogram of **racemate TP_A4N4CY-R21**



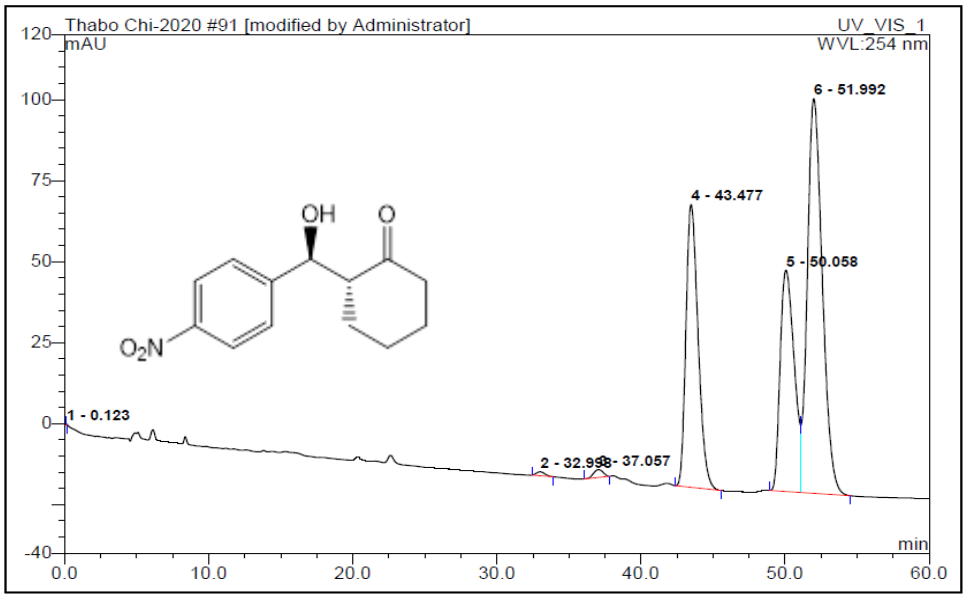
No.	Ret.Time min	Peak Name	Height mAU	Area mAU*min	Rel.Area %	Amount	Type
1	34.07	n.a.	1.720	2.175	0.41	n.a.	BMB*
2	39.61	n.a.	1.567	2.126	0.40	n.a.	BMB*
3	44.44	n.a.	89.782	95.791	17.89	n.a.	BMB*
4	51.10	n.a.	76.011	85.149	15.91	n.a.	M *
5	52.96	n.a.	252.425	350.115	65.40	n.a.	MB*
Total:			421.505	535.356	100.00	0.000	

Figure S.4-30: Chiral HPLC chromatogram of **TP_A4.21N4CY** (entry 7)



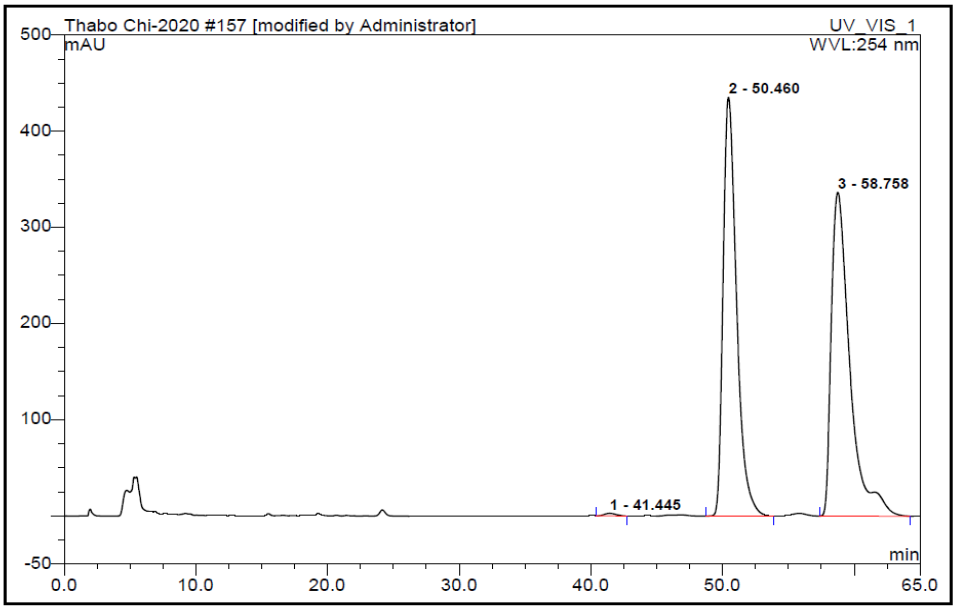
No.	Ret.Time min	Peak Name	Height mAU	Area mAU*min	Rel.Area %	Amount	Type
1	34.58	n.a.	0.066	0.017	0.00	n.a.	BMB*
2	40.58	n.a.	0.008	0.001	0.00	n.a.	BMB*
3	45.26	n.a.	185.230	193.103	49.21	n.a.	BMB*
4	52.02	n.a.	146.419	199.321	50.79	n.a.	BMB*
Total:			331.723	392.442	100.00	0.000	

Figure S.4-R: Chiral HPLC chromatogram of **racemate TP_A4N4CY2-R22**



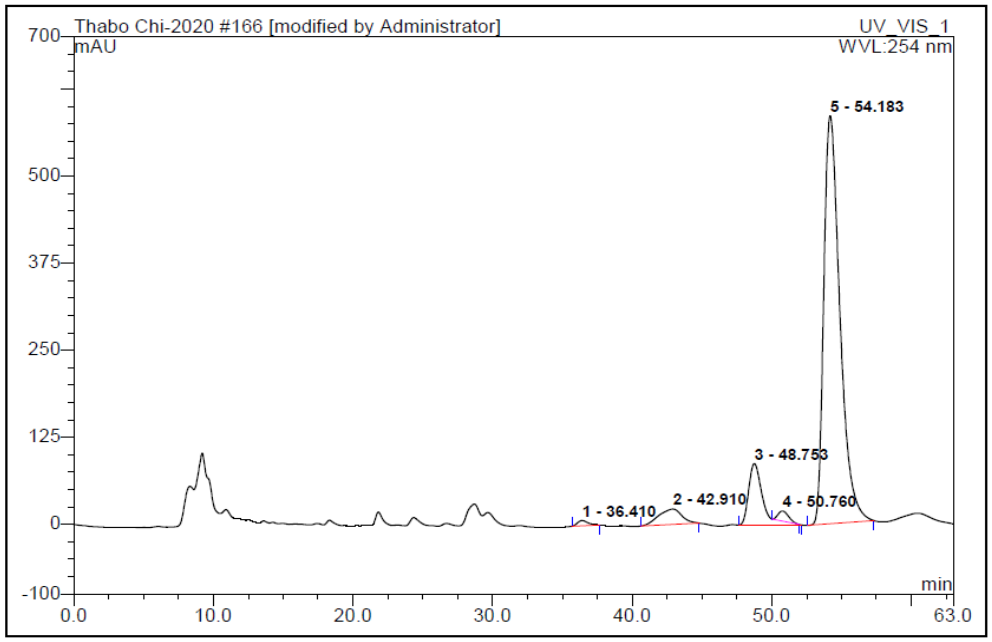
No.	Ret.Time min	Peak Name	Height mAU	Area mAU*min	Rel.Area %	Amount	Type
1	0.12	n.a.	0.109	0.002	0.00	n.a.	BMB
2	33.00	n.a.	1.236	0.834	0.27	n.a.	BMB*
3	37.06	n.a.	2.392	1.807	0.58	n.a.	BMB*
4	43.48	n.a.	87.290	85.243	27.30	n.a.	BMB*
5	50.06	n.a.	68.346	77.060	24.68	n.a.	BM *
6	51.99	n.a.	121.829	147.322	47.18	n.a.	MB
Total:			281.202	312.269	100.00	0.000	

Figure S.4-31: Chiral HPLC chromatogram of **TP_A4.22N4CY** (entry 8)



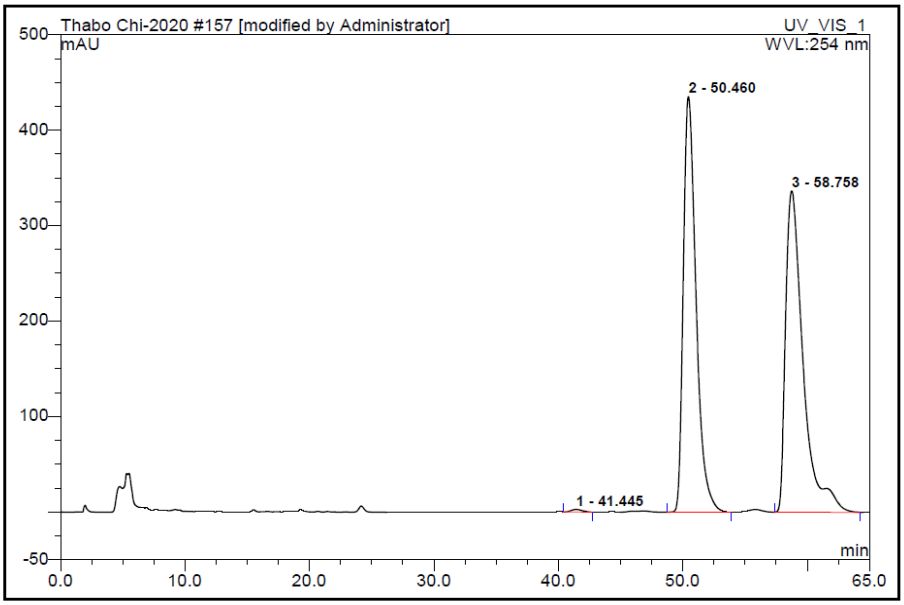
No.	Ret.Time min	Peak Name	Height mAU	Area mAU*min	Rel.Area %	Amount	Type
1	41.45	n.a.	2.604	2.643	0.25	n.a.	BMB*
2	50.46	n.a.	435.305	517.082	48.38	n.a.	BMB
3	58.76	n.a.	336.497	549.047	51.37	n.a.	BMB*
Total:			774.406	1068.772	100.00	0.000	

Figure S.4-R: Chiral HPLC chromatogram of **racemate TP_A4N4CY2-R23**



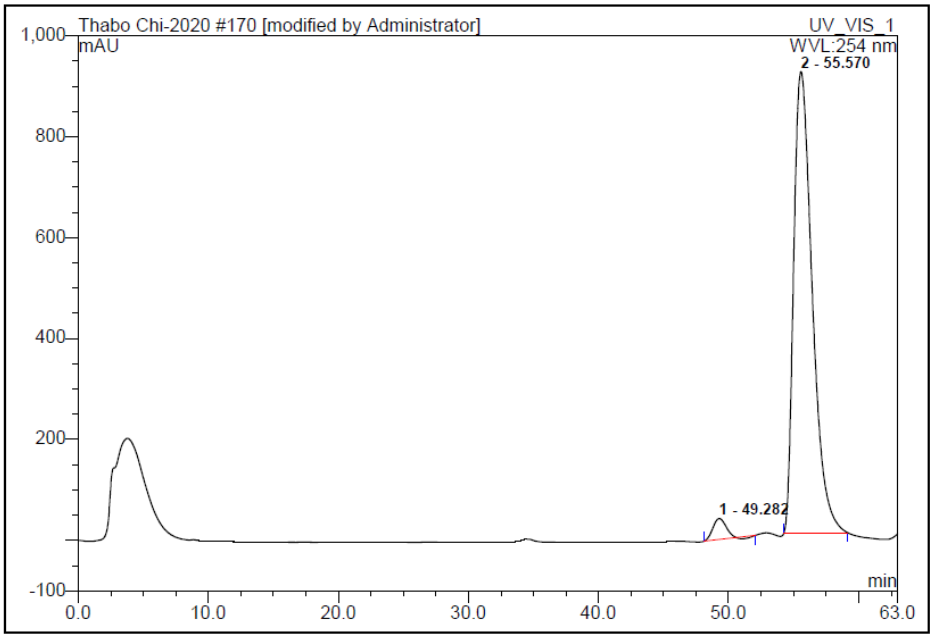
No.	Ret.Time min	Peak Name	Height mAU	Area mAU*min	Rel.Area %	Amount	Type
1	36.41	n.a.	7.606	6.670	0.70	n.a.	BMB*
2	42.91	n.a.	22.219	42.629	4.49	n.a.	BMB*
3	48.75	n.a.	88.286	103.361	10.88	n.a.	BMB*
4	50.76	n.a.	14.477	12.671	1.33	n.a.	Rd
5	54.18	n.a.	585.602	785.073	82.60	n.a.	BMB*
Total:			718.191	950.404	100.00	0.000	

Figure S.4-32: Chiral HPLC chromatogram of **TP_A4.23N4CY** (entry 9)



No.	Ret.Time min	Peak Name	Height mAU	Area mAU*min	Rel.Area %	Amount	Type
1	41.45	n.a.	2.604	2.643	0.25	n.a.	BMB*
2	50.46	n.a.	435.305	517.082	48.38	n.a.	BMB
3	58.76	n.a.	336.497	549.047	51.37	n.a.	BMB*
Total:			774.406	1068.772	100.00	0.000	

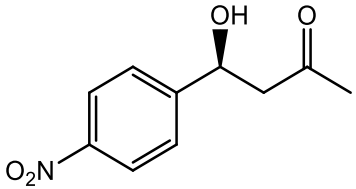
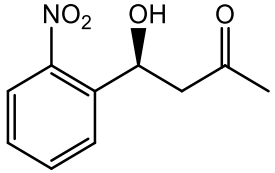
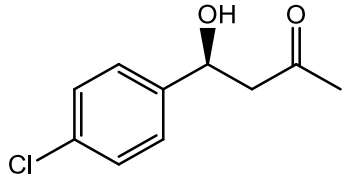
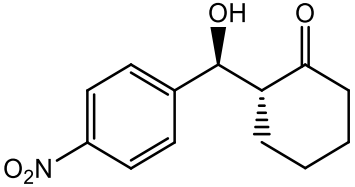
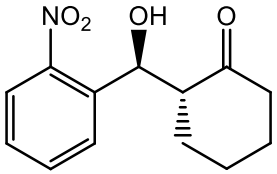
Figure S.4-R: Chiral HPLC chromatogram of **racemate TP_A4N4CY2-R24**

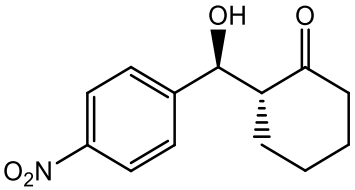
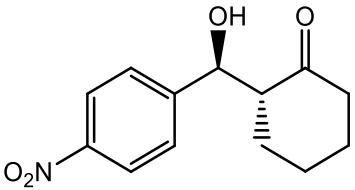
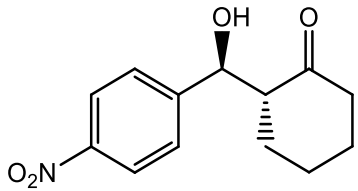


No.	Ret.Time min	Peak Name	Height mAU	Area mAU*min	Rel.Area %	Amount	Type
1	49.28	n.a.	41.384	44.974	2.89	n.a.	BMB*
2	55.57	n.a.	913.659	1508.723	97.11	n.a.	BMB*
Total:			955.043	1553.696	100.00	0.000	

Figure S.4-33: Chiral HPLC chromatogram of **TP_A4.24N4CY** (entry 10)

Table A: Analytical data and Chiral-phase HPLC spectra analysis for selected aldol products using Lux 5μm Cellulose-1 chiral column

Structure	Aldol product	Eluent; **%ratio**	Flow rate; **Wavelength (nm)**	Retention time (min)
	TP_A1.1N4ACE	Hexane/IPA; **85/15**	0.6 mL; **254**	t_{Rmajor} = 23.38; t_{Rminor} = 30.42
	TP_A1.2N4ACE	Hexane/IPA; **85/15**	0.6 mL; **254**	t_{Rmajor} = 24.52; t_{Rminor} = 32.07
	TP_A1.3N4ACE	Hexane/IPA; **85/15**	0.6 mL;**254**	t_{Rminor} = 22.37; t_{Rmajor} = 27.88
	TP_A1.4N4ACE	Hexane/IPA; **85/15**	0.6 mL; **254**	t_{Rminor} = 23.13; t_{Rmajor} = 28.80
	TP_A2.1N2ACE	Hexane/IPA; **90/10**	0.6 mL; **254**	t_{Rmajor} = 22.75; t_{Rmajor} = 26.31
	TP_A2.2N2ACE	Hexane/IPA; **90/10**	0.6 mL; **254**	t_{Rmajor} =19.31; t_{Rminor} = 22.29
	TP_A3Cl4ACE	Hexane/IPA; **85/15**	0.7 mL; **254**	t_{Rminor} = 14.77; t_{Rmajor} = 16.79
	Using cyclohexanone as solvent for reaction between cyclohexanone and aromatic aldehydes **(Table 4-2)**			
	TP_A4.1N4CY	Hexane/IPA; **94/6**	0.6 mL; **254**	t_{Rminor} = 39.09; t_{Rmajor} = 44.17
	TP_A4.2N4CY	Hexane/IPA; **94/6**	0.6 mL; **254**	t_{Rmajor} = 38.63; t_{Rminor}= 43.60
	TP_A5.1N4CY	Hexane/IPA; **95/5**	0.5 mL;**254**	t_{Rmajor} = 39.28; t_{Rminor} = 44.15
	TP-A5.2N4CY	Hexane/IPA; **95/5**	0.5 mL; **254**	t_{Rmajor} =38.63; t_{Rminor}=43.60

	Selected Aldol products using **organic solvents (Table 4-3)**			
	TP_A4.3N4CY	Hexane/IPA; **95/5**	0.7mL, **254**	t_{Rmajor} = 37.91; t_{Rminor} = 42.57
	TP_A4.4N4CY	Hexane/IPA; **95/5**	0.6mL, **254**	t_{Rmajor} = 39.19 t_{Rminor} = 45.06
	TP_A4.5N4CY	Hexane/IPA; **94/6**	0.7mL; **254**	t_{Rminor} = 39.08; t_{Rmajor} = 45.61
	TP_A4.6N4CY	Hexane/IPA; **95/5**	0.6mL; **254**	t_{Rminor} = 43.19; t_{Rmajor} = 48.48
	TP_A4.7N4CY	Hexane/IPA; **96/4**	0.8mL; **254**	t_{Rmajor} = 29.42; t_{Rminor} = 26.19
	Using **8 mol%** catalyst loading **(Table 4-5)**			
	TP_A4.10N4CY	Hexane/IPA; **94/6**	0.6mL; **254**	t_{Rmajor} = 44.50; t_{Rminor} = 51.20
	TP_A4.9N4CY	Hexane/IPA; **94/6**	0.7mL; **254**	t_{Rminor} = 34.49; t_{Rmajor} = 38.65
	TP_A4.13N4CY	Hexane/IPA; **95/5**	0.6mL; **254**	t_{Rminor} = 45.79; t_{Rmajor} = 54.67
	TP_A4.14N4CY	Hexane/IPA; **95/5**	0.6mL; **254**	t_{Rminor} = 43.66; t_{Rmajor} = 50.82
	TP_A4.15N4CY	Hexane/IPA; **94/6**	0.6mL; **254**	t_{Rmajor} = 37.05; t_{Rmajor} = 44.23
	TP_A4.16N4CY	Hexane/IPA; **95/5**	0.7mL; **254**	t_{Rminor} = 48.57; t_{Rmajor} = 55.54
	TP_A4.17N4CY	Hexane/IPA; **95/5**	0.8mL; **254**	t_{Rminor} =42.08; t_{Rmajor} = 50.40
	Aldol products obtained using **peptide-capped AuNPs (Table 5-3)**			
	TP_A4.19N4CY	Hexane/IPA; **95/5**	0.8mL; **254**	t_{Rminor} = 45.08; t_{Rmajor} = 53.93
	TP_A4.20N4CY	Hexane/IPA; **95/5**	0.8mL; **254**	t_{Rminor} = 44.33; t_{Rmajor} = 52.82
	TP_A4.21N4CY	Hexane/IPA; **95/5**	0.8mL; **254**	t_{Rminor} = 44.44; t_{Rmajor} = 52.96
	TP_A4.22N4CY	Hexane/IPA; **95/5**	0.8mL; **254**	t_{Rminor} = 43.48; t_{Rmajor} = 51.99
	TP_A4.23N4CY	Hexane/IPA; 90/10	0.8mL; **254**	t_{Rminor} = 49.14; t_{Rmajor} = 54.59
	TP_A4.24N4CY	Hexane/IPA; 90/10	0.8mL; **254**	t_{Rminor} = 49.45; t_{Rmajor} = 55.57
	TP_A4.25N4CY	Hexane/IPA; 90/10	0.8mL; **254**	t_{Rminor} = 48.75; t_{Rmajor} = 54.18
	Catalyst reusability (Table 4-6)			
	TP_A4.18N4CY	Hexane/IPA; **95/5**	0.8mL; **254**	t_{Rminor} = 40.92; t_{Rmajor} = 48.72

Selected NMR spectra for determination of the syn/anti (dr) for aldol products by ^{1}H NMR

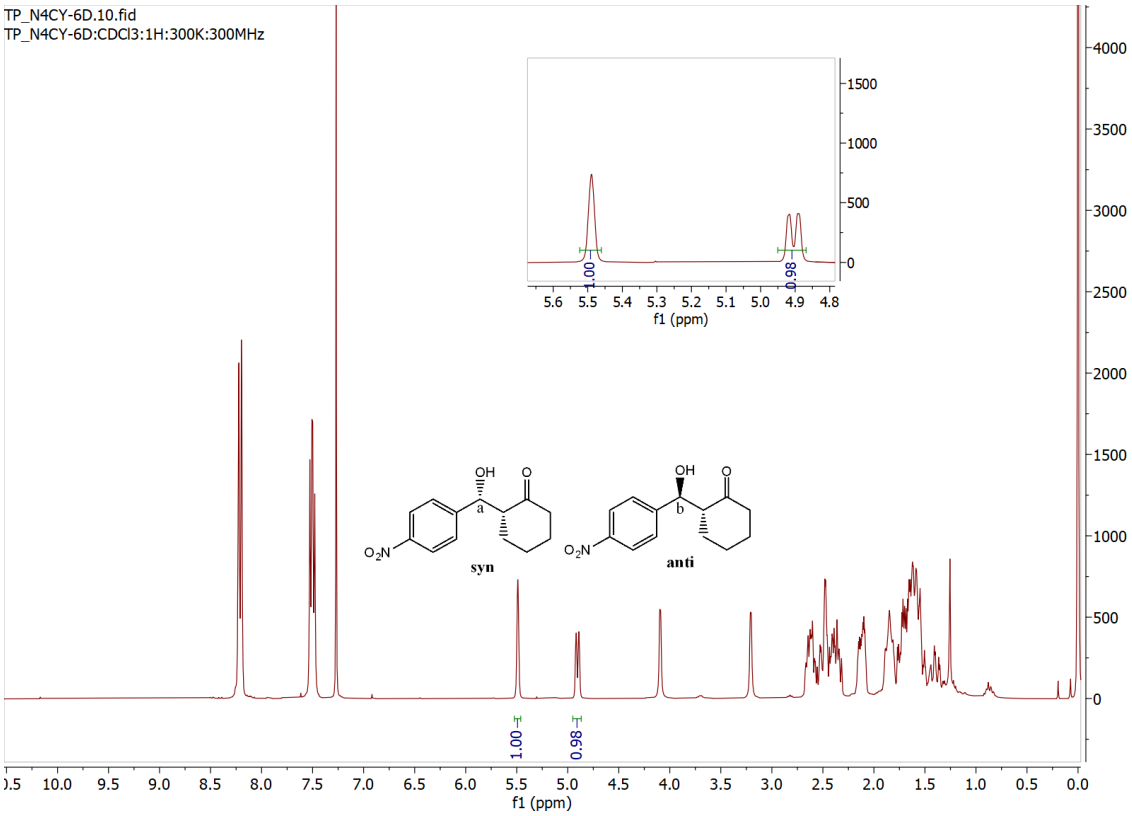


Figure S.4-34: ^{1}H NMR spectrum of the crude product of **TP_A4.2N4CY**

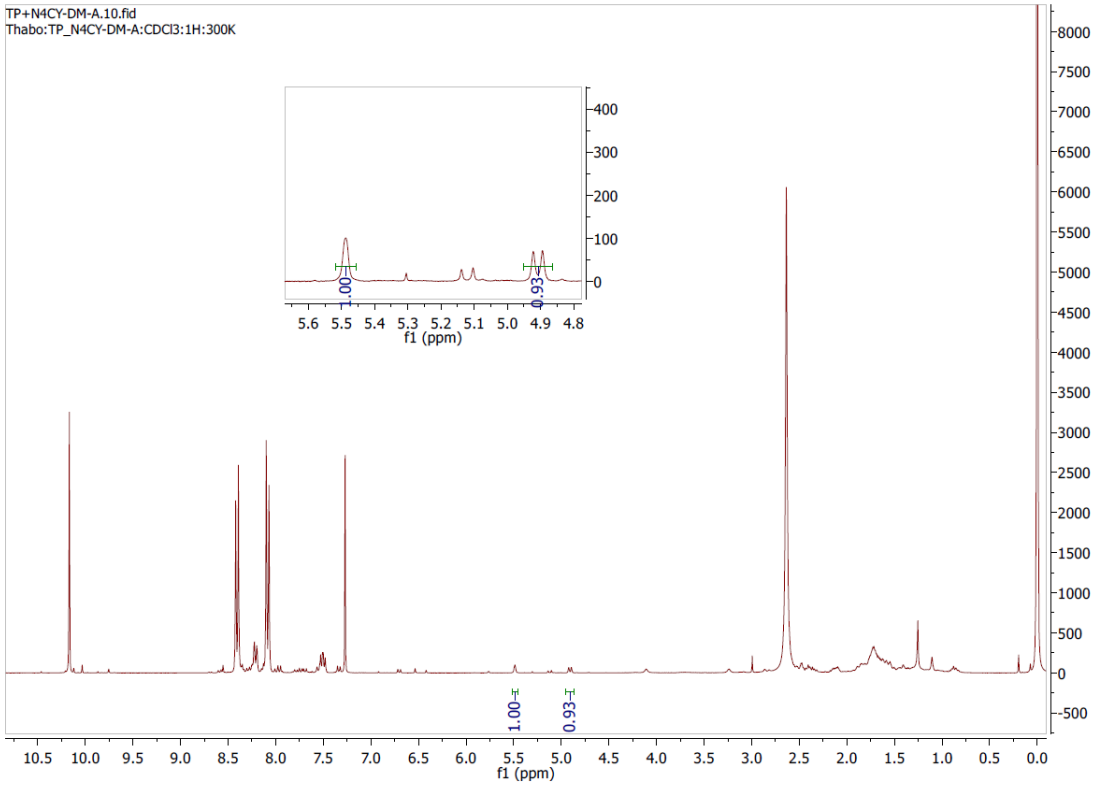


Figure S.4-35: ^{1}H NMR spectrum of the crude product of **TP_A4.3N4CY**

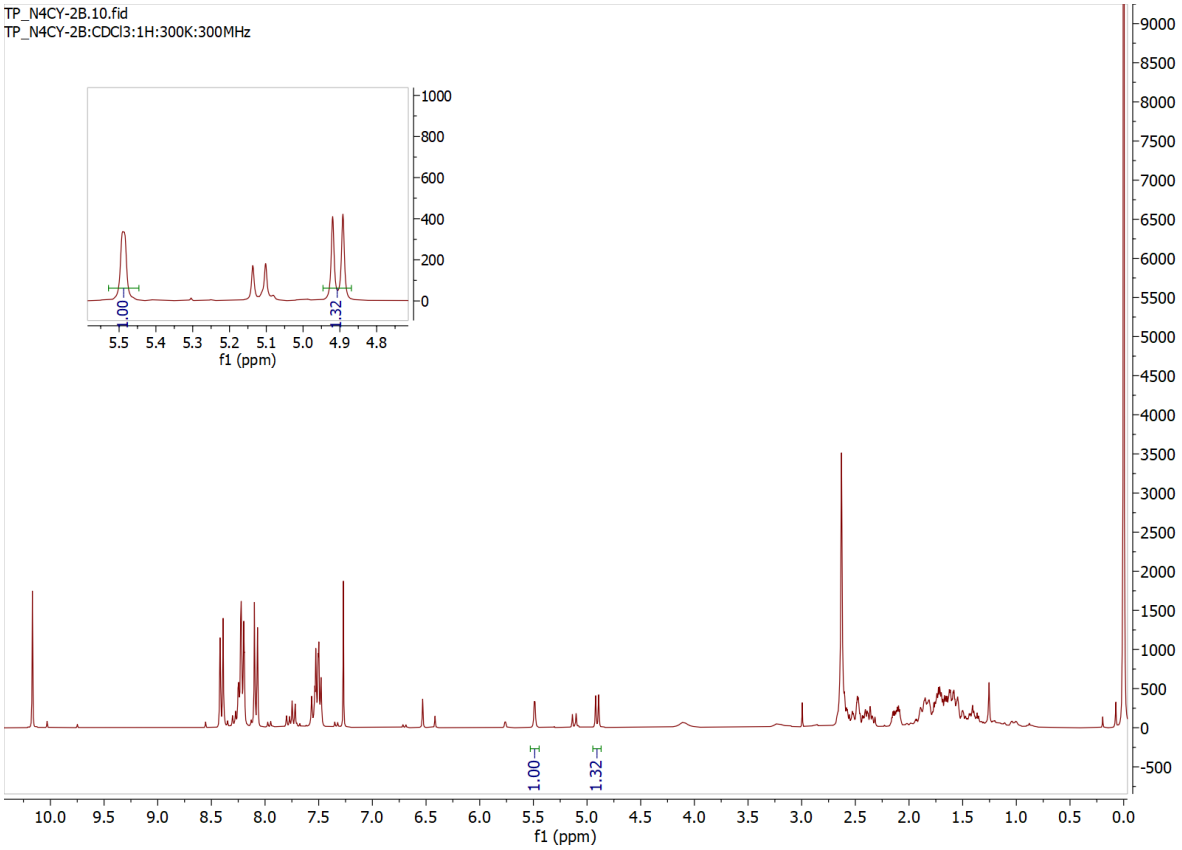


Figure S.4-36: ^{1}H NMR spectrum of the crude product of **TP_A4.4N4CY**

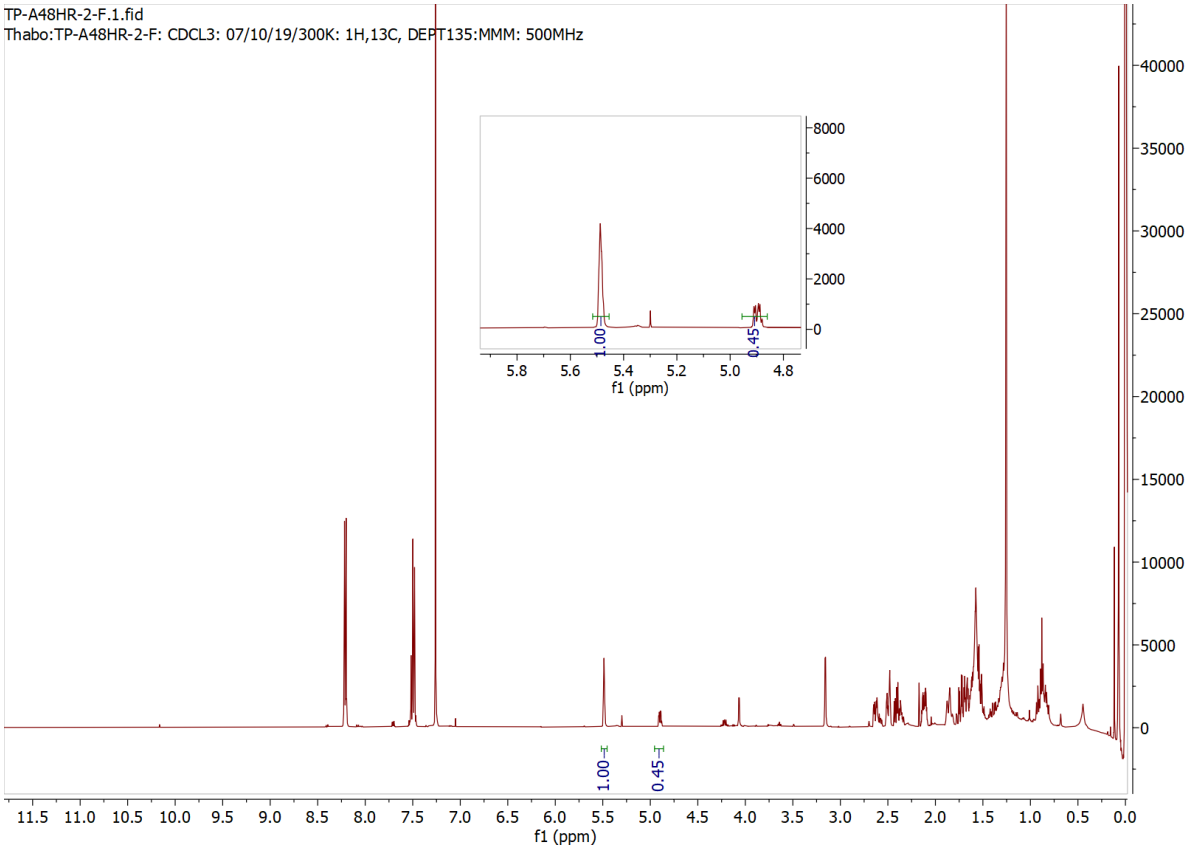


Figure S.4-37: ^{1}H NMR spectrum of the crude product **TP_A4.5N4CY**

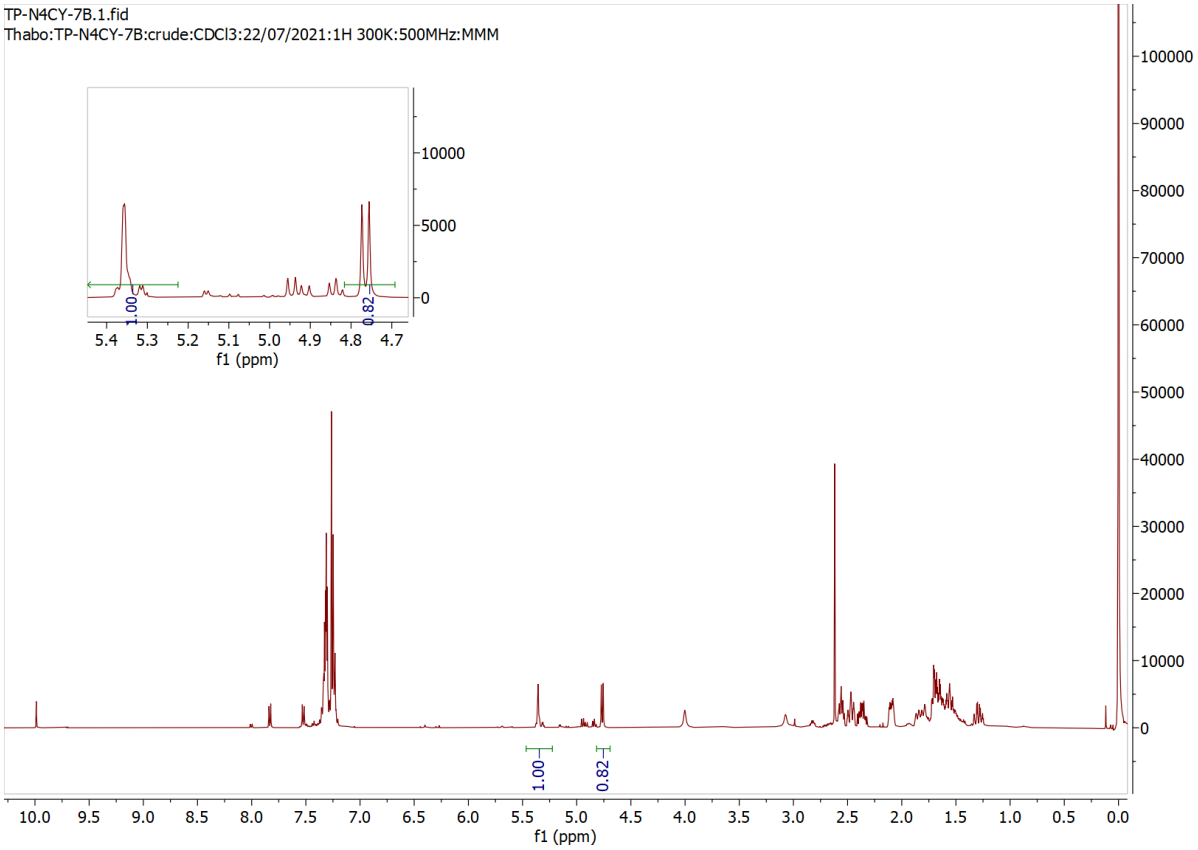


Figure S.4-38: ^{1}H NMR spectrum of the crude product of **TP_A4.6N4CY**

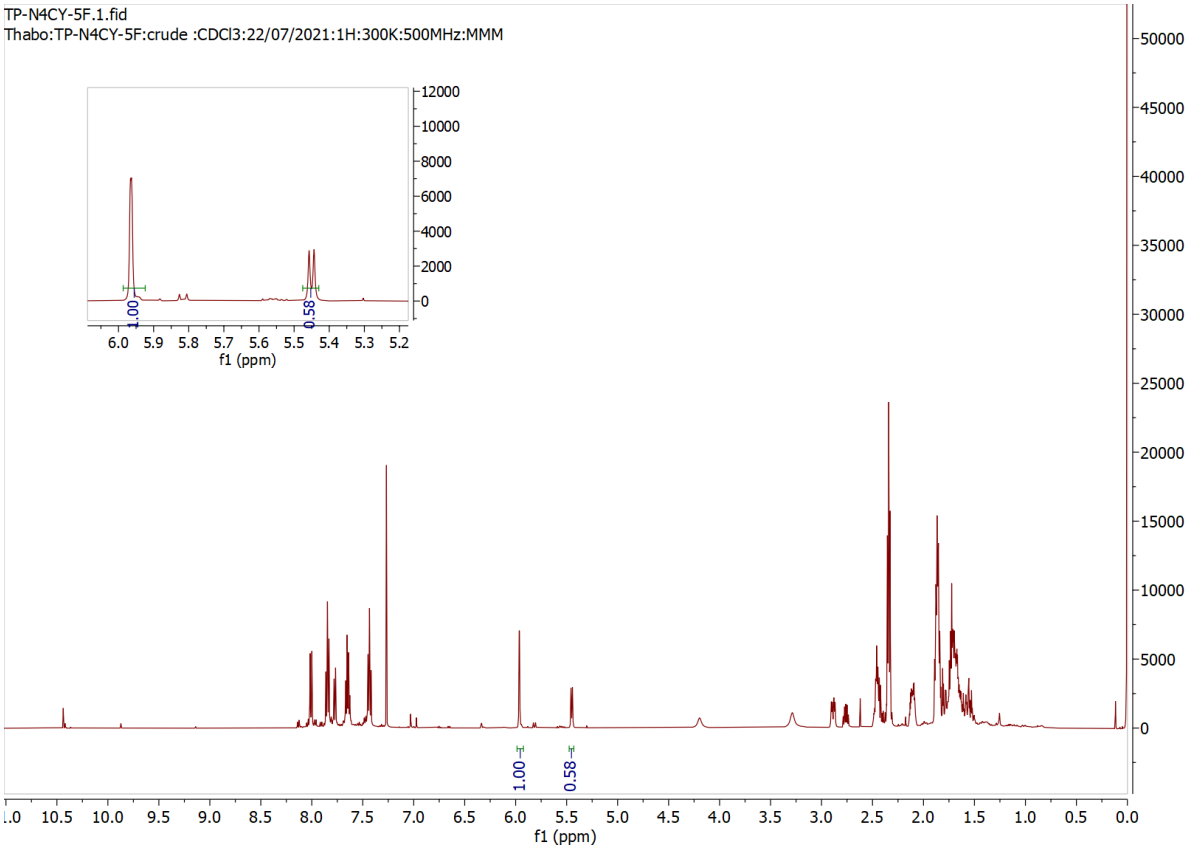


Figure S.4-39: ^{1}H NMR spectrum of the crude product of **TP_A4.8N4CY**

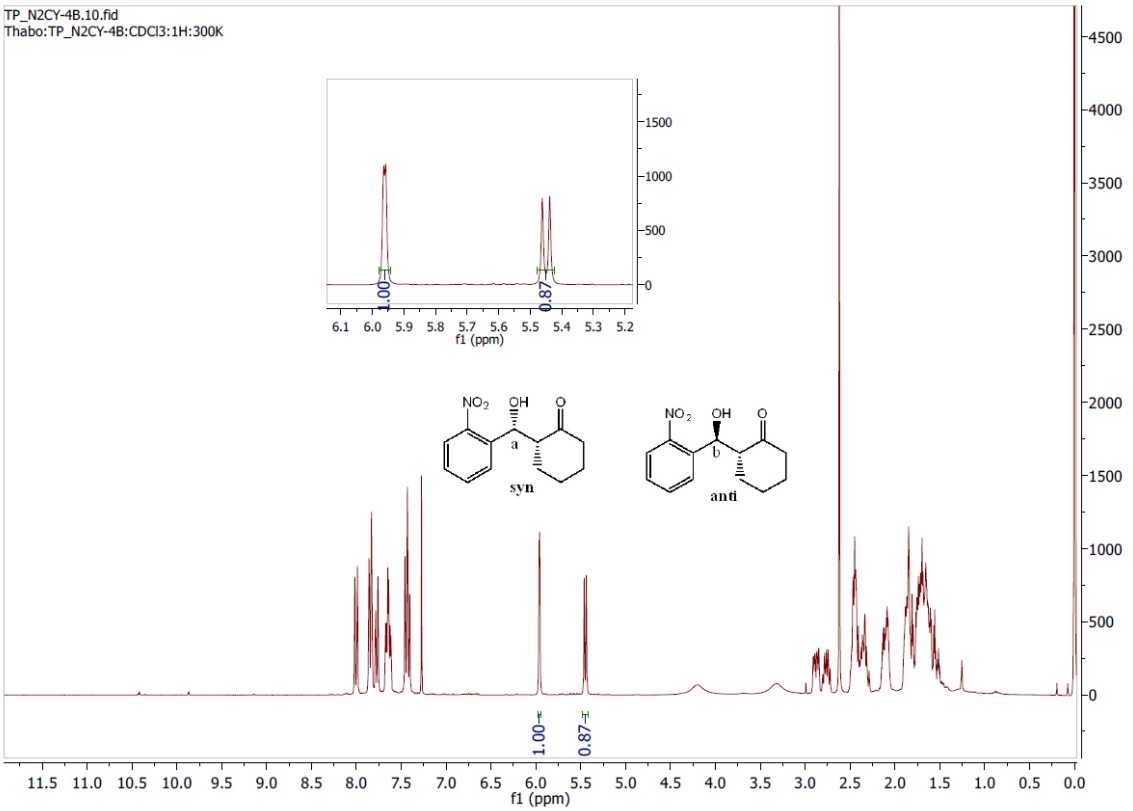


Figure S.4-40: ^{1}H NMR spectrum of the crude product of **TP_A5.1N2CY**

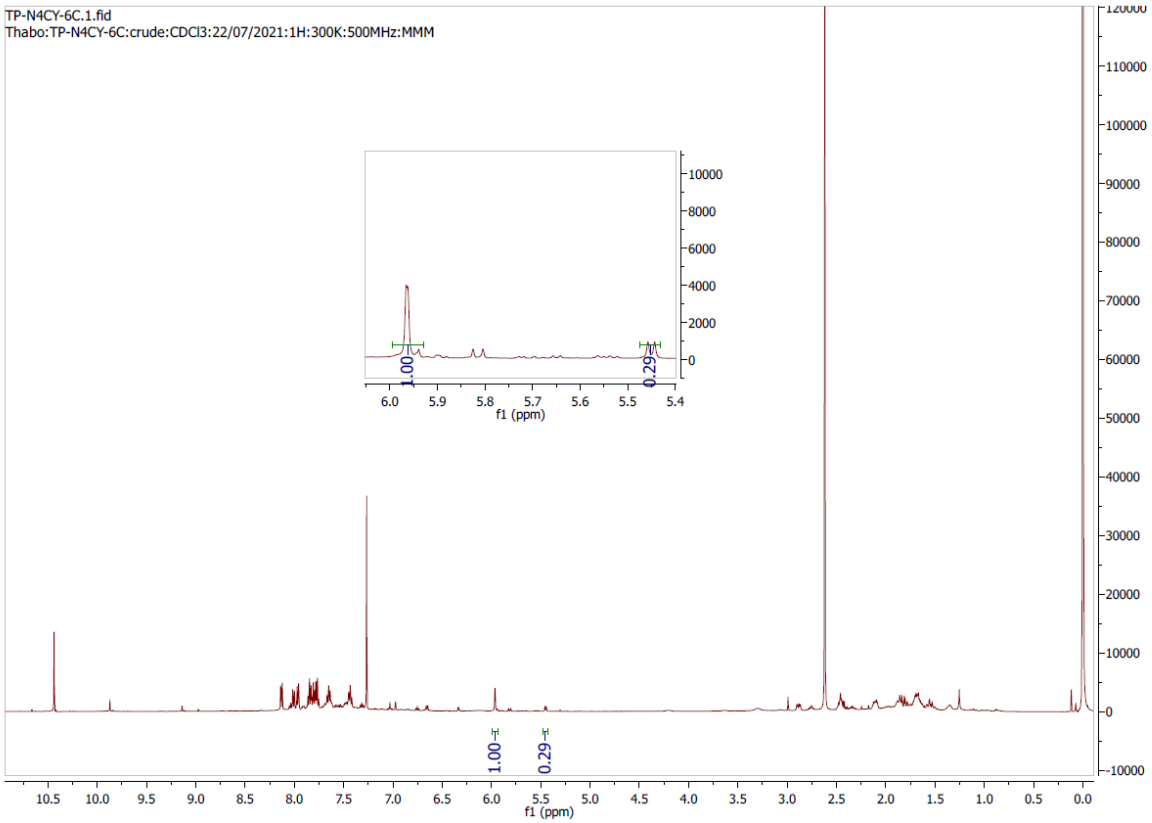


Figure S.4-41:^{1}H NMR spectrum of the crude product of **TP_A5.2N2CY**

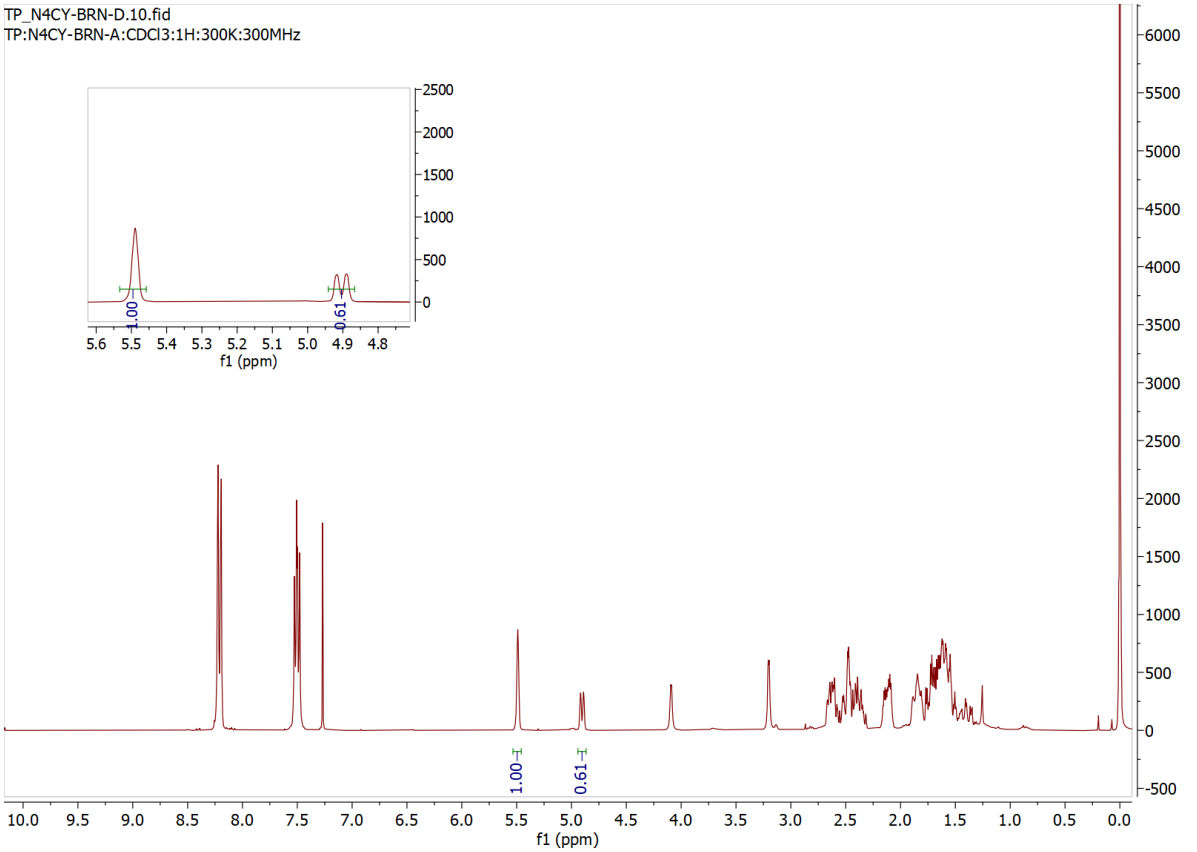


Figure S.4-42: ^{1}H NMR spectrum of the crude product **TP_A4.9N4CY**

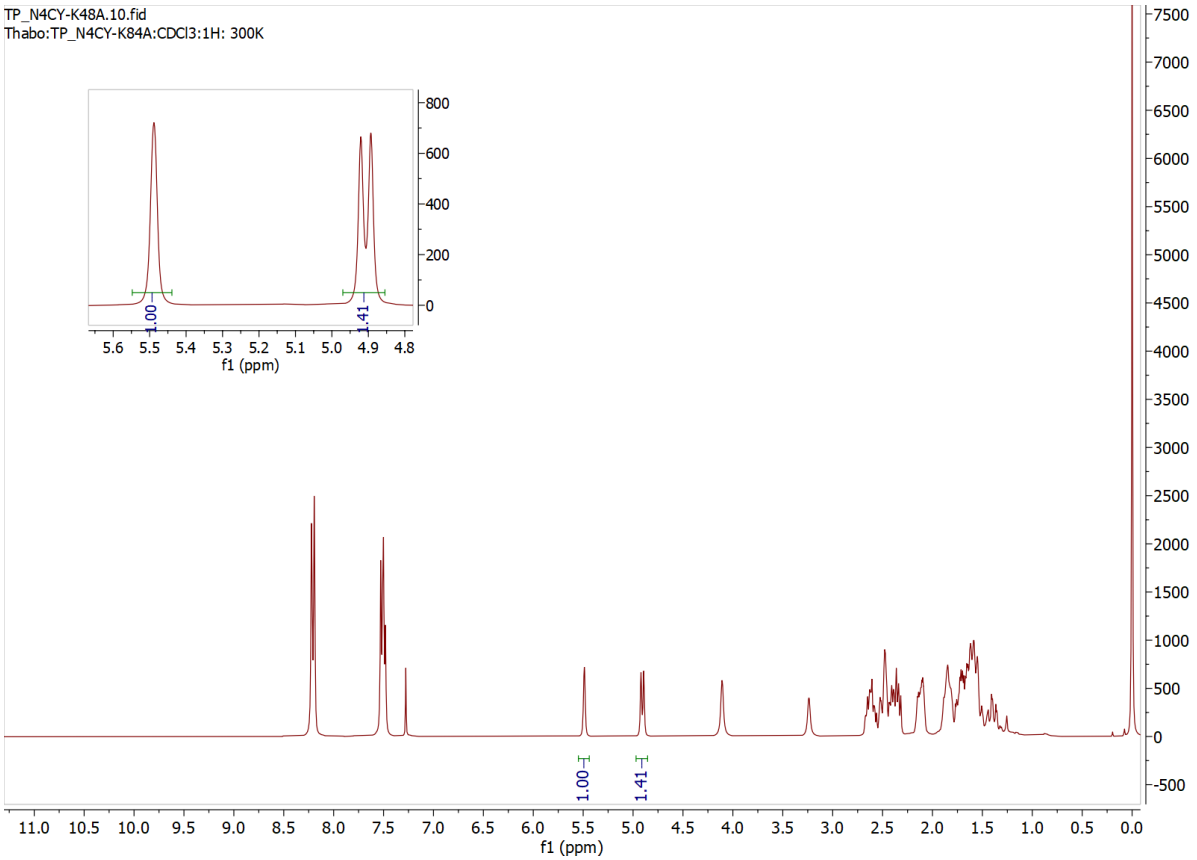


Figure S.4-43: ^{1}H NMR spectrum of the crude product **TP_A4.10N4CY**

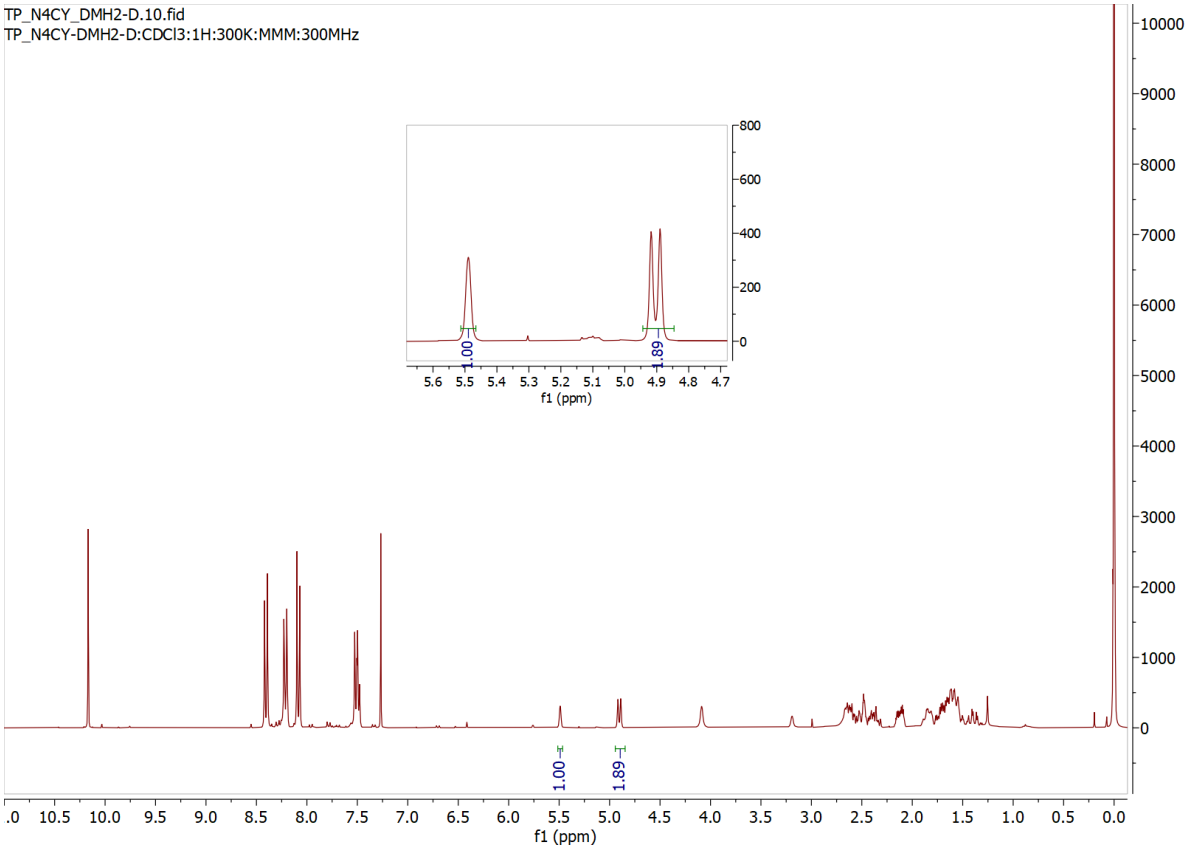


Figure S.4-44: ^{1}H NMR spectrum of the crude product **TP_A4.12N4CY**

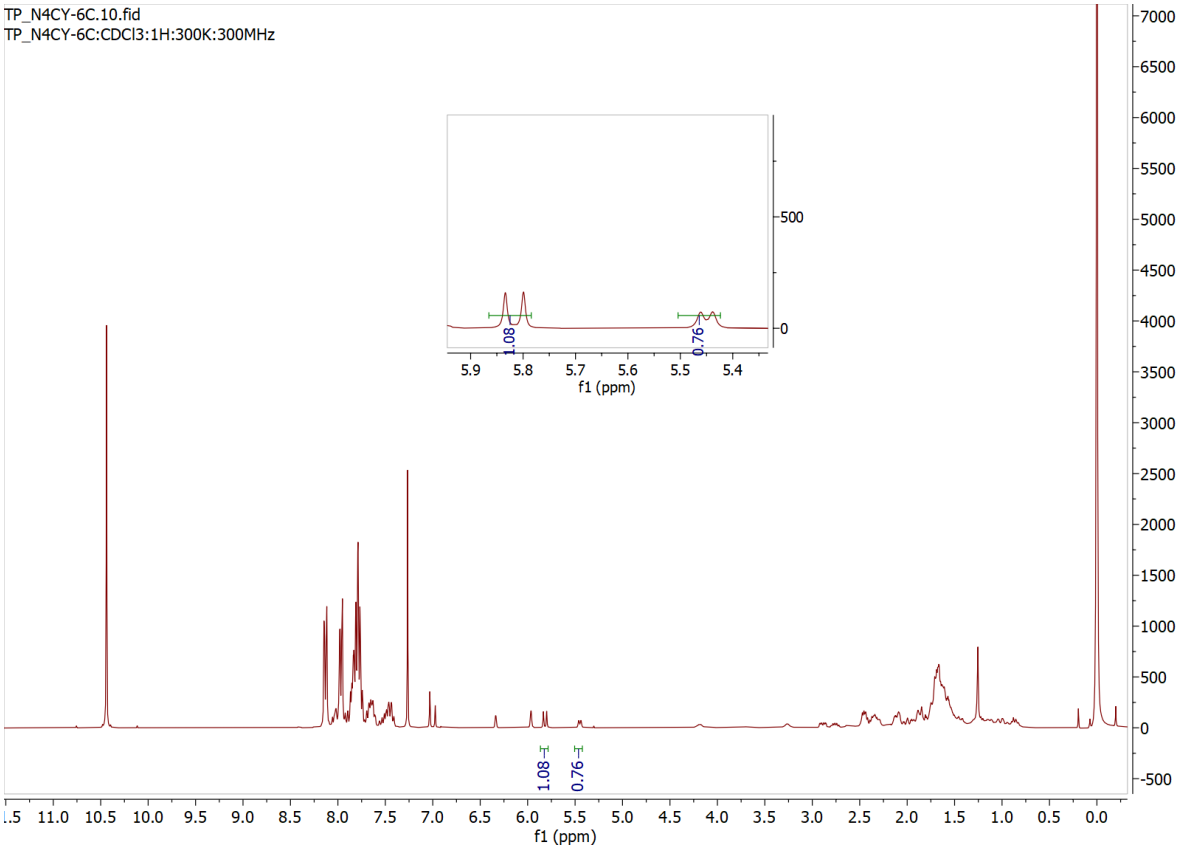


Figure S.4-45: ^{1}H NMR spectrum of the crude product of **TP_A4.14N4CY**

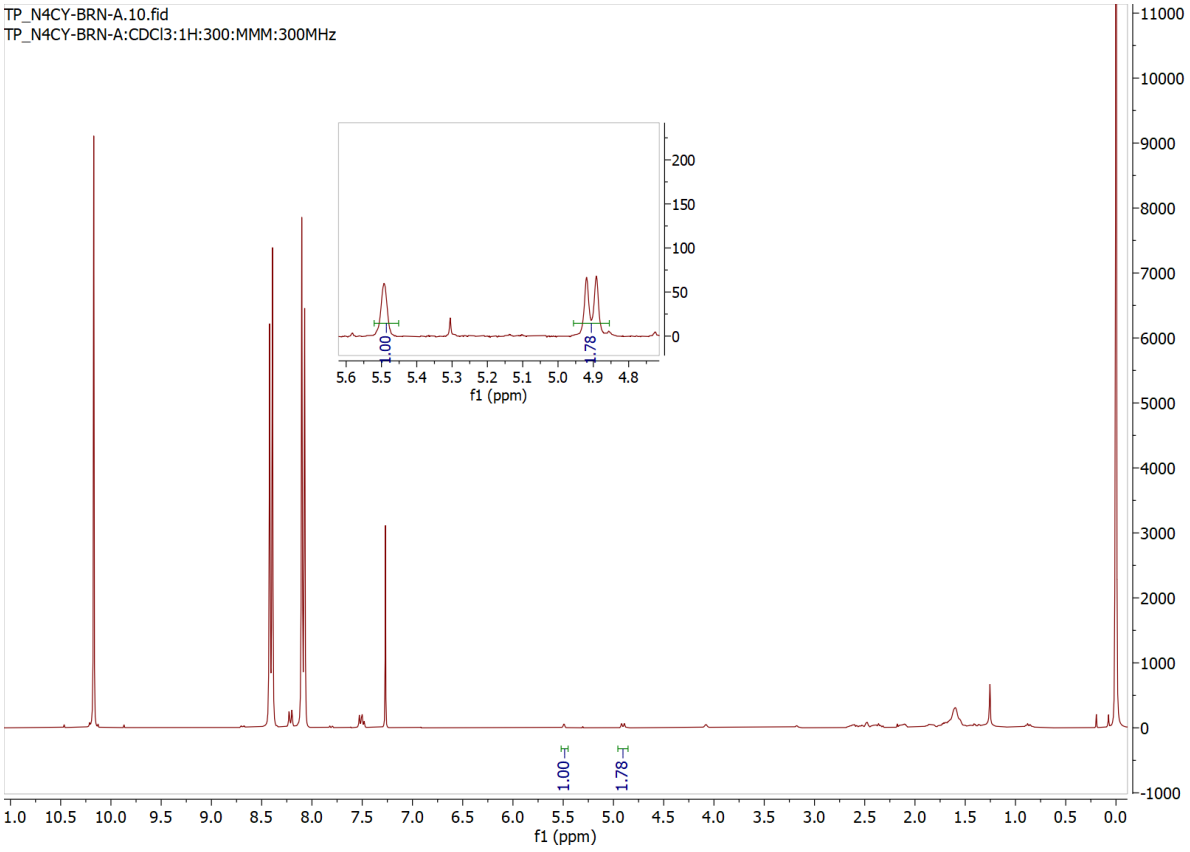


Figure S.4-46: ^{1}H NMR spectrum of the crude product of **TP_A4.16N4CY**

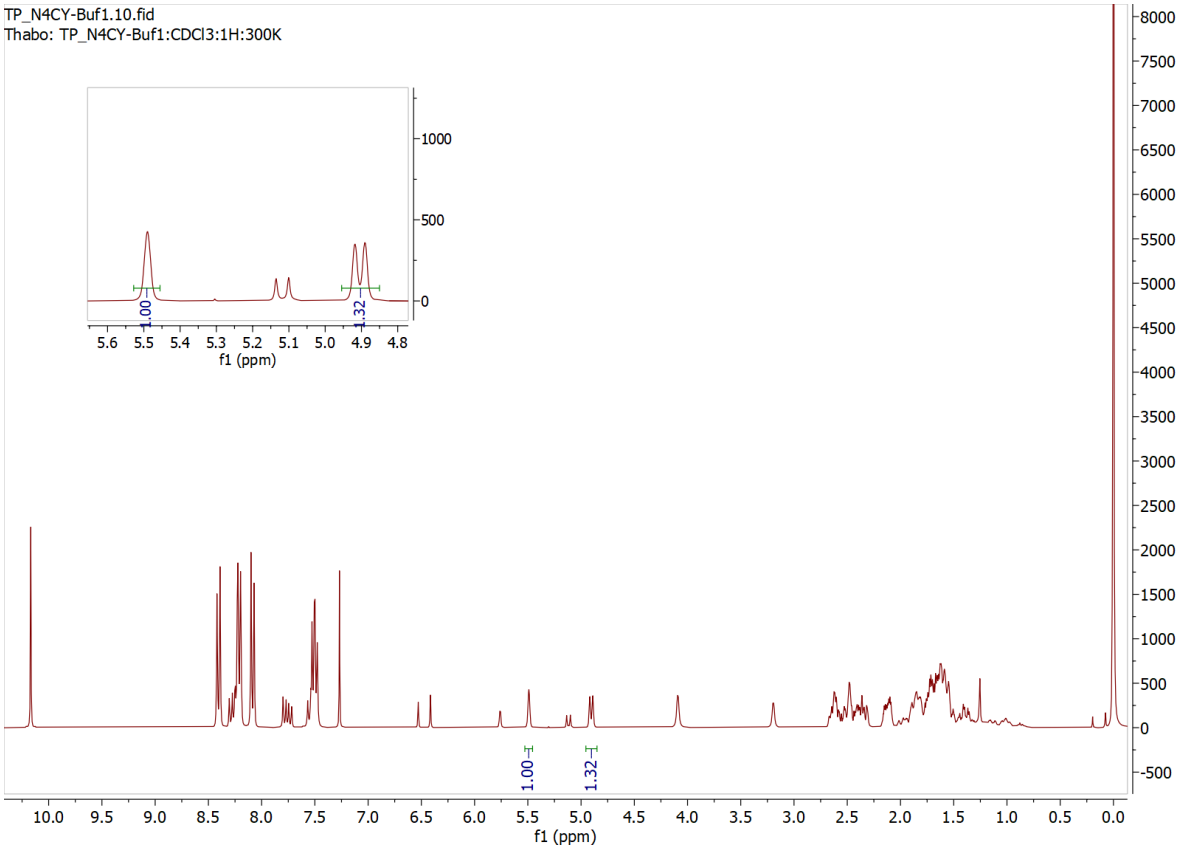


Figure S.4-47: ^{1}H NMR spectrum of the crude product **TP_A4.17N4CY**

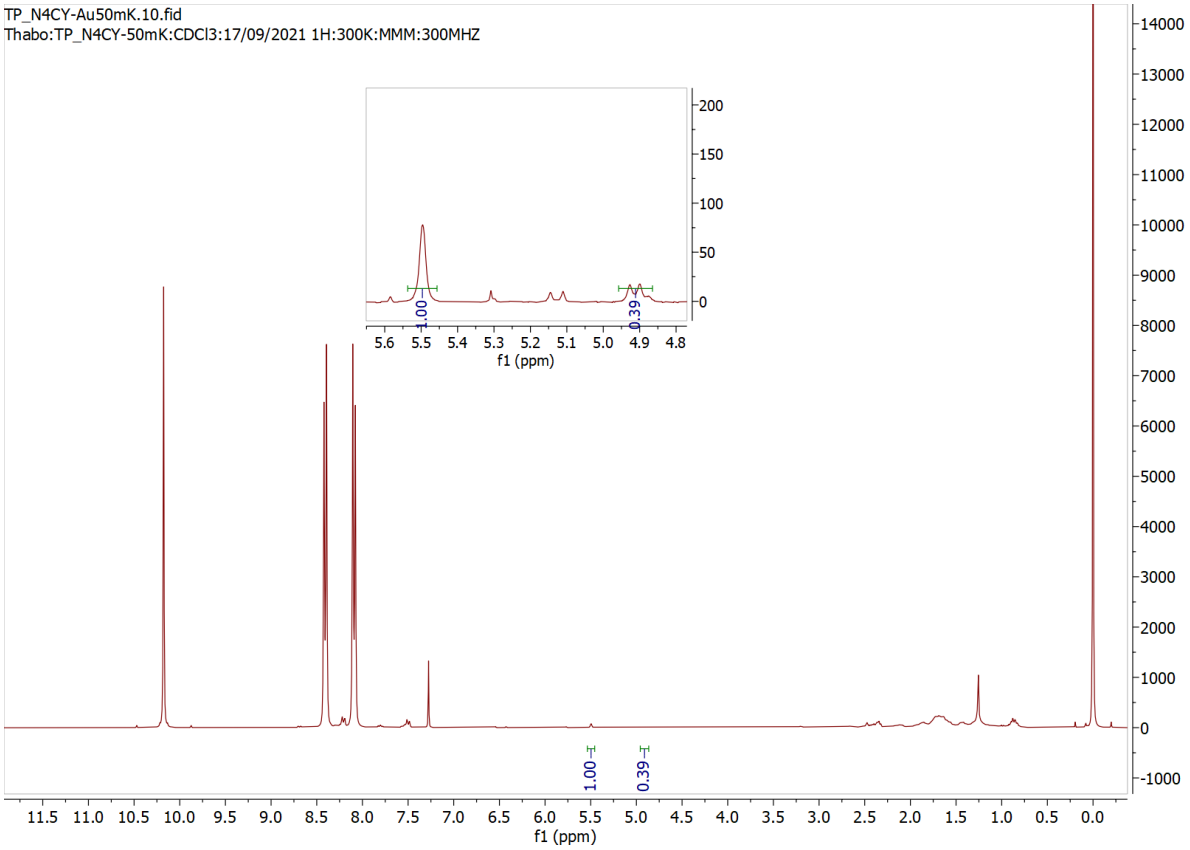


Figure S.4-48: ^{1}H NMR spectrum of the crude product **TP_A4.19N4CY**

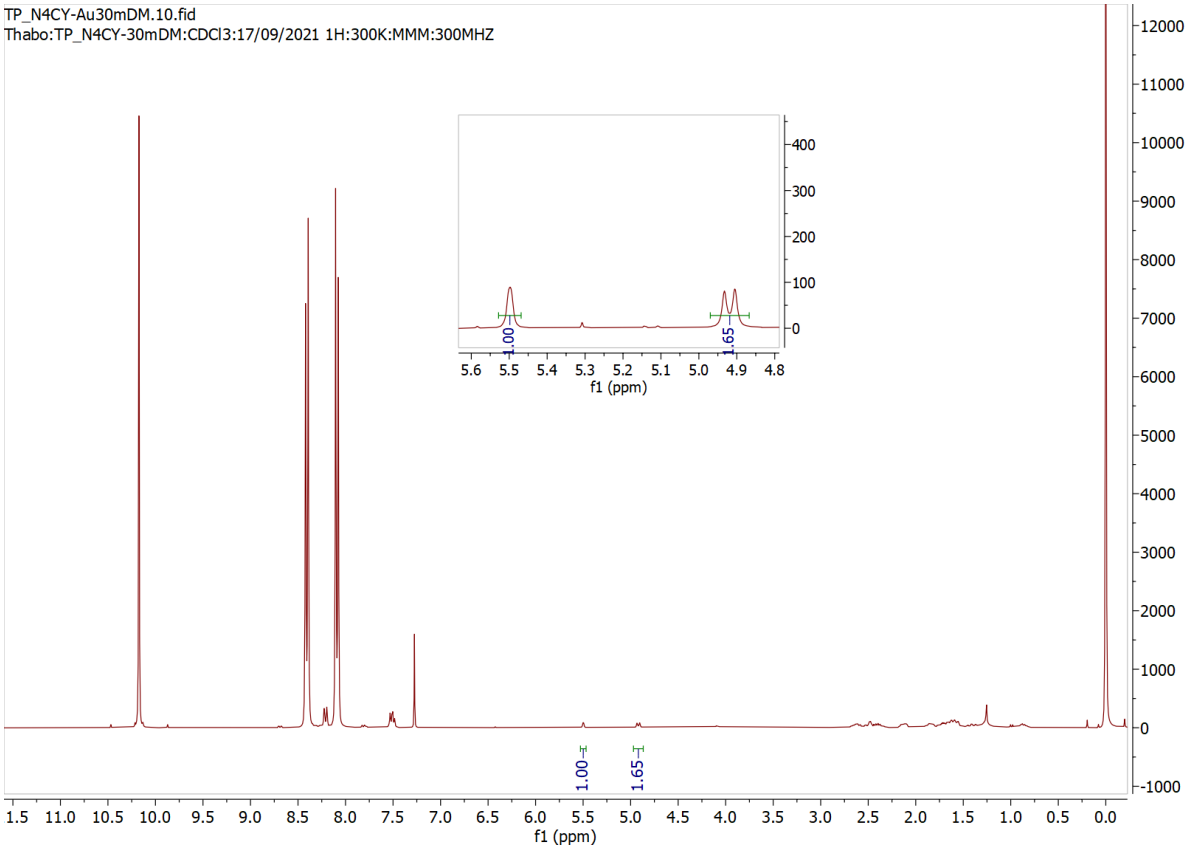


Figure S.4-49: ^{1}H NMR spectrum of the crude product **TP_A4.20N4CY**

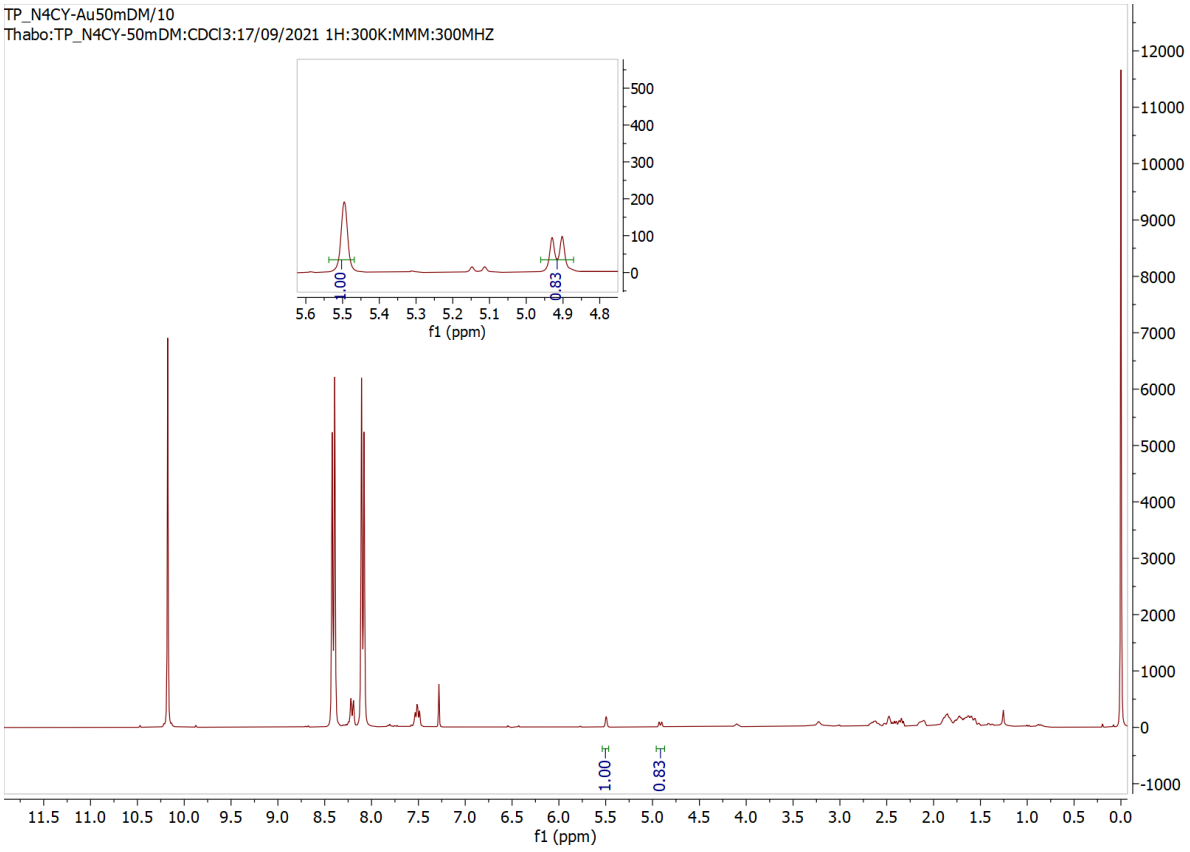


Figure S.4-50: ^{1}H NMR spectrum of the crude product **TP_A4.21N4CY**

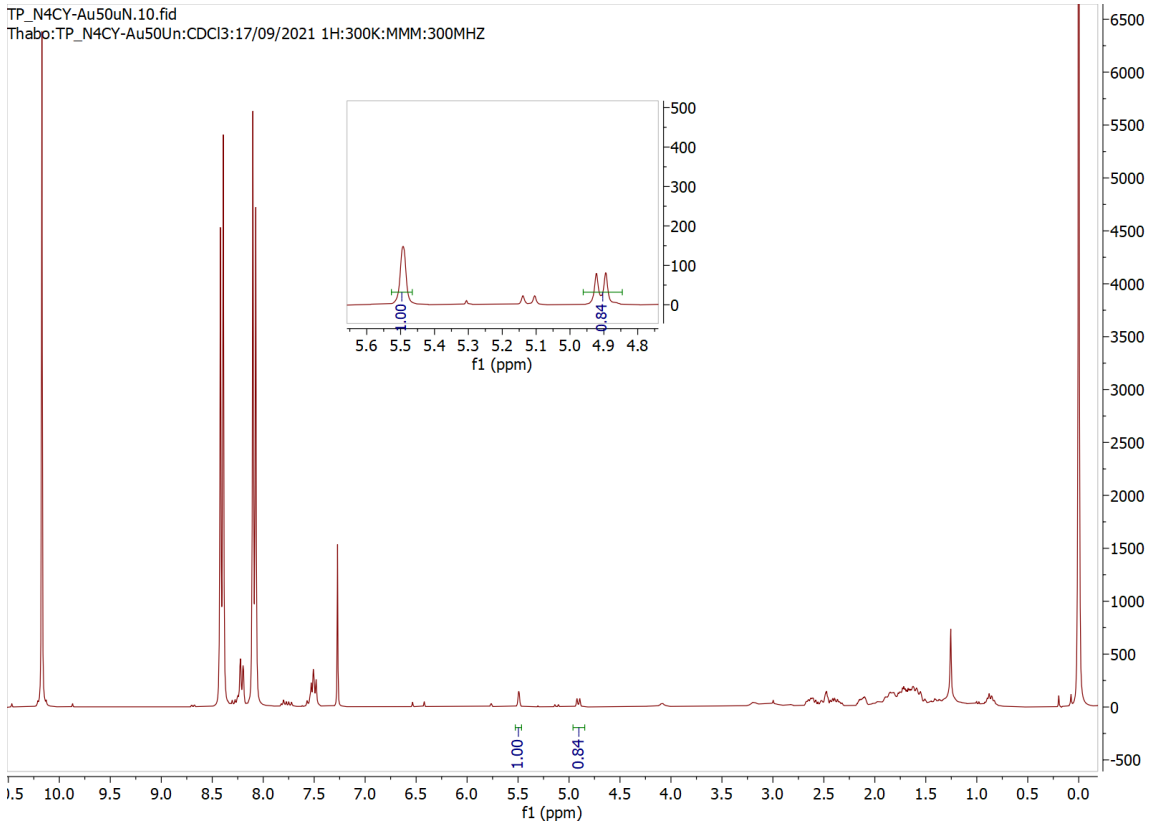


Figure S.4-51:^{1}H NMR spectrum of the crude product **TP_A4.22N4CY**

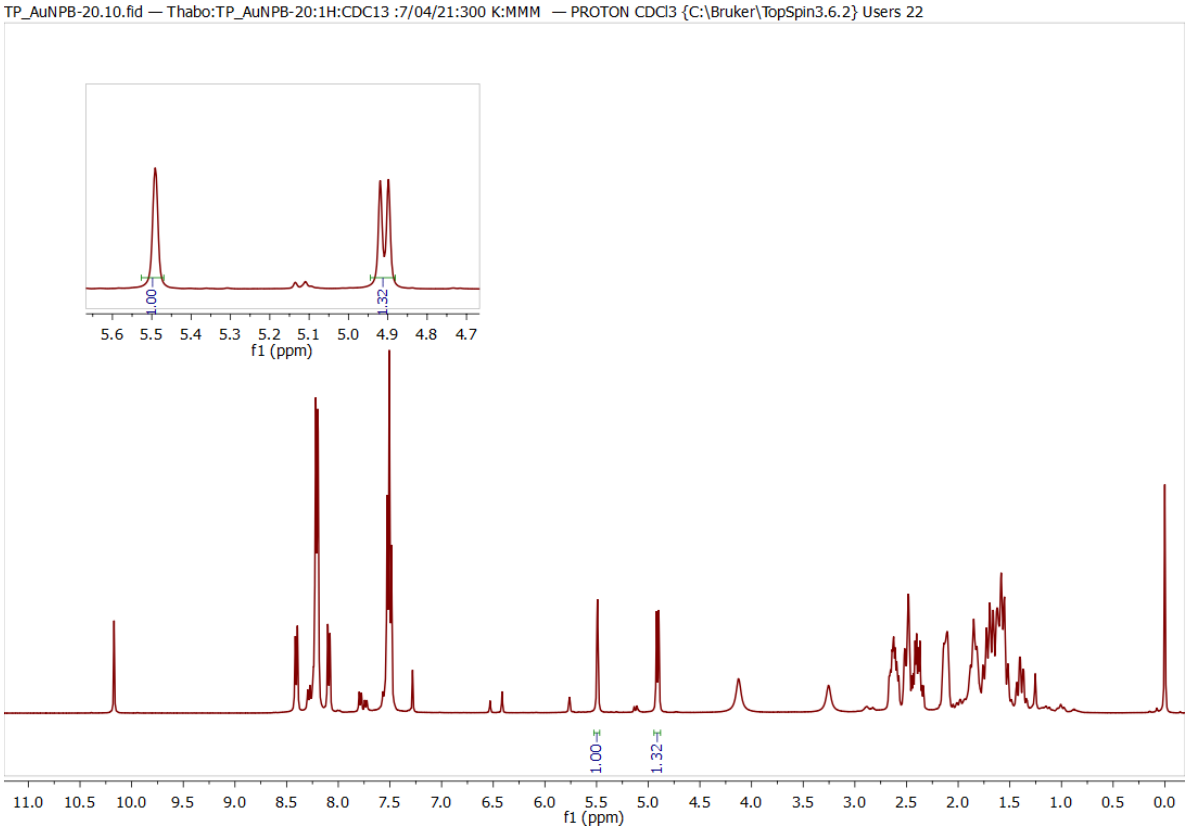


Figure S.4-52:[1]H NMR spectrum of the crude product **TP_A4.23N4CY**

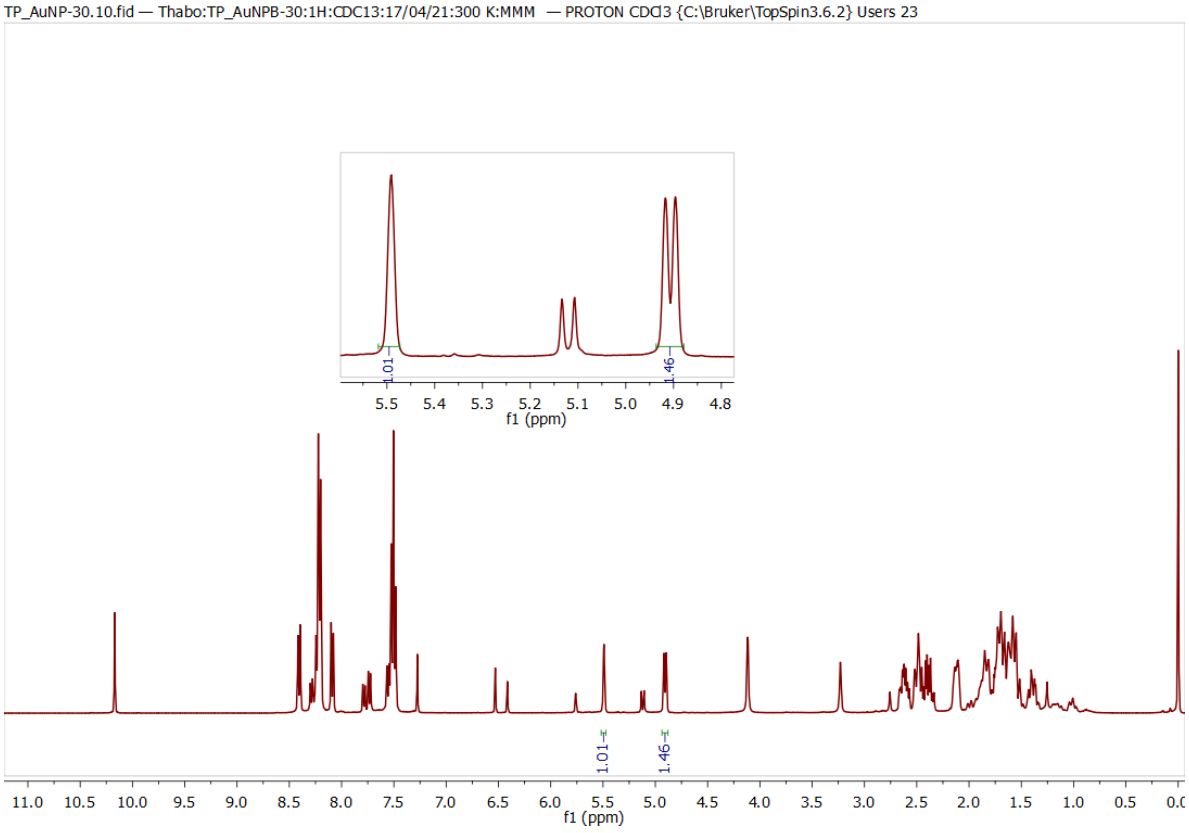


Figure S.4-53:[1]H NMR spectrum of the crude product **TP_A4.24N4CY**

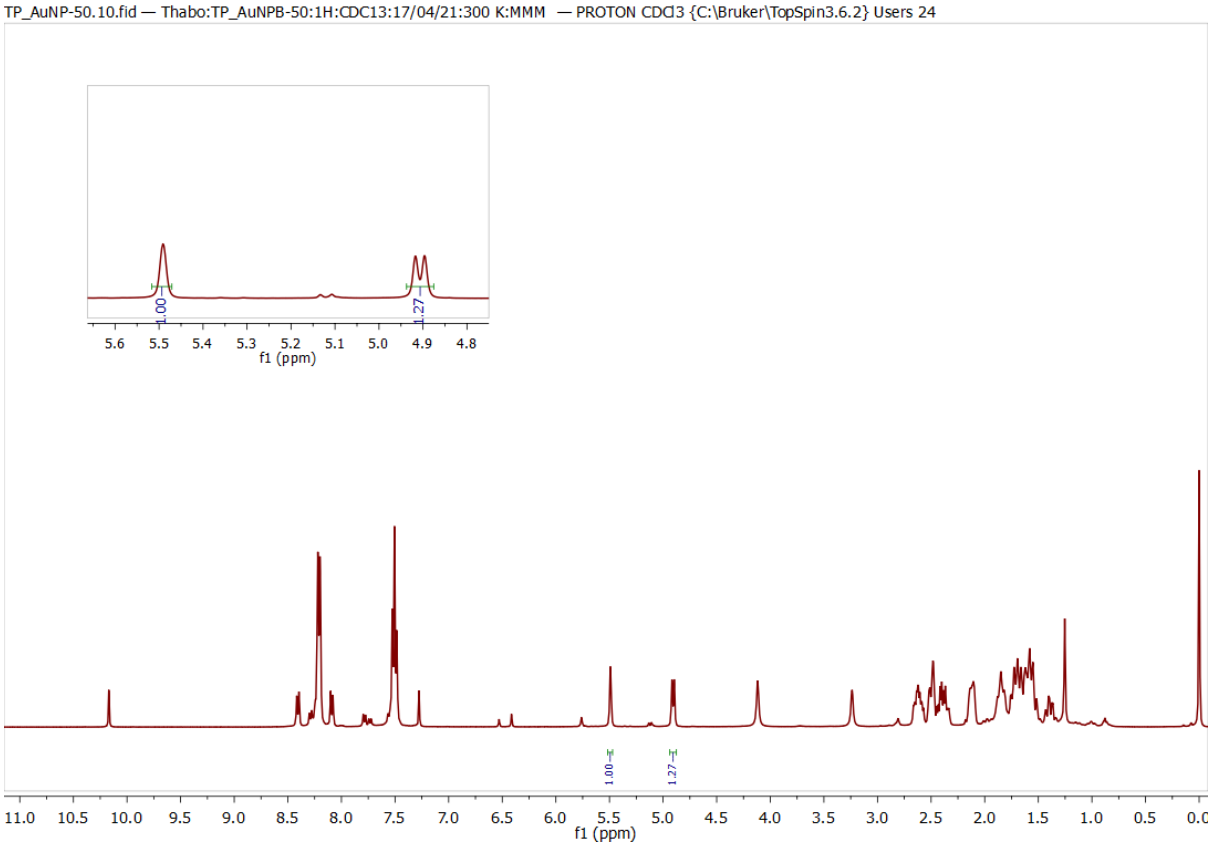


Figure S.4-54:^{1}H NMR spectrum of the crude product **TP_A4.25N4CY**